INTEGRATIVE MULTI-OMICS FOR DIAGNOSIS, TREATMENTS, AND DRUG DISCOVERY OF AGING-RELATED NEURONAL DISEASES

EDITED BY: Min Tang, Tao Huang, Jialiang Yang and Cheng Guo
PUBLISHED IN: Frontiers in Aging Neuroscience

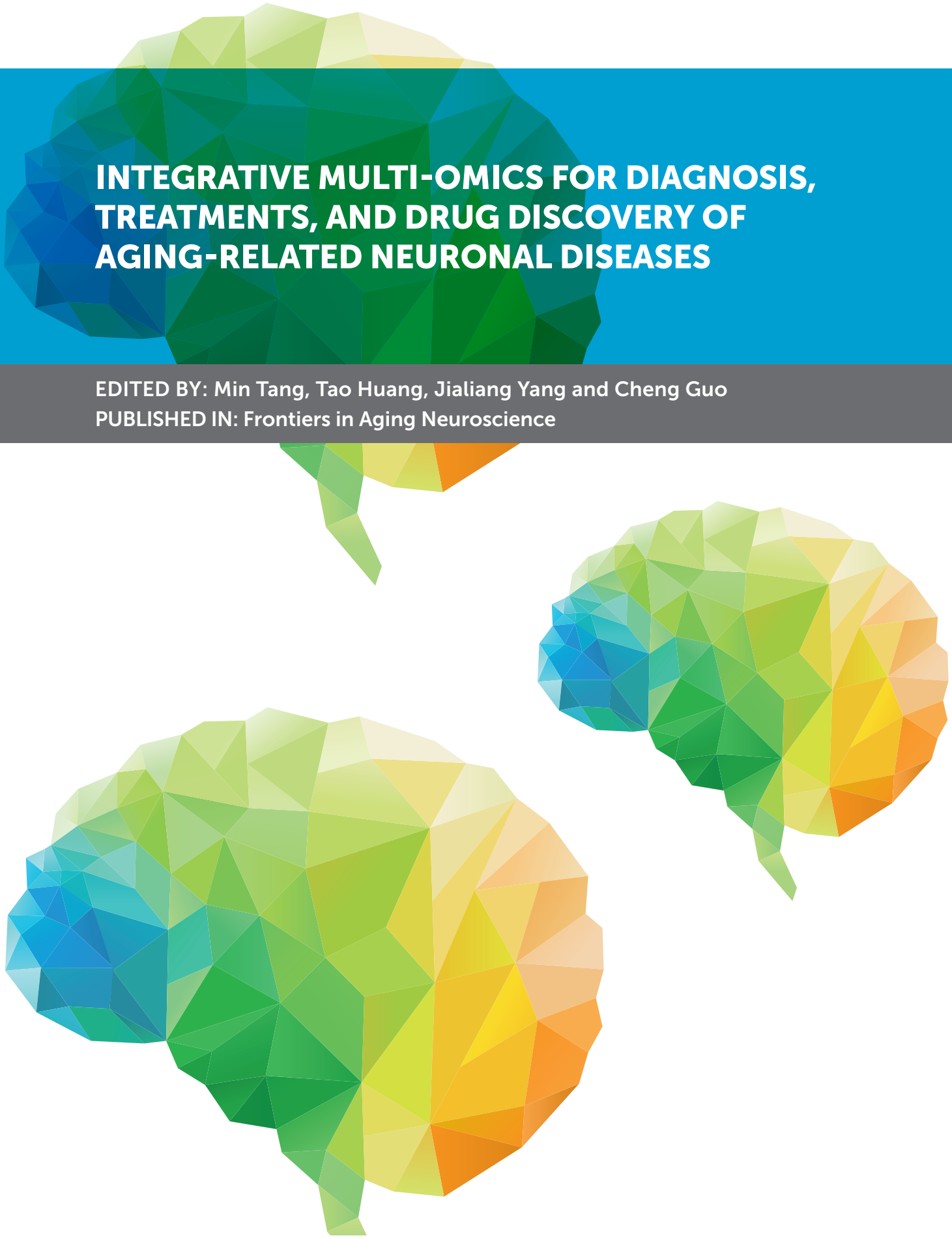

frontiers Research Topics

frontiers

ISSN 1664-8714
ISBN 978-2-83250-667-7
DOI 10.3389/978-2-83250-667-7

About Frontiers

Frontiers is more than just an open-access publisher of scholarly articles: it is a pioneering approach to the world of academia, radically improving the way scholarly research is managed. The grand vision of Frontiers is a world where all people have an equal opportunity to seek, share and generate knowledge. Frontiers provides immediate and permanent online open access to all its publications, but this alone is not enough to realize our grand goals.

Frontiers Journal Series

The Frontiers Journal Series is a multi-tier and interdisciplinary set of open-access, online journals, promising a paradigm shift from the current review, selection and dissemination processes in academic publishing. All Frontiers journals are driven by researchers for researchers; therefore, they constitute a service to the scholarly community. At the same time, the Frontiers Journal Series operates on a revolutionary invention, the tiered publishing system, initially addressing specific communities of scholars, and gradually climbing up to broader public understanding, thus serving the interests of the lay society, too.

Dedication to Quality

Each Frontiers article is a landmark of the highest quality, thanks to genuinely collaborative interactions between authors and review editors, who include some of the world's best academicians. Research must be certified by peers before entering a stream of knowledge that may eventually reach the public - and shape society; therefore, Frontiers only applies the most rigorous and unbiased reviews.
Frontiers revolutionizes research publishing by freely delivering the most outstanding research, evaluated with no bias from both the academic and social point of view. By applying the most advanced information technologies, Frontiers is catapulting scholarly publishing into a new generation.

What are Frontiers Research Topics?

Frontiers Research Topics are very popular trademarks of the Frontiers Journals Series: they are collections of at least ten articles, all centered on a particular subject. With their unique mix of varied contributions from Original Research to Review Articles, Frontiers Research Topics unify the most influential researchers, the latest key findings and historical advances in a hot research area! Find out more on how to host your own Frontiers Research Topic or contribute to one as an author by contacting the Frontiers Editorial Office: frontiersin.org/about/contact

INTEGRATIVE MULTI-OMICS FOR DIAGNOSIS, TREATMENTS, AND DRUG DISCOVERY OF AGING-RELATED NEURONAL DISEASES

Topic Editors:
Min Tang, Jiangsu University, China
Tao Huang, Shanghai Institute of Nutrition and Health, Chinese Academy of Sciences (CAS), China
Jialiang Yang, Geneis (Beijing) Co. Ltd, China
Cheng Guo, Columbia University, United States

Citation: Tang, M., Huang, T., Yang, J., Guo, C., eds. (2022). Integrative Multi-Omics for Diagnosis, Treatments, and Drug Discovery of Aging-Related Neuronal Diseases. Lausanne: Frontiers Media SA.
doi: 10.3389/978-2-83250-667-7

Table of Contents

frontiers | Frontiers in Aging Neuroscience

TYPE Editorial
PUBLISHED 18 October 2022
DOI 10.3389/fnagi.2022.1047076

OPEN ACCESS

EDITED AND REVIEWED BY
Kristy A. Nielson,
Marquette University, United States

*CORRESPONDENCE
Min Tang
mt3138@ujs.edu.cn

SPECIALTY SECTION
This article was submitted to Neurocognitive Aging and Behavior, a section of the journal Frontiers in Aging Neuroscience

RECEIVED 17 September 2022
ACCEPTED 04 October 2022
PUBLISHED 18 October 2022

CITATION
Shan C, Liu X, Liu Y, Zhang H, Liu J, Guo Y, Gong X and Tang M (2022) Editorial: Integrative multi-omics for diagnosis, treatments, and drug discovery of aging-related neuronal diseases.
Front. Aging Neurosci. 14:1047076.
doi: 10.3389/fnagi.2022.1047076

Editorial: Integrative multi-omics for diagnosis, treatments, and drug discovery of aging-related neuronal diseases

Chaofan Shan[1], Xiaoyan Liu[1], Yi Liu[1,2], Hantao Zhang[1], Junlin Liu[1], Yinglu Guo[1], Xun Gong[3] and Min Tang[1]*

[1]School of Life Sciences, Jiangsu University, Zhenjiang, China, [2]Institute of Animal Science, Jiangsu Academy of Agricultural Sciences, Nanjing, China, [3]Affiliated Hospital of Jiangsu University, Zhenjiang, China

KEYWORDS

multi-omics, drug discovery, Alzheimer's disease, ischemic stroke, Parkinson's disease

Editorial on the Research Topic
Integrative multi-omics for diagnosis, treatments, and drug discovery of aging-related neuronal diseases

The prevalence of aging-related neuronal diseases is increasing. However, there is still a huge unmet need for diagnosis, treatments, and drug discovery of these diseases. With the development of modern high-throughput omic measurement platforms, vast amounts of biological data have been generated which can be integrated in multi-omics studies to examine the complex molecular underpinnings of diseases, thus impacting the development of aging-related neuronal diseases' therapy.

In this editorial, we presented an account of how integrative multi-omics studies have greatly facilitated the diagnosis, treatments, and drug discovery of aging-related neuronal diseases. This editorial is based on 13 research articles and 3 regular reviews which shed light on the power of integrative multi-omics studies to improve aging-related neuronal diseases' therapy including but not limited to Alzheimer's disease (AD), ischemic stroke (IS), and Parkinson's disease (PD).

Several research articles analyze variables for prediction. In Han et al.'s cross-sectional study, chi square test, correlation analysis, and regression analysis were employed to analyze the influencing factors of cognitive impairment. Consequently, gender, age, education level, hypertension, and LDL-C were found to have significant differences in the incidence of cognitive impairment, providing a basis for the early screening and intervention in the elderly (Han et al.). Two research articles create prediction models based on variables of interest. Kang et al. developed an accurate, efficient nomogram with a model created by Cox regression method and further built a corresponding website to help clinicians improve their assessment of patient outcomes. In Li J. et al.'s study, they applied machine learning classification model light

gradient boosting machine (LightGBM) to analyze presurgical variables of endovascular treatment (EVT) for acute ischemic stroke (AIS) induced by large-vessel occlusion (LVO) and construct a unique prediction model which was used to establish feasible and accurate presurgical prediction scale in identifying unfavorable outcomes of AIS after EVT.

Eight research articles capture gene signature (models) by integrating multi-omics information through different bioinformatics analysis and machine learning approaches. Zhang C. et al. first employed the limma R package to the got the significant differentially expressed genes (DGEs) in Depression. These DEGS were then put into weighted gene co-expression network analysis (WGCNA) and protein–protein interaction (PPI) analysis and at last the common gene general transcription factor IIF polypeptide 2 (GTF2F2) which may serve as a promising diagnostic biomarker and treatment target of depression was thus identified (Zhang C. et al.). Most of the bioinformatic approaches in this study were implemented in the article of Gu et al., where Stepwise regression and logistic regression analyses were employed to get hub genes and diagnostic model related to Iron Metabolism in AD. They also retrieved eight drugs targeting hub genes from the DrugBank database (Gu et al.). A similar study in IS was completed by Wang X. et al. where Boruta algorithm was used for genes' further screening. Importantly, they validated the gene signature with many methods, such as enrichment analyses through GO, KEGG, and GSEA pathways, ROC curves, and immune cell infiltration. Moreover, Li D. et al. demonstrated that gene methylation can also be utilized as signatures. In their research, least absolute shrinkage and selection operator cox regression analysis were carried out to construct a diagnostic signature related to PD (Li D. et al.). In Zhang W. et al.'s study, the molecular mechanism of Xingnao Kaiqiao Pill in the treatment of perioperative neurocognitive disorder (PND) was investigated from the perspective of network pharmacology and molecular docking technology. They constructed the network of "Xingnao Kaiqiao Pill–traditional Chinese medicine–compound–common target" by Cytoscape software. Molecular docking stimulation was used to further verify the interaction between the active components and key targets (Zhang W. et al.). Huang et al. and Chen Y. et al. both performed multi-omics integration analysis based on single cell technology. In their study, scRNA analysis, differential expression analysis, cell-cell communication analyses, and cell trajectory inference analyses were performed to identify candidate ligands or receptors, as well as the corresponding cell types. Combined with molecular docking, Huang et al. found that Quercetin targets VCAM1 to prevent diabetic cerebrovascular endothelial cell injury (Huang et al.), while Chen Y. et al. further identified differentially expressed transcription factors in AD associated with exercise using a modified SCENIC method. Chen Y. et al. finally constructed a network of exercise-regulating TFs in monocytes, revealing the mechanism by which exercise regulated monocytes to confer therapeutic benefits against AD and its complications. Furthermore, through target gene's knockdown and bioassays, Xia et al. found that GDF15 effectively alleviated neuronal ferroptosis post Spinal cord injury (SCI) *via* the p62-Keap1-Nrf2 signaling pathway and promoted locomotor recovery of SCI mice, which is suggested as a potential target on SCI pathogenesis and treatment.

Notably, two research articles focus on the development of computational approaches which can integrate multi-omics information. Based on topological features extracted from a protein-protein interaction (PPI) network and functional features extracted by integrating subcellular localization and homologous information of proteins, Zhu et al. exploited a novel iterative method called linear neighborhood similarity-based protein multifeatures fusion (LNSPF) to predict potential key proteins. The gene expression data downloaded from the benchmark database are used for further optimization through linear neighborhood similarity (Zhu et al.). To find biologically important imaging genetic relations more powerfully, Wang et al. imposed the GraphNet regularization penalty on the existing model and presented an improved fusion paired group lasso structured sparse canonical correlation analysis algorithm (FGLGNSCCA). Experiment results shown that the new FGLGNSCCA model proposed in their manuscript is superior or equivalent to traditional methods. With FGLGNSCCA algorithm, more AD-related biomarkers can been found (Wang et al.).

Finally, three reviews give a comprehensive understanding of the progress in the field of aging-related neuronal diseases from different aspects. Chen W. et al.'s review focuses on optogenetics in neurobiology, including how to use optogenetics to control nerve cells, study neural circuits, and treat diseases by changing the state of neurons. Wang Y. et al. revealed potential protective role of polysaccharides of Neurodegenerative Diseases (NDs), highlighting the contributions of polysaccharides and the prospects of their mechanism studies for the treatment of NDs. Ji et al. concentrated on body fluids biomarkers of early neurological deterioration (END) that have shown potential to be transferred into clinical practice.

In conclusion, the research articles and reviews in this Research Topic show how integrative multi-omics are applied to better understand and treat aging-related neuronal disease. For fully utilizing data from various omics sources to gain insights into disease, multi-omics approaches are becoming more relevant every day.

Author contributions

This editorial was designed by MT and XG and written by CS and XL. YL, HZ, and YG had revised it. All authors have made a direct and intellectual contribution to this topic and approved the article for publication.

Funding

This work was supported by grants from Jiangsu University (19JDG039) and the National Natural Science Foundation of China (32002235).

Conflict of interest

The authors declare that the research was conducted in the absence of any commercial or financial relationships that could be construed as a potential conflict of interest.

Publisher's note

All claims expressed in this article are solely those of the authors and do not necessarily represent those of their affiliated organizations, or those of the publisher, the editors and the reviewers. Any product that may be evaluated in this article, or claim that may be made by its manufacturer, is not guaranteed or endorsed by the publisher.

frontiers in Aging Neuroscience

ORIGINAL RESEARCH
published: 06 January 2022
doi: 10.3389/fnagi.2021.817520

An Improved Fusion Paired Group Lasso Structured Sparse Canonical Correlation Analysis Based on Brain Imaging Genetics to Identify Biomarkers of Alzheimer's Disease

Shuaiqun Wang†, Xinqi Wu†, Kai Wei and Wei Kong*

College of Information Engineering, Shanghai Maritime University, Shanghai, China

OPEN ACCESS

Edited by:
Tao Huang,
Shanghai Institute of Nutrition and Health, Chinese Academy of Sciences (CAS), China

Reviewed by:
Xiaoqi Zheng,
Shanghai Normal University, China
Zhe Xu,
Changzhou Institute of Technology, China

***Correspondence:**
Shuaiqun Wang
wangsq@shmtu.edu.cn

†*These authors share first authorship*

Specialty section:
This article was submitted to Alzheimer's Disease and Related Dementias, a section of the journal Frontiers in Aging Neuroscience

Received: *18 November 2021*
Accepted: *14 December 2021*
Published: *06 January 2022*

Citation:
Wang S, Wu X, Wei K and Kong W (2022) An Improved Fusion Paired Group Lasso Structured Sparse Canonical Correlation Analysis Based on Brain Imaging Genetics to Identify Biomarkers of Alzheimer's Disease. Front. Aging Neurosci. 13:817520. doi: 10.3389/fnagi.2021.817520

Brain imaging genetics can demonstrate the complicated relationship between genetic factors and the structure or function of the humankind brain. Therefore, it has become an important research topic and attracted more and more attention from scholars. The structured sparse canonical correlation analysis (SCCA) model has been widely used to identify the association between brain image data and genetic data in imaging genetics. To investigate the intricate genetic basis of cerebrum imaging phenotypes, a great deal of other standard SCCA methods combining different interested structed have now appeared. For example, some models use group lasso penalty, and some use the fused lasso or the graph/network guided fused lasso for feature selection. However, prior knowledge may not be completely available and the group lasso methods have limited capabilities in practical applications. The graph/network guided approaches can use sample correlation to define constraints, thereby overcoming this problem. Unfortunately, this also has certain limitations. The graph/network conducted methods are susceptible to the sign of the sample correlation of the data, which will affect the stability of the model. To improve the efficiency and stability of SCCA, a sparse canonical correlation analysis model with GraphNet regularization (FGLGNSCCA) is proposed in this manuscript. Based on the FGLSCCA model, the GraphNet regularization penalty is imposed in our study and an optimization algorithm is presented to optimize the model. The structural Magnetic Resonance Imaging (sMRI) and gene expression data are used in this study to find the genotype and characteristics of brain regions associated with Alzheimer's disease (AD). Experiment results shown that the new FGLGNSCCA model proposed in this manuscript is superior or equivalent to traditional methods in both artificially synthesized neuroimaging genetics data or actual neuroimaging genetics data. It can select essential features more powerfully compared with other multivariate methods and identify significant canonical correlation coefficients as well as captures more significant typical weight patterns which demonstrated its excellent ability in finding biologically important imaging genetic relations.

Keywords: sparse canonical correlation analysis (SCCA), GraphNet regularization, Alzheimer's disease (AD), brain imaging genetics, SNP, gene expression

INTRODUCTION

Alzheimer's disease (AD) is an irreversible long-time neurodegenerative disease and not only brings misfortune to the patient, but also brings a heavy economic and emotional burden to the family (Alzheimer's Association, 2013). AD is the most common form of dementia and its incidence increases with the aging of the population (Goldberg, 2007). In the past ten years, image genetics has become a crucial research topic in biomedicine and bioinformatics. The reason is that the potential influence of genes on brain structure and function can be found by genetic research. As a powerful tool for data-driven association analysis, statistical learning methods can make full use of the inherent structural information of biomarker data to build models to analyze the correlation between susceptible genes and brain structure or function which can indicate the pathogenesis of brain cognitive behavior or related diseases well. Image genetics can be used to identify the relationship between imaging results and genetic variables (Chen et al., 2013; Hashimoto et al., 2015; Aghakhanyan et al., 2018). Therefore, imaging genetics has become a hot research topic in biomedicine and bioinformatics research.

Correlated canonical analysis (CCA) (Hotelling, 1936) is a classic algorithm and a hot spot in imaging genetics. CCA can be used to mine the correlation between data. However, when using the traditional CCA method, a serious over-fitting phenomenon may appear. For the sake of dealing with this issue, some scholars have introduced sparse canonical correlation analysis (SCCA), which can be used to identify bivariate contacts between a great number of genes and dozens of imaging quantitative traits (QTs). Then, to more effectively distinguish the bivariate correlation about a series of genes with a large number of imaging QTs, some researchers have made different amendments for SCCA. The GraphNet based sparse canonical correlation analysis model (GNSCCA) used graph-constrained resilient network regularization, which not only can find meaningful connections, but also contribute to the smoothness between adjacent coefficients (Du et al., 2015). The an improved GNSCCA method (AGNSCCA) introduced one new penalty to improve SCCA model and developed an effective optimization algorithm to get a better typical correlation coefficient (Du et al., 2016). Sparse canonical correlation analysis based on joint connectivity (JCBSCCA) proposed a connectivity-based penalty measure to incorporate prior biological information and had sound anti-noise performance (Kim et al., 2020). Some scholars have considered that genetic data and imaging features had different group-level structures. Because prior knowledge is not fully available in real life, they improved the lasso penalty combined lasso with graph/network guidance in structured sparse learning. Du et al. (2020) proposed the FGLSCCA (Grosenick et al., 2013) adding two new penalty conditions to the SCCA model, namely, the fusion paired group lasso (FGL) as well as the graph guided paired group lasso (GGL). However, FGLSCCA also has certain shortcomings. The stability and anti-interference of the FGLSCCA algorithm are not good enough, and it cannot incorporate physiological restraints such as connectivity.

In response to the above problems, FGLGNSCCA algorithm is proposed in our present study. First of all, GraphNet regularization (Grosenick et al., 2013) is added to the punitive measure in FGLGNSCCA model. GraphNet regularization is an upgraded version of resilient network regularization and can validly incorporate physiological restraints. Moreover, JCBSCCA has confirmed its stability and noise resistance. To make the model's results more biological explanatory power, this manuscript applies it as prior knowledge to the model. Secondly, this manuscript derives an efficient iterative optimization algorithm, which proves that the algorithm converges to the optimal local solution. Firstly, we use synthetic data for testing. These experiments illustrate that the algorithm has better noise immunity than other algorithms. When the data set is small, it has more smoothness. Then we use the accurate data set. These results suggest that it has a better canonical correlation coefficient. It is effective to recognize salient features on the actual data set.

METHOD

Sparse Canonical Correlation Analysis

In the formulas, bold lowercase letters represent vectors and bold uppercase letters describe matrices. Expressly, we set $\mathbf{X} \in R^{n \times p}$, $\mathbf{Y} \in R^{n \times q}$ in this article. $\mathbf{X}$ has n samples and p features, while $\mathbf{Y}$ has n samples and q features. Meanwhile, $\mathbf{X}$ is the genotype data set as well as $\mathbf{Y}$ is the image data set. CCA is used to analyze the correlation between two data sets. The purpose of the CCA model is to find the weight vectors $\mathbf{u}$ and $\mathbf{v}$ of the features in $\mathbf{X}$ and $\mathbf{Y}$ that maximize the relation. The formula is as follows:

$$\max_{\mathrm{u,v}} \mathbf{u}^{\mathrm{T}} \boldsymbol{X}^{\boldsymbol{T}} \boldsymbol{Y} \mathbf{v} \tag{1}$$

$$\text{s.t.} \mathbf{u}^{\mathrm{T}} \boldsymbol{X}^{\boldsymbol{T}} \boldsymbol{X} \mathbf{u} \;=\; \mathbf{v}^{\mathrm{T}} \boldsymbol{Y}^{\boldsymbol{T}} \boldsymbol{Y} \mathbf{v} \;=\; 1,$$

In image genetics, the feature dimensions of data are often much higher than the sample size which lead to over-fitting. Witten et al., proposed sparse SCCA (Parkhomenko et al., 2009; Du et al., 2020) to solve excessive feature dimensionality. The definition is as follows:

$$\min_{u,v} -\mathbf{u}^{\mathrm{T}} \mathbf{X}^{\mathrm{T}} \mathbf{Y} v \;+\; \lambda_{\mathrm{u}} \left| |\mathbf{u}| \right|_1^1 {}_{+\,\lambda_{\mathrm{v}}} \left| |\mathbf{v}| \right|_1^1 \tag{2}$$

$$s.t. \left| |\mathbf{u}| \right|_2^2 \;=\; \left| |\mathbf{v}| \right|_2^2 \;=\; 1$$

FGLSCCA Model

Du et al. (2020) imposed two new penalties FGL and GGL on the SCCA model (Grosenick et al., 2013).

$$\min_{u,v} -\mathbf{u}^{\mathrm{T}} \mathbf{X}^{\mathrm{T}} \mathbf{Y} v \;+\; \Omega_{\mathrm{FGL}} (\mathbf{u}) \;+\; \Omega_{\mathrm{GGL}} (\mathbf{v}) \tag{3}$$

$$s.t. ||\mathbf{X}\mathbf{u}||^2 \;\leq\; 1, ||\mathbf{Y}\mathbf{v}||^2 \;\leq\; 1$$

Among them, the FGL and GGL penalties are defined as:

$$\Omega_{FGL} (\mathbf{u}) \;=\; \lambda_1 \sum_{i=1}^{p-1} \omega_{i,i+1} \sqrt{u_i^2 \;+\; u_{i+1}^2} \tag{4}$$

$$\Omega_{\mathrm{GGL}} (\mathbf{v}) \;=\; \lambda_2 \sum_{(j,k) \in E} \omega_{j,k} \sqrt{v_j^2 \;+\; v_k^2} \tag{5}$$

Here, $\omega_{j,k}$ is the weight value of the edge. GGL is an effective technique for estimating the inverse covariance matrix.

New Connectivity Penalties

This article used a new penalty term based on connectivity, and it was graphed (Grosenick et al., 2013). GraphNet regularization is one restraint by an amended version of the resilient network regularization, which allows the effective integration of physical constraints of connectivity (Grosenick et al., 2013).

First of all, connectivity methods can quantify meaningful neurobiological measurements and are a good source of information (Hagmann et al., 2008). Second, the GraphNet regularization program encourages the similarity of the relevant elements of the canonical vector (Du et al., 2016). The formula is as follows:

$$\begin{aligned} \mathrm{P}(\mathbf{u}) &= \sum_{\mathrm{i,j}} \mathrm{C}_{\mathbf{u}(\mathrm{i,j})} (\mathbf{u}_\mathrm{i} - \mathbf{u}_\mathrm{j})^2 \\ \mathrm{P}(\mathbf{v}) &= \sum_{\mathrm{i,j}} \mathrm{C}_{\mathbf{v}(\mathrm{i,j})} (\mathbf{v}_\mathrm{i} - \mathbf{v}_\mathrm{j})^2 \end{aligned} \tag{6}$$

From the literature (Grosenick et al., 2013), the following formula can be obtained:

$$\mathrm{P}(\mathbf{u}) = \mathbf{u}^\mathrm{T}\mathbf{L}_\mathbf{u}\mathbf{u},\ \mathrm{P}(\mathbf{v}) = \mathbf{v}^\mathrm{T}\mathbf{L}_\mathbf{v}\mathbf{v} \tag{7}$$

$\mathbf{L_u}$ and $\mathbf{L_v}$ mean the Laplacian matrix.

The Proposed FGLGNSCCA Model

A new structured sparse canonical correlation analysis method (FGLGNSCCA) was proposed in this manuscript. In the presented model, $X \in R^{n \times p}$ and $\mathbf{Y} \in R^{n \times q}$represented the gene variable matrix and the brain image variable matrix, respectively. Meanwhile, $\mathbf{u}$ and $\mathbf{v}$ represented the characteristic weights or regular loads of $\boldsymbol{X}$ and $\boldsymbol{Y}$, respectively.

The model formula is as follows:

$$\begin{aligned} \min_{\mathrm{u,v}} -\mathbf{u}^\mathrm{T}\boldsymbol{X}^\mathrm{T}\boldsymbol{Y}\mathbf{v} + \Omega_{\mathrm{FGL}}(\mathbf{u}) + \Omega_{\mathrm{GGL}}(\mathbf{v}) + \frac{\gamma_1}{2}(||\mathbf{Xu}||^2 - 1) \\ + \frac{\gamma_2}{2}(||\boldsymbol{Y}\mathbf{v}||^2 - 1) + \frac{\lambda_1}{2}\mathbf{u}^T L_u \mathbf{u} + \frac{\lambda_2}{2}\mathbf{v}^T L_v \mathbf{v} \\ s.t. ||\mathbf{Xu}||^2 \le 1, ||\mathbf{Yv}||^2 \le 1, \end{aligned} \tag{8}$$

Figure 1 is the schematic diagram of the proposed algorithm FGLSCCA.

Agency Goals and Optimization Algorithms

If this article directly used the Lagrangian method to find the partial derivatives of $\mathbf{u}$ and $\mathbf{v}$ in equation (8), it was quite difficult. Therefore, we used the results of Grosenick et al. (2013), Du et al. (2020) and used the substitution functions $\Omega_{FGL}^{APP}(\mathbf{u})$ and $\Omega_{GGL}^{APP}(\mathbf{v})$ derived when processing the data. In addition, set $||\mathbf{Xu}||^2 = 1$ and $||\mathbf{Yv}||^2 = 1$, and $L(\mathbf{u}, \mathbf{v})$ is as follows:

$$\begin{aligned} L(\mathbf{u}, \mathbf{v}) = -\mathbf{u}^\mathrm{T}\boldsymbol{X}^\mathrm{T}\boldsymbol{Y}\mathbf{v} + \Omega_{FGL}^{APP}(\mathbf{u}) + \Omega_{GGL}^{APP}(\mathbf{v}) + \frac{\gamma_1}{2}(||\boldsymbol{X}\mathbf{u}||^2 - 1) \\ + \frac{\gamma_2}{2}(||\boldsymbol{Y}\mathbf{v}||^2 - 1) + \frac{\lambda_1}{2}\mathbf{u}^T \mathbf{L}_\mathbf{u} \mathbf{u} + \frac{\lambda_2}{2}\mathbf{v}^T \mathbf{L}_\mathbf{v} \mathbf{v} \end{aligned} \tag{9}$$

$\gamma_1, \gamma_2, \lambda_1$, and λ_2 are artificially set positive tuning parameters, and this Lagrangian function is continuous. Therefore, the vectors $\mathbf{u}$ and $\mathbf{v}$ can be differentiated. The partial derivatives of U and V need to be calculated, and then set $L(\mathbf{u}, \mathbf{v}) = 0$ to get

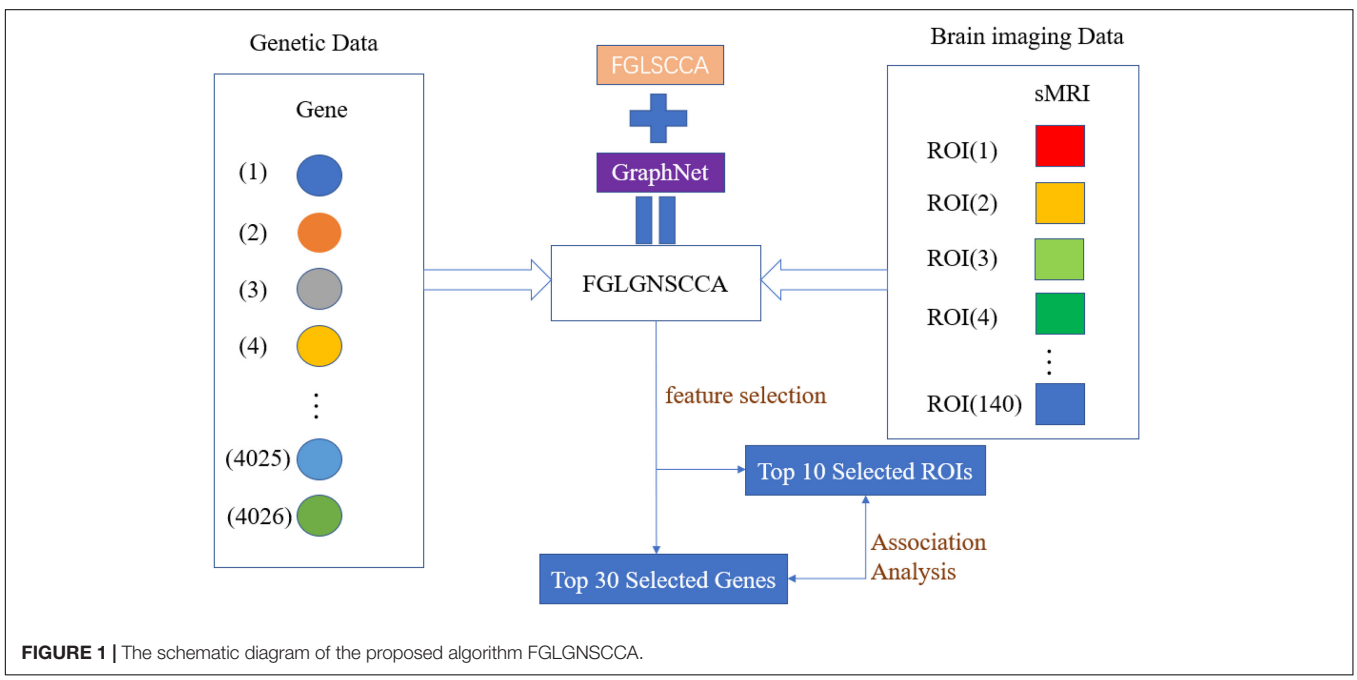

FIGURE 1 | The schematic diagram of the proposed algorithm FGLGNSCCA.

TABLE 1 | Pseudo code for FGLGNSCCA.

Algorithm 1: Algorithm for FGLGNSCCA

Require: Normalized data $\mathbf{X} \in R^{n \times p}, Y \in R^{n \times q}$, *set* parameters $\lambda_1, \lambda_2, \gamma_1, \gamma_2$
Ensure: Canonical vectors **u**, **v**
1:Initialize $\mathbf{u} \in R^{p \times 1}, \mathbf{v} \in R^{q \times 1}$
2:**While** not converged **do**
3: Update the diagonal matrix $\mathbf{D_X}$, P (**u**)
4: Fix **v** and solve $\mathbf{u} = \frac{\mathbf{X^T Y v}}{\lambda_1 \boldsymbol{D_X} + \gamma_1 \boldsymbol{X^T X} + \lambda_1 \mathbf{L_u}}$
5: Scale $\mathbf{u} = \mathbf{u}./sqrt(\mathbf{u^T X^T X u})$
6: Update the diagonal matrix $\boldsymbol{D_Y}$, P (**v**)
7: Fix **u** and solve $\mathbf{v} = \frac{\boldsymbol{Y^T X u}}{\lambda_2 \boldsymbol{D_Y} + \gamma_2 \boldsymbol{Y^T Y} + \lambda_2 \mathbf{L_v}}$
8: Scale $\mathbf{v} = \mathbf{v}./sqrt(\mathbf{v^T Y^T Y v})$
9:End while

the extreme value:

$$\mathbf{0} = -\mathbf{X^T Y v} + \left(\lambda_1 \boldsymbol{D_X} + \gamma_1 \boldsymbol{X^T X} + \lambda_1 \mathbf{L_u}\right) \mathbf{u}, \quad (10)$$

$$\mathbf{0} = -\mathbf{Y^T X u} + \left[\lambda_2 \mathbf{D_Y} + \gamma_2 \mathbf{Y^T Y} + \lambda_2 \mathbf{L_v}\right] \mathbf{v}, \quad (11)$$

Here, $\mathbf{D_X} \in R^{p \times p}$ and $\mathbf{D_Y} \in R^{q \times q}$ are diagonal matrix.

$$d_{X_i^i} = \frac{\omega_{i-1,i}}{\sqrt{u_{i-1}^2 + u_i^2}} + \frac{\omega_{i,i+1}}{\sqrt{u_i^2 + u_{i+1}^2}}$$
$$s.t. \omega_{0,1} = \omega_{p,p+1} = 0, \quad (12)$$

$$d_{Y_j^j} = \sum_{m=1,(j,m) \in E}^{q} \frac{\omega_{j,m}}{\sqrt{v_j^2 + v_m^2}} \quad (13)$$

Here, $d_{X_i^i}$ is the i-th element of $\mathbf{D_X}$, and $d_{Y_j^j}$ is the j-th element of $\mathbf{D}_Y$.

The following formula can be obtained by the formulas (10) and (11):

$$\mathbf{u} = \frac{\boldsymbol{X^T Y v}}{\lambda_1 \mathbf{D_X} + \gamma_1 \boldsymbol{X^T X} + \lambda_1 \mathbf{L_u}}, \quad (14)$$

$$\mathbf{v} = \frac{\mathbf{Y^T X} u}{\lambda_2 \mathbf{D_Y} + \gamma_2 \boldsymbol{Y^T Y} + \lambda_2 \mathbf{L_v}}, \quad (15)$$

The pseudo code of the model is shown in **Table 1**.

RESULTS

Simulation Data Experiment

In this part, simulated data has been used for experiments. Therefore, the accuracy of the proposed algorithm for detecting highly correlated biomarkers can be more intuitively estimated. First, we simulated the generation of two loading vectors as ground truth to simulate gene and image features. The number of the samples was set up n. In the data (gene data and image data), the gene data had p = 800 feature dimensions, and the image data had q = 100 dimensions. Secondly, this manuscript generated a latent variable $\varepsilon N(0, \delta^2)$ to express the correlation between genetic data and images (Lin et al., 2014). Finally, this manuscript imposed different noise levels on the generated data matrix to evaluate the anti-noise performance of the model. We compared with the proposed model with FGLSCCA, L1-SCCA, AGNSCCA as shown in **Figure 2** which shown the influence of different noise levels on the sample correlation results under 100 times of fivefold cross-validation.

In **Figure 2**, it can be seen that as the noise level continues to increase, the calculated typical correlation coefficients of each model are decreasing, and the stability of the correlation results also decreases to varying degrees. Under the low-level noise,

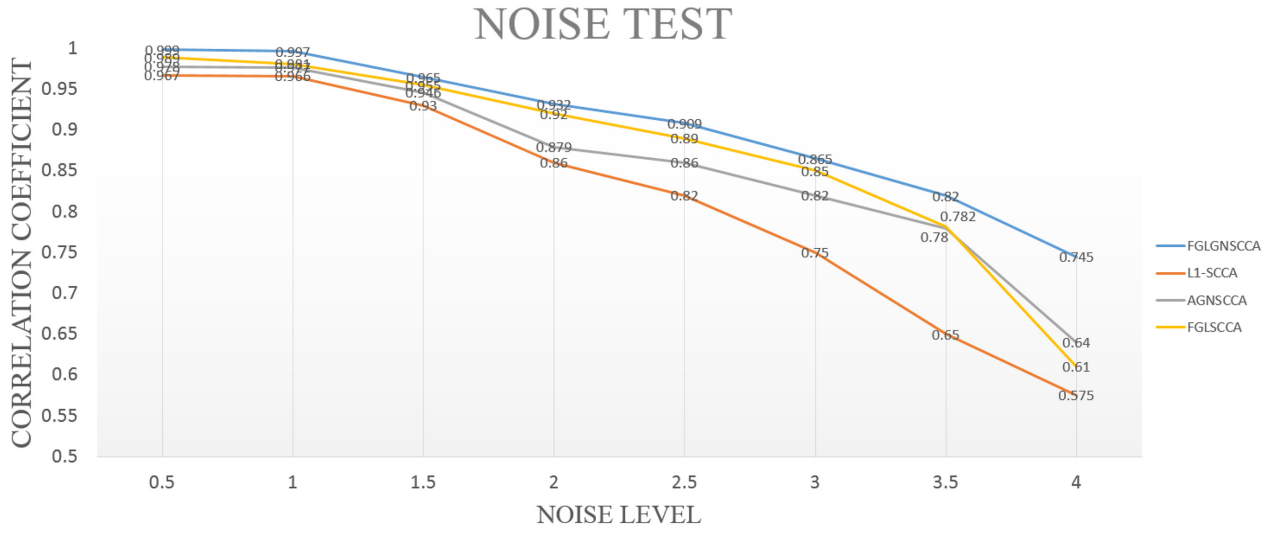

FIGURE 2 | The test results of different models under different noise levels. The horizontal axis is the noise level, and the vertical axis is the typical correlation coefficient.

TABLE 2 | Characteristics of the subjects.

Groups	AD	EMCI	LMCI	HC
Number	25	186	62	113
Gender (M/F)	10/15	101/85	32/30	58/55
Age (mean ± SD)	75.99 ± 10.22	71.56 ± 7.51	72.91 ± 6.82	75.06 ± 5.68

EMCI stands for Early Mild Cognitive Impairment, LMCI stands for Late mild cognitive impairment, HC stands for Healthy Contro.

the difference in the typical correlation coefficients of different models is slight, but the proposed algorithm FGLGNSCCA still has a weak advantage. Under the high-level noise, the new model presented has higher correlation typical coefficients. Therefore, our model is better than other three models. In general, under the same conditions, the model proposed in this manuscript has better anti-noise performance and sample correlation, which is more conducive to the analysis of data correlation results and the discovery of the pathogenic mechanism of AD's related biomarkers.

Subject Data and Preprocessing

The genetic data and imaging phenotype data used in this article are all from the Alzheimer's Disease Neuroimaging Project (ADNI) database[1]. The main contribution of ADNI is the development of clinical, imaging, genetic and biomarkers for early detection and tracking of AD.

Consistent with the previous preprocessing method, this article downloaded the data of 386 non-Hispanic white subjects in ADNI1, including imaging and genotyping data (Wei et al., 2021). First, for raw structure magnetic resonance imaging (sMRI), DiffusionKit (Gorski et al., 2007) is used to perform head movement correction on sMRI. Secondly, using the SPM software package (Saykin et al., 2010). CA T toolkit to achieve sMRI segmentation, the image phenotype feature comprises 140 regions of interest (ROI).

This article uses PLINK (Jung and Hu, 2015) to preprocess the genotype data and screen it according to the following criteria: $HWEp < 10^{-6}$, extract genes with variance more significant than 0.5. In the end, 4,026 genes were obtained in this article. The characteristics of the subjects are counted in **Table 2**.

Experimental Setup and Parameter Selection

In this part, this article will use the algorithm to experiment on accurate data, and finally select the appropriate parameters. In the FGLGNSCCA model, there are four parameters ($\lambda_1, \lambda_2, \gamma_1, \gamma_2$) that need to be set manually. In this study, the values of $\lambda_1$and λ_2 will be fixed, and the values of γ_1 and γ_2 will be constantly changed for experimentation. When a certain set of values makes the experiment get the largest canonical correlation coefficient, then a set of parameters needed in this research is obtained.

Because of the limited number of samples collected in this article, this article finally chose fivefold cross-validation (Wang et al., 2010). After a complete fivefold cross-validation, this study obtained five typical correlation coefficients (CC).

In this article, $\lambda_1 = \lambda_2 = 1$ will be fixed. This article applies the proposed algorithm to image data and gene expression data. The goal of this article is to obtain the most significant canonical correlation coefficient (CC) between gene and image data. Therefore, when the CC is the largest, the parameter results required in this article can be obtained. Then by repeating the experiment 50 times, the average CC and standard deviation are calculated, which are used as the experimental results of this

[1]http://ADNI.loni.usc.edu/

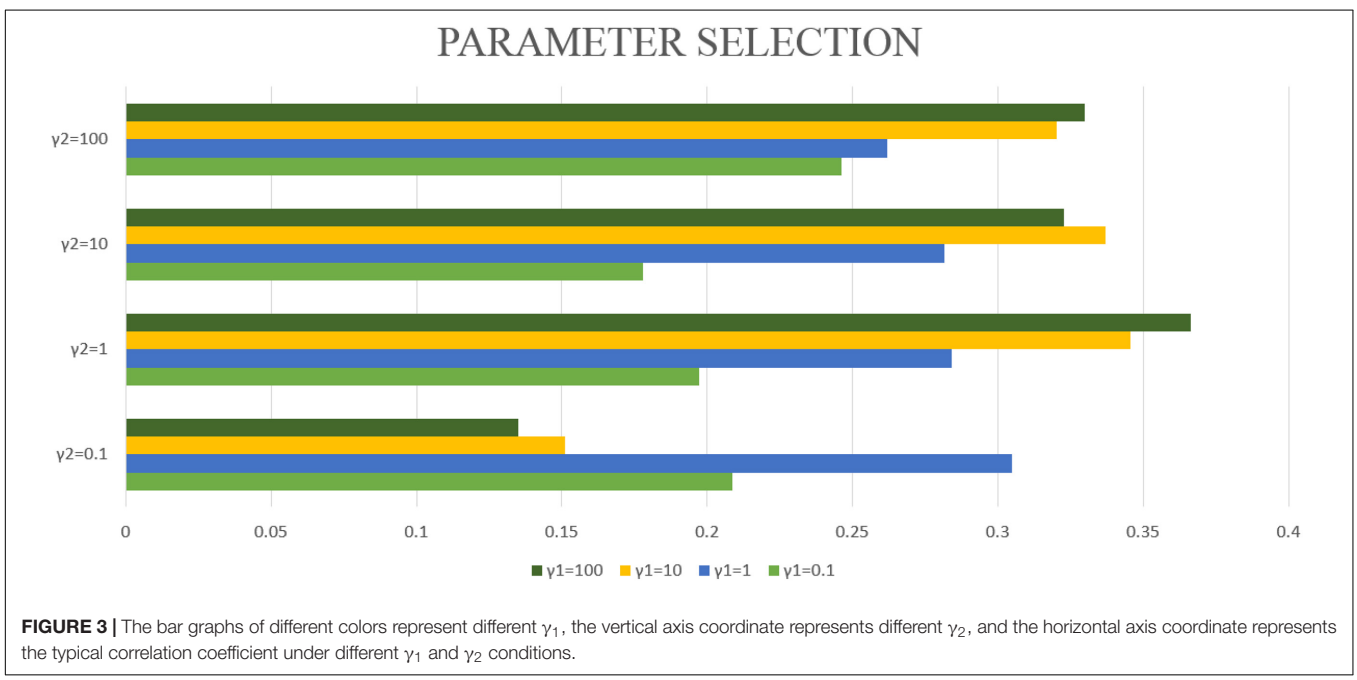

FIGURE 3 | The bar graphs of different colors represent different γ_1, the vertical axis coordinate represents different γ_2, and the horizontal axis coordinate represents the typical correlation coefficient under different γ_1 and γ_2 conditions.

article. However, the blind grid search of parameters is very time-consuming. Therefore, this article matches the values of γ_1 and γ_2 one by one from (0.1, 1, 10, 100). After testing with different parameters, $\gamma_1 = 100$ and $\gamma_2 = 1$ are selected in this article. Finally, the maximum correlation coefficient of the model in this manuscript is CC = 0.3665 ± 0.0126. The correlation coefficients obtained by different parameters are shown in **Figure 3**.

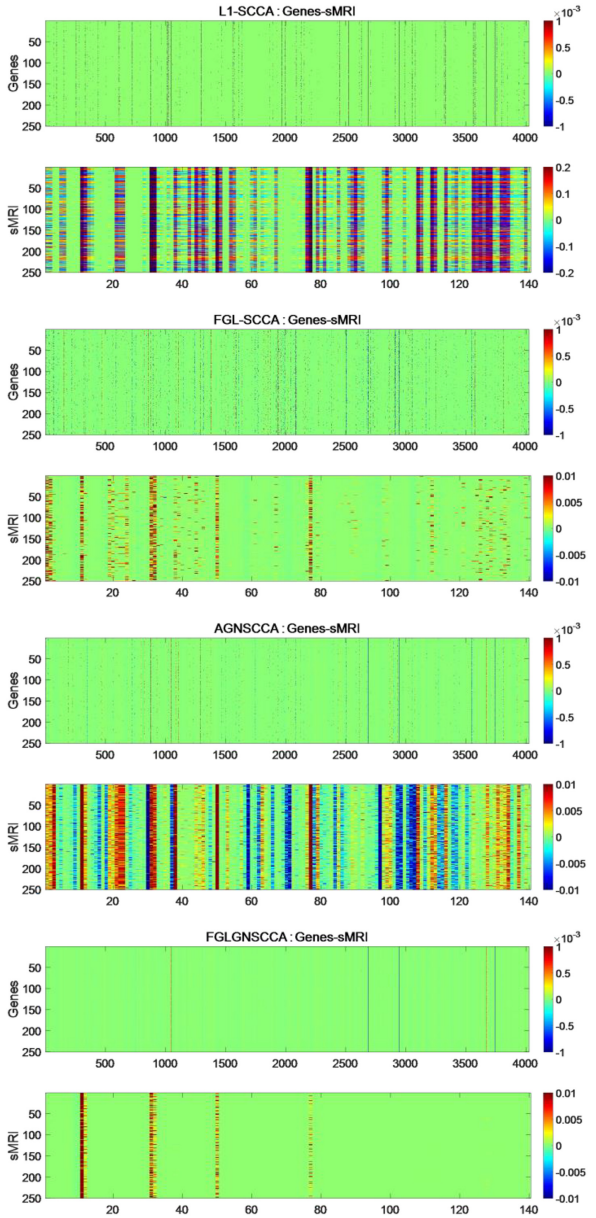

FIGURE 4 | The heat maps obtained by 250 runs of different models. The upper figure in each part is the canonical weight of the genes which is u and the following figure is the image canonical weight which is v. The dimension of standard gene weight is $R^{250 \times 4026}$ (each row represents the number of the algorithm runs, and each column represents a feature). The size of the standard sMRI weight is $R^{250 \times 140}$.

TABLE 3 | TOP10 Brain ROI.

ROI	Weight
lCau	3.39E-02
rThaPro	1.24E-02
rAngGy	5.22E-03
lVenVen	2.63E-03
lMedFroCbr	2.31E-03
rCau	2.14E-03
rSupMarGy	9.65E-05
rPosIns	7.22E-05
rCbeLoCbe6-7	6.15E-05
rPoCGy	5.37E-05

Experimental Results of Real Data

The fresh model proposed in this study does not use the common generalized fusion lasso, but uses the penalty term using FGL, GGL, and GraphNet normalized form. This study selected 386 sample data, including genetic data and image data. This manuscript compares the FGLGNSCCA model with other models, and finally can confirm whether the algorithm in this manuscript has better performance. To ensure the reliability of the experimental results, this manuscript uses FGLGNSCCA and the other three models to conduct 50 times fivefold cross-validation training, respectively. Each time, a load vector is generated and stored in the matrix. In the end, this research will get a 250 × 4026 matrix and a 250 × 140 matrix. For the above research results, respectively, as shown in **Figure 4**.

It can be seen from **Figure 4** that the L1-SCCA model cannot accurately identify the brain regions and genes from a large amount of data. Although the FGLSCCA and AGNSCCA models can identify a certain number of brain regions and genes, some of their features show disorder and do not have excellent stability. The models of L1-SCCA,FGLSCCA, and AGNSCCA extract too many feature genes and brain regions, which may not be used as effective biomarkers related to AD. First of all, the heat map of the FGLGNSCCA algorithm in **Figure 4** clearly displayed the significant genes and brain regions, which is helpful for accurate positioning. Secondly, fewer distinctive features eliminate some interferences, and may help drug research for the treatment of AD. In general, the method in this manuscript was more conducive to discovering relevant biomarkers for the pathogenesis of AD by analyzing the correlation and biological significance between gene expression data and sMRI.

In addition, the TOP10 brain regions identified by the proposed model has been shown and the absolute values of the average weight of 50 × 5 times are listed in **Table 3**. Due to the high dimensionality of the genes, this article separately displayed the TOP30 genes and average weights identified by the new model proposed in this article in **Table 4**. At the same time, this article also gave the typical correlation coefficients (Mean ± SD) between gene and sMRI of different models. Through 50 times fivefold cross-validation, the comparison results of canonical correlation coefficients are shown in **Table 5**.

This research, respectively, counted the TOP30 genes and the TOP10 brain regions obtained by the four algorithms, and respectively, drew the gene venn diagram and the brain region

TABLE 4 | TOP30 gene genetic feature weight.

Gene	Weight
PRKY	9.79E-03
RPS4Y1	8.62E-03
PRKX| | PRXY	8.37E-03
RPS4Y2	6.81E-03
KDM5D	5.26E-03
EIF1AY	4.83E-03
TXLNG2P	4.51E-03
DDX3Y	3.54E-03
UTY	3.19E-03
XIST	2.76E-03
KDM6A	1.03E-03
EIF1AX	7.13E-04
TXLNG	6.23E-04
TTTY10	3.08E-04
DDX58	1.23E-04
USP9Y	1.13E-05
ZFX	9.10E-06
DDX3X	8.64E-06
PPAPDC1B	8.51E-06
POU2AF1	6.65E-06
ZFY	6.55E-06
DDX60	6.01E-06
FCRL1	3.60E-06
NT5E	3.21E-06
PTPRK	2.37E-06
CXCR5	2.09E-06
E2F5	1.23E-06
AFF3	1.15E-06
CXCL5	1.08E-06
FCRL2	9.98E-07

TABLE 5 | Canonical correlation coefficients of different models.

Model	CC (Mean ± SD)
FGLGNSCCA	0.3665 ± 0.0126
FGLSCCA	0.2891 ± 0.0296
AGNSCCA	0.3056 ± 0.0362
L1-SCCA	0.3102 ± 0.0281

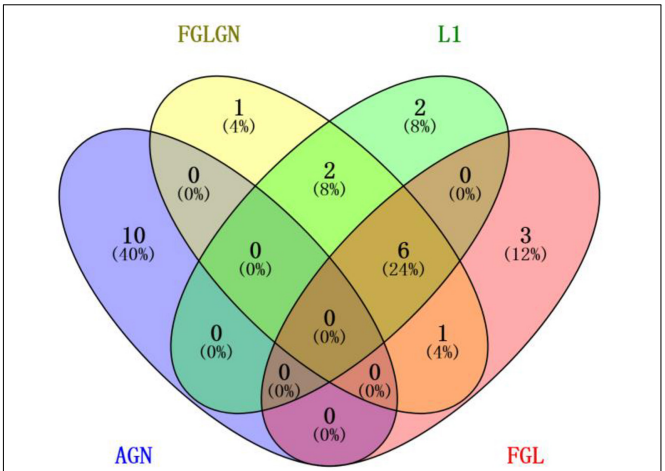

FIGURE 5 | The venn diagram of the brain area.

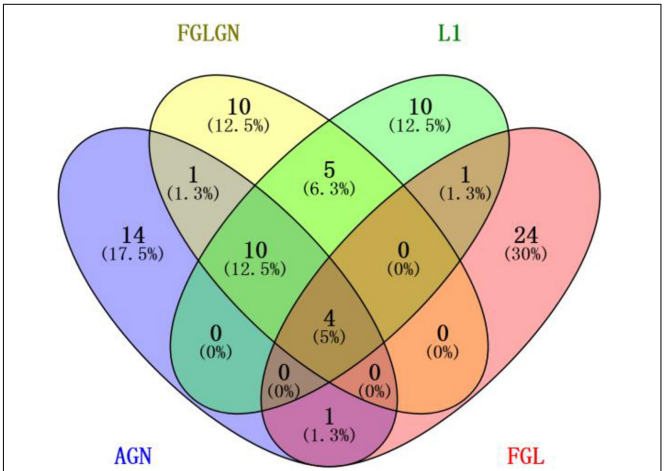

FIGURE 6 | The venn diagram of the gene.

venn diagram as shown in **Figures 5**, **6** (Jia et al., 2021). It can be seen from **Figure 6** that the FGLGNSCCA algorithm has obtained ten genes that are not duplicated with other algorithms. The genes, E2F5 and PTPRK, have been confirmed to be related to AD. In the venn diagram of the brain area, the TOP10 brain areas selected by AGNSCCA are not repeated with other algorithms, indicating that the effect of AGNSCCA is not good. FGLGNSCCA, L1-SCCA, and FGLSCCA obtained a total of six identical brain regions, some of which proved to be related to AD, while FGLGNSCCA alone has a brain region named Right Caudate (rCau), which may be a biomarker of AD. With FGLGNSCCA algorithm, more AD-related biomarkers have been found. Therefore, the algorithm proposed in this manuscript is more superior.

DISCUSSION

In the research of this article, this article used data from 386 samples, including genetic data and image data. When comparing with different models, the new models presented in this article all show better performance. First of all, the new model proposed in this article can display several brain areas more prominently. In contrast, the display of other models is more confusing and cannot effectively identify the prominent brain areas. Secondly, the new model proposed in this article can also identify significant genes and the correlation between image and genetic data, which is incomparable to the other three models.

Prediction of Region of Interest

Figure 7 shows a schematic diagram of the first ten brain regions. The color in **Figure 7** represents the typical weight of the TOP10 brain regions, which is **v**. The value indicated by the color has been shown on the right side of the picture. The new model

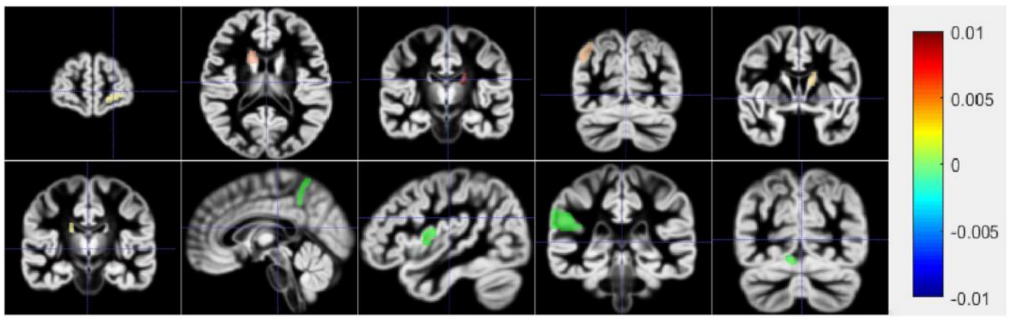

FIGURE 7 | The first row is 1–5 brain areas, and the second row is 6–10 brain areas.

proposed in this manuscript identifies the first ten brain regions, among which Left Supramarginal Gyrus (lSupMarGy) (Penniello et al., 1995), Right Thalamus Proper (rThaPro) (de Jong et al., 2008), Left Caudate (lCau) (Baik et al., 2021), and Left Medial Frontal Cerebrum (lMedFroCbr) (Johannsen et al., 1999) are associated with AD. And Left Caudate has the most remarkable correlation in the recognition results of this manuscript, so it further proves the reliability and authenticity of the algorithm in this manuscript, which is due to the excellent performance of the algorithm in this manuscript. Although the other three algorithms can also identify a certain number of brain regions to a certain extent, the algorithm in this article has significant differences. It can identify brain regions that are significantly related to AD. In addition, the Right Angular Gyrus (rAngGy) and self-awareness are functionally associated with the physical disconnection (de Boer et al., 2020), which may be related to the loss of self-awareness in patients with advanced AD. Moreover, Right Angular Gyrus plays an essential role in language function (Rosselli et al., 2015), which may be related to a series of symptoms such as aphasia in AD patients. Right Angular Gyrus, which has a high correlation, has not yet been confirmed to be highly correlated with AD. This may be the next direction for clinical research.

Over-Representation Analysis

Gene Ontology Enrichment Analysis

DAVID is a robust database. It has two absolute advantages. First, there are many identifiers. Second, there are many types of background species. It has data on a small number of research objects, and its operation is convenient. Since 2003 Since its inception, it has always had a good reputation. Therefore, this article chooses the DAVID database for data analysis. First, this article uses DAVID Bioinformatics Resources 6.8[2] to perform gene ontology (GO) enrichment analysis on the first 500 genes identified by the algorithm in this article (Ding and Zhang, 2017). In the results of GO enrichment analysis, this article finally selected the first four more significant terms, as shown in **Table 6**. A total of 16 different genes are enriched in these four terms. From this result, it can be concluded that these 16 genes are all involved in biological processes (BP), and the detailed GO enrichment analysis is shown in the GO string diagram **Figure 8**.

Alzheimer's disease not only damages the human brain, but also can cause damage to other human organs. The early stage of AD is not fatal, but in the middle and late stages, AD will bring various complications (heart disease, thromboembolism, stroke, and renal failure, etc.), which will bring death threats to the patient. From this, we know that AD is not a simple neurological disease, but a comprehensive disease. Mental functions such as early and mid-term characteristic memory of AD patients are weakened. Still the late symptoms of AD are aphasia, a decline in physical fitness and loss of bodily control. It can be seen that AD is a chronic disease with multiple genes working together, and its pathogenesis includes a large number of biological processes. Because AD's toxic proteins can erode brain cells, the innate immune response of the brain mucosa is a critical protective mechanism. It can also be seen in the analysis results, innate immune response in the mucosa is one of the most effective terms. It has been confirmed in the literature (Stylianaki et al., 2019) that when the antibacterial response of neutrophils outside the patient's body is damaged, the probability of getting sepsis will increase, and sepsis is one of the complications of AD. This can also be reflected in the analysis of this article. That is, the antibacterial humoral response is one of the first four significant terms. The above reveals the link between some diseases and AD.

Kyoto Encyclopedia of Genes and Genomes Pathway Analysis

In this part, this article also used the DAVID database to perform the Kyoto Encyclopedia of Genes and Genomes (KEGG) pathway analysis on the first 1000 genes identified by the algorithm (Kanehisa et al., 2017). The DAVID database identified 987 genes. Other genes did not match. It may be because the database has not

TABLE 6 | Four sets of significant terms obtained by GO analysis.

Category	ID	Term	FDR
BP	GO:0002227	innate immune response in mucosa	6.24E-02
BP	GO:0050832	defense response to fungus	6.24E-02
BP	GO:0019731	antibacterial humoral response	7.99E-02
BP	GO:0009615	response to virus	7.99E-02

[2]https://david.ncifcrf.gov/

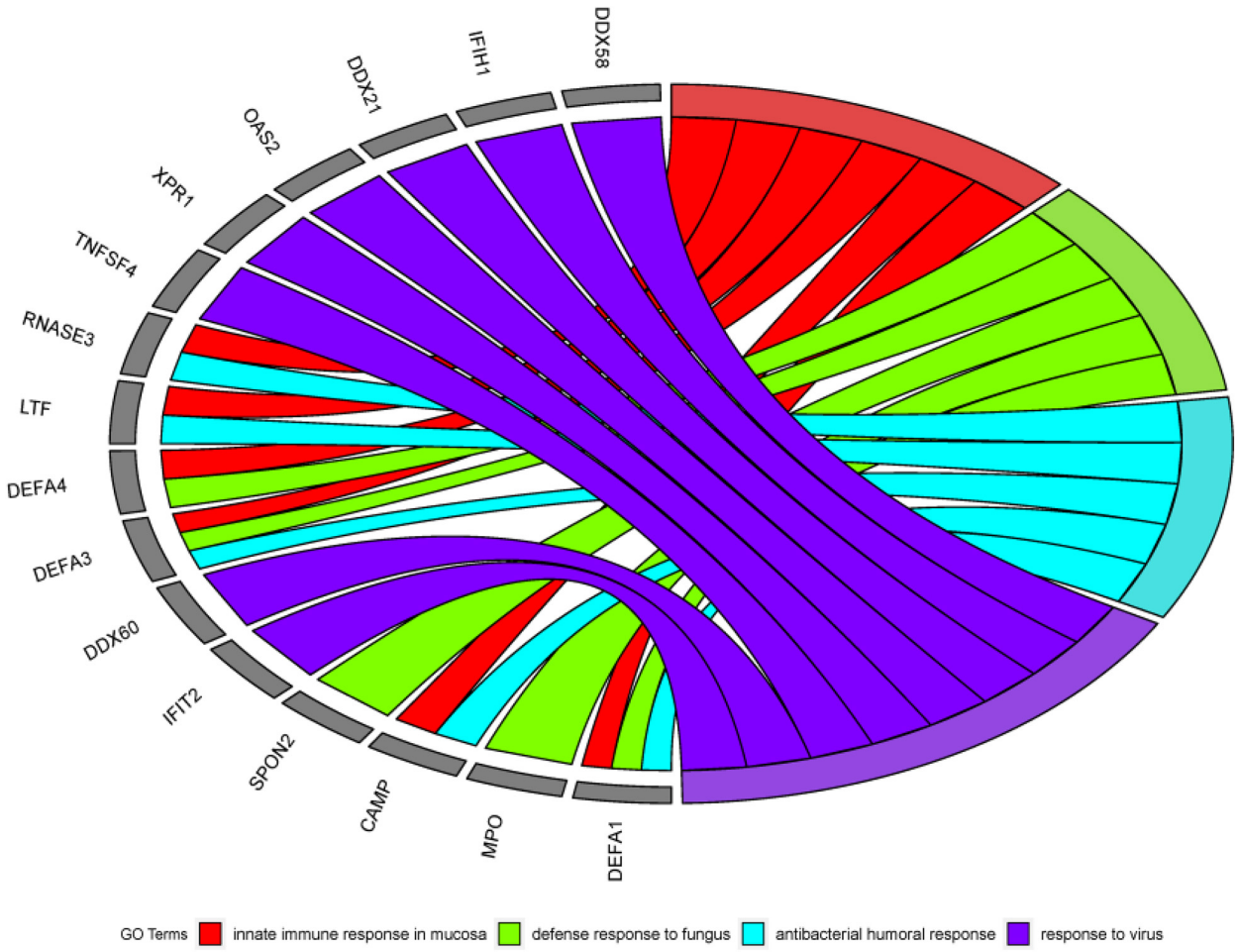

FIGURE 8 | Chord diagram obtained through GO analysis in the experiment. Among the first 500 genes entered, 16 genes were significantly enriched in 4 GO term.

been updated in time or the gene names are outdated. Among all the genes compared to the database, a total of 351 genes were enriched in the KEGG signal path, accounting for about 35.6%. To observe the significance of the input gene enrichment in the pathway, after artificially setting P-value < 0.05, 11 signal pathways were screened, as shown in **Figure 9**.

From **Figure 9** that the cell adhesion molecules (CAMS) signal pathway enrichment analysis is more significant than other pathways. In the literature (Leshchyns'ka and Sytnyk, 2016), it is shown that the loss of synapses between brain neurons is inevitable with Alzheimer's disease (AD). The article describes in detail that changes in synaptic adhesion play a vital role in the destruction of neuronal networks in AD. From **Figure 10** that these 11 signal pathways can be divided into three major categories, namely environmental information processing, Organismal Systems, and Human Diseases. The signal pathways we have identified are highly related to organism systems and human diseases.

The above analysis proves that the new algorithm proposed in this manuscript has identified the signal pathways related to AD, proving that FGLGNSCCA has powerful performance.

Refinement Analysis

Among the TOP30 genes identified by FGLGNSCCA, genes such as ZFX (Soleimani et al., 2020), XIST (Wang et al., 2018), E2F5 (Johanson et al., 2008), KDM6A (Davis et al., 2020), TXLNG (Hotokezaka et al., 2015), and PTPRK (Chen et al., 2018) have been confirmed to play an eventful role in the AD process or participation in related biological processes. The RPS4Y1 gene is associated with Parkinson's disease (Sun et al., 2014). The literature (Yue et al., 2020) deemed that XIST may become a new underlying aim for the remedy of AD. At the same time, the literature (Chanda and Mukhopadhyay, 2020) also discussed the possibility of XIST-mediated therapeutic intervention and the relationship between XIC and women's preference for AD. The PTPRK gene is associated with an increased risk of neuropsychiatric diseases and cancer, and the literature (Sun et al., 2014) provided evidence that the PTPRK gene is associated with the risk of AD. The relationship between other genes and AD needs to be studied in the future.

In addition, the paired correlation heat maps of TOP30 genes and TOP10 brain regions are shown in **Figure 11** in this article which in **Tables 3**, **4**. The Y-axis direction is the typical weights of

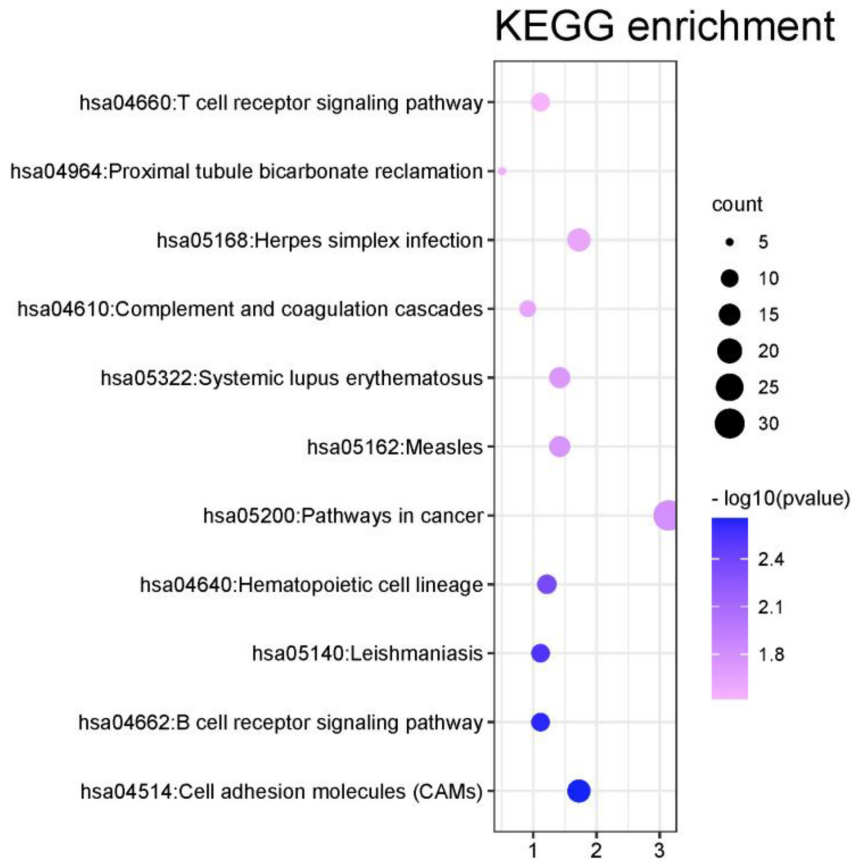

FIGURE 9 | KEGG enrichment analysis results of the first 1000 genes.

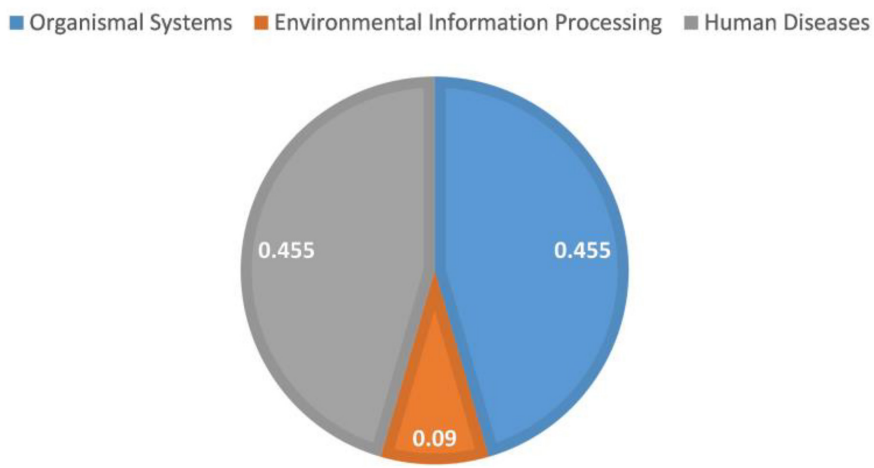

FIGURE 10 | Environmental information processing includes 1 signal path. Organismal systems includes five signal paths; human diseases includes five signal paths.

genes arranged from small to large, and the *X*-axis is the typical weights of brain regions from high to low. As expected in this article, all Gene-ROI pairs have a strong correlation. And it can be observed in this article that the first nine genes (PRKY, RPS4Y1, PRKX | | PRKY, RPS4Y2, KDM5D, EIF1AY, TXLNG2P, DDX3Y, and UTY) are negatively correlated with all brain regions. And

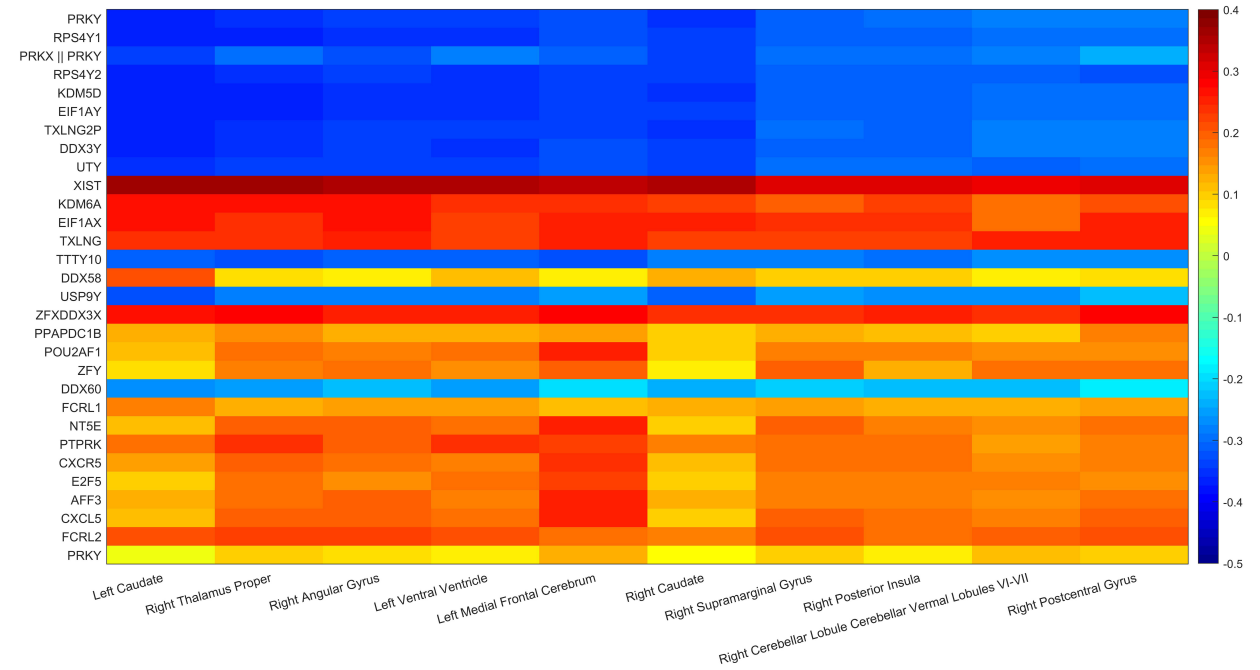

FIGURE 11 | Gene-ROI pairwise correlation.

it can be found that the effects of the same genetic variable on different brain regions show the same positive or negative relationship as a whole.

This article used the z-test to analyze the pairwise correlation of the Gene-ROI we got. The number of Gene-ROI pairwise correlation coefficient is 300, z-test is selected in this article. Next, this article selected the TOP10 data with *p*-value less than 0.01 which are shown in **Table 7**. It can be seen from the **Table 7** that the XIST gene is extremely related to five brain regions, and the XIST gene has been confirmed to be related to AD. Caudate brain region is extremely related to six genes, and Caudate has also been shown to be related to AD. Therefore, this article believes that XIST gene and Caudate brain region are likely to be biomarkers of AD.

TABLE 7 | The TOP10 pairs with p <0.01.

Gene-ROI	*P*-value
XIST-Left Caudate	0.00291
XIST-Right Thalamus Proper	0.00366
XIST-Left Ventral Ventricle	0.00441
XIST-Right Angular Gyrus	0.00470
KDM5D-Left Caudate	0.00534
XIST-Right Caudate	0.00546
RPS4Y2-Left Caudate	0.00577
PRKX | | PRKY-Left Caudate	0.00597
EIF1AY-Left Caudate	0.00604
TXLNG2P-Left Caudate	0.00609

Of course, the algorithm proposed in this article also has certain shortcomings. First of all, the collected samples limited the performance of the model. Due to the small number of samples, various penalty items may cause over-fitting problems. At the same time, we have not collected more image data to get a closer image genetic association in addition to sMRI.

CONCLUSION

This article dedicates identifying biomarkers related to AD through image genetics. Once they are clinically verified, they can better predict the possibility of a person becoming an AD patient and guide clinical decision-making. In this study, this manuscript adds GraphNet regularization based on FGLSCCA. GraphNet regularization is a constraint by a modified version of the resilient network regularization, which allows the physical limitations of connectivity to be effectively integrated. First of all, in the research using artificially synthesized highly correlated data sets for testing, these findings indicate that the algorithm in this manuscript has better anti-noise capability than the three methods (L1-SCCA, FGLSCCA, and AGNSCCA). Secondly, on the actual ADNI data set, we used the data set of 386 non-Hispanic white subjects. After the FGLGNSCCA model was run through 50-fold cross-validation, it obtains a higher canonical correlation coefficient of gene-ROI than other models, and more significant biomarkers have been identified. Again, this article uses the David database in the biological analysis. In the GO and KEGG enrichment analysis, this study found that 16 genes are present in 4 significant GO Term, and 351 genes are present in 11 signal pathways. These intuitive biological analyses can

make it easier for us to interpret AD pathology-related problems. Finally, by displaying the pairwise correlation heat map of genetic variables and image variables, this article shows that the effects of the same gene on different brain regions are all related in the same direction as a whole. And we found a combination of ROI and gene, and this combination may be contacted to AD. It further shows the close relationship between genetic variables and brain regions. In the future, we will undertake to add other data together for research, hoping to more effectively explore the biological relationship between genetic data and imaging data.

Most people only think that AD is a chronic neurological disease, which only has the characteristics of dementia, memory loss, and other non-lethal features. But in fact, AD is a fatal chronic neurological disease. The early stage of AD is just some trivial things such as memory decline, and these things will naturally occur with age, and people will naturally not pay more attention. But in most cases, when a person is diagnosed as an AD patient, his condition has reached the middle or late stage, and at this time, the doctor is unable to recover. Therefore, it is hoped that the new algorithm proposed in this article can effectively and earlier identify patients with early AD or ordinary people who may become AD patients.

DATA AVAILABILITY STATEMENT

The original contributions presented in the study are included in the article/supplementary material, further inquiries can be directed to the corresponding author.

AUTHOR CONTRIBUTIONS

SW, XW, and WK: research conception and design. XW and KW: data collection, analysis, and interpretation. XW and SW: statistical analysis and manuscript drafting. SW, XW, KW, and WK: reviewing important academic content. All authors contributed to the article.

FUNDING

This work was supported by the National Natural Science Foundation of China (No. 61803257) and Natural Science Foundation of Shanghai (No. 18ZR1417200).

REFERENCES

Aghakhanyan, G., Vergallo, A., Gennaro, M., Mazzarri, S., Guidoccio, F., Radicchi, C., et al. (2018). The precuneus - a witness for excessive aβ gathering in alzheimer's disease pathology.*Neurodegener. Dis.* 18, 302–309. doi: 10.1159/000492945

Alzheimer's Association. (2013). 2013 Alzheimer's disease facts and figures. *Alzheimers Dement.* 9, 208–245. doi: 10.1016/j.jalz.2013.02.003

Baik, K., Yang, J. J., Jung, J. H., Lee, Y. H., Chung, S. J., Yoo, H. S., et al. (2021). Structural connectivity networks in Alzheimer's disease and Lewy body disease. *Brain Behav.* 11:e02112. doi: 10.1002/brb3.2112

Chanda, K., and Mukhopadhyay, D. (2020). LncRNA Xist, X-chromosome instability and Alzheimer's disease. *Curr Alzheimer Res.* 17, 499–507. doi: 10.2174/1567205017666200807185624

Chen, J., Bushman, F. D., Lewis, J. D., Wu, G. D., and Li, H. (2013). Structure -constrained sparse canonical correlation analysis with an application to microbiome data analysis. *Biostatistics* 14, 244–258.

Chen, Y., Xu, C., Harirforoosh, S., Luo, X., and Wang, K. S. (2018). Analysis of PTPRK polymorphisms in association with risk and age at onset of Alzheimer's disease, cancer risk, and cholesterol. *J. Psychiatr Res.* 96, 65–72. doi: 10.1016/j.jpsychires.2017.09.021

Davis, E. J., Broestl, L., Abdulai-Saiku, S., Worden, K., Bonham, L. W., Miñones-Moyano, E., et al. (2020). A second X chromosome contributes to resilience in a mouse model of Alzheimer's disease. *Sci. Transl. Med.* 12:eaaz5677. doi: 10.1126/scitranslmed.aaz5677

de Boer, D. M. L., Johnston, P. J., Kerr, G., Meinzer, M., and Cleeremans, A. (2020). A causal role for the right angular gyrus in self-location mediated perspective taking. *Sci. Rep.* 10:19229. doi: 10.1038/s41598-020-76235-7

de Jong, L. W., van der Hiele, K., Veer, I. M., Houwing, J. J., Westendorp, R. G., Bollen, E. L., et al. (2008). Strongly reduced volumes of putamen and thalamus in Alzheimer's disease: an MRI study. *Brain* 131(Pt 12), 3277–3285. doi: 10.1093/brain/awn278

Ding, J., and Zhang, Y. (2017). Analysis of key GO terms and KEGG pathways associated with carcinogenic chemicals. *Comb. Chem. High. Throughput Screen* doi: 10.2174/1386207321666171218120133 Epub ahead of print.

Du, L., Huang, H., Yan, J., Kim, S., Risacher, S. L., Inlow, M., et al. (2016). Alzheimer's Disease neuroimaging initiative. Structured sparse canonical correlation analysis for brain imaging genetics: an improved GraphNet method. *Bioinformatics* 32, 1544–1551. doi: 10.1093/bioinformatics/btw033

Du, L., Liu, K., Yao, X., Risacher, S. L., Han, J., Saykin, A. J., et al. (2020). Detecting genetic associations with brain imaging phenotypes in Alzheimer's disease via a novel structured SCCA approach. *Med Image Anal.* 61:101656. doi: 10.1016/j.media.2020.101656

Du, L., Yan, J., Kim, S., Risacher, S. L., Huang, H., Inlow, M., et al. (2015). GN-SCCA: GraphNet based sparse canonical correlation analysis for brain imaging genetics. *Brain Inform. Health* 9250, 275–284. doi: 10.1007/978-3-319-23344-4_27

Goldberg, R. J. (2007). Alzheimer's disease. *Compr. Ther.* 33, 58–64. doi: 10.1007/s12019-007-8000-0

Gorski, J., Pfeuffer, F., and Klaproths, K. (2007). Biconvex sets and optimization with biconvex functions: a survey and extensions. *Math. Methods Oper. Res.* 66, 373–407.

Grosenick, L., Klingenberg, B., Katovich, K., Knutson, B., and Taylor, J. E. (2013). Interpretable whole-brain prediction analysis with GraphNet. *Neuroimage* 72, 304–321. doi: 10.1016/j.neuroimage.2012.12.062

Hagmann, P., Cammoun, L., Gigandet, X., Meuli, R., Honey, C. J., Wedeen, V. J., et al. (2008). Mapping the structural core of human cerebral cortex. *PLoS Biol.* 6:e159. doi: 10.1371/journal.pbio.0060159

Hashimoto, R., Ohi, K., Yamamori, H., Yasuda, Y., Fujimoto, M., Umeda-Yano, S., et al. (2015). Imaging genetics and psychiatric disorders. *Curr. Mol. Med.* 15, 168–175. doi: 10.2174/1566524015666150303104159

Hotelling, H. (1936). Relations between two sets of variates. *Biometrika* 28, 321–377.

Hotokezaka, Y., Katayama, I., van Leyen, K., and Nakamura, T. (2015). GSK-3β-dependent downregulation of γ-taxilin and αNAC merge to regulate ER stress responses. *Cell Death Dis.* 6:e1719. doi: 10.1038/cddis.2015.90

Jia, A., Xu, L., and Wang, Y. (2021). Venn diagrams in bioinformatics. *Brief Bioinform.* 22:bbab108. doi: 10.1093/bib/bbab108

Johannsen, P., Jakobsen, J., Bruhn, P., and Gjedde, A. (1999). Cortical responses to sustained and divided attention in Alzheimer's disease. *Neuroimage* 10(3 Pt 1), 269–281. doi: 10.1006/nimg.1999.0475

Johanson, C. E., Duncan, J. A. III, Klinge, P. M., Brinker, T., Stopa, E. G., and Silverberg, G. D. (2008). Multiplicity of cerebrospinal fluid functions: new challenges in health and disease. *Cerebrospinal Fluid Res.* 5:10. doi: 10.1186/1743-8454-5-10

Jung, Y., and Hu, J. (2015). A K-fold averaging cross-validation procedure. *J. Nonparametr. Stat.* 27, 167–179. doi: 10.1080/10485252.2015.1010532

Kanehisa, M., Furumichi, M., Tanabe, M., Sato, Y., and Morishima, K. (2017). KEGG: new perspectives on genomes, pathways, diseases and drugs. *Nucleic Acids Res.* 45, D353–D361. doi: 10.1093/nar/gkw1092

Kim, M., Won, J. H., Youn, J., and Park, H. (2020). Joint-connectivity-based sparse canonical correlation analysis of imaging genetics for detecting biomarkers of Parkinson's Disease. *IEEE Trans. Med. Imaging* 39, 23–34. doi: 10.1109/TMI.2019.2918839

Leshchyns'ka, I., and Sytnyk, V. (2016). Synaptic cell adhesion molecules in Alzheimer's disease. *Neural Plast.* 2016:6427537. doi: 10.1155/2016/6427537

Lin, D., Calhoun, V. D., and Wang, Y. P. (2014). Correspondence between fMRI and SNP data by group sparse canonical correlation analysis. *Med. Image Anal.* 18, 891–902. doi: 10.1016/j.media.2013.10.010

Parkhomenko, E., Tritchler, D., and Beyene, J. (2009). Sparse canonical correlation analysis with application to genomic data integration. *Stat. Appl. Genet. Mol. Biol.* 8, 2–34. doi: 10.2202/1544-6115.1406

Penniello, M. J., Lambert, J., Eustache, F., Petit-Taboué, M. C., Barré, L., Viader, F., et al. (1995). A PET study of the functional neuroanatomy of writing impairment in Alzheimer's disease. The role of the left supramarginal and left angular gyri. *Brain* 118(Pt3), 697–706. doi: 10.1093/brain/118.3.697

Rosselli, M., Ardila, A., and Bernal, B. (2015). Modelo de conectividad de la circunvolución angular en el lenguaje: metaanálisis de neuroimágenes funcionales [Angular gyrus connectivity model for language: a functional neuroimaging meta-analysis]. *Rev Neurol.* 60, 495–503. Spanish,

Saykin, A. J., Shen, L., Foroud, T. M., Potkin, S. G., Swaminathan, S., Kim, S., et al. (2010). Alzheimer's disease neuroimaging initiative. Alzheimer's disease neuroimaging initiative biomarkers as quantitative phenotypes: genetics core aims, progress, and plans. *Alzheimer's Dement* 6, 265–273. doi: 10.1016/j.jalz.2010.03.013

Soleimani, S., Nasim, N., Esfandi, F., Karimipoor, M., Kholghi-Oskooei, V., Naby Gol, M., et al. (2020). SE translocation gene but not zinc finger or X-linked factor is down-regulated in gastric cancer. *Gastroenterol. Hepatol. Bed. Bench.* 13, 8–13.

Stylianaki, A., Stanic, B., Morgenstern, M., Richards, G. R., Moriarty, F. T., and Thompson, K. (2019). Humoral factors from musculoskeletal polytrauma patients impair antibacterial responses of neutrophils in vitro. *J. Bone Jt Infect.* 4, 280–284. doi: 10.7150/jbji.35424

Sun, A. G., Wang, J., Shan, Y. Z., Yu, W. J., Li, X., Cong, C. H., et al. (2014). Identifying distinct candidate genes for early Parkinson's disease by analysis of gene expression in whole blood. *Neuro Endocrinol. Lett.* 35, 398–404.

Wang, K., Li, M., and Hakonarson, H. (2010). ANNOVAR: functional annotation of genetic variants from high-throughput sequencing data. *Nucleic Acids Res.* 38:e164. doi: 10.1093/nar/gkq603

Wang, X., Wang, C., Geng, C., and Zhao, K. (2018). LncRNA XIST knockdown attenuates Aβ25-35-induced toxicity, oxidative stress, and apoptosis in primary cultured rat hippocampal neurons by targeting miR-132. *Int. J. Clin. Exp. Pathol.* 11, 3915–3924.

Wei, K., Kong, W., and Wang, S. (2021). An improved multi-task sparse canonical correlation analysis of imaging genetics for detecting biomarkers of Alzheimer's disease. *IEEE Access* 9, 30528–30538.

Yue, D., Guanqun, G., Jingxin, L., Sen, S., Shuang, L., Yan, S., et al. (2020). Silencing of long noncoding RNA XIST attenuated Alzheimer's disease-related BACE1 alteration through miR-124. *Cell Biol. Int.* 44, 630–636. doi: 10.1002/cbin.11263

Conflict of Interest: The authors declare that the research was conducted in the absence of any commercial or financial relationships that could be construed as a potential conflict of interest.

Publisher's Note: All claims expressed in this article are solely those of the authors and do not necessarily represent those of their affiliated organizations, or those of the publisher, the editors and the reviewers. Any product that may be evaluated in this article, or claim that may be made by its manufacturer, is not guaranteed or endorsed by the publisher.

frontiers in Aging Neuroscience

ORIGINAL RESEARCH
published: 24 January 2022
doi: 10.3389/fnagi.2021.799500

An Iterative Method for Predicting Essential Proteins Based on Multifeature Fusion and Linear Neighborhood Similarity

Xianyou Zhu[1†], Yaocan Zhu[2†], Yihong Tan[2], Zhiping Chen[1,2] and Lei Wang[2*]*

[1] College of Computer Science and Technology, Hengyang Normal University, Hengyang, China, [2] College of Computer Engineering and Applied Mathematics, Changsha University, Changsha, China

OPEN ACCESS

Edited by:
Min Tang,
Jiangsu University, China

Reviewed by:
Weinan Zhou,
University of Illinois at Urbana-Champaign, United States
Qianqian Song,
Wake Forest School of Medicine, United States

***Correspondence:**
Yaocan Zhu
1930204639@qq.com
Lei Wang
wanglei@xtu.edu.cn

[†]These authors share first authorship

Specialty section:
This article was submitted to Neurocognitive Aging and Behavior, a section of the journal Frontiers in Aging Neuroscience

Received: *21 October 2021*
Accepted: *02 December 2021*
Published: *24 January 2022*

Citation:
Zhu X, Zhu Y, Tan Y, Chen Z and Wang L (2022) An Iterative Method for Predicting Essential Proteins Based on Multifeature Fusion and Linear Neighborhood Similarity. Front. Aging Neurosci. 13:799500. doi: 10.3389/fnagi.2021.799500

Growing evidence have demonstrated that many biological processes are inseparable from the participation of key proteins. In this paper, a novel iterative method called linear neighborhood similarity-based protein multifeatures fusion (LNSPF) is proposed to identify potential key proteins based on multifeature fusion. In LNSPF, an original protein-protein interaction (PPI) network will be constructed first based on known protein-protein interaction data downloaded from benchmark databases, based on which, topological features will be further extracted. Next, gene expression data of proteins will be adopted to transfer the original PPI network to a weighted PPI network based on the linear neighborhood similarity. After that, subcellular localization and homologous information of proteins will be integrated to extract functional features for proteins, and based on both functional and topological features obtained above. And then, an iterative method will be designed and carried out to predict potential key proteins. At last, for evaluating the predictive performance of LNSPF, extensive experiments have been done, and compare results between LNPSF and 15 state-of-the-art competitive methods have demonstrated that LNSPF can achieve satisfactory recognition accuracy, which is markedly better than that achieved by each competing method.

Keywords: key protein, entropy, linear neighborhood similarity, iterative method, multi-feature fusion

INTRODUCTION

In the past few years, with the development of high-throughput and bioinformatics technologies, recognition of potential key proteins based on protein-protein interaction (PPI) networks has become a new research hotspot (Dai et al., 2021; Zhang et al., 2021). Essential proteins play an important role in cell growth and regulation, and researches on essential proteins can deepen the understanding of biological life processes. Existing key protein prediction methods can be roughly divided into two categories: one is based on the topological characteristics of PPI networks and the other is based on the fusion of topological structures of PPI networks and biological information of protein such as the gene expression data, the subcellular localization data, the homologous

data, and the gene ontology of protein. For example, based on topological characteristics of PPI networks, Li et al. (2015) proposed a method called LAC, in which, the local average connectivity of nodes in the PPI network was adopted to estimate the essentiality of proteins. Qi and Luo (2016) introduced a model named LID by measuring the importance of proteins by the local interaction density between neighboring nodes in the PPI network. Lin designed two predictive models called MNC (maximum neighborhood connectivity) and DMNC (density of maximum neighborhood connectivity) based on the maximum neighborhood connectivity and density of maximum neighborhood connectivity of modes in the PPI network separately (Lin et al., 2011). In addition, researchers have proposed a series of methods to identify key proteins based on the centrality of nodes in PPI networks, such as DC (degree centrality) (Hahn and Kern, 2005), EC (eigenvector centrality) (Bonacich, 1987), CC (closeness centrality) (Wuchty and Stadler, 2003), IC (information centrality) (Stephenson and Zelen, 1989), SC (subgraph centrality) (Estrada and Rodríguez-Velázquez, 2005), BC (betweenness centrality) (Joy et al., 2005), and NC (neighbor centrality) (Wang et al., 2012). In all these methods, since only topological characteristics of PPI networks were considered, then unknown interactions between proteins might greatly affect the identification accuracy of potential key proteins. Hence, to improve the recognition accuracy, some other methods based on the fusion of biological information and topological features were proposed successively. For instance, Tang and Li proposed two methods called WDC (weighted degree centrality) (Tang et al., 2014) and PEC (integration ECC and Pearson correlation) (Li et al., 2012), respectively, by fusing topological features of PPI networks with gene expression information of proteins to measure the importance of proteins. Peng et al. (2012) designed two methods, namely, UDoNC (united the domain features and the normalized ECC) and ION (integration of the properties of orthologous and the features of neighbors) (Peng et al., 2015a), through combining homology and domain information of proteins with topological features of PPI networks separately. Zhang et al. (2013) introduced a prediction model called CoEWC by integrating topological characteristics of PPI networks with co-expression characteristics of proteins in gene expression profiles. Li et al. (2018) proposed a method named subnetwork partition and prioritization by fusing subcellular localization information of proteins with PPI networks. Zhao et al. (2019) designed an iterative computing method called RWHN by combining homology, domain, and subcellular localization information of proteins with topological features of PPI networks. Zhao et al. (2014) proposed a prediction method called POEM by integrating gene expression data of proteins and topology features of PPI networks. Lei et al. (2020) designed a method based on gene expression data and Drosophila optimization algorithm (FOCA), which combines PPI network, subcellular localization, gene ontology annotation, gene expression data, and artificial fish swarm optimization (AFSO) algorithm (Lei et al., 2016) to predict key proteins. In addition, a prediction method based on the combination of a learning system and specific scoring matrix was proposed by Wang (Wang et al., 2017), and a prediction method based on the deep learning model proposed by Chen (Chen et al., 2019). Chen et al. (2020) proposed an identification method called NPRI by integrating heterogeneous networks. Dai et al. (2020) identified key proteins based on PPI network embedding. Zhang et al. (2019) proposed a method by fusing dynamic PPI networks. Sun et al. (2021) designed an iterative method called IoMCD (iteration based on multiple characteristic differences) based on cross-entropy. Li et al. (2020) proposed an iterative method called CVIM (character vector iteration method) based on the fusion of topological structures of PPI networks and functional characteristics of proteins.

Experimental results show that the fusion of network topological features and biological information of proteins can improve the accuracy of identifying potential key proteins effectively. However, in most existing methods, due to the limited categories of topological structures of PPI networks and functional characteristics of proteins fused, the predictive performances of these methods are not satisfactory. Hence, in this study, through combining a series of topological features of PPI networks and abundant biological information of proteins, a new predictive method called LNSPF (linear neighborhood similarity-based protein multifeatures fusion) is proposed to identify potential key proteins. In LNSPF, an original PPI network will be constructed first based on known PPI data downloaded from benchmark databases, and then, topological features will be extracted from the original PPI network. Next, the protein nodes in the original PPI network are defined as data points, the protein gene expression data are defined as the characteristics of the corresponding data points, and the data points are reconstructed to calculate the linear neighborhood similarity between the data points in the feature space. After that, subcellular location and homologous information of proteins will be integrated to extract functional features for proteins. At last, based on both functional and topological features extracted above, an iterative method will be designed to predict key proteins. Experimental results show that LNSPF can achieve reliable prediction accuracies of 100%, 90%, and 87% in top 1%, 5%, and 10% ranked key proteins separately based on the GAVIN database, which is markedly superior to 15 state-of-the-art competitive methods, namely, DC (Hahn and Kern, 2005), CC (Wuchty and Stadler, 2003), IC (Stephenson and Zelen, 1989), SC (Estrada and Rodríguez-Velázquez, 2005), BC (Joy et al., 2005), NC (Wang et al., 2012), PEC (Li et al., 2012), LAC (Li et al., 2015), COEWC (Zhang et al., 2013), POEM (Zhao et al., 2014), ION (Peng et al., 2015a), TEGS (Li et al., 2018), RWHN (Zhao et al., 2019), IoMCD (Sun et al., 2021), and CVIM (Li et al., 2020) simultaneously.

MATERIALS AND METHODS

As shown in **Figure 1**, the process of LNSPF consists of the following four main steps:

Step 1: First, based on known PPI data downloaded from the benchmark database, an original PPI network is constructed, from which, topological features, namely,

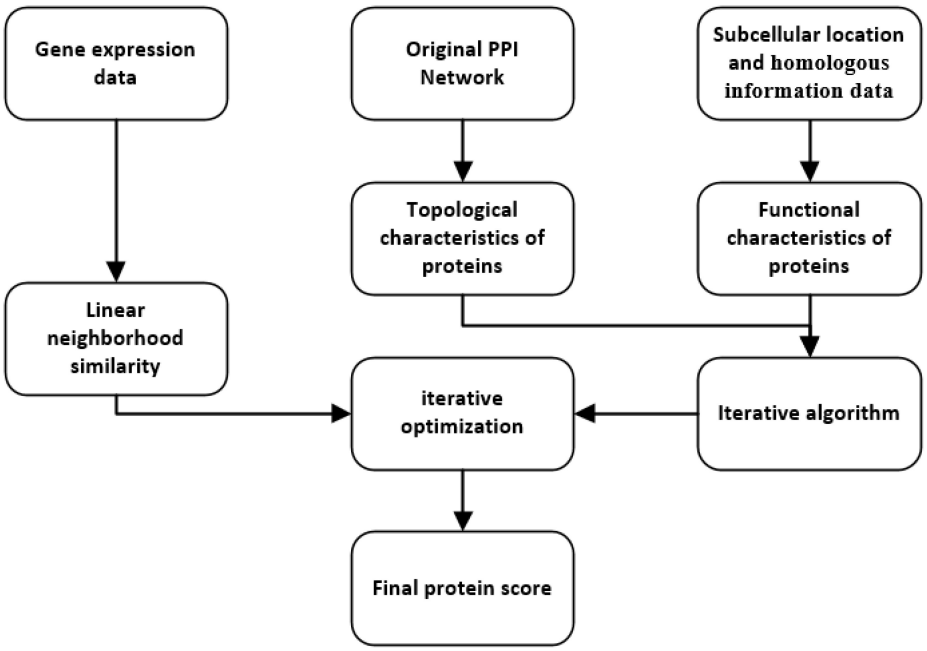

FIGURE 1 | Flowchart of the LNSPF.

degree, two hops degree, and triangle are extracted successively.

Step 2: Next, subcellular location and homologous information of proteins will be integrated to extract functional features for proteins.

Step 3: Moreover, based on the topological and biological properties obtained above, an iterative method is designed to estimate the importance of proteins.

Step 4: At last, based on the gene expression data downloaded from the benchmark database, the score was further optimized by using linear neighborhood similarity.

Extraction of Functional Features for Proteins

Let $G = (V, E)$ denote the original PPI network constructed from a dataset of known PPIs downloaded from any given benchmark database D, $V = \{p_1, p_2, \cdots p_N\}$ represent a set of different proteins, and $E = \{e(p_i, p_j) | p_i, p_j \in V\}$ represent a collection of edges between proteins in G. Here, if and Based a known interaction between any two given proteins in V, there is a side $e(p_i, p_j)$ between them. Obviously, based on the original PPI network G, we can obtain a $N \times N$ dimensional adjacency matrix $A = (a_{ij})_{N\times N}$,where there is $a_{ij} = 1$, if and only if there is an edge $e(p_i, p_j)$ between p_i and p_j, otherwise, there is $a_{ij} = 0$.

For any given protein p_i in G, let $NG(p_i)$ denote the set of nodes neighboring to p_i in G, then it is obvious that there is:

$$NG(p_i) = \{p_j | \exists\, e(p_i, p_j) \in E, p_j \in V\} \quad (1)$$

According to Equation 1, it is easy to know that the nodes in $NG(p_i)$ are one-hop from p_i in G, for convenience, we define $NG(p_i)$ as the set of one-hop neighbors of p_i in G, based on which, we can obtain a new set of two-hops neighbors of p_i in G as follows:

$$THNG(p_i) = \{p_j | \exists\, e(p_j, p_k) \in E, p_k \in NG(p_i)\} \quad (2)$$

Where $|NG(p_i)|$ denotes the number of different nodes in the set $NG(p_i)$.

According to Equations 1, 2, based on the fact that key proteins and their neighbors often form tight junction clusters (Li et al., 2015; Peng et al., 2015a), we can define two kinds of topological properties for any given protein p_i in G as follows:

$$TP_1(p_i) = \sum_{p_j \in NG(p_i)} TZ_1(p_i, p_j) \quad (3)$$

$$TP_2(p_i) = \sum_{p_j \in NG(p_i)} TZ_2(p_i, p_j) \quad (4)$$

Where,

$$TZ_1(p_i, p_j) = \begin{cases} \frac{|NG(p_i) \cap NG(p_j)|}{|NG(p_i)|}; & p_j \in NG(p_i) \\ 0; & \text{otherwise} \end{cases} \quad (5)$$

$$TZ_2(p_i, p_j) = \begin{cases} \frac{|THNG(p_i) \cap NG(p_j)|}{|THNG(p_i)|}; & p_j \in NG(p_i) \\ 0; & \text{otherwise} \end{cases} \quad (6)$$

From observing Equations 3, 4, it can be seen that, for any two given proteins p_i and p_j in G, the more the number of common one-hop or two-hops neighboring nodes between them,

the bigger the values of $TZ_1\left(p_i, p_j\right)$ and $TZ_2(p_i, p_j)$ will be. Hence, it is obvious that $TZ_1\left(p_i, p_j\right)$ and $TZ_2(p_i, p_j)$ can to a certain extent reflect the tightness and the aggregation degree between p_i and p_j, respectively.

Extraction of Functional Features for Proteins

Key proteins tend to connect with each other rather than exist independently, and the key of proteins is usually expressed through protein complexes or functional modules, rather than a single protein (Min et al., 2017). Existing studies have shown that key proteins are closely related to the subcellular structures of proteins (Peng et al., 2015b; Li et al., 2016; Fan et al., 2017). In this section, we will adopt the subcellular locations to extract functional features for proteins. First, for any given protein p_i, let $Sub\left(p_i\right)$ denote the set of different subcellular locations relating to p_i, and $\left|Sub\left(p_i\right)\right|$ represent the number of different elements in $Sub\left(p_i\right)$, then, we can calculate one kind of functional property for p_i as follows:

$$FP_1(p_i) = \frac{\sum_{p_j \in NG(p_i)} TZ_3\left(p_i, p_j\right)}{\left|NG\left(p_i\right)\right|} + 1 \tag{7}$$

Where,

$$TZ_3(p_i, p_j) = \begin{cases} \dfrac{\left|Sub\left(p_i\right) \cap Sub\left(p_j\right)\right|^2}{\left|Sub\left(p_i\right)\right| * \left|Sub(p_j)\right|}; \\ \qquad \left|Sub\left(p_i\right) | * |Sub(p_j)\right| > 0 \\ 0; \qquad otherwise \end{cases} \tag{8}$$

In addition, in the study of Peng et al. (2012), key proteins were proved to be relatively conserved. Through whether each protein has homology, the homology score of each protein is obtained to indicate the degree of conservation of each protein. Based on the homology information of proteins, for any given protein p_i, let $os(p_i)$ denote the homology fraction of p_i, then we can obtain another kind of functional property for p_i as follows:

$$FP_2(p_i) = \frac{os(p_i)}{\underset{p_j \in V}{max}\left\{os(p_j)\right\}} \tag{9}$$

Construction of Linear Neighborhood Similarity-Based Protein Multifeatures Fusion

Initial Iteration

For generality, supposing that we have extracted M_1 different topological features (such as TP_1, TP_2,. . ., TP_{M_1}) and M_2 different functional features (such as FP_1, FP_2,. . .,FP_{M_2}), moreover, there is $M_1 + M_2 = M$, then, for any given protein p_i, we can construct a feature vector for it as follows:

$$\begin{aligned} V_i &= < TP_1, TP_2, \ldots, TP_{M_1}, FP_1, FP_2, \ldots, FP_{M_2} > \\ &= < P_1, P_2, \ldots, P_M > \end{aligned} \tag{10}$$

Based on Equation 10, we can further obtain a feature matrix for all N proteins in G as follows:

$$Z = [\, V_1 \cdots V_N \,]^T = \left[z_{ij}\right]_{N \times M} \tag{11}$$

Based on Equation 11, it is obvious that we can adopt entropy to measure the weight of each feature in all M different features as follows:

$$w_j = (1 - e_j) / \sum_{i=1}^{M} (1 - e_i) \tag{12}$$

Where,

$$e_j = -\sum_{i=1}^{N} z_{ij} \ln z_{ij} / \ln N \tag{13}$$

TABLE 1 | A brief description of the existing representative prediction models.

Algorithm	Network topology	Biological information	Particular year
DC (Hahn and Kern, 2005)	Degree centrality	NO	2005
EC (Bonacich, 1987)	Eigenvector centrality	NO	1987
CC (Wuchty and Stadler, 2003)	Closeness centrality	NO	2003
IC (Stephenson and Zelen, 1989)	Information centrality	NO	1989
SC (Estrada and Rodríguez-Velázquez, 2005)	Subgraph centrality	NO	2005
BC (Joy et al., 2005)	Betweenness centrality	NO	2005
NC (Wang et al., 2012)	Neighbor centrality	NO	2012
PEC (Li et al., 2012)	Edge clustering coefficient	Gene expression data	2012
LAC (Li et al., 2015)	Degree centrality, common neighbor node	NO	2011
CoEWC (Zhang et al., 2013)	Clustering coefficient	Gene expression data	2013
POEM (Zhao et al., 2014)	Degree centrality, subgraph, edge clustering coefficient, closeness centrality	Gene expression data	2014
ION (Peng et al., 2015a)	Edge clustering coefficient	Orthologous data	2012
TEGS (Li et al., 2018)	Subnetwork partition and prioritization	subcellular localization data	2018
RWHN (Zhao et al., 2019)	Degree centrality, protein-domain	Orthologous data, subcellular localization	2019
IoMCD (Sun et al., 2021)	Common neighbor node, degree Centrality	Gene expression data, orthologous data	2021
CVIM (Li et al., 2020)	Degree centrality, common neighbor node	Gene expression data, orthologous data	2020

Moreover, according to Equation 13, we can further calculate the feature-based score of p_i for any given protein as follows:

$$CScore(p_i) = \sum_{j=1}^{M} w_j Z_{ij} \tag{14}$$

Based on Equation 14, we can construct a new matrix H as follows:

$$H_{ij} = \begin{cases} \dfrac{CScore(p_i)}{\sum_{l=1}^{N} CScore(p_l)}; & if\ i = j \\ \dfrac{min\left\{CScore(p_i), CScore(p_j)\right\}}{\sum_{l=1}^{N} CScore(l)}; & else \end{cases} \tag{15}$$

Hence, according to Equation 15, we can obtain stable scores for all proteins in an iterative way as follows:

$$Y^{t+1} = \alpha H Y^t + (1-\alpha)\, Y^0 \tag{16}$$

Where the parameter $\alpha \in (0,\ 1)$and $Y^0 = < FP_2\left(p_1\right), FP_2\left(p_2\right), \ldots, FP_2(p_N) >$ is the vector consisting of initial scores of all proteins. Moreover, for convenience, we define the final stable scores obtained by Equation 16 as Y^{Final}.

Further Optimization

Proteins can be considered as data points in the feature space, and how to predict the similarity between potential essential proteins in the feature space is very important for the prediction of essential proteins. Wang and Zhang (2008) found that every data point in a high-dimensional space can be reconstructed by its neighbors. Zhang et al. (2017) proposed a new similarity measure to predict drug side effects based on characteristics of drugs. Hence, based on above concepts, in this section, we will first define protein nodes in the original PPI network as data points, and the gene expression data of proteins as features of corresponding data points. And for convenience, for any given protein p_i, let $g_i = < g_{i1}, g_{i2}, \ldots, g_{i36} >$ represent its gene expression data, where g_{it} represents the gene expression level of p_i at the tth time point, then, we can further reconstruct each data point p_i based on features of its neighbors by minimizing the following reconstruction error ε_i:

$$\begin{aligned} \varepsilon_i &= \left\| g_i - \sum_{p_j \in NG(p_i)} s_{i,j} g_j^2 \right\| + \|s_i^2\| \\ &= \left\| \sum_{p_j \in NG(p_i)} s_{i,j} \left(g_i - g_j\right)^2 \right\| + \sum_{p_j \in NG(p_i)} \left(s_{i,j}\right)^2 \\ &= \sum_{p_j, p_k \in NG(p_i)} s_{i,j} s_{i,k} \left(g_i - g_j\right)^T \left(g_i - g_j\right) + \sum_{p_j \in NG(p_i)} \left(s_{i,j}\right)^2 \\ &= \sum_{p_j, p_k \in NG(p_i)} s_{i,j} \left(G^i + I\right) s_{i,k} \\ &= s_i^T \left(G^i + I\right) s_i \\ s.t. \quad & \sum_{p_j \in NG(p_i)} s_{i,j} = 1, s_{i,j} \geq 0 \end{aligned} \tag{17}$$

Here, $G^i = (g_i - g_j)^T (g_i - g_j)$, $s_i = (s_{i,1},\ s_{i,2} \cdots s_{i,k})^T$, $\|g_i - \sum_{p_j \in NG(p_i)} s_{i,j} g_j^2\|$ is the item of reconstruction error, $\|s_i^2\|$ is used for regularization and I is the identity matrix.

Obviously, according to Equation 17, let $S_{i,j} = \begin{cases} s_{i,j} : & if\ p_j \in NG\left(p_i\right) \\ 1 : & i = j \\ 0 : & otherwise \end{cases}$, then we can obtain a $N \times N$-dimensional similarity matrix S as follows:

$$S = \begin{bmatrix} S_{11} & \cdots & S_{1N} \\ \vdots & \ddots & \vdots \\ S_{N1} & \cdots & S_{NN} \end{bmatrix} \tag{18}$$

In addition, for any given protein node p_i in G, we can calculate the similarity $s_{i,j}$ between it and its neighboring node

TABLE 2 | Influence of parameter α on the effect of initial iteration algorithm in Gavin database.

	α								
Rank	**0.1**	**0.2**	**0.3**	**0.4**	**0.5**	**0.6**	**0.7**	**0.8**	**0.9**
Top1% (19)	16	17	18	18	18	**18**	17	15	15
Top5% (93)	75	80	83	83	82	80	80	78	79
Top10% (186)	147	155	156	159	162	162	**163**	160	161
Top15% (278)	198	205	213	219	218	**220**	220	219	217
Top20% (371)	249	259	264	268	271	267	**274**	278	272
Top25% (464)	303	306	309	314	317	**322**	322	320	321

The bold values represent the best predictive performance achieved by LNSPF under different conditions.

TABLE 3 | Effect of parameter β on prediction performance of LNSPF in Gavin database.

	β								
Rank	**0.1**	**0.2**	**0.3**	**0.4**	**0.5**	**0.6**	**0.7**	**0.8**	**0.9**
Top1% (19)	18	**19**	**19**	**19**	18	18	18	18	17
Top5% (93)	81	83	83	**84**	82	82	82	81	78
Top10% (186)	164	**165**	164	163	164	166	164	163	161
Top15% (278)	221	**223**	221	**223**	222	219	220	219	210
Top20% (371)	271	274	274	**278**	274	272	272	270	262
Top25% (464)	324	324	325	**326**	325	321	319	314	310

The bold values represent the best predictive performance achieved by LNSPF under different conditions.

TABLE 4 | Effect of parameter β on prediction performance of LNSPF based on DIP database.

	β								
Rank	**0.1**	**0.2**	**0.3**	**0.4**	**0.5**	**0.6**	**0.7**	**0.8**	**0.9**
Top1% (51)	46	**47**	47	46	46	46	44	44	43
Top5% (255)	203	**208**	205	203	203	200	198	197	189
Top10% (510)	347	**352**	350	**352**	**352**	349	342	334	330
Top15% (764)	468	468	467	**469**	467	459	457	458	429
Top20% (1019)	547	546	544	**548**	547	542	542	535	519
Top25% (1274)	626	**630**	628	625	622	622	623	615	608

The bold values represent the best predictive performance achieved by LNSPF under different conditions.

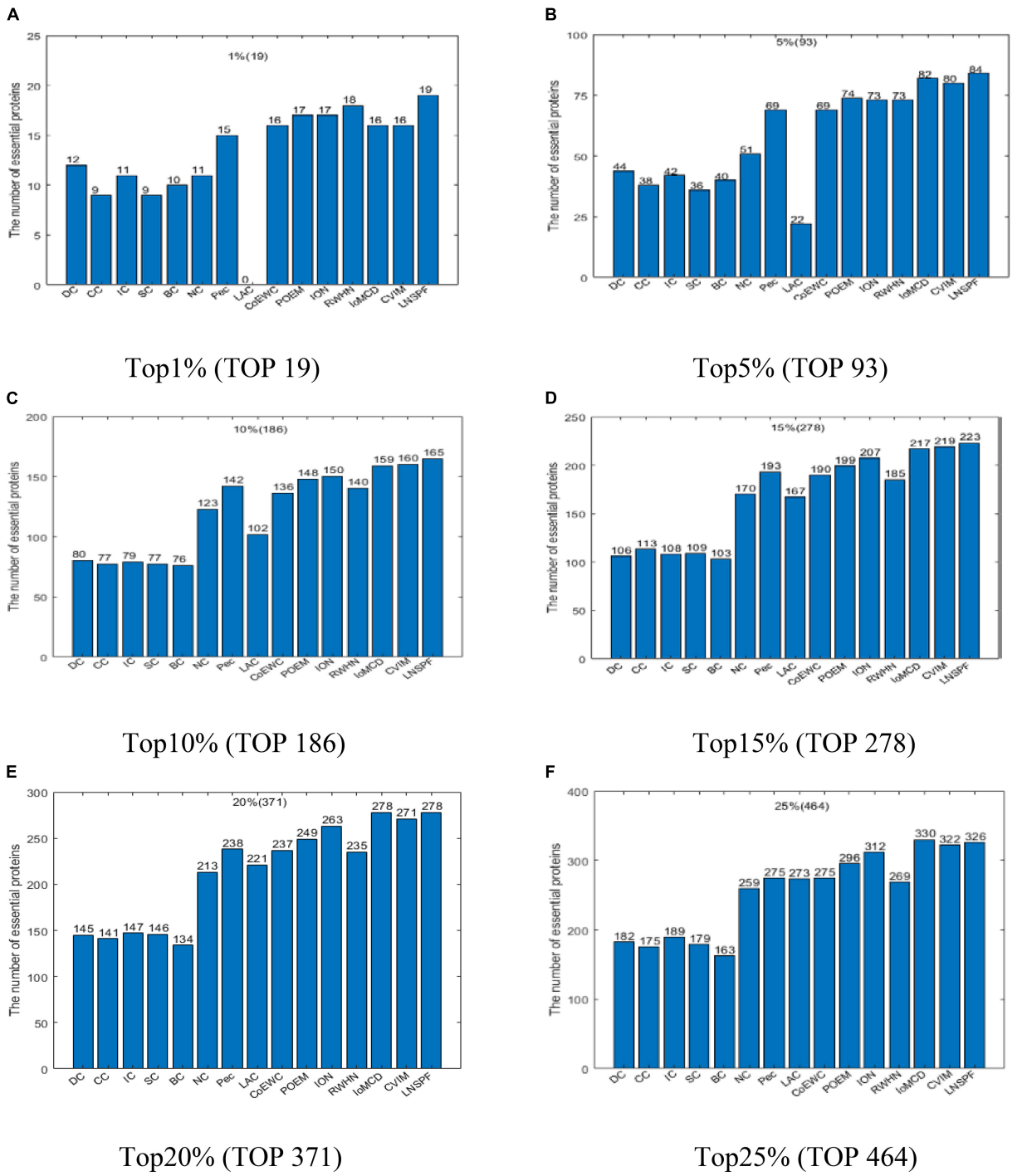

FIGURE 2 | Comparison results of the numbers of real key proteins predicted by LNSPF, DC, CC, IC, SC, BC, NC, PEC, LAC, CoEWC, POEM, ION, RWHN, IoMCD, and CVIM based on the GAVIN database. **(A)** Top 1% ranked proteins. **(B)** Top 5% ranked proteins. **(C)** Top 10% ranked proteins. **(D)** Top 15% ranked proteins. **(E)** Top 20% ranked proteins. **(F)** Top 25% ranked proteins.

$p_j \in NG(p_i)$ as follows:

$$\begin{aligned} &min \;\; s_i^T \left(G^i + \mu I\right) s_i \\ &s.t. \quad \sum_{p_j \in NG(p_i)} s_{i,j} = 1 \,, s_{i,j} \geq 0 \end{aligned}$$

Thereafter, let $T^0 = Y^{Final}$, based on above newly obtained matrix S, we can further optimize the scores for all proteins in an iterative way as follows:

$$T^{\sigma+1} = \beta S T^{\sigma} + (1-\beta) T^0 \tag{19}$$

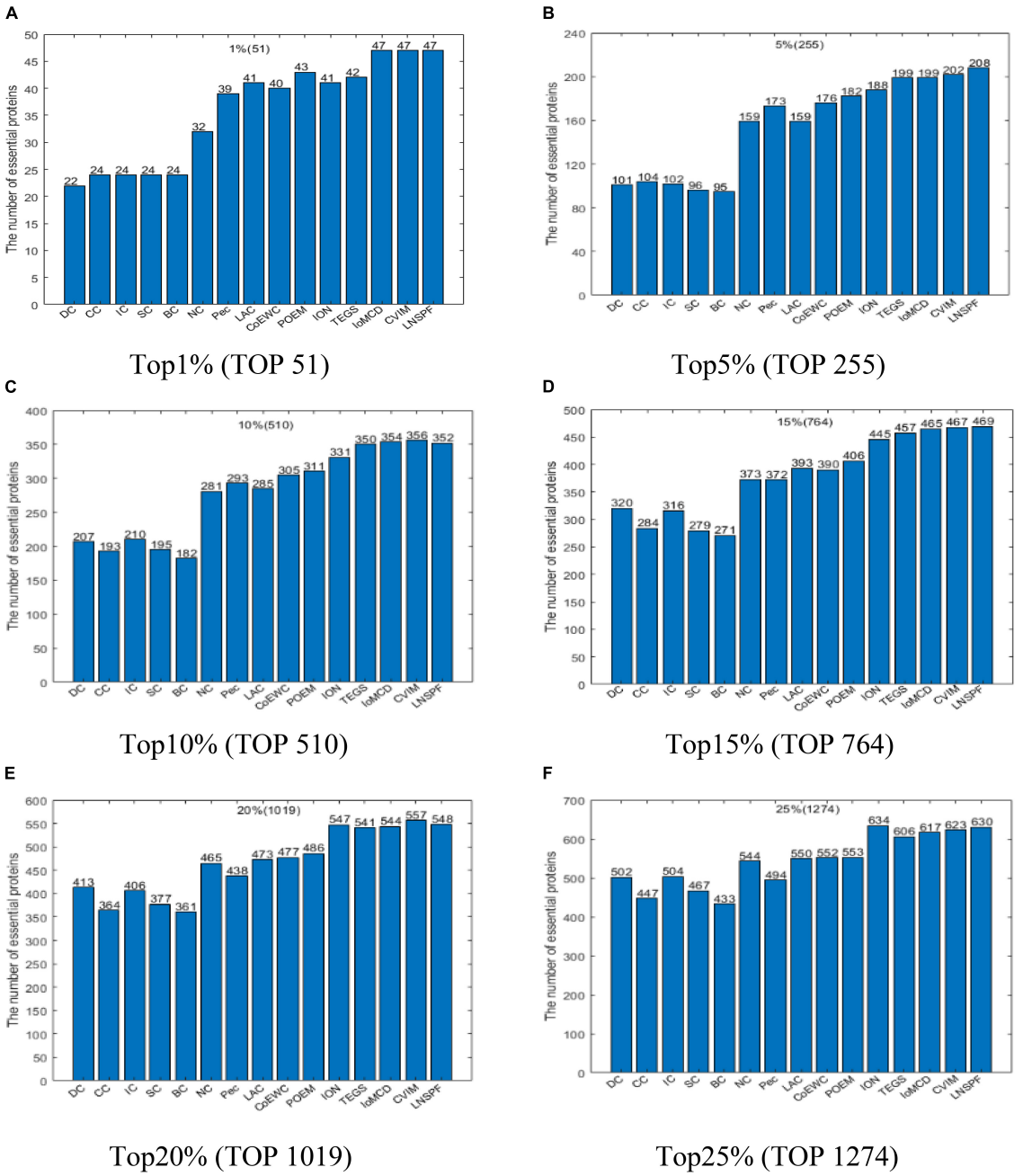

FIGURE 3 | Comparison results of the numbers of real key proteins predicted by LNSPF, DC, CC, IC, SC, BC, NC, PEC, LAC, CoEWC, POEM, ION, RWHN, IoMCD, and CVIM based on the DIP database. **(A)** Top 1% ranked proteins. **(B)** Top 5% ranked proteins. **(C)** Top 10% ranked proteins. **(D)** Top 15% ranked proteins. **(E)** Top 20% ranked proteins. **(F)** Top 25% ranked proteins.

Here, there is $\beta \in (0, \quad 1)$.

Based on the above descriptions, the process of LNSPF can be described in detail as follows:

Algorithm: LNSPF.

Input: Original PPI network, gene expression data, subcellular location data and homologous data, parameters δ and K.

Output: Rank the proteins in descending order according to T^{Final} value, and output TOP K%.

Step 1: According to Equations 3, 4, an original PPI network $G = (V, E)$ is generated, based on which, topological features are extracted;

Step 2: According to Equations 7, 9, functional characteristics are extracted from the subcellular location data and homologous data, respectively.

Step 3: According to Equation 15, the matrix H is obtained;

Step 4: let $t = t + 1$; calculate Y^{t+1} according to Equation 16;

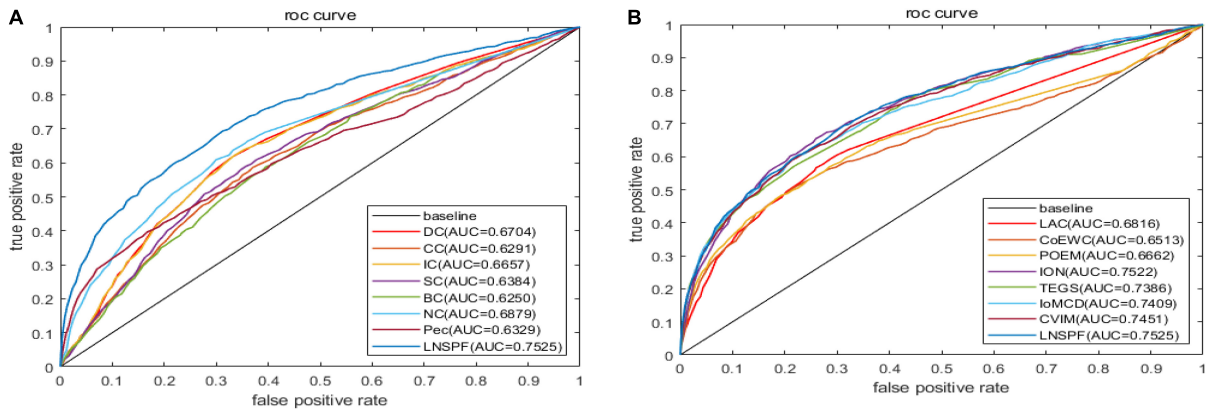

FIGURE 4 | The ROC curves of LNSPF method based on DIP dataset and DC, CC, IC, SC, BC, NC, Pec, and LAC CoEWC, POEM, ION, TEGS, IoMCD, and CVIM 14 prediction methods. **(A)** Comparison between LNSPF and DC, CC, IC, SC, BC, NC, PEC. **(B)** Comparison between LNSPF and LAC, CoEWC, POEM, ION, TEGS, IoMCD, CVIM.

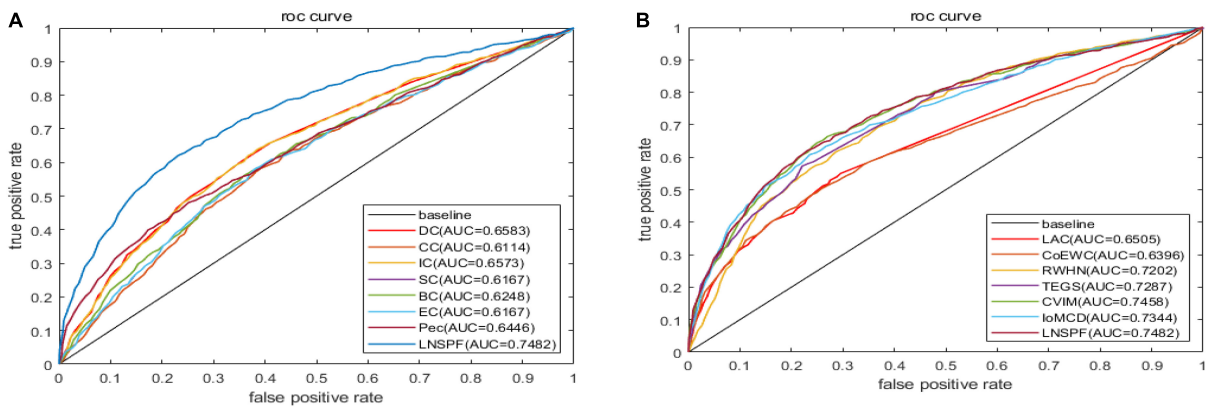

FIGURE 5 | The ROC curves of LNSPF method based on Krogan dataset and DC, CC, IC, SC, BC, EC, PEC, and LAC, CoEWC, RWHN, TEGS, CVIM, and IOMCD 13 prediction methods. **(A)** Comparison between LNSPF and DC, CC, IC, SC, BC, EC, PEC. **(B)** Comparison between LNSPF and LAC, CoEWC, RWHN, TEGS, CVIM, IOMCD.

Step 5: Repeat step 4 until $||Y^{t+1} - Y^t|| < \delta$, the matrix Y^{Final} is obtained;

Step 6: According to Equation 18, the similarity matrix S is obtained;

Step 7: let $T^0 = Y^{Final}$ and $\sigma = \sigma + 1$, the matrix Y^{Final} is further optimized according to Equation 19;

Step 8: Repeat step 7 until $||T^{\sigma+1} - T^{\sigma}|| < \delta$, the matrix T^{Final} is obtained;

Step 9: The values of T^{Final} are sorted in descending order, and the top K% proteins with the highest final scores are output.

EXPERIMENTAL RESULTS

Experimental Data

During experiments, we first downloaded known PPIs from three different databases such as the Gavin (Gavin et al., 2006) database, the DIP (Xenarios et al., 2002) database, and the Krogan (Cherry, 1998) database, and then, after filtering repeated interactions and self-interactions, we finally obtained 24,743 interactions between 5,093 proteins based on the DIP database, 7,669 interactions between 1,855 proteins based on the Gavin database, and 14,317 interactions between 3,672 proteins based on the Krogan database, respectively. Moreover, we obtained a group of 1,285 essential proteins in Saccharomyces cerevisiae from the databases of SGDP (Holman et al., 2009), SGD (Holman et al., 2009), DEG (Zhang and Lin, 2009), and MIPS (Bruno et al., 2012) as well. Furthermore, we

TABLE 5 | Based on DIP database, LNSPF and AUC of 14 competitive methods.

Method	LNSPF	DC	CC	IC	SC	BC	NC	Pec
AUC	0.7525	0.6704	0.6293	0.6657	0.6384	0.6250	0.6879	0.6329
Method	**LNSPF**	**LAC**	**CoEWC**	**POEM**	**ION**	**TEGS**	**IoMCD**	**CVIM**
AUC	0.7525	0.6816	0.6513	0.6662	0.7522	0.7386	0.7409	0.7451

TABLE 6 | AUC values of LNSPF and 13 competing methods based on Krogan dataset.

Method	LNSPF	DC	CC	IC	SC	BC	EC
AUC	0.7482	0.6583	0.6114	0.6573	0.6167	0.6248	0.6167
Method	**PEC**	**LAC**	**CoEWC**	**RWHN**	**TEGS**	**CVIM**	**IoMCD**
AUC	0.6446	0.6505	0.6396	0.7202	0.7287	0.7458	0.7344

downloaded the homology information of proteins from the Inparanoid database (Gabriel et al., 2010), the gene expression dataset composing of 6,776 proteins representing the gene expression level of proteins in continuous metabolic cycles from the database provided by Tu et al. (2005), and the dataset of subcellular location information from the part-means database (Binder et al., 2014) separately. Especially, the dataset of subcellular location information consists of 11 kinds of subcellular localization, namely, the extracellular, peroxisome, nucleus, plasma, endosome, mitochondrion, vacuole, cytosol, golgi, cytoskeleton, and endoplasmic, which are closely related to known key proteins. At last, to evaluate the recognition rate of true essential proteins predicted by LNSPF, we compared LNSPF with 16 representative predictive models, as shown in **Table 1**, namely, DC, EC, CC, IC, SC, BC, NC, Pec, LAC, CoEWC, POEM, ION, TEGS, RWHN, IoMCD, and CVIM.

Influence of Parameters on Linear Neighborhood Similarity-Based Protein Multifeatures Fusion Performance

In LNSPF, we set parameters α and β, the value ranges of both α and β are (0, 1), to adjust the final protein score. During experiments, we will set different values to the parameter α or β first based on the Gavin database and the DIP database, respectively, and then, the setting value with the highest

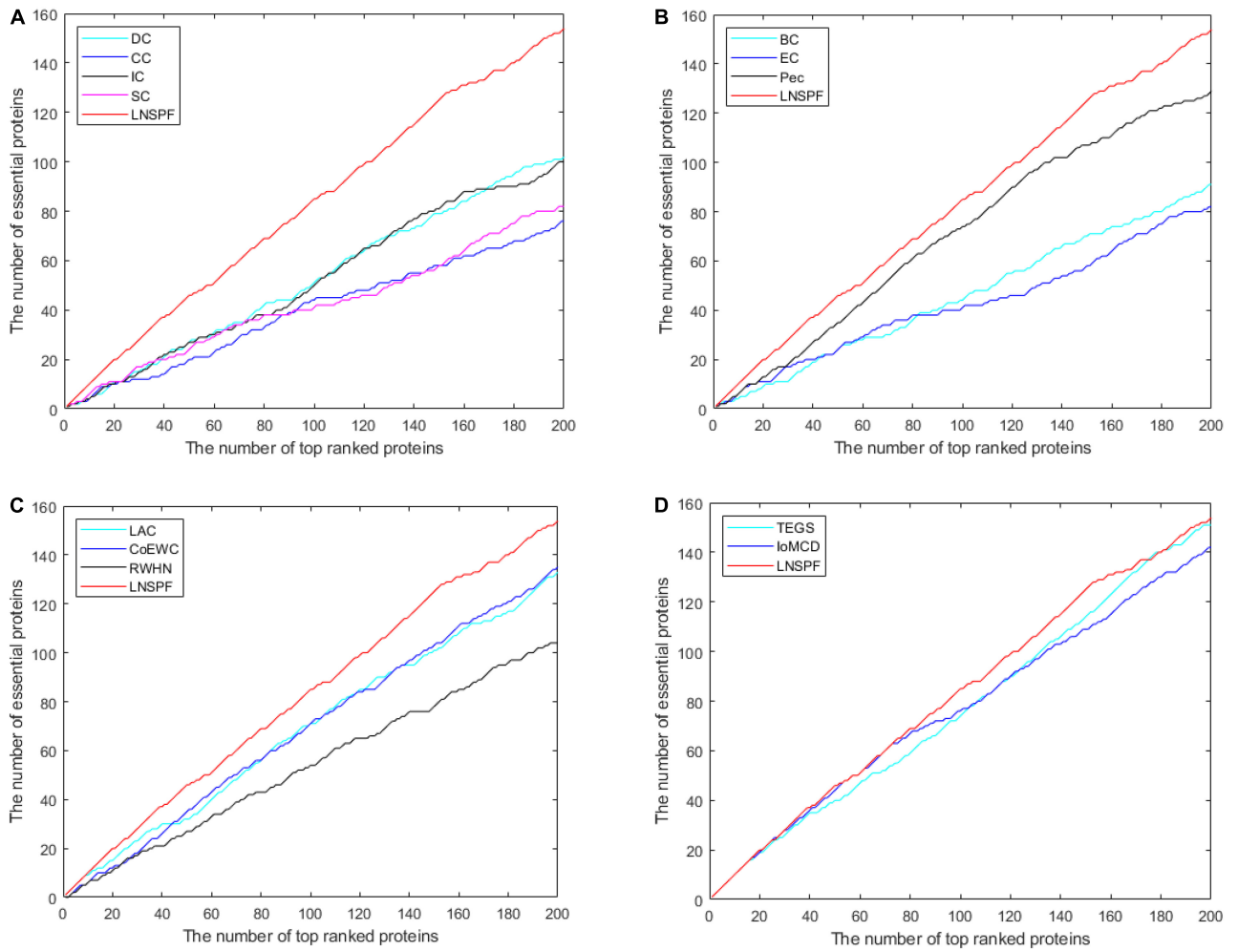

FIGURE 6 | The figure shows the Jackknife curves of LNSPF and DC, CC, IC, SC, BC, EC, and PEC based on Krogan dataset, and LAC, CoEWC, RWHN, TEGS, and IOMCD 12 prediction methods. The X-axis represents the number of potentially critical proteins ranked in the top 200, and the Y-axis represents the number of truly essential proteins identified by these models. **(A)** Comparison between LNSPF and DC, CC, IC, SC. **(B)** Comparison between LNSPF and BC, EC, PEC. **(C)** Comparison between LNSPF and LAC, CoEWC, RWHN. **(D)** Comparison between LNSPF and TEGS, IOMCD.

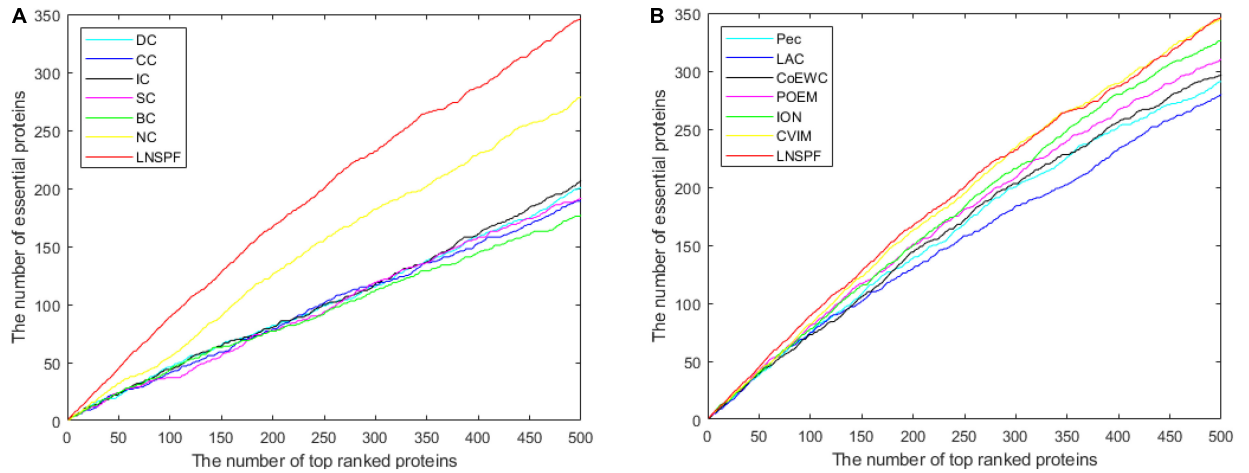

FIGURE 7 | The figure, respectively, shows the Jackknife curve of LNSPF and DC, CC, IC, SC, BC, NC, and PEC, LAC, COEWC, POEM, ION, and CVIM 12 prediction methods based on DIP data set. The X-axis represents the number of potentially critical proteins ranked in the top 500, and the Y-axis represents the number of truly essential proteins identified by these models. **(A)** Comparison between LNSPF and DC, CC, IC, SC, BC, NC. **(B)** Comparison between LNSPF and PEC, LAC, COEWC, POEM, ION, CVIM.

prediction accuracy of essential protein will be selected as the final value of parameter α or β. Based on the Gavin dataset, we set α to 0.1., 0.8, and 0.9 to predict the effect of the preliminary iterative algorithm. From observing **Table 2**, it is obvious that when $\alpha = 0.6$, the protein score with obvious effect and the most stable one can be obtained. At this time, the setting value of α in Gavin dataset is 0.6 and that in DIP database is 0.8. β set 0.1, . . ., 0.8, 0.9. The prediction results based on Gavin data set ($\alpha = 0.6$) and dip data set ($\alpha = 0.8$) are shown in **Tables 3**, **4**, respectively. By observing **Table 3**, it is easy to see that the prediction performance of LNSPF is the highest at 1%, 5%, 15%, 20%, and 25% when $\beta = 0.4$ is used. Therefore, based on Gavin data set, it is appropriate to set β as 0.4. By observing **Table 4**, it is easy to see that the prediction performance of LNSPF is the highest at 1%, 5%, 10%, and 25% when $\beta = 0.2$ is used. Therefore, based on the DIP data set, it is more appropriate to set β as 0.2.

COMPARISON OF LNSPF WITH OTHER METHODS

Comparison of the Number of Real Essential Proteins Between Linear Neighborhood Similarity-Based Protein Multifeatures Fusion and 14 Representative Methods

According to above descriptions, it is easy to see that LNSPF can achieve it best predictive performance while we set α to 0.6 and β to 0.4 based on the Gavin database. Hence, in this section, in order to estimate the actual predictive performance of LNSPF, we will first compare it with 14 advanced predictive methods based on the Gavin database while setting α to 0.6 and β to 0.4, and the comparison results are shown in **Figure 2**. From observing the **Figure 2**, it is easy to see that, in the ranking of the number of true essential proteins inferred by these 15 predictive methods, LNSPF can achieve better predictive performance than all these competitive methods in top 1, 5, 10, 15, and 20% predicted key proteins simultaneously. For instance, from the top 1% to top 20% predicted key proteins, the predictive accuracies of LNSPF are 15.8, 4.3, 2.6, 1.4, and 1.8% higher than that of the method of CVIM, respectively.

Similarly, according to above descriptions, it is easy to see that LNSPF can achieve it best predictive performance while we set α to 0.6 and β to 0.2 based on the DIP database. Hence, in this section, in order to estimate the actual predictive performance of LNSPF, we will further compare it with 14 advanced predictive methods based on the DIP database while setting α to 0.6 and β to 0.2, and the comparison results are shown in **Figure 3**. From observing the **Figure 3**, it is easy to see that, the numbers of essential proteins detected by LNSPF in the top 1, 5, 10, 15, 20, and 25% ranked proteins are significantly better than that of all competitive methods as a whole.

Receiver Operating Characteristic Curve Verification

Receiver operating characteristic curve (ROC) is used to compare the prediction performance of LNSPF with DC, CC, IC, SC, BC, NC, PEC, LAC, CoEWC, POEM, ION, TEGS, IoMCD, and CVIM based on DIP data set. The larger the area of ROC curve, the better the performance of the model, it can be seen from **Figure 4** and **Table 5** that the performance of this model is significantly higher than that of the 14 competitive methods. The prediction performance of LNSPF method based on Krogan dataset compared with DC, CC, IC, SC, BC, EC, PEC, and LAC, CoEWC, RWHN, TEGS, CVIM, and IoMCD 13 competing methods. It can be seen from **Figure 5** and **Table 6** that the performance of this model is significantly higher than that of these 13 competing methods.

Verification of Jackknife Method

In this section, I'll use the Jackknife method to verify the performance of the LNSPF against the other models. The performance of LNSPF was compared with DC, CC, IC, SC, BC, EC, PEC, and LAC, CoEWC, RWHN, TEGS, and IOMCD based on Krogan data set. As shown in **Figure 6**. It is obvious that this method is superior to other models. The performance of LNSPF is compared with DC, CC, IC, SC, BC, NC, PEC, and LAC, COEWC, POEM, ION, and CVIM based on DIP data set, as shown in **Figure 7**.

DISCUSSION

Essential proteins play an important role in cell growth and regulation, for the past few years, accumulating computational methods have been proposed to detect potential key proteins, however, the predictive performances of these existing methods are not very satisfactory yet. In this study, a novel predictive model called LNSPF was designed by combining topological features of PPI networks with a series of biological characteristics of proteins to detect potential key proteins. In LNSPF, a new entropy-based method for feature fusion and a linear neighborhood similarity method for optimization were adopted. Comparing with traditional identification methods, LNSPF can achieve better predictive performance, which demonstrates that the method based on the fusion of biological information of proteins and topological features of PPI networks can improve the prediction accuracy of essential proteins effectively. In addition, there are some limitations in current version of LNSPF as well, for example, the loss of gene time expression data or homologous data of some proteins will affect the recognition accuracy of LNSPF to some degree.

CONCLUSION

In this paper, an iterative model of protein multifeature fusion based on linear neighborhood similarity (LNSPF) is proposed to predict essential proteins by fusing biological and topological information of proteins. In LNSPF, first, the topological features are extracted from the original PPI network, and then the functional features are extracted from the subcellular location data. Second, an entropy weight method is used to fuse the features, and then a stable protein score is obtained by an iterative method. At last, a linear neighborhood similarity method is used to optimize the score effectively. The experimental results show that based on Gavin data sets, the Krogan data sets, and DIP held several experimental data sets, through a variety of methods to verify the effectiveness of the new model LNSPF and stability. Compared with many advanced prediction models, the new model LNSPF has better prediction effect.

DATA AVAILABILITY STATEMENT

The original contributions presented in the study are included in the article/supplementary material, further inquiries can be directed to the corresponding author/s.

AUTHOR CONTRIBUTIONS

XZ and YZ conceived the study, implemented the algorithms corresponding to the study, and wrote the manuscript. LW and ZC improved the study based on the original model. YT and LW supervised the study. XZ and YZ revised the manuscript. All authors reviewed and improved the manuscript.

FUNDING

This research is partly sponsored by the Research Foundation of Education Bureau of Hunan Province (No. 20B080), the Natural Science Foundation of Hunan Province (No. 2019JJ70010), the Hunan Provincial Natural Science Foundation of China (2020JJ4152), the Science and Technology Plan Project of Hunan Province (2016TP1020), the Hunan Province Science and Technology Project Funds (2018TP1036), and the National Scientific Research Foundation of Hunan Province Education Commission (18B367).

ACKNOWLEDGMENTS

The authors thank Shiyuan Li and the anonymous referees for suggestions that helped improve the manuscript substantially.

REFERENCES

Binder, J. X., Pletscher-Frankild, S., Tsafou, K., Stolte, C., O'Donoghue, S. I., Schneider, R., et al. (2014). COMPARTMENTS: unification and visualization of protein subcellular localization evidence. *Database* 2014:bau012. doi: 10.1093/database/bau012

Bonacich, P. (1987). 'Power and centrality: a family of measures. *Am. J. Sociol.* 92, 1170–1182. doi: 10.1086/228631

Bruno, A., Jef, B., and Carla, C. (2012). *SGDP: Saccharomyces Genome Deletion Project [EB/OL]*. Available online at: http://yeastdeletion.stanford.edu/ (accessed June 20, 2012).

Chen, Z., Meng, Z., Liu, C., Wang, X., Kuang, L., Pei, T., et al. (2020). A novel model for predicting essential proteins based on heterogeneous protein-domain network. *IEEE Access* 8, 8946–8958. doi: 10.1109/access.2020.2964571

Chen, Z.-H., You, Z.-H., Li, L.-P., Guo, Z. H., Hu, P. W., Jiang, H. J., et al. (2019). "Combining LSTM network model and wavelet transform for predicting self-interacting proteins," in *Intelligent Computing Theories and Application. ICIC 2019. Lecture Notes in Computer Science*, eds D. S. Huang, V. Bevilacqua, and P. Premaratne (Cham: Springer).

Cherry, J. (1998). SGD: *Saccharomyces* genome database. *Nucleic Acids Res.* 26, 73–79. doi: 10.1093/nar/26.1.73

Dai, W., Chang, Q., Peng, W., Zhong, F., and Li, Y. (2020). Network embedding the protein-pro tein interaction network for human essential genes identification. *Genes* 11:153. doi: 10.3390/genes11020153

Dai, W., Chen, B., Peng, W., Li, X., Zhong, J., and Wang, J. (2021). A novel multi-ensemble method for identifying essential proteins. *J. Comp. Biol.* 28, 637–649. doi: 10.1089/cmb.2020.0527

Estrada, E., and Rodríguez-Velázquez, J. A. (2005). Subgraph centrality in complex networks. *Phys. Rev. E, Stat. Phys. Plasmas Fluids Relat. Interdiscip. Top.* 71, 33–122.

Fan, Y., Tang, X., Hu, X., Wu, W., and Ping, Q. (2017). Prediction of essential proteins bases on subcellular localization and gene expression correlation. *BMC Bioinformatics* 18(Suppl. 13):470. doi: 10.1186/s12859-017-1876-1875

Gabriel, O., Thomas, S., Kristoffer, F., Köstler, T., Messina, D. N., Roopra, S., et al. (2010). InParanoid 7: new algorithms and tools for eukaryotic orthology analysis. *Nucleic Acids Res.* 38, D196–D203. doi: 10.1093/nar/gkp931

Gavin, A. C., Aloy, P., Grandi, P., Krause, R., Boesche, M., Marzioch, M., et al. (2006). Proteome survey reveals modularity of the yeast cell machinery. *Nature* 440:631. doi: 10.1038/nature04532

Hahn, M. W., and Kern, A. D. (2005). Comparative genomics of centrality and essentiality in three eukaryotic protein-interaction networks. *Mol. Biol. Evol.* 22, 803–806. doi: 10.1093/molbev/msi072

Holman, A. G., Davis, P. J., Foster, J. M., Carlow, C. K., and Kumar, S. (2009). Computational prediction of essential genes in an unculturable endosymbiotic bacterium. Wolbachia of Brugia Malayi. *BMC Microbiol.* 9:243. doi: 10.1186/1471-2180-9-243

Joy, M. P., Brock, A., Ingber, D. E., and Huang, S. (2005). High-betweenness proteins in the yeast protein interaction network. *J. Biomed. Biotechnol.* 2005, 96–103. doi: 10.1155/JBB.2005.96

Lei, X., Ding, Y., Fujita, H., and Aidong, Z. (2016). Identification of dynamic protein complexes based on fruit fly optimization algorithm. *Knowl Base Syst.* 105, 270–277. doi: 10.1038/s41598-018-28680-8

Lei, X., Yang, X., and Wu, F.-X. (2020). Artificial fish swarm optimization-based method to identify essential proteins. *IEEE/ACM Trans Comput Biol Bioinform.* 17, 495–495. doi: 10.1109/TCBB.2018.2865567

Li, G., Min, L., Wang, J., Wu, J., Wu, F. X., Pan, Y., et al. (2016). Predicting essential proteins based on subcellular localization, orthology and PPI networks. *BMC Bioinformatics* 17:279. doi: 10.1186/s12859-016-1115-5

Li, M., Li, W., Wu, F. X., Pan, Y., and Wang, J. (2018). Identifying essential proteins based on sub-network partition and prioritization by integrating subcellular localization information. *J. Theoretical Biol.* 447, 65–47. doi: 10.1016/j.jtbi.2018.03.029

Li, M., Lu, Y., Wang, J., Wu, F.-X., and Pan, Y. (2015). 'A topology potential-based method for identifying essential proteins from PPI networks. *IEEE/ACM Trans. Comput. Biol. Bioinf.* 12, 372–383. doi: 10.1109/TCBB.2014.2361350

Li, M., Zhang, H., Wang, J. X., and Pan, Y. (2012). A new essential protein discovery method based on the integration of protein-protein interaction and gene expression data. *BMC Syst. Biol.* 6:15. doi: 10.1186/1752-0509-6-15

Li, S., Chen, Z., He, X., Zhang, Z., Pei, T., Tan, Y., et al. (2020). An iteration method for identifying yeast essential proteins from weighted PPI network based on topological and functional features of proteins. *IEEE Access* 8, 90792–90804. doi: 10.1109/access.2020.2993860

Lin, C. Y., Chin, C. H., and Wu, H. H. (2011). Hubba: hub objects analyzer-a framework of interactome hubs identification for network biology. *Comp. Biol. Chem.* 35:143. doi: 10.1093/nar/gkn257

Min, L., Yu, L., Niu, Z., and Wu, F. X. (2017). United complex centrality for identification of essential proteins from PPI networks. *IEEE/ACM Trans. on Comp. Biol. Bioinform. (TCBB)* 14, 370–380. doi: 10.1109/TCBB.2015.2394487

Peng, W., Wang, J. X., Cheng, Y., Lu, Y., Wu, F., Pan, Y., et al. (2015a). UDoNC: an algorithm for identifying essential proteins based on protein domains and protein-protein interaction networks. *IEEE/ACM Trans. Comp. Biol. Bioinform.* 12, 276–288. doi: 10.1109/TCBB.2014.2338317

Peng, W., Wang, J. X., Wang, W., Liu, Q., Wu, F. X., Pan, Y., et al. (2012). Iteration method for predicting essential proteins based on orthology and protein-protein interaction networks. *BMC Syst. Biol.* 6:87. doi: 10.1186/1752-0509-6-87

Peng, X., Wang, J., Zhong, J., Luo, J., and Pan, Y. (2015b). "An efficient method to identify essential proteins for different species by integrating protein subcellular localization information," in *Proceedings of the IEEE International Conference on Bioninformatics and Biomedicine*, (Piscataway, NJ: IEEE).

Qi, Y., and Luo, J. (2016). Prediction of essential proteins based on local interaction density. *IEEE/ACM Trans. Comp. Biol. Bioinform.* 13, 1170–1182. doi: 10.1109/TCBB.2015.2509989

Stephenson, K., and Zelen, M. (1989). Rethinking centrality: methods and examples. *Soc. Netw.* 11, 1–37.

Sun, W., Wang, L., Peng, J., Zhang, Z., Pei, T., Tan, Y., et al. (2021). A cross-entropy-based method for essential protein identification in yeast protein-protein interaction network. *Curr. Bioinform.* 16, 565–575. doi: 10.2174/1574893615999201116210840

Tang, X., Wang, J., Zhong, J., and Pan, Y. (2014). Predicting essential proteins based on weighted degree centrality. *IEEE/ACM Trans. Comp. Biol. Bioinform.* 11, 407–418. doi: 10.1109/TCBB.2013.2295318

Tu, B. P., Kudlicki, A., Rowicka, M., and McKnight, S. L. (2005). Logic of the yeast metabolic cycle: temporal compartmentalization of cellular processes. *Science* 310, 1152–1158. doi: 10.1126/science.1120499

Wang, F., and Zhang, C. (2008). Label propagation through linear neighborhoods. *Knowledge Data Eng. IEEE Trans.* 20, 55–67. doi: 10.1109/tkde.2007.190672

Wang, J. X., Li, M., and Wang, H. (2012). Identifification of essential proteins based on edge clustering coeffificient. *IEEE/ACM Trans. Comput. Biol. Bioinf.* 9, 1070–1080. doi: 10.1109/tcbb.2011.147

Wang, L., You, Z.-H., Xia, S.-X., Liu, F., Chen, X., Yan, X., et al. (2017). Advancing the prediction accuracy of protein-protein interactions by utilizing evolutionary information from position-specific scoring matrix and ensemble classifier. *J. Theor. Biol.* 418, 105–110. doi: 10.1016/j.jtbi.2017.01.003

Wuchty, S., and Stadler, P. F. (2003). Centers of complex networks. *J. Theor. Biol.* 223, 45–53. doi: 10.1016/s0022-5193(03)00071-7

Xenarios, I., Salwinski, L., Duan, X. J., Higney, P., Kim, S. M., Eisenberg, D., et al. (2002). DIP, the database of interacting proteins: a research tool for studying cellular networks of protein interactions. *Nucleic Acids Res.* 30, 303–305. doi: 10.1093/nar/30.1.303

Zhang, F., Peng, W., Yang, Y., Dai, W., and Song, J. (2019). A novel method for identifying essential genes by fusing dynamic protein–protein interactive networks. *Genes* 10:31. doi: 10.3390/genes10010031

Zhang, R., and Lin, Y. (2009). DEG 5.0, a database of essential genes in both prokaryotes and eukaryotes. *Nucleic Acids Res.* 37, D455–D458. doi: 10.1093/nar/gkn858

Zhang, W., Xue, X., Xie, C., Li, Y., Liu, J., Chen, H., et al. (2021). CEGSO: boosting essential proteins prediction by integrating protein complex, gene expression, gene ontology, subcellular localization and orthology information. *Interdisciplinary Sci. Comp. Life Sci.* 13, 349–361. doi: 10.1007/s12539-021-00426-7

Zhang, W., Yue, X., Liu, F., Chen, Y., Tu, S., Zhang, X., et al. (2017). A unified frame of predicting side effects of drugs by using linear neighborhood similarity. *BMC Syst. Biol.* 11:101. doi: 10.1186/s12918-017-0477-472

Zhang, X., Xu, J., and Xiao, W. (2013). A new method for the discovery of essential proteins. *PLoS One* 8:e58763. doi: 10.1371/journal.pone.0058763

Zhao, B., Wang, J., Li, M., Wu, F.-X., and Pan, Y. (2014). Prediction of essential proteins based on overlapping essential modules. *IEEE Trans. Nanobiosci.* 13, 415–424. doi: 10.1109/TNB.2014.2337912

Zhao, B., Zhao, Y., Zhang, X., Zhang, Z., Zhang, F., and Wang, L. (2019). An iteration method for identifying yeast essential proteins from heterogeneous network. *BMC Bioinf.* 20:355. doi: 10.1186/s12859-019-2930-2

Conflict of Interest: The authors declare that the research was conducted in the absence of any commercial or financial relationships that could be construed as a potential conflict of interest.

Publisher's Note: All claims expressed in this article are solely those of the authors and do not necessarily represent those of their affiliated organizations, or those of the publisher, the editors and the reviewers. Any product that may be evaluated in this article, or claim that may be made by its manufacturer, is not guaranteed or endorsed by the publisher.

frontiers in Aging Neuroscience

ORIGINAL RESEARCH
published: 10 February 2022
doi: 10.3389/fnagi.2022.830494

Is Immune Suppression Involved in the Ischemic Stroke? A Study Based on Computational Biology

*Xin Wang[1], Qian Wang[2], Kun Wang[2], Qingbin Ni[2], Hu Li[3], Zhiqiang Su[1] and Yuzhen Xu[3]**

[1] Department of Neurology, First Affiliated Hospital of Harbin Medical University, Harbin, China, [2] Postdoctoral Workstation, Taian City Central Hospital, Taian, China, [3] Department of Rehabilitation, The Second Affiliated Hospital of Shandong First Medical University, Taian, China

Objective: To identify the genetic mechanisms of immunosuppression-related genes implicated in ischemic stroke.

Background: A better understanding of immune-related genes (IGs) involved in the pathophysiology of ischemic stroke may help identify drug targets beneficial for immunomodulatory approaches and reducing stroke-induced immunosuppression complications.

Methods: Two datasets related to ischemic stroke were downloaded from the GEO database. Immunosuppression-associated genes were obtained from three databases (i.e., DisGeNET, HisgAtlas, and Drugbank). The CIBERSORT algorithm was used to calculate the mean proportions of 22 immune-infiltrating cells in the stroke samples. Differential gene expression analysis was performed to identify the differentially expressed genes (DEGs) involved in stroke. Immunosuppression-related crosstalk genes were identified as the overlapping genes between ischemic stroke-DEGs and IGs. Feature selection was performed using the Boruta algorithm and a classifier model was constructed to evaluate the prediction accuracy of the obtained immunosuppression-related crosstalk genes. Functional enrichment analysis, gene-transcriptional factor and gene-drug interaction networks were constructed.

Results: Twenty two immune cell subsets were identified in stroke, where resting CD4 T memory cells were significantly downregulated while M0 macrophages were significantly upregulated. By overlapping the 54 crosstalk genes obtained by feature selection with ischemic stroke-related genes obtained from the DisGenet database, 17 potentially most valuable immunosuppression-related crosstalk genes were obtained, ARG1, CD36, FCN1, GRN, IL7R, JAK2, MAFB, MMP9, PTEN, STAT3, STAT5A, THBS1, TLR2, TLR4, TLR7, TNFSF10, and VASP. Regulatory transcriptional factors targeting key immunosuppression-related crosstalk genes in stroke included STAT3, SPI1, CEPBD, SP1, TP53, NFIL3, STAT1, HIF1A, and JUN. In addition, signaling pathways enriched by the crosstalk genes, including PD-L1 expression and PD-1 checkpoint pathway,

OPEN ACCESS

Edited by:
Min Tang,
Jiangsu University, China

Reviewed by:
Zeman Qin,
Sun Yat-sen Memorial Hospital, China
Rui Sun,
Chinese Academy of Medical Sciences and Peking Union Medical College, China

****Correspondence:***
Yuzhen Xu
tianyayizhe@126.com

Specialty section:
This article was submitted to Neuroinflammation and Neuropathy, a section of the journal Frontiers in Aging Neuroscience

Received: *07 December 2021*
Accepted: *20 January 2022*
Published: *10 February 2022*

Citation:
Wang X, Wang Q, Wang K, Ni Q, Li H, Su Z and Xu Y (2022) Is Immune Suppression Involved in the Ischemic Stroke? A Study Based on Computational Biology. Front. Aging Neurosci. 14:830494. doi: 10.3389/fnagi.2022.830494

NF-kappa B signaling, IL-17 signaling, TNF signaling, and NOD-like receptor signaling, were also identified.

Conclusion: Putative crosstalk genes that link immunosuppression and ischemic stroke were identified using bioinformatics analysis and machine learning approaches. These may be regarded as potential therapeutic targets for ischemic stroke.

Keywords: immunosuppression, ischemic stroke, genes, transcription factors, bioinformatics

INTRODUCTION

Ischemic stroke is the second most common cause of mortality worldwide and imposes a tremendous healthcare burden owing to significant disability. Aging populations are likely to further compound the gravity of the burden imposed by stroke (Katan and Luft, 2018). The prevention and clinical management of stroke assume critical importance. As currently widely applied modalities are limited in their clinical efficacy, a need for the advent of novel approaches is recognized. Molecular mechanisms involved in the pathophysiology of stroke resulting from cerebral ischemia and consequent brain tissue damage, involve immune activation, which leads to a host of both neuroprotective and neuro-toxic effects (Iadecola and Anrather, 2011; Iadecola et al., 2020). Further, stroke is frequently followed by post-stroke infection, which results from systemic immunosuppression that occurs after stroke and is associated with a worse prognosis (Shi et al., 2018). This occurs as a bi-directional brain-immune system interaction, when catecholamines and glucocorticoids are produced by an activated HPA-axis in attempts to limit local inflammation, which leads to natural killer T-cell (NKT) and T-cell activation, alongside reactive oxygen species production (Shim and Wong, 2016). Immune-modulatory approaches involving T-cell transfer, natural killer T-cell (NKT) activators and interferon-gamma (IFN-γ) have shown benefit in reducing post-stroke immunosuppression (Wong et al., 2011; Liu et al., 2017). Immunomodulatory approaches that target multiple elements of the immune system are now recognized as the most promising directions in stroke and its complication management (Fu et al., 2015). Several established drugs such as Azithromycin and Metformin have shown neuroprotective action in stroke via modulation of innate immune responses (Amantea and Giacinto, 2016) and the repurposing of such drugs may offer therapeutic potential, thus underscoring the importance of uncovering immunosuppression mechanisms in stroke.

However, at present, the immune mechanisms implicated in stroke and stroke-associated systemic immunosuppression are still poorly understood. A comprehensive understanding of the immune mechanisms relevant to stroke has the potential to identify target genes and functional pathways, which can direct therapeutic interventions including drug development and repurposing. Integrated bioinformatics analysis of gene expression or transcriptomic datasets associated with disease can leverage higher scales of data to generate valuable insights. Gene expression data can also enable *in silico* identification of heterogeneous cell populations within a sample, including immune activate cell subsets (Newman et al., 2015). Furthermore, the application of machine learning-based feature selection algorithms can highlight potentially the most important genes linked to a disease or condition (Kursa, 2014). Therefore, in the current study, we aimed to utilize bioinformatics tools combined with feature selection to perform comprehensive secondary analysis of multiple transcriptomic datasets in stroke to reveal key immunosuppression related genes implicated in its pathogenesis. This approach could help highlight genes and pathways of high value for clinical and therapeutic translation for managing stroke and related immunosuppression.

MATERIALS AND METHODS

Gene Expression Datasets in Stroke and Immunosuppression-Related Gene Data

Two gene-expression microarray datasets pertaining to ischemic stroke were identified and downloaded from the NCBI Gene Expression Omnibus (GEO) database,[1] GSE16561 and GSE22255. GSE16561 included peripheral blood samples from 39 stroke patients and 24 controls in a total of 63 samples analyzed using the "Illumina HumanRef-8 v3.0 Expression BeadChip" array (Barr et al., 2010) and GSE22255 included peripheral blood mononuclear cells from 20 stroke patients and 20 controls in a total of 40 samples analyzed using the "Affymetrix Human Genome U133 Plus 2.0" array (Krug et al., 2012).

Next, immunosuppression-related genes were downloaded from DisGenet[2] and HisgAtlas.[3] In addition, drugs related to immunosuppressive agents were sourced from Drugbank.[4] Here, 311 immunosuppressive drugs were identified and the relevant immunosuppressive related genes were downloaded. The immunosuppression-related genes obtained from these three databases (DisGeNET, HisgAtlas, and Drugbank) were merged to obtain a total of 1,332 genes, and the expression profiles of these specific immunosuppression-related genes in the GSE16561 and GSE22255 datasets were extracted.

[1]http://www.ncbi.nlm.nih.gov/geo

[2]http://www.disgenet.org

[3]http://biokb.ncpsb.org.cn/HisgAtlas/

[4]https://www.drugbank.ca/

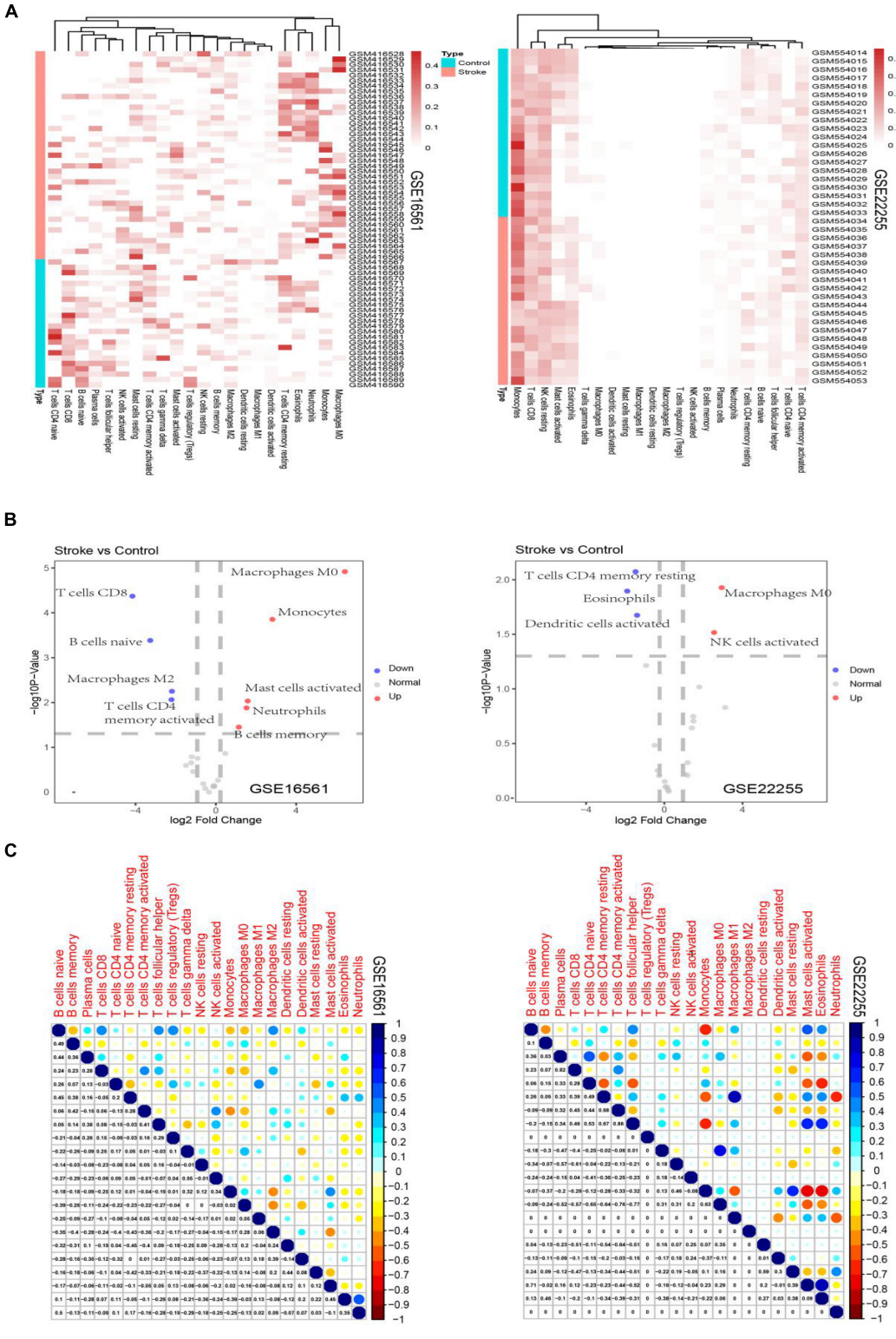

FIGURE 1 | Heatmaps depicting the proportion of immune cell subtypes in the GSE16561 and the GSE22255 datasets **(A)**. Volcano plots depict the log2fold change of significantly up-regulated and down-regulated cellular subsets in the GSE16561 and the GSE22255 datasets **(B)**. Correlogram plots depicting the correlations between immune cell subtypes **(C)**.

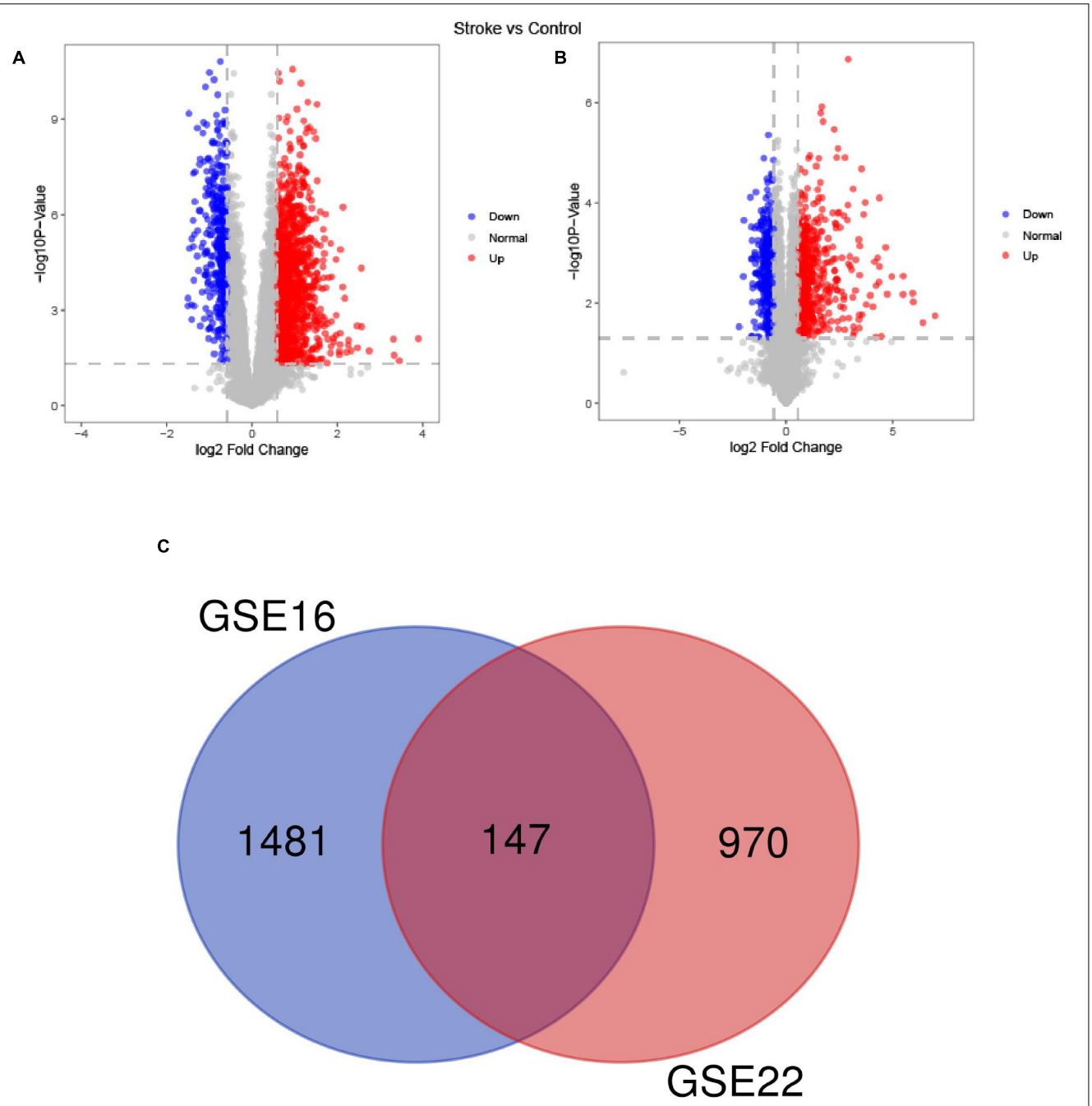

FIGURE 2 | A Venn diagram of the up- and down-regulated DEGs in the GSE16561 **(A)** and GSE22255 **(B)** datasets and the Venn diagram depicts DEGs shared by the GSE16561 and GSE22255 series of samples **(C)**.

Analysis of Immune-Cell Subsets Enriched in Stroke

The expression levels of immunosuppression-related genes in stroke were normalized and the "CIBERSORT" deconvolution algorithm (Newman et al., 2019) in the R statistical environment was applied to predict the infiltrating immune cell subsets that are highly related to stroke. The expression matrix of immunosuppression-related genes in stoke was used as the input, with 1,000 permutations and quantile normalization. A heatmap was then constructed to display immune cell subsets in each sample.

Differential Gene Expression Analysis and Functional Enrichment Analysis

The downloaded GSE16561 and GSE22255 gene expression datasets were subjected to preprocessing and filtration.

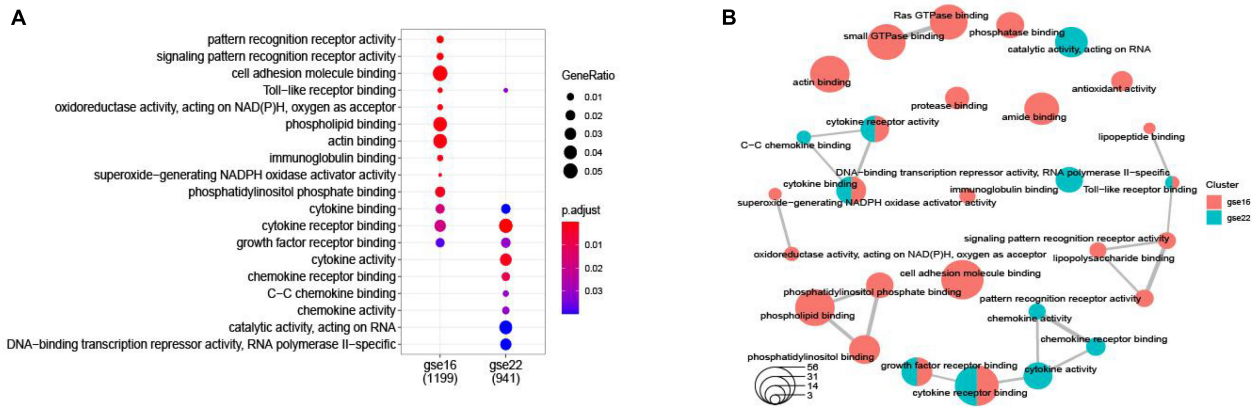

FIGURE 3 | A dotplot of the GO function enrichment nodes of DEGs in the GSE16561 and GSE22255 datasets **(A)**; an emapplot of the GO function enrichment nodes in GSE16561 and GSE22255 datasets **(B)**.

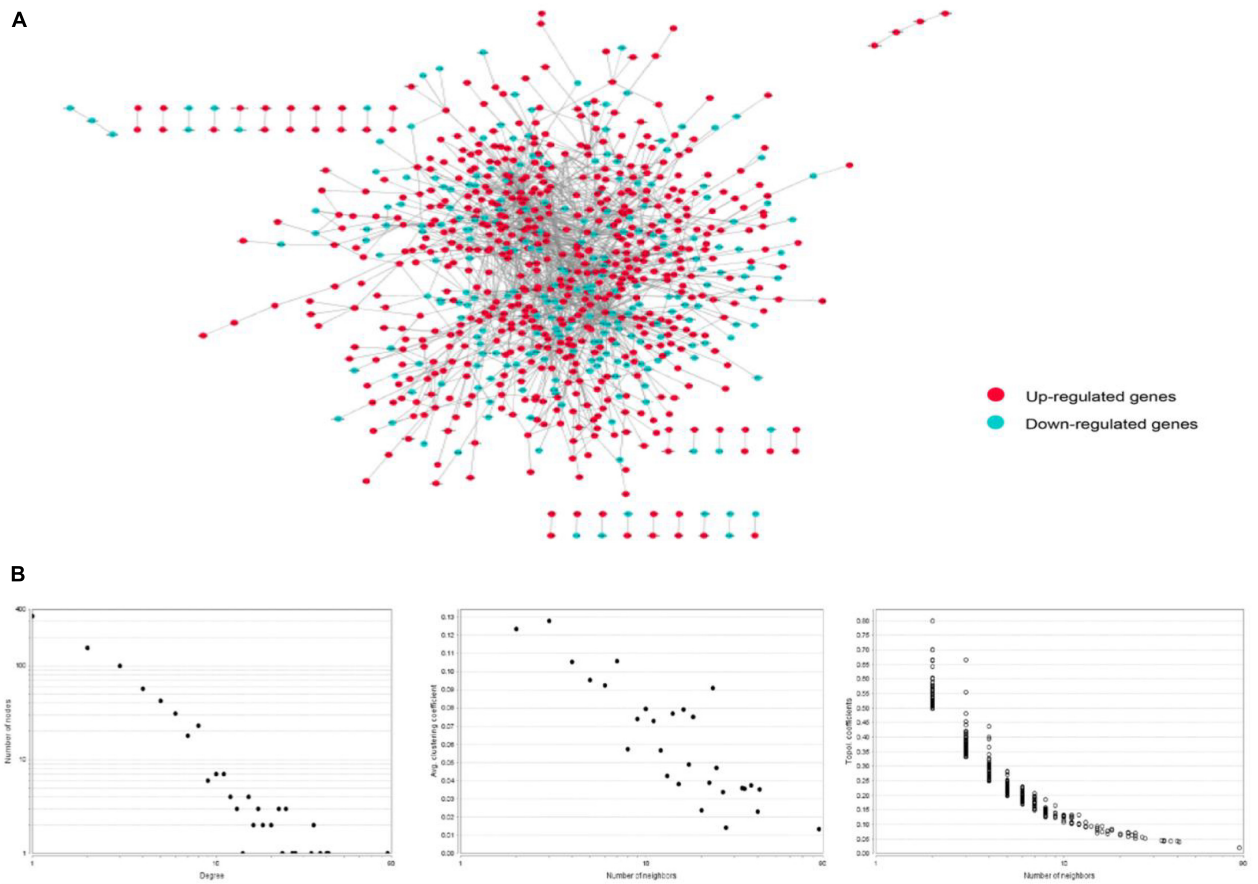

FIGURE 4 | (A) The protein-protein interaction network consisted by integrating the differentially expressed genes in two datasets. There are 1,460 relational pairs and 821 nodes in the network. **(B)** The various statistical indicators in the PPI network shown in **(A)**.

Differential gene expression was performed using the R package "limma" with a P-value < 0.05 and logFC change > 0.58 set as thresholds to determine differentially expressed genes (DEGs) and volcano plots were plotted to display the results. Gene ontology (GO) functional profiles of the significant differentially expressed genes from these two data sets were clustered based on similarity using the "compareCluster_go" function of the "clusterProfiler" R package (Yu et al., 2012).

TABLE 1 | Top 30 ranked genes in the PPI network of integrated DEGs.

Symbol	Degree	Average Shortest Path Length	Betweenness Centrality	Closeness Centrality	Clustering Coefficient	Topological Coefficient
GRB2	86	2.76315789	0.24334414	0.36190476	0.01340629	0.02064727
MAPK1	41	2.86973684	0.10984015	0.34846401	0.03536585	0.03951394
TP53	40	3.05921053	0.07761154	0.32688172	0.02307692	0.04166667
FYN	37	2.95263158	0.08285592	0.33868093	0.03753754	0.0418483
PXN	34	2.88552632	0.10707404	0.34655723	0.04278075	0.04506822
CREBBP	34	3.25	0.06912861	0.30769231	0.0285205	0.04338757
CASP3	33	3.02105263	0.09005441	0.33101045	0.03598485	0.04453627
YWHAG	27	3.30921053	0.04671586	0.30218688	0.01424501	0.05149051
SMAD3	26	3.19736842	0.06550871	0.3127572	0.03384615	0.05560704
LYN	24	3.18552632	0.03191512	0.31391987	0.05072464	0.06045279
JUN	24	3.23157895	0.03011403	0.30944625	0.0615942	0.06934932
MAPK14	24	3.11184211	0.0477154	0.32135307	0.02898551	0.05197368
SP1	23	2.91710526	0.0673405	0.34280559	0.09090909	0.06418972
MAPK3	22	3.14473684	0.02389596	0.31799163	0.06060606	0.07029309
STAT3	22	3.26315789	0.03607932	0.30645161	0.03896104	0.07188161
YWHAH	22	3.375	0.03049526	0.2962963	0.01731602	0.05947324
PIK3R1	20	3.39605263	0.03433461	0.29445951	0.01578947	0.069
HSP90AB1	20	3.11184211	0.04933295	0.32135307	0.03157895	0.0642132
HSPA8	18	3.02368421	0.05323372	0.33072237	0.08496732	0.0790687
PRKCD	18	3.28289474	0.02483384	0.30460922	0.06535948	0.08389262
STAT1	17	3.28947368	0.04105675	0.304	0.01470588	0.0681606
PRKDC	17	3.09210526	0.0327038	0.32340426	0.08088235	0.07782405
HSPA1A	17	3.36710526	0.03019882	0.29699101	0.05147059	0.07769145
VCL	16	3.48157895	0.02689397	0.287226	0.03333333	0.07515823
PAK2	16	3.14342105	0.02459102	0.31812474	0.125	0.09440104
TNFRSF1A	15	3.47368421	0.02722882	0.28787879	0.11428571	0.09318996
SNCA	15	3.40263158	0.03034559	0.29389018	0.02857143	0.08539945
CDC42	15	3.53289474	0.02840219	0.283054	0.00952381	0.07843137
LRIF1	15	3.81842105	0.02597249	0.26188835	0	0.07083333
VIM	14	3.30526316	0.02247123	0.30254777	0.07692308	0.09307359

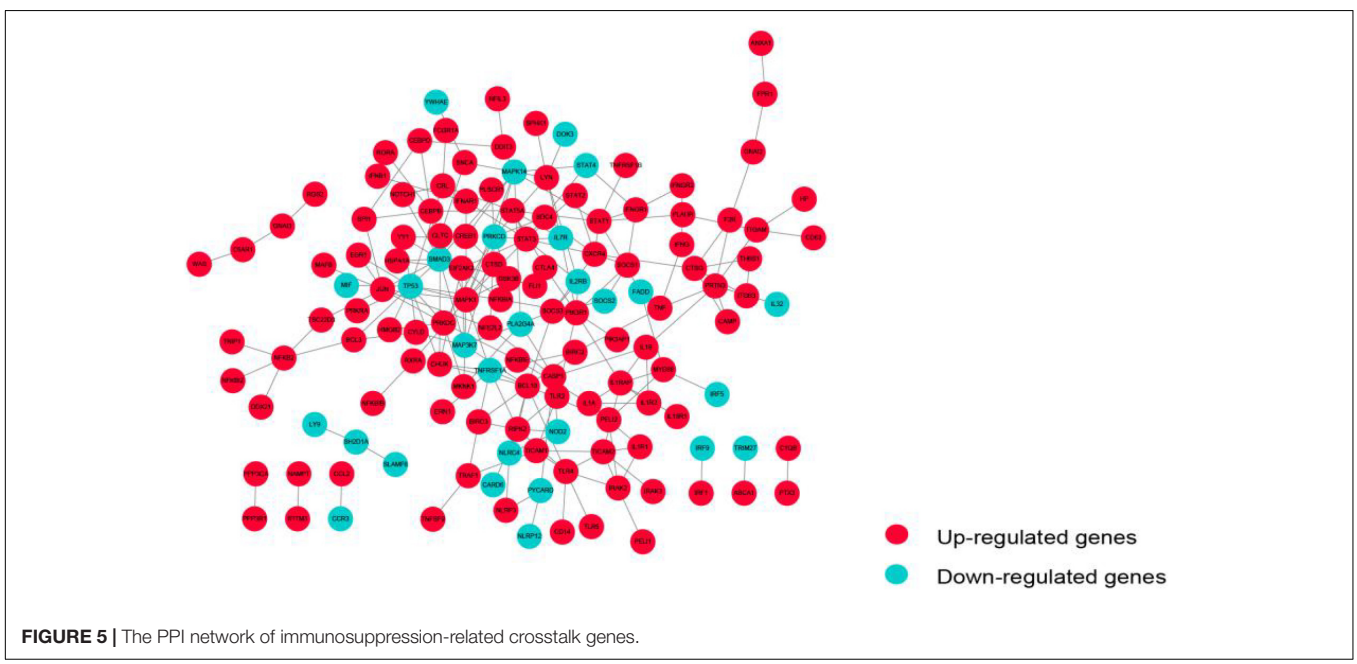

FIGURE 5 | The PPI network of immunosuppression-related crosstalk genes.

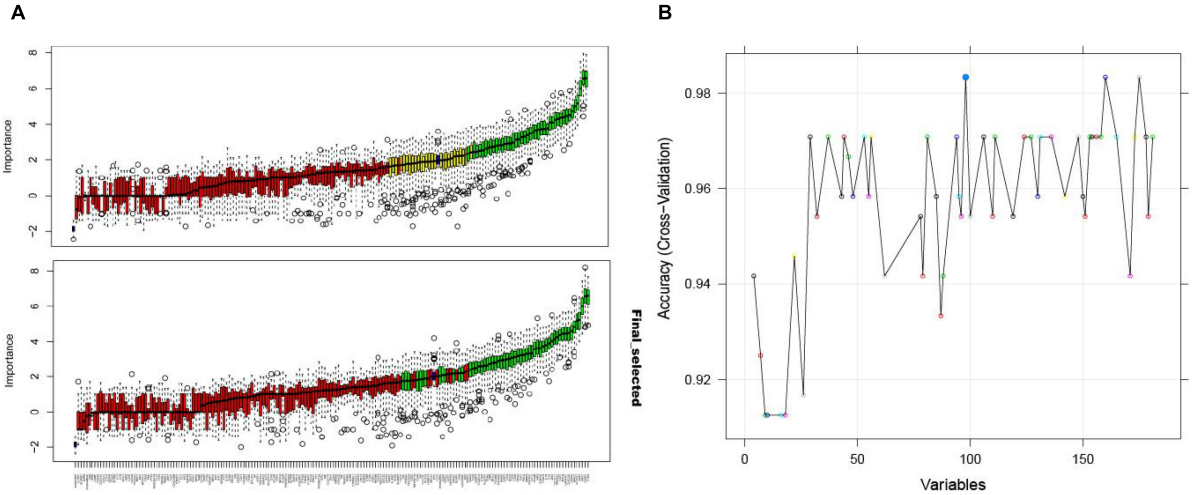

FIGURE 6 | The Boruta algorithm feature selection results of the GSE16561 dataset showing the results before and after the "TentativeRoughFix" function to remove undetermined features **(A)**; accuracy score of the number of feature selections using the RFE algorithm for the GSE16561 dataset **(B)**.

Among these, pathways with P-value < 0.05 were considered as significantly enriched.

Protein-Protein Interaction Network

Protein-protein interaction (PPI) data was downloaded from multiple databases including PBIND (currently offline), BioGRID),[5] MINT,[6] HPRD,[7] IntAct[8] and OPHID[9] and were integrated and the PPI relationship pairs of the immunosuppression-related DEGs were extracted from the integrated PPI data. A PPI network was constructed using Cytoscape and topological properties were analyzed using the "networkanalyzer" tool (Gustavsen et al., 2019). Gene nodes with the highest degree (indicating network connectivity) were considered to be of high functional importance in stroke and the top 30 genes were thus annotated as important stroke-related genes.

Identification of Immunosuppression-Related Crosstalk Genes and Protein-Protein Interaction Network

Immunosuppression-related genes were downloaded from the InnateDB[10] database and intersecting DEGs in the GSE16561 and GSE22255 datasets were identified among these, merged with the earlier identified immunosuppression-related DEGs, and labeled as immunosuppression-related crosstalk genes. PPI relationship pairs for these genes were extracted and a crosstalk gene PPI network was constructed using Cytoscape.

[5]http://thebiogrid.org/

[6]https://mint.bio.uniroma2.it/

[7]http://www.hprd.org/

[8]https://www.ebi.ac.uk/intact/

[9]http://ophid.utoronto.ca/ophidv2.204/

[10]https://www.innatedb.ca/

Feature Selection of Most Important Immunosuppression-Related Crosstalk Genes

The immunosuppression-related crosstalk genes were considered as stroke-related features and the Boruta algorithm was applied using the R package "Boruta" (Kursa and Rudnicki, 2010) to select the most representative features. Boruta algorithm is a supervised classification feature selection method that is based on random forest and identifies all relevant features for classification task. The central concept in this algorithm is the iterative comparison of the actual predictor variables to generated shadow variables using random forest, thus sequentially identifying the variables relevant to classification. In the first step, the gene expression profiles of these crosstalk genes in the GSE16561 dataset were extracted. In the second step, the Boruta algorithm was applied to group features based on the category of each sample, with a p-value < 0.01 and the default maximum run at 100 times. The outcome grouped the crosstalk gene features into three categories: tentative temporary/pending features (not enough to accept or reject), confirmed features, and rejected features. For the tentative features, the "TentativeRoughFix" function was applied. Assuming that the Boruta algorithm might have preference errors, a traditional recursive feature elimination algorithm (RFE) was also applied to perform feature screening on the extracted immune gene expression values and the outcomes were compared.

Classifier Models Based on Crosstalk Immunosuppression-Related Crosstalk Genes

First of all, considering that the expression values in the GSE16561 and GSE22255 data sets were of different magnitudes and the GSE16561 data was normalized but GSE22255 was not, the GSE22255 data was normalized so that the two datasets

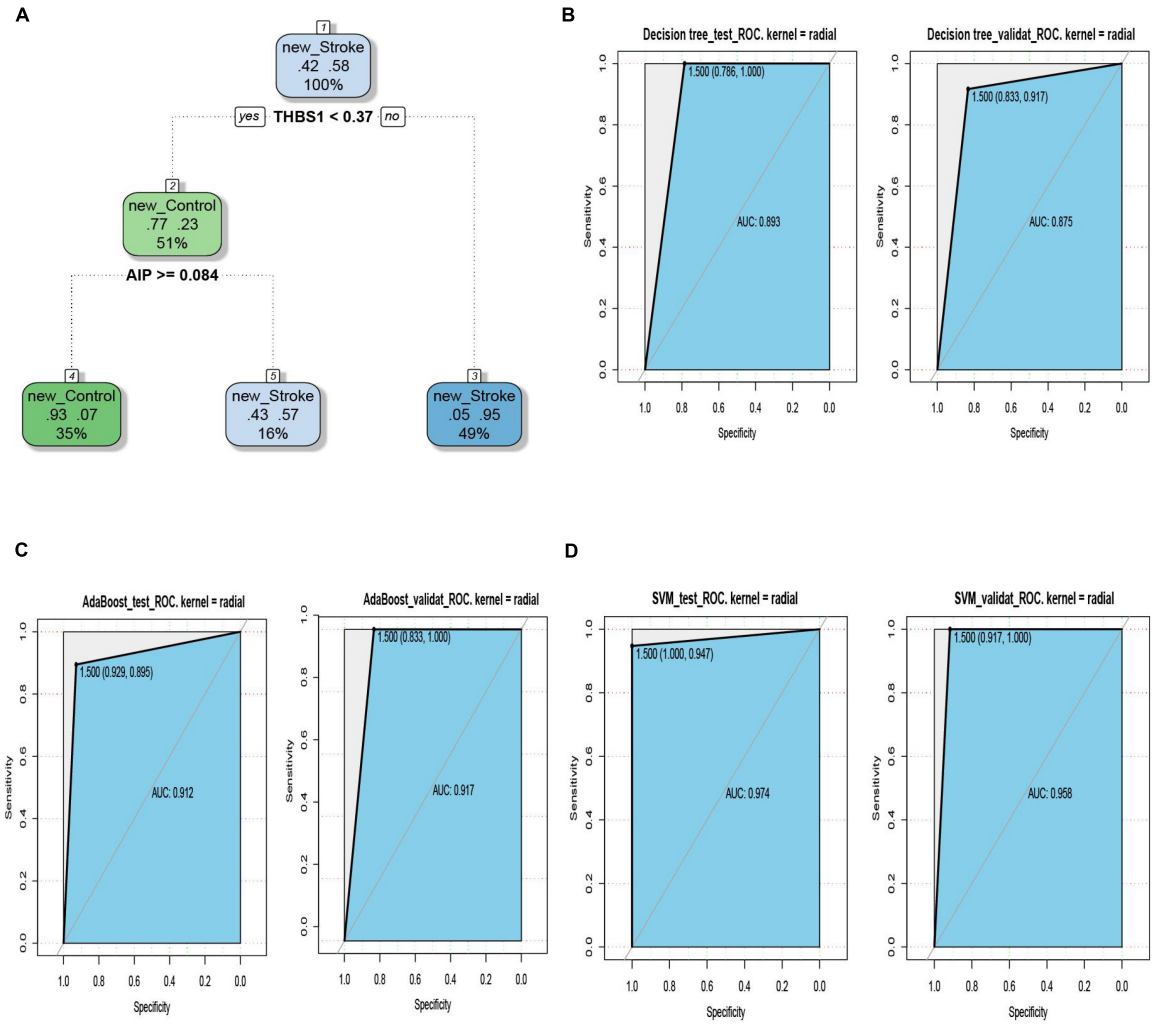

FIGURE 7 | The decision tree diagram of the classifier model **(A)**. ROC curves of the test and validation sets of three classifiers; Decision tree **(B)**, AdaBoost **(C)** and SVM **(D)**.

were consistent. Next, the crosstalk genes obtained using the Boruta algorithm were verified using the two standardized data sets, and the "k nearest neighbor" method was applied to fill in missing (NA) values. The Decision tree, AdaBoost, and SVM algorithms were used to build classifier models. Here, randomly selected samples from the GSE16561 and GSE22255 datasets were used as a training set. Randomly selected 70% samples from the GSE16561 series were set as a test set and the crosstalk gene expression data from the GSE22255 data set was used as the verification set. To predict the accuracy of the classifier models, the test set data was input into the trained classifier for verification, and the receiver operating curves (ROC) curves of the prediction results were plotted using the "pROC" R package. Next, 1,159 genes related to ischemic stroke were downloaded from the "DisGenet" database. The crosstalk immunosuppression-related genes obtained were intersected with these to identify the potentially most valuable classifier genes and the accuracy of the selected genes was examined.

Pathway Analysis of the Immunosuppression-Related Crosstalk Genes

The crosstalk genes were subjected to KEGG pathway analysis and the top 30 enriched pathways were represented as key pathways of interest.

Crosstalk Gene-Transcription Factor Network Analysis

Transcription factors (TF) and target gene pairs were downloaded from the TRRUST[11] and ORTI[12] databases and the data were pooled. The TF-target gene relationship pairs of the crosstalk genes were extracted the TF-crosstalk gene network was plotted in Cytoscape. The topological properties of the top

[11]https://www.grnpedia.org/trrust/

[12]http://orti.sydney.edu.au/about.html

10 genes ranked by outdegree were analyzed to gain insights into the transcriptional regulation of immunosuppression-related genes in stroke pathogenesis.

Biological Pathways Analysis Enriched by the Transcription Regulatory Crosstalk Genes

The TF-target gene relationship pairs were extracted from the transcriptional regulatory network, and these genes were divided into two gene sets, genes that were up-regulated and those that were down-regulated. The "enrichGO()" function of the "clusterprofiler" R package was applied to separately analyze biological pathways enriched in these two gene sets, with a p-value < 0.05. The top 30 enriched biological pathways were reported as those being most significant pathways.

Crosstalk Gene- Drug Target Network Analysis

To identify drugs that may be potentially relevant to stroke by immune modulation, gene-drug interaction pair data was downloaded from the DIGDB database.[13] Drugs related to the most significant crosstalk genes identified earlier to construct a gene-drug network.

RESULTS

Immune-Cell Subsets Enriched in Stroke

The derived cellular component subsets in the samples are displayed as heatmaps and volcano plots (**Figure 1**) and significant differences were noted in the immune cell components between the stroke and normal samples. As samples were not labeled correctly, filtering was applied. Thereafter, GSE16561 retained 48 samples while GSE22255 retained 24 samples. Two subtypes of immune cells, resting CD4 memory T cells and M0 Macrophages were significantly different between the cases and controls. CD4 memory T cells were significantly down-regulated in stroke whereas M0 Macrophages were noted as significantly up-regulated.

Differentially Expressed Genes and Functional Enrichment Analysis

Among the DEGs determined in the two datasets, 147 DEGs were shared (**Figure 2**). The top 10 most highly significantly enriched pathways are depicted in **Figure 3**. Nodes representing regulatory pathways that control cell growth and division were found overlapping amongst the results from the two datasets. Other sets of functional pathways enriched in the DEGs varied between the two datasets, plausibly owing to sample heterogeneity.

Protein-Protein Interaction Network in Stroke

The PPI network of integrated DEGs of the two datasets is represented in **Figure 4**. The network consisted of 1,460 PPI pairs and 821 nodes. The gene nodes with topmost degree ranks in the PPI network included GRB2, MAPK1, TP53, FYN, PXN and **Table 1** presents the top 10 gene nodes in the network.

Immunosuppression-Related Crosstalk Genes

The PPI network of these immunosuppression-related crosstalk genes comprising of 213 PPI pairs and 140 nodes is depicted in **Figure 5**. There are 213 international pairs and 140 nodes in the network.

Feature Selection From Immunosuppression-Related Crosstalk Genes

Using the Boruta algorithm, 54 immune-related crosstalk gene features were selected as representative features (**Figure 6A**). 98 feature genes were selected by the RFE algorithm (**Figure 6B**), which included all 54 genes selected using the Boruta algorithm, validating its good performance.

Classifier Models Based on Immunosuppression-Related Crosstalk Genes

The ROC curves pertaining to the dataset used to evaluate the classifier models are represented in **Figure 7**. The SVM classifier showed the best performance. The AUC values for the test set and validation set were 0.974 and 0.958, respectively, indicating the excellent performance of the classifier model to predict stroke patients and normal samples (**Table 2**). Among the 54 crosstalk immune-related genes, 17 genes were noted in the DisGenet database including, "ARG1" "CD36" "FCN1" "GRN" "IL7R" " JAK2" "MAFB" "MMP9" "PTEN" "STAT3" "STAT5A" "THBS1" "TLR2" "TLR4" "TLR7" "TNFSF10" "VASP."

Among the 54 crosstalk immune-related genes, 17 genes were noted in the DisGenet database including, "ARG1" "CD36" "FCN1" "GRN" "IL7R" " JAK2" "MAFB" "MMP9" "PTEN" "STAT3" "STAT5A" "THBS1" "TLR2" "TLR4" "TLR7" "TNFSF10" "VASP." Another classifier model was constructed using these 17 genes and the ROC curves were plotted (**Figure 8**).

Pathway Analysis of the Immunosuppression-Related Crosstalk Genes

The top 30 KEGG pathways enriched in the immune-related crosstalk genes are represented in a barplot and dotplot (**Figure 9**). NOD-like receptor signaling pathway showed the highest significance and gene ratio values. TNF-signaling, Measles, Tuberculosis, C-type leptin receptor signaling

TABLE 2 | Test results of 3 classifiers.

Number	Dataset	Decision tree	AdaBoost	SVM
1	Test set	0.893	0.912	0.974
2	validation set	0.875	0.917	0.958

[13]http://www.dgidb.org/search_interactions

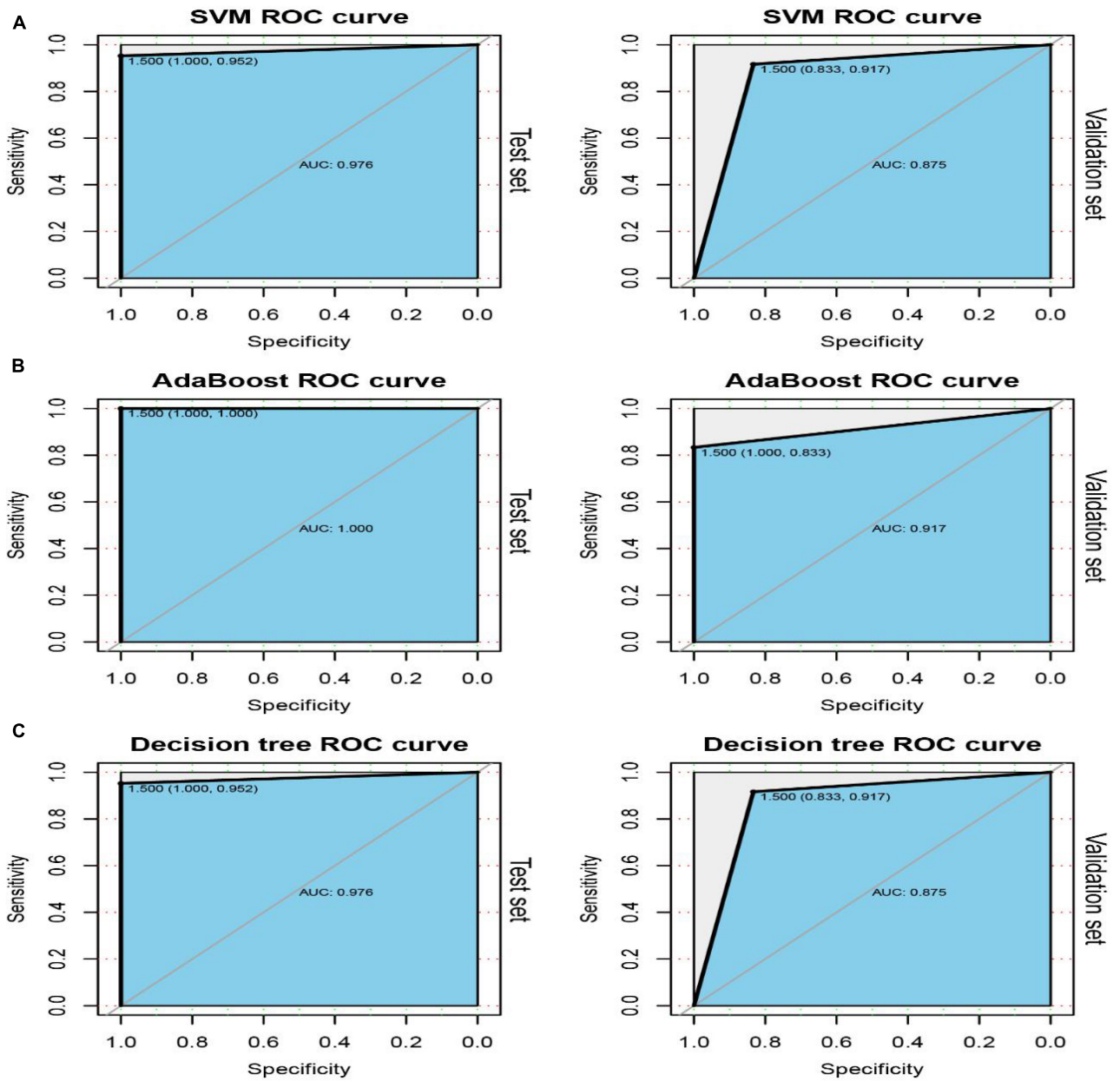

FIGURE 8 | ROC curves of the test and validation sets of three classifiers: SVM **(A)**, AdaBoost **(B)** and Decision tree **(C)**.

and osteoclast differentiation were among the topmost enriched pathways.

Immunosuppression-Related Crosstalk Gene-Transcription Factor Network Analysis

The TF-target gene network consisted of 146 nodes and 208 TF-target gene pairs (**Figure 10**). The topological properties of top 10 genes in the network ranked by outdegree is presented in **Table 3**. STAT3, SPI1, CEBPD, STAT5A, and SP1 were ranked the highest in this network.

Biological Pathways Analysis Enriched by the Transcription Regulatory Immunosuppression-Related Crosstalk Genes

The up-regulated crosstalk immunosuppression-related genes were mainly enriched in biological pathways related to cell growth and proliferation, and energy metabolism, while the down-regulated genes were mainly enriched in positive cell apoptosis. The biological pathways related to cell differentiation and migration indicated that up- and down-regulated genes function together to promote the occurrence and development

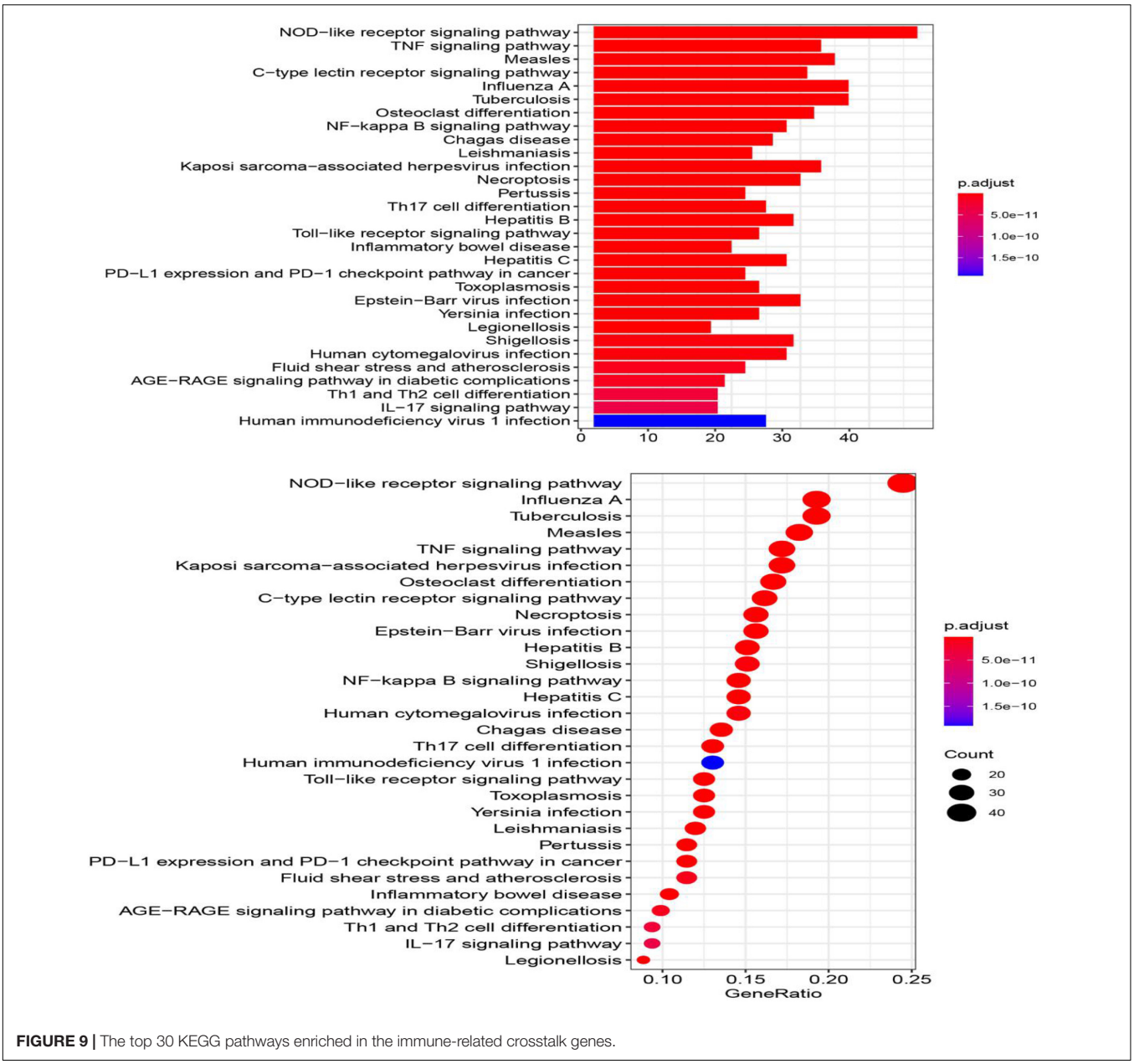

FIGURE 9 | The top 30 KEGG pathways enriched in the immune-related crosstalk genes.

of stroke (**Figure 11A**). Expression levels of 10 key genes screened in the transcriptional regulatory network showed that the STAT3 gene and HIF1A gene showed similar transcriptional regulatory relationship in both the datasets, whereas TP53 as a transcription factor and its target gene JUN did not consistency in the expression pattern (**Figure 11B**) suggesting immune type heterogeneity in stroke.

Drugs Targeted by Immunosuppression-Related Crosstalk Genes

Drugs related to the 17 immunosuppression-related cross talk genes were screened and 11 genes were found to have target drugs. A gene-drug network is presented in **Figure 12**. The maximum numbers of drug targets were noted for the PTEN gene, followed by the JAK2 gene.

DISCUSSION

The current study provides insights into the immune landscape of stroke via a comprehensive bioinformatic analysis of key immunosuppression-related genes underpinning the pathogenesis of stroke. Using a machine learning approach, a small number of 17 potentially most relevant immunosuppression-related crosstalk gene features were identified, which showed high performance accuracy in

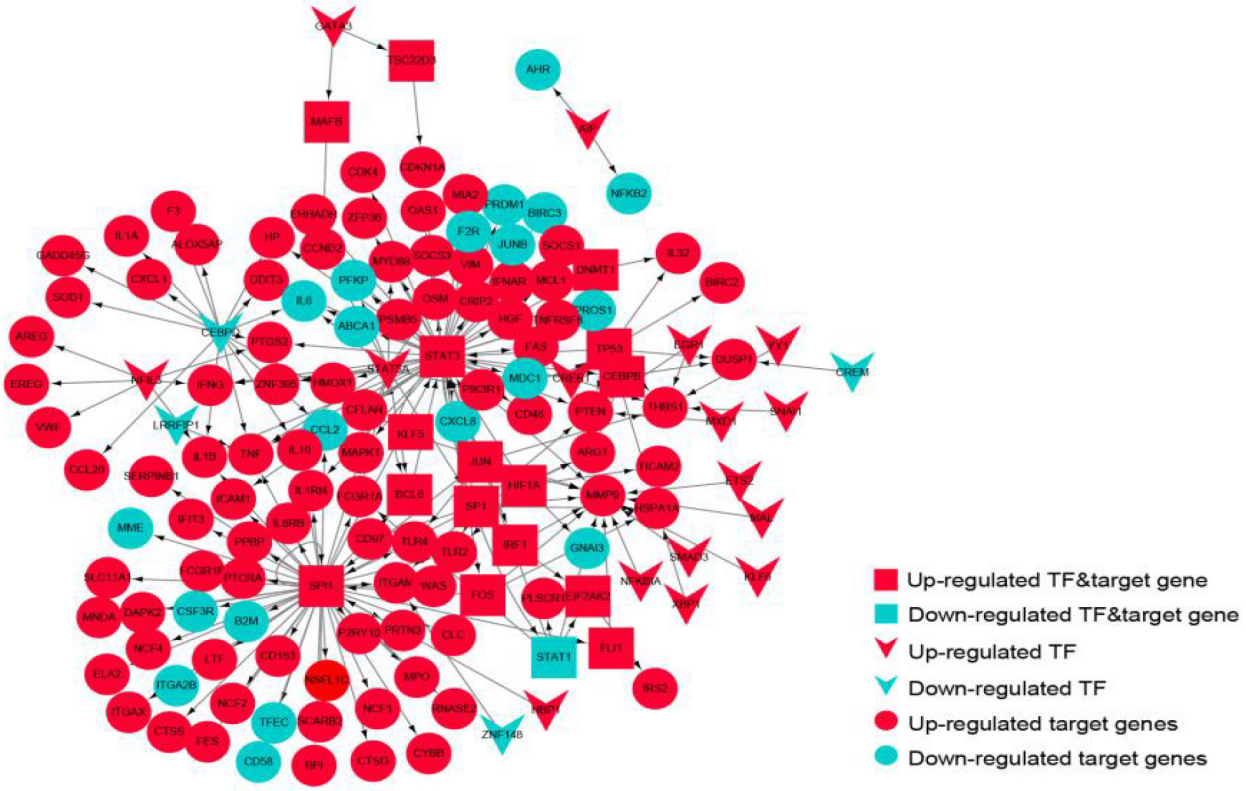

FIGURE 10 | The transcriptional regulatory network of the crosstalk genes. Red represents up-regulated genes, blue represents down-regulated genes, circles represent target genes, arrows represent transcription factors, and rectangles represent targets.

TABLE 3 | Top 10 ranked genes in the transcription factor-crosstalk gene regulatory network.

SYMBOL	Outdegree	Average Shortest Path Length	Betweenness Centrality	Closeness Centrality	Clustering Coefficient	Expression_type
STAT3	56	1.83333333	0.04281957	0.54545455	0.00526008	*Up*
SPI1	50	1.65740741	0.0308494	0.60335196	0.00580552	*Up*
CEBPD	16	1.05882353	0	0.94444444	0	*Down*
STAT5A	13	2.76576577	0	0.36156352	0	*Up*
SP1	10	2	0.00361269	0.5	0.05454545	*Up*
TP53	7	2.72222222	0.00152332	0.36734694	0.02380952	*Up*
NFIL3	6	1	0	1	0	*Up*
STAT1	5	2.74074074	0.00134852	0.36486486	0.05	*Down*
HIF1A	5	2.75	0.0015483	0.36363636	0	*Up*
JUN	4	2.58333333	0.00621816	0.38709677	0.15	*Up*

classifying stroke from healthy samples suggesting their potential value in molecular diagnosis and as biological targets.

The initial findings showed that CD4 memory T cells were significantly downregulated while M0 Macrophages were upregulated in stroke. CD4 T cell infiltration has been implicated in stroke-associated neuroinflammation (Yilmaz et al., 2006; Gu et al., 2013) and CD4 cell deficit has shown beneficial effects by reducing infarction. The seemingly contrasting finding from our study may be accounted for by the temporal sequence of T cell infiltration in ischemic stroke, whereby animal models of stroke have shown that the peak of T cell infiltration appears after 3–5 days in transient ischemia, while other report CD4 T cells showed a rise beginning from 7 to 30 days after stroke (Gelderblom et al., 2009; Shichita et al., 2009; Stubbe et al., 2012). The samples used in the present study included blood collected within 24 h of symptom onset (Barr et al., 2010) and whereas the exact duration was not specified in one dataset (Krug et al., 2012), therefore, the temporal variation in immune cell infiltration could not be assessed. Macrophages and microglia play key roles in mediating tissue injury during the acute phase of ischemic stroke (Mabuchi et al., 2000; Hu et al., 2012). Infiltration of blood monocytes through a breached blood-brain

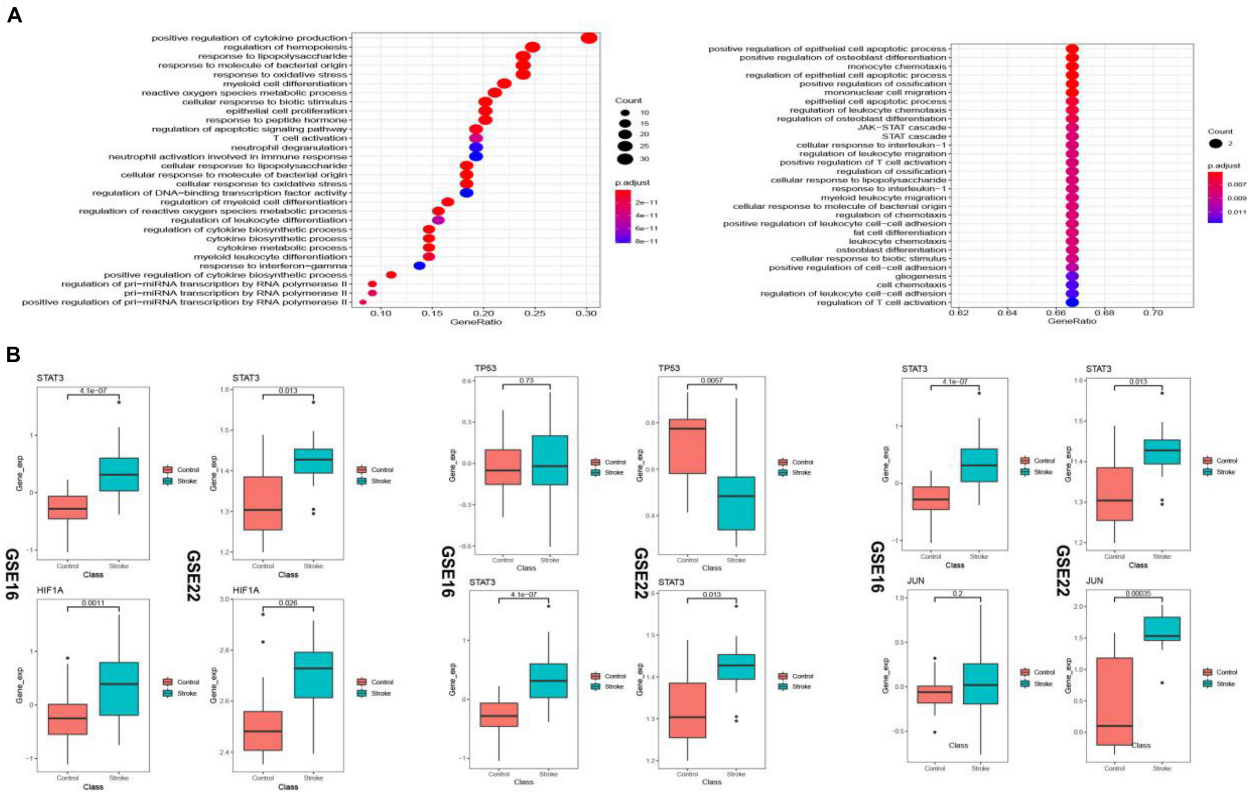

FIGURE 11 | Biological pathways (BP) enriched in the up- and down-regulated transcriptional regulatory immunosuppression-related crosstalk genes **(A)**. Expression levels of key transcription factors and corresponding target crosstalk genes in the stroke and control samples in the two datasets **(B)**.

barrier is an important early event in the neuroinflammation of post-stroke brain tissue (Mo et al., 2013). C-C chemokine receptor 2 (CCR2) + Mo/MΦ have been found to spread through the brain tissue in the early phase of stroke and have been implicated in both early stage inflammation and later functional recovery (Garcia-Bonilla et al., 2016; Fang et al., 2018; Pedragosa et al., 2020).

The PPI network of DEGs in stroke indicated that the top genes of relevance were GRB2, MAPK1, TP53, FYN, and PXN. The involvement of these genes in stroke pathology is largely supported by experimental data. GRB2 encodes for a protein that binds the epidermal growth factor receptor leading to downstream mitogen-activated protein kinase (MAPK) signaling and is implicated in the development of atherosclerotic lesions (Proctor et al., 2007). GRB2 has been implicated in neuronal autophagy in stroke neuropathology via the suppression of the Akt/mTOR pathway (Luo et al., 2020). p38 mitogen-activated protein kinase (MAPK) signaling is a key mediator of inflammation, being a critical mediator of cell responses to cytokines and MAPK signaling has been widely implicated in the pathogenesis of stroke (Sun and Nan, 2016), although the specific upstream and downstream mechanisms remain unclarified, and different brain tissue types are marked by varying MAPK signaling patterns after ischemic stroke (Sawe et al., 2008). Animal data have shown that inhibition of p38 MAPKα starting in the early period after stroke led to improvement in motor and somatosensory function (Alam et al., 2020), whereas others have reported that MAPK-1 signaling plays an endogenous protective role in stroke and its inhibition accelerated stroke-induced injury via its anti-apoptotic and anti-inflammatory actions (Liu et al., 2014). MAPK inhibitors are emerging as promising anti-inflammatory agents for acute stages of brain inflammation (Kaminska et al., 2009) including cerebrovascular disorders (Ansar et al., 2013).

TP53 polymorphism has been found associated with the prognosis of post-stroke functional recovery (Gomez-Sanchez et al., 2011) and neuroprotection after ischemia (Ramos-Araque et al., 2018). Furthermore, methylation of TP53 promoter has been associated with ischemic stroke (Wei et al., 2019). A recent bioinformatic study investigating ischemic stroke-related targets for the herbal medication *Calculus Bovis* reported MAPK1 and TP53 among the top target genes (Liu et al., 2021).

FYN is a type of Src Family Kinase (SFK) gene, that code for a non-receptor protein tyrosine kinase and SFK inhibitors have shown protective action against ischemic stroke in animals (Takenaga et al., 2009). FYN is shown to interact with NMDAR during the ischemic response (Takagi et al., 1999) and phosphorylation of several proteins, which is implicated in cell death in stroke via reactive oxygen species generation and calcium flux (Knox and Jiang, 2015). In a rabbit, increased

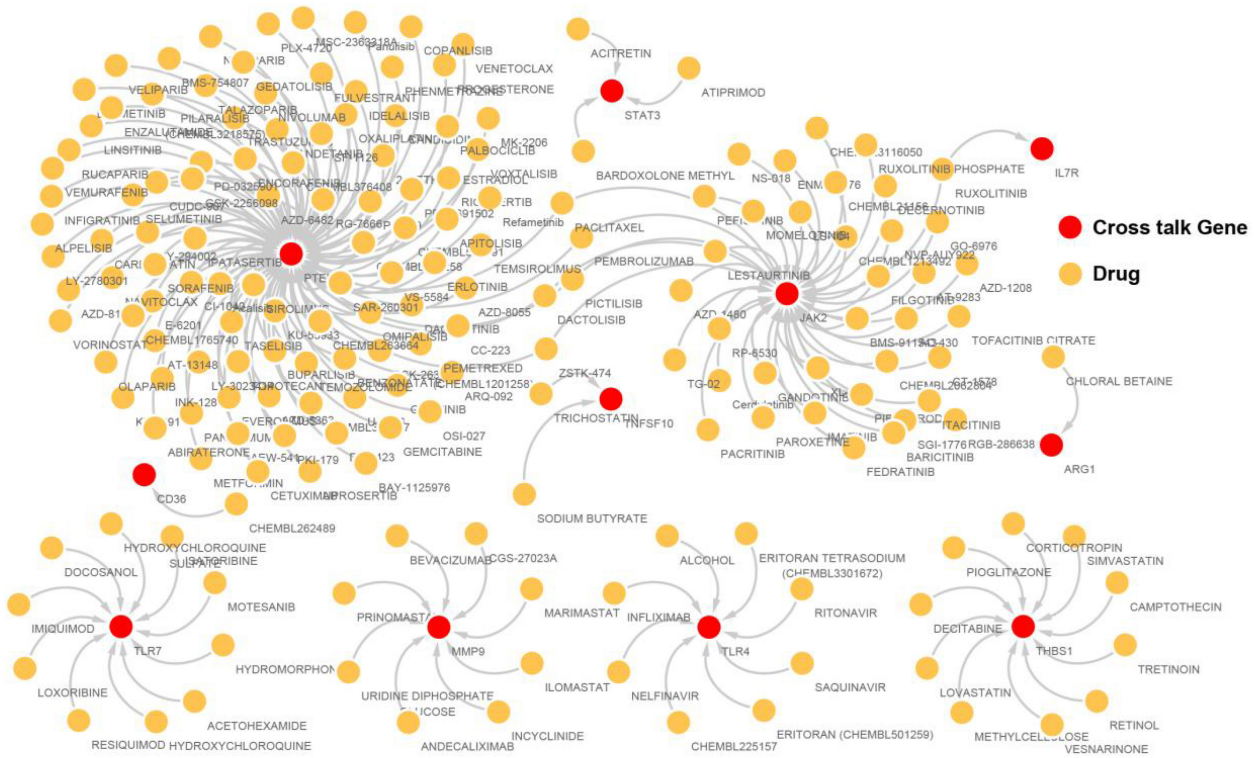

FIGURE 12 | The immunosuppression-related crosstalk genes-target drugs network.

expression of FYN gene after ischemic stroke has been documented, and the authors suggested that GP6 induced activation of FYN initiated phosphorylation events eventually accelerating platelet adhesion (Gu et al., 2021).

Paxillin or PXN is implicated in oligodendrocyte differentiation (Yamauchi et al., 2006). Downregulation of PXN in response to treatment of ischemic stroke with two Chinese medicine derived bioactive compounds has been documented (Liu et al., 2012). Similar downregulation of PXN by Diphenyleneiodonium for the treatment of stroke has been also documented (Nagel et al., 2012) although experimental evidence describing functional pathways of PXN involvement in stroke pathology is scarce. In a concordant finding, a bioinformatics analysis of inflammation associated competing endogenous RNA network in ischemic stroke has reported FYN and PXN among the most significantly enriched modules from the hub genes (Zhang et al., 2020).

The SVM classifier showed excellent AUC values for discrimination of ischemic stroke and pathway analysis of the immunosuppression-related crosstalk genes showed TNF-signaling among the topmost enriched pathways. TNF-signaling plays pleiotropic and multiple roles in ischemic stroke, including acute inflammation and cell death during the early stages and tissue repair during the later recovery phase (Sairanen et al., 2001). The disease-related KEGG pathways enriched in the 17 key immunosuppression-related crosstalk genes including Measles and Tuberculosis pathways and osteoclast differentiation have been similarly reported as top pathways implicated in stroke (Diao and Liu, 2017). Leptin receptors are expressed by astrocytes (Schwartz and Baskin, 2013) and treatment with Leptin has shown improvements in post-stroke edema and functional recovery (Busch et al., 2010). In the transcriptional regulatory network of the immunosuppression-related crosstalk genes, STAT3 and SPI1 showed very high degrees. Activation of the JAK/STAT3 pathway in stroke is well-documented (Planas et al., 1996; Choi et al., 2003; Satriotomo et al., 2006) and its inhibition is found to significantly reduce the inflammatory process (Wu et al., 2018). In agreement with our findings, transcriptomic analysis of astrocytes has shown Stat3, Sp1, and Spi1 as the most significant transcription factors in stroke (Rakers et al., 2018).

Along with STAT3, HIF1A showed a consistent transcriptional regulatory relationship in both datasets. HIF1A or hypoxia-inducible factor 1, is implicated in cellular adaptation to hypoxia and its inhibition was found to increase mortality and infarct volume size, while its downstream genes were found to increase ischemia-induced blood-brain barrier permeability on one hand, but also induce neuroprotection on the other hand (Yan et al., 2011). HIF1A has been considered an important target for the management of stroke (Pan et al., 2021). Analysis of drug targets for the immunosuppression-related crosstalk genes showed PTEN and JAK2 as the most prominent targets. PTEN or Phosphatase and tensin homolog deleted on chromosome 10 inhibitor drugs administration after stroke is found to confer neuroprotection via improvement of axonal growth and

activation of the Akt/mTOR activation (Mao et al., 2013). Small molecule PTEN inhibitors currently under investigation include BPV that has shown protective effects in experimental stroke (Mao et al., 2013) and SF1670 (Li et al., 2011). JAK2 is a part of the Janus Kinase family and are implicated in cytokine and growth factor-related signaling and JAK targeting has been proposed as a strategy for the management of multiple immune and inflammatory diseases (Schwartz et al., 2017).

The findings of the present study must be considered in light of its limitations. The included microarray datasets were of small sample size and RNA-seq datasets were not included. Large sampled transcriptome datasets with detailed metadata including time after stroke are essential to decipher the molecular events in the immune cascade following stroke. Additionally, experimental *in vitro* and *in vivo* investigations to verify the identified relevant immunosuppression-related genes in stroke were not conducted. In addition, the functional pathways involved remain to be investigated in future targeted studies. Therefore, future studies are necessary to confirm the involvement of the highlighted immune crosstalk genes and their related mechanistic pathways in ischemic stroke, in order to facilitate the clinical translation of these findings. At the same time, the strength of the current study includes the application of multiple bioinformatics and machine learning approaches to identify the most relevant immunosuppression-related genes in stroke.

CONCLUSION

The present bioinformatic study utilized a comprehensive approach to analyze immunosuppression-related genes implicated in stroke and identified key immunosuppression-related genes, transcriptional regulatory factors and signaling pathways implicated in the molecular pathogenesis of ischemic stroke. The most prominent molecular mechanisms included 17 immunosuppression-related key crosstalk genes including ARG1, CD36, FCN1, GRN, IL7R, JAK2, MAFB, MMP9, PTEN, STAT3, STAT5A, THBS1, TLR2, TLR4, TLR7, TNFSF10, and VASP, transcription factors targeting STAT3, SPI1, CEPBD, SP1, TP53, NFIL3, STAT1, HIF1A, and JUN, and, enriched signaling pathways, PD-L1 expression and PD-1 checkpoint pathway, NF-kappa B signaling, IL-17 signaling, TNF signaling, and NOD-like receptor signaling.

DATA AVAILABILITY STATEMENT

The original contributions presented in the study are included in the article/**Supplementary Material**, further inquiries can be directed to the corresponding author/s.

AUTHOR CONTRIBUTIONS

XW: conceptualization, funding acquisition, methodology, formal analysis, and writing—original draft. QW, KW, and QN: methodology, formal analysis, and writing—original draft. HL and ZS: formal analysis, methodology and writing—review and editing. YX: project administration, supervision, and writing—review and editing. All authors contributed to the article and approved the submitted version.

FUNDING

This present study was funded by the China Postdoctoral Science Foundation (2020M681398), the Shandong Medical and Health Technology Development Fund (2018WS147 and 202103070325), and the Natural Science Foundation of Shandong Province (ZR2020MH141 and ZR2021MH0025).

SUPPLEMENTARY MATERIAL

The Supplementary Material for this article can be found online at: https://www.frontiersin.org/articles/10.3389/fnagi.2022.830494/full#supplementary-material

REFERENCES

Alam, J. J., Krakovsky, M., Germann, U., and Levy, A. (2020). Continuous administration of a p38α inhibitor during the subacute phase after transient ischemia-induced stroke in the rat promotes dose-dependent functional recovery accompanied by increase in brain BDNF protein level. *PLoS One* 15:e0233073. doi: 10.1371/journal.pone.0233073

Amantea, D., and Giacinto, B. (2016). Drug repurposing for immune modulation in acute ischemic stroke. *Curr. Opin. Pharmacol.* 26, 124–130. doi: 10.1016/j.coph.2015.11.006

Ansar, S., Eftekhari, S., Waldsee, R., Nilsson, E., Nilsson, O., Säveland, H., et al. (2013). MAPK signaling pathway regulates cerebrovascular receptor expression in human cerebral arteries. *BMC Neurosci.* 14:12. doi: 10.1186/1471-2202-14-12

Barr, T. L., Conley, Y., Ding, J., Dillman, A., Warach, S., Singleton, A., et al. (2010). Genomic biomarkers and cellular pathways of ischemic stroke by RNA gene expression profiling. *Neurology* 75, 1009–1014. doi: 10.1212/wnl.0b013e3181f2b37f

Busch, H.-J., Schirmer, S. H., Jost, M., van Stijn, S., Peters, S. L. M., Piek, J. J., et al. (2010). Leptin augments cerebral hemodynamic reserve after three-vessel occlusion: distinct effects on cerebrovascular tone and proliferation in a nonlethal model of hypoperfused rat brain. *J. Cereb. Blood Flow Metab.* 31, 1085–1092. doi: 10.1038/jcbfm.2010.192

Choi, J.-S., Kim, S. Y., Cha, J.-H., Choi, Y.-S., Sung, K.-W., Oh, S. T., et al. (2003). Upregulation of gp130 and STAT3 activation in the rat hippocampus following transient forebrain ischemia. *Glia* 41, 237–246. doi: 10.1002/glia.10186

Diao, X., and Liu, A. (2017). Identification of core pathways based on attractor and crosstalk in ischemic stroke. *Exp. Ther. Med.* 15, 1520–1524. doi: 10.3892/etm.2017.5563

Fang, W., Zhai, X., Han, D., Xiong, X., Wang, T., Zeng, X., et al. (2018). CCR2-dependent monocytes/macrophages exacerbate acute brain injury but promote functional recovery after ischemic stroke in mice. *Theranostics* 8, 3530–3543. doi: 10.7150/thno.24475

Fu, Y., Liu, Q., Anrather, J., and Shi, F.-D. (2015). Immune interventions in stroke. *Nat. Rev. Neurol.* 11, 524–535. doi: 10.1038/nrneurol.2015.144

Garcia-Bonilla, L., Faraco, G., Moore, J., Murphy, M., Racchumi, G., Srinivasan, J., et al. (2016). Spatio-temporal profile, phenotypic diversity, and fate of recruited monocytes into the post-ischemic brain. *J. Neuroinflammation* 13:285. doi: 10.1186/s12974-016-0750-0

Gelderblom, M., Leypoldt, F., Steinbach, K., Behrens, D., Choe, C.-U., Siler, D. A., et al. (2009). Temporal and spatial dynamics of cerebral immune cell

accumulation in stroke. *Stroke* 40, 1849–1857. doi: 10.1161/strokeaha.108.534503

Gomez-Sanchez, J. C., Delgado-Esteban, M., Rodriguez-Hernandez, I., Sobrino, T., Perez de la Ossa, N., Reverte, S., et al. (2011). The human Tp53 Arg72Pro polymorphism explains different functional prognosis in stroke. *J. Exp. Med.* 208, 429–437. doi: 10.1084/jem.20101523

Gu, L., Xiong, X., Wei, D., Gao, X., Krams, S., and Zhao, H. (2013). T cells contribute to stroke-induced Lymphopenia in rats. *PLoS One* 8:e59602. doi: 10.1371/journal.pone.0059602

Gu, Y., Wu, Y., and Chen, L. (2021). GP6 promotes the development of cerebral ischemic stroke induced by atherosclerosis via the FYN-PKA-pPTK2/FAK1 signaling pathway. *Adv. Clin. Exp. Med.* 30, 823–829. doi: 10.17219/acem/135510

Gustavsen, J. A., Pai, S., Isserlin, R., Demchak, B., and Pico, A. R. (2019). RCy3: network biology using Cytoscape from within R. *F1000Res.* 8:1774. doi: 10.12688/f1000research.20887.3

Hu, X., Li, P., Guo, Y., Wang, H., Leak, R. K., Chen, S., et al. (2012). Microglia/Macrophage polarization dynamics reveal novel mechanism of injury expansion after focal cerebral ischemia. *Stroke* 43, 3063–3070. doi: 10.1161/strokeaha.112.659656

Iadecola, C., and Anrather, J. (2011). The immunology of stroke: from mechanisms to translation. *Nat. Med.* 17, 796–808. doi: 10.1038/nm.2399

Iadecola, C., Buckwalter, M. S., and Anrather, J. (2020). Immune responses to stroke: mechanisms, modulation, and therapeutic potential. *J. Clin. Invest.* 130, 2777–2788. doi: 10.1172/jci135530

Kaminska, B., Gozdz, A., Zawadzka, M., Ellert-Miklaszewska, A., and Lipko, M. (2009). MAPK signal transduction underlying brain inflammation and gliosis as therapeutic target. *Anat. Rec.* 292, 1902–1913. doi: 10.1002/ar.21047

Katan, M., and Luft, A. (2018). Global burden of stroke. *Semin. Neurol.* 38, 208–211. doi: 10.1055/s-0038-1649503

Knox, R., and Jiang, X. (2015). Fyn in neurodevelopment and ischemic brain injury. *Dev. Neurosci.* 37, 311–320. doi: 10.1159/000369995

Krug, T., Gabriel, J. P., Taipa, R., Fonseca, B. V., Domingues-Montanari, S., Fernandez-Cadenas, I., et al. (2012). TTC7B emerges as a novel risk factor for ischemic stroke through the convergence of several genome-wide approaches. *J. Cereb. Blood Flow Metab.* 32, 1061–1072. doi: 10.1038/jcbfm.2012.24

Kursa, M. B. (2014). Robustness of Random Forest-based gene selection methods. *BMC Bioinformatics* 15:8. doi: 10.1186/1471-2105-15-8

Kursa, M. B., and Rudnicki, W. R. (2010). Feature selection with theBorutaPackage. *J. Stat. Softw.* 36, 1–13. doi: 10.18637/jss.v036.i11

Li, Y., Prasad, A., Jia, Y., Roy, S. G., Loison, F., Mondal, S., et al. (2011). Pretreatment with phosphatase and tensin homolog deleted on chromosome 10 (PTEN) inhibitor SF1670 augments the efficacy of granulocyte transfusion in a clinically relevant mouse model. *Blood J. Am. Soc. Hematol.* 117, 6702–6713. doi: 10.1182/blood-2010-09-309864

Liu, F., Li, L., Chen, J., Wu, Y., Cao, Y., and Zhong, P. (2021). A network pharmacology to explore the mechanism of calculus bovis in the treatment of ischemic stroke. *Biomed Res. Int.* 2021:6611018. doi: 10.1155/2021/6611

Liu, J., Zhou, C.-X., Zhang, Z.-J., Wang, L.-Y., Jing, Z.-W., and Wang, Z. (2012). Synergistic mechanism of gene expression and pathways between jasminoidin and ursodeoxycholic acid in treating focal cerebral ischemia-reperfusion injury. *CNS Neurosci. Ther.* 18, 674–682. doi: 10.1111/j.1755-5949.2012.00348.x

Liu, L., Doran, S., Xu, Y., Manwani, B., Ritzel, R., Benashski, S., et al. (2014). Inhibition of mitogen-activated protein kinase phosphatase-1 (MKP-1) increases experimental stroke injury. *Exp. Neurol.* 261, 404–411. doi: 10.1016/j.expneurol.2014.05.009

Liu, Q., Jin, W.-N., Liu, Y., Shi, K., Sun, H., Zhang, F., et al. (2017). Brain ischemia suppresses immunity in the periphery and brain via different neurogenic innervations. *Immunity* 46, 474–487. doi: 10.1016/j.immuni.2017.02.015

Luo, H.-C., Yi, T.-Z., Huang, F.-G., Wei, Y., Luo, X.-P., and Luo, Q.-S. (2020). Role of long noncoding RNA MEG3/miR-378/GRB2 axis in neuronal autophagy and neurological functional impairment in ischemic stroke. *J. Biol. Chem.* 295, 14125–14139. doi: 10.1074/jbc.ra119.010946

Mabuchi, T., Kitagawa, K., Ohtsuki, T., Kuwabara, K., Yagita, Y., Yanagihara, T., et al. (2000). Contribution of microglia/macrophages to expansion of infarction and response of oligodendrocytes after focal cerebral ischemia in rats. *Stroke* 31, 1735–1743. doi: 10.1161/01.str.31.7.1735

Mao, L., Jia, J., Zhou, X., Xiao, Y., Wang, Y., Mao, X., et al. (2013). Delayed administration of a PTEN inhibitor BPV improves functional recovery after experimental stroke. *Neuroscience* 231, 272–281. doi: 10.1016/j.neuroscience.2012.11.050

Mo, X., Li, T., Ji, G., Lu, W., and Hu, Z. (2013). Peripheral polymorphonuclear leukocyte activation as a systemic inflammatory response in ischemic stroke. *Neurol. Sci.* 34, 1509–1516. doi: 10.1007/s10072-013-1447-0

Nagel, S., Hadley, G., Pfleger, K., Grond-Ginsbach, C., Buchan, A. M., Wagner, S., et al. (2012). Suppression of the inflammatory response by diphenyleneiodonium after transient focal cerebral ischemia. *J. Neurochem.* 123, 98–107. doi: 10.1111/j.1471-4159.2012.07948.x

Newman, A. M., Liu, C. L., Green, M. R., Gentles, A. J., Feng, W., Xu, Y., et al. (2015). Robust enumeration of cell subsets from tissue expression profiles. *Nat. Methods* 12, 453–457. doi: 10.1038/nmeth.3337

Newman, A. M., Steen, C. B., Liu, C. L., Gentles, A. J., Chaudhuri, A. A., Scherer, F., et al. (2019). Determining cell type abundance and expression from bulk tissues with digital cytometry. *Nat. Biotechnol.* 37, 773–782. doi: 10.1038/s41587-019-0114-2

Pan, Z., Ma, G., Kong, L., and Du, G. (2021). Hypoxia-inducible factor-1: regulatory mechanisms and drug development in stroke. *Pharmacol. Res.* 170:105742. doi: 10.1016/j.phrs.2021.105742

Pedragosa, J., Miró-Mur, F., Otxoa-de-Amezaga, A., Justicia, C., Ruíz-Jaén, F., Ponsaerts, P., et al. (2020). CCR2 deficiency in monocytes impairs angiogenesis and functional recovery after ischemic stroke in mice. *J. Cereb. Blood Flow Metab.* 40, S98–S116. doi: 10.1177/0271678x20909055

Planas, A. M., Soriano, M. A., Berruezo, M., Justicia, C., Estrada, A., Pitarch, S., et al. (1996). Induction of Stat3, a signal transducer and transcription factor, in reactive microglia following transient focal cerebral ischaemia. *Eur. J. Neurosci.* 8, 2612–2618. doi: 10.1111/j.1460-9568.1996.tb01556.x

Proctor, B. M., Ren, J., Chen, Z., Schneider, J. G., Coleman, T., Lupu, T. S., et al. (2007). Grb2 Is required for atherosclerotic lesion formation. *Arterioscler. Thromb. Vasc. Biol.* 27, 1361–1367. doi: 10.1161/atvbaha.106.134007

Rakers, C., Schleif, M., Blank, N., Matušková, H., Ulas, T., Händler, K., et al. (2018). Stroke target identification guided by astrocyte transcriptome analysis. *Glia* 67, 619–633. doi: 10.1002/glia.23544

Ramos-Araque, M. E., Rodriguez, C., Vecino, R., Cortijo Garcia, E., de Lera Alfonso, M., Sanchez Barba, M., et al. (2018). The neuronal ischemic tolerance is conditioned by the Tp53 Arg72Pro polymorphism. *Transl. Stroke Res.* 10, 204–215. doi: 10.1007/s12975-018-0631-1

Sairanen, T., Carpeìn, O., Karjalainen-Lindsberg, M.-L., Paetau, A., Turpeinen, U., Kaste, M., et al. (2001). Evolution of cerebral tumor necrosis factor-α production during human ischemic stroke. *Stroke* 32, 1750–1758. doi: 10.1161/01.str.32.8.1750

Satriotomo, I., Bowen, K. K., and Vemuganti, R. (2006). JAK2 and STAT3 activation contributes to neuronal damage following transient focal cerebral ischemia. *J. Neurochem.* 98, 1353–1368. doi: 10.1111/j.1471-4159.2006.04051.x

Sawe, N., Steinberg, G., and Zhao, H. (2008). Dual roles of the MAPK/ERK1/2 cell signaling pathway after stroke. *J. Neurosci. Res.* 86, 1659–1669. doi: 10.1002/jnr.21604

Schwartz, D. M., Kanno, Y., Villarino, A., Ward, M., Gadina, M., and O'Shea, J. J. (2017). JAK inhibition as a therapeutic strategy for immune and inflammatory diseases. *Nat. Rev. Drug Discov.* 16, 843–862. doi: 10.1038/nrd.2017.201

Schwartz, M. W., and Baskin, D. G. (2013). Leptin and the brain: then and now. *J. Clin. Invest.* 123, 2344–2345. doi: 10.1172/jci69346

Shi, K., Wood, K., Shi, F.-D., Wang, X., and Liu, Q. (2018). Stroke-induced immunosuppression and poststroke infection. *Stroke Vasc. Neurol.* 3, 34–41. doi: 10.1136/svn-2017-000123

Shichita, T., Sugiyama, Y., Ooboshi, H., Sugimori, H., Nakagawa, R., Takada, I., et al. (2009). Pivotal role of cerebral interleukin-17–producing γδT cells in the delayed phase of ischemic brain injury. *Nat. Med.* 15, 946–950. doi: 10.1038/nm.1999

Shim, R., and Wong, C. H. Y. (2016). Ischemia, immunosuppression and infection—tackling the predicaments of post-stroke complications. *Int. J. Mol. Sci.* 17:64. doi: 10.3390/ijms17010064

Stubbe, T., Ebner, F., Richter, D., Engel, O. R., Klehmet, J., Royl, G., et al. (2012). Regulatory T cells accumulate and proliferate in the ischemic hemisphere for up to 30 days after MCAO. *J. Cereb. Blood Flow Metab.* 33, 37–47. doi: 10.1038/jcbfm.2012.128

Sun, J., and Nan, G. (2016). The mitogen-activated protein kinase (MAPK) signaling pathway as a discovery target in stroke. *J. Mol. Neurosci.* 59, 90–98. doi: 10.1007/s12031-016-0717-8

Takagi, N., Cheung, H. H., Bissoon, N., Teves, L., Wallace, M. C., and Gurd, J. W. (1999). The Effect of transient global ischemia on the interaction of Src and Fyn with the N-Methyl-d-Aspartate receptor and postsynaptic densities: possible involvement of Src homology 2 domains. *J. Cereb. Blood Flow Metab.* 19, 880–888. doi: 10.1097/00004647-199908000-00007

Takenaga, Y., Takagi, N., Murotomi, K., Tanonaka, K., and Takeo, S. (2009). Inhibition of Src activity decreases tyrosine phosphorylation of occludin in brain capillaries and attenuates increase in permeability of the blood-brain barrier after transient focal cerebral ischemia. *J. Cereb. Blood Flow Metab.* 29, 1099–1108. doi: 10.1038/jcbfm.2009.30

Wei, Y., Sun, Z., Wang, Y., Xie, Z., Xu, S., Xu, Y., et al. (2019). Methylation in the TP53 promoter is associated with ischemic stroke. *Mol. Med. Report* 20, 1404–1410. doi: 10.3892/mmr.2019.10348

Wong, C. H. Y., Jenne, C. N., Lee, W.-Y., Léger, C., and Kubes, P. (2011). Functional innervation of hepatic iNKT cells is immunosuppressive following stroke. *Science* 334, 101–105. doi: 10.1126/science.1210301

Wu, Y., Xu, J., Xu, J., Zheng, W., Chen, Q., and Jiao, D. (2018). Study on the mechanism of JAK2/STAT3 signaling pathway-mediated inflammatory reaction after cerebral ischemia. *Mol. Med. Report* 17, 5007–5012. doi: 10.3892/mmr.2018.8477

Yamauchi, J., Miyamoto, Y., Sanbe, A., and Tanoue, A. (2006). JNK phosphorylation of paxillin, acting through the Rac1 and Cdc42 signaling cascade, mediates neurite extension in N1E-115 cells. *Exp. Cell Res.* 312, 2954–2961. doi: 10.1016/j.yexcr.2006.05.016

Yan, J., Zhou, B., Taheri, S., and Shi, H. (2011). Differential effects of HIF-1 inhibition by YC-1 on the overall outcome and blood-brain barrier damage in a rat model of ischemic stroke. *PLoS One* 6:e27798. doi: 10.1371/journal.pone.0027798

Yilmaz, G., Arumugam, T. V., Stokes, K. Y., and Granger, D. N. (2006). Role of T lymphocytes and interferon-γ in ischemic stroke. *Circulation* 113, 2105–2112. doi: 10.1161/circulationaha.105.593046

Yu, G., Wang, L.-G., Han, Y., and He, Q.-Y. (2012). clusterProfiler: an R package for comparing biological themes among gene clusters. *OMICS* 16, 284–287. doi: 10.1089/omi.2011.0118

Zhang, L., Liu, B., Han, J., Wang, T., and Han, L. (2020). Competing endogenous RNA network analysis for screening inflammation-related long non-coding RNAs for acute ischemic stroke. *Mol. Med. Rep.* 22, 3081–3094. doi: 10.3892/mmr.2020.11415

Conflict of Interest: The authors declare that the research was conducted in the absence of any commercial or financial relationships that could be construed as a potential conflict of interest.

Publisher's Note: All claims expressed in this article are solely those of the authors and do not necessarily represent those of their affiliated organizations, or those of the publisher, the editors and the reviewers. Any product that may be evaluated in this article, or claim that may be made by its manufacturer, is not guaranteed or endorsed by the publisher.

frontiers | Frontiers in Aging Neuroscience

REVIEW
published: 19 April 2022
doi: 10.3389/fnagi.2022.867863

The Roles of Optogenetics and Technology in Neurobiology: A Review

Wenqing Chen[1,2†], Chen Li[3†], Wanmin Liang[2], Yunqi Li[2], Zhuoheng Zou[2], Yunxuan Xie[2], Yangzeng Liao[2], Lin Yu[2], Qianyi Lin[2], Meiying Huang[2], Zesong Li[4] and Xiao Zhu[1,2]**

[1] Department of Laboratory Medicine, Hangzhou Medical College, Hangzhou, China, [2] Zhu's Team, Guangdong Medical University, Zhanjiang, China, [3] Department of Biology, Chemistry, Pharmacy, Free University of Berlin, Berlin, Germany, [4] Guangdong Provincial Key Laboratory of Systems Biology and Synthetic Biology for Urogenital Tumors, Shenzhen Key Laboratory of Genitourinary Tumor, Department of Urology, The First Affiliated Hospital of Shenzhen University, Shenzhen Second People's Hospital (Shenzhen Institute of Translational Medicine), Shenzhen, China

OPEN ACCESS

Edited by:
Min Tang,
Jiangsu University, China

Reviewed by:
Ling Li,
University of North Dakota, United States
Kaihua Guo,
Sun Yat-sen University, China

***Correspondence:**
Zesong Li
lzssc@email.szu.edu.cn
Xiao Zhu
bioxzhu@yahoo.com

[†]These authors have contributed equally to this work

Specialty section:
This article was submitted to Cellular and Molecular Mechanisms of Brain-aging, a section of the journal Frontiers in Aging Neuroscience

Received: *01 February 2022*
Accepted: *21 March 2022*
Published: *19 April 2022*

Citation:
Chen W, Li C, Liang W, Li Y, Zou Z, Xie Y, Liao Y, Yu L, Lin Q, Huang M, Li Z and Zhu X (2022) The Roles of Optogenetics and Technology in Neurobiology: A Review. Front. Aging Neurosci. 14:867863. doi: 10.3389/fnagi.2022.867863

Optogenetic is a technique that combines optics and genetics to control specific neurons. This technique usually uses adenoviruses that encode photosensitive protein. The adenovirus may concentrate in a specific neural region. By shining light on the target nerve region, the photosensitive protein encoded by the adenovirus is controlled. Photosensitive proteins controlled by light can selectively allow ions inside and outside the cell membrane to pass through, resulting in inhibition or activation effects. Due to the high precision and minimally invasive, optogenetics has achieved good results in many fields, especially in the field of neuron functions and neural circuits. Significant advances have also been made in the study of many clinical diseases. This review focuses on the research of optogenetics in the field of neurobiology. These include how to use optogenetics to control nerve cells, study neural circuits, and treat diseases by changing the state of neurons. We hoped that this review will give a comprehensive understanding of the progress of optogenetics in the field of neurobiology.

Keywords: nanoparticles, nervous system, neural circuits, neurobiology, neuron, optogenetics

INTRODUCTION

In 2005, optogenetics was born and appeared in the public (Boyden et al., 2005). Since the advent of optogenetics, many top medical journals have described it as a core technology for the future of humanity (Method of the year, 2010; News, 2010; Adamantidis et al., 2015). Optogenetics can be combined with molecular biology, viral biology and other methods to introduce foreign light-sensitive protein genes into living cells (Amitrano et al., 2021; Di Ventura and Weber, 2021). Therefore, optogenetics has made many achievements in the field of neurobiology. Such as exploring unknown neuron functions (**Figure 1**), the discovery of neural circuits (**Figure 2**), and treatment of neurological diseases (**Figure 3**). By using the technology of optogenetics, the research of many difficult diseases has been advanced greatly. Using optogenetics to induce the differentiation of neural progenitor cells, the researchers were able to treat stroke in mice (Yu et al., 2019; Peters et al., 2021; Vassalli et al., 2021). The mice were able to remove and reactivate a memory by changing the connections between related neurons in the brain with different frequencies of light (Nabavi et al., 2014). Blindness can

be treated by using optogenetics to activate the photogene expression of the related photoactivation channels or pumps in retinal cells (Ostrovsky and Kirpichnikov, 2019). This technology have led us into a higher research field.

OPTOGENETIC RESEARCH METHODS

Nerve Cells

Induce Neuronal Differentiation

In 2019, Luo et al. (2019) used photoelectric fullerene-bound photosensitive protein (HEBR) to reprogram and differentiate human fibroblasts. In this study, researchers transfected HEBR plastids into human fibroblasts using fullerene as a cell culture substrate (**Figure 1**). Previous research has shown that environmental stresses, such as acidity, can stimulate cell reprogramming. When the researchers illuminated HERB transfected fibroblasts with green light, the pH in and out of the transfected fibroblasts changed momentously, causing the fibroblasts to differentiate into neuron-like cells. This study has clinical significance in nerve repair.

In other studies, researchers combined a variety of technologies, such as optogenetics, synthetic biology (Padmanabhan et al., 2019; Hemmati et al., 2020; Yi et al., 2020; Zhang et al., 2020), for the first time to achieve far red light to control the expression of genomic genes. The far-red light-regulated CRISPR-dCas9 endogenous gene transcription activation device was developed for the first time (Gjaltema and Schulz, 2018), which successfully induced the pluripotent stem cells into functional neural cells (Shao et al., 2018). By combining BphS, which respond to red light proteins in rhodobacter, transcription factors BldD in streptococcus, and protein dCas9 in streptococcus pyogenes, this device can accurately realize the reversible activation of target genes inside and outside the organism, with high precision. Meanwhile, the frequency of light used in the study is in the physiological range and has no side effects on organisms. In theory, the results of this research can be widely used for precise epigenetic regulation (Hori and Kikuchi, 2019). And, in the future, this technology may be applied in the clinical field to treat diseases such as muscular dystrophy (Vajtay et al., 2019).

Control the Behavior of Nerve Cells

In earlier studies, optogenetics simply stimulated neurons (Nowak et al., 2010). Early applications of optogenetic control neurons were mainly two: driving proton pumps with light to charge mitochondria (Hallett et al., 2016), and polarizing or depolarizing neurons (Yao et al., 2012). By making a single neuron hyperpolarized, the function of this neuron can be studied (Aquili et al., 2014). In the latest study, researchers can decode and control signaling pathways in neurons (**Figure 1**; Melero-Fernandez de Mera et al., 2017). In this study, the intracellular signaling pathways of the organism can be controlled by light, using the main bioresonance effect of the organism. Using light to control specific signaling pathways that regulate the behavior of nerve cells, researchers can learn which neurons are involved in those pathways. In related studies, we can learn more about the JNK signaling pathway by inhibiting p38MAPK with OptoJNKI (a photosensitive substance that inhibits p38MAPK) (Melero-Fernandez de Mera et al., 2017). Moreira et al. (2019) managed to control the taste of fruit flies by shining different LEDs on different taste neurons. In this study, the researchers managed to alter feeding behavior in fruit flies by manipulating taste receptors. This technique can be used to study the progression of clinical diseases and to discover new therapies.

Study Neuronal Function

Studies have shown that people with schizophrenia and other psychiatric and neurological disorders have gamma oscillations in their brains (Gao et al., 2021a,b). But exactly how gamma oscillations are produced is not clear (Fan et al., 2020; Lu W. et al., 2020; Song et al., 2020). Cardin et al. (2009) discovered how the brain produces gamma oscillations by using optogenetics to manipulate the activity of nerve cells. By manipulating the interneurons' related behavior with different frequencies of light, the researchers were able to observe the extent of the gamma oscillations produced by the interneurons. The research will contribute to a range of neurological disorders.

In 2014, researchers used optogenetics to inactivate cells in parts of the rat brain (**Figure 1**) to identify the neurons responsible for behavioral decision-making (Aquili et al., 2014). This study is the first to show that optogenetics inhibition of nucleus accumbens neurons during reward and false feedback can increase the behavioral complexity of individuals (Aquili et al., 2014). In the same year, another researcher used optogenetics to identify neurons that control aggression in the hypothalamus of mice (Lee et al., 2014). In 2017, scientists used optogenetics to find neurons in the brains of mice that control hunting behavior (Han et al., 2017). Because the hypothalamus in humans and mice is structurally similar, these findings are also useful for studying human behavior.

Neural Circuits

The Neural Circuits That Regulate Sodium Appetite

Sodium ions are important ions in the nervous system that regulate neurons. If sodium ion is not ingested for a long time, it will cause symptoms such as loss of appetite, weakness of limbs and dizziness. When a variety of animals are deficient in sodium ions, they will consume a large amount of salt rich in sodium ions, which is called sodium appetite (Thornton and Fitzsimons, 1995; Geerling and Loewy, 2008; Molnar and Labouesse, 2021). After a large intake of salt, the body will produce a sense of satisfaction to prevent further intake (Wolf et al., 1984). Previous studies on sodium appetite were flawed and did not conform to the single variable principle of the experiment. Until 2019, Lee et al. (2019) demonstrated that the pre-LCPDYN neurons are the core neurons in the regulation of sodium appetite by combining optogenetics with other techniques, and are regulated by the homeostatic and sense-related brain regions (**Table 1** and **Figure 2**). In this study, researchers used optogenetic techniques to inhibit pre-LCPDYN neurons, and found that the pre-LCPDYN neurons are essential in the neural circuits that regulate sodium appetite. This experiment has revealed the mechanism of nerve circuits regulating sodium appetite and related conclusions.

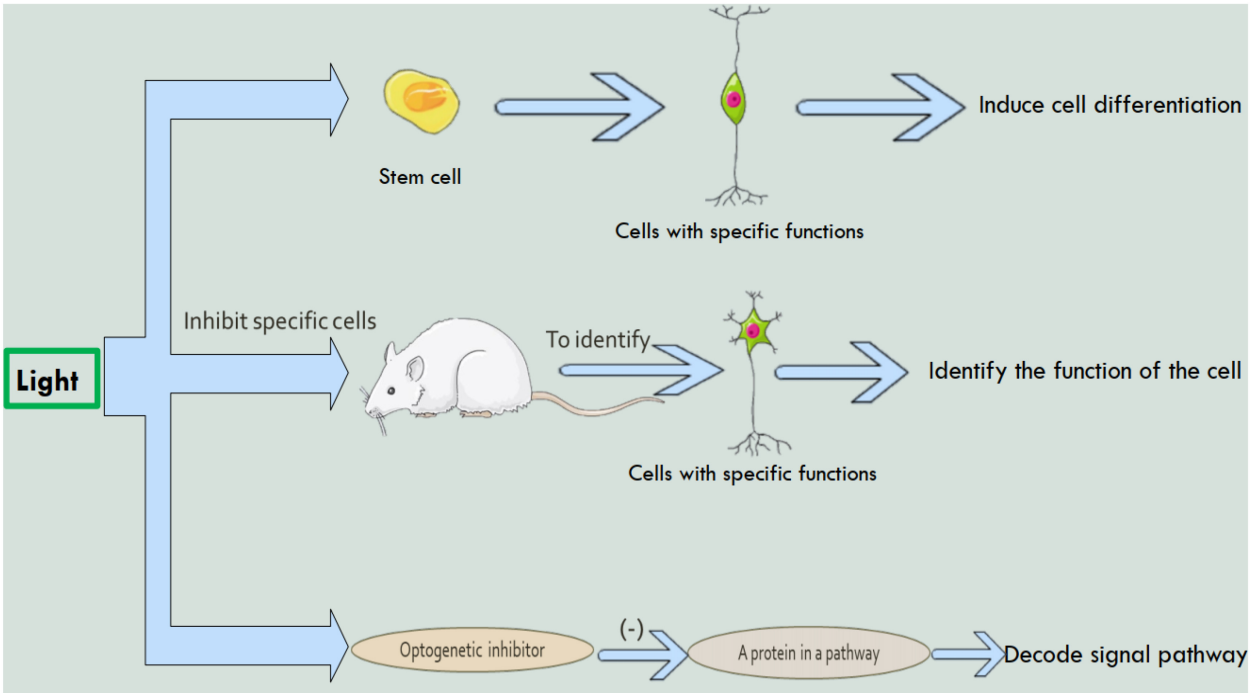

FIGURE 1 | The study of optogenetics in the field of neurons. Using optogenetics, it is possible to induce stem cell differentiation, identify cell function, and decode intercellular signaling pathways.

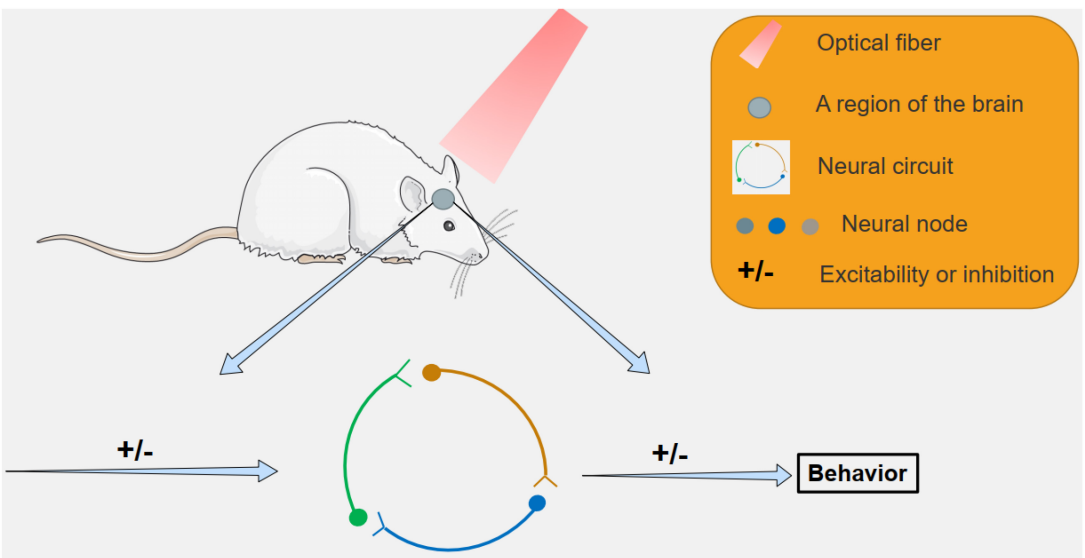

FIGURE 2 | The study of neural circuits by optogenetic methods. By targeting specific areas with light, specific neural circuits can be inhibited or activated, leading to behavioral changes in mice, and related neural circuits can be studied.

The Nerve Basis of Compulsive Feeding

Globally, obesity (Hosseinpanah et al., 2019; Lu D. et al., 2020) and type 2 diabetes (Broder et al., 2014; Song et al., 2020; Liu Y. et al., 2021) are among the major diseases that endanger human health. Bad eating habits can bring about many diseases. Clinically, the treatment for severely obese patients is usually gastric bypass surgery. This approach is extremely traumatic. Optogenetics separates normal eating behavior from reward-seeking eating (Cardi et al., 2018), providing new ideas for the treatment of this disease.

Nieh et al. (2015) demonstrated that the hypothalamic-ventral tegmental pathway is involved in controlling feeding in

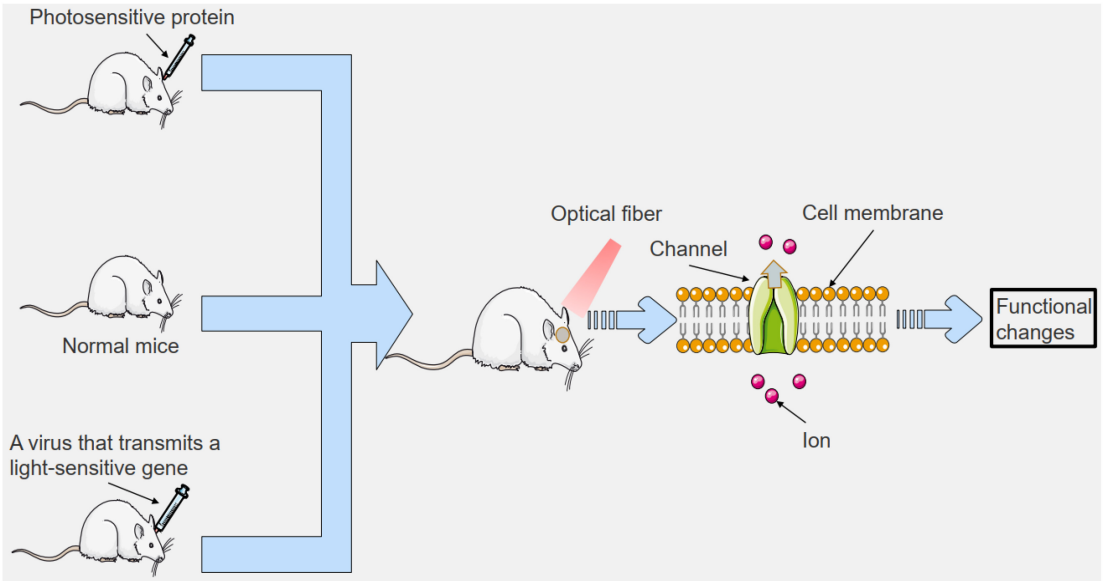

FIGURE 3 | To study the mechanisms of clinical diseases using optogenetics. We can introduce photosensitive proteins outside the body, or we can introduce viruses that transmit photosensitive genes, or we can shine light directly on specific areas. This can lead to changes in cell membrane pathways in the irradiated area, which can affect cell function. The related functions of organisms can be altered to study clinical diseases.

TABLE 1 | The study of optogenetics in neurobiology.

The field of optogenetics	The specific research		References
Nerve cells	Induce neuronal differentiation		Shao et al., 2018
	Control the behavior of nerve cells		Moreira et al., 2019
	Study neuronal function		Aquili et al., 2014
Neural circuits	The neural circuits that regulate sodium appetite		Lee et al., 2019
	The nerve basis of compulsive feeding		Nieh et al., 2015; Kim et al., 2021
	Social behavioral neural circuits		Zhao et al., 2017; Yang Y. et al., 2021
	Body temperature regulating neural circuit		Zhao et al., 2017
	Spatial learning and memory circuits		Yang et al., 2018; Huang et al., 2021
	Neural circuit mechanisms that activate addictive memory		Alaghband et al., 2014
Nervous system-based clinical research	Nervous system	Alzheimer's disease	Roy et al., 2016
		Parkinson's disease	Ztaou et al., 2016
		Epilepsy	Chen et al., 2018
		Stroke	Yu et al., 2019
	Skeletal system		Bryson et al., 2014
	Urinary system		Mickle et al., 2019
	Pain		Samineni et al., 2017; Harriott et al., 2021
	Vision		Berry et al., 2019; Gilhooley et al., 2021
	Memory		Vetere et al., 2019

starving mice by activating or inhibiting specific neurons using optogenetics (Jennings et al., 2015; **Table 1** and **Figure 2**). In this study, the researchers introduced light-sensitive proteins that control the activity of neurons into the lateral hypothalami-ventral tegmental region (VTA) and activated the region with light, causing already satiated mice to take longer to eat.

In another study, Sternson et al. successfully distinguished appetitive behavior (Sternson and Atasoy, 2014) from neurons that satisfy behavior (Atasoy et al., 2012; Gatto and Goulding, 2018). In the study, the mice were given food freely or a reward for completing a task. Neuronal activity in the lateral hypothalamus of mice was also imaged. Based on this study, researchers were able to identify the neural basis of compulsive eating.

In 2021, the researchers used an AVV virus vector to deliver the ChR2 light-sensitive protein gene to a specific vagus nerve in the stomach (Kim et al., 2021; **Table 1** and **Figure 2**). By using a tiny LED was inserted into the end of a flexible shaft

in the stomach. Mice were successfully induced to feel full by external stimulation of specific gastric vagus nerve with remote radio frequency source. In 2022, researchers used optogenetics to inhibit neuropod cells in mice intestinal mucosa and found that mice consumed less sucrose (Buchanan et al., 2022). These studies suggest that optogenetics has a role to play in understanding the neural circuit of compulsive feeding.

Social Behavioral Neural Circuits

Social behavior is one of the characteristics of biology, but the social behavior neural circuits of biology is hardly understood. But through optogenetics, scientists are unraveling the mysteries of biological social behavior. Chiang and his colleagues developed an automatic laser tracking and optogenetic manipulation system (Hsiao et al., 1408; Wu et al., 2014) (ALTOMS) that can be used to study the social memory of fruit flies. After the expression of photosensitive proteins in neurons at specific sites, neurons involved in pain expression photosensitive pathways can be activated when laser irradiation is applied to specific sites (Karim et al., 2006; **Table 1** and **Figure 2**). Using the system, the researchers were able to get certain males to quickly learn to avoid females, while other males continued to approach. At the same time, automated laser tracking and optogenetic manipulation systems (ALTOMS) (Hsiao et al., 1408; Wu et al., 2014) are expected to help identify the neural circuits responsible for specific drosophila behavior and understand the circuitry behind the ability to form memories based on social interaction learning.

In the latest study, researchers implanted tiny wireless optogenetic electronic devices into the brains of mice. The synchrony between brain neurons in the medial prefrontal cortex of mice induced social preference in mice (Yang Y. et al., 2021; **Table 1** and **Figure 2**). The micro technique used in this study was less invasive and had less effect on the natural behavior of mice. Now, optogenetics not only controls the behavior of rodents but also primates (Rajalingham et al., 2021). These studies demonstrates the broad application of optogenetics in human social behavior circuits.

Body Temperature Regulating Neural Circuits

Thermoregulation is important for many life activities (Davison, 1976). Human beings have known for the last century that the thermoregulatory center is located in the hypothalamus (Hamilton and Ciaccia, 1971), but it is difficult to use traditional methods to analyze the thermoregulatory mechanism. In order to elucidate the neurons and neural circuits of hypothalamus involved in body temperature regulation, relevant researchers used optogenetics combined with physiological calcium signal recording (Tretyn, 1999) and other means to conduct experiments from the level of neural circuits on the hypothalamus of mice (Zhao et al., 2017). This study found neurons in the preoptic region of the hypothalamus that regulate thermally driven cooling behavior, as well as neurons in the dorsolateral part of the dorsolateral part of the hypothalamus responsible for the thermogenesis mechanism caused by cold stimulation. By using optogenetics to activate vLPO neurons, the researchers found that vLPO neurons are at the core neuron in thermoregulatory neural circuit (**Table 1** and **Figure 2**; Zhao et al., 2017). In addition, a new marker for heat-sensitive neurons, brain-derived neurotrophic factor (BDNF), was identified (Ciszowski et al., 2016). This study provides new clues for physiological and pathological research based on thermoregulation.

Spatial Learning and Memory Circuits

Using techniques such as optogenetics, single synapse tracing (Spreafico et al., 1981) and *in vivo* multi-channel electrophysiological recording (Brozoski et al., 2006), the researchers found that the excitatory pyramidal cells of the entorhinal cortex (ECIIPN) (Shu et al., 2016) formed a single synaptic connection(eciipn-ca1pv synapses) with the inhibitory small abruption protein cells of the hippocampus CA1 region (CA1PV) (Shu et al., 2016; Yang et al., 2018). In the transgenic mouse model of Alzheimer's disease, this memory loop is selectively damaged (Yang et al., 2018). Researchers used optogenetics stimulation therapy to repair eciipn-ca1pv synaptic degeneration damage and effectively treat memory loss in Alzheimer's disease (**Table 1** and **Figure 2**). This experiment proves that this loop is involved in regulating spatial learning and memory (Yang et al., 2018). In another study, researchers combined optogenetic technology with multi-channel synchronous optical stimulation and electrical recording technology, and found a circuit of emotional influence on spatial learning and memory in terms of structure and function (Zhang et al., 2017). Vahaba et al. (2017) used optogenetics to manipulate the NIF and HVC regions in the brains of zebra finches (Spierings and ten Cate, 2014). By controlling the interaction of these two regions, the researchers managed to encode the finches' memories (Vahaba et al., 2017). Huang et al. (2021) (**Table 1** and **Figure 2**), Huang et al. treated mice with phototherapy and recorded the potential changes in the hippocampal CA1 region of mice. The results showed that light therapy improved spatial memory and was associated with changes in the activity patterns of hippocampal neurons. These studies on spatial learning and memory could provide insights into the treatment of Alzheimer's disease and some psychiatric disorders.

Neural Circuit Mechanisms That Activate Addictive Memory

Drug addiction (Martinez-Gonzalez et al., 2016; Xu et al., 2021) is an abnormal learning and memory process. Withdrawal scenarios can reactivate the addictive memory when the patient enters a scene that was previously associated with withdrawal symptoms (Hellemans et al., 2006). According to previous studies, the basolateral amygdala (BLA) plays an important role in inducing addictive memory retrieval (Wang et al., 2014; Khakpoor et al., 2016; Yi et al., 2021). However, its downstream neural circuits remain unknown. In this study, researchers combined neural tracer, optogenetics, chemical genetics and other methods. It was found that after activation of BLA -PrL loop, PrL was induced to transmit information back to BLA by projecting neurons, so as to activate the increase of Arc protein expression level in another group of BLA neurons and cause the recall of addictive memory (**Table 1** and **Figure 2**; Alaghband et al., 2014). The study revealed the important role of

the prefrontal cortex as a hub of the neural circuits in reactivating addictive memories in withdrawal scenarios, providing support for the treatment of drug addiction.

NERVOUS SYSTEM-BASED CLINICAL RESEARCH

Central Nervous System

Alzheimer's Disease

Currently, none of the drugs used to improve cognitive function can fundamentally treat Alzheimer's disease, but can only alleviate the symptoms. In 2016, Roy's team successfully restored memory in mice using optogenetics (**Table 1** and **Figure 3**; Roy et al., 2016). In the study, the researchers implanted light-sensitive proteins into the hippocampus of mice with memory loss. In response to light, memory cells in the hippocampus of the mice were activated. The next day, without light, the mice lost their memory again. As shown in the study, the hippocampus of the memory recovery mice established a strong connection with the entorhinal cortex (Meda et al., 2013) which is missing in Alzheimer's patients (Liu and Zhang, 2019; Vallee et al., 2020). Another study used optogenetics stimulation therapy to repair eciipn-ca1pv synaptic degeneration damage and effectively treat memory damage caused by Alzheimer's disease (**Figure 3**; Yang et al., 2018). At the same time, an important research achievement in Alzheimer's disease is the treatment of cognitive dysfunction with near-infrared bioluminescence (Saltmarche et al., 2017; Arenas et al., 2020). Up to now, many studies have demonstrated that near-infrared bioluminescence therapy can improve cognitive function (Chao, 2019; Kinouchi et al., 2021). The above research may provide ideas for the radical cure of Alzheimer's disease.

Parkinson's Disease

Parkinson's disease is a chronic disease with no clinical cure (Guo et al., 2019; Altinoz et al., 2020). However, Parkinson's disease can be alleviated and treated with optogenetics. Ztaou et al. (2016) found that bilateral activation of indirect pathway MSNs by optogenetics can produce Parkinson's-like presentation. However, activation of MSNs in the direct pathway alleviates symptoms such as freezing, bradykinesia, and difficulty in initiating movement (Kravitz et al., 2010; de Almeida and da Silva, 2021; Malaquias et al., 2021; Yang X. et al., 2021). Yang et al. (2018) found that the use of optogenetics combined with deep brain stimulation (DBS) (Castano-Candamil et al., 2019) to stimulate the afferent axons of the subthalamic nucleus region at high frequency can significantly treat Parkinson's disease (**Table 1** and **Figure 3**). Carter et al. (2010) used optogenetic targeting to control the LC-NE region of the cerebral cortex of mice, and were able to treat sleep disorders in mice with Parkinson's disease (**Figure 3**). Steinbeck et al. (2015) induced rapid and reversible reactivation of motor defects in mice that had recovered from Parkinson's motor defects induced by injury (**Figure 3**). And a recent study showed that photogenetic stimulation of the deep brain can relieve Parkinson's disease in rats (Ingram et al., 2020; Yu et al., 2020). These studies suggest that optogenetics has great potential in the clinical treatment of Parkinson's disease.

Epilepsy

More than 20% of epileptic patients develop stubborn resistance to epileptic drugs (Zhou et al., 2013; Murawiec et al., 2020), which eventually develops into refractory epilepsy (Martinez-Juarez et al., 2012; Tsai et al., 2021). The researchers injected green light-emitting nanoparticles into the hippocampus of mice (Roet et al., 2019), and irradiated the cranium surface with infrared light, and found that the epileptic neurons of mice were effectively silenced (**Table 1** and **Figure 3**; Chen et al., 2018). The nanoparticles used in this experiment are stable, biocompatible and can be used for a long time. Lu et al. (2016) conducted *in vivo* and *in vitro* experiments, and the excitatory photosensitive protein was expressed in inhibitory neurons to inhibit epileptoid activity up to 70.0 and 82.4%, respectively. These studies indicate that optogenetic techniques are superior to other methods in the treatment of epilepsy.

Stroke

Cerebral apoplexy (Ng et al., 2019) is caused by the obstruction of blood flow to the brain tissues caused by vascular obstruction, which often occurs suddenly, with such symptoms as fainting, hemiplegia, and slant of the tongue, with a high mortality and disability rate. There is still a lack of effective treatment drugs, and transplantation of nerve progenitor cells is a good way to restore the function of nerve neurons in the brain (Cabral-Costa and Kowaltowski, 2020; Ostolaza et al., 2020; Roy-O'Reilly et al., 2020). Yu et al. (2019) provided luciferin CTZ to the brain of mice by intranasal administration (**Table 1**). When CTZ encounters luminescent proteins, it emits the required light. This study showed that survival rates for the growth and differentiation of neural progenitor cells increased significantly, more intact axons and nerve connections were produced, and better responses to electrical stimulation were achieved. The affected limb also showed better recovery. In young mice, stroke affected limb function was restored to normal levels, and even in older mice, stroke symptoms were partially recovered (**Table 1** and **Figure 3**). The findings offer hope for an effective treatment for stroke.

Memory

A memory can bring either pleasure or fear (Kirmayer et al., 1995; Riksen and Netea, 2020). And relevant neurobiological studies have shown that an experience can cause changes in multiple brain areas, such as the cerebral cortex, hippocampus and amygdala, thus producing memory (Josselyn et al., 2015). In the following studies, optogenetics can manipulate memories and erase bad memories by manipulating neurons in the brain. In 2014, researchers successfully removed and reactivated a certain memory by changing the connections of related neurons in the brain of rats with different frequencies of light (**Table 1** and **Figure 3**; Nabavi et al., 2014). In 2017, researchers used optogenetic technology in conjunction with electrophysiological technology and behavioral experiments (Ishikawa and Sakaguchi, 2013) to study the role of specific neural pathways in fear memory (Klavir et al., 2017; Yilmaz et al., 2020). In 2019, relevant studies

for the first time found the subgroup of neurons that regulate the new memory of fear extinction, which improved people's cognition of fear memory (Lacagnina et al., 2019). Also, in 2019, people used optogenetic methods to manipulate memory-related neurons to encode memory imprinting without experience for the first time (**Table 1** and **Figure 3**; Vetere et al., 2019). The above research indicates that optogenetics plays an important role in the study of the mechanism of memory generation and memory-related diseases.

Peripheral Nervous System

Skeletal System

In the past, electric stimulation was often used for patients who lost motor function, and the electric stimulation treatment was prone to muscle fatigue and inaccurate discharge (Asakawa et al., 2021). However, optogenetics can stimulate a certain muscle fiber accurately and with low trauma, which can be used to study the treatment of motor system injury. In 2010, researchers started to apply optogenetics to the treatment of motor impairment (**Table 1** and **Figure 3**). Llewellyn et al. (2010) utilized light stimulation of muscle fibers, and after 20 min of light stimulation of muscle fibers, the muscle still maintained a third of the maximum stress (**Table 1** and **Figure 3**). Bryson et al. (2014) constructed a mouse model of muscle loss innervation and transplanted the embryoid containing ChR2 motor neurons into the mouse. By shining blue light on the transplant site, the researchers were able to restore leg muscle function (**Table 1** and **Figure 3**). Srinivasan et al. (2018) used tiny LED lights to control light-sensitive proteins expressed in the legs of mice. The study succeeded in controlling ankle movement in mice. These studies suggest that optogenetics has great potential in controlling biological motor systems, especially in the treatment of paralysis and the treatment of muscle degeneration.

Urinary System

Related researchers developed a full closed-loop optogenetic control system (Mickle et al., 2019) and implanted it into female mice with drug-induced bladder dysfunction. This system can detect bladder filling, and the system can also irradiate the bladder for optogenetic control (Kessler et al., 2019). Shown in the study, photosensitive proteins are expressed in nerve cells of the bladder in mice by optogenetics technique, which makes the neurons in the bladder of mice in a hyperpolarized state. For 7 days after the system was implanted, the mice did well. Finally, the rats returned to normal bladder function (**Table 1** and **Figure 3**; Mickle et al., 2019). Through further research and testing, this method is of clinical value.

Pain

Pain is one of the common clinical symptoms. Prolonged severe pain can seriously affect the patient's quality of life. At present, photogenetic technology can solve the pain problem very well. In 2017, a new in-spinal optogenetics device was used for pain treatment and research (**Table 1** and **Figure 3**; Samineni et al., 2017; Mai et al., 2020). Using this device, the researchers activated the afferent nerve of trpv1-chr2 channel protein, causing pain response behavior in mice (Jacob and Szerb, 1951; Zhu et al., 2020; Ji et al., 2021; Zhang et al., 2021). The researchers then ran a real-time comparison experiment, and the results were the same. Now that the device's function is clear, it can be widely used in pain research. Another study used the selective silencing of related neurons by a wirelessly controlled electro-optical system to reduce ongoing pain and induced skin allergic reactions in mice under cystitis conditions (**Table 1** and **Figure 3**; Samineni et al., 2017). And it had no bad effect on the mice. Hua et al. (2020) discovered a class of inhibitory neurons called "CeAga." It turns off pain. Inhibition of the expression of CeAga neurons by optogenetics stopped the pain behavior in mice (Mai et al., 2020). Due to its high accuracy and low side effects, optogenetics may be widely used in the field of pain in the near future.

Vision

Special neurons in the retina react to light and transmit it to the brain to produce vision (Pozarickij et al., 2020; Creeden et al., 2021; Liu H. et al., 2021; Yu et al., 2021; Elkhalifa et al., 2022). When neurons in the retina stop working properly, the eye can't work properly. Nowadays, optogenetic can be used to treat eye diseases such as color blindness (**Table 1** and **Figure 3**; Cideciyan et al., 2016). The researchers sensitized the cells to light by the expression of light genes that encode light-activated channels or pumps in the remaining retinal cells (Ostrovsky and Kirpichnikov, 2019; Blomeier et al., 2021; He et al., 2021; Kramer et al., 2021; Mickoleit et al., 2021). Relevant research has achieved good results in recent years. In 2017, Russian scientists injected drugs with certain genetic structure into the blind eyes of experimental rodents, and the sight of experimental animals was partially restored (Aung et al., 2017). Berry et al. (2019) restored vision to blind mice (**Table 1** and **Figure 3**). In 2021, the company of Bionic Sight successfully used optogenetics to enable patients with advanced retinitis pigmentosa to see light and motion (Harris and Gilbert, 2022).

CONCLUSION, CHALLENGES AND PERSPECTIVES

Since the advent of optogenetics, the technology has occupied the research field of neurobiology. Using optogenetics, researchers have decoded many neural circuits that cannot be decoded with other techniques. Such as social behavioral neural circuits, body temperature regulating neural circuits, spatial learning and memory circuits and so on. In view of the minimally invasive and high accuracy of optogenetics, optogenetics has a broad prospect in clinical treatment. Many irreversible diseases, especially neurodegenerative changes, can be solved by optogenetics. And the related research has entered the clinical trial stage.

Although optogenetics has achieved a lot in many fields, it still faces many challenges. Many scientists have proposed that exogenous light exposure causes neurons to respond in a non-physiological way, leading to incorrect physiological conclusions (Oh et al., 2021). And whether exogenous photosensitive proteins can have potential effects on nerve cells. Due to economic and other factors, optogenetics is mostly used in mouse experiments. Clinical trials of optogenetics are rare. Therefore,

it will take a long time to prove that optogenetics can be widely applied to humans.

At present, optogenetics continues to flourish. Photogenetic treatments for retinal degeneration (Cehajic-Kapetanovic et al., 2019; Gilhooley et al., 2021) and pain (Harriott et al., 2021) are also in clinical trials. Researchers are also developing more precise (Adesnik and Abdeladim, 2021) and less invasive optogenetic devices, such as SOUL (Gong et al., 2020). At the same time, optogenetics has strong compatibility, it can be used to study a variety of diseases, such as diabetes (Li et al., 2021), inflammation (Baumschlager and Khammash, 2021; Bhat et al., 2021; Dos Santos et al., 2021; Jamaluddin et al., 2021; Michoud et al., 2021; Santos et al., 2021; Senok et al., 2021), tumors (Kim et al., 2017; Adampourezare et al., 2021; Esmaeili et al., 2022), depression (Hare et al., 2019), epilepsy (Zhang and Wang, 2021) and so on. And in 2020, 45 laboratories around the world integrated all optogenetics resources and create an optogenetics experimental database (Tremblay et al., 2020). According to the current progress, optogenetics has a broad prospect. It is believed that soon, optogenetics will become a major technique in neurobiology.

AUTHOR CONTRIBUTIONS

XZ and ZL designed this study and supervised the research. WC wrote the manuscript. WL, YLi, ZZ, YX, YLiao, LY, QL, and MH discussed the manuscript. CL, ZL, and XZ edited the manuscript. All authors read and approved the final manuscript.

FUNDING

This work was supported partly by the National Natural Science Foundation of China (81972366), Guangdong Key Laboratory funds of Systems Biology and Synthetic Biology for Urogenital Tumors (2017B030301015), and its Open Grant (2021B030301015-3).

REFERENCES

Adamantidis, A., Arber, S., Bains, J. S., Bamberg, E., Bonci, A., Buzsaki, G., et al. (2015). Optogenetics: 10 years after ChR2 in neurons–views from the community. *Nat. Neurosci.* 18, 1202–1212. doi: 10.1038/nn.4106

Adampourezare, M., Dehghan, G., Hasanzadeh, M., and Hosseinpoure Feizi, M. A. (2021). Application of lateral flow and microfluidic bio-assay and biosensing towards identification of DNA-methylation and cancer detection: recent progress and challenges in biomedicine. *Biomed Pharmacother* 141:111845. doi: 10.1016/j.biopha.2021.111845

Adesnik, H., and Abdeladim, L. (2021). Probing neural codes with two-photon holographic optogenetics. *Nat Neurosci* 24, 1356–1366. doi: 10.1038/s41593-021-00902-9

Alaghband, Y., O'Dell, S. J., Azarnia, S., Khalaj, A. J., Guzowski, J. F., and Marshall, J. F. (2014). Retrieval-induced NMDA receptor-dependent arc expression in two models of cocaine-cue memory. *Neurobiol. Learn. Mem.* 116, 79–89. doi: 10.1016/j.nlm.2014.09.001

Altinoz, M. A., Elmaci, I., Hacimuftuoglu, A., Ozpinar, A., Hacker, E., and Ozpinar, A. (2020). PPARdelta and its ligand erucic acid may act anti-tumoral, neuroprotective, and myelin protective in neuroblastoma, glioblastoma, and Parkinson's disease. *Mol. Aspects Med.* 2020:100871. doi: 10.1016/j.mam.2020.100871

Amitrano, A. M., Berry, B. J., Lim, K., Kim, K. D., Waugh, R. E., Wojtovich, A. P., et al. (2021). Optical control of CD8(+) T cell metabolism and effector functions. *Front. Immunol.* 12:666231. doi: 10.3389/fimmu.2021.666231

Aquili, L., Liu, A. W., Shindou, M., Shindou, T., and Wickens, J. R. (2014). Behavioral flexibility is increased by optogenetic inhibition of neurons in the nucleus accumbens shell during specific time segments. *Learn Mem.* 21, 223–231. doi: 10.1101/lm.034199.113

Arenas, F., Castro, F., Nunez, S., Gay, G., Garcia-Ruiz, C., and Fernandez-Checa, J. C. (2020). STARD1 and NPC1 expression as pathological markers associated with astrogliosis in post-mortem brains from patients with Alzheimer's disease and down syndrome. *Aging* 12, 571–592. doi: 10.18632/aging.102641

Asakawa, K., Handa, H., and Kawakami, K. (2021). Illuminating ALS motor neurons with optogenetics in zebrafish. *Front. Cell Dev. Biol.* 9:640414. doi: 10.3389/fcell.2021.640414

Atasoy, D., Betley, J. N., Su, H. H., and Sternson, S. M. (2012). Deconstruction of a neural circuit for hunger. *Nature* 488, 172–177. doi: 10.1038/nature11270

Aung, T., Ozaki, M., Lee, M. C., Schlotzer-Schrehardt, U., Thorleifsson, G., Mizoguchi, T., et al. (2017). Genetic association study of exfoliation syndrome identifies a protective rare variant at LOXL1 and five new susceptibility loci. *Nat. Genet.* 49, 993–1004. doi: 10.1038/ng.3875

Baumschlager, A., and Khammash, M. (2021). Synthetic biological approaches for optogenetics and tools for transcriptional light-control in bacteria. *Adv. Biol.* 5:e2000256. doi: 10.1002/adbi.202000256

Berry, M. H., Holt, A., Salari, A., Veit, J., Visel, M., Levitz, J., et al. (2019). Restoration of high-sensitivity and adapting vision with a cone opsin. *Nat. Commun.* 10:1221. doi: 10.1038/s41467-019-09124-x

Bhat, S. V., Price, J. D. W., and Dahms, T. E. S. (2021). AFM-based correlative microscopy illuminates human pathogens. *Front. Cell Infect. Microbiol.* 11:655501. doi: 10.3389/fcimb.2021.655501

Blomeier, T., Fischbach, P., Koch, L. A., Andres, J., Minambres, M., Beyer, H. M., et al. (2021). Blue light-operated CRISPR/Cas13b-mediated mRNA knockdown (lockdown). *Adv. Biol.* 5:e2000307. doi: 10.1002/adbi.202000307

Boyden, E. S., Zhang, F., Bamberg, E., Nagel, G., and Deisseroth, K. (2005). Millisecond-timescale, genetically targeted optical control of neural activity. *Nat. Neurosci.* 8, 1263–1268. doi: 10.1038/nn1525

Broder, H. L., Tormeti, D., Kurtz, A. L., Baah-Odoom, D., Hill, R. M., Hirsch, S. M., et al. (2014). Type II diabetes and oral health: perceptions among adults with diabetes and oral/health care providers in Ghana. *Commun. Dent Health* 31, 158–162.

Brozoski, T. J., Caspary, D. M., and Bauer, C. A. (2006). Marking multi-channel silicon-substrate electrode recording sites using radiofrequency lesions. *J. Neurosci. Methods* 150, 185–191. doi: 10.1016/j.jneumeth.2005.06.012

Bryson, J. B., Machado, C. B., Crossley, M., Stevenson, D., Bros-Facer, V., Burrone, J., et al. (2014). Optical control of muscle function by transplantation of stem cell-derived motor neurons in mice. *Science* 344, 94–97. doi: 10.1126/science.1248523

Buchanan, K. L., Rupprecht, L. E., Kaelberer, M. M., Sahasrabudhe, A., Klein, M. E., Villalobos, J. A., et al. (2022). The preference for sugar over sweetener depends on a gut sensor cell. *Nat. Neurosci.* 25, 191–200. doi: 10.1038/s41593-021-00982-7

Cabral-Costa, J. V., and Kowaltowski, A. J. (2020). Neurological disorders and mitochondria. *Mol. Aspects Med.* 71:100826. doi: 10.1016/j.mam.2019.10.003

Cardi, V., Mallorqui-Bague, N., Albano, G., Monteleone, A. M., Fernandez-Aranda, F., and Treasure, J. (2018). Social difficulties as risk and maintaining factors in anorexia nervosa: a mixed-method investigation. *Front. Psychiatry* 9:12. doi: 10.3389/fpsyt.2018.00012

Cardin, J. A., Carlen, M., Meletis, K., Knoblich, U., Zhang, F., Deisseroth, K., et al. (2009). Driving fast-spiking cells induces gamma rhythm and controls sensory responses. *Nature* 459, 663–667. doi: 10.1038/nature08002

Carter, M. E., Yizhar, O., Chikahisa, S., Nguyen, H., Adamantidis, A., Nishino, S., et al. (2010). Tuning arousal with optogenetic modulation of locus coeruleus neurons. *Nat. Neurosci.* 13, 1526–1533. doi: 10.1038/nn.2682

Castano-Candamil, S., Piroth, T., Reinacher, P., Sajonz, B., Coenen, V. A., and Tangermann, M. (2019). An easy-to-use and fast assessment of patient-specific DBS-induced changes in hand motor control in Parkinson's disease. *IEEE Trans. Neural. Syst. Rehabil. Eng.* 27, 2155–2163. doi: 10.1109/TNSRE.2019.2941453

Cehajic-Kapetanovic, J., Birtel, J., McClements, M. E., Shanks, M. E., Clouston, P., Downes, S. M., et al. (2019). Clinical and molecular characterization of PROM1-related retinal degeneration. *JAMA Netw Open* 2:e195752. doi: 10.1001/jamanetworkopen.2019.5752

Chao, L. L. (2019). Effects of home photobiomodulation treatments on cognitive and behavioral function, cerebral perfusion, and resting-state functional connectivity in patients with dementia: a pilot trial. *Photobiomodul Photomed Laser Surg* 37, 133–141. doi: 10.1089/photob.2018.4555

Chen, S., Weitemier, A. Z., Zeng, X., He, L., Wang, X., Tao, Y., et al. (2018). Near-infrared deep brain stimulation via upconversion nanoparticle-mediated optogenetics. *Science* 359, 679–684. doi: 10.1126/science.aaq1144

Cideciyan, A. V., Roman, A. J., Jacobson, S. G., Yan, B., Pascolini, M., Charng, J., et al. (2016). Developing an outcome measure with high luminance for optogenetics treatment of severe retinal degenerations and for gene therapy of cone diseases. *Invest. Ophthalmol. Vis. Sci.* 57, 3211–3221. doi: 10.1167/iovs.16-19586

Ciszowski, K., Gomolka, E., Gawlikowski, T., Szpak, D., Potoczek, A., and Boba, M. (2016). [Brain-derived neurotrophic factor (BDNF) and nerve growth factor (NGF) blood levels in patients with acute carbon monoxide poisoning - a preliminary observations]. *Przegl. Lek* 73, 552–559.

Creeden, J. F., Imami, A. S., Eby, H. M., Gillman, C., Becker, K. N., Reigle, J., et al. (2021). Fluoxetine as an anti-inflammatory therapy in SARS-CoV-2 infection. *Biomed. Pharmacother* 138:111437. doi: 10.1016/j.biopha.2021.111437

Davison, J. (1976). Hydra hymanae: regulation of the life cycle by time and temperature. *Science* 194, 618–620. doi: 10.1126/science.982029

de Almeida, W. S., and da Silva, D. A. (2021). Does polysaccharide quaternization improve biological activity? *Int. J. Biol. Macromol.* 182, 1419–1436. doi: 10.1016/j.ijbiomac.2021.05.012

Di Ventura, B., and Weber, W. (2021). The rise of molecular optogenetics. *Adv. Biol.* 5:e2100776. doi: 10.1002/adbi.202100776

Dos Santos, A. G. A., da Silva, M. G. L., Carneiro, E. L., de Lima, L. L., Fernandes, A., Silveira, T. G. V., et al. (2021). A new target organ of leishmania (viannia) braziliensis chronic infection: the intestine. *Front. Cell Infect. Microbiol.* 11:687499. doi: 10.3389/fcimb.2021.687499

Elkhalifa, D., Rayan, M., Negmeldin, A. T., Elhissi, A., and Khalil, A. (2022). Chemically modified mRNA beyond COVID-19: Potential preventive and therapeutic applications for targeting chronic diseases. *Biomed. Pharmacother* 145:112385. doi: 10.1016/j.biopha.2021.112385

Esmaeili, Y., Khavani, M., Bigham, A., Sanati, A., Bidram, E., Shariati, L., et al. (2022). Mesoporous silica@chitosan@gold nanoparticles as "on/off" optical biosensor and pH-sensitive theranostic platform against cancer. *Int. J. Biol. Macromol.* 202, 241–255. doi: 10.1016/j.ijbiomac.2022.01.063

Fan, W., Mai, L., Zhu, X., Huang, F., and He, H. (2020). The role of microglia in perioperative neurocognitive disorders. *Front. Cell Neurosci.* 14:261.

Gao, G., Fan, C., Li, W., Liang, R., Wei, C., Chen, X., et al. (2021a). Mesenchymal stem cells: ideal seeds for treating diseases. *Hum. Cell.* 34, 1585–1600.

Gao, G., Li, C., Fan, W., Zhang, M., Li, X., Chen, W., et al. (2021b). Brilliant glycans and glycosylation: seq and ye shall find. *Int. J. Biol. Macromol.* 189, 279–291. doi: 10.1016/j.ijbiomac.2021.08.054

Gatto, G., and Goulding, M. (2018). Locomotion control: brainstem circuits satisfy the need for speed. *Curr. Biol.* 28, R256–R259. doi: 10.1016/j.cub.2018.01.068

Geerling, J. C., and Loewy, A. D. (2008). Central regulation of sodium appetite. *Exp. Physiol.* 93, 177–209. doi: 10.1113/expphysiol.2007.039891

Gilhooley, M. J., Hickey, D. G., Lindner, M., Palumaa, T., Hughes, S., Peirson, S. N., et al. (2021). ON-bipolar cell gene expression during retinal degeneration: implications for optogenetic visual restoration. *Exp. Eye Res.* 207:108553. doi: 10.1016/j.exer.2021.108553

Gjaltema, R. A. F., and Schulz, E. G. (2018). CRISPR/dCas9 switch systems for temporal transcriptional control. *Methods Mol. Biol.* 1767, 167–185. doi: 10.1007/978-1-4939-7774-1_8

Gong, X., Mendoza-Halliday, D., Ting, J. T., Kaiser, T., Sun, X., Bastos, A. M., et al. (2020). An ultra-sensitive step-function opsin for minimally invasive optogenetic stimulation in mice and macaques. *Neuron* 107:e8.

Guo, H. M., Zhou, Z. Y., Huang, Y. Q., Li, X., and Wang, X. J. (2019). Investigation of the roles of dysbindin-1 and SATB2 in the progression of Parkinson's disease. *Eur. Rev. Med. Pharmacol. Sci.* 23, 7510–7516. doi: 10.26355/eurrev_201909_18865

Hallett, R. A., Zimmerman, S. P., Yumerefendi, H., Bear, J. E., and Kuhlman, B. (2016). Correlating *in vitro* and *in vivo* activities of light-inducible dimers: a cellular optogenetics guide. *ACS Synth. Biol.* 5, 53–64. doi: 10.1021/acssynbio.5b00119

Hamilton, C. L., and Ciaccia, P. J. (1971). Hypothalamus, temperature regulation, and feeding in the rat. *Am. J. Physiol.* 221, 800–807. doi: 10.1152/ajplegacy.1971.221.3.800

Han, W., Tellez, L. A., Rangel, M. J. Jr., Motta, S. C., Zhang, X., Perez, I. O., et al. (2017). Integrated control of predatory hunting by the central nucleus of the amygdala. *Cell* 168:e18. doi: 10.1016/j.cell.2016.12.027

Hare, B. D., Shinohara, R., Liu, R. J., Pothula, S., DiLeone, R. J., and Duman, R. S. (2019). Optogenetic stimulation of medial prefrontal cortex Drd1 neurons produces rapid and long-lasting antidepressant effects. *Nat. Commun.* 10:223. doi: 10.1038/s41467-018-08168-9

Harriott, A. M., Chung, D. Y., Uner, A., Bozdayi, R. O., Morais, A., Takizawa, T., et al. (2021). Optogenetic spreading depression elicits trigeminal pain and anxiety behavior. *Ann. Neurol.* 89, 99–110. doi: 10.1002/ana.25926

Harris, A. R., and Gilbert, F. (2022). Restoring vision using optogenetics without being blind to the risks. *Graefes Arch. Clin. Exp. Ophthalmol.* 260, 41–45. doi: 10.1007/s00417-021-05477-6

He, L., Tan, P., Huang, Y., and Zhou, Y. (2021). Design of smart antibody mimetics with photosensitive switches. *Adv. Biol.* 5:e2000541. doi: 10.1002/adbi.202000541

Hellemans, K. G., Everitt, B. J., and Lee, J. L. (2006). Disrupting reconsolidation of conditioned withdrawal memories in the basolateral amygdala reduces suppression of heroin seeking in rats. *J. Neurosci.* 26, 12694–12699. doi: 10.1523/JNEUROSCI.3101-06.2006

Hemmati, S., Behzadipour, Y., and Haddad, M. (2020). Decoding the proteome of severe acute respiratory syndrome coronavirus 2 (SARS-CoV-2) for cell-penetrating peptides involved in pathogenesis or applicable as drug delivery vectors. *Infect Genet. Evol.* 85:104474. doi: 10.1016/j.meegid.2020.104474

Hori, Y., and Kikuchi, K. (2019). Chemical tools with fluorescence switches for verifying epigenetic modifications. *Acc. Chem. Res.* 52, 2849–2857. doi: 10.1021/acs.accounts.9b00349

Hosseinpanah, F., Serahati, S., Barzin, M., Aryannezhad, S., Rezaie, M., Valizadeh, M., et al. (2019). Trends of obesity in 10-years of follow-up among tehranian children and adolescents: tehran lipid and glucose study (TLGS). *Iran J. Public Health* 48, 1714–1722.

Hsiao, P. Y., Wu, M. C., Lin, Y. Y., Fu, C. C., and Chiang, A. S. (1408). Optogenetic manipulation of selective neural activity in free-moving drosophila adults. *Methods Mol. Biol.* 37:2016. doi: 10.1007/978-1-4939-3512-3_26

Hua, T., Chen, B., Lu, D., Sakurai, K., Zhao, S., Han, B. X., et al. (2020). General anesthetics activate a potent central pain-suppression circuit in the amygdala. *Nat. Neurosci.* 23, 854–868. doi: 10.1038/s41593-020-0632-8

Huang, X., Huang, P., Huang, L., Hu, Z., Liu, X., Shen, J., et al. (2021). A visual circuit related to the nucleus reuniens for the spatial-memory-promoting effects of light treatment. *Neuron* 109, 347–362e7. doi: 10.1016/j.neuron.2020.10.023

Ingram, T. L., Shephard, F., Sarmad, S., Ortori, C. A., Barrett, D. A., and Chakrabarti, L. (2020). Sex specific inflammatory profiles of cerebellar mitochondria are attenuated in Parkinson's disease. *Aging* 12, 17713–17737. doi: 10.18632/aging.103937

Ishikawa, T., and Sakaguchi, Y. (2013). Both movement-end and task-end are critical for error feedback in visuomotor adaptation: a behavioral experiment. *PLoS One* 8:e55801. doi: 10.1371/journal.pone.0055801

Jacob, J., and Szerb, J. (1951). [Effect of various alarm stimuli on reaction to pain in mice]. *Arch. Int. Pharmacodyn Ther.* 87, 251–253.

Jamaluddin, N. D., Mazlan, N. F., Tan, L. L., Yusof, N. Y. M., and Khalid, B. (2021). G-quadruplex microspheres-based optical RNA biosensor for arthropod-borne virus pathogen detection: a proof-of-concept with dengue serotype 2. *Int. J. Biol. Macromol.* 199, 1–9. doi: 10.1016/j.ijbiomac.2021.12.047

Jennings, J. H., Ung, R. L., Resendez, S. L., Stamatakis, A. M., Taylor, J. G., Huang, J., et al. (2015). Visualizing hypothalamic network dynamics for appetitive and consummatory behaviors. *Cell* 160, 516–527. doi: 10.1016/j.cell.2014.12.026

Ji, J., He, Q., Luo, X., Bang, S., Matsuoka, Y., McGinnis, A., et al. (2021). IL-23 enhances C-fiber-mediated and blue light-induced spontaneous pain in female mice. *Front. Immunol.* 12:787565. doi: 10.3389/fimmu.2021.787565

Josselyn, S. A., Kohler, S., and Frankland, P. W. (2015). Finding the engram. *Nat. Rev. Neurosci.* 16, 521–534. doi: 10.1038/nrn4000

Karim, F., Hu, H. J., Adwanikar, H., and Kaplan, D. (2006). Gereau RWt: impaired inflammatory pain and thermal hyperalgesia in mice expressing neuron-specific dominant negative mitogen activated protein kinase kinase (MEK). *Mol. Pain* 2:2. doi: 10.1186/1744-8069-2-2

Kessler, T. M., Birder, L. A., and Gomery, P. (2019). Neuromodulation of urinary tract function. *New Engl. J. Med.* 380, 2067–2069.

Khakpoor, M., Nasehi, M., Vahdati, A., Hoseyni, S. E., and Zarrindast, M. R. (2016). Additive effect of BLA GABAA receptor mechanism and (+)-MK-801 on memory retention deficit, an isobologram analysis. *Pharmacol. Biochem. Behav.* 143, 57–64. doi: 10.1016/j.pbb.2016.02.001

Kim, K. D., Bae, S., Capece, T., Nedelkovska, H., de Rubio, R. G., Smrcka, A. V., et al. (2017). Targeted calcium influx boosts cytotoxic T lymphocyte function in the tumour microenvironment. *Nat. Commun.* 8:15365. doi: 10.1038/ncomms15365

Kim, W. S., Hong, S., Gamero, M., Jeevakumar, V., Smithhart, C. M., Price, T. J., et al. (2021). Organ-specific, multimodal, wireless optoelectronics for high-throughput phenotyping of peripheral neural pathways. *Nat. Commun.* 12:157. doi: 10.1038/s41467-020-20421-8

Kinouchi, K., Mikami, Y., Kanai, T., and Itoh, H. (2021). Circadian rhythms in the tissue-specificity from metabolism to immunity: insights from omics studies. *Mol. Aspects Med.* 80:100984. doi: 10.1016/j.mam.2021.100984

Kirmayer, L. J., Young, A., and Hayton, B. C. (1995). The cultural context of anxiety disorders. *Psychiatr. Clin. North Am.* 18, 503–521. doi: 10.1016/s0193-953x(18)30037-6

Klavir, O., Prigge, M., Sarel, A., Paz, R., and Yizhar, O. (2017). Manipulating fear associations via optogenetic modulation of amygdala inputs to prefrontal cortex. *Nat. Neurosci.* 20, 836–844. doi: 10.1038/nn.4523

Kramer, M. M., Muhlhauser, W. W. D., Weber, W., and Radziwill, G. (2021). Multichromatic control of signaling pathways in mammalian cells. *Adv. Biol.* 5:e2000196. doi: 10.1002/adbi.202000196

Kravitz, A. V., Freeze, B. S., Parker, P. R., Kay, K., Thwin, M. T., Deisseroth, K., et al. (2010). Regulation of parkinsonian motor behaviours by optogenetic control of basal ganglia circuitry. *Nature* 466, 622–626. doi: 10.1038/nature09159

Lacagnina, A. F., Brockway, E. T., Crovetti, C. R., Shue, F., McCarty, M. J., Sattler, K. P., et al. (2019). Distinct hippocampal engrams control extinction and relapse of fear memory. *Nat. Neurosci.* 22, 753–761. doi: 10.1038/s41593-019-0361-z

Lee, H., Kim, D. W., Remedios, R., Anthony, T. E., Chang, A., Madisen, L., et al. (2014). Scalable control of mounting and attack by Esr1+ neurons in the ventromedial hypothalamus. *Nature* 509, 627–632. doi: 10.1038/nature13169

Lee, S., Augustine, V., Zhao, Y., Ebisu, H., Ho, B., Kong, D., et al. (2019). Chemosensory modulation of neural circuits for sodium appetite. *Nature* 568, 93–97. doi: 10.1038/s41586-019-1053-2

Li, T., Chen, X., Qian, Y., Shao, J., Li, X., Liu, S., et al. (2021). A synthetic BRET-based optogenetic device for pulsatile transgene expression enabling glucose homeostasis in mice. *Nat. Commun.* 12:615. doi: 10.1038/s41467-021-20913-1

Liu, D. Y., and Zhang, L. (2019). MicroRNA-132 promotes neurons cell apoptosis and activates tau phosphorylation by targeting GTDC-1 in Alzheimer's disease. *Eur. Rev. Med. Pharmacol. Sci.* 23, 8523–8532. doi: 10.26355/eurrev_201910_19166

Liu, H., Cheng, Y., Chu, J., Wu, M., Yan, M., Wang, D., et al. (2021). Baicalin attenuates angiotensin II-induced blood pressure elevation and modulates MLCK/p-MLC signaling pathway. *Biomed. Pharmacother* 143:112124. doi: 10.1016/j.biopha.2021.112124

Liu, Y., Li, N., Zhu, X., and Qi, Y. (2021). How wide is the application of genetic big data in biomedicine. *Biomed. Pharmacother.* 133:111074. doi: 10.1016/j.biopha.2020.111074

Llewellyn, M. E., Thompson, K. R., Deisseroth, K., and Delp, S. L. (2010). Orderly recruitment of motor units under optical control *in vivo*. *Nat. Med.* 16, 1161–1165. doi: 10.1038/nm.2228

Lu, D., Huang, Y., Kong, Y., Tao, T., and Zhu, X. (2020). Gut microecology: why our microbes could be key to our health. *Biomed Pharmacother* 131:110784. doi: 10.1016/j.biopha.2020.110784

Lu, W., Yao, J., Zhu, X., and Qi, Y. (2020). Nanomedicines: redefining traditional medicine. *Biomed Pharmacother* 134:111103. doi: 10.1016/j.biopha.2020.111103

Lu, Y., Zhong, C., Wang, L., Wei, P., He, W., Huang, K., et al. (2016). Optogenetic dissection of ictal propagation in the hippocampal-entorhinal cortex structures. *Nat. Commun.* 7:10962.

Luo, P. W., Han, H. W., Yang, C. S., Shrestha, L. K., Ariga, K., and Hsu, S. H. (2019). Optogenetic modulation and reprogramming of bacteriorhodopsin-transfected human fibroblasts on self-assembled fullerene C60 nanosheets. *Adv. Biosyst.* 3:e1800254. doi: 10.1002/adbi.201800254

Mai, L., Zhu, X., Huang, F., He, H., and Fan, W. (2020). p38 mitogen-activated protein kinase and pain. *Life Sci.* 256:117885. doi: 10.1016/j.lfs.2020.117885

Malaquias, A. D. M., Marques, L. E. C., Pereira, S. S., de Freitas Fernandes, C., Maranhao, A. Q., Stabeli, R. G., et al. (2021). A review of plant-based expression systems as a platform for single-domain recombinant antibody production. *Int. J. Biol. Macromol.* 193, 1130–1137. doi: 10.1016/j.ijbiomac.2021.10.126

Martinez-Gonzalez, J. M., Vilar Lopez, R., Becona Iglesias, E., and Verdejo-Garcia, A. (2016). Self-deception as a mechanism for the maintenance of drug addiction. *Psicothema* 28, 13–19. doi: 10.7334/psicothema2015.139

Martinez-Juarez, I. E., Lopez-Zapata, R., Gomez-Arias, B., Bravo-Armenta, E., Romero-Ocampo, L., Estevez-Cruz, Z., et al. (2012). [Refractory epilepsy: use of the new definition and related risk factors. a study in the mexican population of a third-level centre]. *Rev. Neurol.* 54, 159–166.

Meda, S. A., Koran, M. E., Pryweller, J. R., Vega, J. N., and Thornton-Wells, T. A. (2013). Alzheimer's disease neuroimaging i: genetic interactions associated with 12-month atrophy in hippocampus and entorhinal cortex in Alzheimer's disease neuroimaging initiative. *Neurobiol. Aging* 34:1518.e9. doi: 10.1016/j.neurobiolaging.2012.09.020

Melero-Fernandez de Mera , R. M., Li, L. L., Popinigis, A., Cisek, K., Tuittila, M., Yadav, L., et al. (2017). A simple optogenetic MAPK inhibitor design reveals resonance between transcription-regulating circuitry and temporally-encoded inputs. *Nat. Commun.* 8:15017. doi: 10.1038/ncomms15017

Method of the year (2010). Method of the year. *Nat. Methods* 8:1. doi: 10.1038/nmeth.f.321

Michoud, F., Seehus, C., Schonle, P., Brun, N., Taub, D., Zhang, Z., et al. (2021). Epineural optogenetic activation of nociceptors initiates and amplifies inflammation. *Nat. Biotechnol.* 39, 179–185. doi: 10.1038/s41587-020-0673-2

Mickle, A. D., Won, S. M., Noh, K. N., Yoon, J., Meacham, K. W., Xue, Y., et al. (2019). A wireless closed-loop system for optogenetic peripheral neuromodulation. *Nature* 565, 361–365. doi: 10.1038/s41586-018-0823-6

Mickoleit, F., Rosenfeldt, S., Toro-Nahuelpan, M., Schaffer, M., Schenk, A. S., Plitzko, J. M., et al. (2021). High-yield production, characterization, and functionalization of recombinant magnetosomes in the synthetic bacterium rhodospirillum rubrum "magneticum". *Adv. Biol.* 5:e2101017. doi: 10.1002/adbi.202101017

Molnar, K., and Labouesse, M. (2021). The plastic cell: mechanical deformation of cells and tissues. *Open Biol.* 11:210006. doi: 10.1098/rsob.210006

Moreira, J. M., Itskov, P. M., Goldschmidt, D., Baltazar, C., Steck, K., Tastekin, I., et al. (2019). optoPAD, a closed-loop optogenetics system to study the circuit basis of feeding behaviors. *Elife* 8:e43924.

Murawiec, S., Chudek, J., Nieves, W., Almgren-Rachtan, A., and Jedrzejczak, J. (2020). Increasing the dosage of pregabalin in patients with focal epilepsy decreases the frequency of seizures and ameliorates symptoms of anxiety, depression and insomnia. *Eur. Rev. Med. Pharmacol. Sci.* 24, 13015–13024. doi: 10.26355/eurrev_202012_24207

Nabavi, S., Fox, R., Proulx, C. D., Lin, J. Y., Tsien, R. Y., and Malinow, R. (2014). Engineering a memory with LTD and LTP. *Nature* 511, 348–352. doi: 10.1038/nature13294

News, S. (2010). Insights of the decade. stepping away from the trees for a look at the forest. introduction. *Science* 330, 1612–1613. doi: 10.1126/science.330.6011.1612

Ng, Y. S., Bindoff, L. A., Gorman, G. S., Horvath, R., Klopstock, T., Mancuso, M., et al. (2019). Consensus-based statements for the management of mitochondrial stroke-like episodes. *Wellcome Open Res.* 4:201. doi: 10.12688/wellcomeopenres.15599.1

Nieh, E. H., Matthews, G. A., Allsop, S. A., Presbrey, K. N., Leppla, C. A., Wichmann, R., et al. (2015). Decoding neural circuits that control compulsive sucrose seeking. *Cell* 160, 528–541. doi: 10.1016/j.cell.2015.01.003

Nowak, V. A., Pereira, E. A., Green, A. L., and Aziz, T. Z. (2010). Optogenetics–shining light on neurosurgical conditions. *Br. J. Neurosurg.* 24, 618–624. doi: 10.3109/02688697.2010.520764

Oh, T. J., Fan, H., Skeeters, S. S., and Zhang, K. (2021). Steering molecular activity with optogenetics: recent advances and perspectives. *Adv. Biol.* 5:e2000180. doi: 10.1002/adbi.202000180

Ostolaza, A., Blanco-Luquin, I., Urdanoz-Casado, A., Rubio, I., Labarga, A., Zandio, B., et al. (2020). Circular RNA expression profile in blood according to ischemic stroke etiology. *Cell Biosci.* 10:34. doi: 10.1186/s13578-020-00394-3

Ostrovsky, M. A., and Kirpichnikov, M. P. (2019). Prospects of optogenetic prosthesis of the degenerative retina of the eye. *Biochemistry* 84, 479–490. doi: 10.1134/S0006297919050031

Padmanabhan, S., Perez-Castano, R., and Elias-Arnanz, M. (2019). B12-based photoreceptors: from structure and function to applications in optogenetics and synthetic biology. *Curr. Opin Struct. Biol.* 57, 47–55. doi: 10.1016/j.sbi.2019.01.020

Peters, A. E., Caban, S. J., McLaughlin, E. A., Roman, S. D., Bromfield, E. G., Nixon, B., et al. (2021). The Impact of Aging on Macroautophagy in the Pre-ovulatory Mouse Oocyte. *Front Cell Dev Biol* 9:691826. doi: 10.3389/fcell.2021.691826

Pozarickij, A., Williams, C., and Guggenheim, J. A. (2020). and the UKBE, vision C: non-additive (dominance) effects of genetic variants associated with refractive error and myopia. *Mol. Genet. Genom.* 295, 843–853. doi: 10.1007/s00438-020-01666-w

Rajalingham, R., Sorenson, M., Azadi, R., Bohn, S., DiCarlo, J. J., and Afraz, A. (2021). Chronically implantable LED arrays for behavioral optogenetics in primates. *Nat. Methods* 18, 1112–1116. doi: 10.1038/s41592-021-01238-9

Riksen, N. P., and Netea, M. G. (2020). Immunometabolic control of trained immunity. *Mol. Aspects Med.* 77:100897. doi: 10.1016/j.mam.2020.100897

Roet, M., Hescham, S. A., Jahanshahi, A., Rutten, B. P. F., Anikeeva, P. O., and Temel, Y. (2019). Progress in neuromodulation of the brain: a role for magnetic nanoparticles? *Prog. Neurobiol.* 177, 1–14. doi: 10.1016/j.pneurobio.2019.03.002

Roy, D. S., Arons, A., Mitchell, T. I., Pignatelli, M., Ryan, T. J., and Tonegawa, S. (2016). Memory retrieval by activating engram cells in mouse models of early Alzheimer's disease. *Nature* 531, 508–512. doi: 10.1038/nature17172

Roy-O'Reilly, M. A., Ahnstedt, H., Spychala, M. S., Munshi, Y., Aronowski, J., Sansing, L. H., et al. (2020). Aging exacerbates neutrophil pathogenicity in ischemic stroke. *Aging* 12, 436–461. doi: 10.18632/aging.102632

Saltmarche, A. E., Naeser, M. A., Ho, K. F., Hamblin, M. R., and Lim, L. (2017). Significant improvement in cognition in mild to moderately severe dementia cases treated with transcranial plus intranasal photobiomodulation: case series report. *Photomed. Laser Surg.* 35, 432–441. doi: 10.1089/pho.2016.4227

Samineni, V. K., Mickle, A. D., Yoon, J., Grajales-Reyes, J. G., Pullen, M. Y., Crawford, K. E., et al. (2017). Optogenetic silencing of nociceptive primary afferents reduces evoked and ongoing bladder pain. *Sci. Rep.* 7:15865. doi: 10.1038/s41598-017-16129-3

Santos, D. S., Morais, J. A. V., Vanderlei, I. A. C., Santos, A. S., Azevedo, R. B., Muehlmann, L. A., et al. (2021). Oral delivery of fish oil in oil-in-water nanoemulsion: development, colloidal stability and modulatory effect on *in vivo* inflammatory induction in mice. *Biomed Pharmacother* 133:110980. doi: 10.1016/j.biopha.2020.110980

Senok, A., Monecke, S., Nassar, R., Celiloglu, H., Thyagarajan, S., Muller, E., et al. (2021). Lateral flow immunoassay for the detection of panton-valentine leukocidin in staphylococcus aureus from skin and soft tissue infections in the united arab emirates. *Front. Cell Infect Microbiol.* 11:754523. doi: 10.3389/fcimb.2021.754523

Shao, J., Wang, M., Yu, G., Zhu, S., Yu, Y., Heng, B. C., et al. (2018). Synthetic far-red light-mediated CRISPR-dCas9 device for inducing functional neuronal differentiation. *Proc. Natl. Acad. Sci. U.S.A.* 115, E6722–E6730. doi: 10.1073/pnas.1802448115

Shu, S., Zhu, H., Tang, N., Chen, W., Li, X., Li, H., et al. (2016). Selective degeneration of entorhinal-CA1 synapses in Alzheimer's disease via activation of DAPK1. *J. Neurosci.* 36, 10843–10852. doi: 10.1523/JNEUROSCI.2258-16.2016

Song, C., Kong, Y., Huang, L., Luo, H., and Zhu, X. (2020). Big data-driven precision medicine: starting the custom-made era of iatrology. *Biomed. Pharmacother* 129:110445. doi: 10.1016/j.biopha.2020.110445

Spierings, M. J., and ten Cate, C. (2014). Zebra finches are sensitive to prosodic features of human speech. *Proc. Biol. Sci.* 281:20140480. doi: 10.1098/rspb.2014.0480

Spreafico, R., Hayes, N. L., and Rustioni, A. (1981). Thalamic projections to the primary and secondary somatosensory cortices in cat: single and double retrograde tracer studies. *J. Comput. Neurol.* 203, 67–90. doi: 10.1002/cne.902030107

Srinivasan, S. S., Maimon, B. E., Diaz, M., Song, H., and Herr, H. M. (2018). Closed-loop functional optogenetic stimulation. *Nat. Commun.* 9:5303. doi: 10.1038/s41467-018-07721-w

Steinbeck, J. A., Choi, S. J., Mrejeru, A., Ganat, Y., Deisseroth, K., Sulzer, D., et al. (2015). Optogenetics enables functional analysis of human embryonic stem cell-derived grafts in a Parkinson's disease model. *Nat. Biotechnol.* 33, 204–209. doi: 10.1038/nbt.3124

Sternson, S. M., and Atasoy, D. (2014). Agouti-related protein neuron circuits that regulate appetite. *Neuroendocrinology* 100, 95–102. doi: 10.1159/000369072

Thornton, S. M., and Fitzsimons, J. T. (1995). The effects of centrally administered porcine relaxin on drinking behaviour in male and female rats. *J. Neuroendocrinol.* 7, 165–169. doi: 10.1111/j.1365-2826.1995.tb00743.x

Tremblay, S., Acker, L., Afraz, A., Albaugh, D. L., Amita, H., Andrei, A. R., et al. (2020). An open resource for non-human primate optogenetics. *Neuron* 108:e6. doi: 10.1016/j.neuron.2020.09.027

Tretyn, A. (1999). Calcium-dependent signal transduction pathways in plants–phytochrome mechanism of action as an example. *Pol. J. Pharmacol.* 51, 145–151.

Tsai, Z. R., Zhang, H. W., Tseng, C. H., Peng, H. C., Kok, V. C., Li, G. P., et al. (2021). Late-onset epilepsy and subsequent increased risk of dementia. *Aging* 13, 3573–3587. doi: 10.18632/aging.202299

Vahaba, D. M., Macedo-Lima, M., and Remage-Healey, L. (2017). Sensory coding and sensitivity to local estrogens shift during critical period milestones in the auditory cortex of male songbirds. *eNeuro* 4:ENEURO.0317-17.2017. doi: 10.1523/ENEURO.0317-17.2017

Vajtay, T. J., Bandi, A., Upadhyay, A., Swerdel, M. R., Hart, R. P., Lee, C. R., et al. (2019). Optogenetic and transcriptomic interrogation of enhanced muscle function in the paralyzed mouse whisker pad. *J. Neurophysiol.* 121, 1491–1500. doi: 10.1152/jn.00837.2018

Vallee, A., Vallee, J. N., Guillevin, R., and Lecarpentier, Y. (2020). Riluzole: a therapeutic strategy in Alzheimer's disease by targeting the WNT/beta-catenin pathway. *Aging* 12, 3095–3113. doi: 10.18632/aging.102830

Vassalli, Q. A., Colantuono, C., Nittoli, V., Ferraioli, A., Fasano, G., Berruto, F., et al. (2021). Onecut regulates core components of the molecular machinery for neurotransmission in photoreceptor differentiation. *Front. Cell Dev. Biol.* 9:602450. doi: 10.3389/fcell.2021.602450

Vetere, G., Tran, L. M., Moberg, S., Steadman, P. E., Restivo, L., Morrison, F. G., et al. (2019). Memory formation in the absence of experience. *Nat. Neurosci.* 22, 933–940. doi: 10.1038/s41593-019-0389-0

Wang, J. J., Yao, W. Q., Chen, Y. J., Ma, L., and Tao, Y. Z. (2014). [Neurons in NAc core and BLA are activated during cocaine context-associated reward memory retrieval in mice]. *Sheng Li Xue Bao* 66, 545–558.

Wolf, G., Schulkin, J., and Simson, P. E. (1984). Multiple factors in the satiation of salt appetite. *Behav. Neurosci.* 98, 661–673. doi: 10.1037//0735-7044.98.4.661

Wu, M. C., Chu, L. A., Hsiao, P. Y., Lin, Y. Y., Chi, C. C., Liu, T. H., et al. (2014). Optogenetic control of selective neural activity in multiple freely moving drosophila adults. *Proc. Natl. Acad. Sci. U.S.A.* 111, 5367–5372. doi: 10.1073/pnas.1400997111

Xu, Q., Zhang, J., Qin, T., Bao, J., Dong, H., Zhou, X., et al. (2021). The role of the inflammasomes in the pathogenesis of uveitis. *Exp. Eye Res.* 208:108618. doi: 10.1016/j.exer.2021.108618

Yang, X., Sun, X., Liu, J., Huang, Y., Peng, Y., Xu, Y., et al. (2021). Photo-crosslinked GelMA/collagen membrane loaded with lysozyme as an antibacterial corneal implant. *Int. J. Biol. Macromol.* 191, 1006–1016. doi: 10.1016/j.ijbiomac.2021.09.144

Yang, X., Yao, C., Tian, T., Li, X., Yan, H., Wu, J., et al. (2018). A novel mechanism of memory loss in Alzheimer's disease mice via the degeneration of entorhinal-CA1 synapses. *Mol. Psychiatry* 23, 199–210. doi: 10.1038/mp.2016.151

Yang, Y., Wu, M., Vazquez-Guardado, A., Wegener, A. J., Grajales-Reyes, J. G., Deng, Y., et al. (2021). Wireless multilateral devices for optogenetic studies of individual and social behaviors. *Nat. Neurosci.* 24, 1035–1045. doi: 10.1038/s41593-021-00849-x

Yao, J. P., Hou, W. S., and Yin, Z. Q. (2012). Optogenetics: a novel optical manipulation tool for medical investigation. *Int. J. Ophthalmol.* 5, 517–522. doi: 10.3980/j.issn.2222-3959.2012.04.22

Yi, M., Ma, Y., Zhu, S., Luo, C., Chen, Y., Wang, Q., et al. (2020). Comparative proteomic analysis identifies biomarkers for renal aging. *Aging* 12, 21890–21903. doi: 10.18632/aging.104007

Yi, Y., Li, Y., Meng, Q., Li, Q., Li, F., Lu, B., et al. (2021). A PRC2-independent function for EZH2 in regulating rRNA 2'-O methylation and IRES-dependent translation. *Nat. Cell Biol.* 23, 341–354. doi: 10.1038/s41556-021-00653-6

Yilmaz, I., Karaarslan, N., Yasar Sirin, D., and Ozbek, H. (2020). Pharmaco-molecular assessment of the effects of anandamide and its antagonists on hippocampal tissue in Wistar albino rats. *Eur. Rev. Med. Pharmacol. Sci.* 24, 11871–11882. doi: 10.26355/eurrev_202011_23845

Yu, C., Cassar, I. R., Sambangi, J., and Grill, W. M. (2020). Frequency-specific optogenetic deep brain stimulation of subthalamic nucleus improves parkinsonian motor behaviors. *J. Neurosci.* 40, 4323–4334. doi: 10.1523/JNEUROSCI.3071-19.2020

Yu, L., Wang, J., Zou, Y., Zeng, H., Cheng, W., and Jing, X. (2021). Qingfei oral liquid inhibited autophagy to alleviate inflammation via mTOR signaling pathway in RSV-infected asthmatic mice. *Biomed. Pharmacother* 138: 111449. doi: 10.1016/j.biopha.2021.111449

Yu, S. P., Tung, J. K., Wei, Z. Z., Chen, D., Berglund, K., Zhong, W., et al. (2019). Optochemogenetic stimulation of transplanted iPS-NPCs enhances neuronal repair and functional recovery after ischemic stroke. *J. Neurosci.* 39, 6571–6594. doi: 10.1523/JNEUROSCI.2010-18.2019

Zhang, D., Chen, H. D., Zulfiqar, H., Yuan, S. S., Huang, Q. L., Zhang, Z. Y., et al. (2021). iBLP: an xgboost-based predictor for identifying bioluminescent proteins. *Comput. Math Methods Med.* 2021:6664362. doi: 10.1155/2021/6664362

Zhang, L., and Wang, Y. (2021). Gene therapy in epilepsy. *Biomed Pharmacother* 143:112075.

Zhang, M., Eshraghian, E. A., Jammal, O. A., Zhang, Z., and Zhu, X. (2020). CRISPR technology: the engine that drives cancer therapy. *Biomed Pharmacother* 133:111007. doi: 10.1016/j.biopha.2020.111007

Zhang, Z., Liu, Q., Wen, P., Zhang, J., Rao, X., Zhou, Z., et al. (2017). Activation of the dopaminergic pathway from VTA to the medial olfactory tubercle generates odor-preference and reward. *Elife* 6:e25423. doi: 10.7554/eLife.25423

Zhao, Z. D., Yang, W. Z., Gao, C., Fu, X., Zhang, W., Zhou, Q., et al. (2017). A hypothalamic circuit that controls body temperature. *Proc. Natl. Acad. Sci. U.S.A.* 114, 2042–2047. doi: 10.1073/pnas.1616255114

Zhou, M., Zhu, J. Q., and Kang, L. Y. (2013). [Progress on chemical components and anti-cerebral injury effects of storax]. *Zhongguo Zhong Yao Za Zhi* 38, 3825–3828.

Zhu, R., Guo, W., Xu, X. J., and Zhu, L. (2020). An integrating immune-related signature to improve prognosis of hepatocellular carcinoma. *Comput. Math Methods Med.* 2020:8872329. doi: 10.1155/2020/8872329

Ztaou, S., Maurice, N., Camon, J., Guiraudie-Capraz, G., Kerkerian-Le Goff, L., Beurrier, C., et al. (2016). Involvement of striatal cholinergic interneurons and M1 and M4 muscarinic receptors in motor symptoms of Parkinson's disease. *J. Neurosci.* 36, 9161–9172. doi: 10.1523/JNEUROSCI.0873-16.2016

Conflict of Interest: The authors declare that the research was conducted in the absence of any commercial or financial relationships that could be construed as a potential conflict of interest.

Publisher's Note: All claims expressed in this article are solely those of the authors and do not necessarily represent those of their affiliated organizations, or those of the publisher, the editors and the reviewers. Any product that may be evaluated in this article, or claim that may be made by its manufacturer, is not guaranteed or endorsed by the publisher.

frontiers | Frontiers in Aging Neuroscience

ORIGINAL RESEARCH
published: 03 May 2022
doi: 10.3389/fnagi.2022.881488

Exercise Modifies the Transcriptional Regulatory Features of Monocytes in Alzheimer's Patients: A Multi-Omics Integration Analysis Based on Single Cell Technology

Yisheng Chen[1†], Yaying Sun[1†], Zhiwen Luo[1†], Xiangjun Chen[1], Yi Wang[1], Beijie Qi[1], Jinrong Lin[1], Wei-Wei Lin[2], Chenyu Sun[3], Yifan Zhou[4,5], Jiebin Huang[6], Yuzhen Xu[7], Jiwu Chen[8]* and Shiyi Chen[1]**

[1] Huashan Hospital, Fudan University, Shanghai, China, [2] Department of Neurosurgery, The Second Affiliated Hospital of Zhejiang University School of Medicine, Zhejiang University, Hangzhou, China, [3] AMITA Health Saint Joseph Hospital Chicago, Chicago, IL, United States, [4] Department of Ophthalmology, Shanghai General Hospital, Shanghai Jiao Tong University School of Medicine, Shanghai, China, [5] Department of Ophthalmology, Putuo People' s Hospital, Tongji University, Shanghai, China, [6] Department of Pediatrics, Ruijin Hospital, Shanghai Jiao Tong University School of Medicine, Shanghai, China, [7] Department of Rehabilitation, The Second Affiliated Hospital of Shandong First Medical University, Taian, China, [8] Department of Orthopedics, Shanghai General Hospital, Shanghai Jiao Tong University School of Medicine, Shanghai Jiao Tong University, Shanghai, China*

Monocytes have been reported to be important mediators of the protective effect of exercise against the development of Alzheimer's disease (AD). This study aims explored the mechanism by which monocytes achieve this. Using single cell transcriptome analysis, results showed that CD14 + and CD16 + monocytes interacted with other cells in the circulating blood. *TNF*, *CCR1*, *APP*, and *AREG*, the key ligand-receptor-related genes, were found to be differentially expressed between exercise-treated and AD patients. The SCENIC analysis was performed to identify individual clusters of the key transcription factors (TFs). Nine clusters (M1-M9) were obtained from the co-expression network. Among the identified TFs, *MAFB*, *HES4*, and *FOSL1* were found to be differentially expressed in AD. Moreover, the M4 cluster to which *MAFB*, *HES4*, and *FOSL1* belonged was defined as the signature cluster for AD phenotype. Differential analysis by bulkRNA-seq revealed that the expression of *TNF*, *CCR1*, and *APP* were all upregulated after exercise ($p < 0.05$). And *ATF3*, *MAFB*, *HES4*, and *KLF4* that were identified in M4 clusters may be the TFs that regulate *TNF*, *CCR1*, and *APP* in exercise prescription. After that, *APP*, *CCR1*, *TNF*, *ATF3*, *KLF4*, *HES4*, and *MAFB* formed a regulatory network in the ERADMT gene set, and all of them were mechanistically linked. The ERADMT gene set has been found to be a potential risk marker for the development of AD and can be used as an indicator of compliance to exercise therapy in AD patients. Using single-cell integration analysis, a network of exercise-regulating TFs in monocytes was constructed for AD disease. The constructed network reveals the mechanism by which exercise regulated monocytes to confer therapeutic benefits against AD and its complications. However, this study, as a bioinformatic research, requires further experimental validation.

Keywords: Alzheimer's disease, exercise, monocyte, transcription factors, cell communication

OPEN ACCESS

Edited by:
Min Tang,
Jiangsu University, China

Reviewed by:
Mingming Li,
Changzheng Hospital, Second Military Medical University, China
Zhizhong Ye,
Shenzhen Futian Hospital for Rheumatic Diseases, China
Hong Jiang,
Shanghai Ninth People's Hospital, China

***Correspondence:**
Yuzhen Xu
ianyayizhe@126.com
Jiwu Chen
jeevechen@gmail.com
Shiyi Chen
cshiyi@163.com

† These authors have contributed equally to this work

Specialty section:
This article was submitted to Alzheimer's Disease and Related Dementias, a section of the journal Frontiers in Aging Neuroscience

Received: *22 February 2022*
Accepted: *11 April 2022*
Published: *03 May 2022*

Citation:
Chen Y, Sun Y, Luo Z, Chen X, Wang Y, Qi B, Lin J, Lin W-W, Sun C, Zhou Y, Huang J, Xu Y, Chen J and Chen S (2022) Exercise Modifies the Transcriptional Regulatory Features of Monocytes in Alzheimer's Patients: A Multi-Omics Integration Analysis Based on Single Cell Technology. Front. Aging Neurosci. 14:881488. doi: 10.3389/fnagi.2022.881488

INTRODUCTION

Alzheimer's disease (AD) is a degenerative disease of the central nervous system characterized by progressive cognitive dysfunction and behavioral impairment. The disease is common in aged individuals and accounts for about 50–70% of all cases of dementia. Patients with AD present with progressive memory impairment, decreased ability to perform daily living activities, and abnormal mental behavior. Therefore, it imposes a heavy burden on society and families, making it the largest global public health issue facing humanity (Pfeffer et al., 1987). In terms of pathogenesis, it is thought to be caused by extracellular amyloid β-protein (Aβ) deposition and tau hyperphosphorylation. However, the exact pathogenesis of the disease is unknown, and there is no effective treatment available (Lei et al., 2021). The immune profile of peripheral blood has been found to be closely associated with the development of AD (Mancuso et al., 2013; Noble et al., 2014). Some pathogens (*Chlamydia pneumoniae*) may enter the brain with infected mononuclear cells (MacIntyre et al., 2003). Pathogenic invasion can trigger the increase in Aβ, thus causing long-term chronic inflammation, thus leading to AD development (Miklossy, 2011). Therefore, targeting monocytes may be a promising therapeutic approach for AD (Dobri et al., 2021).

The role of physical activity in AD prevention has received much attention in recent years (Macpherson et al., 2017; Kivipelto et al., 2018; López-Ortiz et al., 2021). However, the specific mechanisms by which exercise prevents the onset of AD should be further explored. Physical exercise can influence the transcriptome characteristics of monocytes (Strohacker et al., 2012). For instance, moderate exercise increases monocyte adhesion, molecule expression, and oxidized low-density lipoprotein (ox-LDL)-induced transendothelial migration. Monocytes are then stimulated to migrate through the endothelium (Wang et al., 2005) and thus may act as a regulator of AD prevention through exercise. Therefore, studying the effect of exercise on the transcriptional characteristics of monocytes can provide insights into the potential mechanisms of AD prevention through exercise.

Single-cellomics is a rapidly growing discipline based on single-cell sequencing, a novel high-throughput sequencing technology. Single-cell sequencing has various unique advantages in various areas, including early disease diagnosis, biological marker detection and prognosis prediction. For example, scRNA-seq analysis showed that nucleated cells in the blood play a key role in preventing AD development (Xu and Jia, 2021). Besides uncovering monocytes and their subpopulations involved in AD pathophysiology, single cell sequencing can also disclose their distinct transcriptional profiles and presumably unique functional qualities (Khan and Kaihara, 2019; Masuda et al., 2020; Tuzlak et al., 2021). Single cell sequencing can be used to elucidate the pathogenesis and identify novel therapeutic targets for immune diseases affecting the central nervous system by focusing on the immune cells (B cells, T cells, monocytes, macrophages, microglia, dendritic cells) and tissue cells (oligodendrocytes, astrocytes, neurons).

This study aimed to investigate transcriptional profile changes of monocytes after exercise using an integrative analysis based on single-cell technology to address the gap in exercise-mediated monocyte prevention and therapy of AD. We also examined the potential expression and regulatory mechanisms of the post-exercise monocyte transcriptome to establish a biological basis for the beneficial mechanism of exercise prescriptions for AD patients.

MATERIALS AND METHODS

Data Acquisition

The dataset was obtained from GEO, an international public open source database (Barrett et al., 2012). The nucleated cell dataset from peripheral blood of three AD patients (aged > 60 years with positive amyloid positron emission tomography) and two age-matched cognitively normal controls (NC) were obtained from GSE181279. The scRNA-seq was used to analyze 36,849 nucleated peripheral blood cells in the GSE181279 dataset through the Cell Ranger standard analysis procedure (Xu and Jia, 2021). The Affymetrix Human Genome U133 Plus 2. 0 Array was used to analyze the GSE51835 dataset, a bulk RNA-seq dataset based on the GPL570 platform. The GSE51835 dataset consisted of mononuclear cells in 24 peripheral blood samples of 12 pre-exercise and 12 post-exercise (20 min) individuals (Radom-Aizik et al., 2014). The humanht-12 v4 Expression bead chip was used to assess GSE140831 dataset, which is based on the GPL15988 platform, using circulating blood mRNA expression data of 204 AD and 530 normal controls. The limma package of the R software was used to analyze variance as previously described. The log fold change (logFC) and mean expression values of all genes were also recorded. Adjusted *p*-values less than 0.05 were considered to be statistically significantly different (Costa-Silva et al., 2017; Chen et al., 2021; Lin W. et al., 2021; Shi et al., 2021; Wu et al., 2021). The "pheatmap" package of the R software was used for heat m*APP*ing. The "rcircos" package was used to draw a circle map describing the chromosomal location of the target gene (Zhang et al., 2013). All raw data were stored in text form.

Single-Cell Transcriptional Profiling and Clustering

As previously described, scRNA analysis was performed using the Seurat package of R software, which included quality control, downscaling, and clustering of the GSE181279 dataset (Chen et al., 2021; Lin W.-W. et al., 2021; Mangiola et al., 2021; Pereira et al., 2021; Shi et al., 2021; Wu et al., 2021). All genes were expressed in at least three cells. At least 200 genes were expressed in each cell, and the number of mitochondrial genes was less than 10. "FindVariableFeatures" was used to calculate the variable genes between samples after normalization of gene expression. Further non-linear dimensionality reduction analysis was conducted using the UMAP method (Becht et al., 2018). Initial annotation of cell clustering was performed using SingleR (Deng et al., 2020). The cell clusters were further corrected based on the methods described in some previous studies (Zhang et al., 2020; Xu and Jia, 2021). The differential expression analysis of

single-cell mimetic bulk RNA data obtained from the specific cells was conducted using DEseq2 to obtain the differentially expressed genes (DEGs) in AD patients (Mou et al., 2020). P-value < 0.05 was considered a statistically significant difference.

Cell Communication Analysis

Ligand-receptor complex-mediated intercellular communication is key in a wide range of biological processes. In this study, the analysis of intercellular ligand-receptor complex interactions was conducted using the CellPhoneDB database. Intercellular interactions with p-values < 0.01 were considered statistically significant (Efremova et al., 2020). Additionally, cell chat was used as an additional method to describe intercellular signaling communication and conserved and context-specific pathways (Jin et al., 2021).

Scenic-Based Analysis of Key Transcription Factors

Key TFs within single-cell clusters were analyzed using a modified SCENIC method as previously described (20, 22, 33, 34). The regulon activity score (RAS) for each cell was repeated thrice to determine the stability of the regulatory relationship (Suo et al., 2018). An entropy-based strategy was used to quantify the cell-type specificity of the regulation (Cabili et al., 2011). Next, the correlations of the different TF overall regulatory activities were analyzed using Pearson correlation coefficients. It is worth noting that this method can currently only be used to analyze positively associated transcriptional regulatory networks, so only positively associated transcriptional regulators of target genes can be explored.

Single-Cell Pseudotime Analysis

The pseudotime analysis measures the transcriptional difference a single cell can achieve during cell differentiation. The Monocle package ranks each cell relative to its progress on the learning trajectory. In this study, pseudotime analysis was performed using Monocle2 package (Qiu et al., 2017).

Enrichment Analysis of Pathways and Functions

Enrichment analyses, including KEGG and gene ontology (GO) were conducted using clusterprofiler package for R software [version 3. 14. 3] (Yu et al., 2012). The org. Hs. eg. db package [version 3. 10. 0] was used for ID conversion. "Homo sapiens" was selected as the species. P-value < 0.05 was considered a statistically significant difference.

Construction of Predictive Models

The neural network model was constructed as described previously using the R packages "neuralnet" and "neuralnettools" (Beck, 2018). The "pacman" package of the R software was used to construct the random forest (RF) and support vector machine (SVM) models. The models were selected based on the receiver operating characteristic curve (ROC) and the characteristics of the |residuals|. The nomogram prediction model was then built using the "rms" function. Finally, calibration curves for the model were plotted (Kang et al., 2020; Ying et al., 2021). The DCA curves and clinical effectiveness curves were plotted to further evaluate the predictive power of the model (Van Calster et al., 2018; Olivieri, 2021).

RESULTS

Transcriptome Analysis of Peripheral Blood Nucleated Cells From Alzheimer's Disease Patients

GSE181279 dataset contained 36,849 peripheral blood nucleated cells of three AD patients (aged > 60 years) and two age-matched non-AD patients (NC). All genes were expressed in at least three cells. (**Supplementary Figure 1A**). At least 200 genes were expressed in each cell, and the number of mitochondrial genes was less than 10. UMAP plots were used to show the distribution of different samples in the tissues of AD and NC groups (**Supplementary Figure 1B**). Feature RNA, counted RNA, mitochondrial RNA, and hemoglobin RNA are shown in **Supplementary Figure 1C**. SingleR was used for initial annotation of cell clustering. Key genes defining cell types in circulating blood, including *CD3D*, *CD3E*, *CD3G*, *CD4*, *CD8A*, *CD8B*, *S100A4*, *GPR183*, *SELL*, *CCR7*, *GZMK*, *GNLY*, *MS4A1*, *KLRF1*, *LYZ*, *CD14*, and *FCGR3A* were further determined after initial annotation of cell clustering, based on previous studies (13, 29). Violin plots were used to show the expression of these marker genes in different cell clusters (**Figure 1A**). The cell types of the different clusters were further annotated based on the expression patterns of the marker genes (**Figures 1B,C**). The dotted heat map showed that the marker gene expression between the AD and NC groups was consistent, suggesting that this cellular annotation can distinguish different cell types (**Figure 1D**).

Cellular Communication Characteristics of $CD14^+$ and $CD16^+$ Monocytes in Alzheimer's Disease Based on Exercise

The proportion of each cell type in different patients was expressed in bar chart to analyze the cellular composition changes of circulating blood in AD patients (**Figure 2A**). The proportions of $CD14^+$ and $CD16^+$ monocytes were not significantly different between the AD and NC groups. This result indicates that monocyte differences in AD patients are mainly due to transcription differences and not proportion differences of cell types. The "deseq2" package and the "FindVariableFeatures" function were then used to analyze the major differentially expressed genes (DEGs) in $CD14^+$ and $CD16^+$ monocytes (**Figures 2B–D**). Cellchat was used to analyze the communication between CD14 + and CD16 + monocytes and other cells along a number of pathways, including the MIF signaling pathway (**Figure 2E**), GALECTIN signaling pathway (**Figure 2F**), *TNF* signaling pathway (**Figure 2G**), IL16 signaling pathway (**Figure 2H**), ANNEXIN signaling pathway (**Supplementary Figure 2A**), RESISTIN signaling pathway was assessed using Cellchat (**Supplementary Figure 2B**). This suggests that CD14 + and CD16 + monocytes are communicate

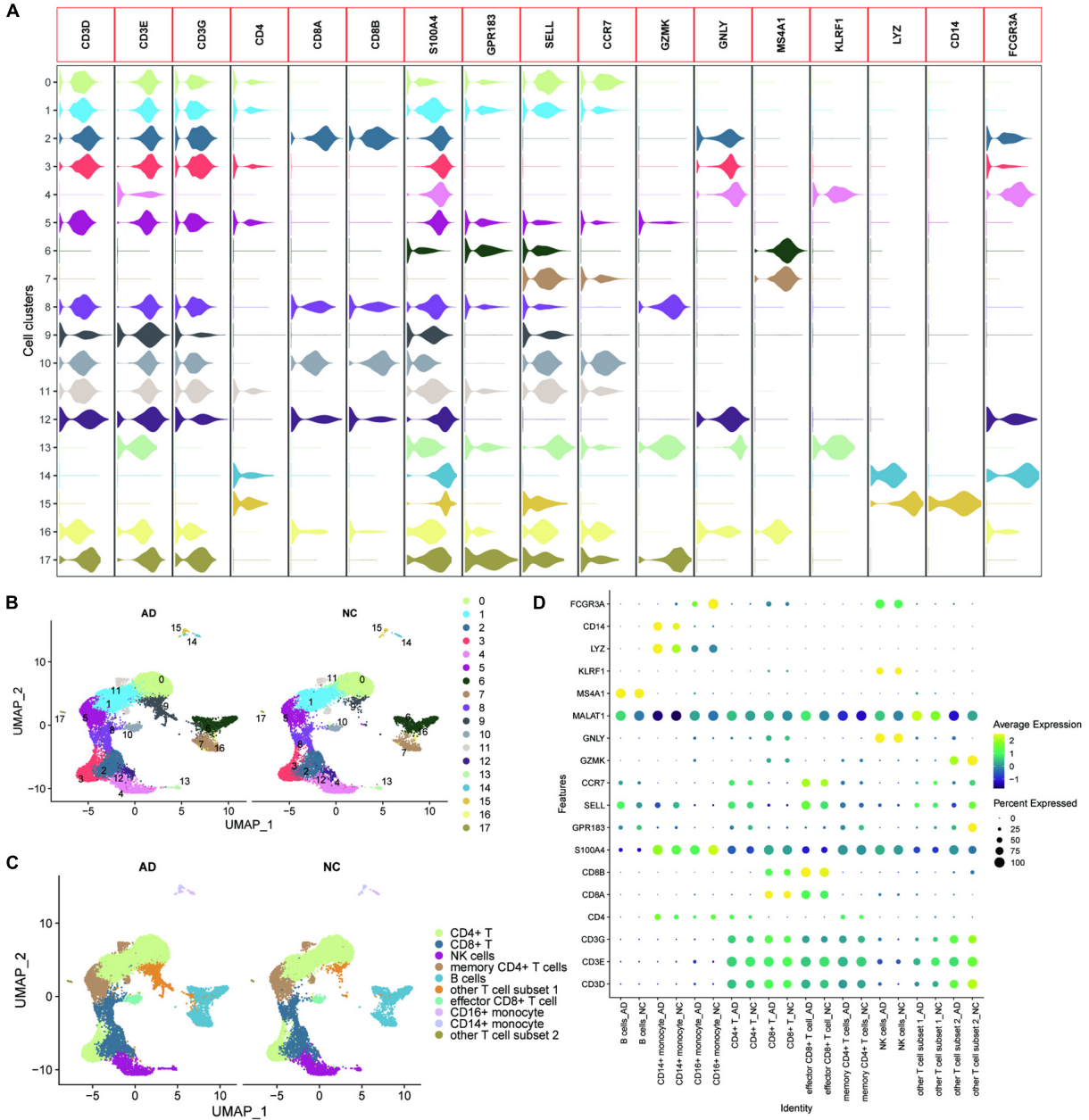

FIGURE 1 | Heterogeneity of the transcriptome of peripheral blood nucleated cells from patients with AD. **(A)** Violin plots showing the expression of the marker genes in different cell clusters; **(B)** UMAPs show the distribution of the 17 cell clusters in the AD and NC groups, with different colors representing different cell clusters; **(C)** The cells are annotated according to the expression characteristics of the cell clusters and marker genes; **(D)** The dotted heat map showing good agreement and characteristic expression of marker genes between AD and NC groups, where MALAT1 as a characteristic gene of other T cell subset 1 was significantly upregulated in other T cell subset 1.

with other cells, and that monocytes may regulate the circulating blood microenvironment.

The effect of exercise on monocyte transcription in circulating blood was evaluated to analyze the mechanisms by which exercise regulates mRNA transcription levels in monocytes of AD patients. The "limma" package was used for differential analysis of the GSE51835 bulk RNA-seq, and 1811 DEGs were obtained. The main DEGs are shown on the heat map (**Figure 3A**). GO, and KEGG enrichment analyses of these DEGs are shown in **Figure 3B**. The GO functional enrichment analysis showed that the DEGs were significantly enriched in: response to lipopolysaccharide, response to molecule of bacterial origin, signal transduction by p53 class mediator, ubiquitin ligase complex, nuclear transcription factor complex, transferase complex, transferring phosphorus-containing groups, methylation-dependent protein binding, methylated histone

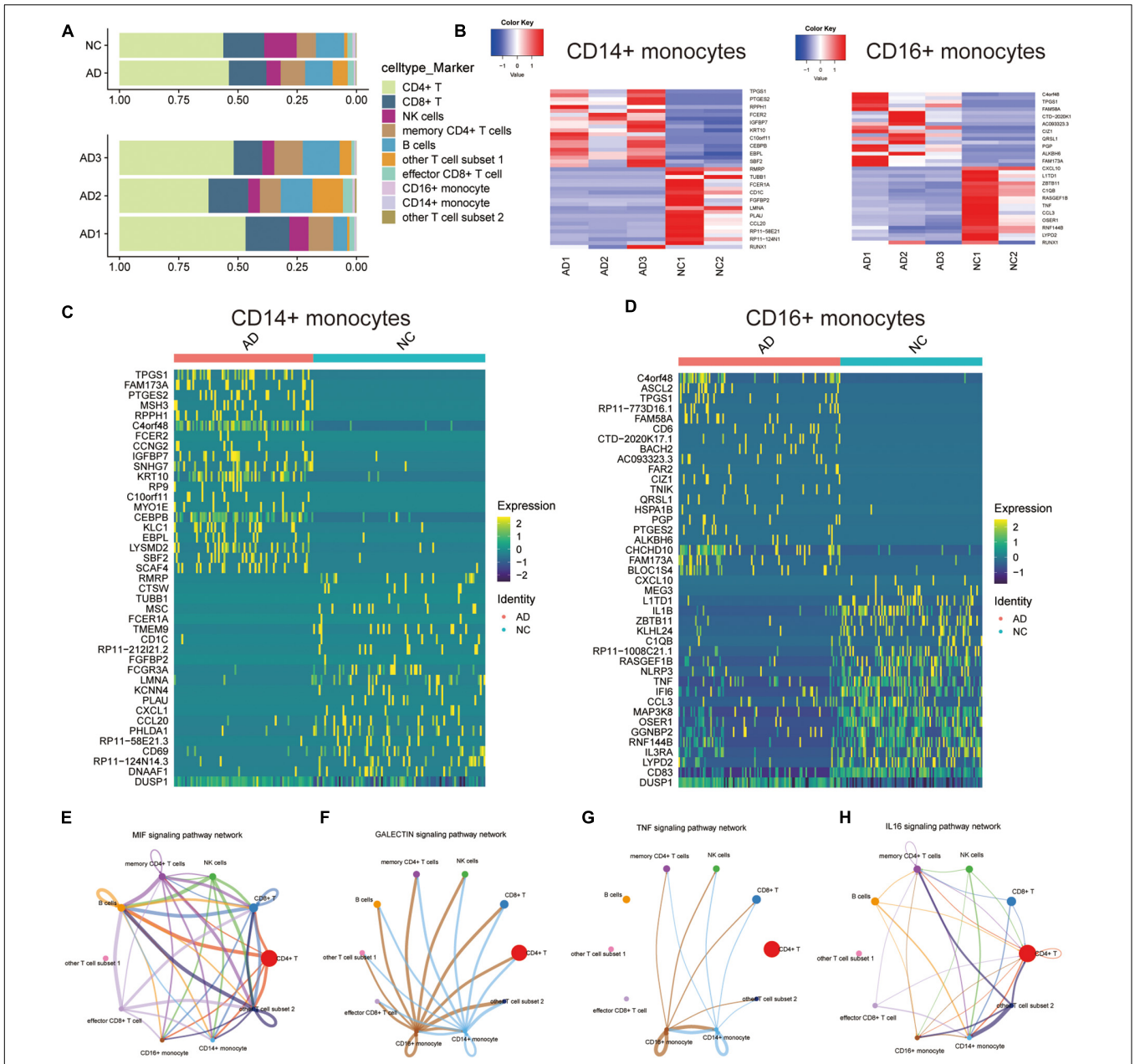

FIGURE 2 | Differential expression and cellular communication characteristics of CD14$^+$ and CD16$^+$ monocytes in patients with AD. **(A)** Horizontal bars show the proportion of each cell type in different patients; **(B)** Deseq2 obtained the main DEGs in CD14$^+$ and CD16$^+$ monocytes; **(C,D)** Major DEGs in CD14$^+$ and CD16$^+$ monocytes obtained by *APP*lying the "FindVariableFeatures" function; **(E–H)** Cellchat-based results showing the association of specific cell populations with other cell populations in different key cellular pathways: MIF signaling pathway **(E)**, GALECTIN signaling pathway **(F)**, *TNF* signaling pathway **(G)**, IL16 signaling pathway **(H)**.

binding, and transcription corepressor activity. Moreover, the KEGG enrichment analysis showed that the DEGs were significantly enriched in the FOXO signaling pathway, Natural killer cell-mediated cytotoxicity, and Th17 cell differentiation. The enrichment analyses suggest that transcriptional and immune microenvironmental homeostasis regulation are the main effects of exercise on monocytes (**Figure 3B**). A total of 57 and 39 DEGs were associated with AD at the single-cell level in CD14$^+$ and CD16$^+$ monocytes, respectively (**Supplementary Figure 2C**). GO, and KEGG enrichment analyses showed that these DEGs were mainly enriched in functions and pathways related to immune differentiation and transcriptional regulation (**Supplementary Figures 2D,E**). These analyses indicate that CD14$^+$ and CD16$^+$ monocytes play a crucial cellular communication function in regulating blood microenvironment in AD. These results show that exercise can influence the immune microenvironment in circulating blood by regulating the transcription of monocytes, and thus may be

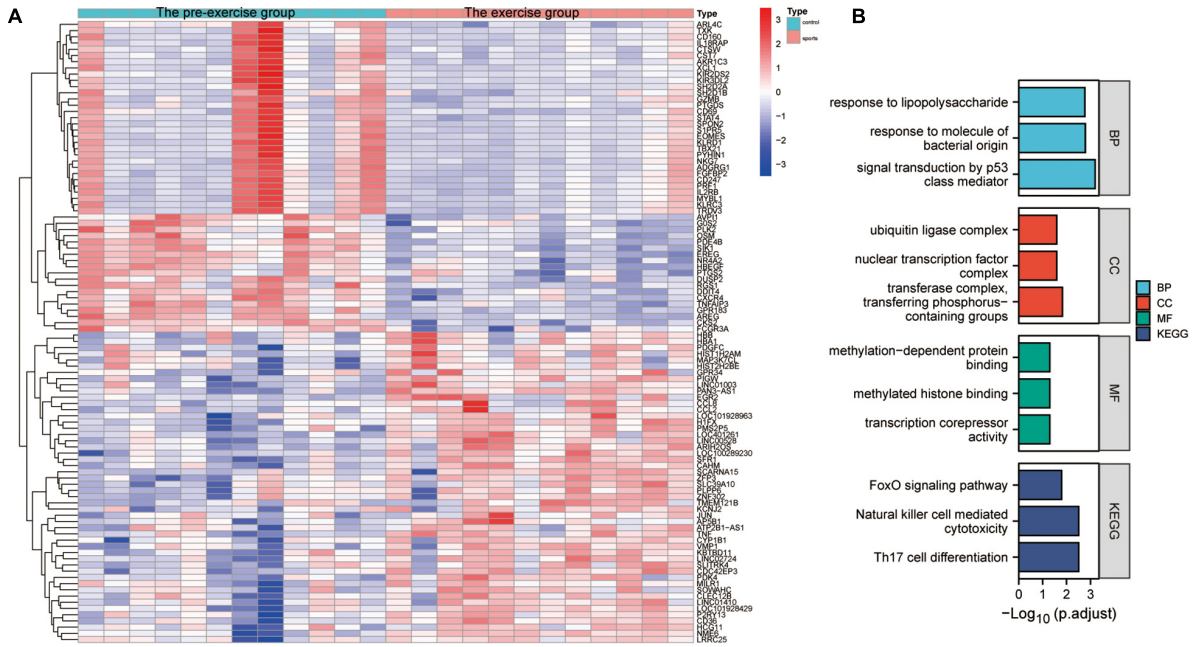

FIGURE 3 | Characterization of the effect of the exercise group on the expression profile of monocytes. **(A)** Heat map of the major DEGs in monocytes from the GSE51835 bulk RNA dataset before versus after the patients received exercise; **(B)** GO and KEGG enrichment analysis of the major DEGs in monocytes.

a mechanism for AD prevention through exercise. However, further studies are needed to assess the effect of exercise on monocyte transcriptional regulators to provide an initiating factor for the prevention of AD development through exercise. Moreover, further exploration of exercise-regulated changes in cellular communication can reveal the specific mechanisms by which these transcriptional regulators modulate the blood microenvironment.

TNF, CCR1, APP, and *AREG* Are Key Ligand-Receptor-Related Genes Associated With Exercise Prescription

Ligand-receptor complex-mediated intercellular communication is essential for various biological processes. This study conducted intercellular ligand-receptor complex interaction analysis using the CellPhoneDB database. Any pair with $p < 0.05$ was considered key ligand-receptor pair. Intersection analysis was performed to explore cellular communication changes under exercise regulation (shown in the Venn diagram, **Figure 4A**). *CD74*, *ANXA1*, *HLA-DPB1*, *GRN*, and *ICAM1* were DEGs of $CD14^+$ monocytes intersecting with key ligand-receptor intersection genes. Moreover, *TNF*, *CCL3*, *CD52*, and *LAMP1* were DEGs of $CD16^+$ monocytes intersecting with key ligand-receptor intersection genes. A dotted heat map of key ligand-receptor relationship pairs associated with *CD74*, *ANXA1*, *HLA-DPB1*, *GRN*, *ICAM1*, *TNF*, *CCL3*, *CD52*, and *LAMP* is shown in **Figure 4B**. Of the 32 ligand-receptor relationship pairs, exercise regulated the transcript levels of four genes (*TNF*, *CCR1*, *APP*, and *AREG*). A dotted heat map demonstrated the differential expression profile of *TNF*, *CCR1*, *APP*, and *AREG* genes in the AD and normal control (NC) groups (**Figure 4D**). UMAP plots were used to demonstrate the transcriptional profiles of *TNF*, *CCR1*, *APP*, and *AREG* in the GSE181279 single-cell dataset (**Figure 4E**), suggesting that *TNF*, *CCR1*, *APP*, and *AREG* may be key ligand-receptor-related genes associated with exercise prescription.

MAFB, *HES4*, and *FOSL1* Are Differentially Expressed Transcription Factors in Alzheimer's Disease

A SCENIC analysis was performed on all cells of GSE181279 to further identify differentially expressed transcription factors in AD associated with exercise. An unsupervised cluster analysis of the GSE181279 dataset was re-performed using the t-SNE method. The t-SNE plot demonstrated the clustering results for $CD14^+$ and $CD16^+$ monocytes (**Figures 5A,B**), suggesting that $CD14^+$ and $CD16^+$ monocytes were well clustered. According to SCENIC analysis, the top 10 TFs of $CD14^+$ and $CD16^+$ monocytes were ranked based on the regulon specificity score (RSS; **Figure 5C**). Venn diagrams of DEGs in $CD14^+$ and $CD16^+$ monocytes from AD patients were plotted against the top 10 key TFs in $CD14^+$ and $CD16^+$ monocytes via intersection analysis to screen the key transcriptional regulators that are differentially expressed in the AD blood microenvironment (**Figure 5D**). These 10 key transcription factors could be possible targets for exercise to regulate AD onset if exercise can influence AD onset by modulating transcription factors in monocytes. *MAFB*, *HES4*, and *FOSL1* were differentially expressed in AD. The dotted heat map demonstrated the differential expression profile of *MAFB*, *HES4*, and *FOSL1* genes in the AD and NC groups (**Figure 5E**),

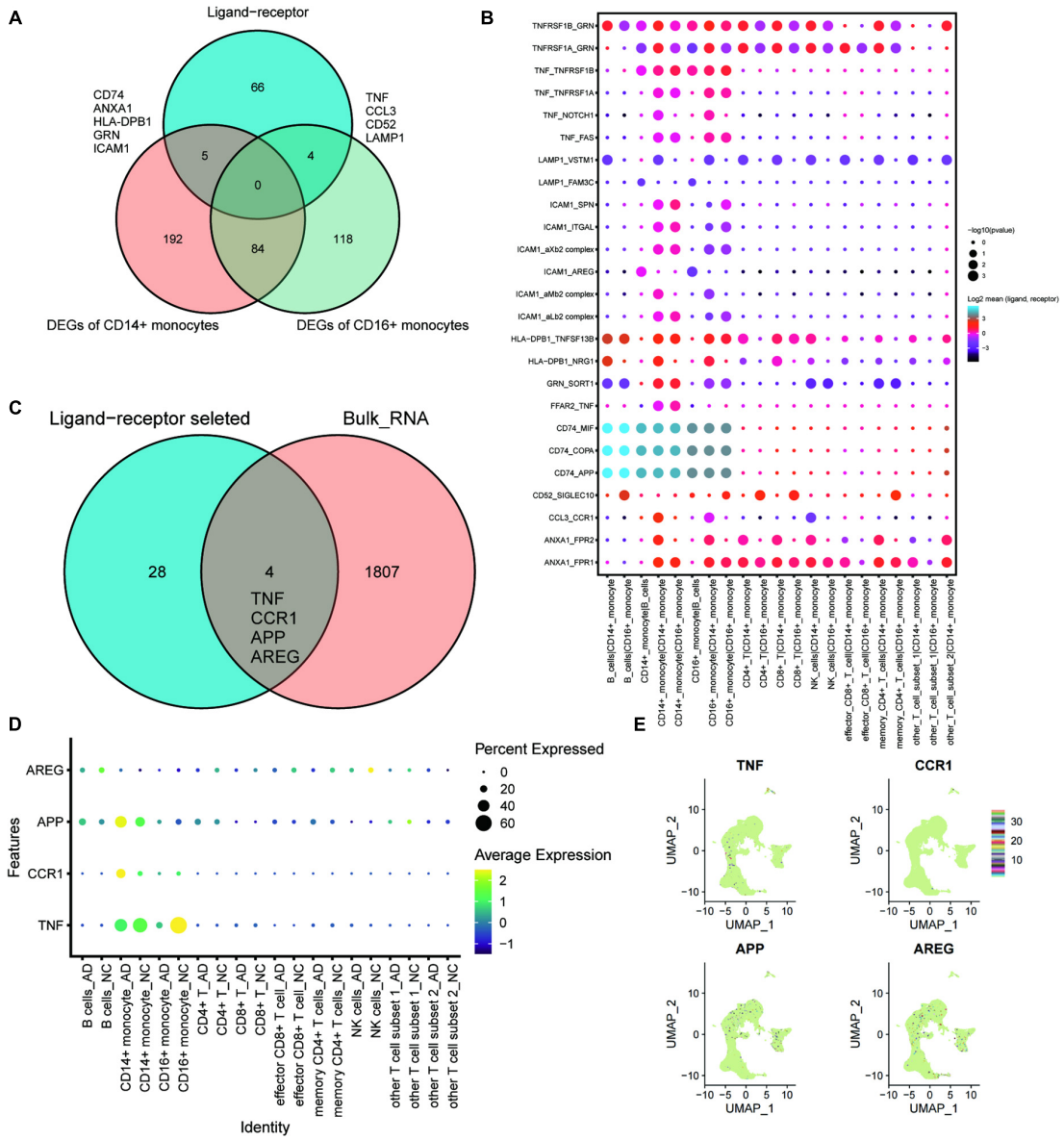

FIGURE 4 | The key ligand-receptor-related genes associated with exercise prescription. **(A)** Venn diagram analysis identifies CD74, ANXA1, HLA-DPB1, GRN, and ICAM1 as the intersections of DEGs of $CD14^+$ monocytes with intersecting genes of key ligand-receptors, whereas the *TNF*, CCL3, CD52, and LAMP1 were intersections of DEGs of $CD16^+$ monocytes with key ligand-receptor intersection genes; **(B)** Pointwise heat map of key ligand-receptor relationship pairs associated with CD74, ANXA1, HLA-DPB1, GRN, ICAM1, *TNF*, CCL3, CD52, and LAMP1. **(C)** Wayne plots showing that *TNF*, *CCR1*, *APP*, and *AREG* in these selected ligand-receptor relationship pairs were found to be differentially expressed in post-exercise monocytes; **(D)** Dot heat map demonstrating the differential expression profile of *TNF*, *CCR1*, *APP*, and *AREG* genes in the AD and NC groups; **(E)** Transcriptional features of *TNF*, *CCR1*, *APP*, and *AREG* genes in the GSE181279 single cell dataset demonstrated using UMAP plots.

indicating that these genes are transcription factors differentially expressed in AD patients.

Transcription Factors in M4 Cluster Are Target Genes for Exercise Regulation of Alzheimer's Disease Monocytes

Transcription factors represent functional and differentiation trajectories of cells. Herein, the expression of transcription factors was quantified using an entropic strategy, then underwent re-cluster analysis to determine the transcription factor clusters where the transcriptional regulators *MAFB*, *HES4*, and *FOSL1* are located (**Figure 5F**). We used the UMAP method for the cell type clustering analysis, and the tSNE clustering strategy for the transcriptional regulatory network analysis. The t-SNE plots were used to characterize the transcriptional activity of the M1–M9 modules, where *FOSL1*, *HES4*, and *MAFB* were found to be the characteristic transcription factors of the

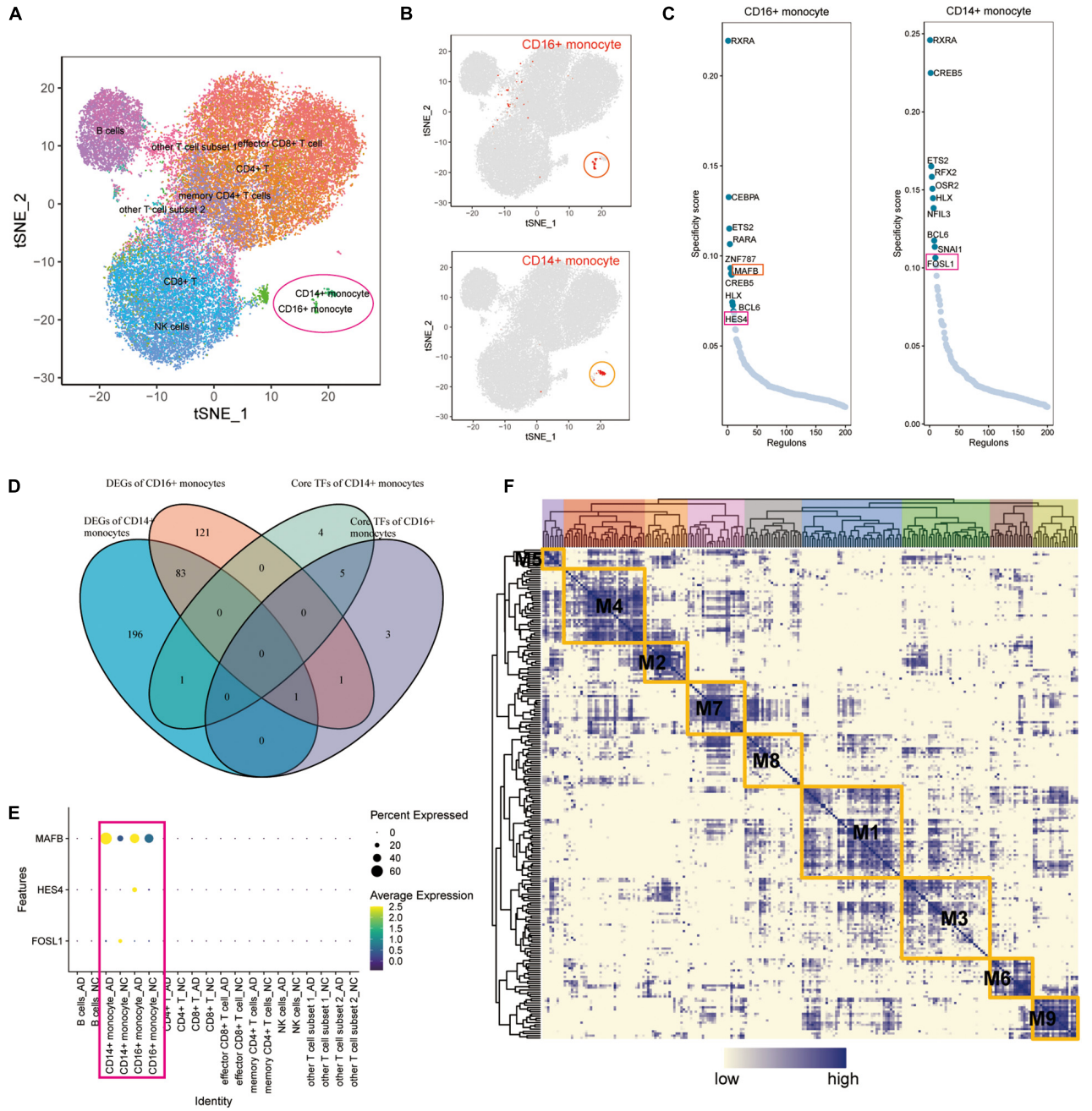

FIGURE 5 | The key transcription factors of monocytes affected by exercise in patients with AD. **(A)** Unsupervised clustering analysis of the GSE181279 dataset was re-performed using the t-SNE method; **(B)** The t-SNE plot showing the clustering results of $CD14^+$ and $CD16^+$ monocytes, which suggest that the monocytes are well clustered; **(C)** The top 10 TFs of $CD14^+$ and $CD16^+$ monocytes based on RSS ranking positions; **(D)** Venn diagram of intersection analysis of DEGs in $CD14^+$ and $CD16^+$ monocytes from patients with AD and having key TFs in top10 of $CD14^+$ and $CD16^+$ monocytes; **(E)** Dotted heat map demonstrating the differential expression profile of *MAFB*, *HES4*, and *FOSL1* genes in the AD and NC groups; **(F)** Expression of transcription factors quantified using an entropic strategy and re-clustered in the same way.

M4 module (**Figures 6A,B** and **Supplementary Table 2**). In this investigation, both UMAP and tSNE clustering methods performed well, examined the effect of hierarchical clustering in this study. The transcriptional activity of the various cell types in the different cell modules is shown in **Figures 6A,B**. $CD14^+$ and $CD16^+$ monocytes were significantly enriched in the M4 module (**Supplementary Figure 3A**). GO, and KEGG enrichment analyses were used to explore the function of transcription factors in the M4 cluster (**Figure 6C**). These transcription factors were found to play a role in muscle organ

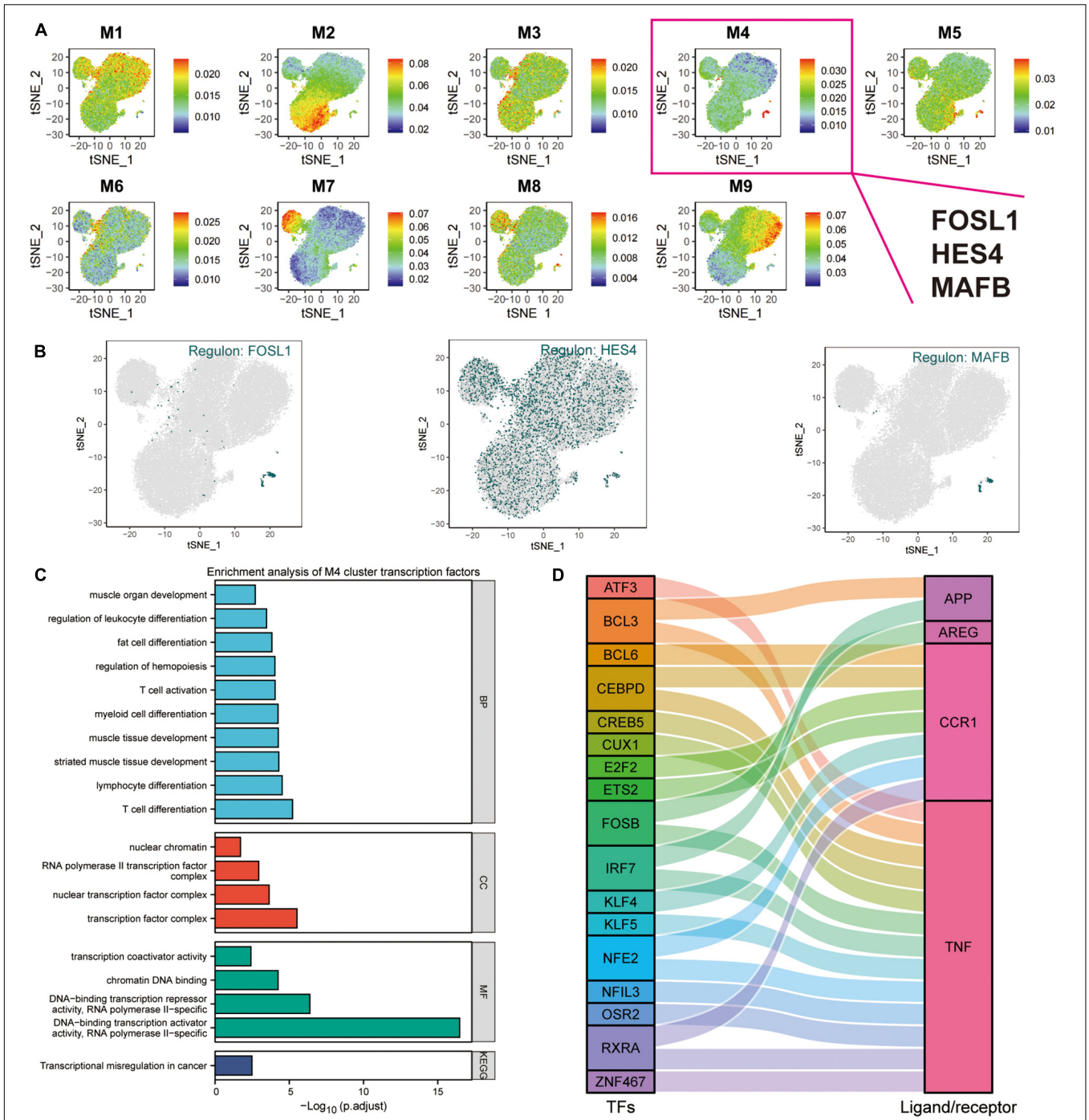

FIGURE 6 | Cluster analysis of target genes in exercise-regulated AD monocytes. **(A)** The transcriptional activity profile of the M1–M9 module is illustrated using t-SNE plots, where *FOSL1*, *HES4*, and *MAFB* are the signature transcription factors of the M4 module; **(B)** Expression profiles of key transcription factors *FOSL1*, *HES4*, and *MAFB* are shown using t-SNE plots; **(C)** GO and KEGG enrichment analysis of M4 transcription factor clusters; **(D)** Sangi diagram demonstrating the key ligands or receptors that may be regulated by the transcription factors in the M4 cluster.

development, regulation of leukocyte differentiation, fat cell differentiation, hemopoiesis regulation, T cell activation, myeloid cell differentiation, muscle tissue development, lymphocyte differentiation, T cell differentiation, nuclear chromatin, RNA polymerase II transcription factor complex, nuclear transcription factor complex, transcription factor complex, transcription coactivator activity, and chromatin DNA binding. Moreover, the M4 cluster was significantly enriched in various pathways and functions, such as chromatin DNA binding, and DNA-binding transcription repressor activity. These results suggest

that transcription factors in the M4 cluster are closely related to muscle tissue development, immune cell differentiation, and cellular transcriptional regulatory functions and pathways. *TNF*, *CCR1*, *APP*, and *AREG* were identified as key ligand-receptor-related genes associated with exercise prescription. Sankey maps were drawn based on the results of previous SCENIC analyses to reveal transcriptional regulators that may regulate *TNF*, *CCR1*, *APP*, and *AREG* (**Figure 6D**). Differential analysis by bulkRNA-seq revealed that the expression of TNF, CCR1, and APP were all upregulated after exercise ($p < 0.05$). These findings show that transcription factors in the M4 cluster (TNF, CCR1, and APP) may have a role in the prevention of Alzheimer's disease through exercise.

Construction of a Transcriptional Regulatory Network for Exercise-Altered Alzheimer's Disease Monocytes via Combined Bulk RNA-seq and Single-Cell Mimetic Timing Analysis

And an intersection analysis of 17 key transcription factors from the M4 cluster with 1811 DEG that were differentially expressed after exercise was performed to screen the key differentially expressed transcriptional regulators in the AD blood microenvironment affected by exercise (**Figure 7A**). The transcription factors *ATF3*, *BCL3*, *KLF4*, and *NFIL3* were the key TFs regulated by AD and exercise. The expression profiles of *ATF3*, *NFIL3*, *BCL3*, and *KLF4* on the t-SNE plot are shown in **Figure 7B**. The key transcription factors were predominantly expressed in $CD14^+$ and $CD16^+$ monocytes. Subsequently, the sankey diagram demonstrated the key ligands or receptors (*APP*, *CCR1*, and *TNF*) that may be regulated by the co-differentially expressed transcription factors (*ATF3*, *BCL3*, *KLF4*, and *NFIL3*; **Figure 7C**). *APP*, *CCR1*, *TNF*, *ATF3*, *KLF4*, *HES4*, and *MAFB* were considered exercise-regulated AD monocyte transcription (ERADMT) gene sets. Pseudo-temporal analysis measures the transcriptional variation that can be achieved by single cells during cell differentiation. In this study, pseudo-timing analysis was conducted using the Monocle2 package. First, a principal component (PCA) analysis of all $CD14^+$ and $CD16^+$ monocytes was performed (**Supplementary Figure 3B**), and results showed that $CD14^+$ and $CD16^+$ monocytes could be distinguished. Scatter plots were used to further characterize the expression profiles of *APP*, *CCR1*, *TNF*, *ATF3*, *KLF4*, *HES4*, and *MAFB* (**Supplementary Figure 3C**). The distribution of $CD14^+$, $CD16^+$ monocytes, and pseudotime values and the branching of the proposed chronological trajectory were also further plotted on the proposed chronological trajectory (**Supplementary Figure 3D**). The distribution of *APP*, *CCR1*, *TNF*, *ATF3*, *KLF4*, *HES4*, and *MAFB* expression values on the pseudo-temporal trajectory based on pseudo-time was also assessed (**Figures 7D,E**) (**Supplementary Figure 3E**). The ERADMT gene set of *APP*, *CCR1*, *TNF*, *ATF3*, *HES4*, and *KLF4* were significantly differentially expressed in the post-exercise bulk RNA dataset (**Supplementary Figure 3F**). Furthermore, ERADMT gene set was concentrated in the state 1 branch of the pseudo-temporal track and enriched in $CD14^+$ monocyte. These results indicate that exercise can improve the microenvironment in AD circulating blood mainly by driving $CD14^+$ monocyte.

ERADMT Gene Set Can Be Used as an Indicator for Assessing Exercise Therapy Compliance in Alzheimer's Disease Patients

To validate the regulatory relationships in the ERADMT gene set, we analyzed the expression correlation of *APP, CCR1, TNF, ATF3, KLF4, HES4,* and *MAFB* in CD14 + and CD16 + monocytes using the Pearson correlation method based on the GSE181279 single cell dataset (**Figures 8A,B**). In addition, we also analyzed the correlations among the expression levels of *APP, CCR1, TNF, ATF3, KLF4, HES4,* and *MAFB* in monocytes based on the GSE51835 bulk RNA dataset using the Pearson correlation method (**Figure 8C**). The results were similar to those of the SCENIC analysis, i.e., The expression of genes in the ERADMT gene set was positively correlated with each other's expression. To assess the function of these monocyte genes for exercise adherence, a neural network model was constructed using *APP, CCR1, TNF, ATF3, KLF4, HES4,* and *MAFB* (**Figure 8D**). In addition, ROC analysis suggested that all elements in the ERADMT gene set had good ability to assess whether exercise was received (**Figure 8E**). The ROC curves indicated that the neural network model could accurately assess patients' exercise compliance (**Figure 8F**). The location of the ERADMT gene set (*APP, CCR1, TNF, ATF3, KLF4, HES4*, and *MAFB*) on the chromosomes in this study is also shown as a circle plot (**Figure 8G**). The above study suggests that the level of expression of genes in the ERADMT gene set may reflect exercise therapy adherence in AD patients. It can also predict whether the subjects are receiving adequate amounts of physical activity. In summary, *ATF3*, *MAFB*, *HES4*, and *KLF4* were defined as potential transcription factors for *TNF*, *CCR1* and *APP* under the regulation of exercise prescription by Bulk RNA-seq and single cell mimetic timing analysis. Accordingly, a network of exercise-altered monocyte transcriptional regulation was constructed (**Figure 9**).

ERADMT Gene Set Found to Be a Potential Risk Marker for the Development of Alzheimer's Disease Patients

To further assess the predictive power of the ERADMT gene set for the onset of AD in patients, we performed further analysis with the GSE140831 dataset. We obtained circulating blood mRNA expression data from a total of 204 patients with Alzheimer's disease and 530 normal controls. Correlation analysis based on the GSE140831 dataset suggested that the expression in the ERADMT gene set was positively correlated with each other, except for *APP*, which was negatively correlated with *ATF3* and *HES4* (**Supplementary Figure 4A**). Next, RF models and SVM models were constructed to assess the predictive power of the ERADMT gene set on the onset of AD patients. The box plot and Reverse cumulative distribution of |residual|

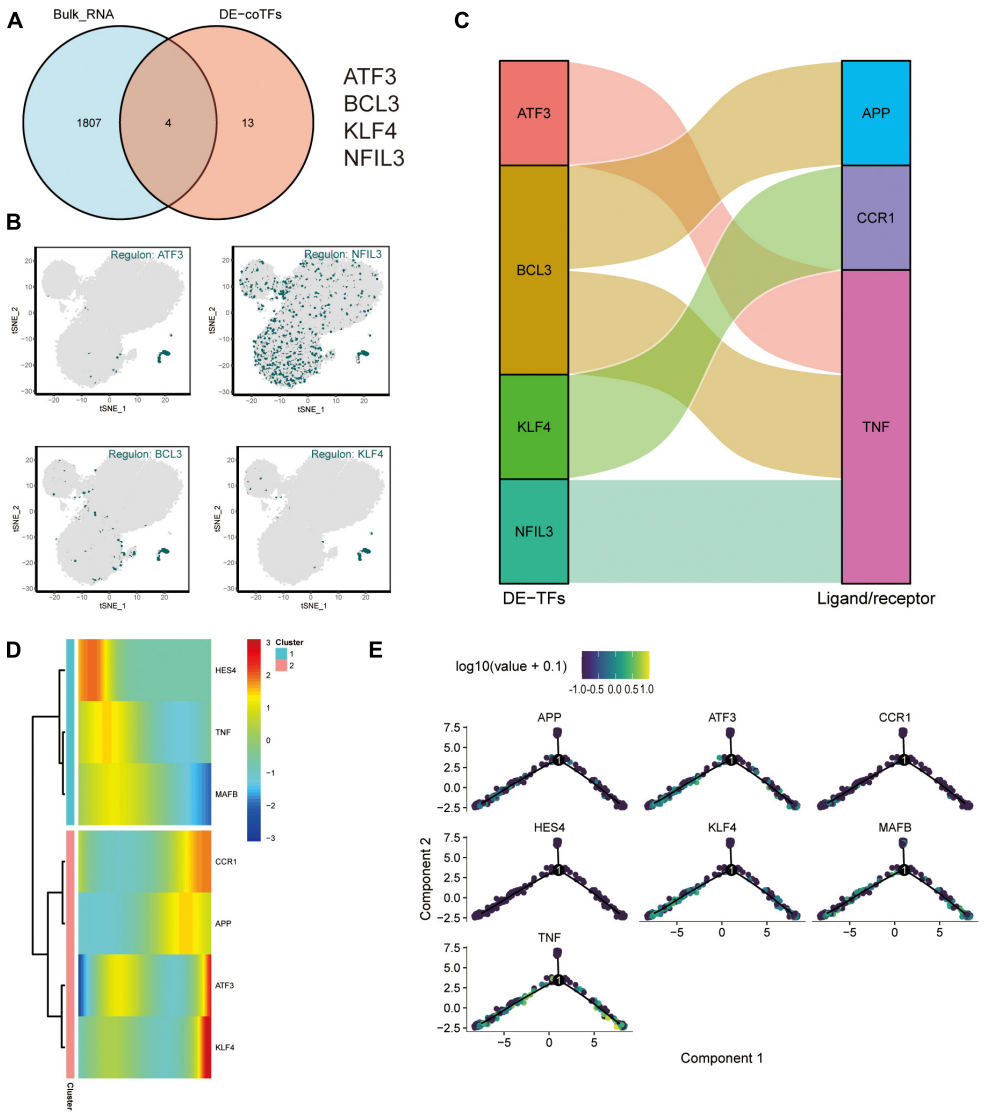

FIGURE 7 | Exercise regulates AD monocyte transcription (ERADMT) gene sets. **(A)** Intersection analysis of 17 key transcription factors from the M4 cluster with 1811 DEGs after exercise; **(B)** Expression characteristics of the intersecting genes *ATF3*, *NFIL3*, *BCL3*, and *KLF4* on the t-SNE plot; **(C)** Sangi diagram showing the key ligands or receptors (including: *APP*, *CCR1*, and *TNF*) that may be regulated by the co-differentially expressed transcription factors (including: *ATF3*, *BCL3*, *KLF4*, and *NFIL3*); **(D)** Heat map indicating the relationship between *APP*, *CCR1*, *TNF*, *ATF3*, *KLF4*, *HES4*, and *MAFB* expression and pseudo-time; **(E)** Expression characteristics of *APP*, *CCR1*, *TNF*, *ATF3*, *KLF4*, *HES4*, and *MAFB* on the pseudotime trajectory.

indicate that the model residuals of the SVM model are larger than those of the RF model (**Supplementary Figures 4B,C**). The relationship between the "error" of the RF model and the number of trees selected for the model is shown in **Supplementary Figure 4D**. The importance of ERADMT genes was also ranked (**Supplementary Figure 4E**). The AUC values of the RF model were significantly higher than those of the SVM model (**Supplementary Figure 4F**). To visualize the model, we constructed a nomogram prediction model using the ERADMT gene set expression profile (**Supplementary Figure 4G**). The calibration curve of this ERADMT gene set nomogram prediction model suggests that the model prediction results fit well with the actual results (**Supplementary Figure 4H**). The DCA curve of the nomogram prediction model based on this ERADMT gene set suggests that the model has potentially good clinical utility (**Supplementary Figures 5A,B**). According to the results of the logistic prediction model, the ERADMT gene set is a potential risk marker for the development of AD patients.

DISCUSSION

Peripheral blood nucleated cells of AD patients annotated nine cell subsets, including $CD4^+$ T cells, $CD8^+$ T cells, NK cells, memory $CD4^+$ T cells, B cells, effector $CD8^+$ T cells, $CD14^+$ monocytes, $CD16^+$ monocytes, other T cell subset

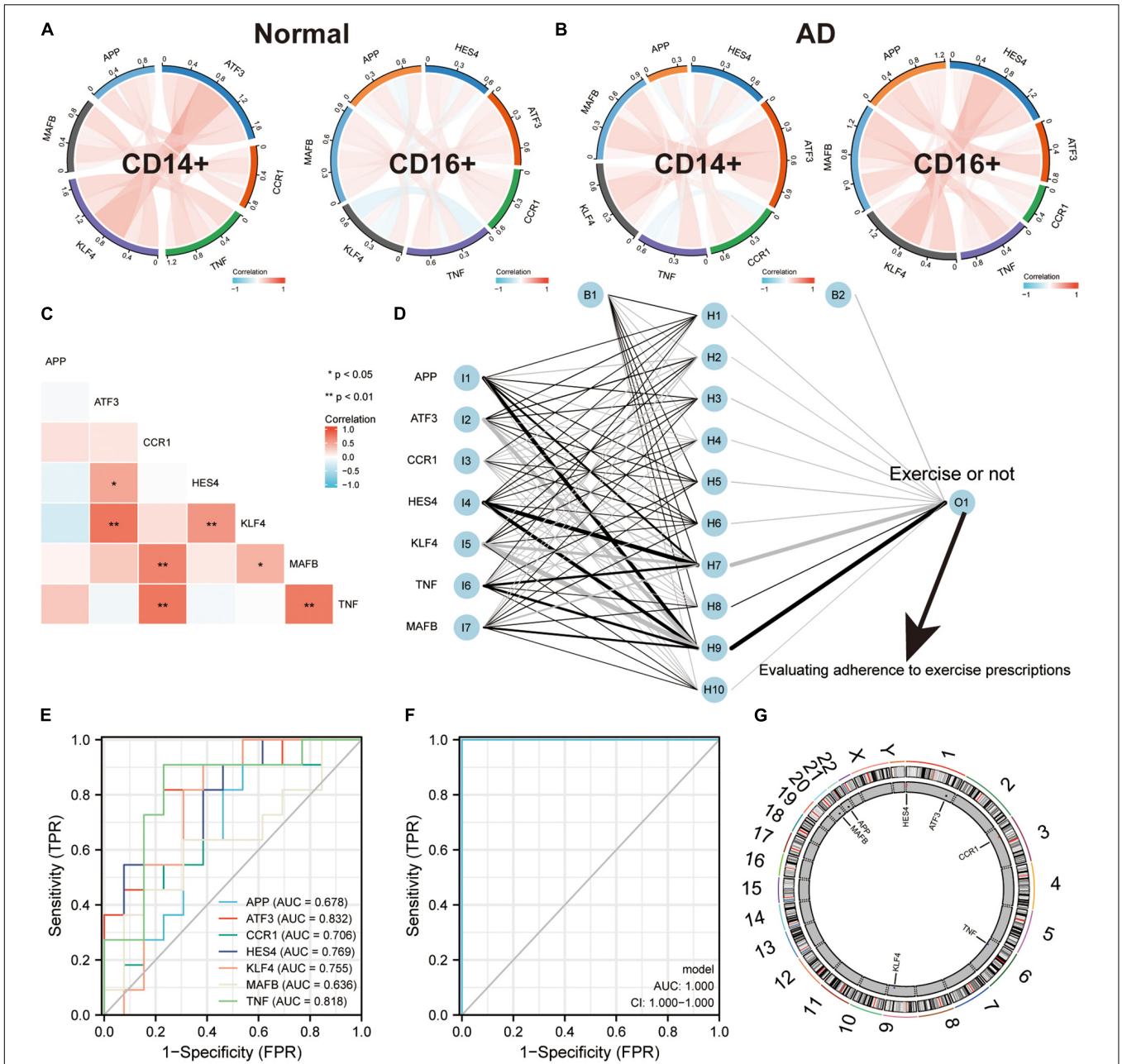

FIGURE 8 | ERADMT gene set as an indicator for assessing adherence to exercise prescription in patients with AD. **(A,B)** Correlation of *APP*, *CCR1*, *TNF*, *ATF3*, *KLF4*, *HES4*, and *MAFB* expression in $CD14^+$ and $CD16^+$ monocytes based on the GSE181279 single cell dataset, analyzed using Person method, including NC group (A) and AD group (B), red indicates positive correlation whereas blue indicates negative correlation; **(C)** Expression correlations of *APP*, *CCR1*, *TNF*, *ATF3*, *KLF4*, *HES4*, and *MAFB* in monocytes were analyzed using the Person method based on the GSE181279 bulk RNA dataset; **(D)** Schematic diagram of a neural network model for determining whether to exercise using *APP*, *CCR1*, *TNF*, *ATF3*, *KLF4*, *HES4*, and *MAFB*; **(E)** The predictive ability of the ERADMT gene set (*APP*, *CCR1*, *TNF*, *ATF3*, *KLF4*, *HES4*, and *MAFB*) to separately predict whether to undergo exercise or not; **(F)** ROC curve indicating that the neural network model can accurately predict patients' exercise compliance; **(G)** The position of the ERADMT gene set (*APP*, *CCR1*, *TNF*, *ATF3*, *KLF4*, *HES4*, and *MAFB*) on the chromosome is indicated by the circle plot.

1 and other T Cell subset 2. Cell communication analysis revealed that $CD14^+$ and $CD16^+$ monocytes have a close cellular communication with other cells. $CD14^+$ and $CD16^+$ monocytes play a key cellular communication function in the regulation of the AD blood microenvironment, consistent with previous studies (Gu et al., 2016; Kapellos et al., 2019). Moreover, four genes (*TNF*, *CCR1*, *APP*, and *AREG*) were identified as potentially key ligand-receptor-related genes associated with exercise prescription. Enrichment analyses suggested that regulation of transcriptional and immune microenvironment

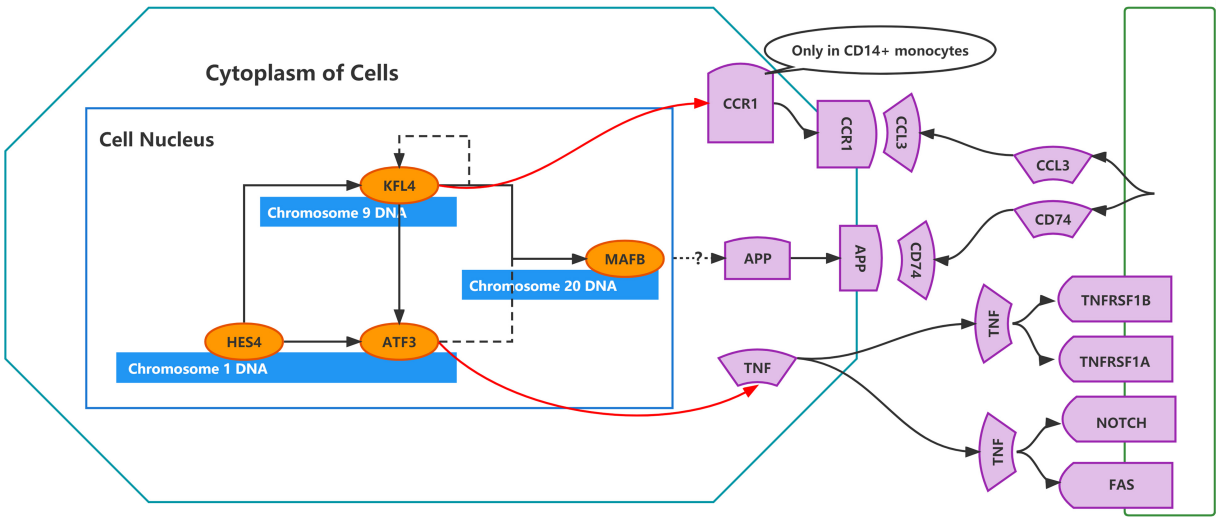

FIGURE 9 | Schematic representation of the regulatory network constructed using the ERADMT gene set.

homeostasis are the main effects of exercise on monocytes, indicating the potential mechanism for AD prevention. SCENIC analysis identified *MAFB*, *HES4*, and *FOSL1* as differentially expressed transcription factors in AD patients. Moreover, *FOSL1*, *HES4*, and *MAFB* were identified as characteristic transcription factors of the M4 module. The transcription factors in the M4 cluster were closely associated with muscle tissue development, immune cell differentiation, and transcriptional regulatory functions and pathways of cells. These results suggest that the transcription factors in the M4 cluster may be key target genes for exercise regulation.

The expression of transcription factors in each module had a substantial positive connection, and *FOSL1*, *HES4*, and *MAFB* identified the genes in the M4 module as a possible cluster of transcriptional regulators linked to the start of Alzheimer's disease. M4 module genes *ATF3*, *BCL3*, *KLF4*, and *NFIL3* are differentially expressed in the exercise group; therefore, *ATF3*, *BCL3*, *KLF4*, and *NFIL3* are regarded pivotal genes in the prevention of AD incidence by exercise. Therefore, *APP*, *CCR1*, *TNF*, *ATF3*, *KLF4*, *HES4*, and *MAFB* were identified as ERADMT gene set. ERADMT gene set, as a set of genes in the regulatory network, is a potential risk marker for AD development and an indicator for the assessment of exercise therapy adherence in AD patients.

The pseudo-timing analysis showed that ERADMT gene set was concentrated in the state 1 branch of the pseudo-timing trajectory and enriched in $CD14^+$ monocyte, indicating that exercise can improve the microenvironment in AD circulating blood mainly by driving $CD14^+$ monocyte. The ERADMT gene set was also concentrated in the state 1 branch of the pseudo-temporal trajectory and enriched in $CD14^+$ monocyte, indicating that exercise can improve the microenvironment in AD circulating blood mainly by driving $CD14^+$ monocyte. Neural network models were then constructed using *APP*, *CCR1*, *TNF*, *ATF3*, *KLF4*, *HES4*, and *MAFB*. Subsequently, *ATF3*, *MAFB*, *HES4*, and *KLF4* were identified as potential transcription factors for *TNF*, *CCR1* and *APP* under the regulation of exercise prescription. A network of exercise-altered transcriptional regulation of monocytes was also constructed. Finally, predictive models constructed based on RF and SVM suggested that the ERADMT gene set is a potential risk marker for AD development.

The three TFs (*ATF3*, *KFL4*, and *HES4*) were located in the M4 cluster and enriched in AD-related pathways. A previous study showed that *ATF3* is a TF regulated by locomotion (Park et al., 2021). Moreover, exercise upregulates *ATF3* transcription in skeletal muscle after exercise (Fernández-Verdejo et al., 2017). Treadmill exercise can promote sciatic nerve injury regeneration through *ATF3* upregulation (Kim et al., 2020). In contrast, silencing of the *ATF3* family gene can inhibit exercise-induced angiogenesis (Fan et al., 2021). *ATF3* can also promote the progression of neurodegenerative diseases (Bao et al., 2021). Previous studies have revealed that KFL4, as a tumor stem cell marker, promotes cell differentiation and development (Li et al., 2019; Chen et al., 2020; Paterson et al., 2021). It modulates the development of non-hematopoietic cell lineage and is also regarded as a cellular marker (Pessina et al., 2010). However, in a recent study, KFL4 was found to be associated with the onset of dementia, which is consistent with our findings (Santiago et al., 2020). This is the first study to suggest that motor regulation can affect *KFL4*. *HES4* is a key transcription factor in the NOTCH pathway (Wagley et al., 2020) that promotes the initiation of early t-cell development. It may also be associated with mediation of NOTCH pathway-dependent differences in human hematopoietic cell lines (De Decker et al., 2020). Epigenetic dysregulation of *HES4* may be closely associated with the

development of Huntington's disease in the nervous system (Bai et al., 2015). In the present study, *ATF3*, *KFL4*, and *HES4* were identified for the first time as potential TFs mediating the effects of exercise therapy.

Moreover, *APP*, *CCR1*, and *TNF* were identified as key ligand-receptor genes. *APP* was differentially expressed after exercise. *APP* mutations cause AD (Lee et al., 2018). Amyloid hypothesis shows that secretases cleave APP to form toxic amyloid-B (AB) peptides and plaques, thus causing AD (Selkoe and Hardy, 2016). Herein, *APP* expression and its expression ratio in $CD14^+$ monocytes were significantly increased in AD patients. The monocyte-macrophage-microglial cell lineage of the cerebrovascular pericyte lineage produces fibrillar A beta in the capillary wall (Wisniewski et al., 2000). *APP* is significantly upregulated in $CD14^+$ monocytes of AD patients, indicating that *APP* may be a key cause of amyloid deposition. Moreover, this study showed that the key transcription factor ATF3 can positively regulate the key ligand TNF. TNF is a ligand for TNFRSF1B, TNFRSF1A, NOTCH and FAS. In a previous study on the GSE51835 dataset, it was found that high-intensity exercise may influence the monocyte immune function by regulating ATF3 via the TNF and FoxO signaling pathways. Hence, it may improve the body's resistance to chronic inflammatory diseases (Li and Luo, 2021). Chemokine and its receptors play a key role in the development of neurodegenerative diseases (Savarin-Vuaillat and Ransohoff, 2007). CCR1 is a receptor for CCL3. Herein, KLF4 could positively regulate the key receptor CCR1. It was earlier reported that CCR1 was a potential target in AD. However, the relationship between CCR1 and exercise has not been clarified (Liu et al., 2014). Overall, the key ligand-receptor genes (*APP*, *CCR1*, and *TNF*) play crucial cellular communication functions in the regulation of the AD blood microenvironment. Exercise can affect the immune microenvironment in circulating blood by regulating the transcription of monocytes, and thus may be a potential mechanism for AD prevention through exercise.

In this study, the integration analysis of scRNA-seq and bulk RNA-seq data revealed that exercise improves cellular communication in circulating blood of AD patients probably by altering the transcriptional regulatory network of monocytes. Moreover, the M4 clustered TFs were enriched in AD-related pathways. In the M4 cluster, ATF3, MAFB, HES4, and KLF4 TFs regulated the transcription of exercise-related ligand receptor genes (*TNF, CCR1,* and *APP*). The ERADMT gene set comp'rises *APP, CCR1, TNF, ATF3, KLF4, HES4,* and *MAFB*. Abnormal function of APP protein has been linked to extracellular β-amyloid deposition. Further analysis revealed that the ERADMT gene set is a potential indicator of exercise therapy adherence in AD patients and a risk marker for AD development. In conclusion, the proposed ERADMT gene set regulated by locomotion provides insights for further mechanistic studies. Although this study included three datasets with large sample sizes and multidimensional and multilevel analyses were performed, this study, as a bioinformatic analysis, requires further experimental validation. Additionally, further clinical studies are needed.

CONCLUSION

This study constructed a network of movement-altered AD monocyte transcriptional regulatory features using single-cell integration analysis, mainly composed of ERADMT gene set (*APP*, *CCR1*, *TNF*, *ATF3*, *KLF4*, *HES4*, and *MAFB*). The results showed that the ERADMT gene set can be potential markers for AD development and an indicator of adherence to exercise therapy in AD patients.

DATA AVAILABILITY STATEMENT

The datasets presented in this study can be found in online repositories. The names of the repository/repositories and accession number(s) can be found in the article/**Supplementary Material**.

AUTHOR CONTRIBUTIONS

YC: methodology, writing – review and editing, conceptualization, software, validation, formal analysis, data curation, and writing – original draft. YS: conceptualization, methodology, supervision, and writing – original draft. ZL: methodology, conceptualization, and writing – original draft. XC: supervision, writing – review and editing. YW: supervision, writing – review and editing. BQ: data curation, writing – review and editing. JL: data curation and methodology. W-WL: software, validation, and language polishing. CS: validation and language polishing. YZ: conceptualization and validation. JH: validation and data curation. YX: writing – original draft, conceptualization, supervision, methodology, and funding acquisition. JC: conceptualization, supervision, project administration, and funding acquisition. SC: conceptualization, supervision, project administration and funding acquisition.

FUNDING

This study was supported by grants from the National Natural Science Foundation of China (No. 82102634, 81972062, and 81772419), Medical and Health Science and Technology Development Project of Shandong Province (2018WS147). This work was also supported by Project of the Key Clinical Medicine Center of Shanghai (No. 2017ZZ01006), Sanming Project of Medicine in Shenzhen (No. SZSM201612078), Development Project of Shanghai Peak Disciplines-Integrative Medicine (No. 20180101), Shanghai Committee of Science and Technology (No. 19441901600).

ACKNOWLEDGMENTS

We thank the reviewers for their contribution to the successful publication of this study. We thank Home for Researchers editorial team (https://www.home-for-researchers.com) for language editing service.

SUPPLEMENTARY MATERIAL

The Supplementary Material for this article can be found online at: https://www.frontiersin.org/articles/10.3389/fnagi.2022.881488/full#supplementary-material

Supplementary Figure 1 | Quality control for the scRNA-seq data of GSE181279 dataset. **(A)** The plot on the left represents a scatter plot of the number of mitochondria in individual cells and number of RNAs detected. The plot in the middle represents a scatter plot of the number of signature genes in relation to the number of RNAs detected. The plot on the right represents a scatter plot of the number of erythrocyte proteins mixed in the sample in relation to number of RNAs detected; **(B)** Distribution of all clusters is represented with a UMAP plot, where different colors represent different samples; **(C)** Differences in signature RNA expression, the total number of RNAs detected, pMT, and pHB in different clinical samples. pMT: percent of mitochondrial counts; pHB: percent of hemoglobin RNA counts.

Supplementary Figure 2 | Intersection and enrichment analysis of DEGs in $CD14^+$ and $CD16^+$ monocytes from Alzheimer's Disease (AD) patients for the GSE51835 bulk RNA dataset. **(A,B)** Cellchat-based results demonstrating the association of specific cell populations with other cell populations on various cellular pathways, including the ANNEXIN signaling pathway (A), and RESISTIN signaling pathway (B); **(C)** Venn diagram showing results of intersection analysis of DEGs in $CD14^+$ and $CD16^+$ monocytes from AD patients for the GSE51835 bulk RNA dataset; **(D)** Differentially expressed genes co-expressed in CD14 + monocytes from AD patients after exercise; **(E)** Differentially expressed genes co-expressed in CD16 + monocytes from AD patients after exercise.

Supplementary Figure 3 | Key transcriptome clusters of monocytes affected by exercise in AD patients with pseudotime analysis. **(A)** Distinct cell types' transcriptional regulatory activity in different cell modules; **(B)** All $CD14^+$ and $CD16^+$ monocytes were subjected to a principal component analysis (PCA); **(C)** Scatter plots of *APP*, *CCR1*, *TNF*, *ATF3*, *KLF4*, *HES4*, and *MAFB* expression profiles; **(D)** Distribution of $CD14^+$ and $CD16^+$ monocytes on pseudotime trajectories, pseudotime value distribution plots, and pseudotime trajectories branching **(E)**. *APP*, *CCR1*, *TNF*, *ATF3*, *KLF4*, *HES4*, and *MAFB* expression levels in relation to pseudo-time; **(F)** In the post-exercise bulk RNA collection, these seven important genes of *APP*, *CCR1*, *TNF*, *ATF3*, *HES4*, and *KLF4* were discovered to be tightly related.

Supplementary Figure 4 | The ERADMT gene set was found to be a potential risk marker for the development of patients with AD. **(A)** Correlation analysis of *APP*, *CCR1*, *TNF*, *ATF3*, *KLF4*, *HES4*, and *MAFB* in the GSE140831 dataset; **(B,C)** The box plot shows that the model residuals of SVM are larger than those of RF model; **(D)** Relationship between the "error" of the RF model and number of selected trees of the model; **(E)** Ranking of ERADMT genes according to their importance; **(F)** Predictive power of RF and SVM models with predictive power demonstrated by the ROC curves; **(G)** The nomogram prediction model constructed with the expression features of the ERADMT gene set; **(H)** The nomogram prediction model's calibration curve based on the ERADMT gene set.

Supplementary Figure 5 | The ERADMT gene set prediction AD risk column nomogram prediction model's predictive power was evaluated; **(A)** Decision Curve Analysis (DCA) curves of the nomogram prediction model based on the ERADMT gene set; **(B)** The nomogram prediction model based on the ERADMT gene set underwent DCA.

REFERENCES

Bai, G., Cheung, I., Shulha, H. P., Coelho, J. E., Li, P., Dong, X., et al. (2015). Epigenetic dysregulation of hairy and enhancer of split 4 (HES4) is associated with striatal degeneration in postmortem Huntington brains. *Hum. Mol. Genet.* 24, 1441–1456. doi: 10.1093/hmg/ddu561

Bao, C., He, C., Shu, B., Meng, T., Cai, Q., Li, B., et al. (2021). Aerobic exercise training decreases cognitive impairment caused by demyelination by regulating ROCK signaling pathway in aging mice. *Brain Res. Bull.* 168, 52–62. doi: 10.1016/j.brainresbull.2020.12.010

Barrett, T., Wilhite, S. E., Ledoux, P., Evangelista, C., Kim, I. F., Tomashevsky, M., et al. (2012). NCBI GEO: archive for functional genomics data sets—update. *Nucleic Acids Res.* 41, D991–D995. doi: 10.1093/nar/gks1193

Becht, E., McInnes, L., Healy, J., Dutertre, C.-A., Kwok, I. W. H., Ng, L. G., et al. (2018). Dimensionality reduction for visualizing single-cell data using UMAP. *Nat. Biotechnol.* 37, 38–44. doi: 10.1038/nbt.4314

Beck, M. W. (2018). NeuralNetTools: visualization and analysis tools for neural networks. *J. Stat. Softw.* 85, 1–20. doi: 10.18637/jss.v085.i11

Cabili, M. N., Trapnell, C., Goff, L., Koziol, M., Tazon-Vega, B., Regev, A., et al. (2011). Integrative annotation of human large intergenic noncoding RNAs reveals global properties and specific subclasses. *Genes Dev.* 25, 1915–1927. doi: 10.1101/gad.17446611

Chen, M., Ye, A., Wei, J., Wang, R., and Poon, K. (2020). Deoxycholic acid upregulates the reprogramming factors KFL4 and OCT4 through the IL-6/STAT3 pathway in esophageal adenocarcinoma cells. *Technol. Cancer Res. Treat.* 19:153303382094530. doi: 10.1177/1533033820945302

Chen, Y., Sun, Y., Xu, Y., Lin, W.-W., Luo, Z., Han, Z., et al. (2021). Single-cell integration analysis of heterotopic ossification and fibrocartilage developmental lineage: endoplasmic reticulum stress effector Xbp1 transcriptionally regulates the notch signaling pathway to mediate fibrocartilage differentiation. *Oxid. Med. Cell. Longev.* 2021:7663366. doi: 10.1155/2021/7663366

Costa-Silva, J., Domingues, D., and Lopes, F. M. (2017). RNA-Seq differential expression analysis: an extended review and a software tool. *PLoS One* 12:e0190152. doi: 10.1371/journal.pone.0190152

De Decker, M., Lavaert, M., Roels, J., Tilleman, L., Vandekerckhove, B., Leclercq, G., et al. (2020). HES1 and HES4 have non-redundant roles downstream of notch during early human T-cell development. *Haematologica* 106, 130–141. doi: 10.3324/haematol.2019.226126

Deng, H., Sun, Y., Zeng, W., Li, H., Guo, M., Yang, L., et al. (2020). New classification of macrophages in plaques: a revolution. *Curr. Atheroscler. Rep.* 22:31. doi: 10.1007/s11883-020-00850-y

Dobri, A.-M., Dudău, M., Enciu, A.-M., and Hinescu, M. E. (2021). CD36 in Alzheimer's disease: an overview of molecular mechanisms and therapeutic targeting. *Neuroscience* 453, 301–311. doi: 10.1016/j.neuroscience.2020.11.003

Efremova, M., Vento-Tormo, M., Teichmann, S. A., and Vento-Tormo, R. (2020). CellPhoneDB: inferring cell–cell communication from combined expression of multi-subunit ligand–receptor complexes. *Nat. Protoc.* 15, 1484–1506. doi: 10.1038/s41596-020-0292-x

Fan, Z., Turiel, G., Ardicoglu, R., Ghobrial, M., Masschelein, E., Kocijan, T., et al. (2021). Exercise-induced angiogenesis is dependent on metabolically primed $ATF3/4^+$ endothelial cells. *Cell Metab.* 33, 1793–1807.e9. doi: 10.1016/j.cmet.2021.07.015

Fernández-Verdejo, R., Vanwynsberghe, A. M., Essaghir, A., Demoulin, J., Hai, T., Deldicque, L., et al. (2017). Activating transcription factor 3 attenuates chemokine and cytokine expression in mouse skeletal muscle after exercise and facilitates molecular adaptation to endurance training. *FASEB J.* 31, 840–851. doi: 10.1096/fj.201600987R

Gu, B. J., Huang, X., Ou, A., Rembach, A., Fowler, C., Avula, P. K., et al. (2016). Innate phagocytosis by peripheral blood monocytes is altered in Alzheimer's disease. *Acta Neuropathol.* 132, 377–389. doi: 10.1007/s00401-016-1596-3

Jin, S., Guerrero-Juarez, C. F., Zhang, L., Chang, I., Ramos, R., Kuan, C.-H., et al. (2021). Inference and analysis of cell-cell communication using CellChat. *Nat. Commun.* 12:1088. doi: 10.1038/s41467-021-21246-9

Kang, X., Chen, B., Chen, Y., Yi, B., Yan, X., Jiang, C., et al. (2020). A prediction modeling based on SNOT-22 score for endoscopic nasal septoplasty: a retrospective study. *PeerJ* 8:e9890. doi: 10.7717/peerj.9890

Kapellos, T. S., Bonaguro, L., Gemünd, I., Reusch, N., Saglam, A., Hinkley, E. R., et al. (2019). Human monocyte subsets and phenotypes in major chronic inflammatory diseases. *Front. Immunol.* 10:2035. doi: 10.3389/fimmu.2019.02035

Khan, S., and Kaihara, K. A. (2019). "Single-cell RNA-sequencing of peripheral blood mononuclear cells with ddSEQ," in *Single Cell Methods*, ed. V. Proserpio (New York, NY: Springer New York), 155–176. doi: 10.1007/978-1-4939-9240-9_10

Kim, J.-E., Cho, Y.-H., and Seo, T.-B. (2020). Treadmill exercise activates ATF3 and ERK1/2 downstream molecules to facilitate axonal regrowth after sciatic nerve injury. *J. Exerc. Rehabil.* 16, 141–147. doi: 10.12965/jer.2040188.094

Kivipelto, M., Mangialasche, F., and Ngandu, T. (2018). Lifestyle interventions to prevent cognitive impairment, dementia and Alzheimer disease. *Nat. Rev. Neurol.* 14, 653–666. doi: 10.1038/s41582-018-0070-3

Lee, M.-H., Siddoway, B., Kaeser, G. E., Segota, I., Rivera, R., Romanow, W. J., et al. (2018). Somatic APP gene recombination in Alzheimer's disease and normal neurons. *Nature* 563, 639–645. doi: 10.1038/s41586-018-0718-6

Lei, P., Ayton, S., and Bush, A. I. (2021). The essential elements of Alzheimer's disease. *J. Biol. Chem.* 296:100105. doi: 10.1074/jbc.REV120.008207

Li, P., and Luo, L. (2021). Identification of critical genes and signaling pathways in human monocytes following high-intensity exercise. *Healthcare* 9:618. doi: 10.3390/healthcare9060618

Li, X. M., Kim, S. J., Hong, D.-K., Jung, K. E., Choi, C. W., Seo, Y.-J., et al. (2019). KLF4 suppresses the tumor activity of cutaneous squamous cell carcinoma (SCC) cells via the regulation of SMAD signaling and SOX2 expression. *Biochem. Biophys. Res. Commun.* 516, 1110–1115. doi: 10.1016/j.bbrc.2019.07.011

Lin, W., Wang, Y., Chen, Y., Wang, Q., Gu, Z., and Zhu, Y. (2021). Role of calcium signaling pathway-related gene regulatory networks in ischemic stroke based on multiple WGCNA and single-cell analysis. *Oxid. Med. Cell. Longev.* 2021:8060477. doi: 10.1155/2021/8060477

Lin, W.-W., Xu, L.-T., Chen, Y.-S., Go, K., Sun, C., and Zhu, Y.-J. (2021). Single-cell transcriptomics-based study of transcriptional regulatory features in the mouse brain vasculature. *Biomed Res. Int.* 2021:7643209. doi: 10.1155/2021/7643209

Liu, C., Cui, G., Zhu, M., Kang, X., and Guo, H. (2014). Neuroinflammation in Alzheimer's disease: chemokines produced by astrocytes and chemokine receptors. *Int. J. Clin. Exp. Pathol.* 7, 8342–8355.

López-Ortiz, S., Pinto-Fraga, J., Valenzuela, P. L., Martín-Hernández, J., Seisdedos, M. M., García-López, O., et al. (2021). Physical exercise and Alzheimer's disease: effects on pathophysiological molecular pathways of the disease. *Int. J. Mol. Sci.* 22:2897. doi: 10.3390/ijms22062897

MacIntyre, A., Abramov, R., Hammond, C. J., Hudson, A. P., Arking, E. J., Little, C. S., et al. (2003). Chlamydia pneumoniae infection promotes the transmigration of monocytes through human brain endothelial cells. *J. Neurosci. Res.* 71, 740–750. doi: 10.1002/jnr.10519

Macpherson, H., Teo, W.-P., Schneider, L. A., and Smith, A. E. (2017). A life-long approach to physical activity for brain health. *Front. Aging Neurosci.* 9:147. doi: 10.3389/fnagi.2017.00147

Mancuso, R., Baglio, F., Cabinio, M., Calabrese, E., Hernis, A., Nemni, R., et al. (2013). Titers of herpes simplex virus type 1 antibodies positively correlate with grey matter volumes in Alzheimer's disease. *J. Alzheimers Dis.* 38, 741–745. doi: 10.3233/JAD-130977

Mangiola, S., Doyle, M. A., and Papenfuss, A. T. (2021). Interfacing seurat with the R tidy universe. *Bioinformatics* 37, 4100–4107. doi: 10.1093/bioinformatics/btab404

Masuda, T., Sankowski, R., Staszewski, O., and Prinz, M. (2020). Microglia heterogeneity in the single-cell era. *Cell Rep.* 30, 1271–1281. doi: 10.1016/j.celrep.2020.01.010

Miklossy, J. (2011). Emerging roles of pathogens in Alzheimer disease. *Expert Rev. Mol. Med.* 13:e30. doi: 10.1017/S1462399411002006

Mou, T., Deng, W., Gu, F., Pawitan, Y., and Vu, T. N. (2020). Reproducibility of methods to detect differentially expressed genes from single-cell RNA sequencing. *Front. Genet.* 10:1331. doi: 10.3389/fgene.2019.01331

Noble, J. M., Scarmeas, N., Celenti, R. S., Elkind, M. S. V., Wright, C. B., Schupf, N., et al. (2014). Serum IgG antibody levels to periodontal microbiota are associated with incident Alzheimer disease. *PLoS One* 9:e114959. doi: 10.1371/journal.pone.0114959

Olivieri, A. C. (2021). A down-to-earth analyst view of rotational ambiguity in second-order calibration with multivariate curve resolution - a tutorial. *Anal. Chim. Acta* 1156:338206. doi: 10.1016/j.aca.2021.338206

Park, J.-W., Kim, K.-H., Choi, J.-K., Park, T. S., Song, K.-D., and Cho, B.-W. (2021). Regulation of toll-like receptors expression in muscle cells by exercise-induced stress. *Anim. Biosci.* 34, 1590–1599. doi: 10.5713/ab.20.0484

Paterson, C., Kilmister, E. J., Brasch, H. D., Bockett, N., Patel, J., Paterson, E., et al. (2021). Cell populations expressing stemness-associated markers in lung adenocarcinoma. *Life* 11:1106. doi: 10.3390/life11101106

Pereira, W. J., Almeida, F. M., Conde, D., Balmant, K. M., Triozzi, P. M., Schmidt, H. W., et al. (2021). Asc-seurat: analytical single-cell Seurat-based web application. *BMC Bioinformatics* 22:556. doi: 10.1186/s12859-021-04472-2

Pessina, A., Bonomi, A., Sisto, F., Baglio, C., Cavicchini, L., Ciusani, E., et al. (2010). $CD45^{+}/CD133^{+}$ positive cells expanded from umbilical cord blood expressing PDX-1 and markers of pluripotency. *Cell Biol. Int.* 34, 783–790. doi: 10.1042/CBI20090236

Pfeffer, R. I., Afifi, A. A., and Chance, J. M. (1987). Prevalence of Alzheimer's disease in a retirement community. *Am. J. Epidemiol.* 125, 420–436. doi: 10.1093/oxfordjournals.aje.a114548

Qiu, X., Mao, Q., Tang, Y., Wang, L., Chawla, R., Pliner, H. A., et al. (2017). Reversed graph embedding resolves complex single-cell trajectories. *Nat. Methods* 14, 979–982. doi: 10.1038/nmeth.4402

Radom-Aizik, S., Zaldivar, F. P., Haddad, F., and Cooper, D. M. (2014). Impact of brief exercise on circulating monocyte gene and microRNA expression: implications for atherosclerotic vascular disease. *Brain Behav. Immunity* 39, 121–129. doi: 10.1016/j.bbi.2014.01.003

Santiago, J. A., Bottero, V., and Potashkin, J. A. (2020). Transcriptomic and network analysis identifies shared and unique pathways across dementia spectrum disorders. *Int. J. Mol. Sci.* 21:2050. doi: 10.3390/ijms21062050

Savarin-Vuaillat, C., and Ransohoff, R. M. (2007). Chemokines and chemokine receptors in neurological disease: raise, retain, or reduce? *Neurotherapeutics* 4, 590–601. doi: 10.1016/j.nurt.2007.07.004

Selkoe, D. J., and Hardy, J. (2016). The amyloid hypothesis of Alzheimer's disease at 25 years. *EMBO Mol. Med.* 8, 595–608. doi: 10.15252/emmm.201606210

Shi, Q., Yan, X., Wang, J., and Zhang, X. (2021). Collagen family genes associated with risk of recurrence after radiation therapy for vestibular schwannoma and pan-cancer analysis. *Dis. Markers* 2021:7897994. doi: 10.1155/2021/7897994

Strohacker, K., Breslin, W. L., Carpenter, K. C., Davidson, T. R., Agha, N. H., and McFarlin, B. K. (2012). Moderate-intensity, premeal cycling blunts postprandial increases in monocyte cell surface CD18 and CD11a and endothelial microparticles following a high-fat meal in young adults. *Appl. Physiol. Nutr. Metab.* 37, 530–539. doi: 10.1139/h2012-034

Suo, S., Zhu, Q., Saadatpour, A., Fei, L., Guo, G., and Yuan, G.-C. (2018). Revealing the critical regulators of cell identity in the mouse cell atlas. *Cell Rep.* 25, 1436–1445.e3. doi: 10.1016/j.celrep.2018.10.045

Tuzlak, S., Dejean, A. S., Iannacone, M., Quintana, F. J., Waisman, A., Ginhoux, F., et al. (2021). Repositioning TH cell polarization from single cytokines to complex help. *Nat. Immunol.* 22, 1210–1217. doi: 10.1038/s41590-021-01009-w

Van Calster, B., Wynants, L., Verbeek, J. F. M., Verbakel, J. Y., Christodoulou, E., Vickers, A. J., et al. (2018). Reporting and interpreting decision curve analysis: a guide for investigators. *Eur. Urol.* 74, 796–804. doi: 10.1016/j.eururo.2018.08.038

Wagley, Y., Chesi, A., Acevedo, P. K., Lu, S., Wells, A. D., Johnson, M. E., et al. (2020). Canonical notch signaling is required for bone morphogenetic protein-mediated human osteoblast differentiation. *Stem Cells* 38, 1332–1347. doi: 10.1002/stem.3245

Wang, J.-S., Chen, Y.-W., Chow, S.-E., Ou, H.-C., and Sheu, W. H.-H. (2005). Exercise paradoxically modulates oxidized LDL-induced adhesion molecules expression and trans-endothelial migration of monocyte in men. *Thromb. Haemost.* 94, 846–852. doi: 10.1160/TH05-02-0139

Wisniewski, H. M., Wegiel, J., Vorbrodt, A. W., Mazur-Kolecka, B., and Frackowiak, J. (2000). Role of perivascular cells and myocytes in vascular amyloidosis. *Ann. N. Y. Acad. Sci.* 903, 6–18. doi: 10.1111/j.1749-6632.2000.tb06344.x

Wu, J., Qin, J., Li, L., Zhang, K., Chen, Y., Li, Y., et al. (2021). Roles of the immune/methylation/autophagy landscape on single-cell genotypes and stroke risk in breast cancer microenvironment. *Oxid. Med. Cell. Longev.* 2021:5633514. doi: 10.1155/2021/5633514

Xu, H., and Jia, J. (2021). Single-cell RNA sequencing of peripheral blood reveals immune cell signatures in Alzheimer's disease. *Front. Immunol.* 12:645666. doi: 10.3389/fimmu.2021.645666

Ying, C., Guo, C., Wang, Z., Chen, Y., Sun, J., Qi, X., et al. (2021). A prediction modeling based on the Hospital for Special Surgery (HSS) knee score for poor postoperative functional prognosis of elderly patients with patellar fractures. *Biomed Res. Int.* 2021:6620504. doi: 10.1155/2021/6620504

Yu, G., Wang, L.-G., Han, Y., and He, Q.-Y. (2012). clusterProfiler: an R Package for comparing biological themes among gene clusters. *Omics* 16, 284–287. doi: 10.1089/omi.2011.0118

Zhang, H., Meltzer, P., and Davis, S. (2013). RCircos: an R package for Circos 2D track plots. *BMC Bioinformatics.* 14:244. doi: 10.1186/1471-2105-14-244

Zhang, J.-Y., Wang, X.-M., Xing, X., Xu, Z., Zhang, C., Song, J.-W., et al. (2020). Single-cell landscape of immunological responses in patients with COVID-19. *Nat. Immunol.* 21, 1107–1118. doi: 10.1038/s41590-020-0762-x

Conflict of Interest: The authors declare that the research was conducted in the absence of any commercial or financial relationships that could be construed as a potential conflict of interest.

Publisher's Note: All claims expressed in this article are solely those of the authors and do not necessarily represent those of their affiliated organizations, or those of the publisher, the editors and the reviewers. Any product that may be evaluated in this article, or claim that may be made by its manufacturer, is not guaranteed or endorsed by the publisher.

frontiers | Frontiers in Aging Neuroscience

ORIGINAL RESEARCH
published: 27 May 2022
doi: 10.3389/fnagi.2022.918217

General Transcription Factor IIF Polypeptide 2: A Novel Therapeutic Target for Depression Identified Using an Integrated Bioinformatic Analysis

Chi Zhang[1], Min Cheng[1], Naifu Dong[1], Dongjie Sun[2] and Haichun Ma[1]**

[1] Department of Anesthesiology, The First Hospital of Jilin University, Changchun, China, [2] College of Basic Medical Sciences, Jilin University, Changchun, China

OPEN ACCESS

Edited by:
Min Tang,
Jiangsu University, China

Reviewed by:
Hao Chen,
Hunan University, China
Yalin Wu,
Lushan Botanical Garden (CAS), China

***Correspondence:**
Dongjie Sun
sunparrow@126.com
Haichun Ma
mahc@jlu.edu.cn

Specialty section:
This article was submitted to Neuroinflammation and Neuropathy, a section of the journal Frontiers in Aging Neuroscience

Received: 12 April 2022
Accepted: 09 May 2022
Published: 27 May 2022

Citation:
Zhang C, Cheng M, Dong N, Sun D and Ma H (2022) General Transcription Factor IIF Polypeptide 2: A Novel Therapeutic Target for Depression Identified Using an Integrated Bioinformatic Analysis. Front. Aging Neurosci. 14:918217. doi: 10.3389/fnagi.2022.918217

Depression currently affects 4% of the world's population; it is associated with disability in 11% of the global population. Moreover, there are limited resources to treat depression effectively. Therefore, we aimed to identify a promising novel therapeutic target for depression using bioinformatic analysis. The GSE54568, GSE54570, GSE87610, and GSE92538 gene expression data profiles were retrieved from the Gene Expression Omnibus (GEO) database. We prepared the four GEO profiles for differential analysis, protein–protein interaction (PPI) network construction, and weighted gene co-expression network analysis (WGCNA). Gene Ontology functional enrichment and Kyoto Encyclopedia of Genes and Genomes metabolic pathway analyses were conducted to determine the key functions of the corresponding genes. Additionally, we performed correlation analyses of the hub genes with transcription factors, immune genes, and N6-methyladenosine (m6A) genes to reveal the functional landscape of the core genes associated with depression. Compared with the control samples, the depression samples contained 110 differentially expressed genes (DEGs), which comprised 56 downregulated and 54 upregulated DEGs. Moreover, using the WGCNA and PPI clustering analysis, the blue module and cluster 1 were found to be significantly correlated with depression. *GTF2F2* was the only common gene identified using the differential analysis and WGCNA; thus, it was used as the hub gene. According to the enrichment analyses, GTF2F2 was predominantly involved in the cell cycle and JAK-STAT, PI3K-Akt, and p53 signaling pathways. Furthermore, differential and correlation analyses revealed that 9 transcription factors, 12 immune genes, and 2 m6A genes were associated with GTF2F2 in depression samples. GTF2F2 may serve as a promising diagnostic biomarker and treatment target of depression, and this study provides a novel perspective and valuable information to explore the molecular mechanism of depression.

Keywords: depression, GTF2F2, therapeutic target, bioinformatics, WGCNA

INTRODUCTION

Depression is a common mental health disorder that currently affects 4% of the world's population, and it is associated with disability in 11% of the global population. It has been recognized as one of the most serious public health concerns with limited global public health progression (Hao et al., 2019). In some cases, psychiatric symptoms such as hallucinations and delusions may occur, accompanied by suicidal behavior (Chambers et al., 1982). The prevalence rate of depression in the United States of America exceeds 24% and is associated with other health and behavioral issues, including 800,000 annual suicides predominantly among young people. Millions of people die of the disease every year (Maurer et al., 2018). Moreover, depression increases the likelihood of early mortality, substance use, and anxiety (Casey, 2017; Kandola et al., 2019). Although the clinical symptoms of depression can be alleviated, the treatment and recurrence rates of the disease are not very optimistic because of patients' inadequate knowledge and unwillingness to obtain regular treatments such as psychological and pharmacological therapies (Hardeveld et al., 2010). Indeed, half of the patients with major depressive disorder (MDD) do not respond to antidepressants (Hennings et al., 2009). To date, the specific cause of depression is not clear, and the dynamics and potential mechanisms of its onset and development remain poorly understood, thereby impeding the development and application of treatment strategies.

The recent rapid development of bioinformatics with high-throughput gene expression detection and hub gene screening methods, as well as weighted gene co-expression network analysis (WGCNA), has been advantageous in identifying the genes or specific molecular cascades involved in complex diseases, providing strategies for elucidating the molecular mechanisms of depression. Some molecular characterization and gene signatures have been shown to have pathophysiological significance in the mechanism of depression (Iwamoto et al., 2004; Bian et al., 2021; see also Liu et al., 2020). However, their biological functions need to be clarified, and integrated bioinformatic analyses of the transcription factors (TFs) and immune and methyladenosine gene characteristics in depression are still lacking.

In this study, four gene expression data profiles were retrieved from the GEO database, with an aim to discern some promising biomarkers in depression using integrative bioinformatic methods. We then conducted Gene Ontology (GO) functional enrichment and Kyoto Encyclopedia of Genes and Genomes (KEGG) metabolic pathway enrichment analyses of the core differentially expressed genes (DEGs) to estimate the underlying functions of the corresponding genes. After WGCNA and protein–protein interaction (PPI) analysis, general transcription factor IIF polypeptide 2 (*GTF2F2*) was identified as the hub gene. GTF2F2 combines with general transcription factor IIF polypeptide 1 (GTF2F1) to form a heteromeric general transcription initiation factor (TFIIF), which subsequently binds to DNA-dependent RNA polymerase II (Sasaki et al., 2013; Tsymbal et al., 2016). RNA polymerase II plays a critical role in mRNA synthesis, and GTF2F2 is essential for the initiation and elongation phases of gene transcription (Sasaki et al., 2013). Moreover, GTF2F2 is responsible for neurogenesis, neuroplasticity, and synaptogenesis by the mediation of Nuclear respiratory factor-1 (NRF-1) expression (Tong et al., 2013). Recently, GTF2F2 has also been reported to be involved in the potential development of SARS-CoV-2 (Pierzynowska et al., 2020). Therefore, *GTF2G2* was further analyzed, and the correlation of GTF2G2 with TFs, immune genes, and m6A genes was investigated.

MATERIALS AND METHODS

Data Collection

The GSE54568, GSE54570, GSE87610, and GSE92538 gene expression data profiles were collected from the GEO database. These four profiles contained 15, 13, 72, and 56 normal and 15, 13, 76, and 29 depression samples, respectively. The R packages "limma" and "sva" were used to combine the four GEO profiles and to normalize the data matrix. Thereafter, the R package "ggplot2" was used to present sample distribution.

Differential Analysis

The R packages "limma" and "impute" were utilized to identify the DEGs in the normal and depression samples. Furthermore, the cutoff criteria used were adjusted p-value < 0.05 and $\log_2|$ fold change$| > 0.5$. The DEGs were then presented in a volcano plot and heat map.

Weighted Gene Co-expression Network Analysis

We also conducted WGCNA using the R package "WGCNA" to select genes of interest. WGCNA transformed the adjacency matrix into a topological overlap matrix (TOM) in accordance with the soft threshold power. Subsequently, the genes were divided into different modules using the TOM-based dissimilarity measure. The cutoff threshold for minModuleSize and mergeCutHeight was set to 30 and 0.25, respectively.

Protein–Protein Interaction Network Construction

The interaction information of proteins with a combined score > 0.7 was obtained from the search tool for the Retrieval of Interacting Genes/Proteins database.[1] Cytoscape software (version 3.8.2) and its plugin, MCODE, were used to visualize the network and conduct clustering analysis of the network.

Functional and Pathway Enrichment Analyses

FunRich software (version 3.1) was used to perform biological process and pathway enrichment analyses of the corresponding gene sets. Additionally, the R packages "org.Hs.eg.db" and "clusterProfiler" were used to conduct the GO and KEGG enrichment analyses of certain gene sets. Database for Annotation, Visualization, and Integrated Discovery (DAVID)[2] was used to investigate the enrichment of genes in TFs.

[1] https://string-db.org/

[2] https://david.ncifcrf.gov

Correlation Analysis

The correlation information of genes was retrieved using the R package "corrplot" and the correlation heat map was plotted with the R package "heatmap." The R packages "ggplot2," "ggpubr," and "ggExtra" were used to plot correlation density images. Moreover, the depression samples were grouped into high and low hub gene subgroups based on the median expression of the hub genes. We also used the R packages "limma" and "vioplot" to visualize the violin plots for the DEGs.

RESULTS

General Transcription Factor IIF Polypeptide 2 Identified as the Hub Gene

Samples from the four GEO profiles (GSE54568, GSE54570, GSE87610, and GSE92538) were uniformly and logically scattered in the principal component analysis (PCA) plot after normalization using the R package (as shown in **Figures 1A,B**). Compared with the normal samples, the depression samples contained 110 DEGs, which comprised 56 downregulated and 54 upregulated DEGs (as shown in **Figure 1C**). These DEGs presented different expression profiles in patients with depression compared with those in the corresponding normal controls (as shown in **Figure 1D**). The DEGs were substantially enriched in energy pathways, protein metabolism, metabolism, and other biological processes (as shown in **Supplementary Figure 1A** and **Supplementary Table 1**). For the biological pathway, the DEGs were predominantly associated with the adaptive immune system, interferon signaling, and antigen processing-cross presentation (as shown in **Supplementary Figure 1B** and **Supplementary Table 2**).

After considering the distribution of clinical traits within all 289 samples, no outliers were removed when the samples were clustered according to the WGCNA and differential analysis (as

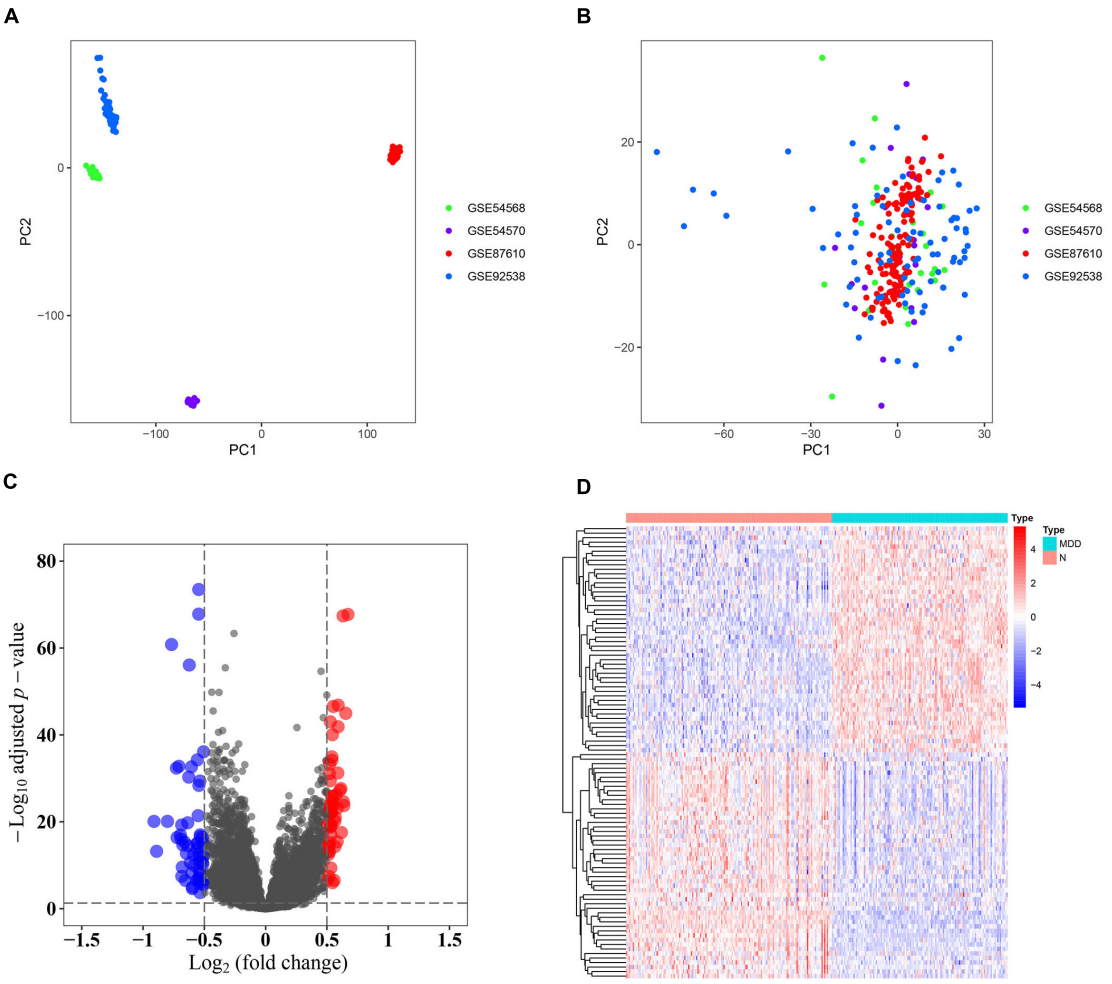

FIGURE 1 | Identification of differentially expressed genes (DEGs). **(A)** Principal component analysis (PCA) of the four profiles (GSE54568, GSE54570, GSE87610, and GSE92538) was conducted using the pre-normalized data matrix. **(B)** PCA of the four profiles (GSE54568, GSE54570, GSE87610, and GSE92538) was performed using the normalized data matrix. **(C)** Volcano plot of the DEGs in normal and depression samples, wherein the blue and red dots represent downregulated and upregulated DEGs, respectively. **(D)** Heat map plot of the expression profile of the DEGs in normal and depression samples.

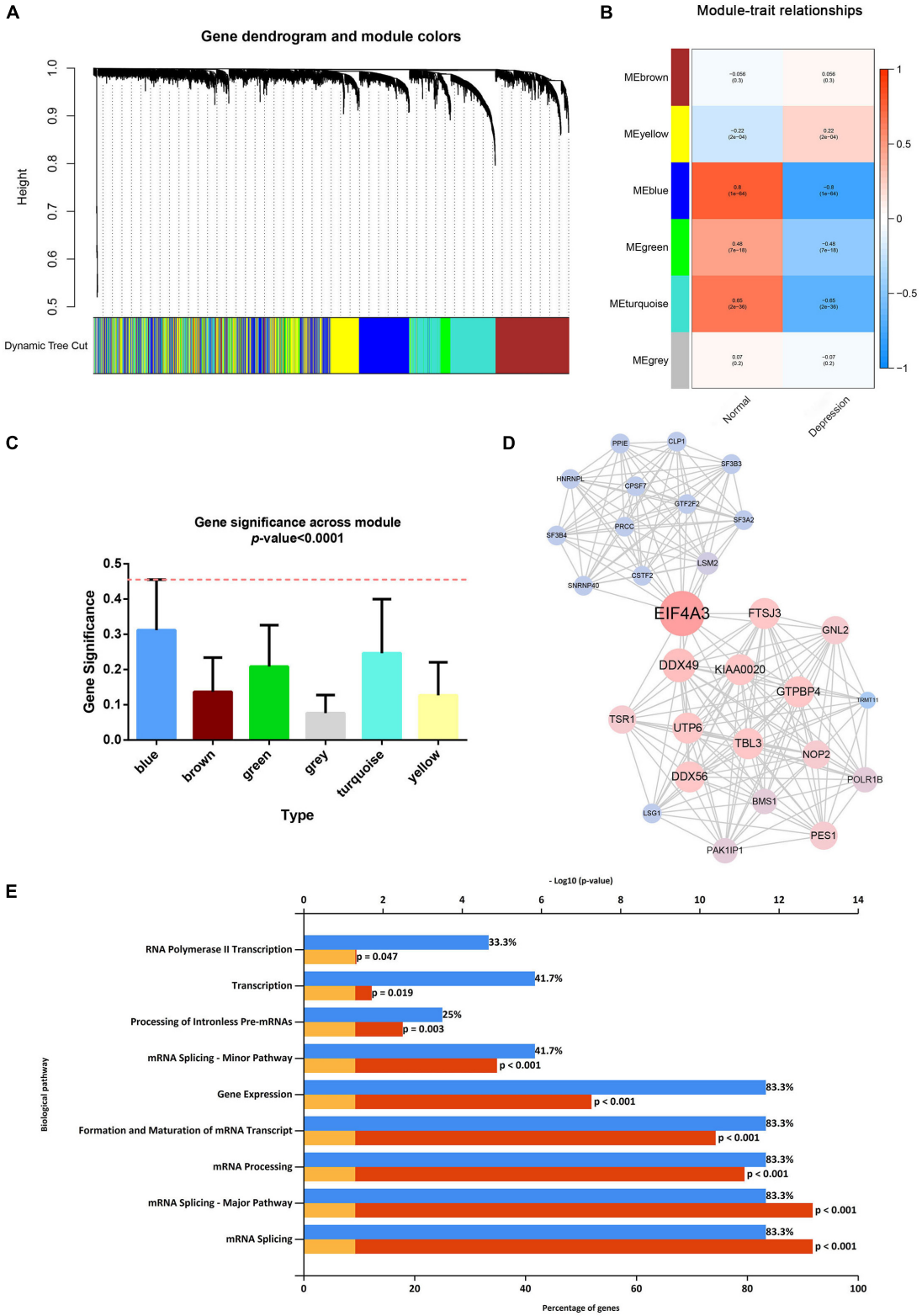

FIGURE 2 | Weighted gene co-expression network analysis and protein–protein analysis. **(A)** Image of a clustering dendrogram for the Gene Expression Omnibus profiles using the dissimilarity measure 1-TOM. **(B)** Heat map of the correlation between the module eigengenes and sample type. **(C)** Histogram for module significance of the distribution of the average gene significance and module errors for patients with depression. **(D)** Image of the network of the highest-scoring cluster in the protein–protein interaction network. **(E)** The typical pathways are enriched by the differentially expressed genes in the highest-scoring cluster.

shown in **Supplementary Figure 1**). A soft-thresholding power of 10 and a scale-free R^2 of 0.80 were identified and used to construct a scale-free network (as shown in **Supplementary Figures 3A,B**). Subsequently, six modules were identified; the blue module was significantly correlated with depression, and it presented a higher module significance than other modules (as shown in **Figures 2A–C**). Genes within the blue module were used to construct a PPI network containing 284 nodes and 764 edges (as shown in **Supplementary Figure 4**). We then analyzed the three clusters with the highest clustering scores within the PPI network, of which cluster 1 with the highest clustering score (14.427) comprised 29 nodes and 202 edges (as shown in **Figure 2D**) compared to cluster 2 (as shown in **Supplementary Figure 5**), and cluster 2 (as shown in **Supplementary Figure 6**). Cluster 1 was associated with mRNA splicing, processing, and formation; mRNA transcript maturation; and other pathways (as shown in **Figure 2E**). Additional details are provided in **Supplementary Tables 3–5**.

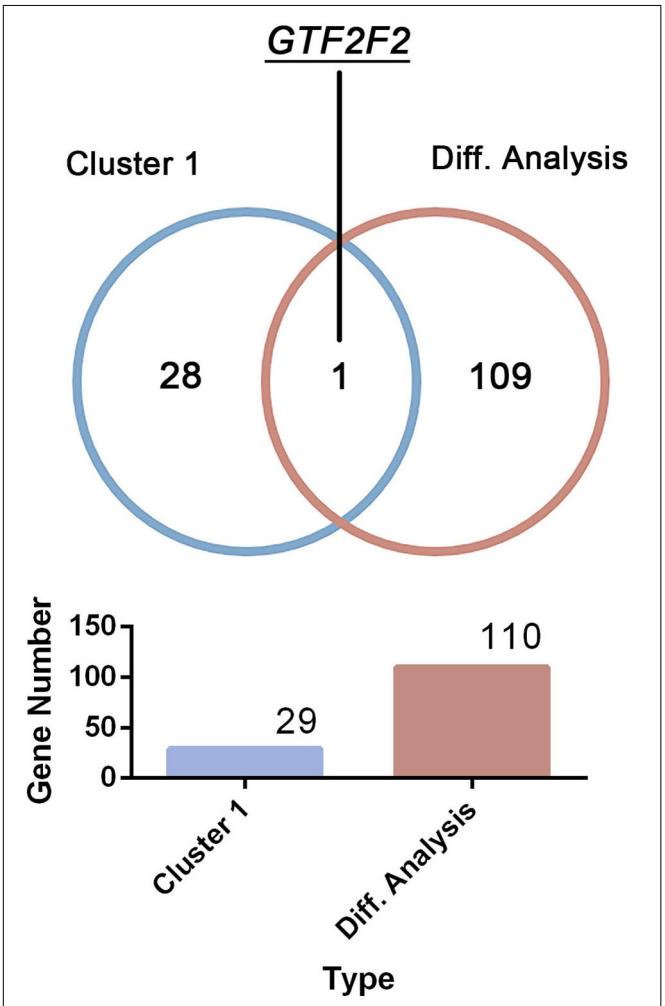

FIGURE 3 | Determination of the core gene. *GTF2F2* was the only common gene identified using the clustering analysis within cluster 1 and the differential analysis of both normal and depression samples.

Only one common gene, *GTF2F2*, was identified using the DEGs in the differential analysis and genes within cluster 1 (as shown in **Figure 3**). Therefore, *GTF2F2* was used as the hub gene in this study.

Functional Analysis of General Transcription Factor IIF Polypeptide 2

According to the differential analysis results, *GTF2F2* was significantly upregulated in depression samples compared with that in the corresponding controls (as shown in **Supplementary Figure 7A**), and the depression samples were grouped into high and low GTF2F2 expression subgroups based on the median GTF2F2 expression levels (as shown in **Supplementary Figure 7B**). Additionally, the DEGs in the high and low GTF2F2 expression subgroups were enriched using R software to determine the potential functions of GTF2F2. We found that GTF2F2 was significantly associated with responses to steroid hormones, rhythmic processes, intracellular receptor signaling pathways, and other biological processes (as shown in **Figure 4A**). The transcription regulator complex, photoreceptor cell cilium, and nuclear envelope were the main cellular components enriched. In terms of molecular function, GTF2F2 was only related to protein serine/threonine phosphatase activity. Further details are provided in **Supplementary Table 6**. Furthermore, GTF2F2 may be involved in the cell cycle and cell senescence. It may also be involved in JAK-STAT, PI3K-Akt, p53, TGF-β, and other biological signaling pathways (as shown in **Figure 4B**). Additional details are provided in **Supplementary Table 7**. Moreover, a heat map was plotted to depict the association between the top 10 downregulated and upregulated DEGs in the high GTF2F2 subgroup, compared with that in the low GTF2F2 subgroup (as shown in **Supplementary Figure 8**). *YEATS4* and *ARMCX5* had a positive correlation with *GTF2F2*, whereas *XPO6* and *C3* had a negative correlation with *GTF2F2* (as shown in **Figure 5**).

General Transcription Factor IIF Polypeptide 2 Associated With Transcription Factors

Using the DAVID platform, the 20 DEGs in the correlation analysis were found to be predominantly enriched in the five TFs: RORA2, TCF11, PPARA, GATA2, and LMO2COM (as shown in **Supplementary Figure 9**). Additionally, we established the correlation between GTF2F2 and TFs based on their mRNA expression levels, whereby the TFs with the top 10 positive and negative correlations are depicted in a heat map (as shown in **Supplementary Figure 10**). We used 20 TFs for further analysis, 16 of which were significantly differentially expressed in depression samples compared with those in normal samples as shown in **Figure 6A**, and 11 TFs were significantly related to GTF2F2, based on their expression levels in the high and low GTF2F2 expression subgroups (as shown in **Figure 6B**). Moreover, nine TFs overlapped in the differential and correlation analyses (as shown in **Figure 6C**).

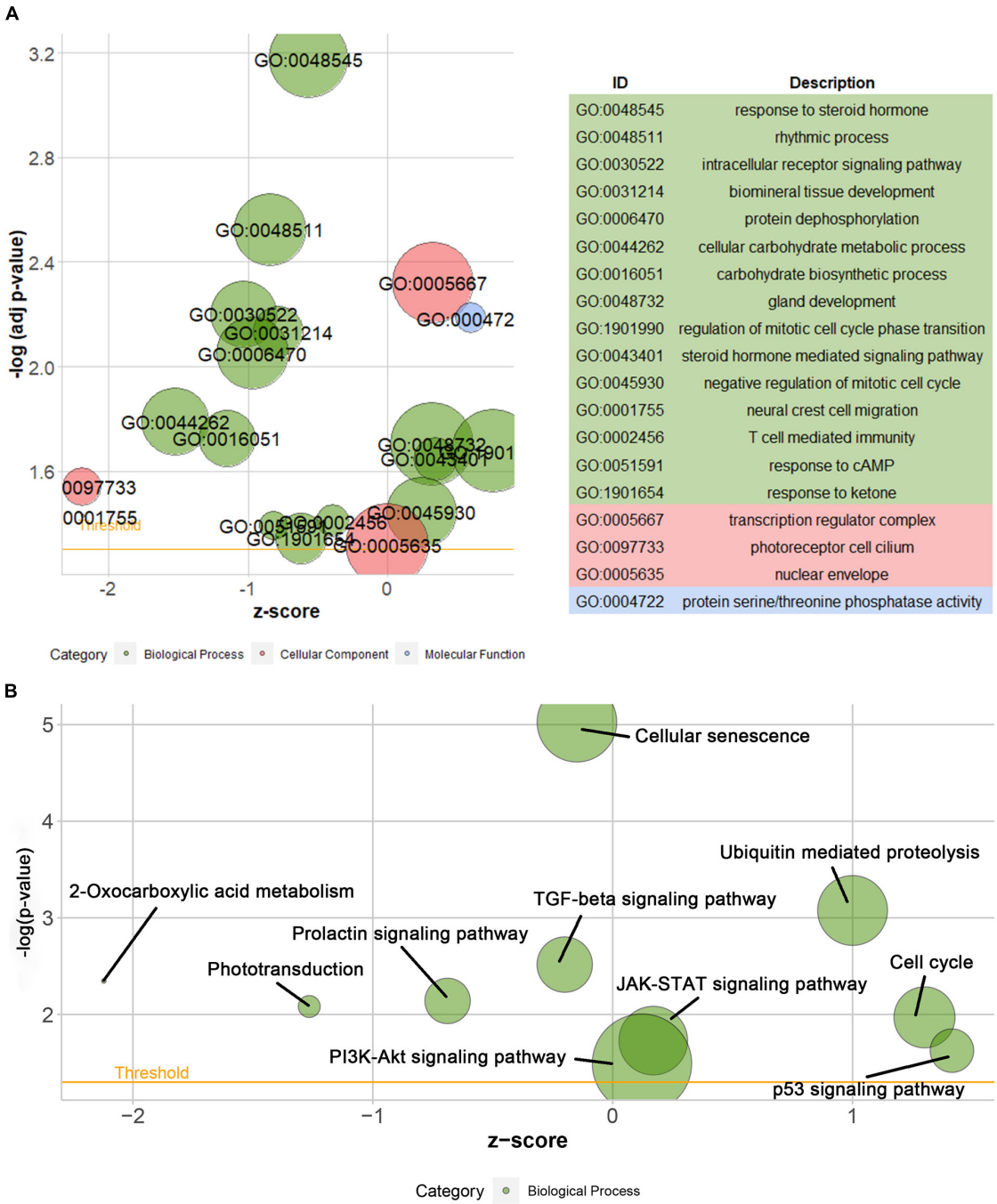

FIGURE 4 | Gene Ontology (GO) and Kyoto Encyclopedia of Genes and Genomes (KEGG) enrichment analyses of GTF2F2 function. **(A)** Bubble plot of the GO function analysis of the differentially expressed genes (DEGs) in the low and high GTF2F2 subgroups (grouped according to the median GTF2F2 expression levels). **(B)** Bubble plot of the KEGG pathway analysis of the DEGs in the low and high GTF2F2 expression subgroups. A higher z-score represents a higher expression of enriched terms.

General Transcription Factor IIF Polypeptide 2 Associated With Immune Genes

The correlation of GTF2F2 with immune genes was also determined based on their mRNA expression levels using R software, and the genes with the top 10 positive and negative association coefficients are presented in **Supplementary Figure 11**. Twenty immune genes were utilized to perform further differential and correlation analyses; 18 immune genes were significantly differentially expressed in depression samples compared with those in the corresponding controls (as shown in

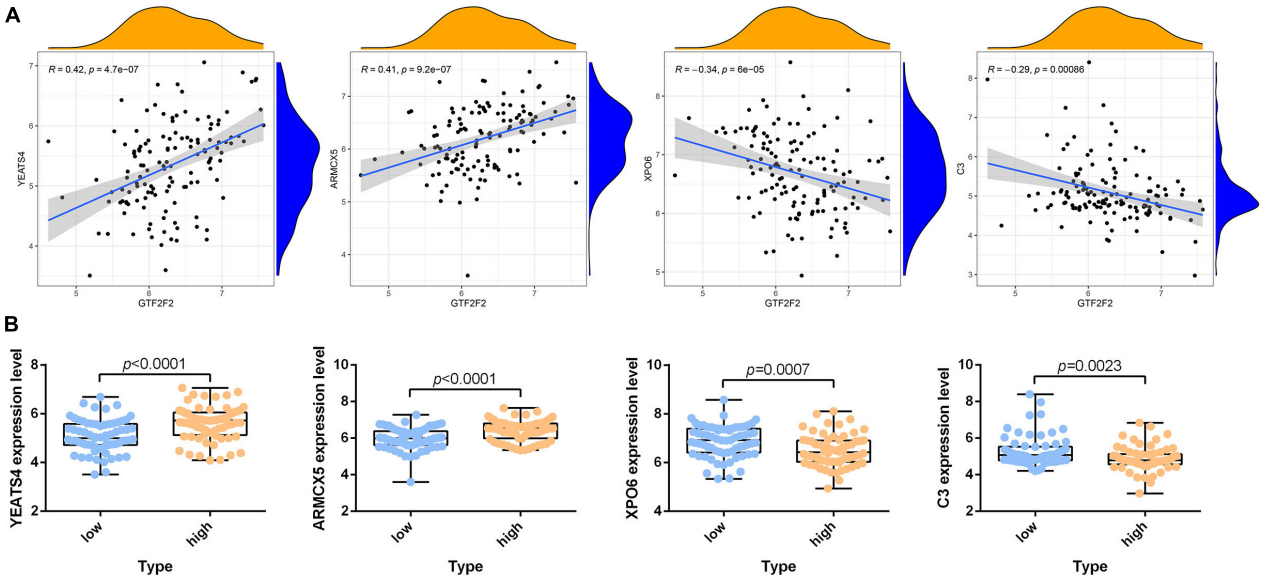

FIGURE 5 | Correlation of *GTF2F2* with *YEATS4*, *ARMCX5*, *XPO6*, and *C3*. **(A)** Scatter plots of the correlation of *GTF2F2* with *YEATS4*, *ARMCX5*, *XPO6*, and *C3*. **(B)** Histograms of the expression profiles of *YEATS4*, *ARMCX5*, *XPO6*, and *C3* in the low and high GTF2F2 subgroups (grouped according to the median GTF2F2 expression levels).

Figure 7A), and 13 immune genes were significantly associated with GTF2F2 based on their expression levels in the high and low GTF2F2 expression subgroups as shown in **Figure 7B**. Furthermore, 12 genes overlapped in the differential and correlation analyses (as shown in **Figure 7C**).

General Transcription Factor IIF Polypeptide 2 Associated With N6-Methyladenosine Genes

We investigated the association of GTF2F2 with m6A genes; **Supplementary Figure 12** presents a heat map of the correlation between 20 m6A genes with the top 10 positive and negative correlation coefficients. The differential and correlation analyses revealed that 12 m6A genes were significantly different in depression samples compared with those in their corresponding controls (as shown in **Figure 8A**). Moreover, three m6A genes were significantly correlated with GTF2F2 based on their expression levels in the high and low GTF2F2 expression subgroups (as shown in **Figure 8B**). Additionally, *METTL3* and *YTHDC1* were the only overlapping genes identified in the differential and correlation analyses (as shown in **Figure 8C**).

DISCUSSION

Depression with heterogeneous characteristics has been poorly reported, diagnosed, and treated. Patients with depression are suspected of being socially abandoned and having reduced interactions with others to manage their complex matters. Depression also affects the educational status, professional lives, and romantic relationships of individuals during their transition to adulthood (Park et al., 2018). In particular, MDD becomes a serious mental disorder that profoundly affects an individual's quality of life. Most patients with MDD are not effectively treated, and it is not clear why they discontinue treatment. The low response rates and high adverse effect burden of antidepressants mean that depression would require a longer time to attain therapeutic benefits. To date, there is no efficient biomarker for early diagnosis or for predicting or monitoring the pathogenesis of MDD in clinical trials, because the etiology and pathogenic mechanisms are undefined. Patients with depression have been reported to have reduced gray matter volume in the dorsolateral prefrontal cortex (DLPFC), and this may be associated with suicidal ideation (Zhang et al., 2020). Moreover, DLPFC-mediated cognitive control may also be related to emotional regulation, cognitive dysfunction, and motivation (Jones and Graff-Radford, 2021). Therefore, we collected the datasets containing DLPFC tissues of MDD, with an aim to identify a promising novel therapeutic target using an integrated bioinformatic analysis to provide valuable findings for further examinations of the pathogenic mechanisms of depression.

In our study, GTF2F2 was identified as the hub gene associated with MDD. GTF2F2 has a potential role in regulating neurite outgrowth. Neurite outgrowth is an intricate process, regulated by numerous genes. It is reported that GTF2F2 positively regulates neurite outgrowth through NRF-1 mediation. After silencing NRF-1, the mRNA levels of GTF2F2 increased, whereas the knockdown of GTF2F2 significantly decreased NRF-1-regulated neurite outgrowth (Tong et al., 2013; Preciados et al., 2016). Our results showed that GTF2F2 was significantly associated with rhythmic processes. Dysregulation of the circadian system increases the susceptibility to pathological conditions, including depression. Over 90% of the patients have sleep complaints. The successful treatment of depression

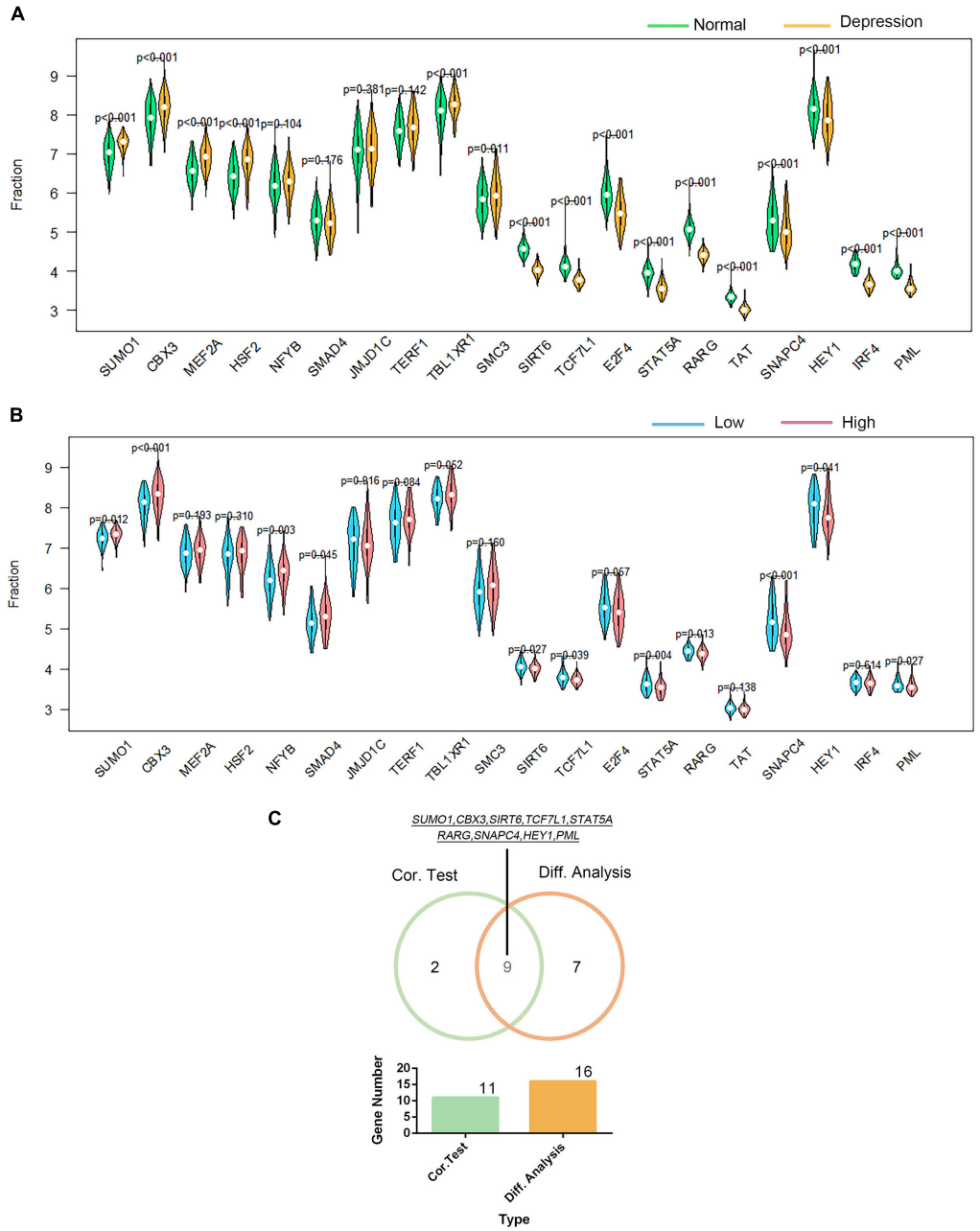

FIGURE 6 | Correlation of GTF2F2 with transcription factors. **(A)** Violin plot of the differential analysis of the top 20 transcription factors (TFs) in non-psychiatric control samples and depression samples. The top 20 TFs were determined using the correlation coefficient of GTF2F2 with TFs. **(B)** Violin plot of the expression profiles of the top 20 TFs in the subgroups with low and high GTF2F2 expression levels. **(C)** Venn plot of the nine common TFs that overlapped in the normal and depression samples and the subgroups with low and high GTF2F2 expression levels.

frequently leads to an improvement in altered circadian rhythm (Satyanarayanan et al., 2018; Geoffroy and Palagini, 2021). Furthermore, our results illustrated that higher expression of GTF2F2 foreboded higher expression of retinoid-related orphan receptor alpha (RORA), which has been linked to MDD (Ming et al., 2015; Min et al., 2017). RORA is involved in the regulation of circadian rhythms, and it has been suggested to be correlated with depression vulnerability (Chen et al., 2021). GTF2F2 may affect pathogenesis of depression through the circadian process. However, further verification needs to be carried out for identification.

Depression is associated with abnormalities in the immune system. The central nervous system, endocrine system, and immune system share the same neurotransmitters, cytokines, and hormones to communicate within and among each other (Kovaru et al., 2009). There is considerable evidence that

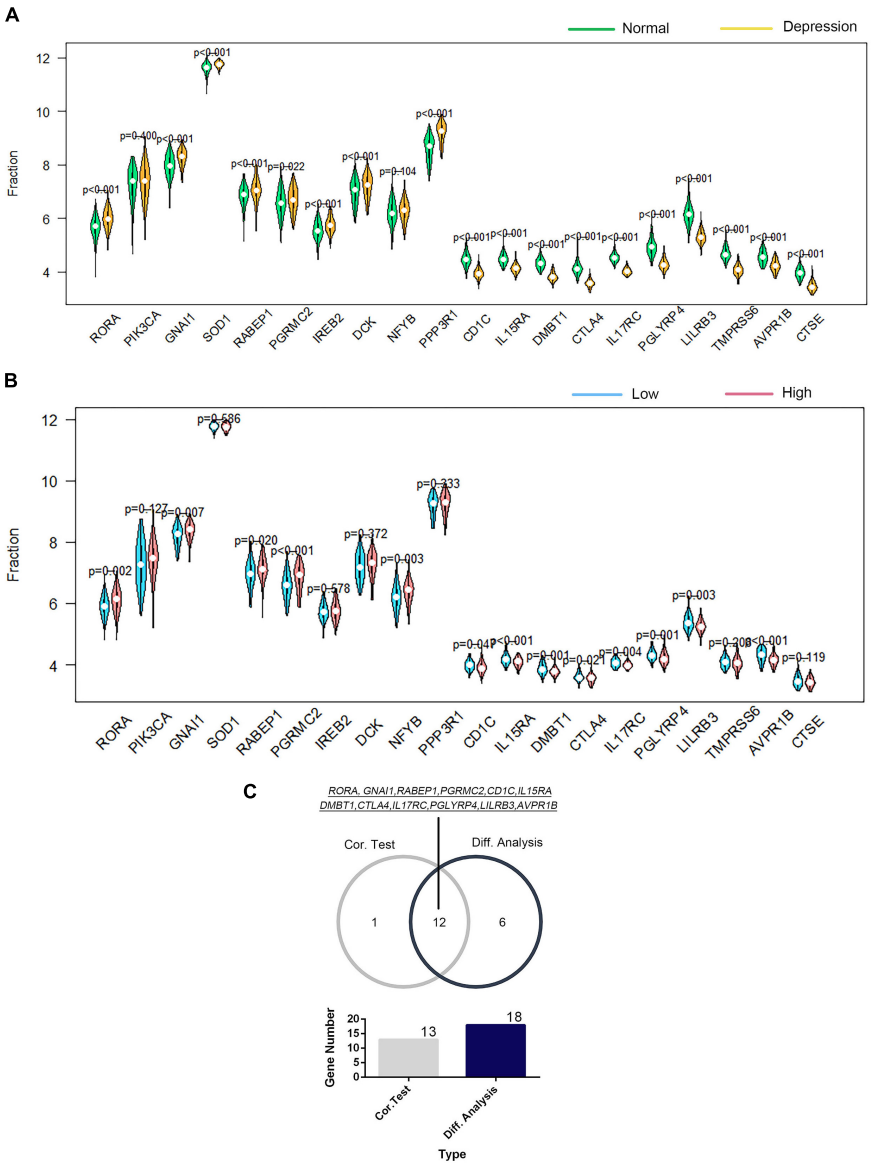

FIGURE 7 | Correlation of GTF2F2 with immune genes. **(A)** Violin plot of the differential analysis of the top 20 immune genes in normal and depression samples. The top 20 immune genes were determined using the correlation coefficient of GTF2F1 with immune genes. **(B)** Violin plot of the expression profiles of the top 20 immune genes in the subgroups with low and high GTF2F2 expression levels. **(C)** Venn plot of the 12 common immune genes that overlapped between the normal and depression samples and between the subgroups with low and high GTF2F2 expression levels.

inflammatory response and immune system changes are a part of depression. Inflammation is likely a critical disease modifier, promoting susceptibility to depression (Leonard, 2001). We showed that GTF2F2 is involved in JAK-STAT, PI3K-Akt, p53, TGF-β, and other biological signaling pathways related to immune response. The transforming growth factor (TGF)-β pathway, with its role as a regulatory cytokine, has been involved in the pathophysiology of MDD (Lee and Kim, 2010). It is known that NRF-1, as an important regulator of GTF2F2, can interfere with the TGF-β/SMAD pathway with a novel negative regulation of SMAD4 (Rajasekaran et al., 2021). From our results, GTF2F2 may affect the TGF-β pathway through NRF-1, and therefore, associate with MDD progression. Besides, JAK-STAT signaling pathway was reported in the MDD (Gao et al., 2022; Maes et al., 2022), which may also act as a target of GTF2F2 affecting MDD.

Moreover, higher GTF2F2 levels were associated with lower IL15Rα receptor levels. Interleukin-15 affects the serotonin system and exerts anti-depressive effects through the IL15Rα receptor. Additionally, IL15Rα knockout mice show depressive phenotypes (Wu et al., 2011). RORA is also involved in the regulation of types 2 and 3 innate lymphoid cells, macrophages, and Treg cells (De Matteis et al., 2018; Lo et al., 2019; L'homme et al., 2020; Haim-Vilmovsky et al., 2021). Using overexpression in CD4-conditional *RORA*-knockout mice,

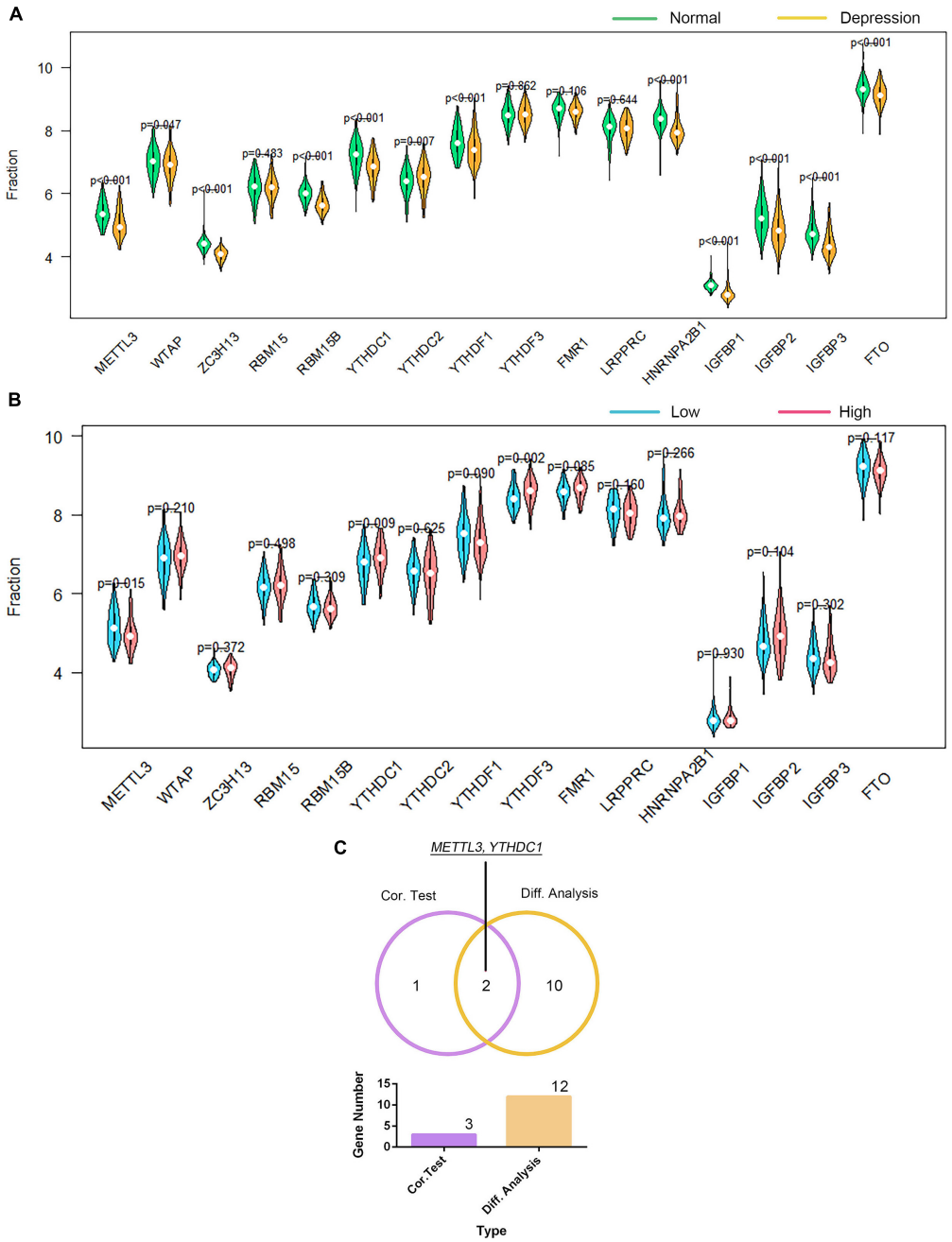

FIGURE 8 | Correlation of GTF2F2 with *m6A* genes. **(A)** Violin plot of the differential analysis of the top 20 *m6A* genes in normal and depression samples. The top 20 *m6A* genes were determined using the correlation coefficient of GTF2F2 with *m6A* genes. **(B)** Violin plot of the expression profiles of the top 20 *m6A* genes in the subgroups with low and high GTF2F2 expression levels. **(C)** Venn plot of the two common *m6A* genes that overlapped between the normal and depression samples and between the subgroups with low and high GTF2F2 expression levels.

Haim-Vilmovsky et al. (2021) investigated the role of RORA in regulating inflammation in CD4 + T cells and found that RORA could negatively regulate the immune system. Moreover, the RORA activity is regulated by interleukin-33, chemokine (CC motif) ligand 7, and the local microenvironment (Jiang et al., 2019; Yang et al., 2019; Haim-Vilmovsky et al., 2021; Zou et al., 2021). C3, the key molecule in the complement cascade reaction, is primarily produced by astrocytes (Lian et al., 2016). In an MDD model, CUMS mice, injected with a C3aR antagonist, accumulate the expression of C3a and C3aR, and the microglial polarization was observed (Li et al., 2020). Our result shows that high GTF2F2 has a negative correlation with C3, which may involve in the regulation process. These results revealed that GTF2F2 may play a role in the immune function of depressive behaviors, and

suppression of GTF2F2 may be a way to effectively ameliorate depressive symptoms.

GTF2F2 is essential for the initiation and elongation phases of gene transcription (Sasaki et al., 2013; Tsymbal et al., 2016; Ramayo-Caldas et al., 2019). Sasaki et al. (2013) suggested that mutations in the 3′ UTR of GTF2F2 could influence the RNA expression of GTF2F2. Additionally, the allelic imbalance contributes to GTF2F2 expression, which may be responsible for the slight increase in RNA polymerase II activity (Sasaki et al., 2013). Moreover, GTF2F2, COPS4, PSMA6, GTF2B, and SSB have been identified as dysregulated TFs that are correlated with Alzheimer's disease and diabetes mellitus. These five TFs are differentially expressed in the corresponding tissue, such as the brain in Alzheimer's disease and the pancreas in diabetes mellitus (Lee and Lee, 2021). Lee and Lee found that *GTF2F2*, *COPS4*, *PSMA6*, *GTF2B*, and *SSB* comprised a gene module, which was dysregulated in blood samples of patients with Alzheimer's disease and diabetes mellitus (Lee and Lee, 2021). GTF2F2 interacts with GTF2F1 to construct the TFIIF complex that is necessary to form RNA polymerase II, which is essential for the initiation and elongation of transcription (Aso et al., 1993; Purrello et al., 1995; Tsymbal et al., 2016). During transcription elongation, GTF2F2 competes with Gdown1, the substoichiometric 13th subunit of RNA polymerase II, and it is involved in pausing the early stage of elongation to regulate the activity of RNA polymerase II.

TFs, a group of DNA-binding proteins, are essential for the molecular state of a cell (Goossens et al., 2017; Li and Leonard, 2018; Tian et al., 2018; Vishnoi et al., 2020). Several studies have recognized the importance of understanding the behaviors and functions of TFs (Füllgrabe and Moore, 2018; Martínez Corrales and Alic, 2020). For example, HEY1, a transcription factor, is an effector molecule of the NOTCH signaling pathway (Watanabe et al., 2020; Xie et al., 2020). In salivary adenoid cystic carcinoma, NOTCH is positively associated with HEY1 activation, and HEY1 affects the expression of NOTCH and contributes to cellular proliferation, apoptosis inhibition, and spheroid formation *in vitro* (Xie et al., 2020). Additionally, recent studies have revealed that the immune system plays pivotal roles in brain function, such as learning and memory, and in positively regulating neural plasticity and neurogenesis (Dougherty et al., 1987; Dantzer, 2018; Besedovsky, 2019). Recently, several studies have demonstrated the essential functions of post-translational modifications, particularly in influencing the transcriptomic landscape of the brain (Hendee et al., 2017; Park et al., 2018; Elsamadicy et al., 2021). Additionally, methylation of the adenosine base at the N6 position is the most common internal modification shaping eukaryotic mRNAs (Widagdo and Anggono, 2018); m6A exerts additional regulatory effects on RNA in a context- and stimulus-dependent manner (Chen et al., 2019; Zhao et al., 2020). GTF2F2 is correlated with post-transcriptional modification in protein molecules, including *METTL3* and *YTHDC1*. The abnormal expression of m6A-related proteins occurs in the nervous system, thereby affecting neuritogenesis, brain volume, learning and memory, memory formation and consolidation, and is implicated in the pathogenesis of depression (Zhang et al., 2022). This revealed that GTF2F2 might act as a satisfactory indicator for abundant mRNA modifications that regulate transcript processing and translation in depression.

This study contributes to our understanding of the potential mechanisms underlying depression and provides novel insights into the therapeutic strategies for this mental health condition. However, this study had some limitations. First, this study was solely conducted using bioinformatic analysis; thus, the results were not validated with new experimental data. Second, the molecular mechanisms of GTF2F2 in depression and the correlation of GTF2F2 with the corresponding genes, such as the key functions of GTF2F2 in its interactions with the immune system and m6A genes, were not examined in detail. Finally, GTF2F2 was identified as a core gene for depression using GEO profiles with small sample sizes and imbalanced clinical data. Therefore, these limitations should be addressed in future research.

CONCLUSION

Using an integrated bioinformatical analysis, for the first time to our knowledge, *GTF2F2* was identified as a hub gene that may be vital for the onset and development of depression, which may serve as a promising novel indicator for the pathogenesis of depression. Further studies are needed to explore the correlation of GTF2F2 with immune response pathways such as the JAK-STAT and PI3K-Akt pathways and with inflammatory factors, which may improve the treatment of patients with depression.

DATA AVAILABILITY STATEMENT

The original contributions presented in the study are included in the article/**Supplementary Material**, further inquiries can be directed to the corresponding author/s.

AUTHOR CONTRIBUTIONS

HM and DS conceived and designed the experiments. CZ and MC conducted the acquisition, analysis, and interpretation of data. CZ and ND confirmed the authenticity of the raw data. CZ wrote the manuscript. All authors read and approved the final manuscript.

ACKNOWLEDGMENTS

We are grateful to the reviewers for their input in improving this manuscript.

SUPPLEMENTARY MATERIAL

The Supplementary Material for this article can be found online at: https://www.frontiersin.org/articles/10.3389/fnagi.2022.918217/full#supplementary-material

REFERENCES

Aso, T., Tsai, P., Kawaguchi, T., Menninger, J. C., Kitajima, S., Yasukochi, Y., et al. (1993). Assignment of the human GTF2F1 gene to chromosome 19p13.3. *Genomics* 16, 252–253. doi: 10.1006/geno.1993.1168

Besedovsky, H. O. (2019). The immune system as a sensorial system that can modulate brain functions and reset homeostasis. *Ann. N. Y. Acad. Sci.* 1437, 5–14. doi: 10.1111/nyas.13935

Bian, Q., Chen, J., Wu, J., Ding, F., Li, X., Ma, Q., et al. (2021). Bioinformatics analysis of a TF-miRNA-lncRNA regulatory network in major depressive disorder. *Psychiatry Res.* 299:113842. doi: 10.1016/j.psychres.2021.113842

Casey, D. A. (2017). Depression in older adults: a treatable medical condition. *Prim. Care.* 44, 499–510. doi: 10.1016/j.pop.2017.04.007

Chambers, W. J., Puig-Antich, J., Tabrizi, M. A., and Davies, M. (1982). Psychotic symptoms in prepubertal major depressive disorder. *Arch. Gen. Psychiatry* 39, 921–927. doi: 10.1001/archpsyc.1982.04290080037006

Chen, X. Y., Zhang, J., and Zhu, J. S. (2019). The role of m6A RNA methylation in human cancer. *Mol. Cancer* 18:103. doi: 10.1186/s12943-019-1033-z

Chen, Z., Tao, S., Zhu, R., Tian, S., Sun, Y., Wang, H., et al. (2021). Aberrant functional connectivity between the suprachiasmatic nucleus and the superior temporal gyrus: bridging RORA gene polymorphism with diurnal mood variation in major depressive disorder. *J. Psychiatr. Res.* 132, 123–130. doi: 10.1016/j.jpsychires.2020.09.037

Dantzer, R. (2018). Neuroimmune interactions: from the brain to the immune system and vice versa. *Physiol. Rev.* 98, 477–504. doi: 10.1152/physrev.00039.2016

De Matteis, S., Molinari, C., Abbati, G., Rossi, T., Napolitano, R., Ghetti, M., et al. (2018). Immunosuppressive Treg cells acquire the phenotype of effector-T cells in chronic lymphocytic leukemia patients. *J. Transl. Med.* 16:172. doi: 10.1186/s12967-018-1545-0

Dougherty, P. M., Drath, D. B., and Dafny, N. (1987). Evidence of an immune system to brain communication axis that affects central opioid functions: muramyl peptides attenuate opiate withdrawal. *Eur. J. Pharmacol.* 141, 253–260. doi: 10.1016/0014-2999(87)90270-6

Elsamadicy, A. A., Koo, A. B., David, W. B., Lee, V., Zogg, C. K., Kundishora, A. J., et al. (2021). Post-traumatic seizures following pediatric traumatic brain injury. *Clin. Neurol. Neurosurg.* 203:106556. doi: 10.1016/j.clineuro.2021.106556

Füllgrabe, C., and Moore, B. C. J. (2018). The association between the processing of binaural temporal-fine-structure information and audiometric threshold and age: a meta-analysis. *Trends Hear.* 22:2331216518797259. doi: 10.1177/2331216518797259

Gao, Y., Zhao, H., Xu, T., Tian, J., and Qin, X. (2022). Identification of crucial genes and diagnostic value analysis in major depressive disorder using bioinformatics analysis. *Comb. Chem. High. Throughput. Screen* 25, 13–20. doi: 10.2174/1386207323999201124204413

Geoffroy, P. A., and Palagini, L. (2021). Biological rhythms and chronotherapeutics in depression. *Prog. Neuropsychopharmacol. Biol. Psychiatry.* 106:110158. doi: 10.1016/j.pnpbp.2020.110158

Goossens, S., Vandamme, N., Van Vlierberghe, P., and Berx, G. (2017). EMT transcription factors in cancer development re-evaluated: beyond EMT and MET. *Biochim. Biophys. Acta Rev. Cancer.* 1868, 584–591. doi: 10.1016/j.bbcan.2017.06.006

Haim-Vilmovsky, L., Henriksson, J., Walker, J. A., Miao, Z., Natan, E., Kar, G., et al. (2021). Mapping rora expression in resting and activated CD4+ T cells. *PLoS One* 16:e0251233. doi: 10.1371/journal.pone.0251233

Hao, Y., Ge, H., Sun, M., and Gao, Y. (2019). Selecting an appropriate animal model of depression. *Int. J. Mol. Sci.* 20:4827. doi: 10.3390/ijms20194827

Hardeveld, F., Spijker, J., De Graaf, R., Nolen, W. A., and Beekman, A. T. (2010). Prevalence and predictors of recurrence of major depressive disorder in the adult population. *Acta Psychiatr. Scand.* 122, 184–191. doi: 10.1111/j.1600-0447.2009.01519.x

Hendee, K., Wang, L. W., Reis, L. M., Rice, G. M., Apte, S. S., and Semina, E. V. (2017). Identification and functional analysis of an ADAMTSL1 variant associated with a complex phenotype including congenital glaucoma, craniofacial, and other systemic features in a three-generation human pedigree. *Hum. Mutat.* 38, 1485–1490. doi: 10.1002/humu.23299

Hennings, J. M., Owashi, T., Binder, E. B., Horstmann, S., Menke, A., Kloiber, S., et al. (2009). Clinical characteristics and treatment outcome in a representative sample of depressed inpatients - findings from the Munich Antidepressant Response Signature (MARS) project. *J. Psychiatr. Res.* 43, 215–229. doi: 10.1016/j.jpsychires.2008.05.002

Iwamoto, K., Kakiuchi, C., Bundo, M., Ikeda, K., and Kato, T. (2004). Molecular characterization of bipolar disorder by comparing gene expression profiles of postmortem brains of major mental disorders. *Mol. Psychiatry* 9, 406–416. doi: 10.1038/sj.mp.4001437

Jiang, M., Tao, S., Zhang, S., Wang, J., Zhang, F., Li, F., et al. (2019). Type 2 innate lymphoid cells participate in IL-33-stimulated Th2-associated immune response in chronic obstructive pulmonary disease. *Exp. Ther. Med.* 18, 3109–3116. doi: 10.3892/etm.2019.7924

Jones, D. T., and Graff-Radford, J. (2021). Executive dysfunction and the prefrontal cortex. *Continuum (Minneap. Minn.)* 27, 1586–1601. doi: 10.1212/CON.0000000000001009

Kandola, A., Ashdown-Franks, G., Hendrikse, J., Sabiston, C. M., and Stubbs, B. (2019). Physical activity and depression: towards understanding the antidepressant mechanisms of physical activity. *Neurosci. Biobehav. Rev.* 107, 525–539. doi: 10.1016/j.neubiorev.2019.09.040

Kovaru, H., Pav, M., Kovaru, F., Raboch, J., and Fiserova, A. (2009). Cell signalling in CNS and immune system in depression and during antidepressant treatment: focus on glial and natural killer cells. *Neuro Endocrinol. Lett.* 30, 421–428.

L'homme, L., Sermikli, B. P., Molendi-Coste, O., Fleury, S., Quemener, S., Le Maître, M., et al. (2020). Deletion of the nuclear receptor RORα in macrophages does not modify the development of obesity, insulin resistance and NASH. *Sci. Rep.* 10:21095. doi: 10.1038/s41598-020-77858-6

Lee, H. Y., and Kim, Y. K. (2010). Transforming growth factor-beta1 and major depressive disorder with and without attempted suicide: preliminary study. *Psychiatry Res.* 178, 92–96. doi: 10.1016/j.psychres.2009.03.023

Lee, T., and Lee, H. (2021). Shared blood transcriptomic signatures between Alzheimer's disease and diabetes mellitus. *Biomedicines* 9:34. doi: 10.3390/biomedicines9010034

Leonard, B. E. (2001). The immune system, depression and the action of antidepressants. *Prog. Neuropsychopharmacol. Biol. Psychiatry* 25, 767–780. doi: 10.1016/s0278-5846(01)00155-5

Li, J., Wang, H., Du, C., Jin, X., Geng, Y., Han, B., et al. (2020). hUC-MSCs ameliorated CUMS-induced depression by modulating complement C3 signaling-mediated microglial polarization during astrocyte-microglia crosstalk. *Brain Res. Bull.* 163, 109–119. doi: 10.1016/j.brainresbull.2020.07.004

Li, P., and Leonard, W. J. (2018). Chromatin accessibility and interactions in the transcriptional regulation of T cells. *Front. Immunol.* 9:2738. doi: 10.3389/fimmu.2018.02738

Lian, H., Litvinchuk, A., Chiang, A. C., Aithmitti, N., Jankowsky, J. L., and Zheng, H. (2016). Astrocyte-Microglia cross talk through complement activation modulates amyloid pathology in mouse models of Alzheimer's disease. *J. Neurosci.* 36, 577–589. doi: 10.1523/JNEUROSCI.2117-15.2016

Liu, W., Zhang, L., and Zheng, D. (2020). Umbilical cord blood-based gene signatures related to prenatal major depressive disorder. *Medicine* 98:e16373.

Lo, B. C., Canals Hernaez, D., Scott, R. W., Hughes, M. R., Shin, S. B., Underhill, T. M., et al. (2019). The transcription factor RORα preserves ILC3 lineage identity and function during chronic intestinal infection. *J. Immunol.* 203, 3209–3215. doi: 10.4049/jimmunol.1900781

Maes, M., Rachayon, M., Jirakran, K., et al. (2022). The immune profile of major dysmood disorder: proof of concept and mechanism using the precision nomothetic psychiatry approach. *Cells* 11:1183. doi: 10.3390/cells11071183

Martínez Corrales, G., and Alic, N. (2020). Evolutionary conservation of transcription factors affecting longevity. *Trends Genet.* 36, 373–382. doi: 10.1016/j.tig.2020.02.003

Maurer, D. M., Raymond, T. J., and Davis, B. N. (2018). Depression: screening and diagnosis. *Am. Fam. Phys.* 98, 508–515.

Min, J. A., Lee, H. J., Lee, S. H., Park, Y. M., Kang, S. G., Park, Y. G., et al. (2017). RORA polymorphism interacts with childhood maltreatment in determining anxiety sensitivity by sex: a preliminary study in healthy young adults. *Clin. Psychopharmacol. Neurosci.* 15, 402–406. doi: 10.9758/cpn.2017.15.4.402

Ming, Q., Wang, X., Chai, Q., Yi, J., and Yao, S. (2015). Retinoid-related orphan receptor alpha (RORA) gene variation is associated with trait depression. *Psychiatry Res.* 229, 629–630. doi: 10.1016/j.psychres.2015.07.014

Park, J. S., Ahn, H. K., Na, J., Lee, H. H., Yoon, Y. E., Yoon, M. G., et al. (2018). Development of a screening tool to predict chronic kidney disease risk in

post-nephrectomy living kidney donors. *Transplant. Proc.* 50, 993–997. doi: 10.1016/j.transproceed.2018.01.034

Pierzynowska, K., Gaffke, L., and Węgrzyn, G. (2020). Transcriptomic analyses suggest that mucopolysaccharidosis patients may be less susceptible to COVID-19. *FEBS Lett.* 594, 3363–3370. doi: 10.1002/1873-3468.13908

Preciados, M., Yoo, C., and Roy, D. (2016). Estrogenic endocrine disrupting chemicals influencing NRF1 regulated gene networks in the development of complex human brain diseases. *Int. J. Mol. Sci.* 17:2086. doi: 10.3390/ijms17122086

Purrello, M., Di Pietro, C., Rapisarda, A., Mirabile, E., Motta, S., Sichel, G., et al. (1995). Genetic characterization of general transcription factors TFIIF and TFIIB of Homo sapiens sapiens. *Cytogenet. Cell Genet.* 69, 75–80. doi: 10.1159/000133942

Rajasekaran, N., Song, K., Lee, J. H., et al. (2021). Nuclear respiratory Factor-1, a Novel SMAD4 binding protein, represses TGF-β/SMAD4 signaling by functioning as a transcriptional cofactor. *Int. J. Mol. Sci.* 22:5595. doi: 10.3390/ijms22115595

Ramayo-Caldas, Y., Mármol-Sánchez, E., Ballester, M., Sánchez, J. P., González-Prendes, R., Amills, M., et al. (2019). Integrating genome-wide co-association and gene expression to identify putative regulators and predictors of feed efficiency in pigs. *Genet. Sel. Evol.* 51:48. doi: 10.1186/s12711-019-0490-6

Sasaki, S., Ibi, T., Watanabe, T., Matsuhashi, T., Ikeda, S., and Sugimoto, Y. (2013). Variants in the 3′ UTR of general transcription factor IIF, polypeptide 2 affect female calving efficiency in Japanese Black cattle. *BMC Genet.* 14:41. doi: 10.1186/1471-2156-14-41

Satyanarayanan, S. K., Su, H., Lin, Y. W., and Su, K. P. (2018). Circadian rhythm and melatonin in the treatment of depression. *Curr. Pharm. Des.* 24, 2549–2555. doi: 10.2174/1381612824666180803112304

Tian, Z., Zhao, Q., Biswas, S., and Deng, W. (2018). Methods of reactivation and reprogramming of neural stem cells for neural repair. *Methods* 133, 3–20. doi: 10.1016/j.ymeth.2017.08.014

Tong, C. W., Wang, J. L., Jiang, M. S., Hsu, C. H., Chang, W. T., and Huang, A. M. (2013). Novel genes that mediate nuclear respiratory factor 1-regualted neurite outgrowth in neuroblastoma IMR-32 cells. *Gene* 515, 62–70. doi: 10.1016/j.gene.2012.11.026

Tsymbal, D. O., Minchenko, D. O., Kryvdiuk, I. V., Riabovo, O. O., Halkin, O. O., Ratushna, O. O., et al. (2016). Expression of proliferation related transcription factor genes in U87 glioma cells with IRE1 knockdown: upon glucose and glutamine deprivation. *Fiziol. Zh.* 62, 3–15. doi: 10.15407/fz62.01.003

Vishnoi, K., Viswakarma, N., Rana, A., and Rana, B. (2020). Transcription factors in cancer development and therapy. *Cancers* 12:32824207.

Watanabe, Y., Seya, D., Ihara, D., Ishii, S., Uemoto, T., Kubo, A., et al. (2020). Importance of endothelial Hey1 expression for thoracic great vessel development and its distal enhancer for Notch-dependent endothelial transcription. *J. Biol. Chem.* 295, 17632–17645. doi: 10.1074/jbc.RA120.015003

Widagdo, J., and Anggono, V. (2018). The m6A-epitranscriptomic signature in neurobiology: from neurodevelopment to brain plasticity. *J. Neurochem.* 147, 137–152. doi: 10.1111/jnc.14481

Wu, X., Hsuchou, H., Kastin, A. J., He, Y., Khan, R. S., Stone, K. P., et al. (2011). Interleukin-15 affects serotonin system and exerts antidepressive effects through IL15Rα receptor. *Psychoneuroendocrinology* 36, 266–278. doi: 10.1016/j.psyneuen.2010.07.017

Xie, J., Lin, L. S., Huang, X. Y., Gan, R. H., Ding, L. C., Su, B. H., et al. (2020). The NOTCH1-HEY1 pathway regulates self-renewal and epithelial-mesenchymal transition of salivary adenoid cystic carcinoma cells. *Int. J. Biol. Sci.* 16, 598–610. doi: 10.7150/ijbs.36407

Yang, Y., Yuan, G., Xie, H., Wei, T., Zhu, D., Cui, J., et al. (2019). Circadian clock associates with tumor microenvironment in thoracic cancers. *Aging* 11, 11814–11828. doi: 10.18632/aging.102450

Zhang, N., Ding, C., Zuo, Y., Peng, Y., and Zuo, L. (2022). N6-methyladenosine and neurological diseases. *Mol. Neurobiol.* 59, 1925–1937. doi: 10.1007/s12035-022-02739-0

Zhang, R., Wei, S., Chang, M., Jiang, X., Tang, Y., and Wang, F. (2020). Dorsolateral and ventrolateral prefrontal cortex structural changes relative to suicidal ideation in patients with depression. *Acta Neuropsychiatr.* 32, 84–91. doi: 10.1017/neu.2019.45

Zhao, W., Qi, X., Liu, L., Ma, S., Liu, J., and Wu, J. (2020). Epigenetic regulation of m6A modifications in human cancer. *Mol. Ther. Nucleic Acids.* 19, 405–412. doi: 10.1016/j.omtn.2019.11.022

Zou, Y., Sun, H., Guo, Y., Shi, Y., Jiang, Z., Huang, J., et al. (2021). Integrative pan-cancer analysis reveals decreased melatonergic gene expression in carcinogenesis and RORA as a prognostic marker for hepatocellular carcinoma. *Front. Oncol.* 11:643983. doi: 10.3389/fonc.2021.643983

Conflict of Interest: The authors declare that the research was conducted in the absence of any commercial or financial relationships that could be construed as a potential conflict of interest.

Publisher's Note: All claims expressed in this article are solely those of the authors and do not necessarily represent those of their affiliated organizations, or those of the publisher, the editors and the reviewers. Any product that may be evaluated in this article, or claim that may be made by its manufacturer, is not guaranteed or endorsed by the publisher.

frontiers | Frontiers in Aging Neuroscience

REVIEW
published: 30 May 2022
doi: 10.3389/fnagi.2022.918473

A Systematic Review of Body Fluids Biomarkers Associated With Early Neurological Deterioration Following Acute Ischemic Stroke

*Xiaotan Ji[1,2], Long Tian[3], Shumei Yao[1], Fengyue Han[1], Shenna Niu[3] and Chuanqiang Qu[1,3]**

[1] Department of Neurology, Shandong Provincial Hospital, Shandong University, Jinan, China, [2] Department of Neurology, Jining No. 1 People's Hospital, Jining, China, [3] Department of Neurology, Shandong Provincial Hospital Affiliated to Shandong First Medical University, Jinan, China

OPEN ACCESS

Edited by:
Min Tang,
Jiangsu University, China

Reviewed by:
Xinyan Wang,
Xi'an Peihua University, China
Jian Su,
Nanjing University of Information Science and Technology, China

***Correspondence:**
Chuanqiang Qu
drquchuanqiang@sina.com

Specialty section:
This article was submitted to Cellular and Molecular Mechanisms of Brain-aging, a section of the journal Frontiers in Aging Neuroscience

Received: *12 April 2022*
Accepted: *10 May 2022*
Published: *30 May 2022*

Citation:
Ji XT, Tian L, Yao SM, Han FY, Niu SN and Qu CQ (2022) A Systematic Review of Body Fluids Biomarkers Associated With Early Neurological Deterioration Following Acute Ischemic Stroke. Front. Aging Neurosci. 14:918473. doi: 10.3389/fnagi.2022.918473

Biomarkers are objectively measured biological properties of normal and pathological processes. Early neurological deterioration (END) refers to the deterioration of neurological function in a short time after the onset of acute ischemic stroke (AIS) and is associated with adverse outcomes. Although multiple biomarkers have been found to predict END, there are currently no suitable biomarkers to be applied in routine stroke care. According to the Preferred Reporting Items for Systematic Review standards, we present a systematic review, concentrating on body fluids biomarkers that have shown potential to be transferred into clinical practice. We also describe newly reported body fluids biomarkers that can supply different insights into the mechanism of END. In our review, 40 scientific papers were included. Depending on the various mechanisms, sources or physicochemical characteristics of body fluids biomarkers, we classified related biomarkers as inflammation, protease, coagulation, metabolism, oxidative stress, and excitatory neurotoxicity. The body fluids biomarkers whose related articles are limited or mechanisms are unknown are categorized as other biomarkers. The inflammation-related biomarkers, such as neutrophil-to-lymphocyte ratio and hypersensitive C-reactive protein, play a crucial role among the mentioned biomarkers. Considering the vast heterogeneity of stroke progression, using a single body fluids biomarker may not accurately predict the risk of stroke progression, and it is necessary to combine multiple biomarkers (panels, scores, or indices) to improve their capacity to estimate END.

Keywords: acute ischemic stroke, early neurological deterioration, biomarkers, body fluids, inflammation

Abbreviations: TNF-α, tumor necrosis factor α; IL-1, interleukin 1; IL-6, interleukin 6; NLR, neutrophil-to-lymphocyte ratio; Hs-CRP, hypersensitive C-reactive protein; MMP-9, matrix metalloproteinase-9; ALP, Alkaline phosphatase; F2-isoP, F2-isoprostanes; HT, Hemorrhagic transformation; END, early neurological deterioration; CLEC-2, C-Type Lectin-Like Receptor; GLT-1, glutamate transporter 1; TMAO, Trimethylamine N-oxide.

INTRODUCTION

Stroke (also known as apoplexia, cerebrovascular accident) is a worldwide disease burden due to its high morbidity, mortality, and disability rates. Especially it has been the first leading cause of mortality in China (GBD 2016 Stroke Collaborators, 2019). Stroke, including ischemic stroke and hemorrhagic stroke, is characterized by damage to brain tissue caused by the sudden rupture of the blood vessels in the brain or blockage that prevents blood from flowing to the brain. Ischemic stroke, accounting for about 87% of stroke cases, is caused by obstruction of the cerebral arteries (Writing Group Members et al., 2016). In acute ischemic stroke (AIS), a sudden drop in blood flow to the brain causes all or part of the supply of oxygen and glucose to be reduced to neurons and other brain cells. The result is to trigger multiple physiological, biochemical, and molecular mechanisms that ultimately result in massive cell death and changes in the basic neural function of the ischemic cell (Seners et al., 2015).

Early neurological deterioration (END) is the deterioration of nerve function in the hours or days following AIS and leads to adverse outcomes (Seners et al., 2015). The incidence of END ranges from 2.2 to 37.5% (Siegler et al., 2013; Seners et al., 2015), depending on the severity threshold and interval of clinical evaluation. The occurrence of END is affected by multiple factors and mechanisms, which cause disability or an increase in mortality. Collateral circulation disorder, primary site thrombus enlargement, recurrent stroke, cerebral edema, hemorrhagic transformation (HT) and epilepsy are risk factors that cause END following AIS (Siegler et al., 2013). Malignant edema and symptomatic intracranial hemorrhage are the two leading direct causes of END (Seners and Baron, 2018). The definition of END is not uniform at present, with most studies using the National Institutes of Health Stroke Score (NIHSS) definition of an increase of four points between admission and 24 h (Seners et al., 2015). It is well known that END is closely related to poor prognosis in stroke patients. Consequently, predictive factors for END are also of great importance. The ability to identify stroke patients with a high risk of END is critical for clinicians. Current methods of identifying the high-risk individuals depend to a large extent on the evaluations of clinical and neuroimaging features which exist at the time of onset, as well as the initial response to treatment.

Biomarkers refer to biochemical indicators that can mark structural or functional changes in systems, organs, tissues, cells and subcell structure, which can be used for a wide range of aims, such as risk stratification, treatment evaluation strategy, clinical trial design, and drug development (Biomarkers Definitions Working Group, 2001). Biomarkers are mostly derived from human tissues or body fluids, including physiological, biochemical, immune, cellular and molecular changes, which have biological materiality, and human physiological and pathological correlation of measurement, and are divided into diagnostic biomarkers, prognostic biomarkers, predictive biomarkers, pharmacodynamic biomarkers, safety biomarkers and detection biomarkers (Biomarkers Definitions Working Group, 2001). In patients with AIS, according to the expression of biomarkers, patients' conditions can be assessed and intervened as early as possible to reduce the incidence of END, and additional clinical information independent of imaging and clinical characteristics can be provided. Considering the apparent values of predicting stroke progression, we summarize recent progress in the relationships between biomarkers and END following AIS. We expect to provide the current new knowledge of biomarkers for END in AIS, aiming to distinguish these high-risk stroke patients and obtain closer monitoring and aggressive treatment, improving long-term clinical prognosis. In the meantime, we look forward to providing direction for future research and could potentially lead to the development of novel therapeutic approaches.

METHODS

The present systematic review was performed according to the Preferred Reporting Items for Systematic Review and Meta-analyses (PRISMA) standards (Liberati et al., 2009). The collected studies were systematically searched and critically reviewed. A literature search of the electronic database PubMed, Science Direct Scopus, Google Scholar, and Excerpta Medica Database (EMBASE) from database inception to October 2021 was conducted. The search terms were "acute ischemic stroke," "cerebral infarction," "early neurological deterioration," "biomarker" in the title and abstract. Early neurological deterioration refers to the deterioration of neurological function in a short time after the onset of acute stroke, without regard to severity threshold and interval of clinical evaluation. The references of all articles retrieved were examined and cross-referenced to further identify the related literature. The selection criteria were as follows: (1) original research articles; and (2) reviews, and mini-reviews. In addition, non-English papers and case reports/series were excluded. Preprint articles were also excluded. The literature search was conducted by two researchers (TL, YSM). Two researchers (JXT, TL) independently reviewed the papers whose titles or abstracts appeared to be relevant and selected those which analyzed biomarkers associated with END flowing AIS. The dispute over the qualifications of the two researchers was resolved through negotiation. Critical appraisal and assessment of bias were accomplished by two investigators (HFY, YSM). Data extraction was conducted by two investigators (JXT, TL) and confirmed by other investigators (HFY, NSN). Synthesis of results was completed by one researcher (JXT).

RESULTS

We reviewed the titles and abstracts, as well as manually searched the reference lists. The reference lists of all included articles were checked to avoid missing literatures. A total of 178 articles were found in the search and then screened based on their abstracts. These included papers were further viewed full-text critically, considering the primary purposes of the review. This assessment left 40 related articles comprising original research articles, reviews, or mini-reviews. **Figure 1** showed our search strategy. **Table 1** demonstrated related studies on the body fluids

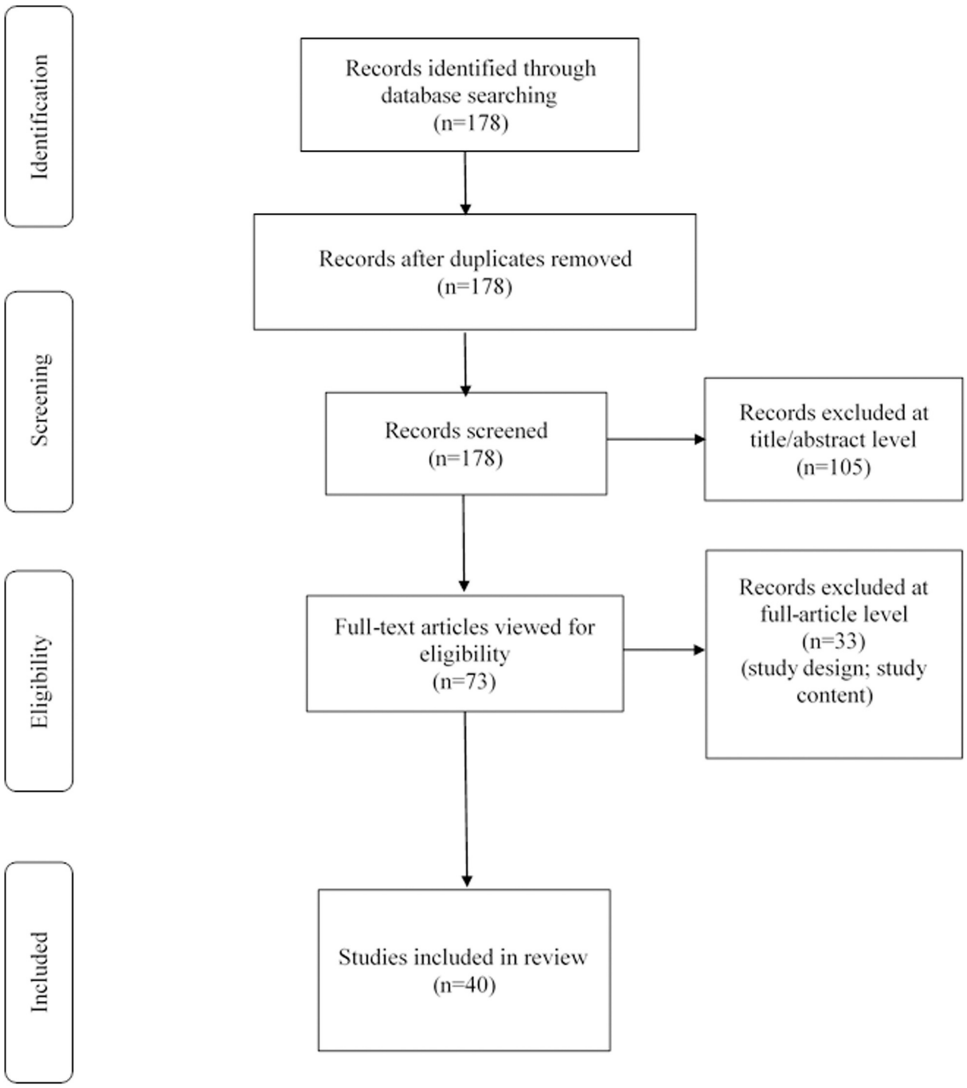

FIGURE 1 | Search strategy: A methodological evaluation of each study was examined according to the PRISMA standards, including an assessment of bias.

biomarkers of END flowing AIS, excluding the review, mini-review, animal experiment, and the research not mentioning the indicator of sensitivity, specificity and adjusted odds ratio (aOR) and 95% confidence interval (95% CI).

Biomarkers Related to Inflammation

Neutrophil-to-Lymphocyte Ratio (NLR)

Previous studies have shown that neuroinflammation plays an essential role in the pathophysiologic process and progression of cerebral infarction (Shi et al., 2019; Stoll and Nieswandt, 2019; Parikh et al., 2020; Schuhmann et al., 2020). Neutrophils are the primary inflammatory cells in AIS, releasing pro-inflammatory cytokines and other cytotoxic products (proteases, reactive oxygen species) that cause secondary brain damage in the ischemic penumbra (Ceulemans et al., 2010). At the same time, neutrophils are the source of matrix metalloproteinase-9 (MMP-9), which directly induces blood-brain barrier (BBB) disruption and HT (Duan et al., 2018). On the other hand, specific lymphocyte subtypes, such as regulatory T cells (Tregs), are the primary brain-protective immunomodulators of ischemic injury after AIS. They have been shown associated with reduced infarct volume and improved neurological function (Kim et al., 2012; Liesz et al., 2013). Therefore, a single biochemical indicator is limited in reflecting the progression of AIS. NLR, platelet-to-lymphocyte ratio (PLR), and lymphocyte-to-monocyte ratio (LMR) are comprehensive parameters that can preferably reflect the immune activity of cells and has a better role in prediction. Recent studies suggest that NLR, PLR, and LMR are potential novel biomarkers of underlying inflammatory processes that may serve as better predictors of ischemic stroke (Lux et al., 2020). Especially elevated NLR is associated with an increased risk of carotid artery stenosis (Koklu et al., 2016) and intracranial atherosclerosis (Nam et al., 2018). Patients with large artery atherosclerosis stroke (LAAS) are prone to END and therefore

TABLE 1 | Published studies on the biomarkers of END following AIS.

Type	Biomarker	AIS subtype	Cut-off	First sample collection (after admission)	Se (%)	Sp (%)	References
inflammation	NLR	LAAS	N/A	<24 h	N/A	N/A	Nam et al., 2019
		single subcortical infarctions	N/A	<24 h	aOR = 1.24	95%CI 1.04–1.49	Nam et al., 2021
		First-ever AIS treated with intravenous thrombolysis within 4.5 h	4.43	<4.5 h	70.9	79.3	Gong et al., 2019b
		AIS treated with intravenous thrombolysis within 4.5 h	N/A	<4.5 h	1.385	95%CI 1.238–1.551	Gong et al., 2021
		AIS received intravenous thrombolysis or endovascular thrombectomy of the anterior circulation	7	<24 h	60	60	Ferro et al., 2021
	Hs-CRP	First-ever AIS	N/A	days 1, 3, 7, 14	N/A	N/A	Zang et al., 2016
		AIS with AF	N/A	<24 h	2.78	95%CI 1.067–7.240	Duan et al., 2020
		penetrating artery infarction	3.48 mg/L	day 2	73.64	82.35	Gong et al., 2019a
	IL-6	AIS received endovascular therapy	28.04 pg/mL	days 1, 2, 3, 7 <24 h	1.98	95%CI 1.05–6.69	Deng et al., 2021
protease	MMP-9	AIS within 24 h	181.7 ng/mL	<24 h	0.829	0.813	Yuan et al., 2018
	ALP	AIS with AF and/or rheumatic heart disease	N/A	<48 h	aOR = 8.96	95%CI 1.33–60.21	Liu et al., 2016
		AIS caused by intracranial atherosclerosis	N/A	<day 1	N/A	N/A	Uehara et al., 2020
	Lp-PLA 2	first-ever AIS	2.99	<48 h	1.96	95%CI 1.02–4.27	Wang et al., 2019
coagulation	P-selectin	AIS	N/A	days 1, 3, 7 and 14	N/A	N/A	Wang et al., 2013
	CLEC-2	AIS within 7 days	235.48 pg/ml	<7 days	76.8	54.2	Zhang et al., 2018
	D-dimer	AIS	N/A	<24 h	1.87	95%CI 1.38–2.54	Barber et al., 2004
		AIS	N/A	<24 h	N/A	N/A	Barber et al., 2006
		AIS within 24 h	N/A	<24 h	3.622	95%CI 1.732–7.573	Liu et al., 2020
metabolite	blood glucose	AIS treated with recanalization treatment (EVT after IV rt-PA, EVT, or IV rt-PA alone)	107.1 mg/dL	<24 h	100	53	Huang Z. X. et al., 2020
	glycemic variability	AIS with type 2 diabetes	N/A	<72 h	1.479	95%CI 1.162–1.882	Hui et al., 2018
	glycated albumin	AIS with prediabetes	N/A	<12 h	4.58	95%CI 1.64–12.81	Lee et al., 2021
	HDL-cholesterol	AIS within 24 h	N/A	<24 h	0.42	95% CI 0.19–0.94	Ryu et al., 2016
	apoB/apoA-I ratio	AIS within 24 h	N/A	<24 h	2.37	95% CI 1.02–5.53	Ryu et al., 2016
	triglyceride	AIS	N/A	<24 h	N/A	N/A	Choi et al., 2012
	Cystatin C	AIS and TIA in elderly patients without chronic kidney disease	N/A	<24 h	N/A	N/A	Kim et al., 2017
		cardiogenic cerebral embolism	1.41 mg/L	<24 h	49.1	75.7	Cong and Ma, 2021
	WBPC	AIS within 4.5 h	6.05 μMc	at admission	N/A	N/A	Martin et al., 2019;
	TMAO	AIS within 24 h	5.0 μmol/L	<24 h	2.14	95%CI 1.19–3.82	Hou et al., 2020
others	Albuminuria	acute small subcortical infarcts in the lenticulostriate artery territory within 24 h	N/A	the first morning after admission	6.64	1.62–27.21	Umemura et al., 2014
		AIS	N/A	at admission	5.58	95%CI 2.24–14.82	Kanamaru et al., 2017
	cTnI	AF related AIS	N/A	<24 h	1.16	95%CI 1.00–1.34	Nam et al., 2020
	homocysteine	AIS within 48 h	11.4 μmol/L	<24 h	3.45	95%CI 1.25–9.50	Kwon et al., 2014

Wherever appropriate, the sensitivity (Se) and specificity (Sp) have been replaced by the adjusted odds ratio (aOR) and the corresponding 95% confidence interval (CI), respectively. 1. An indicated combination of D-dimer level and platelet count. 2. Prediabetes, including impaired fasting glucose and/or impaired glucose tolerance (IGT) and/or impaired hemoglobin A1c (HbA1c), is an intermediate metabolic state between normal glucose metabolism and diabetes. Not included the review, mini-review, animal experiment, and the research not mentioned the indicator of Se, Sp, and aOR. AIS, acute ischemic stroke; TIA, transient ischemic attack; AF, atrial fibrillation; LAAS, large artery atherosclerosis stroke; EVT, endovascular treatment; IV rt–PA, intravenous recombinant tissue plasminogen activator; N/A, not applicable or not available; NLR, neutrophil-to-lymphocyte ratio; Hs-CRP, hypersensitive C-reactive protein; interleukin-6, IL-6; MMP-9, matrix metalloproteinase-9; ALP, Alkaline phosphatase; Lp-PLA 2, Lipoprotein-associated phospholipase A 2; F2-isoP, F2-isoprostanes; CLEC-2, C-Type Lectin-Like Receptor; HDL-cholesterol, high-density lipoprotein-cholesterol; apoB/apoA-I ratios, apolipoprotein B/apolipoprotein A-I ratios; Hcy, homocysteine; WBPC, whole blood purine concentration; TMAO, Trimethylamine N-oxide; cTnI, cardiac troponin I; GA, glycated albumin; h, hour.

have a poorer clinical prognosis (Lee and Lee, 2017). Nam et al. reported that NLR level was independently associated with END events in patients with LAAS. The mechanism might be involved in the degree of large artery stenosis, the number of stenotic lesions, and the stability of atherosclerotic plaque (Nam et al., 2019). The NLR level was also related to END in patients with single subcortical infarctions which were defined as an infarct in the area of penetrating arteries and its prognosis is relatively favorable (Nam et al., 2021).

Intravenous thrombolysis and endovascular treatment are the main methods in the treatment of AIS. However, the overall efficacy of these treatments is limited, with only 30 to 50% of patients achieving good long-term outcomes (Semerano et al., 2019). Possible causes include BBB dysfunction, brain injury secondary to cerebral edema, HT, and infarct enlargement (Mizuma et al., 2018; Shi et al., 2019). Previous studies showed that an elevated level of NLR may predict post-thrombolysis END in ischemic stroke patients. It also indicated that the optimal cutoff value of NLR indicating post-thrombolysis END was 4.43, with corresponding sensitivity and specificity of 70.9 and 79.3%, respectively (Gong et al., 2019b). The results of another observational study also demonstrated that NLR, PLR, and LMR are associated with post-thrombolysis END, where NLR and PLR may have the ability to predict (Gong et al., 2021). However, neither research explored related mechanisms. Ferro et al. showed that NLR level within 24 h was following the severity of cerebral edema and END in patients with anterior circulation infarction who received reperfusion therapy (including intravenous thrombolysis and intravascular thrombectomy), and cerebral edema might be an essential mechanism linking systemic inflammation to secondary brain injury (Ferro et al., 2021).

Hypersensitive C-Reactive Protein (Hs-CRP)

Hypersensitive C-reactive protein is a systemic marker of inflammation that is produced in large quantities by hepatocytes, and is caused by IL-1, IL-6 and TNF-α stimulation (Lakhan et al., 2009). Ischemic brain tissue releases inflammatory cytokines and chemokines, and Hs-CRP is one of the mediators of ischemic brain injury. Cytokines and inflammatory factors cause neuron necrosis, vascular endothelial cell permeability, and BBB destruction, inducing cell apoptosis (Esenwa and Elkind, 2016). The previous study has found that patients with progressive cerebral infarction had higher Hs-CRP levels than patients with non-progressive cerebral infarction in 3, 7, and 14 days after the onset of AIS (Zang et al., 2016). However, the research did not analyze the subtypes of AIS. A recent study showed that Hs-CRP levels were independently associated with END in cerebral embolism caused by atrial fibrillation (AF) (Duan et al., 2020). Although the exact mechanism behind this association is unclear, there are two possible explanations. First of all, cerebral edema after an acute cerebral infarction can trigger the body's inflammatory response, promote inflammation in the brain, and worsen the cerebral infarction. Therefore, cerebral edema may be one of the leading causes of END. As an acute-phase reactant and systemic inflammatory indicator, Hs-CRP levels may also be elevated by cerebral edema in acute cerebral infarction (Paquissi, 2016). In addition, previous reports indicated that patients with AF are at an increased risk of thrombosis. This tendency to thrombosis is thought to be associated with abnormal changes in inflammatory biomarkers such as Hs-CRP. Therefore, elevated Hs-CRP may further increase the risk of thrombosis in patients with AF, which may lead to infarction enlargement or new thromboembolic events (Seo et al., 2012; Ryu et al., 2016).

Penetrating artery infarctions account for about 25% of all ischemic strokes, and progressive motor deficits (PMD) are common in penetrating artery infarctions during the acute stage and sometimes lead to severe disability (Li et al., 2015). Previous studies have suggested that PMD is associated with a poor prognosis of perforating artery infarction (Li et al., 2015). Gong et al. suggested that Hs-CRP was independently correlated with PMD, and its optimal cutoff value for Hs-CRP as a predictor for PMD was 3.48 mg/L, with its sensitivity and specificity were 73.64 and 82.35%, respectively (area under the curve was 0.792) (Gong et al., 2019a). Hence, it is believed that PMD is caused by biochemical abnormalities such as inflammation.

Interleukin-6 (IL-6)

Vascular disease is the basis of ischemic stroke, and the role of inflammatory factors in it can't be ignored. IL-6 is a multipotent cytokine that plays an important role in host defense by modulating immune and inflammatory responses (Lambertsen et al., 2012). IL-6 is mainly produced by macrophages, T lymphocytes and B lymphocytes, and can be induced by a variety of cytokines such as viruses, endotoxins and tumor necrosis factors in tissue damage or infection. The expression of IL-6 is strictly regulated, but persistent dysregulation of IL-6 synthesis has pathological effects on chronic inflammation and autoimmunity. As an important member of the cytokine regulatory network, IL-6 plays a core role in acute severe reactions. Moreover, IL-6 can promote the expression of intercellular adhesion molecules, promote the adhesion and aggregation of inflammatory cells, accelerate the rupture of plaques, cause vulnerable plaques and thrombosis, and induce C-reactive protein (CRP) production in the liver (Lambertsen et al., 2012). Vila et al. (2000) found that the level of IL-6 increased sharply within 24 h of experimental stroke. At the same time, the patients with END after AIS have a higher expression level of IL-6 in cerebrospinal fluid and plasma than those whose clinical symptoms improved or stabilized (Vila et al., 2000). Recent research reported that AIS patients with END had an increased expression level of IL-6 compared with AIS patients without END. A previous study has suggested that IL-6 could exacerbate the damage to the brain and disrupt the proliferation of neural stem cells (Acalovschi et al., 2003). IL-6 can diagnose early inflammation more quickly. Above all, the level of IL-6 may be a reliable predictive marker and further study is required to verify the prediction.

Biomarkers Related to Protease

Matrix Metalloproteinase-9 (MMP-9)

Hemorrhagic transformation is a common complication of AIS, especially in patients with cerebral embolism and intravenous thrombolysis. It can delay effective treatment and lead to a

poor prognosis for AIS patients. A recent study reported that HT is an independent risk factor for END in ischemic stroke patients receiving endovascular thrombectomy (Kim et al., 2019). Therefore, early identification of patients at high risk of HT is of great significance (Alvarez-Sabin et al., 2013). Since disruption of the BBB is associated with HT, current studies have suggested that the early BBB disruption can be used as a predictor of HT. Previous studies have indicated that MMP-9 helps to break down the extracellular matrix and the basal membrane of brain blood vessels during AIS (Lucivero et al., 2007), and it can activate numerous proinflammatory cytokines and chemokines containing interleukin and tumor necrosis factor (Candelario-Jalil et al., 2009), facilitate leukocytes transport across the endothelium (Kurzepa et al., 2014). In the meanwhile, MMP-9 plays an essential role in BBB destruction, neuronal damage, and HT (Hill et al., 2012). A meta-analysis of 12 clinical studies showed that serum MMP9 levels had high sensitivity (85%) but low specificity (79%) for HT after AIS (Wang et al., 2018). Another clinical study from China also demonstrated that serum MMP-9 levels in AIS patients with spontaneous HT were significantly higher than those in patients with non-spontaneous HT and healthy controls (Yuan et al., 2018). In this research, 181.7 ng/mL was used as the cutoff value of MMP-9, with a positive predictive value of 48% and a negative predictive value of 96%. Considering MMP-9 activity is controlled by single nucleotide polymorphisms (SNPs) of the MMP-9 gene, Yi et al. (2019) pointed out that MMP-9 polymorphisms were independently associated with a higher risk of END in AIS patients with AF. In conclusion, MMP-9 is essential to HT after AIS, and further studies are needed to confirm the diverse mechanisms of MMP-9 in AIS.

Alkaline Phosphatase (ALP)

Alkaline phosphatase is a molecular marker of vascular calcification and plays a vital role in atherosclerosis, leading to increased vascular stiffness and decreased compliance. In addition, ALP is considered a surrogate marker for systemic inflammation, malnutrition, and metabolic syndrome, which may lead to a worsening clinical outcome in AIS patients (Kim et al., 2013). Previous research demonstrated that increased ALP levels might help identify high-risk symptomatic HT in cardioembolic stroke patients (Liu et al., 2016). The related mechanism concerned neuroinflammation and the immature and unstable vasculature (Liu et al., 2016). Uehara et al. (2020) recently found that the elevated serum ALP level on admission may predict END in symptomatic intracranial atherosclerotic cerebral infarction. The results were only statistically significant in the symptomatic intracranial artery stenosis group, not in the symptomatic intracranial artery occlusion group. These results suggest that END is due to inter-arterial re-embolization of vulnerable plaques resulting from symptomatic intracranial atherosclerosis rather than a hemodynamic mechanism due to occlusion. Increased ALP level is a surrogate marker of instability in symptomatic intracranial artery stenosis plaques (Uehara et al., 2020). Considering the multifunction of ALP, further investigations are needed to discover the potential significance of AIS progression.

Lipoprotein-Associated Phospholipase A2 (Lp-PLA2)

Lipoprotein-associated phospholipase A2 also known as platelet-activating factor ethylene phthalide hydrolase, is a phospholipase that facilitates the hydrolysis of oxidized phospholipids, and is secreted by macrophages T cells and mast cells in the intima of blood vessels (Huang F. et al., 2020). Lp-PLA2 is classified as secretory (PLA2-I and PLA2-II) and cytoplasmic (PLA2-III and PLA2-IV), and is a kind of vascular-specific inflammatory marker (Huang F. et al., 2020). Studies have found that Lp-PLA2 is associated with the development of cardiovascular disease. Lp-PLA2 can hydrolyze and oxidize low-density lipoprotein to release lipid proinflammatory substances such as lysophosphatidylcholine and oxidized free fatty acids which further damage vascular endothelial cells through oxidative stress mechanism, and induce the expression of adhesion factors, thus promoting the aggregation of monocytes into the lumen to form macrophages. Macrophages, in turn, phagocytose oxidize low-density lipoprotein to form foam cells, which further stimulate the proliferation of vascular endothelial cells and ultimately participate in the formation of atherosclerotic plaques (Sofogianni et al., 2018). Furthermore, Packard et al. found that Lp-PLA2 was more closely associated with cardiovascular events than CRP (Ge et al., 2016). And a Multi-Ethnic study showed that the elevated level of Lp-PLA2 increased mortality in patients with coronary heart disease and stroke, so Lp-PLA2 has a marked relation with coronary heart disease and stroke (Ge et al., 2016). Serum Lp-PLA2 level in patients with atherosclerosis and ischemic stroke was higher than that in the normal population (Li et al., 2017; Sofogianni et al., 2018). Zhou et al. analyzed 488 patients with AIS. Patients were managed according to the NIHSS score, with 3 as the median. It was found that patients above the median had a higher level of Lp-PLA2 than that below the median, which implied that Lp-PLA2 might be independently related to the severity of ischemic stroke (Zhou et al., 2018). Recent research expounded that Lp-PLA2 was a risk factor for END following AIS. In the study, 181 patients with AIS were included and 31 patients were diagnosed END within 10 days after first-ever AIS, and the detection results showed that the probability of END increases with the increase of Lp-PLA2 level (Wang et al., 2019). The study suggested that Lp-PLA2 may as an independent predictor for END following AIS.

Biomarkers Related to Coagulation

P-Selectin and C-Type Lectin-Like Receptor 2 (CLEC-2)

Thrombosis is caused by abnormal adhesion and accumulation of platelets onto blood vessel walls, resulting in interruption of blood flow to the brain. Platelet activation plays an essential role in the occurrence and development of AIS. P-selectin and CLEC-2 are both markers of platelet activation. The level of P-selectin reflects the degree of platelet activation and platelet function status, and mediates the adhesion of platelets, neutrophils and endothelial cells, which increases reperfusion injury after AIS (Wang et al., 2013). It has two types: surface membrane type and soluble type. Wang et al. found that soluble P-selectin level was high in patients with progressive AIS, especially in the

progressive aortic atherosclerosis group. Meanwhile, this result was closely correlated with the onset time of progressive AIS (Wang et al., 2013). CLEC-2 is a C-Type Lectin-Like Receptor that is highly expressed on platelets, and is also closely related to platelet activation (Wu et al., 2019). Recent results suggested that elevated plasma CLEC-2 levels were significantly associated with progression in patients with AIS, and the optimal cutoff point for predicting stroke progression was 235.48 pg/mL with a specificity of 54.2%, the sensitivity of 76.8%, respectively (Zhang et al., 2018). At the same time, the author proposed several probable hypotheses to interpret the relationship. Firstly, plasma CLEC-2 takes part in continuous arterial thrombosis and atherosclerotic development, which are predictors of progression and poor outcomes of AIS. Secondly, CLEC-2 has been shown to facilitate thrombo-inflammation which may be important pathogenesis for infarct growth and neurological deterioration (Nieswandt et al., 2011).

D-Dimer

D-dimer is one of the degradation products of fibrin in circulating blood and can represent total fibrin concentration and thus serve as a biomarker for intravascular thrombosis (Zhang et al., 2021). Previous study found that D-dimer levels were significantly higher in patients with progressive AIS than in patients without progressive stroke (Barber et al., 2004). Barber et al. (2006) confirmed that D-dimer was an independent predictor of AIS progression using three different measurement methods (Barber et al., 2006). Furthermore, A recent meta-analysis demonstrated that high D-dimer levels on admission significantly increased the risk of recurrence on the 5-day diffusion-weighted imaging (DWI) in AIS patients (Yuan et al., 2021). As previous research noted, elevated D-dimer levels may reflect the ongoing or potential thrombosis and hypercoagulability (Haapaniemi and Tatlisumak, 2009). In addition, D-dimer may stimulate inflammatory processes. There have had an evidence that D-dimer itself can stimulate the synthesis and release of pro-inflammatory cytokines in monocytes (Kang et al., 2009), which may provide another mechanism in the progression of AIS. What is interesting, recent clinical research from China combined two biological predictors of D-dimer and platelet count, showing that patients with elevated D-dimer level and abnormal platelet count at the same time are at greater risk for END (Liu et al., 2020).

Biomarkers Related to Metabolism

Blood Glucose

Previous research found patients with END had higher levels of blood glucose (Simonsen et al., 2016). In a retrospective study, 213 patients were included in the analysis, indicating that blood glucose level at admission may be an important predictor of END in female AIS patients, but not in males. In the meanwhile, the study pointed out the cutoff value of admission blood glucose level is 107.1 mg/dL (Huang Z. X. et al., 2020). Another indicator is blood sugar variability taking into account the continuous fluctuation in blood sugar, which is another vital part of dysglycemia (Gonzalez-Moreno et al., 2014). In diabetic patients with AIS, initial glycemic variability has been shown related to END (Hui et al., 2018). The glycemic variability assessment was obtained by calculating the standard deviation and the average amplitude of glycemic excursions from the glucose monitoring within the initial 3 hospital days (Hui et al., 2018). Recent research analyzing 215 acute ischemic stroke patients with prediabetes demonstrates that pre-stroke glycemic variability was associated with END occurrence (Lee et al., 2021). In this research, the glycemic variability was defined by glycated albumin ($\geq$16.0%), which showed glycemic fluctuation prior to 4 weeks of stroke onset (Freitas et al., 2017). The authors considered that oxidative stress and insulin resistance played a crucial role in the association. Rapid blood sugar variability created more oxidative stress and reactive oxygen species than chronic hyperglycemia, which progressed to microvascular and macrovascular injury (Lee et al., 2021).

Glycated Albumin (GA)

Glycated albumin is the product of the non-enzymatic glycated reaction between glucose and serum albumin, which can reflect the blood glucose fluctuation level during 14–21 days. Glycated albumin is not only an indicator for screening and diagnosing of prediabetes and diabetes mellitus, but also a good predictor of diabetes mellitus complicated with macrovascular disease (Hsu et al., 2015). As an important glycosylated product, GA has a close correlation with diabetes, nephropathy, retinopathy, coronary heart disease and atherosclerosis (Li et al., 2013). Moreover, GA is closely related to the assessment of prognosis and recurrence risk of atherosclerotic cardiovascular disease and ischemic stroke, and has important clinical significance for monitoring the occurrence of cardiovascular and cerebrovascular adverse events. For example, clinical research reported that serum GA was associated with subclinical atherosclerosis when the concentration of GA was greater than 15.5%, and closely associated with carotid intima-media thickness and high sensitivity of C-reactive protein in non-diabetic residents, which hinted that GA might as assessment factor of carotid atherosclerosis (Li et al., 2013). Lee et al. detected the GA level in 215 patients with acute ischemic stroke with prediabetes, and found that the END occurrence rate was higher in the high level of GA group than that in the low GA group (Lee et al., 2021). In conclusion, glycated albumin may be an important risk factor for atherosclerosis, coronary heart disease, ischemic stroke and END following AIS.

Blood Lipid

Elevated total cholesterol and low-density lipoprotein (LDL)-cholesterol levels are well-known risk factor for cerebrovascular disease. Like the general expectation, a previous study from South Korea, including 410 AIS patients, has pointed out that low high-density lipoprotein-cholesterol levels and high apolipoprotein B/apolipoprotein A-I ratios were independently associated with END (Ryu et al., 2016). The research also pointed out that the association between high-density lipoprotein-cholesterol and END did not differ regardless of subtypes. However, the apolipoprotein B/apolipoprotein A-I ratio was independently related to END in large-artery atherosclerotic stroke only (Ryu et al., 2016). However, as for triglyceride (TG), both hypertriglyceridemia and low TG might be risk factors for poor outcomes in patients with AIS (Choi et al., 2012).

Choi et al. (2012) found that TG had a non-linear, J-shaped association with END following AIS, which further emphasized both hyper TG and hypo TG can be risk factors for adverse early outcomes in AIS.

Cystatin C

The similarities in the hemodynamics between cerebral and renal vascular beds have drawn attention to the association between cerebral infarction and kidney damage (Umemura et al., 2014; Kanamaru et al., 2017). Although Cystatin C is a sensitive indicator of renal function, high levels of Cystatin C are an independent and significant predictor of END in elderly AIS patients with normal renal function in a Korean clinical study (Kim et al., 2017). As for the mechanism, the authors pointed out that the elevated serum Cystatin C may reflect an imbalance in elastolytic activity. This imbalance between proteases and inhibitors affects the cardiovascular system (Sai et al., 2016). Meanwhile, a high Cystatin C concentration is associated with inflammation and endothelial dysfunction, which is involved in the pathogenesis of atherosclerosis (Balta et al., 2013). These factors might explain the relation between microcirculation disorders and impaired vasodilation, which leads to END. Another recent research from China furtherly confirmed the essential role of Cystatin C in the END. Patients with cardiogenic cerebral embolism were enrolled in the study, and the results demonstrated Cystatin C was associated with END within 3 days of cardiogenic cerebral embolism (Cong and Ma, 2021). However, this study had several limitations that excluded other types of cerebral infarction and not investigated the potential mechanism deeply.

Whole Blood Purine Concentration (WBPC)

Purines are nitrogen-containing compounds with a short half-life released by the breakdown of adenosine triphosphate (ATP) and consumed again during oxidative phosphorylation. A recent study observed the relationship between END and WBPC in patients with AIS. Although the results lacked statistical significance, it still suggested that early WBPC may be a simple biomarker for predicting END in AIS patients (Martin et al., 2019). Overall, WBPC was higher for the END group than the non-END group, and the optimal ROC threshold was 6.05 μM. The impossible cellular mechanism is that the ischemic core ceased ATP metabolism and then increased purine production, whereas the penumbral tissue will consume ATP without replenishment, thereby elevating WBPC until perfusion is restored or cell death occurs (Martin et al., 2019). As AIS is the blockage of the cerebral artery, and the lack of blood supplying the brain results in energy metabolism disturbance. Considering the relationship between purine and cell metabolism, the potential function of purine in cerebral infarction is complicated. However, relevant researches are still lacking and more basic or clinical study should be implemented in the future.

Trimethylamine N-Oxide (TMAO)

TMAO is an enterogenic microbiota-associated metabolite synthesized mainly in the liver of the host. Intestinal microbes metabolize lecithin, choline and other nutrients to produce trimethylamine (TMA) which circulates into the liver through portal veins, and is oxidized by flavin monooxygenase 3 (FMO3) or another flavin monooxygenase (FMOx) to produce TMAO (Brunt et al., 2021). Circulating levels of choline, betaine and carnitine are associated with the development of cardiovascular disease and predict the risk of adverse cardiac events. But their prognostic assessment of disease depends on serum TMAO levels (Thomas and Fernandez, 2021). TMA/TMAO is a new crossover between diet, gut microbiome, atherosclerosis and thrombosis. Elevated plasma TMAO level has been shown to independently predict the risk of adverse cardiac events, which includes myocardial infarction, stroke and intervention with conventional cardiac risk factors and renal failure induced death (Xie et al., 2021). Research reported that high plasma TMAO levels were related to atherosclerosis (Xie et al., 2021). Clinical studies have found that patients with 3-year high plasma TMAO levels are more likely to develop atherosclerosis under the same conditions of cardiovascular risk factors (Tang et al., 2013). Wang et al. (2011) also verified that raised TMAO levels in mice by feeding cholinergic food or TMAO, and after a period of time, they found that atherosclerotic plaques appeared in the aortic root of the mice, and the area was proportional to the plasma TMAO level. At the same time, clinical data and *in vivo* studies in mice indicated that TMAO could increase platelet reactivity to agonists and shorten the clotting time of platelets, and raise the risk of thrombus formation (Zhu et al., 2016).

As a metabolite of an exogenous diet, TMAO has many direct or indirect associations with neurological diseases, and plays an important role in the development of neurological diseases. In Alzheimer's disease, TMAO induces mitochondrial function and synaptic dysfunction, activates astrocytes to induce neuroinflammation, damages the BBB (Botchway et al., 2022). For example, the expression level of inflammatory factor CD44 was raised in primary human astrocytes treated with TMAO compared with the control group (Brunt et al., 2021). In Parkinson's disease, TMAO can be used as an osmotic regulator to regulate the conformation of α -synuclein polypeptides (Chung et al., 2021). A recent study reported that patients with END following AIS were detected to have a higher TMAO level and the median concentration was 4.8 μmol/L (Hou et al., 2020). The research indicated that TMAO might be a predictive factor of END following AIS.

Biomarkers Related to Oxidative Stress and Excitatory Neurotoxicity

F2-Isoprostanes (F2-isoP)

Oxidative stress has been shown to play an important role in the occurrence and development of ischemic brain injury (Kelly et al., 2008). F2-isoP is a product of non-cyclooxygenase free radical-induced neuronal arachidonic acid peroxidation of membrane phospholipids and lipoproteins (Morrow, 2005). Compared with other biomarkers of oxidative stress, F2-isoP was a stable, sensitive, and specific marker of oxidative stress (El Kossi and Zakhary, 2000). At the same time, it can be easily measured in serum, urine, and cerebrospinal fluid (Kelly et al., 2008). Lorenzano et al. (2018) found that increased

plasma F2-isoP concentration in the hyperacute phase could independently predict the occurrence of increased infarct volume in patients with acute cerebral infarction. The result suggested the essential role of oxidative stress in promoting cerebral infarction progression, helping to understand the pathophysiological mechanism of ischemia and stroke progression. Indeed, the complicated relationship between oxidative stress and ischemic stroke should be validated in future studies.

MicroRNA-107 (miR-107)

Researches have shown that glutamate-induced neuron toxicity, known as excitatory neurotoxicity, could trigger ischemic neuron damage (Kostandy, 2012). Glutamate is the most common excitatory neurotransmitter in the nervous system, involving various physiological functions such as learning and memory in the brain (Kostandy, 2012). In the normal brain, glutamate transporters play an essential role in clearing the glutamate released in the synaptic cleft to maintain glutamate homeostasis and prevent neurotoxicity (Yang et al., 2014). To date, five glutamate transporter subtypes (EAAT1-EAAT5) have been identified. Of these, glutamate transporter 1 (GLT-1) is the most abundant subtype and is responsible for most glutamate clearance in the central nervous system (Yang et al., 2011; Kostandy, 2012). Down-regulation of GLT-1 expression leads to glutamate accumulation after cerebral ischemia, which in turn aggravates neuronal damage. Yang et al. (2014) found that plasma miR-107 level increased glutamate accumulation after cerebral ischemia by downregulating GLT-1 expression, which could be used as a new biomarker for monitoring excitatory toxicity in patients with ischemic stroke. Similarly, a recent bioinformatics analysis suggested that miR-107-5p is involved in stroke progression by inhibiting *furin* expression (Zhang et al., 2019). *Furin* is a gene belonging to the subtilisin-like proprotein convertase family, and is a critical mRNA function in the central nervous system (Sawada et al., 1997; Johansson, 1999), which directly leads to stroke by interfering with the formation of hypertension (Sawada et al., 1997; Johansson, 1999). These results suggest that plasma miR-107 may be a biomarker for predicting stroke progression.

Serum Total Bilirubin

Serum bilirubin is produced by hemoglobin released by the lysis of aging red blood cells in the body. It includes indirect bilirubin and direct bilirubin. Direct bilirubin is produced by indirect bilirubin in response to hepatocytes in the liver. Bilirubin is a powerful antioxidant. Its oxidative metabolites and biological proteins are sensitive markers of oxidative stress (Shibama et al., 2019). Studies have found that serum total bilirubin is related to the occurrence and prognosis of ischemic stroke (Thakkar et al., 2019). Physiological antioxidant and anti-inflammatory functions of serum total bilirubin can inhibit lipid oxidation and prevent plaque formation, and has protective effects on oxidative stress-mediated inflammation, atherosclerosis and ischemic cardiovascular and cerebrovascular diseases. In Fang et al' s. study, 1,156 patients with symptomatic intracranial atherosclerotic stenosis were registered and the result showed that downregulated level of total bilirubin was detected in patients with severe and multiple atherosclerotic stenoses (Yu et al., 2021). In addition, the level of serum total bilirubin was decreased in patients with END compared with patients without END, which indicated serum total bilirubin may be a novel biomarker for the prediction of END following AIS (Sheng et al., 2021).

Other Biomarkers

Considering the similarities in the hemodynamics between cerebral and renal vascular beds, as is mentioned above, Umemura et al. (2014) reported that after small subcortical infarcts in the lenticulostriate artery territory, proteinuria was independently associated with END. Another clinical research showed albuminuria quantified by the urinary albumin/creatinine ratio (UACR), was independently associated with END in patients with any subtype of AIS (Kanamaru et al., 2017).

As a routine diagnostic index of acute myocardial infarction, serum cardiac troponin I (cTnI) has high sensitivity and specificity (Thygesen et al., 2018). Meanwhile, cTnI can reflect AF-related cardiac structural changes (such as left atrial enlargement, endothelial dysfunction, and fibrosis) and secondary thrombosis (such as left atrial thrombosis, etc.) (Providencia et al., 2013a,b). Interestingly, elevated cTnI is also common in up to 34% of patients with acute ischemic stroke (Bugnicourt et al., 2010), but its exact cause is unknown. A recent clinical study from Korea found that elevated serum cTnI levels were associated with END in patients with AF-related stroke (Nam et al., 2020). However, the exact mechanism is still unclear, and further prospective studies are needed to verify.

Homocysteine is a sulfur-containing amino acid, which is an important intermediate product in the metabolism of methionine and cysteine. Under normal circumstances, homocysteine can be catabolized and its concentration is maintained at low levels. About 99% of homocysteine in the body is in the form of oxidized dimercapto and about 1% reduced free mercapto homocysteine. More and more studies have shown that hyperhomocysteine can cause vascular damage and lead to cardiovascular and cerebrovascular diseases (Ganguly and Alam, 2015). In 1969, the theory that homocysteine is involved in atherosclerosis was first proposed (Boushey et al., 1995). Reports suggested that homocysteine mediated vascular endothelial injury, smooth muscle cell proliferation, inflammation and oxidative stress, which were the progression of stroke and atherosclerosis, and homocysteine promoted the expression of thrombotic factors, platelet adhesion and aggregation (Zhang et al., 2020). In ischemic stroke risk factors analysis, a higher level of homocysteine was verified in the ischemic stroke group, compared with the control group (Zhang et al., 2020). Meanwhile, homocysteine plays an important role in the nervous system (Ganguly and Alam, 2015). A high level of homocysteine was an important factor to induce Alzheimer's and Parkinson's disease (Yin et al., 2021). Research showed that patients with a high level of serum homocysteine had a higher probability of END, which suggested that serum homocysteine could be an independent predictor for END following AIS (Kwon et al., 2014).

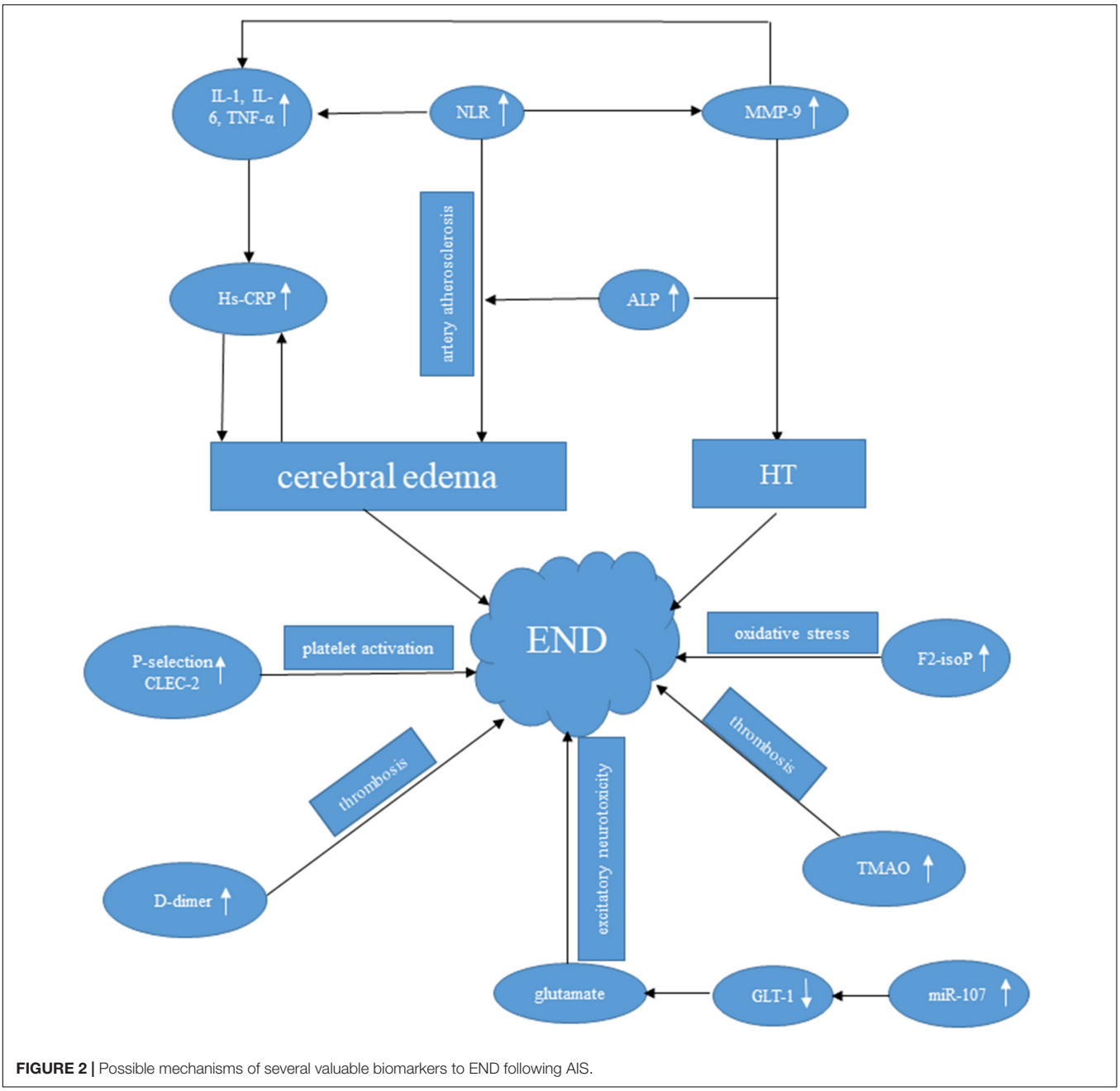

FIGURE 2 | Possible mechanisms of several valuable biomarkers to END following AIS.

CONCLUSION

There are a variety of biomarkers for END (**Figure 2**), which provide new clues for the related mechanisms of stroke progression. Furtherly, biomarkers supply a basis for selecting clinical treatment plans, thus improving the treatment effect of END. Above all, the inflammation-related biomarkers, such as NLP, Hs-CRP, and IL-6 play a crucial role among the mentioned biomarkers. On one hand, the increased NLP indicates a high level of neutrophils, which promote the release of MMP-9 and reactive oxygen species (Ceulemans et al., 2010; Duan et al., 2018). MMP-9 then destructs BBB (Hill et al., 2012), leading to the HT occurrence. On the other hand, Hs-CRP can be triggered by cerebral edema after AIS (Paquissi, 2016) and elevated CRP may further increase the risk of thrombosis (Ryu et al., 2016). However, there is currently no biomarker used for clinical practice because of lacking high sensitivity and specificity. Further research should focus more on prospective studies and standardize the analytical methods. Considering the vast heterogeneity of stroke progression, using a single biomarker may not accurately predict the risk of stroke progression, and it is necessary to combine multiple biomarkers (panels, scores, or indices) to improve their capacity to estimate END. There is no doubt that translating biomarkers

of stroke progression into clinical practice will be of great importance in improving the early identification of such patients, so that treatment regimens can be adjusted in time to improve clinical prognosis.

AUTHOR CONTRIBUTIONS

CQ and XJ: conceptualization. LT: methodology. FH: validation. SY and SN: formal analysis. XJ: writing original draft preparation. CQ: Reviewing and editing. All authors contributed to the drafting, critical revision of the work, and read and agreed to the published version of the manuscript.

FUNDING

This work was supported by the National Natural Science Foundation of China (81771263) and Key Research and Development Program of Shandong Province (2019GSF108030).

REFERENCES

Acalovschi, D., Wiest, T., Hartmann, M., Farahmi, M., Mansmann, U., Auffarth, G. U., et al. (2003). Multiple levels of regulation of the interleukin-6 system in stroke. *Stroke* 34, 1864–1869. doi: 10.1161/01.STR.0000079815.38626.44

Alvarez-Sabin, J., Maisterra, O., Santamarina, E., and Kase, C. S. (2013). Factors influencing haemorrhagic transformation in ischaemic stroke. *Lancet Neurol.* 12, 689–705. doi: 10.1016/S1474-4422(13)70055-3

Balta, S., Demirkol, S., Ay, S. A., Cakar, M., Sarlak, H., and Celik, T. (2013). Serum cystatin-C levels correlate with endothelial dysfunction in patients with the metabolic syndrome. *J. Intern. Med.* 274, 200–201. doi: 10.1111/joim.12078

Barber, M., Langhorne, P., Rumley, A., Lowe, G. D., and Stott, D. J. (2004). Hemostatic function and progressing ischemic stroke: D-dimer predicts early clinical progression. *Stroke* 35, 1421–1425. doi: 10.1161/01.STR.0000126890.63512.41

Barber, M., Langhorne, P., Rumley, A., Lowe, G. D., and Stott, D. J. (2006). D-dimer predicts early clinical progression in ischemic stroke: confirmation using routine clinical assays. *Stroke* 37, 1113–1115. doi: 10.1161/01.STR.0000209240.63821.1a

Biomarkers Definitions Working Group (2001). Biomarkers and surrogate endpoints: preferred definitions and conceptual framework. *Clin. Pharmacol. Ther.* 69, 89–95. doi: 10.1067/mcp.2001.113989

Botchway, B. O., Okoye, F. C., Chen, Y., Arthur, W. E., and Fang, M. (2022). Alzheimer Disease: recent Updates on Apolipoprotein E and Gut Microbiome Mediation of Oxidative Stress, and Prospective Interventional Agents. *Aging Dis.* 13, 87–102. doi: 10.14336/AD.2021.0616

Boushey, C. J., Beresford, S. A., Omenn, G. S., and Motulsky, A. G. (1995). A quantitative assessment of plasma homocysteine as a risk factor for vascular disease. Probable benefits of increasing folic acid intakes. *JAMA* 274, 1049–1057. doi: 10.1001/jama.1995.03530130055028

Brunt, V. E., Larocca, T. J., Bazzoni, A. E., Sapinsley, Z. J., Miyamoto-Ditmon, J., Gioscia-Ryan, R. A., et al. (2021). The gut microbiome-derived metabolite trimethylamine N-oxide modulates neuroinflammation and cognitive function with aging. *Geroscience* 43, 377–394. doi: 10.1007/s11357-020-00257-2

Bugnicourt, J. M., Rogez, V., Guillaumont, M. P., Rogez, J. C., Canaple, S., and Godefroy, O. (2010). Troponin levels help predict new-onset atrial fibrillation in ischaemic stroke patients: a retrospective study. *Eur. Neurol.* 63, 24–28. doi: 10.1159/000258679

Candelario-Jalil, E., Yang, Y., and Rosenberg, G. A. (2009). Diverse roles of matrix metalloproteinases and tissue inhibitors of metalloproteinases in neuroinflammation and cerebral ischemia. *Neuroscience* 158, 983–994. doi: 10.1016/j.neuroscience.2008.06.025

Ceulemans, A. G., Zgavc, T., Kooijman, R., Hachimi-Idrissi, S., Sarre, S., and Michotte, Y. (2010). The dual role of the neuroinflammatory response after ischemic stroke: modulatory effects of hypothermia. *J. Neuroinflammation* 7:74. doi: 10.1186/1742-2094-7-74

Choi, K. H., Park, M. S., Kim, J. T., Chang, J., Nam, T. S., Choi, S. M., et al. (2012). Serum triglyceride level is an important predictor of early prognosis in patients with acute ischemic stroke. *J. Neurol. Sci.* 319, 111–116. doi: 10.1016/j.jns.2012.04.018

Chung, S. J., Rim, J. H., Ji, D., Lee, S., Yoo, H. S., Jung, J. H., et al. (2021). Gut microbiota-derived metabolite trimethylamine N-oxide as a biomarker in early Parkinson's disease. *Nutrition* 83:111090. doi: 10.1016/j.nut.2020.111090

Cong, L., and Ma, W. (2021). Early neurological deterioration in cardiogenic cerebral embolism due to nonvalvular atrial fibrillation: predisposing factors and clinical implications. *Brain Behav.* 11:e01985. doi: 10.1002/brb3.1985

Deng, Q. W., Huang, S., Li, S., Zhai, Q., Zhang, Q., Wang, Z. J., et al. (2021). Inflammatory Factors as Potential Markers of Early Neurological Deterioration in Acute Ischemic Stroke Patients Receiving Endovascular Therapy - The Aisrna Study. *J. Inflamm. Res.* 14, 4399–4407. doi: 10.2147/JIR.S317147

Duan, Z., Guo, W., Tang, T., Tao, L., Gong, K., and Zhang, X. (2020). Relationship between high-sensitivity C-reactive protein and early neurological deterioration in stroke patients with and without atrial fibrillation. *Heart Lung* 49, 193–197. doi: 10.1016/j.hrtlng.2019.10.009

Duan, Z., Wang, H., Wang, Z., Hao, Y., Zi, W., Yang, D., et al. (2018). Neutrophil-Lymphocyte Ratio Predicts Functional and Safety Outcomes after Endovascular Treatment for Acute Ischemic Stroke. *Cerebrovasc. Dis.* 45, 221–227. doi: 10.1159/000489401

El Kossi, M. M., and Zakhary, M. M. (2000). Oxidative stress in the context of acute cerebrovascular stroke. *Stroke* 31, 1889–1892. doi: 10.1161/01.str.31.8.1889

Esenwa, C. C., and Elkind, M. S. (2016). Inflammatory risk factors, biomarkers and associated therapy in ischaemic stroke. *Nat. Rev. Neurol.* 12, 594–604. doi: 10.1038/nrneurol.2016.125

Ferro, D., Matias, M., Neto, J., Dias, R., Moreira, G., Petersen, N., et al. (2021). Neutrophil-to-Lymphocyte Ratio Predicts Cerebral Edema and Clinical Worsening Early After Reperfusion Therapy in Stroke. *Stroke* 52, 859–867. doi: 10.1161/Strokeaha.120.032130

Freitas, P. A. C., Ehlert, L. R., and Camargo, J. L. (2017). Glycated albumin: a potential biomarker in diabetes. *Arch. Endocrinol. Metab.* 61, 296–304. doi: 10.1590/2359-3997000000272

Ganguly, P., and Alam, S. F. (2015). Role of homocysteine in the development of cardiovascular disease. *Nutr. J.* 14:6. doi: 10.1186/1475-2891-14-6

GBD 2016 Stroke Collaborators (2019). Global, regional, and national burden of stroke, 1990-2016: a systematic analysis for the Global Burden of Disease Study 2016. *Lancet Neurol.* 18, 439–458. doi: 10.1016/S1474-4422(19)30034-1

Ge, P. C., Chen, Z. H., Pan, R. Y., Ding, X. Q., Liu, J. Y., Jia, Q. W., et al. (2016). Synergistic Effect of Lipoprotein-Associated Phospholipase A2 with Classical Risk Factors on Coronary Heart Disease: a Multi-Ethnic Study in China. *Cell. Physiol. Biochem.* 40, 953–968. doi: 10.1159/000453153

Gong, P., Liu, Y., Gong, Y., Chen, G., Zhang, X., Wang, S., et al. (2021). The association of neutrophil to lymphocyte ratio, platelet to lymphocyte ratio, and lymphocyte to monocyte ratio with post-thrombolysis early neurological outcomes in patients with acute ischemic stroke. *J. Neuroinflammation* 18:51. doi: 10.1186/s12974-021-02090-6

Gong, P., Xie, Y., Jiang, T., Liu, Y., Wang, M., Sun, H., et al. (2019b). Neutrophil-lymphocyte ratio predicts post-thrombolysis early neurological deterioration in acute ischemic stroke patients. *Brain Behav.* 9:e01426. doi: 10.1002/brb3.1426

Gong, P., Liu, Y., Huang, T., Chen, W., Jiang, T., Gong, Y., et al. (2019a). The association between high-sensitivity C-reactive protein at admission and progressive motor deficits in patients with penetrating artery infarctions. *BMC Neurol.* 19:346. doi: 10.1186/s12883-019-1538-5

Gonzalez-Moreno, E. I., Camara-Lemarroy, C. R., Gonzalez-Gonzalez, J. G., and Gongora-Rivera, F. (2014). Glycemic variability and acute ischemic stroke: the missing link? *Transl. Stroke Res.* 5, 638–646. doi: 10.1007/s12975-014-0365-7

Haapaniemi, E., and Tatlisumak, T. (2009). Is D-dimer helpful in evaluating stroke patients? A systematic review. *Acta Neurol. Scand.* 119, 141–150. doi: 10.1111/j.1600-0404.2008.01081.x

Hill, J. W., Poddar, R., Thompson, J. F., Rosenberg, G. A., and Yang, Y. (2012). Intranuclear matrix metalloproteinases promote DNA damage and apoptosis induced by oxygen-glucose deprivation in neurons. *Neuroscience* 220, 277–290. doi: 10.1016/j.neuroscience.2012.06.019

Hou, L., Zhang, Y., Zheng, D., Shi, H., Zou, C., Zhang, H., et al. (2020). Increasing trimethylamine N-oxide levels as a predictor of early neurological deterioration in patients with acute ischemic stroke. *Neurol. Res.* 42, 153–158. doi: 10.1080/01616412.2019.1710416

Hsu, P., Ai, M., Kanda, E., Yu, N. C., Chen, H. L., Chen, H. W., et al. (2015). A comparison of glycated albumin and glycosylated hemoglobin for the screening of diabetes mellitus in Taiwan. *Atherosclerosis* 242, 327–333. doi: 10.1016/j.atherosclerosis.2015.07.037

Huang, F., Wang, K., and Shen, J. (2020). Lipoprotein-associated phospholipase A2: the story continues. *Med. Res. Rev.* 40, 79–134. doi: 10.1002/med.21597

Huang, Z. X., Huang, Y., Zeng, J., Hao, H., Petroski, G. F., Lu, H., et al. (2020). Admission Glucose Levels May Increase the Risk for Early Neurological Deterioration in Females With Acute Ischemic Stroke. *Front. Neurol.* 11:548892. doi: 10.3389/fneur.2020.548892

Hui, J., Zhang, J., Mao, X., Li, Z., Li, X., Wang, F., et al. (2018). The initial glycemic variability is associated with early neurological deterioration in diabetic patients with acute ischemic stroke. *Neurol. Sci.* 39, 1571–1577. doi: 10.1007/s10072-018-3463-6

Johansson, B. B. (1999). Hypertension mechanisms causing stroke. *Clin. Exp. Pharmacol. Physiol.* 26, 563–565. doi: 10.1046/j.1440-1681.1999.03081.x

Kanamaru, T., Suda, S., Muraga, K., Okubo, S., Watanabe, Y., Tsuruoka, S., et al. (2017). Albuminuria predicts early neurological deterioration in patients with acute ischemic stroke. *J. Neurol. Sci.* 372, 417–420. doi: 10.1016/j.jns.2016.11.007

Kang, D. W., Yoo, S. H., Chun, S., Kwon, K. Y., Kwon, S. U., Koh, J. Y., et al. (2009). Inflammatory and hemostatic biomarkers associated with early recurrent ischemic lesions in acute ischemic stroke. *Stroke* 40, 1653–1658. doi: 10.1161/Strokeaha.108.539429

Kelly, P. J., Morrow, J. D., Ning, M., Koroshetz, W., Lo, E. H., Terry, E., et al. (2008). Oxidative stress and matrix metalloproteinase-9 in acute ischemic stroke: the Biomarker Evaluation for Antioxidant Therapies in Stroke (Beat-Stroke) study. *Stroke* 39, 100–104. doi: 10.1161/STROKEAHA.107.488189

Kim, J. M., Bae, J. H., Park, K. Y., Lee, W. J., Byun, J. S., Ahn, S. W., et al. (2019). Incidence and mechanism of early neurological deterioration after endovascular thrombectomy. *J. Neurol.* 266, 609–615. doi: 10.1007/s00415-018-09173-0

Kim, J., Song, T. J., Park, J. H., Lee, H. S., Nam, C. M., Nam, H. S., et al. (2012). Different prognostic value of white blood cell subtypes in patients with acute cerebral infarction. *Atherosclerosis* 222, 464–467. doi: 10.1016/j.atherosclerosis.2012.02.042

Kim, J., Song, T. J., Song, D., Lee, H. S., Nam, C. M., Nam, H. S., et al. (2013). Serum alkaline phosphatase and phosphate in cerebral atherosclerosis and functional outcomes after cerebral infarction. *Stroke* 44, 3547–3549. doi: 10.1161/STROKEAHA.113.002959

Kim, T. J., Kang, M. K., Jeong, H. G., Kim, C. K., Kim, Y., Nam, K. W., et al. (2017). Cystatin C is a useful predictor of early neurological deterioration following ischaemic stroke in elderly patients with normal renal function. *Eur. Stroke J.* 2, 23–30. doi: 10.1177/2396987316677197

Koklu, E., Yuksel, I. O., Arslan, S., Bayar, N., Cagirci, G., Gencer, E. S., et al. (2016). Is Elevated Neutrophil-to-Lymphocyte Ratio a Predictor of Stroke in Patients with Intermediate Carotid Artery Stenosis? *J. Stroke Cerebrovasc. Dis.* 25, 578–584. doi: 10.1016/j.jstrokecerebrovasdis.2015.10.031

Kostandy, B. B. (2012). The role of glutamate in neuronal ischemic injury: the role of spark in fire. *Neurol. Sci.* 33, 223–237. doi: 10.1007/s10072-011-0828-5

Kurzepa, J., Kurzepa, J., Golab, P., Czerska, S., and Bielewicz, J. (2014). The significance of matrix metalloproteinase (MMP)-2 and MMP-9 in the ischemic stroke. *Int. J. Neurosci.* 124, 707–716. doi: 10.3109/00207454.2013.872102

Kwon, H. M., Lee, Y. S., Bae, H. J., and Kang, D. W. (2014). Homocysteine as a predictor of early neurological deterioration in acute ischemic stroke. *Stroke* 45, 871–873. doi: 10.1161/STROKEAHA.113.004099

Lakhan, S. E., Kirchgessner, A., and Hofer, M. (2009). Inflammatory mechanisms in ischemic stroke: therapeutic approaches. *J. Transl. Med.* 7:97. doi: 10.1186/1479-5876-7-97

Lambertsen, K. L., Biber, K., and Finsen, B. (2012). Inflammatory cytokines in experimental and human stroke. *J. Cereb. Blood Flow Metab.* 32, 1677–1698. doi: 10.1038/jcbfm.2012.88

Lee, S. H., Kim, Y., Park, S. Y., Kim, C., Kim, Y. J., and Sohn, J. H. (2021). Pre-Stroke Glycemic Variability Estimated by Glycated Albumin Is Associated with Early Neurological Deterioration and Poor Functional Outcome in Prediabetic Patients with Acute Ischemic Stroke. *Cerebrovasc. Dis.* 50, 26–33. doi: 10.1159/000511938

Lee, S. J., and Lee, D. G. (2017). Distribution of atherosclerotic stenosis determining early neurologic deterioration in acute ischemic stroke. *PLoS One* 12:e0185314. doi: 10.1371/journal.pone.0185314

Li, D., Wei, W., Ran, X., Yu, J., Li, H., Zhao, L., et al. (2017). Lipoprotein-associated phospholipase A2 and risks of coronary heart disease and ischemic stroke in the general population: a systematic review and meta-analysis. *Clin. Chim. Acta* 471, 38–45. doi: 10.1016/j.cca.2017.05.017

Li, H., Qiu, W., Hu, B., Kang, Z., Wu, A. M., Dai, Y., et al. (2013). Ischemic volumes and early neurologic deterioration in acute brainstem infarctions with hemoglobin A1c. *Eur. Neurol.* 70, 225–232. doi: 10.1159/000351356

Li, J. B., Cheng, R. D., Zhou, L., Wen, W. S., Zhu, G. Y., Tian, L., et al. (2015). What drives progressive motor deficits in patients with acute pontine infarction? *Neural Regen. Res.* 10, 501–504. doi: 10.4103/1673-5374.153703

Liberati, A., Altman, D. G., Tetzlaff, J., Mulrow, C., Gotzsche, P. C., Ioannidis, J. P., et al. (2009). The PRISMA statement for reporting systematic reviews and meta-analyses of studies that evaluate healthcare interventions: explanation and elaboration. *BMJ* 339:b2700. doi: 10.1136/bmj.b2700

Liesz, A., Zhou, W., Na, S. Y., Hammerling, G. J., Garbi, N., Karcher, S., et al. (2013). Boosting regulatory T cells limits neuroinflammation in permanent cortical stroke. *J. Neurosci.* 33, 17350–17362. doi: 10.1523/JNEUROSCI.4901-12.2013

Liu, J., Wang, D., Li, J., Xiong, Y., Liu, B., Wei, C., et al. (2016). Increased Serum Alkaline Phosphatase as a Predictor of Symptomatic Hemorrhagic Transformation in Ischemic Stroke Patients with Atrial Fibrillation and/or Rheumatic Heart Disease. *J. Stroke Cerebrovasc. Dis.* 25, 2448–2452. doi: 10.1016/j.jstrokecerebrovasdis.2016.06.017

Liu, Y., Li, F., Sun, H., Sun, Y., Sun, H., Zhai, Y., et al. (2020). Combined prognostic significance of D-dimer level and platelet count in acute ischemic stroke. *Thromb. Res.* 194, 142–149. doi: 10.1016/j.thromres.2020.05.021

Lorenzano, S., Rost, N. S., Khan, M., Li, H., Lima, F. O., Maas, M. B., et al. (2018). Oxidative Stress Biomarkers of Brain Damage: hyperacute Plasma F2-Isoprostane Predicts Infarct Growth in Stroke. *Stroke* 49, 630–637. doi: 10.1161/STROKEAHA.117.018440

Lucivero, V., Prontera, M., Mezzapesa, D. M., Petruzzellis, M., Sancilio, M., Tinelli, A., et al. (2007). Different roles of matrix metalloproteinases-2 and -9 after human ischaemic stroke. *Neurol. Sci.* 28, 165–170. doi: 10.1007/s10072-007-0814-0

Lux, D., Alakbarzade, V., Bridge, L., Clark, C. N., Clarke, B., Zhang, L., et al. (2020). The association of neutrophil-lymphocyte ratio and lymphocyte-monocyte ratio with 3-month clinical outcome after mechanical thrombectomy following stroke. *J. Neuroinflammation* 17:60. doi: 10.1186/s12974-020-01739-y

Martin, A. J., Dale, N., Imray, C. H. E., Roffe, C., Smith, C. J., Tian, F., et al. (2019). The association between early neurological deterioration and whole blood purine concentration during acute stroke. *Biomark. Res.* 7:7. doi: 10.1186/s40364-019-0158-y

Mizuma, A., You, J. S., and Yenari, M. A. (2018). Targeting Reperfusion Injury in the Age of Mechanical Thrombectomy. *Stroke* 49, 1796–1802. doi: 10.1161/STROKEAHA.117.017286

Morrow, J. D. (2005). Quantification of isoprostanes as indices of oxidant stress and the risk of atherosclerosis in humans. *Arterioscler. Thromb. Vasc. Biol.* 25, 279–286. doi: 10.1161/01.ATV.0000152605.64964.c0

Nam, K. W., Kim, C. K., Yu, S., Chung, J. W., Bang, O. Y., Kim, G. M., et al. (2020). Elevated troponin levels are associated with early neurological worsening in ischemic stroke with atrial fibrillation. *Sci. Rep.* 10:12626. doi: 10.1038/s41598-020-69303-5

Nam, K. W., Kim, T. J., Lee, J. S., Park, S. H., Jeong, H. B., Yoon, B. W., et al. (2019). Neutrophil-to-lymphocyte ratio predicts early worsening in stroke due to large vessel disease. *PLoS One* 14:e0221597. doi: 10.1371/journal.pone.0221597

Nam, K. W., Kwon, H. M., and Lee, Y. S. (2021). Different Predictive Factors for Early Neurological Deterioration Based on the Location of Single Subcortical Infarction: early Prognosis in Single Subcortical Infarction. *Stroke* 52, 3191–3198. doi: 10.1161/STROKEAHA.120.032966

Nam, K. W., Kwon, H. M., Jeong, H. Y., Park, J. H., Kim, S. H., and Jeong, S. M. (2018). High neutrophil to lymphocyte ratios predict intracranial atherosclerosis in a healthy population. *Atherosclerosis* 269, 117–121. doi: 10.1016/j.atherosclerosis.2017.12.035

Nieswandt, B., Pleines, I., and Bender, M. (2011). Platelet adhesion and activation mechanisms in arterial thrombosis and ischaemic stroke. *J. Thromb. Haemost.* 9, 92–104. doi: 10.1111/j.1538-7836.2011.04361.x

Paquissi, F. C. (2016). The Predictive Role of Inflammatory Biomarkers in Atrial Fibrillation as Seen through Neutrophil-Lymphocyte Ratio Mirror. *J. Biomark.* 2016:8160393. doi: 10.1155/2016/8160393

Parikh, N. S., Merkler, A. E., and Iadecola, C. (2020). Inflammation, Autoimmunity, Infection, and Stroke: epidemiology and Lessons From Therapeutic Intervention. *Stroke* 51, 711–718. doi: 10.1161/STROKEAHA.119.024157

Providencia, R., Barra, S., and Paiva, L. (2013a). Atrial fibrillation, elevated troponin, ischemic stroke and adverse outcomes: understanding the connection. *Clin. Res. Cardiol.* 102, 701–711. doi: 10.1007/s00392-013-0591-0

Providencia, R., Paiva, L., Faustino, A., Botelho, A., Trigo, J., Casalta-Lopes, J., et al. (2013b). Cardiac troponin I: prothrombotic risk marker in non-valvular atrial fibrillation. *Int. J. Cardiol.* 167, 877–882. doi: 10.1016/j.ijcard.2012.01.093

Ryu, W. S., Schellingerhout, D., Jeong, S. W., Nahrendorf, M., and Kim, D. E. (2016). Association between Serum Lipid Profiles and Early Neurological Deterioration in Acute Ischemic Stroke. *J. Stroke Cerebrovasc. Dis.* 25, 2024–2030. doi: 10.1016/j.jstrokecerebrovasdis.2016.05.009

Sai, E., Shimada, K., Miyauchi, K., Masaki, Y., Kojima, T., Miyazaki, T., et al. (2016). Increased cystatin C levels as a risk factor of cardiovascular events in patients with preserved estimated glomerular filtration rate after elective percutaneous coronary intervention with drug-eluting stents. *Heart Vessels* 31, 694–701. doi: 10.1007/s00380-015-0674-0

Sawada, Y., Inoue, M., Kanda, T., Sakamaki, T., Tanaka, S., Minamino, N., et al. (1997). Co-elevation of brain natriuretic peptide and proprotein-processing endoprotease furin after myocardial infarction in rats. *FEBS Lett.* 400, 177–182. doi: 10.1016/s0014-5793(96)01385-3

Schuhmann, M. K., Stoll, G., Bieber, M., Vogtle, T., Hofmann, S., Klaus, V., et al. (2020). CD84 Links T Cell and Platelet Activity in Cerebral Thrombo-Inflammation in Acute Stroke. *Circ. Res.* 127, 1023–1035. doi: 10.1161/CIRCRESAHA.120.316655

Semerano, A., Laredo, C., Zhao, Y., Rudilosso, S., Renu, A., Llull, L., et al. (2019). Leukocytes, Collateral Circulation, and Reperfusion in Ischemic Stroke Patients Treated With Mechanical Thrombectomy. *Stroke* 50, 3456–3464. doi: 10.1161/STROKEAHA.119.026743

Seners, P., and Baron, J. C. (2018). Revisiting 'progressive stroke': incidence, predictors, pathophysiology, and management of unexplained early neurological deterioration following acute ischemic stroke. *J. Neurol.* 265, 216–225. doi: 10.1007/s00415-017-8490-3

Seners, P., Turc, G., Oppenheim, C., and Baron, J. C. (2015). Incidence, causes and predictors of neurological deterioration occurring within 24 h following acute ischaemic stroke: a systematic review with pathophysiological implications. *J. Neurol. Neurosurg. Psychiatry* 86, 87–94. doi: 10.1136/jnnp-2014-308327

Seo, W. K., Seok, H. Y., Kim, J. H., Park, M. H., Yu, S. W., Oh, K., et al. (2012). C-reactive protein is a predictor of early neurologic deterioration in acute ischemic stroke. *J. Stroke Cerebrovasc. Dis.* 21, 181–186. doi: 10.1016/j.jstrokecerebrovasdis.2010.06.002

Sheng, X., Du, H., and Tang, Y. (2021). Decreased Serum Total Bilirubin Level Predicts Early Neurological Deterioration in Patients with Acute Ischemic Stroke. *Neuropsychiatr. Dis. Treat.* 17, 1977–1982. doi: 10.2147/NDT.S315330

Shi, K., Tian, D. C., Li, Z. G., Ducruet, A. F., Lawton, M. T., and Shi, F. D. (2019). Global brain inflammation in stroke. *Lancet Neurol.* 18, 1058–1066. doi: 10.1016/S1474-4422(19)30078-X

Shibama, S., Ugajin, T., Yamaguchi, T., and Yokozeki, H. (2019). Bilirubin oxidation derived from oxidative stress is associated with disease severity of atopic dermatitis in adults. *Clin. Exp. Dermatol.* 44, 153–160. doi: 10.1111/ced.13674

Siegler, J. E., Boehme, A. K., Kumar, A. D., Gillette, M. A., Albright, K. C., and Martin-Schild, S. (2013). What change in the National Institutes of Health Stroke Scale should define neurologic deterioration in acute ischemic stroke? *J. Stroke Cerebrovasc. Dis.* 22, 675–682. doi: 10.1016/j.jstrokecerebrovasdis.2012.04.012

Simonsen, C. Z., Schmitz, M. L., Madsen, M. H., Mikkelsen, I. K., Chandra, R. V., Leslie-Mazwi, T., et al. (2016). Early neurological deterioration after thrombolysis: clinical and imaging predictors. *Int. J. Stroke* 11, 776–782. doi: 10.1177/1747493016650454

Sofogianni, A., Alkagiet, S., and Tziomalos, K. (2018). Lipoprotein-associated Phospholipase A2 and Coronary Heart Disease. *Curr. Pharm. Des.* 24, 291–296. doi: 10.2174/1381612824666180111110550

Stoll, G., and Nieswandt, B. (2019). Thrombo-inflammation in acute ischaemic stroke - implications for treatment. *Nat. Rev. Neurol.* 15, 473–481. doi: 10.1038/s41582-019-0221-1

Tang, W. H., Wang, Z., Levison, B. S., Koeth, R. A., Britt, E. B., Fu, X., et al. (2013). Intestinal microbial metabolism of phosphatidylcholine and cardiovascular risk. *N. Engl. J. Med.* 368, 1575–1584. doi: 10.1056/NEJMOA1109400

Thakkar, M., Edelenbos, J., and Dore, S. (2019). Bilirubin and Ischemic Stroke: rendering the Current Paradigm to Better Understand the Protective Effects of Bilirubin. *Mol. Neurobiol.* 56, 5483–5496. doi: 10.1007/s12035-018-1440-y

Thomas, M. S., and Fernandez, M. L. (2021). Trimethylamine N-Oxide (TMAO), Diet and Cardiovascular Disease. *Curr. Atheroscler. Rep.* 23:12. doi: 10.1007/s11883-021-00910-x

Thygesen, K., Alpert, J. S., Jaffe, A. S., Chaitman, B. R., Bax, J. J., Morrow, D. A., et al. (2018). [Fourth universal definition of myocardial infarction (2018)]. *Kardiol. Pol.* 76, 1383–1415. doi: 10.5603/KP.2018.0203

Uehara, T., Yoshida, K., Terasawa, H., Shimizu, H., and Kita, Y. (2020). Increased serum alkaline phosphatase and early neurological deterioration in patients with atherothrombotic brain infarction attributable to intracranial atherosclerosis. *eNeurologicalSci* 20:100253. doi: 10.1016/j.ensci.2020.100253

Umemura, T., Senda, J., Fukami, Y., Mashita, S., Kawamura, T., Sakakibara, T., et al. (2014). Impact of albuminuria on early neurological deterioration and lesion volume expansion in lenticulostriate small infarcts. *Stroke* 45, 587–590. doi: 10.1161/STROKEAHA.113.003164

Vila, N., Castillo, J., Davalos, A., and Chamorro, A. (2000). Proinflammatory cytokines and early neurological worsening in ischemic stroke. *Stroke* 31, 2325–2329. doi: 10.1161/01.str.31.10.2325

Wang, L., Wei, C., Deng, L., Wang, Z., Song, M., Xiong, Y., et al. (2018). The Accuracy of Serum Matrix Metalloproteinase-9 for Predicting Hemorrhagic Transformation After Acute Ischemic Stroke: a Systematic Review and Meta-Analysis. *J. Stroke Cerebrovasc. Dis.* 27, 1653–1665. doi: 10.1016/j.jstrokecerebrovasdis.2018.01.023

Wang, Q., Zhao, W., and Bai, S. (2013). Association between plasma soluble P-selectin elements and progressive ischemic stroke. *Exp. Ther. Med.* 5, 1427–1433. doi: 10.3892/etm.2013.985

Wang, Y., Hu, S., Ren, L., Lei, Z., Lan, T., Cai, J., et al. (2019). Lp-PLA2 as a risk factor of early neurological deterioration in acute ischemic stroke with TOAST type of large arterial atherosclerosis. *Neurol. Res.* 41, 1–8. doi: 10.1080/01616412.2018.1493850

Wang, Z., Klipfell, E., Bennett, B. J., Koeth, R., Levison, B. S., Dugar, B., et al. (2011). Gut flora metabolism of phosphatidylcholine promotes cardiovascular disease. *Nature* 472, 57–63. doi: 10.1038/nature09922

Writing Group Members, Mozaffarian, D., Benjamin, E. J., Go, A. S., Arnett, D. K., Blaha, M. J., et al. (2016). Heart Disease and Stroke Statistics-2016 Update: a Report From the American Heart Association. *Circulation* 133, e38–e360. doi: 10.1161/CIR.0000000000000350

Wu, X., Zhang, W., Li, H., You, S., Shi, J., Zhang, C., et al. (2019). Plasma C-type lectin-like receptor 2 as a predictor of death and vascular events in patients with acute ischemic stroke. *Eur. J. Neurol.* 26, 1334–1340. doi: 10.1111/ene.13984

Xie, G., Yan, A., Lin, P., Wang, Y., and Guo, L. (2021). Trimethylamine N-oxide-a marker for atherosclerotic vascular disease. *Rev. Cardiovasc. Med.* 22, 787–797. doi: 10.31083/j.rcm2203085

Yang, J. L., Sykora, P., Wilson, D. M. III, Mattson, M. P., and Bohr, V. A. (2011). The excitatory neurotransmitter glutamate stimulates DNA repair to increase neuronal resiliency. *Mech. Ageing Dev.* 132, 405–411. doi: 10.1016/j.mad.2011.06.005

Yang, Z. B., Zhang, Z., Li, T. B., Lou, Z., Li, S. Y., Yang, H., et al. (2014). Up-regulation of brain-enriched miR-107 promotes excitatory neurotoxicity through down-regulation of glutamate transporter-1 expression following ischaemic stroke. *Clin. Sci.* 127, 679–689. doi: 10.1042/CS20140084

Yi, X., Zhou, Q., Sui, G., Fan, D., Zhang, Y., Shao, M., et al. (2019). Matrix metalloproteinase-9 gene polymorphisms are associated with ischemic stroke severity and early neurologic deterioration in patients with atrial fibrillation. *Brain Behav.* 9:e01291. doi: 10.1002/brb3.1291

Yin, G., Gan, Y., Jiang, H., Yu, T., Liu, M., Zhang, Y., et al. (2021). Direct Quantification and Visualization of Homocysteine, Cysteine, and Glutathione in Alzheimer's and Parkinson's Disease Model Tissues. *Anal. Chem.* 93, 9878–9886. doi: 10.1021/acs.analchem.1c01945

Yu, F., Zhang, L., Liao, D., Luo, Y., Feng, X., Liu, Z., et al. (2021). Serum Bilirubin Levels and Extent of Symptomatic Intracranial Atherosclerotic Stenosis in Acute Ischemic Stroke: a Cross-Sectional Study. *Front. Neurol.* 12:714098. doi: 10.3389/fneur.2021.714098

Yuan, B., Yang, T., Yan, T., Cheng, W., and Bu, X. (2021). Relationships Between D-Dimer Levels and Stroke Risk as Well as Adverse Clinical Outcomes After Acute Ischemic Stroke or Transient Ischemic Attack: a Systematic Review and Meta-Analysis. *Front. Neurol.* 12:670730. doi: 10.3389/fneur.2021.670730

Yuan, R., Tan, S., Wang, D., Wu, S., Cao, X., Zhang, S., et al. (2018). Predictive value of plasma matrix metalloproteinase-9 concentrations for spontaneous haemorrhagic transformation in patients with acute ischaemic stroke: a cohort study in Chinese patients. *J. Clin. Neurosci.* 58, 108–112. doi: 10.1016/j.jocn.2018.09.014

Zang, R. S., Zhang, H., Xu, Y., Zhang, S. M., Liu, X., Wang, J., et al. (2016). Serum C-reactive protein, fibrinogen and D-dimer in patients with progressive cerebral infarction. *Transl. Neurosci.* 7, 84–88. doi: 10.1515/tnsci-2016-0013

Zhang, H., Zhang, Q., and Liao, Z. (2019). Microarray Data Analysis of Molecular Mechanism Associated with Stroke Progression. *J. Mol. Neurosci.* 67, 424–433. doi: 10.1007/s12031-018-1247-3

Zhang, P., Wang, C., Wu, J., and Zhang, S. (2021). A Systematic Review of the Predictive Value of Plasma D-Dimer Levels for Predicting Stroke Outcome. *Front. Neurol.* 12:693524. doi: 10.3389/fneur.2021.693524

Zhang, T., Jiang, Y., Zhang, S., Tie, T., Cheng, Y., Su, X., et al. (2020). The association between homocysteine and ischemic stroke subtypes in Chinese: a meta-analysis. *Medicine* 99:e19467. doi: 10.1097/MD.0000000000019467

Zhang, X., Zhang, W., Wu, X., Li, H., Zhang, C., Huang, Z., et al. (2018). Prognostic Significance of Plasma CLEC-2 (C-Type Lectin-Like Receptor 2) in Patients With Acute Ischemic Stroke. *Stroke* doi: 10.1161/STROKEAHA.118.022563 [Epub ahead of print].

Zhou, F., Liu, Y., Shi, H., Huang, Q., and Zhou, J. (2018). Relation between lipoprotein-associated phospholipase A2 mass and incident ischemic stroke severity. *Neurol. Sci.* 39, 1591–1596. doi: 10.1007/s10072-018-3474-3

Zhu, W., Gregory, J. C., Org, E., Buffa, J. A., Gupta, N., Wang, Z., et al. (2016). Gut Microbial Metabolite TMAO Enhances Platelet Hyperreactivity and Thrombosis Risk. *Cell* 165, 111–124. doi: 10.1016/j.cell.2016.02.011

Conflict of Interest: The authors declare that the research was conducted in the absence of any commercial or financial relationships that could be construed as a potential conflict of interest.

Publisher's Note: All claims expressed in this article are solely those of the authors and do not necessarily represent those of their affiliated organizations, or those of the publisher, the editors and the reviewers. Any product that may be evaluated in this article, or claim that may be made by its manufacturer, is not guaranteed or endorsed by the publisher.

frontiers | Frontiers in Aging Neuroscience

ORIGINAL RESEARCH
published: 16 June 2022
doi: 10.3389/fnagi.2022.903794

Risk Factors Affecting Cognitive Impairment of the Elderly Aged 65 and Over: A Cross-Sectional Study

*Fengyue Han[1], Changjiang Luo[2], Duojiao Lv[2], Long Tian[3] and Chuanqiang Qu[1,3]**

[1] Department of Neurology, Shandong Provincial Hospital, Shandong University, Jinan, China, [2] Department of Neurology, Jinan Shizhong District People's Hospital, Jinan, China, [3] Department of Neurology, Shandong Provincial Hospital Affiliated to Shandong First Medical University, Jinan, China

Objectives: Elderly population with cognitive impairment has been accelerating in China. This study aimed to explore the relationship between each risk factor and each cognitive domain to provide evidence for risk prevention of controlling impaired cognitive function in elderly.

Methods: This cross-sectional study analyzed the cognitive status of the elderly aged 65 and above in three communities in Shizhong District of Jinan City. Cognitive status was assessed by MMSE. The influencing factors of cognitive impairment were analyzed by chi square test, correlation analysis and regression analysis.

Results: Among 1,171 participants, 643 were defined as cognitive impairment with an incidence of 54.9%. And we found that there were significant differences in the incidence of cognitive impairment among residents with different gender, age, education level, hypertension and LDL-C ($P < 0.05$). However, BMI, marital status, smoking, physical exercise, T2DM, TC, TG and HDL-C had no significant differences in the incidence of cognitive impairment. In addition, education level ($b = 1.194$, $P < 0.001$), age ($b = -0.040$, $P = 0.001$), LDL-C ($b = 0.169$, $P = 0.018$) had statistical significance on the total score of MMSE according to binary logistic regression analysis.

Conclusion: Gender, age, education level, hypertension and LDL-C had significant differences in the incidence of cognitive impairment. And these risk factors could provide a basis for the early screening and intervention of cognitive impairment in the elderly.

Keywords: cognitive dysfunction, aged, risk factors, logistic regression, cross-sectional

OPEN ACCESS

Edited by:
Min Tang,
Jiangsu University, China

Reviewed by:
Chunjiong Zhang,
Tongji University, China
Jian Su,
Nanjing University of Information Science and Technology, China
Xinyan Wang,
Xi'an Peihua University, China

***Correspondence:**
Chuanqiang Qu
drquchuanqiang@sina.com

Specialty section:
This article was submitted to Neurocognitive Aging and Behavior, a section of the journal Frontiers in Aging Neuroscience

Received: *24 March 2022*
Accepted: *16 May 2022*
Published: *16 June 2022*

Citation:
Han F, Luo C, Lv D, Tian L and Qu C (2022) Risk Factors Affecting Cognitive Impairment of the Elderly Aged 65 and Over: A Cross-Sectional Study. Front. Aging Neurosci. 14:903794. doi: 10.3389/fnagi.2022.903794

INTRODUCTION

Due to the continuous development of medical technology and advancements in nursing approaches, the number of elderly people aged 65 and more continues to rise (Eshkoor et al., 2015). Consequently, evidences showed that the prevalence of cognitive impairment (CI) is also likely to increase (Overton et al., 2019; Pettigrew and Soldan, 2019). Cognitive impairment refers

Abbreviations: MMSE, Mini-mental State Examination; BP, blood pressure; LDL-C, low-density lipoprotein cholesterol; BMI - body mass index; T2DM, type 2 diabetes mellitus; TC, total cholesterol; TG, triglyceride; HDL-C, high-density lipoprotein cholesterol.

to the impairment of one or more cognitive functions, which can be divided into mild cognitive impairment (MCI) and dementia according to the severity of the dysfunction. Compared with healthy older adults, MCI patients, accompanying by subjective cognitive decline with lack of objective cognitive and impaired learning and memory, are at a higher risk of dementia, with progression rates ranging from 16% per year (Fleisher et al., 2007). On average, the previous reports revealed that every four seconds, one more individual gets dementia worldwide (WHO and Alzheimer's Disease International, 2012).

Alzheimer's disease (AD) is the most common type of dementia, followed by vascular dementia (Tadic et al., 2016). Vascular risk factors (VRFs), including hypertension, type 2 diabetes mellitus (T2DM), coronary artery disease (CAD), hyperlipidemia, obesity and other risk factors, can lead to stroke and then vascular dementia. The VRFs also have a significant effect in the pathogenesis of Alzheimer's disease. Besides, increasing studies have reported that several risk factors such as gender, age, education, lifestyle and diet habits are associated with the increased risk of development of MCI (Campbell et al., 2013). However, due to different participants, regions and research methods, different conclusions may be drawn from the impact of various risk factors. In addition, different diagnostic criteria for cognitive impairment can also aggravate the differences.

Besides bringing a huge economic burden to the society and patients' families, the emergence of cognitive impairment reduces the quality of life of patients, resulting in painful physical and psychological pressure. However, as of 2016, there are still no pharmacologic treatments for MCI that have been approved by the FDA, the European Medicines Agency or the Pharmaceuticals and Medical Devices Agency in Japan (Petersen, 2016). Thus, early intervention for cognitive dysfunction, for example changes in lifestyle such as physical exercise and cognitive and memory training, is important for the prevention of dementia. This study explored the correlation between cognitive decline and various risk factors in the elderly over 65 years old in the community to identify the population with higher MCI risk and prevent the expected social and disease burden.

MATERIALS AND METHODS

Ethics Statement

The study was conducted according to the guidelines of the Helsinki Declaration. Ethical approval was obtained prior to the start of the study from the Ethics Committee of Jinan Shizhong District People's Hospital. Written informed consent was obtained from all participants.

Study Population

The samples were collected from three communities in Shizhong District of Jinan City: Weijiazhuang sub-district, Liulishan sub-district and Lingxiucheng community. According to the survey data, as of August 2016, there were about 3,000 people aged 65 and above in these three communities. The sample size was estimated according to $n = [Z^2P\ (1\text{-}p)]/d^2$. $Z = 1.96$, P referring to 8.88% of the prevalence of cognitive impairment in general Chinese communities previously reported in the literature (Kuang et al., 2020), allowable error $d = 0.02$, considering 10% invalid samples, the estimated sample size was 864 people. The study was conducted from October 2016 to June 2017. The electronic ID cards of the elderly aged 65 and above in the three communities were sorted, and the residents were selected by simple random sampling method, after which the survey was conducted. Exclusion criteria included: (1) patients with history of neuropsychiatric disorders who could not understand and/or obey the research procedures and/or follow-up; (2) patients with severe anxiety and depression (HAMD $>$ 24, HAMA $\geq$ 29); (3) history of malignant tumor; (4) history of nervous system disorders causing brain dysfunction; (5) patients with severe liver or renal insufficiency (ALT $>$ 2 times the upper limit of normal or AST $>$ 2 times the upper limit of normal; creatinine $>$ 1.5 times the upper limit of normal).

Data Collection and Definition

Before the survey, the participants were informed of the content and purpose of the survey, and the survey was conducted after obtaining the written informed consent. The survey included three parts: general information questionnaire and Chinese version of Mini-mental State Examination (MMSE) (Katzman et al., 1988), physical examination, and laboratory examination.

The self-made general information questionnaire included gender, age, height, weight, marriage, education level, living habits (smoking, drinking, regular diet, and physical exercise), history of chronic diseases (including T2DM, hypertension, hyperlipidemia, and CAD), and medication of related diseases over three recent years. MMSE scale was used to evaluate the cognitive function of the elderly. The scale included 11 cognitive domains: temporal orientation, spatial orientation, immediate recall, attention, delayed recall, naming, repetition, reading, executive function, expression and drawing.

Physical examination included heart rate and blood pressure measurement, and physical examination in neurology department. Participants were asked to sit for 15 min, and then an electronic sphygmomanometer (HEM-741C, Omron, Tokyo, Japan) was used to measure their heart rate and blood pressure. Continuous measurements were taken 3 times, and the average value was used as the final result. The participants were examined by a professional neurologist.

Laboratory tests included liver function (serum glutamic oxaloacetic transaminase, serum alanine transaminase, total bilirubin), renal function (blood urea nitrogen, creatinine), blood lipid (low-density lipoprotein cholesterol, high-density lipoprotein cholesterol, total cholesterol, triglyceride), blood routine (WBC, PLT, Hb), fasting blood glucose and glycosylated hemoglobin.

The total score of MMSE was 30. Those with score less than 27 were assigned to the cognitive impairment group, and those with score more than 27 were categorized as cognitive normal group. According to the level of education,

participants were divided into four groups: those without systematic and formal education were defined as illiterate; those with 1-6 years of education were defined as primary school; those with 7-12 years of education were defined as secondary school; those with more than 12 years of education were defined as university. According to body mass index (calculated by height and weight), the participants were divided into 4 groups: BMI $<$ 18.5 was defined as emaciation, 18.5 $\leq$ BMI $<$ 24 was defined as normal, 24 $\leq$ BMI $<$ 28 was defined as overweight, and 28 $\leq$ BMI was defined as obesity. According to times of exercise in one week, the participants were divided into 3 groups: never exercise; taking exercise $<$ 3 times/week was defined as occasional exercise; taking exercise $\geq$ 3 times/week was defined as regular exercise. Dyslipidemia was defined as LDL-C $>$ 4.13 mmol/L, TG $>$ 2.25 mmol/L, TC $\geq$ 6.2 mmol/L or HDL $<$ 1.03 mmol/L (Kopin and Lowenstein, 2017). T2DM was defined as diabetes mellitus diagnosed in the past, taking hypoglycemic drugs at present, or fasting blood glucose $\geq$ 7.0 mmol/L this time according to the criteria of the Type 2 Diabetes Mellitus Prevention Guideline in China. Hypertension was defined as having been diagnosed with hypertension in the past, taking antihypertensive drugs or measuring blood pressure $\geq$ 140/80mmHg this time. Hypertension grades were defined according to 2013 ESC/ESH Guidelines for the management of arterial hypertension (Mancia et al., 2013). Controlled BP was defined as systolic blood pressure (SBP) $<$ 140 mmHg and/or diastolic blood pressure (DBP) $<$ 90 mmHg; Grade 1 was defined as SBP 140–159 mmHg and/or DBP 90–99 mmHg; Grade 2 was defined as SBP 160–179 mmHg and/or DBP 100–109 mmHg; Grade 3 was defined as SBP $\geq$ 180 mmHg and/or DBP $\geq$ 110 mmHg.

Statistical Analysis

Excel office software was used to establish the database. All statistical analyses were performed with IBM SPSS Statistics for Windows version 26.0 (IBM Corp., Armonk, NY). The test level was bilateral, $\alpha = 0.05$. The counting data were described by frequency or percentage. χ^2 test was used to compare the differences between groups. The risk factors with statistical significance were analyzed by binary logistic regression. Next, the correlation between the risk factors and 11 sub-cognitive domains was analyzed by correlation analysis.

RESULTS

The Relationship of Risk Factors and Cognitive Impairment in the Elderly

A total of 1,324 community residents were investigated in this study. After excluding invalid data, a total of 1,171 respondents entered the analysis. Details of the respondent recruitment and exclusive process in this study were showed in **Figure 1**. There were 528 (45.1%) with normal cognition and 643 (54.9%) with cognitive impairment.

Total 1,171 respondents included 436 men and 735 women, with a male to female ratio of 0.59:1. The respondents were aged between 65 and 95, of which 494 were aged between 65 and 69, accounting for 42.2%; 345 people aged 70-74, accounting for 29.5%; There were 332 people over the age of 75, accounting for 28.3%. Among the respondents, 171 were illiterate, accounting for 14.6%; 237 people with primary school education, accounting for 20.2%; 703 people with secondary school education, accounting for 60.0%; 60 people with university degrees, accounting for 5.1%. There were 58 people who were single, accounting for 5.0%, 896 people who were married, accounting for 76.5%; 217 people who were divorced or widowed, accounting for 18.5%. There were 434 people with smoking history, accounting for 37.1%; 520 people without smoking history, accounting for 44.4%. There were 217 people who never took exercise, accounting for 18.5%; 434 people who took exercise occasionally, accounting for 37.1%; 520 people who took exercise regularly, accounting for 44.4%; There were 12 people who were thin, accounting for 1.0%; 314 people with normal body shape, accounting for 26.8%; 544 people were overweight, accounting for 46.5%; there are 301 obese people, accounting for 25.7%. There were 956 people without type 2 diabetes, accounting for 81.6%; there were 215 people with type 2 diabetes, accounting for 18.4%. There were 691 people without hypertension, accounting for 59.0%; 317 people suffered from grade 1 hypertension, accounting for 27.1%; 137 patients with grade 2 hypertension, accounting for 11.7%; there were 26 people with grade 3 hypertension, accounting for 2.2%. There were 525 people with TC $<$ 6.2mmol/l, accounting for 44.8%; there were 646 people with TC $\geq$ 6.2mmol/l, accounting for 55.2%. There were 786 people with LDL-C $\leq$ 4.13mmol/l, accounting for 67.1%; there were 385 people with LDL-C $>$ 4.13mmol/l, accounting for 32.9%. There were 835 people with TG $\leq$ 2.25mmol/l, accounting for 71.3%; there were 336 people with TG $>$ 2.25mmol/l, accounting for 28.7%. There were 39 people with HDL-C $<$ 1.03mmol/l, accounting for 3.3%; there were 1,132 people with HDL-C $\geq$ 1.03mmol/l, accounting for 96.7%.

As shown in **Table 1**, there were significant differences in the incidence of cognitive impairment among residents with different gender, age, education level, hypertension and LDL-C ($P < 0.05$). There was no significant difference in the incidence of cognitive impairment among residents with different BMI, marital status, smoking history, physical exercise, T2DM, TC, TG and HDL-C ($P > 0.05$). In addition, between different age groups, the results of χ^2-test showed that there was significant difference between 65-69 years old group and $\geq$ 75 years old group ($P < 0.001$), $\chi^2 = 21.091$; there was significant difference between 70-74 years old group and $\geq$ 75 years old group ($P < 0.001$), $\chi^2 = 14.404$; There was no significant difference between 65-69 years old group and 70-74 years old group, $P = 0.609$. Between groups with different levels of Education χ^2 test showed that there were significant differences between the illiterate group and the primary school group, between the illiterate group and the middle school group, between the illiterate group and the university group and between the university group ($P < 0.001$), $\chi^2 = 31.365,139.598,102.331$; There was statistical significance between primary school group and

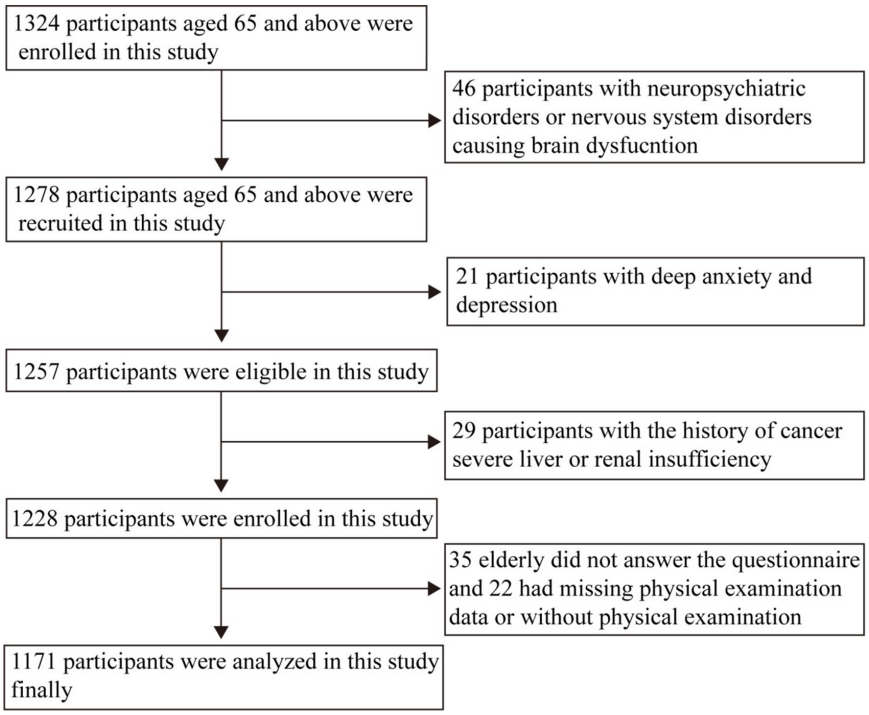

FIGURE 1 | Flow diagram showing the recruitment and exclusive of the residents.

middle school group, primary school group and university group ($P < 0.001$), $\chi^2 = 54.755,36.054$; There was statistical significance between middle school group and university group ($P = 0.03$), $\chi^2 = 4.682$. Between different blood pressure groups χ^2 test showed that there was significant difference between normal group and grade 1 group ($P < 0.001$), $\chi^2 = 14.104$; there was no significant difference between the other two groups.

And, as revealed in **Figure 2A**, the respondents aged between 65 and 69, of which 246 were with cognitive impairment, accounting for 49.8%; the patients aged between 70 and 74, of which 178 were with cognitive impairment, accounting for 51.6%; the respondents aged 75 and over, of which 219 were with cognitive impairment, accounting for 66.0%, the prevalence rate of cognitive impairment was increasing with age. Among the people with illiteracy, 159 people were with cognitive impairment, accounting for 93.0%; among the people with education level of primary school, 167 people were with cognitive impairment, accounting for 70.5%; among the people with education level of middle school, 300 people were with cognitive impairment, accounting for 42.7%; and among the people with education level of high school, 17 people were with cognitive impairment, accounting for 28.3%. The result of **Figure 2B** demonstrated that the morbidity of cognitive impairment was decreasing with the high education level. And we showed that the people with lower LDL-C (less than 4.13 mmol/L), high grade BP and female was more likely to have cognitive impairment (**Figures 2C–E**).

Next, we analyzed the interaction between age and gender, education level, BP, LDL-C in people with cognitive impairment. And we found that prevalence of cognitive impairment was higher among female than male and in lower LDL-C group than higher LDL-C group (**Figures 3A,B**). In addition, in the elderly aged 70-74 years and $\geq$ 75 years, the prevalence of cognitive impairment in all education level group was decreasing with aging, but the percentage of cognitive impairment in people of 65-69 years was significantly high in secondary school group perhaps due to the relatively large deviation of people number recruited to this group (**Figure 3C**). However, in different grade BP group, we found that the prevalence of cognitive impairment in normal group was higher than in the grade 1 group, probably the mild hypertension could improve the cognitive function through cerebral blood circulation and the like a series of positive physiological and biochemical changes (**Figure 3D**). And intriguingly, the effect of grade hypertension on cognitive impairment was different in the elderly aged 65-69 years, 70-74 years and $\geq$ 75 years maybe due to the huge differences of group people number in recruitment (**Figure 3D**).

The variables with statistically significant differences, including gender, age, blood pressure, education level and LDL-C, were used as independent variables for binary logistic regression analysis. The results showed that education level (B = 1.194, OR = 3.302) and LDL-C (B = 0.169, OR = 1.184) were the risk factors of cognitive impairment, while age (B = -0.040, OR = 0.961)was the protective factor. See **Table 2** for details.

TABLE 1 | Basic situation and cognitive impairment of the elderly in three communities, China, 2016.

Characteristics	Cognitive normal	Cognitive impairment	Total	χ^2 value	*p* value
Cases, n (%)	528 (45.1)	643 (54.9)	1171		
Gender, n (%)				11.088	0.001
Male	224 (42.4)	212 (33.0)	436 (37.2)		
Female	304 (57.6)	431 (67.0)	735 (62.8)		
Age group, n (%)				23.132	<0.001
65-69years	248 (47.0)	246 (38.3)	494 (42.2)		
70-74years	167 (31.6)	178 (27.7)	345 (29.5)		
>75years	113 (21.4)	219 (34.0)	332 (28.3)		
Education group, n (%)				182.897	<0.001
Illiteracy	12 (2.3)	159 (24.7)	171 (14.6)		
Primary school	70 (13.3)	167 (26.0)	237 (20.2)		
Secondary school	403 (76.3)	300 (46.7)	703 (60.1)		
University	43 (8.1)	17 (2.6)	60 (5.1)		
Marital status				1.253	0.535
Single	25 (4.7)	33 (5.1)	58 (5.0)		
Married	412 (78.0)	484 (75.3)	896 (76.5)		
Divorced/widowed	91 (17.2)	126 (19.6)	217 (18.5)		
Smoking history				0.645	0.422
NO	313 (59.3)	396 (61.6)	709 (60.5)		
YES	215 (40.7)	247 (38.4)	462 (39.5)		
Physical exercise				5.769	0.056
Never	98 (18.6)	119 (18.5)	217 (18.5)		
Occasional	214 (40.5)	220 (34.2)	434 (37.1)		
Regular	216 (40.9)	304 (47.3)	520 (44.4)		
BMI group, n (%)				7.09	0.069
Thin group	6 (1.1)	6 (0.9)	12 (1.0)		
Normal	133 (25.2)	181 (28.1)	314 (26.8)		
Overweight	267 (50.1)	277 (43.1)	544 (46.5)		
Obese	122 (23.1)	179 (27.8)	301 (25.7)		
T2DM, *n* (%)				0.087	0.768
NO	433 (82.0)	523 (81.3)	956 (81.6)		
YES	95 (18.0)	120 (18.7)	215 (18.4)		
BP, *n* (%)				14.161	0.003
Normal	283 (53.6)	408 (63.4)	691 (59.0)		
Grade 1	170 (32.2)	147 (22.9)	317 (27.1)		
Grade 2	63 (11.9)	74 (11.5)	137 (11.7)		
Grade 3	12 (2.3)	14 (2.2)	26 (2.2)		
TC				1.916	0.166
<6.2 mmol/l	225 (42.6)	300 (46.7)	525 (44.8)		
>6.2 mmol/l	303 (57.4)	343 (53.3)	646 (55.2)		
LDL-C				5.294	0.021
<4.13 mmol/l	336 (63.3)	450 (70.0)	786 (67.1)		
>4.13 mmol/l	192 (36.7)	193 (30.0)	385 (32.9)		
TG				1.521	0.217
<2.25 mmol/l	367 (69.5)	468 (72.8)	835 (71.3)		
>2.25 mmol/l	161 (30.5)	175 (27.2)	336 (28.7)		
HDL-C				2.088	0.148
<1.03 mmol/l	22 (4.2)	17 (2.6)	39 (3.3)		
>1.03 mmol/l	506 (95.8)	626 (97.4)	1132 (96.7)		

BMI - body mass index; T2DM - type 2 diabetes mellitus; BP-blood pressure; TC - total cholesterol; LDL-C– low-density lipoprotein cholesterol; TG– triglyceride; HDL-C–high-density lipoprotein cholesterol.

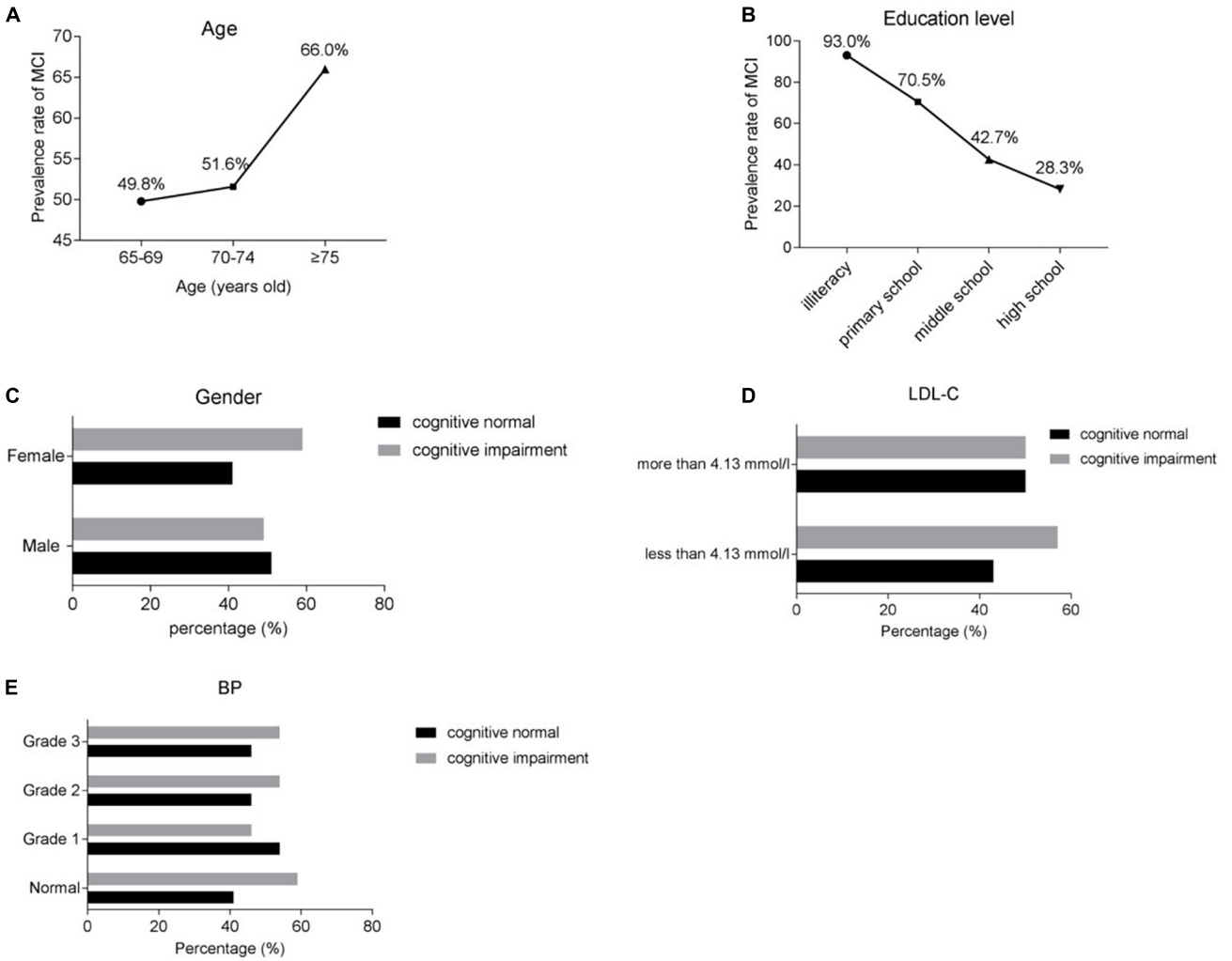

FIGURE 2 | The prevalence rate of cognitive impairment in various risk factors. **(A)** The prevalence rate of cognitive impairment in different ages. **(B)** The prevalence rate of cognitive impairment in different education level. **(C)** The prevalence rate of cognitive normal or impairment in gender level. **(D)** The prevalence rate of cognitive normal or impairment in different level of LDL-C level. **(E)** The prevalence rate of cognitive normal or impairment in different level of BP level. BP, blood pressure. LDL-C, low-density lipoprotein cholesterol.

The Correlation Analysis of Independent Positive Risk Factors and Sub Cognitive Domains

The variables with statistically significant differences, including gender, age, blood pressure, education level and LDL-C, were used as independent variables for correlation analysis with 11 different sub cognitive domains. The results are shown in **Table 3**. The results showed that there were correlations between gender and temporal orientation (r = 0.073), spatial orientation (r = 0.112), immediate memory (r = 0.068), attention (r = 0.142), reading (r = 0.066), expression (r = 0.167) and drawing (r = 0.094). There were correlations between age and 10 sub cognitive domains: temporal orientation (r = −0.082), spatial orientation (r = −0.131), immediate memory (r = −0.220), attention (r = −0.206), delayed memory (r = −0.150), naming (r = −0.113), repetition (r = −0.136), executive ability (r = −0.087), expression (r = 0.167) and drawing (r = 0.094). Education level was correlated with 10 sub cognitive domains: temporal orientation (r = 0.238), spatial orientation (r = 0.282), immediate memory (r = 0.254), attention (r = 0.363), delayed memory (r = 0.226), repetition (r = 0.238), reading (r = 0.277), executive ability (r = 0.172), expression (r = 0.500) and drawing (r = 0.351). There was no correlation between blood pressure, LDL-C and 11 sub cognitive domains.

Taking 11 different sub cognitive domains as dependent variables and age, blood pressure and LDL-C as independent variables for multiple linear regression analysis, the results are shown in **Table 4**. Among them, age was negatively correlated with temporal orientation, spatial orientation, immediate memory, attention, delayed memory, naming, repetition, executive ability, expression and drawing. There was no correlation between blood pressure, LDL-C and these above 11 sub cognitive domains.

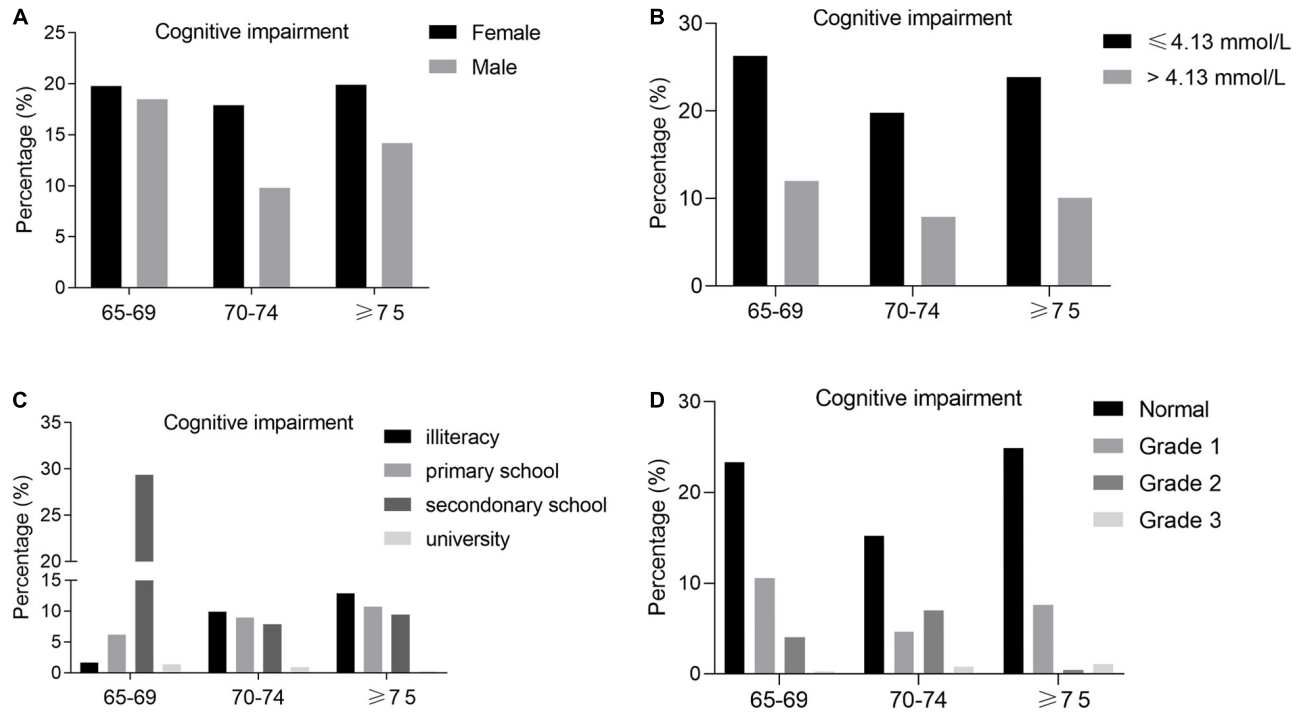

FIGURE 3 | (A) Prevalence of cognitive impairment by gender and age group. **(B)** Prevalence of cognitive impairment by LDL-C and age group. **(C)** Prevalence of cognitive impairment by education level and age group. **(D)** Prevalence of cognitive impairment by BP and age group.

DISCUSSION

The research results of the prevalence of cognitive impairment in the elderly over 65 years old in China have substantially changed over recent years. Kuang et al. (2020) reported that the prevalence of cognitive impairment in the elderly aged 65 years old and more in China was 8.88%, while Yang et al. (2019) indicated that the prevalence of cognitive impairment in the elderly was 15.8%. These inconsistencies may be related to different research methods, diagnostic criteria, participants, and other factors. The incidence of cognitive impairment in this cross-sectional study was 54.9%, which is much higher than that in previous studies and indicates less than optimistic cognitive status in the elderly from these three communities. Since there is no effective drug to reduce cognitive impairment, the prevention of related risk factors is very important. Medical staff must identify the related risk factors of cognitive impairment and promote targeted prevention and treatment so as to reduce the incidence of cognitive impairment in the elderly and improve their quality of life.

In this study, the elderly with cognitive impairment significantly differed in gender, age, education level, BP, and LDL-C compared with the elderly with normal cognition. Among these factors, education level and LDL-C resulted as independent risk factors for cognitive impairment, while age was a protective factor, which is completely different from the results of univariate analysis in **Table 1**.

Age is an important risk factor for cognitive impairment. As we age, the structure of the brain deteriorates. From a macro perspective, the incidence of brain atrophy is an inevitable consequence of aging (Liu-Ambrose et al., 2019). The atrophy of the prefrontal cortex and medial temporal lobe, which is more obvious (Salthouse, 2011), is related to executive function and naming (Harada et al., 2013). In addition, in the process of aging, the reduction of white matter volume is also very obvious. White matter has been shown to be significantly correlated with memory. In the early stage of cognitive impairment (MCI), amnesia is often the first patient complaint (Petersen, 2016). MCI is a cognitive state between normal aging and dementia (Eshkoor et al., 2015, Anderson, 2019)1 16. Eshkoor et al. believe that the diagnosis of MCI is based on the chief complaint of memory impairment (Eshkoor et al., 2015). Therefore, aging is a risk factor for extensive deterioration of multiple cognitive domains such as memory, execution, naming, attention, and reading.

Neurons' death is the possible cause of brain atrophy (Harada et al., 2013). Neurons are non-renewable cells, so the death of neurons is very serious. Still, more theories suggest that the decline of cognitive function in the elderly is related to the decrease of the number of connections between neurons rather than the absolute number of neurons. Synapse is a common connection between neurons, and the information transmission between neurons is also based on a synapse. More studies have been suggesting that the deterioration of cognitive function is based on the decrease of synaptic density. The morphologic

TABLE 2 | Binary logistic regression of gender, age, education, blood pressure and low-density lipoprotein cholesterol on cognitive impairment, China, 2016.

	p value	*B* value	OR value	95% CI
Gender	0.915	−0.014	0.986	0.756-1.285
Age	0.001	−0.040	0.961	0.937-0.985
education	<0.001	1.194	3.302	2.694-4.046
BP	0.269	0.004	1.004	0.997-1.011
LDL-C	0.018	0.169	1.184	1.030-1.361

BP - blood pressure; LDL-C – low-density lipoprotein cholesterol.

TABLE 3 | Correlation analysis of gender, age, education, blood pressure and low-density lipoprotein cholesterol on 11 sub cognitive domains in Mini-mental State Examination, China, 2016.

	Temporal orientation		Spatial orientation		Immediate recall		Attention	
	P value	R	*P* value	r	*P* value	r	*P* value	R
Gender	0.013	0.073	<0.001	0.112	0.019	0.068	<0.001	0.142
Age	0.005	−0.082	<0.001	−0.131	<0.001	−0.220	<0.001	−0.206
BP	0.989	<0.001	0.785	−0.008	0.691	−0.012	0.605	−0.015
LDL-C	0.542	0.018	0.927	−0.003	0.884	0.004	0.187	0.039
Education	<0.001	0.238	<0.001	0.282	<0.001	0.254	<0.001	0.363
	Repetition		**Reading**		**Executive function**		**Expression**	
	P value	R	*P* value	R	*P* value	r	*P* value	R
Gender	0.144	0.043	0.023	0.066	0.060	0.055	<0.001	0.167
Age	<0.001	−0.136	0.987	<0.001	0.003	−0.087	<0.001	−0.159
BP	0.276	−0.032	0.591	0.016	0.348	0.027	0.859	0.005
LDL-C	0.593	−0.016	0.187	0.039	0.329	0.029	0.158	0.041
Education	<0.001	0.238	<0.001	0.277	<0.001	0.172	<0.001	0.500
	Delayed recall		**Naming**		**Drawing**			
	P value	R	*P* value	r	*P* value	r		
Gender	0.265	−0.033	0.680	0.012	0.001	0.094		
Age	<0.001	−0.150	<0.001	−0.113	<0.001	−0.156		
BP	0.527	−0.018	0.648	0.013	0.169	−0.040		
LDL-C	0.234	−0.035	0.908	−0.003	0.955	0.002		
Education	<0.001	0.226	0.056	0.056	<0.001	0.351		

MMSE - Mini-mental State Examination; BP-blood pressure; LDL-C – low-density lipoprotein cholesterol.

changes, including a decrease in the complexity of dendrite arborization, decreased dendrite length and decreased neuritic spines (the major sites for excitatory synapses), directly lead to the decrease of synaptic density (Dickstein et al., 2007).

Currently, it is generally accepted that middle-aged hypertension is related to the decline of cognitive function in old age (Hughes and Sink, 2016; Walker et al., 2017), but the effect the new onset hypertension may have on cognitive function in old age has not yet been consistently defined. It may be that the effect of hypertension on cognitive function is closely related to the duration of hypertension (Walker et al., 2017; Wei et al., 2018). It seems that this theory can be explained by the hypothesis of brain auto-regulation. When the cerebral blood flow perfusion pressure is maintained in a certain range, the cerebral blood flow can maintain a certain steady state. This function is realized by endothelial cells and vascular smooth muscle cells. If long-term persistent hypertension, the cerebral blood perfusion is relatively reduced, resulting in the reduction of the number of cerebral cortex capillaries, fibrosis, smooth muscle cell necrosis, and apoptosis (Tadic et al., 2016). Subsequently, the brain self-regulation starts to be dysfunctional, thus exacerbating the pathological process. This is a chronic, long-term and continuous process.

Hypertension is related to the decline of overall cognitive function, including memory, execution, orientation, reading, repetition, and other cognitive domains. Among these, executive function and information processing speed are the most vulnerable (Hughes and Sink, 2016; Tadic et al., 2016; Walker et al., 2017). The most common lesion associated with hypertension occurs in the frontal cortex, which is the focus of executive function and information processing. Therefore, it can be considered that hypertension affects executive function and information processing speed through the damage of the frontal cortex.

TABLE 4 | Multiple linear regression analysis of age, blood pressure and low-density lipoprotein cholesterol on 11 sub cognitive domains in Mini-mental State Examination, China, 2016.

	Temporal orientation					Spatial orientation					Immediate recall				
	B	SE	β	T	P	B	SE	β	t	P	B	SE	β	t	P
Age	−0.015	0.005	−0.082	−2.806	0.005	−0.019	0.004	−0.131	−4.525	<0.001	−0.021	0.003	−0.220	−7.685	<0.001
BP	<0.001	0.002	0.002	0.065	0.948	<0.001	0.001	−0.003	−0.094	0.925	<0.001	0.001	−0.004	−0.131	0.896
LDL-C	0.016	0.028	0.016	0.552	0.581	−0.004	0.022	−0.005	−0.166	0.868	<0.001	0.015	<0.001	0.014	0.989
	Attention					Delayed recall					Naming				
	B	SE	β	T	P	B	SE	β	t	P	B	SE	β	t	P
Age	−0.060	0.008	−0.205	−7.146	<0.001	−0.028	0.005	−0.150	−5.191	<0.001	−0.004	0.001	−0.113	−3.894	<0.001
BP	−0.001	0.002	−0.011	−0.380	0.704	−0.001	0.002	−0.010	−0.331	0.741	<0.001	<0.001	0.018	0.621	0.535
LDL-C	0.056	0.045	0.036	1.247	0.213	−0.037	0.030	−0.037	−1.262	0.207	−0.001	0.005	−0.007	−0.243	0.808
	Repetition					Reading					Executive function				
	B	SE	B	T	P	B	SE	β	t	P	B	SE	β	t	P
Age	−0.008	0.002	−0.135	−4.653	<0.001	0.896	0.002	0.001	0.024	0.981	−0.011	0.004	−0.087	−2.994	0.003
BP	<0.001	<0.001	−0.025	−0.875	0.382	<0.001	0.001	0.012	0.416	0.677	0.001	0.001	0.028	0.969	0.332
LDL-C	−0.005	0.009	−0.016	−0.541	0.589	0.017	0.013	0.037	1.276	0.202	0.016	0.019	0.024	0.832	0.406
	Expression					Drawing				
	B	SE	B	t	P	B	SE	β	t	P
Age	−0.013	0.002	−0.159	−5.490	<0.001	−0.013	0.002	−0.154	−5.334	<0.001
BP	<0.001	0.001	0.008	0.260	0.795	−0.001	0.001	−0.035	−1.197	0.232
LDL-C	0.017	0.013	0.038	1.300	0.194	0.001	0.013	0.002	0.071	0.944

MMSE - Mini-mental State Examination; BP-blood pressure; LDL-C – low-density lipoprotein cholesterol.

Stern proposed the hypothesis of "cognitive reserve" and defined it as the ability to optimize cognitive performance (Stern, 2002). The cognitive reserve cannot be directly calculated but can only be expressed by different indicators, among which the most commonly used is education level (Kessels et al., 2017; Mungas et al., 2018). The incidence rate of dementia is lower in individuals with higher education levels, and the average age of dementia onset is also delayed by higher education level (Xu et al., 2016). The delay of onset age means the extension of the time without cognitive impairment. To some extent, the improvement of education level improves the quality of life in the elderly. Nevertheless, it is not enough to replace cognitive reserve only by education level. Formal and systematic education years are static, while the cognitive reserve is dynamic. Skilled manual work, good reading habits, and positive social interaction can also be regarded as indicators of cognitive reserve. Moreover, the level of higher education means a better economic level and more extensive interpersonal communication, and the existence of these factors also affects the cognitive status (Kahn and Pearlin, 2006; Shin et al., 2020; Yahirun et al., 2020).

The incidence rates of cognitive impairment were higher in women compared to men (58.6 vs. 48.6%), which is consistent with previous studies (Zhang, 2006; Zhang et al., 2008). In addition to the significant differences in MMSE, there were also significant differences in time orientation, spatial orientation, immediate memory, attention, reading, expression, drawing, and other sub cognitive domains.

The elderly in this study were 65 years of age and above, and most of them were born before the founding of new China in 1949. Previous study indicated that China is a traditionally patriarchal society, where men are dominant in economic level, social status, education level, social activities, and other aspects (Miyawaki and Liu, 2019). South Korea, which has a similar history to China, also records worse cognition in older women (Cho et al., 2017). Especially before 1949, most women had no access to formal education. In addition, the longer life expectancy of women may further aggravate this difference (Hebert et al., 2001, Viña and Lloret, 2010).

LDL-C is a key factor in the formation and development of atherosclerosis and the formation of unstable plaque, which is in the central position in cardiovascular and cerebrovascular diseases (Wang et al., 2018). There are various mechanisms of LDL-C in cognitive decline. Inflammation has an important role in atherosclerosis. Oxidized low-density lipoprotein is phagocytic, forming foam cells, which is the central link of atherosclerosis, eventually leading to thrombosis and cerebral blood flow reduction, neuronal necrosis, apoptosis, and synapse reduction. It is also believed that LDL-C is related to the permeability of the blood-brain barrier and that LDL-C increases the permeability of the blood-brain barrier by reducing the expression of tight junction protein ZO-1 (Dias et al., 2015, Tanaka et al., 2018). However, this theory has not been widely accepted.

The present study has a few limitations in this study. First, this was only a cross-sectional study with a relatively small number of samples and no follow-up data. Second, some important risk factors affecting cognitive function (such as cerebrovascular disease) were not included in the regression equation. Third, our study was performed in Jinan, People's Republic of China, where economic development, labor migration, culture, and lifestyles may influence the prevalence of CI. Finally, there are some limitations related to MMSE: MMSE has a wide range of applications, but its sensitivity is low, and some MCI may be missed. Therefore, a follow-up study needs to be performed in the future.

In conclusion, the present study revealed several risk factors to be the significant predictors of cognitive impairment. Compared with the elderly with normal cognition, the elderly with cognitive impairment has significant differences in gender, age, education level, BP, LDL-C, and so on. Among these factors, education level and LDL-C are the independent risk factors of cognitive impairment, while age is the protective factor, which is quite different from the general cognition in the past. The relationship between other risk factors such as smoking, material status, BMI, T2DM, TC, TG, HDL-C, and cognitive impairment cannot be denied. The study provided an opportunity to targeted cognitive training and intensive intervention for the elderly to delay the progression of cognitive decline.

DATA AVAILABILITY STATEMENT

The original contributions presented in this study are included in the article/supplementary material, further inquiries can be directed to the corresponding authors.

ETHICS STATEMENT

Ethical approval was obtained prior to the start of the study from the Ethics Committee of Jinan Shizhong District People's Hospital. Written informed consent was obtained from all participants.

AUTHOR CONTRIBUTIONS

CQ designed the study. FH analyzed and interpreted the data, wrote and edited the manuscript, administered the project, acquired funding, and reviewed and edited the manuscript. CL, DL, and LT contributed to the acquisition, analysis, and interpretation of the data. All authors contributed to the article and approved the submitted version.

FUNDING

The National Natural Science Fund of China (81771263). The Key Research and Development Program of Shandong Province (2019GSF108030).

ACKNOWLEDGMENTS

We thank all the individuals who participated in this study.

REFERENCES

Anderson, N. D. (2019). State of the science on mild cognitive impairment (MCI). *CNS Spectr.* 24, 78–87. doi: 10.1017/S1092852918001347

Campbell, N. L., Unverzagt, F., LaMantia, M. A., Khan, B. A., and Boustani, M. A. (2013). Risk factors for the progression of mild cognitive impairment to dementia. *Clin. Geriatr. Med.* 29, 873–893.

Cho, J., Jin, Y., Lee, I., Hong, H., Kim, D., Park, S., et al. (2017). Physical inactivity and cognitive impairment in Korean older adults: gender differences in potential covariates. *Ann. Hum. Biol.* 44, 729–737. doi: 10.1080/03014460.2017.1392604

Dias, H. K., Brown, C. L., Polidori, M. C., Lip, G. Y., and Griffiths, H. R. (2015). LDL-lipids from patients with hypercholesterolaemia and Alzheimer's disease are inflammatory to microvascular endothelial cells: mitigation by statin intervention. *Clin. Sci.* 129, 1195–1206. doi: 10.1042/CS20150351

Dickstein, D. L., Kabaso, D., Rocher, A. B., Luebke, J. I., Wearne, S. L., and Hof, P. R. (2007). Changes in the structural complexity of the aged brain. *Aging Cell* 6, 275–284. doi: 10.1111/j.1474-9726.2007.00289.x

Eshkoor, S. A., Hamid, T. A., Mun, C. Y., and Ng, C. K. (2015). Mild cognitive impairment and its management in older people. *Clin. Interv. Aging* 10, 687–693. doi: 10.2147/CIA.S73922

Fleisher, A. S., Sowell, B. B., Taylor, C., Gamst, A. C., Petersen, R. C., Thal, L. J., et al. (2007). Clinical predictors of progression to Alzheimer disease in amnestic mild cognitive impairment. *Neurology* 68, 1588–1595. doi: 10.1212/01.wnl.0000258542.58725.4c

Harada, C. N., Natelson Love, M. C., and Triebel, K. L. (2013). Normal cognitive aging. *Clin. Geriatr. Med.* 29, 737–752.

Hebert, L. E., Scherr, P. A., McCann, J. J., Beckett, L. A., and Evans, D. A. (2001). Is the risk of developing Alzheimer's disease greater for women than for men? *Am. J. Epidemiol.* 153, 132–136. doi: 10.1093/aje/153.2.132

Hughes, T. M., and Sink, K. M. (2016). Hypertension and its role in cognitive function: current evidence and challenges for the future. *Am. J. Hypertens.* 29, 149–157. doi: 10.1093/ajh/hpv180

Kahn, J. R., and Pearlin, L. I. (2006). Financial strain over the life course and health among older adults. *J. Health Soc. Behav.* 47, 17–31. doi: 10.1177/002214650604700102

Katzman, R., Zhang, M. Y., Ya, Q. Ouang, Wang, Z. Y., Liu, W. T., Yu, E., et al. (1988). A Chinese version of the mini-mental state examination; impact of illiteracy in a shanghai dementia survey. *J. Clin. Epidemiol.* 41, 971–978. doi: 10.1016/0895-4356(88)90034-0

Kessels, R. P., Eikelboom, W. S., Schaapsmeerders, P., Maaijwee, N. A., Arntz, R. M., van Dijk, E. J., et al. (2017). Effect of formal education on vascular cognitive impairment after stroke: a meta-analysis and study in young-stroke patients. *J. Int. Neuropsychol. Soc.* 23, 223–238. doi: 10.1017/S1355617716001016

Kopin, L., and Lowenstein, C. (2017). Dyslipidemia. *Ann. Intern. Med.* 167, ITC81–ITC96.

Kuang, W., Gao, M., Tian, L., Wan, Y., and Qiu, P. (2020). Trends in the prevalence of cognitive impairment in Chinese older adults: based on the Chinese longitudinal healthy longevity survey cohorts from 1998 to 2014. *Int. Health* 12, 378–387. doi: 10.1093/inthealth/ihz114

Liu-Ambrose, T., Barha, C., and Falck, R. S. (2019). Active body, healthy brain: exercise for healthy cognitive aging. *Int. Rev. Neurobiol.* 147, 95–120. doi: 10.1016/bs.irn.2019.07.004

Mancia, G., Fagard, R., Narkiewicz, K., Redon, J., Zanchetti, A., Bohm, M., et al. (2013). 2013 ESH/ESC guidelines for the management of arterial hypertension: the Task Force for the Management of Arterial Hypertension of the European Society of Hypertension (ESH) and of the European Society of Cardiology (ESC). *Eur. Heart J.* 34, 2159–2219.

Miyawaki, C. E., and Liu, M. (2019). Gender differences in cognitive impairment among the old and the oldest-old in China. *Geriatr. Gerontol. Int.* 19, 586–592.

Mungas, D., Gavett, B., Fletcher, E., Farias, S. T., DeCarli, C., and Reed, B. (2018). Education amplifies brain atrophy effect on cognitive decline: implications for cognitive reserve. *Neurobiol. Aging* 68, 142–150. doi: 10.1016/j.neurobiolaging.2018.04.002

Overton, M., Pihlsgard, M., and Elmstahl, S. (2019). Prevalence and incidence of mild cognitive impairment across subtypes, age, and sex. *Dement. Geriatr. Cogn. Disord.* 47, 219–232. doi: 10.1159/000499763

Petersen, R. C. (2016). Mild cognitive impairment. *Continuum* 22, 404–418.

Pettigrew, C., and Soldan, A. (2019). Defining cognitive reserve and implications for cognitive aging. *Curr. Neurol. Neurosci. Rep.* 19:1.

Salthouse, T. A. (2011). Neuroanatomical substrates of age-related cognitive decline. *Psychol. Bull.* 137, 753–784. doi: 10.1037/a0023262

Shin, M., Sohn, M. K., Lee, J., Kim, D. Y., Lee, S. G., Shin, Y. I., et al. (2020). Effect of cognitive reserve on risk of cognitive impairment and recovery after stroke: the KOSCO study. *Stroke* 51, 99–107. doi: 10.1161/STROKEAHA.119.026829

Stern, Y. (2002). What is cognitive reserve? Theory and research application of the reserve concept. *J. Int. Neuropsychol. Soc.* 8, 448–460.

Tadic, M., Cuspidi, C., and Hering, D. (2016). Hypertension and cognitive dysfunction in elderly: blood pressure management for this global burden. *BMC Cardiovasc. Disord.* 16:208. doi: 10.1186/s12872-016-0386-0

Tanaka, H., Iida, Y., Iwaki, T., Suzuki, Y., Sano, H., Miyajima, C., et al. (2018). Elevated plasma levels of LDL cholesterol promote dissecting thoracic aortic aneurysms in angiotensin ii-induced mice. *Ann. Vasc. Surg.* 48, 204–213. doi: 10.1016/j.avsg.2017.10.006

Viña, J., and Lloret, A. (2010). Why women have more Alzheimer's disease than men: gender and mitochondrial toxicity of amyloid-beta peptide. *J. Alzheimers Dis.* 20(Suppl. 2), S527–S533. doi: 10.3233/JAD-2010-100501

Walker, K. A., Power, M. C., and Gottesman, R. F. (2017). Defining the relationship between hypertension, cognitive decline, and dementia: a review. *Curr. Hypertens. Rep.* 19:24. doi: 10.1007/s11906-017-0724-3

Wang, A., Liu, J., Meng, X., Li, J., Wang, H., Wang, Y., et al. (2018). Association between oxidized low-density lipoprotein and cognitive impairment in patients with ischemic stroke. *Eur. J. Neurol.* 25, 185–191. doi: 10.1111/ene.13497

Wei, J., Yin, X., Liu, Q., Tan, L., and Jia, C. (2018). Association between hypertension and cognitive function: a cross-sectional study in people over 45 years old in China. *J. Clin. Hypertens.* 20, 1575–1583. doi: 10.1111/jch.13393

WHO and Alzheimer's Disease International (2012). *Dementia: A Public Health Priority*. Available online at: https://www.who.int/publications/i/item/dementia-a-public-health-priority (accessed August 24, 2012).

Xu, W., Tan, L., Wang, H. F., Tan, M. S., Tan, L., Li, J. Q., et al. (2016). Education and risk of dementia: dose-response meta-analysis of prospective cohort studies. *Mol. Neurobiol.* 53, 3113–3123. doi: 10.1007/s12035-015-9211-5

Yahirun, J. J., Vasireddy, S., and Hayward, M. D. (2020). The education of multiple family members and the life-course pathways to cognitive impairment. *J. Gerontol. B Psychol. Sci. Soc. Sci.* 75, e113–e128. doi: 10.1093/geronb/gbaa039

Yang, L., Jin, X., Yan, J., Jin, Y., Xu, S., Xu, Y., et al. (2019). Comparison of prevalence and associated risk factors of cognitive function status among elderly between nursing homes and common communities of China: a STROBE-compliant observational study. *Medicine* 98:e18248. doi: 10.1097/MD.0000000000018248

Zhang, Z. (2006). Gender differentials in cognitive impairment and decline of the oldest old in China. *J. Gerontol. B Psychol. Sci. Soc. Sci.* 61, S107–S115. doi: 10.1093/geronb/61.2.s107

Zhang, Z., Gu, D., and Hayward, M. D. (2008). Early life influences on cognitive impairment among oldest old Chinese. *J. Gerontol. B Psychol. Sci. Soc. Sci.* 63, S25–S33. doi: 10.1093/geronb/63.1.s25

Conflict of Interest: The authors declare that the research was conducted in the absence of any commercial or financial relationships that could be construed as a potential conflict of interest.

frontiers | Frontiers in Aging Neuroscience

ORIGINAL RESEARCH
published: 30 June 2022
doi: 10.3389/fnagi.2022.942285

A Presurgical Unfavorable Prediction Scale of Endovascular Treatment for Acute Ischemic Stroke

Jingwei Li[1,2,3,4,5†], Wencheng Zhu[6†], Junshan Zhou[7†], Wenwei Yun[8], Xiaobo Li[9], Qiaochu Guan[1], Weiping Lv[1], Yue Cheng[1], Huanyu Ni[10], Ziyi Xie[1], Mengyun Li[1], Lu Zhang[1], Yun Xu[1,2,3,4,5] and Qingxiu Zhang[1,2,3,4,5]*

[1] Department of Neurology of Drum Tower Hospital, Medical School and the State Key Laboratory of Pharmaceutical Biotechnology, Nanjing University, Nanjing, China, [2] Institute of Brain Sciences, Nanjing University, Nanjing, China, [3] Jiangsu Key Laboratory for Molecular Medicine, Medical School of Nanjing University, Nanjing, China, [4] Jiangsu Province Stroke Center for Diagnosis and Therapy, Nanjing, China, [5] Nanjing Neurology Clinic Medical Center, Nanjing, China, [6] The Institute of Software, Chinese Academy of Sciences, Beijing, China, [7] Department of Neurology, Nanjing First Hospital, Nanjing Medical University, Nanjing, China, [8] Department of Neurology, Changzhou No.2 People's Hospital Affiliated to Nanjing Medical University, Changzhou, China, [9] Department of Neurology, Northern Jiangsu People's Hospital, Clinical Medical School of Yangzhou University, Yangzhou, China, [10] Department of Pharmacy of Drum Tower Hospital, Medical School, Nanjing University, Nanjing, China

OPEN ACCESS

Edited by:
Jialiang Yang,
Geneis (Beijing) Co. Ltd., China

Reviewed by:
Tian Xu,
Affiliated Hospital of Nantong University, China
Wenjie Cao,
Fudan University, China

***Correspondence:**
Qingxiu Zhang
zhangqingxiu@163.com

[†]These authors have contributed equally to this work

Specialty section:
This article was submitted to Neuroinflammation and Neuropathy, a section of the journal Frontiers in Aging Neuroscience

Received: *12 May 2022*
Accepted: *02 June 2022*
Published: *30 June 2022*

Citation:
Li J, Zhu W, Zhou J, Yun W, Li X, Guan Q, Lv W, Cheng Y, Ni H, Xie Z, Li M, Zhang L, Xu Y and Zhang Q (2022) A Presurgical Unfavorable Prediction Scale of Endovascular Treatment for Acute Ischemic Stroke. Front. Aging Neurosci. 14:942285. doi: 10.3389/fnagi.2022.942285

Objective: To develop a prognostic prediction model of endovascular treatment (EVT) for acute ischemic stroke (AIS) induced by large-vessel occlusion (LVO), this study applied machine learning classification model light gradient boosting machine (LightGBM) to construct a unique prediction model.

Methods: A total of 973 patients were enrolled, primary outcome was assessed with modified Rankin scale (mRS) at 90 days, and favorable outcome was defined using mRS 0–2 scores. Besides, LightGBM algorithm and logistic regression (LR) were used to construct a prediction model. Then, a prediction scale was further established and verified by both internal data and other external data.

Results: A total of 20 presurgical variables were analyzed using LR and LightGBM. The results of LightGBM algorithm indicated that the accuracy and precision of the prediction model were 73.77 and 73.16%, respectively. The area under the curve (AUC) was 0.824. Furthermore, the top 5 variables suggesting unfavorable outcomes were namely admitting blood glucose levels, age, onset to EVT time, onset to hospital time, and National Institutes of Health Stroke Scale (NIHSS) scores (importance = 130.9, 102.6, 96.5, 89.5 and 84.4, respectively). According to AUC, we established the key cutoff points and constructed prediction scale based on their respective weightings. Then, the established prediction scale was verified in raw and external data and the sensitivity was 80.4 and 83.5%, respectively. Finally, scores >3 demonstrated better accuracy in predicting unfavorable outcomes.

Conclusion: Presurgical prediction scale is feasible and accurate in identifying unfavorable outcomes of AIS after EVT.

Keywords: cerebral infarction, endovascular treatment, LightGBM algorithm, large-vessel occlusion, prediction model

INTRODUCTION

Cerebral infarction induced by acute large-vessel occlusion (LVO) in middle cerebral artery or vertebrobasilar artery has a high rate of disability and mortality (Goyal et al., 2016). In recent years, an increasing number of studies have found that endovascular treatment (EVT), which is used to perform recanalization in occluded large vessels, is an effective and plausible treatment that has further improved clinical outcome of patients (Lin et al., 2019; Jia et al., 2021). However, only about 30–40% patients achieved good outcomes even though intervention treatment was successful and blood flow was restored (Han et al., 2021; Jia et al., 2021). Therefore, it is an urgent task for us to explore a feasible prediction model for the outcomes of EVT of LVO.

According to recent clinical trials that have used new neuroimaging methods or biological markers, many risk factors would indicate poor outcomes for patients who received EVT for acute ischemic stroke (AIS) (Brugnara et al., 2020; Liu et al., 2021). To be specific, the risk factors, including brain edema, reperfusion injury, high National Institutes of Health Stroke Scale (NIHSS) scores, and blood-brain barrier damage were all associated with unfavorable prognosis (Chen et al., 2019; Heo et al., 2019; Brugnara et al., 2020; Butler et al., 2020; Liu et al., 2021). Even though research focused on prediction models using neuroimaging markers, biological markers, and neurological impairments is increasing, these predictors could not be used to make presurgical clinical decisions because they are examined and interpreted mostly during or after treatment.

Although logistic regression (LR) is widely applied in calculating disease-associated risk predictors, it still has limitations: it cannot provide satisfying accuracy, and it struggles with large numbers of variables (Dreiseitl and Ohno-Machado, 2002). Therefore, a prognosis model that predicts mid-term/short-term outcomes established by machine learning algorithm in stroke field began to gain attention (Heo et al., 2019; Brugnara et al., 2020; Liu et al., 2021). Furthermore, machine learning algorithm is able to deal with a huge number of complex variables and provides specific numerical values of different predictors (Deng et al., 2018; He et al., 2020; Castaneda-Vega et al., 2021). Among some widely used algorithms, light gradient boosting machine (LightGBM) is a classification model based on decision tree algorithm, with many advantages such as fast training speed, low memory consumption, high accuracy, and the ability to rapidly process massive data (Zhan et al., 2018; Chen et al., 2019; Shaker et al., 2021; Song et al., 2021; Liao et al., 2022).

In this study, 973 cases receiving EVT from four hospitals were enrolled and divided into favorable outcome and unfavorable outcome groups according to live independent ability. Machine learning model LightGBM was used to assess 20 related presurgical variables and construct prognostic prediction model to explore the major predictors for the first time. Afterward, the prediction scale was then established and further validated using raw data as well as new external data. The results suggested that prediction scoring mechanism would be a simple and pragmatic evaluation tool that can be widely used in clinical practice.

MATERIALS AND METHODS

Data Collection and Processing

Data were retrospectively collected from patients who visited one of the four hospitals in Jiangsu Province in China from January 2018 to December 2020. The inclusion criteria were as follows: (1) age $\geq$18 years old; (2) within 24 h of onset; (3) neuroimaging-confirmed intracranial LVO induced AIS, including anterior cerebral artery (A1/A2), middle cerebral artery (M1/M2), basilar artery, intracranial internal carotid artery (T/L), vertebral artery (V4), and posterior cerebral artery (P1); (4) received EVT, including mechanical thrombectomy, angioplasty, intra-arterial thrombolysis, and stenting; and (5) with complete follow-up data with 90-day modified Rankin scale (mRS). The exclusion criteria were (1) malignant tumor; (2) incomplete data; (3) lost to follow-up; (4) severe heart, lung, and renal disease; and (5) pre-stroke mRS $>$ 2 scores.

The external validation data, including 169 patients, was obtained from two of four hospitals from January to July 2021. The inclusion and exclusion criteria followed the above criteria as well.

Baseline data, including demographic characteristics, medical history, laboratory tests, clinical characteristics, occlusion locations, treatment details, and treatment outcomes, were collected for further analysis.

Classification

The 973 patients from internal data were divided into favorable group (mRS $\leq$ 2 scores) and unfavorable group (mRS $>$ 2 scores) based on 90-day mRS. A total of 20 important variables before EVT were selected to construct predictive model. These variables include general parameters, medical history, stroke etiology, treatments and key time points, laboratory test, and occlusion sites.

Machine Learning Algorithms

We used a traditional statistical method and machine learning algorithms, namely, LR and LightGBM. LR is a classification model. It is widely applied in industrial issues and is simple to implement. However, it has limitations in accuracy because of overfitting and poor ability to handle too many variables. However, LightGBM can be trained quickly, costs low memory consumption, has high accuracy, and can support distributed and fast processing of massive data. More importantly, LightGBM was suitable for handling the structured data used in this study, which are of various types and some are missing. Other models need to perform null value processing, normalization, and other operations.

The LightGBM method involves the following steps: choice of a suitable dataset, selection of meaningful features, undersampling and splitting of dataset, training classification models, evaluation of classifiers'

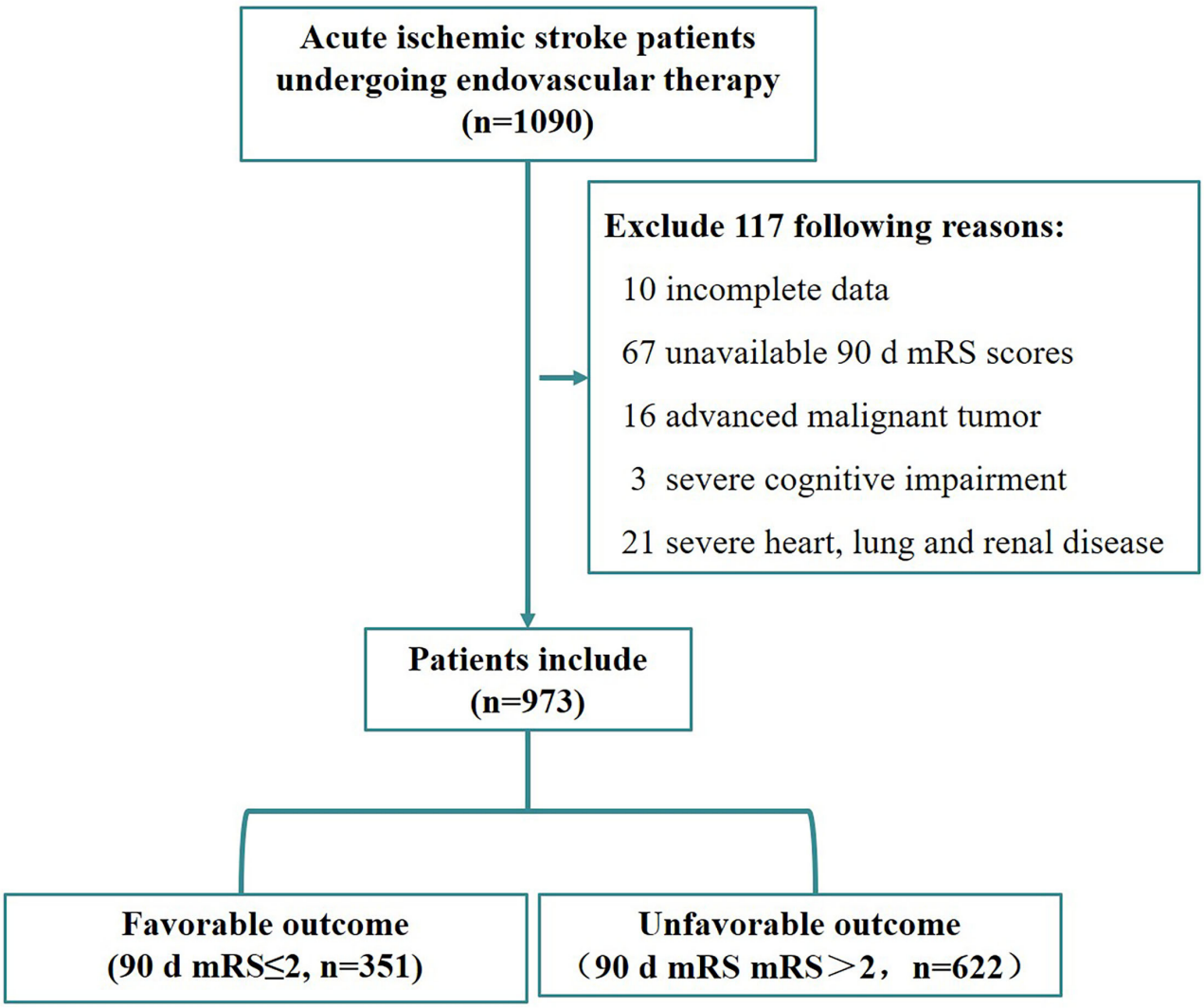

FIGURE 1 | Flowchart of patient selection.

performance, and ranking of the weights of the influence factors.

Machine learning algorithm LightGBM was trained on the dataset consisting of 973 patients. The undersampling method was used to get balanced subsets. Then, the dataset was randomly split into two subsets, namely, training subset (80%) and test subset (20%). The training subset was used for establishing the model and the test subset for evaluating the model generalization on new data. This process was repeated 100 times to obtain average values. In this model, 20 important variables were trained as inputs to classify patients into favorable and unfavorable outcome groups. For the LightGBM model, parameters were set as follows, namely, number of estimators as 65, max depth of the tree as 6, and learning rate as 0.14. We tuned each parameter of the machine learning model and finally selected the optimal parameters. What needs illustration is that 20 presurgical variables are brought into our study based on their importance of influencing prognosis, including admitting blood glucose, age, time from onset to EVT, time from onset to hospital, NIHSS score, intravenous thrombolysis, hospital, stroke etiology, gender, transient ischemic attack (TIA), hypertension, atrial fibrillation, drinking, diabetes mellitus, smoking, time from hospital to puncture, occlusion site, coronary heart disease, hyperlipidemia, and stroke.

Statistical Analysis

If baseline characteristics were in accordance with normal distribution, they were analyzed by one-way ANOVA. If not, the data were analyzed by Mann-Whitney *U*-test. LR with statistical analyses was performed with R (version 3.5.1, https://www.r-project.org/).

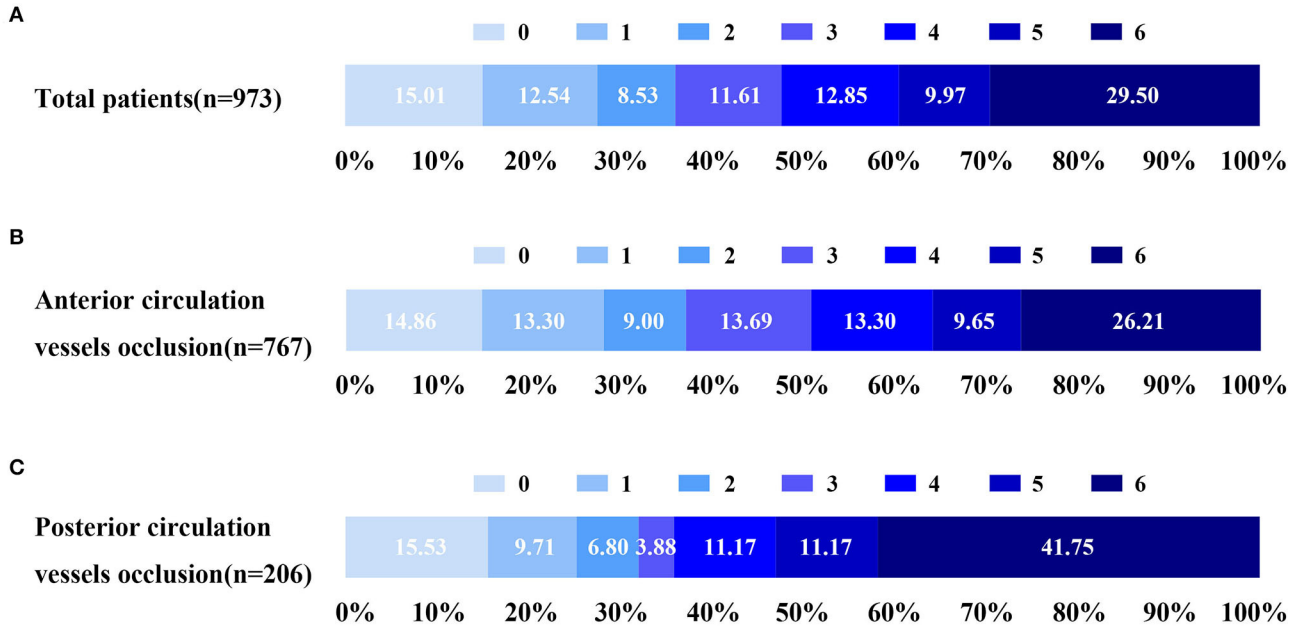

FIGURE 2 | Distribution of 90-day mRS score of EVT for AIS in 973 patients from January 2018 to December 2020. **(A)** Distribution of mRS at 90 days for EVT. **(B)** Distribution of 90-day mRS for EVT at anterior circulation. **(C)** Distribution of 90-day mRS for EVT at posterior circulation. EVT, endovascular treatment; AIS, acute ischemic stroke; mRS, modified Rankin scale.

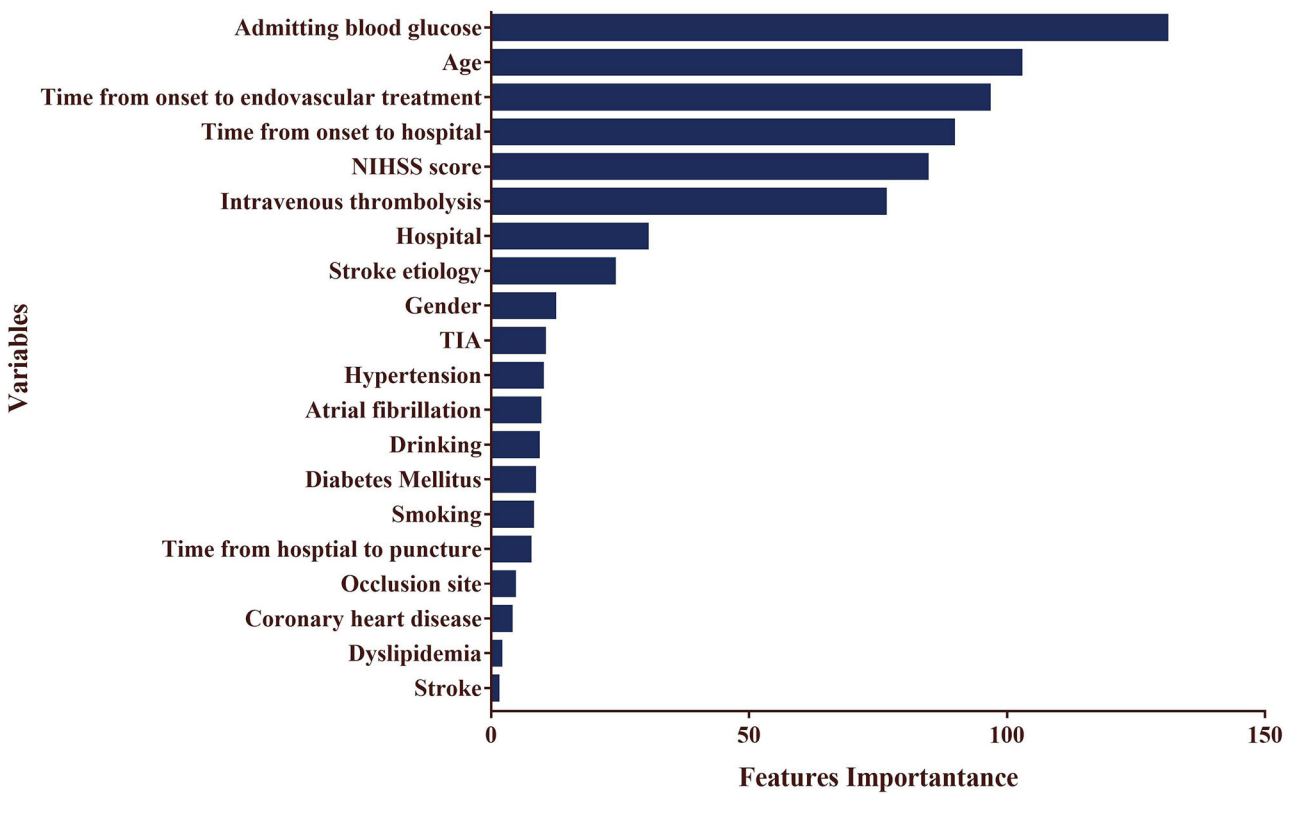

FIGURE 3 | The weighting of outcome after EVT for AIS based on LightGBM model.

TABLE 1 | Baseline characteristics of the patients in two groups.

Characteristics	Postoperative mRS (0–2)	Postoperative mRS (3–6)	*P* (Value)
Age, y, median (IQR)	**65 (57–73)**	**73 (65–80)**	**<0.001*** **
Male, *n* (%)	239 (68.1%)	346 (55.6%)	<0.001***
Female	112 (31.9%)	276 (44.4%)	
NIHSS score, median (IQR)	12 (8–16)	17 (12–25)	<0.001***
Medical history			
Hypertension, *n* (%)	222 (63.2%)	438 (70.4%)	0.021*
Diabetes, *n* (%)	59 (16.8%)	144 (23.2%)	0.019*
Dyslipidemia, *n* (%)	6 (1.7%)	13 (2.1%)	0.68
Atrial fibrillation, *n* (%)	94 (26.8%)	221 (35.5%)	0.005**
Ischemic stroke, *n* (%)	44 (12.5%)	128 (20.6%)	0.002**
TIA, *n* (%)	4 (1.1%)	8 (1.3%)	0.842
Smoking, *n* (%)	121 (34.5%)	147 (23.6%)	<0.001***
Drinking, *n* (%)	84 (23.9%)	89 (14.3%)	<0.001***
Coronary heart disease, *n* (%)	33 (9.4%)	92 (14.8%)	0.016*
Stroke etiology			
Large-artery atherosclerosis, *n* (%)	145 (41.3%)	231 (37.1%)	0.316
Cardioembolic, *n* (%)	155 (44.2%)	282 (45.3%)	
Tandem lesion, *n* (%)	51 (14.5%)	109 (17.5%)	
Treatments and key time points			
Intravenous thrombolysis, *n* (%)	106 (30.2%)	157 (25.2%)	0.094
Time from onset to hospital, min, median (IQR)	210 (120–360)	210 (120–315)	0.795
Time from onset to endovascular treatment, min, median (IQR)	310 (206–442)	300 (207–418)	0.487
Time from Door to Puncture, min, median (IQR)	80 (40–140)	85 (35–143)	0.894
Laboratory test			
Admitting blood glucose (mmol/L), median (IQR)	5.71 (4.97–6.755)	7.02 (5.702–8.908)	<0.001***
Occlusion site			
Anterior circulation	285 (81.2%)	482 (77.5%)	0.174
Posterior circulation	66 (18.8%)	140 (22.5%)	

*Favorable outcome group vs. unfavorable outcome group, *$p < 0.05$, **$p < 0.01$, ***$p < 0.001$. IQR, interquartile range; mRS, modified Rankin scale; NIHSS, national institutes of health stroke scale; TIA, transient ischemic attack.*

RESULTS

Baseline Characteristics

From January 2018 to December 2020, a total of 1,090 patients who underwent EVT for AIS were included in this study, and 117 patients were excluded due to certain reasons (**Figure 1**).

The baseline characteristics of favorable outcome group and unfavorable outcome group are summarized in **Table 1**, with the data presented as *n* (percent) or median [interquartile range (IQR)]. Patients in favorable outcome group were generally younger (65 vs. 73 years), consisted of more men (68.1 vs. 55.6%), had lower baseline NIHSS score (12 vs. 17), and had lower incidence of hypertension (63.2 vs. 70.4%), diabetes (16.8 vs. 23.2%), atrial fibrillation (26.8 vs. 35.5%), ischemic stroke (12.5 vs. 20.6%), and coronary heart disease (9.4 vs. 14.8%).

In addition, as shown in **Supplementary Table 1**, patients in favorable outcome group had higher successful revascularization rate (mTICI $\geq$ 2b, 93.2 vs. 82.8%), fewer mechanical thrombectomy times (2 [IQR, 1–2] vs. 2 [IQR, 1–3]), lower incidence of sICH (14.8 vs. 27.5%), shorter delay from door to reperfusion (151 vs. 180), shorter delay from puncture to reperfusion (60 vs. 85), etc. Compared to patients with unfavorable outcome, drinking and smoking rates were higher in favorable outcome group, which may be associated with a larger proportion of male patients. Furthermore, favorable outcome group showed lower levels of AST, admitting blood glucose, and creatinine.

Clinical Prognostic of EVT for AIS Including Anterior and Posterior Circulation Infarction

The primary outcome assessed by mRS is shown in **Figure 2** and **Supplementary Figure 1** for internal data and external data, respectively. Regarding internal data, favorable outcomes (mRS $\leq$ 2 scores) were achieved in 351/973 (36.07%) patients.

TABLE 2 | Logistic regression analysis of the factors affecting the outcome of EVT for AIS.

Variables	Beta	SE	*P*(Value)
Age, y	0.052	0.007	$6.05*10^{-14***}$
Admitting blood glucose	0.252	0.037	$1.45*10^{-11***}$
Baseline NIHSS Scores	0.097	0.011	$2.00*10^{-16***}$

Favorable outcome group vs. unfavorable outcome group, $^{***}p < 0.001$.

TABLE 3 | Prediction scores of EVT in AIS.

Component	Scoring criteria	Scores
Age, y	≤67	0
	>67	2
NIHSS scores	≤14	1
	>14	2
Admitting blood glucose, mmol/L	≤6.47	0
	>6.47	1
Onset to hospital time, min	≤178	0
	>178	1
Onset to EVT time, min	≤ 380	0
	>380	1

The scores were assigned based on the weighting and clinical research.

In terms of the types of strokes, 767 patients (78.82%) underwent anterior circulation infarction (ACI) and 206 patients (21.18%) underwent posterior circulation infarction (POCI). A comparison of clinical outcomes between ACI and POCI showed that the patients who underwent EVT with ACI presented better clinical outcomes than POCI (37.16% in ACI vs. 32.04% in POCI) (**Figure 2**). Furthermore, the mortality in ACI group (201/767, 26.21%) was significantly lower than that in POCI group (86/206, 41.75%).

In contrast, the external data shown in **Supplementary Figure 1** demonstrated that the percentage of favorable outcome was 72/169 (42.60%) and that of death was 38/169 (22.49%).

Important Predictors for Long-Term Outcome of EVT for AIS

To establish an accurate presurgical prediction model for EVT, we collected as many variables as possible to increase the dimensions so as to avoid overfitting. Altogether 20 closely related parameters before EVT were selected. After training and testing the datasets 100 times, the LightGBM algorithm assigned different weightings to variables based on their significance. The top 5 important parameters for predicting outcomes of EVT for AIS were admitting blood glucose levels, age, onset to EVT time, onset to hospital time, and NIHSS scores (importance = 130.9, 102.6, 96.5, 89.5, and 84.4, respectively) (**Figure 3**).

In contrast, LR analysis showed that the following variables were significantly associated with unfavorable outcomes, namely, advanced age (beta = 0.052, $p < 0.001$), high baseline NIHSS score (beta = 0.097, $p < 0.001$), and high levels of admitting blood glucose (beta = 0.252, $p < 0.001$) (**Table 2**).

Furthermore, we compared the two prediction models and found that LightGBM model performed better than LR model (0.738 vs. 0.701 in accuracy and 0.824 vs. 0.795 in area under the curve) (**Supplementary Table 2**; **Figure 4**). LightGBM method is thus suggested to be an accurate and feasible prediction model for unfavorable outcomes of EVT for AIS.

TABLE 4 | The prognostic impact of prediction scale in EVT for AIS validated by internal and external data.

Different data	Sensitivity [%]	Specificity [%]	AUC
Raw data	80.4	56.7	0.723
External data	83.5	41.7	0.685

Raw data, 973 patients from January 2018 to December 2020; external data, 169 patients from January to July in 2021.

Prediction Scale Might Be an Efficient Tool to Suggest Possible Outcomes of EVT for AIS

To further clarify the validity of important parameters found in LightGBM model in predicting outcomes, we first confirmed critical values and cutoff points using receiver operating characteristic (ROC) curve. The cutoff points of top 5 predictors for the prognosis were as follows: age was 67 years, NIHSS scores were 14, admitting blood glucose was 6.47 mmol/L, onset to EVT time was 380 min, and onset to hospital time was 178 min. In terms of age, we classified patients into two different groups and found that 51.5 and 25.6% patients achieved favorable outcome in ≤67 years age group and >67 years age group [odds ratio (OR), 3.08; 95% confidence interval (CI), 2.35–4.04], respectively (**Supplementary Table 3**). In contrast, we also divided patients into two different groups based on baseline NIHSS score. The results indicated that 52.7 and 21.4% patients gained independence in life in ≤14 scores group and >14 scores group (OR, 4.09; 95% CI, 3.10–5.41), respectively (**Supplementary Table 4**).

Therefore, we further established a prediction scale based on both the cutoff points of these predictors and their weighting values (**Table 3**). The components, scoring criteria, and assigned scores of the prediction scale were as follows: age > 67 years (= 2, if not = 0), NIHSS scores > 14 (= 2, if not = 1), admitting blood glucose > 6.47 mmol/L (= 1, if not = 0), onset to EVT time > 380 min (= 1, if not = 0), and onset to hospital time > 178 min (= 1, if not = 0). The scale was further validated using 973 internal patients' data, and we found that the sensitivity was 80.4% and area under the ROC curve was 0.72 (**Table 4**; **Supplementary Figure 2**). Additionally, we used another 169 external patients' data collected in 2021 to verify the prediction scale, and the resulting sensitivity was 83.5% (**Table 4**). Consequently, a score of 3 was identified as the cutoff

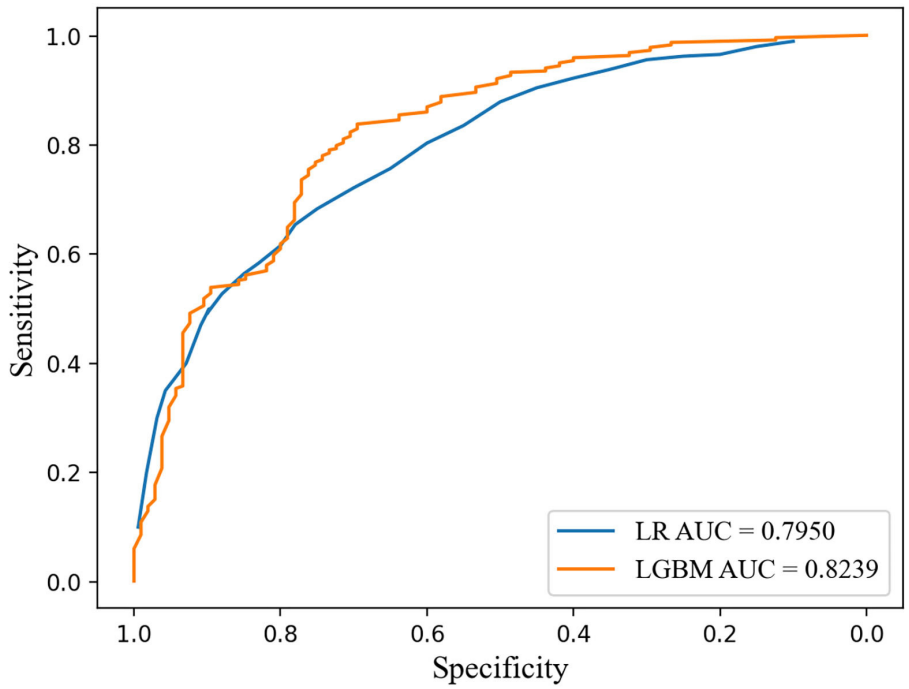

FIGURE 4 | ROC curves of LightGBM model and logistic regression model for predicting unfavorable outcome after EVT for AIS. LightGBM, light gradient boosting machine; ROC, receiver operating characteristic.

point, and we found that prediction scale >3 presented higher accuracy when forecasting unfavorable outcomes at 76.7% (**Supplementary Table 5**). These results suggested that the prediction scale of EVT for AIS will help estimate the proportion of unfavorable prognosis.

DISCUSSION

In this study, we used machine learning LightGBM model to analyze 20 important presurgical variables and constructed a prognostic model of EVT for LVO in real world for the first time and identified several key predictors based on the weightings of multidimensional features, including age, NIHSS scores, admitting blood glucose, onset to hospital time, and onset to EVT time. On this basis, we further established a prediction scale to assess the proportion of patients with unfavorable outcomes and confirmed that score of 3 was the key cutoff point that can distinguish unfavorable outcomes from favorable outcomes.

In recent years, several studies have revealed that brain edema, high mean blood pressure, greater blood pressure variability, and high NIHSS scores were associated with adverse outcome of successful embolectomy of AIS (Chen et al., 2019; Heo et al., 2019; Quinn and Drozdowska, 2019; Butler et al., 2020). In addition, Brugnara et al. (2020) utilized machine learning method to analyze pre- and postinterventional characteristics and found that premorbid mRS and final infarction volume were important predictors for 90-day mRS. However, their study has limitations as they were single-centered and their sample size was small, thus possibly resulting in the overfitting of machine learning algorithms.

In contrast, application of machine learning in disease prediction is widely accepted due to its advantages in processing massive and multidimensional data (Deng et al., 2018; Kamel et al., 2020; Castaneda-Vega et al., 2021). However, although many prediction models have been developed, few have been applied and proved efficient in clinical practice, especially in guiding clinical decision-making (Quinn and Drozdowska, 2019; Kaesmacher et al., 2020; Crowe et al., 2021; Zhu et al., 2021). By contrast, in this study, we incorporated large samples from four clinical centers, and the data were analyzed from many dimensions, including clinical variables, process variables, and biomarkers, to establish a prediction model that predicts long-term outcomes of EVT for AIS. Nevertheless, machine learning has limitations at the interpretation of the results. To avoid "black box" phenomenon of machine learning, we further applied traditional statistical method to analyze the data with the same variables.

In recent years, it is well recognized that age, stroke severity (NIHSS score or infarction volume), and treatment method (intravenous thrombolysis or arterial mechanical thrombectomy) are vital prognostic markers (Drozdowska et al., 2019; Quinn and Drozdowska, 2019; Crowe et al., 2021). In this study, we provided supporting evidence for a conclusion drawn from previous studies that patients

younger than 67 years old and/or NIHSS score below 14 are more likely to achieve positive clinical outcome. These results can facilitate neurologists and patients to make treatment decisions.

In addition, as is consistent with our results, the delay from hospital arrival to puncture or from onset to reperfusion would worsen the outcome of mechanical thrombectomy for acute stroke (Bourcier et al., 2019; Kaesmacher et al., 2020; Snyder et al., 2020; Zhu et al., 2021). In this study, the model demonstrated the top 5 important variables, two of which are related to time, namely, time from onset to hospital, and time from onset to EVT. These results provide important supporting arguments for reducing the intervals of several time points and improving stroke quality control indicators in stroke centers in the future.

Moreover, the results of several randomized controlled studies were controversial on the effect of EVT with or without intravenous alteplase (De Marchis et al., 2019; Suzuki et al., 2021). The results of one-way ANOVA suggested that EVT plus intravenous alteplase was better at restoring functional independence of patients, but the difference was not statistically significant. However, the weighting of intravenous thrombolysis in the prognostic model should be prioritized, even though it needs further clinical trials for validation.

In this study, we applied classification model LightGBM method to predict the prognosis after EVT for AIS. In contrast to traditional LR, LightGBM model showed improved accuracy of prediction. What is worth noting is that established prediction scale based on major predictors might give us an opportunity to help patients and doctors make clinical decisions on the basis of this model.

Strengths and Limitations

Our study has several limitations. First, the data collected from four hospitals were retrospective, which means that data were sometimes incomplete. The sample sizes can still be increased, especially the data in 2021. Secondly, the selected four hospitals were limited to Jiangsu Province and can be expanded to the eastern part of China. Thirdly, the prediction scale focused only on the presurgical variables, which means that the features during or after EVT were overlooked and therefore the specificity of the scoring system was limited. Finally, the lack of external data also limits the accuracy of data validation.

Nevertheless, there are several strengths in this study. The data obtained from four national stroke centers provided huge sample sizes and multiple dimensions. Combining machine learning with traditional statistical methods, we developed better prediction model that can avoid the typical shortcoming of machine learning model: "black box." Furthermore, we established a predictive evaluation system – a prediction scale, validated its accuracy in internal and external data, and identified the cutoff points that can distinguish the higher and lower percentages of positive prognosis.

CONCLUSION

This study demonstrated that the prediction model of EVT for AIS with machine learning algorithm LightGBM model was in general accurate and could be applied to clinical decision-making for LVO. Likewise, the prediction scale established based on the abovementioned model might be an accurate and feasible tool. Two risk factors were identified for unfavorable outcomes of EVT for AIS, namely, age $>$ 67 years and NIHSS score $>$ 14. Better outcomes of EVT could be achieved by minimizing the time intervals of stroke quality control key points and improving the techniques and devices of acute EVT.

DATA AVAILABILITY STATEMENT

The raw data supporting the conclusions of this article will be made available by the authors, without undue reservation.

ETHICS STATEMENT

The studies involving human participants were reviewed and approved by Medical Ethics Committee of Nanjing Drum Tower Hospital. Written informed consent for participation was not required for this study in accordance with the national legislation and the institutional requirements.

AUTHOR CONTRIBUTIONS

QZ and YX designed the study. QZ and LZ wrote the first draft. JL, JZ, WY, and XL performed the EVT operations and quality control for the study. WZ, YC, HN, and QZ performed the statistical analysis. QG, WL, ZX, and ML collected the data. All authors contributed to the further drafts, read, and approved the final manuscript.

FUNDING

This work was supported by the Key Research and Development Program of Jiangsu Province of China (BE2020620 to Dr. YX) and the National Natural Science Foundation of China (Nos. 82071304 and 81671149 to QZ).

ACKNOWLEDGMENTS

We acknowledge all participating centers and investigators for helping data collection. The following centers are involved: Nanjing First Hospital, Nanjing Medical University, Changzhou No. 2 People's Hospital, Subei People's Hospital of Jiangsu Province and The Institute of Software, Chinese Academy of Sciences.

SUPPLEMENTARY MATERIAL

The Supplementary Material for this article can be found online at: https://www.frontiersin.org/articles/10.3389/fnagi.2022.942285/full#supplementary-material

REFERENCES

Bourcier, R., Goyal, M., Liebeskind, D. S., Muir, K. W., Desal, H., Siddiqui, A. H., et al. (2019). Association of time from stroke onset to groin puncture with quality of reperfusion after mechanical thrombectomy: a meta-analysis of individual patient data from 7 randomized clinical trials. *JAMA Neurol.* 76, 405–411. doi: 10.1001/jamaneurol.2018.4510

Brugnara, G., Neuberger, U., Mahmutoglu, M. A., Foltyn, M., Herweh, C., Nagel, S., et al. (2020). Multimodal predictive modeling of endovascular treatment outcome for acute ischemic stroke using machine-learning. *Stroke* 51, 3541–3551. doi: 10.1161/strokeaha.120.030287

Butler, J., Heidari, P., Blayney, S., Hitomi, E., Luby, M., and Leigh, R. (2020). Blood-brain barrier integrity of stroke patients presenting in an extended time window. *BMC Neurol.* 20, 54. doi: 10.1186/s12883-020-01634-2

Castaneda-Vega, S., Katiyar, P., Russo, F., Patzwaldt, K., Schnabel, L., Mathes, S., et al. (2021). Machine learning identifies stroke features between species. *Theranostics* 11, 3017–3034. doi: 10.7150/thno.51887

Chen, X., Huang, Q., Deng, Q., Shen, R., Liu, Y., Lu, M., et al. (2019). A prediction model of brain edema after endovascular treatment in patients with acute ischemic stroke. *J. Neurol. Sci.* 407, 116507. doi: 10.1016/j.jns.2019.116507

Crowe, R. P., Myers, J. B., Fernandez, A. R., Bourn, S., and McMullan, J. T. (2021). The cincinnati prehospital stroke scale compared to stroke severity tools for large vessel occlusion stroke prediction. *Prehosp. Emerg. Care* 25, 67–75. doi: 10.1080/10903127.2020.1725198

De Marchis, G. M., Dankowski, T., König, I. R., Fladt, J., Fluri, F., Gensicke, H., et al. (2019). A novel biomarker-based prognostic score in acute ischemic stroke: the CoRisk score. *Neurology* 92, e1517–e1525. doi: 10.1212/wnl.0000000000007177

Deng, L., Pan, J., Xu, X., Yang, W., Liu, C., and Liu, H. (2018). PDRLGB: precise DNA-binding residue prediction using a light gradient boosting machine. *BMC Bioinform.* 19, 522. doi: 10.1186/s12859-018-2527-1

Dreiseitl, S., and Ohno-Machado, L. (2002). Logistic regression and artificial neural network classification models: a methodology review. *J. Biomed. Inform.* 35, 352–359. doi: 10.1016/s1532-0464(03)00034-0

Drozdowska, B. A., Singh, S., and Quinn, T. J. (2019). Thinking about the future: a review of prognostic scales used in acute stroke. *Front. Neurol.* 10, 274. doi: 10.3389/fneur.2019.00274

Goyal, M., Menon, B. K., van Zwam, W. H., Dippel, D. W., Mitchell, P. J., Demchuk, A. M., et al. (2016). Endovascular thrombectomy after large-vessel ischaemic stroke: a meta-analysis of individual patient data from five randomised trials. *Lancet* 387, 1723–1731. doi: 10.1016/s0140-6736(16)00163-x

Han, B., Sun, X., Liu, R., Tong, X., Jia, B., Mo, D., et al. (2021). Impact of the perioperative blood pressure on clinical outcome after thrombectomy in acute basilar artery occlusion. *J. Stroke Cerebrovasc. Dis.* 30, 105590. doi: 10.1016/j.jstrokecerebrovasdis.2020.105590

He, B., Dai, C., Lang, J., Bing, P., Tian, G., Wang, B., et al. (2020). A machine learning framework to trace tumor tissue-of-origin of 13 types of cancer based on DNA somatic mutation. *Biochim. Biophys. Acta. Mol. Basis Dis.* 1866, 165916. doi: 10.1016/j.bbadis.2020.165916

Heo, J., Yoon, J. G., Park, H., Kim, Y. D., Nam, H. S., and Heo, J. H. (2019). Machine learning-based model for prediction of outcomes in acute stroke. *Stroke* 50, 1263–1265. doi: 10.1161/strokeaha.118.024293

Jia, B., Ren, Z., Mokin, M., Burgin, W. S., Bauer, C. T., Fiehler, J., et al. (2021). Current status of endovascular treatment for acute large vessel occlusion in china: a real-world nationwide registry. *Stroke* 52, 1203–1212. doi: 10.1161/strokeaha.120.031869

Kaesmacher, J., Maamari, B., Meinel, T. R., Piechowiak, E. I., Mosimann, P. J., Mordasini, P., et al. (2020). Effect of pre- and in-hospital delay on reperfusion in acute ischemic stroke mechanical thrombectomy. *Stroke*. 51, 2934–2942. doi: 10.1161/STROKEAHA.120.030208

Kamel, H., Navi, B. B., Parikh, N. S., Merkler, A. E., Okin, P. M., Devereux, R. B., et al. (2020). Machine learning prediction of stroke mechanism in embolic strokes of undetermined source. *Stroke* 51, e203–e210. doi: 10.1161/strokeaha.120.029305

Liao, H., Zhang, X., Zhao, C., Chen, Y., Zeng, X., and Li, H. (2022). LightGBM: an efficient and accurate method for predicting pregnancy diseases. *J. Obstet. Gynaecol.* 42, 620–629. doi: 10.1080/01443615.2021.1945006

Lin, Y., Schulze, V., Brockmeyer, M., Parco, C., Karathanos, A., Heinen, Y., et al. (2019). Endovascular thrombectomy as a means to improve survival in acute ischemic stroke: a meta-analysis. *JAMA Neurol* 76, 850–854. doi: 10.1001/jamaneurol.2019.0525

Liu, D., Nie, X., Pan, Y., Yan, H., Pu, Y., Wei, Y., et al. (2021). Adverse outcomes associated with higher mean blood pressure and greater blood pressure variability immediately after successful embolectomy in those with acute ischemic stroke, and the influence of pretreatment collateral circulation status. *J. Am. Heart Assoc.* 10, e019350. doi: 10.1161/jaha.120.019350

Quinn, T. J., and Drozdowska, B. A. (2019). Stroke prediction and the future of prognosis research. *Nat. Rev. Neurol.* 15, 311–312. doi: 10.1038/s41582-019-0181-5

Shaker, B., Yu, M. S., Song, J. S., Ahn, S., Ryu, J. Y., Oh, K. S., et al. (2021). LightBBB: computational prediction model of blood-brain-barrier penetration based on LightGBM. *Bioinformatics* 37, 1135–1139. doi: 10.1093/bioinformatics/btaa918

Snyder, T., Agarwal, S., Huang, J., Ishida, K., Flusty, B., Frontera, J., et al. (2020). Stroke treatment delay limits outcome after mechanical thrombectomy: stratification by arrival time and ASPECTS. *J. Neuroimag.* 30, 625–630. doi: 10.1111/jon.12729

Song, J., Liu, G., Jiang, J., Zhang, P., and Liang, Y. (2021). Prediction of protein-atp binding residues based on ensemble of deep convolutional neural networks and lightgbm algorithm. *Int. J. Mol. Sci.* 22, 2. doi: 10.3390/ijms22020939

Suzuki, K., Matsumaru, Y., Takeuchi, M., Morimoto, M., Kanazawa, R., Takayama, Y., et al. (2021). Effect of mechanical thrombectomy without vs with intravenous thrombolysis on functional outcome among patients with acute ischemic stroke: the skip randomized clinical trial. *Jama* 325, 244–253. doi: 10.1001/jama.2020.23522

Zhan, Z. H., You, Z. H., Li, L. P., Zhou, Y., and Yi, H. C. (2018). Accurate prediction of ncRNA-protein interactions from the integration of sequence and evolutionary information. *Front Genet* 9, 458. doi: 10.3389/fgene.2018.00458

Zhu, F., Gauberti, M., Marnat, G., Bourcier, R., Kyheng, M., Labreuche, J., et al. (2021). Time from I.V. thrombolysis to thrombectomy and outcome in acute ischemic stroke. *Ann. Neurol.* 89, 511–519. doi: 10.1002/ana.25978

Conflict of Interest: The authors declare that the research was conducted in the absence of any commercial or financial relationships that could be construed as a potential conflict of interest.

frontiers | Frontiers in Aging Neuroscience

REVIEW
published: 04 July 2022
doi: 10.3389/fnagi.2022.917629

Protective Effects of Polysaccharides in Neurodegenerative Diseases

Yinying Wang[1], Rongsha Chen[1], Zhongshan Yang[2], Qian Wen[3], Xia Cao[1], Ninghui Zhao[3] and Jinyuan Yan[1]**

[1] The Central Laboratory of the Second Affiliated Hospital, Kunming Medical University, Kunming, China, [2] Yunnan Provincial Key Laboratory of Molecular Biology for Sino Medicine, Yunnan University of Chinese Medicine, Kunming, China, [3] The Neurosurgery Department of the Second Affiliated Hospital, Kunming Medical University, Kunming, China

Neurodegenerative diseases (NDs) are characterized by progressive degeneration and necrosis of neurons, including Alzheimer's disease (AD), Parkinson's disease (PD), Huntington's disease and others. There are no existing therapies that correct the progression of these diseases, and current therapies provide merely symptomatic relief. The use of polysaccharides has received significant attention due to extensive biological activities and application prospects. Previous studies suggest that the polysaccharides as a candidate participate in neuronal protection and protect against NDs. In this review, we demonstrate that various polysaccharides mediate NDs, and share several common mechanisms characterized by autophagy, apoptosis, neuroinflammation, oxidative stress, mitochondrial dysfunction in PD and AD. Furthermore, this review reveals potential role of polysaccharides *in vitro* and *in vivo* models of NDs, and highlights the contributions of polysaccharides and prospects of their mechanism studies for the treatment of NDs. Finally, we suggest some remaining questions for the field and areas for new development.

Keywords: mechanism, polysaccharides, Alzheimer's disease, Parkinson's disease, Huntington's disease

OPEN ACCESS

Edited by:
Jialiang Yang,
Geneis (Beijing) Co. Ltd, China

Reviewed by:
Shanting Zhao,
Northwest A&F University, China
Ranju Bansal,
Panjab University, India

****Correspondence:***
Ninghui Zhao
zhaoninghui@hotmail.com
Jinyuan Yan
yanjinyuan1011@126.com

Specialty section:
This article was submitted to Parkinson's Disease and Aging-related Movement Disorders, a section of the journal Frontiers in Aging Neuroscience

Received: *11 April 2022*
Accepted: *02 June 2022*
Published: *04 July 2022*

Citation:
Wang Y, Chen R, Yang Z, Wen Q, Cao X, Zhao N and Yan J (2022) Protective Effects of Polysaccharides in Neurodegenerative Diseases. Front. Aging Neurosci. 14:917629. doi: 10.3389/fnagi.2022.917629

INTRODUCTION

Neurodegenerative diseases (NDs) are a series of the central nervous system (CNS) disorders that cause a slowly progressive loss of function of specific neuron populations and their connections including sporadic and hereditary forms (Reith, 2018). Most evidences suggest that approximately 25% of Alzheimer's disease (AD) is familial and 75% is non-familial (Bird, 2018). Approximately 5–10% of Parkinson's disease (PD) is inherited in an autosomal dominant, autosomal recessive, or even X-linked pattern of inheritance (Lesage and Brice, 2009). Moreover, the incidence of genetically confirmed Huntington's disease (HD) in symptomatic individuals with no known family history of HD may be as high as 8% of all individuals with HD (Margolis and Ross, 2003). A number of NDs have an underlying genetic cause, with a 50% recurrence risk when inheritance is autosomal dominant (Roberts et al., 2020). The major pathological hallmarks of NDs are the accumulation and aggregation of proteins in specific neurons aggregation in the CNS. The prevalence of NDs is expected to rise with the increasing life expectancy. The complex and diverse pathological features, unclear molecular mechanisms, limited clinical examination options,

difficulties in early diagnosis, and lack of specificity in treatment have introduced substantial social and economic burdens (Chen-Plotkin, 2014; Kwon et al., 2016; Marsh, 2019; Muddapu et al., 2020). There are various theories on the pathogenesis of AD, the dominant theories include the amyloid beta (Aβ) toxicity hypothesis, the microtubule-associated protein – tau protein functional abnormality hypothesis (Morris et al., 2014), the vascular gene hypothesis (De La Torre, 2010), and the gene mutation hypothesis. AD patients are characterized by accumulation of Aβ into senile plaques and hyperphosphorylated tau into neurofibrillary tangles (Spires-Jones and Hyman, 2014). AD impairs memory and cognitive judgment and is often accompanied by mood swings, disorientation and eventually delirium (Cass, 2017). Despite increases in medication dosage, the efficacy of pharmacological treatments still reduces with disease progresses. The current drugs for AD treatment include neurotransmitter agents such as cholinergic inhibitors (including tacrine, donepezil, rivastigmine, and galantamine; Sharma, 2019), drugs directed at β1 amyloid (E2069, MK-8931; Blume et al., 2018), antioxidant drugs (including monoamine oxidase inhibitors and melatonin; Cardinali et al., 2014; Ostadkarampour and Putnins, 2021), and calcium channel blockers (including nilvadipine, nimodipine, and flunarizine; Nimmrich and Eckert, 2013). Moreover, PD is a severe neurodegenerative disorder that affects around 2–3% of the population over 65 years old (Poewe et al., 2017). PD is characterized by the loss of dopaminergic (DA) neurons in the pars compacta of the substantia nigra and by accumulation of misfolded α-synuclein (α-syn; Balestrino and Schapira, 2020); its cardinal motor symptoms are bradykinesia, rigidity, postural instability, and tremor (Dickson, 2018). Despite significant progress made over the past several decades, PD is still an incurable disorder. The currently available therapeutic approaches focus on stimulation of DA signaling, such as levodopa (L-DOPA), DOPA decarboxylase inhibitors (Bandopadhyay et al., 2022), catechol-O-methyltransferase inhibitors (Salamon et al., 2022), dopamine agonists (Jenner, 2002), and inhibitors of the enzyme monoamine oxidase type B (Nagatsu and Sawada, 2006). Of these, L-DOPA remains the single most effective therapeutic agent for PD patients (Ngwuluka et al., 2010). HD is characterized by a general shrinkage of the brain and degeneration of the striatum (caudate nucleus and putamen) due to the mutation of *Huntingtin* (*HTT*) gene (Jimenez-Sanchez et al., 2017); The symptoms of HD encompasses psychiatric conditions, cognitive defects, motor impairment (e.g., chorea; Huang et al., 2016). Tetrabenazine and Deutetrabenazine, both approved by the Food and Drug Administration (FDA; Potkin and Potkin, 2018), are inhibitors of the vesicular monoamine transporter type 2, and functions through depletion of dopamine in the presynaptic terminals to improve chorea (Dean and Sung, 2018; Kumar et al., 2020), The different drug therapies available for the treatment of NDs are shown in (**Table 1**).

The currently available treatments for NDs are primarily focused on symptom management and no cure is yet available for this devastating disorder, the search for new and effective NDs therapies remains a priority. Herein, this review provides a summary on the pathogenesis and treatment of NDs, and summarizes the application and limitations of different forms of polysaccharides in the most common NDs.

POLYSACCHARIDES

Polysaccharides are naturally and synthetically active macromolecular substances formed by more than ten monosaccharides connected by glycosidic bonds. Natural polysaccharides are widely present in plants, animals, algae, and microorganisms. The polysaccharides are regarded as potential useful agent for the prevention of neuronal damage, and have received considerable attention for wide-ranging bioactivity (Dhahri et al., 2022). Polysaccharides have other beneficial properties including biodegradability, high stability and low toxicity, solubility in water, higher degrees of swelling capability, etc. (Mozammil Hasnain et al., 2019). Moreover, polysaccharide nanoparticles improve the bioavailability and bioactivity of functional ingredients, such as *Ganoderma lucidum*, *Momordica charantia* polysaccharides (Qin et al., 2018) and chitosan (Xue et al., 2020). The polysaccharides mainly include cellulose, chitin and other polysaccharides, and are classified into two major types: indigestible and digestible. The digestible polysaccharides are hydrolyzed to sugar subunits in the stomach, absorbed by the small intestine. Among indigestible polysaccharides, non-fermentable polysaccharides are unable to hydrolyze in the stomach and the small intestine, go through the large intestine, and are finally excreted out in the forms of waste or feces. Only the fermentable and indigestible polysaccharides are metabolized to produce various metabolites by the host intestinal microbiota, such as short chain fatty acids (SCFAs); then these metabolites modulate the host metabolism and pathophysiology process (Ahmadi et al., 2017). The polysaccharides have been widely concerned due to their immunomodulatory function. The polysaccharides bind to polysaccharides receptors, including Toll-like receptor family (TLR), C-type lectin receptor family, complement receptors (CR3), scavenger receptor (SR), mannose receptor family (MR) and so on; these receptors are bound to activate intracellular signaling pathways that generate immune response, such as effects on macrophages, T-lymphocytes, B-lymphocytes, dendritic cells, red blood cells and natural killer cells, affect complement system, and regulate cytokines secretion (Jiang et al., 2010; Zhao et al., 2020).

Recently, polysaccharides have become more prominent as energy sources and supporting tissue structures. The polysaccharides possess many several physiological functions and biological activities, including immune regulation (Lin et al., 2021), anti-tumor (Sha et al., 2022), anti-radiation protection (Li X. et al., 2021), anti-diabetic (Wang P.-C. et al., 2016), anti-virus (Zhang et al., 2022), anti-bacteria (Wang et al., 2021), anti-fatigue functions (Shen et al., 2021), anti-aging (Zhu et al., 2020), and regulation of ubiquitination (Yan et al., 2022), iron metabolism (Ren et al., 2021), intestinal flora (Cai et al., 2021), estrogen (Hwang et al., 2020), and autophagy (Wu et al., 2021b) and so on. Polysaccharides also reduce Aβ deposition (Li G. et al., 2021), inhibit neurotoxicity (Huang et al., 2021), reduce oxidative stress (Liu et al., 2020), exert anti-inflammatory

TABLE 1 | The different drug therapies available for the treatment of NDs.

NDs	Medicine	Treatment mechanisms and disadvantages	References
AD	Cholinergic inhibitors (tacrine, donepezil, rivastigmine, and galantamine)	Increase the cholinergic levels in the brain by inhibiting the biological activity of AChE, and may cause adverse side effects (liver damage, nausea, vomiting, diarrhea, neuromuscular transmission and respiratory paralysis)	Sharma, 2019
	β1 amyloid (E2069, MK-8931)	Lower cerebral Aβ concentrations, may cause adverse side effects (hypomyelination, seizures, axon guidance defects, memory deficits, neurogenesis abnormalities)	Blume et al., 2018
	Antioxidant drugs (Monoamine oxidase inhibitors and melatonin)	Anti-inflammatory effects, cause adverse side effects (hepatotoxicity and hypertensive crisis, neuromuscular, autonomic, and mental status symptoms), and melatonin exerts its inhibitory effect on the generation of Aβ remains undefined	Cardinali et al., 2014; Ostadkarampour and Putnins, 2021
	Calcium channel blockers (nilvadipine, nimodipine, and flunarizine)	Decrease calcium influx through the plasma membrane and impairment of synapse physiology, protect AD cells from Aβ oligomer production	Nimmrich and Eckert, 2013
PD	Levodopa (L-DOPA), DOPA decarboxylase inhibitors	L-DOPA treatment is highly efficient, and is converted to DA and stored in the vesicles of presynaptic DA neurons, prolong use gives rise to motor abnormalities, including dyskinesia	Bandopadhyay et al., 2022
	Catechol-O-methyltransferase inhibitors	Inhibit of catechol-O-methyl transferase enzyme, and results in a higher levodopa concentration in the blood without peripheral degradation to 3-O-methyldopa, increase the bioavailability of L-DOPA, and may cause adverse side effects (liver toxicity, nausea, drowsiness, insomnia, dizziness, hallucination)	Salamon et al., 2022
	Dopamine agonists	Act on either D1-like or D2-like dopamine receptors, and the multiple receptor subtypes present in the brain, produce dyskinesia identical to that of L-dopa	Jenner, 2002
	Inhibitors of the enzyme monoamine oxidase type B	Degrade the neurotransmitter DA that is deficient in the nigro-striatal region in PD, and forms H_2O_2 and toxic aldehyde metabolites of DA, inhibit of DA degradation	Nagatsu and Sawada, 2006
HD	Inhibitors of the vesicular monoamine transporter type 2 (Tetrabenazine and Deutetrabenazine)	Inhibit vesicular monoamine transporter (VMAT) type 2 and consequently decrease available dopamine in the synapse and interaction with postsynaptic dopamine receptors	Potkin and Potkin, 2018

actions (Wen et al., 2022), and inhibit neuronal apoptosis (Guo et al., 2016). These functions and mechanisms of polysaccharides suggest that it is possible for prevention and treatment targets in NDs. In addition, polysaccharides also have some negative effects, such as, lipopolysaccharide (LPS) and zymosan. Zymosan represents an acute inflammation model widely used for the quantification of neutrophils and inflammation-related soluble factors (Cash et al., 2009). LPS is an endotoxin in the outer membrane of most gram-negative bacteria, and is a direct glial-mediated inflammatory stimulus (Kim et al., 2019). LPS is used to model neuroinflammation associated with NDs *via* targeting TLR4 that is primarily expressed on microglial in CNS to produce proinflammatory cytokines (Page et al., 2022). LPS also stimulates glial cells, leads to neuroinflammation for modeling inflammation-mediated DA neurodegeneration in PD animals (Dutta et al., 2008). Nevertheless, low-dose LPS treatment can awake the peripheral immune system, finally delay the further progression of HD (Lee et al., 2018).

In dextran sodium sulfate-induced ulcerative colitis mice, *Ficus carica* polysaccharide changed the abundance of gut microbiota, suppressed the infiltration of inflammatory cell and cytokine formation to prevent the disease development (Zou et al., 2020). Another study demonstrated that *Lycium barbarum* polysaccharide reduced myocardial damage by regulating the intestinal microbiome and fecal metabolome (Zhang et al., 2020b). *Bacteroides fragilis* is an important member of the human gut microbiome, which regulated specific *capsular* polysaccharides to attract IgA binding and deploy specific capsules for immune attraction, potentially enabling stable mucosal colonization and clear pathogens (Donaldson et al., 2018). In nervous system, these receptors, including TLR2, TLR3, TLR4, MR, and SR, are also widely expressed and participate in CNS injury and NDs (Burudi and Régnier-Vigouroux, 2001; Husemann and Silverstein, 2001; Marsh and Stenzel-Poore, 2008; Perez-Pardo et al., 2019; Zhou et al., 2019). If the polysaccharides cross the blood-brain barrier (BBB), they as extrinsic ligands bind to the above receptors to mediate the intracellular signaling in NDs. Due to the poor BBB permeability of most polysaccharides, they may regulate intestinal flora and related metabolic products to exert neuroprotective effects.

In a mouse PD model, *Astragalus* polysaccharides decreased the bax/bcl2 ratio, reversed mitochondrial structural damage and attenuated motor dysfunction (Liu H. et al., 2018). *G. lucidum* polysaccharides regulated expression of apoptosis-associated proteins, inhibited oxidative stress-induced neuronal apoptosis, and had significant neuroprotective effects in cerebellar granule cells (Sun et al., 2017). Wang et al. reported that sulfated hetero-polysaccharides extracted from *Saccharina japonica* may had a "therapeutic anti-apoptosis" utility for PD by enhancing the phosphorylation of PI3K/Akt signaling pathway and impairing caspase-3 levels in H_2O_2-induced SH-SY5Y cells (Wang et al., 2017). *Angelica* polysaccharide significantly alleviated LPS-induced PC-12 cell viability inhibition, apoptosis and expression of inflammatory cytokines, inactivated NF-κB pathway by down-regulating miR-223 (Li R. et al., 2018). *Astragalus* polysaccharide activated the PI3K/AKT/mTOR to increase autophagy, finally elevated cell viability in PD cell model (Tan et al., 2020). Currently, it has reported that the common

mechanisms of polysaccharides against PD and AD involve in neuroinflammation, oxidative stress, autophagy, apoptosis, mitochondrial dysfunction. And, the mechanisms of HD primarily involved in oxidative stress and neurotoxicity. **Figure 1** shows the neuroprotective mechanisms of polysaccharides involved in NDs.

THE ROLE OF POLYSACCHARIDES IN NEURODEGENERATIVE DISEASES

Parkinson's Disease

Parkinson's disease is the second most frequent neurodegenerative disorder of aging, affecting 7–10 million people worldwide, is diagnosed clinically based on typical motor symptoms, including bradykinesia, rigidity, abnormal posture, and resting tremor. Exposure to pesticides or herbicides, carbon monoxide, organic solvents, carbon disulfide, well water, rural environment, plant-derived toxins, and infection are all considered as causes of PD. The pathological feature of PD is the loss of DA neurons, and abnormal accumulation of α-syn. α-syn is a small (140 aa) protein generally enriched in the presynaptic compartment that regulate vesicle dynamics and trafficking, and neurotransmitter release (Emamzadeh, 2016).

Although the etiology of PD remains unclear, the death of DA neurons during PD progress is revealed to be associated with the abnormal aggregation of α-syn (Luk et al., 2012), mitochondrial dysfunction (Mandemakers et al., 2007), overactivated oxidative stress (Ren and Butterfield, 2021), apoptosis (Liu J. et al., 2018), or autophagy (Hou X. et al., 2020), microglia response caused by neuroinflammation (Tiwari and Pal, 2017), microbiota-gut-brain axis (Menozzi et al., 2021), autosomal dominant and recessive sexual heredity-related genetic changes (Filatova et al., 2014), and other factors are closely related. PD is a significant disease that affects human health and life, and brings substantial social and economic burdens to families and society. Since no viable treatment is available for PD to cease or reverse the disease progression, there is an urgent need for novel therapeutic approaches.

Oxidative stress is caused by increasing reactive oxygen species (ROS) product and weakening antioxidant capacity, damaging lipids, proteins, and DNA. ROS in the physiological state are important redox messengers that regulate various signaling pathways and play a crucial role in regulating cellular metabolism, post-transcriptional modification of proteins, and antioxidant defense mechanisms. However, excessive ROS damage lipids, proteins and DNA, and inhibit normal cell function. Oxidative stress is a state of stress damage caused by the imbalance of oxidation and anti-oxidation in the cell (Dröge, 2002). For example, in 1-methyl-4-phenyl-1,2,3,6-tetrahydropyridine (MPTP)-induced mouse PD models, *M. charantia* polysaccharides inhibited oxidative stress products in the brain, thereby increased DA levels, alleviated the impairment of coordination and motor ability by regulating the TLR4/MyD88/NF-κB pathway (Guo et al., 2021). A blue-green alga *spirulina platensis* polysaccharide attenuated the reduction in tyrosine hydroxylase and the dopamine transporter expression (DA-specific markers) *via* increasing in the activities of superoxide dismutase (SOD), and glutathione peroxidase (GSH-Px) in same mouse PD models (Zhang et al., 2015), SOD and GSH-px are important endogenous antioxidants. In 6-hydroxydopamine (6-OHDA) – induced mouse PD model, *Antrodia camphorata* polysaccharide inhibited the activation of ROS *via* increasing the activity and expression of antioxidant enzymes, ultimately reduced DA neuronal damage in the substantia nigra, improves motor performance (Han et al., 2020). Many accumulated evidences show that a prominent feature in many NDs is excessive ROS, it would attack lipid membranes, proteins and DNA (Wu et al., 2006), and eventually contribute to the injury and death of neuronal cells. In H_2O_2 – induced PC12 cells, wild desert plant – drived *Cynomorium songaricum* Rupr polysaccharide maintained the antioxidant system, protected the cells against oxidative damage (Wang F. et al., 2016). A selenium polysaccharide from *Platycodon grandiflorum* attenuated intracellular ROS formation to inhibit the decrease of cell viability against PC12 cells injury (Sheng et al., 2017). *Radix Ophiopogonis* is the one of most widely used Chinese herb in Traditional Chinese Medicine (Wang et al., 2015), this polysaccharide protected PC12 cells through suppressing the increase of the intracellular oxidative stress and endoplasmic reticulum stress (Liu and Li, 2018).

In neuronal cells, mitochondria can be found to enhance at areas of increased energy demand, to alter their motility in axons and at synapses in order to maintain energy homeostasis that is essential for synaptic functions (Sheng, 2017). Mitochondria-derived ATP production provides most of the axonal energy, and damaged mitochondria fail to produce ATP. Biological energy deficits and chronic oxidative stress trigger axonal pathology and synaptic dysfunction, thus contributing to pathogenesis of NDs (Theocharopoulou, 2020). Research showed that sulfated chitosan suppressed rotenone – induced – mitochondrial dysfunction, nuclear condensation, and DNA fragmentation in human neuroblastoma SH-SY5Y cell line (Manigandan et al., 2019). Likewise, in rotenone – induced PD animal model, fucoidan extracted from *Laminaria japonica* enhanced mitochondrial respiratory function through the PGC-1α/NRF2 pathway, alleviated DA degeneration and motor impairments (Zhang L. et al., 2018).

Neuroinflammatory responses are also major pathogenic factors in neurodegeneration, and microglia is key participant in neuroinflammatory. Microglia activation and increased inflammatory cytokines have been implicated in the cognitive decline associated with NDs. Microglia activation produces a variety of pro-inflammatory mediators and pro-inflammatory cytokines, plays a crucial role in various NDs (Luo et al., 2013). These cytokines enter the brain, stimulate microglia to trigger neuroinflammatory responses, induce neuronal degeneration and death. Traditional Chinese medicine – *Schisandra chinensis* protected against DA neurodegeneration by suppressing neuroinflammation *via* the BDNF/Nrf2/NF-κB pathway in 6-OHDA-induced PD mice (Yan et al., 2021). And *G. lucidum* prevented the production of microglia-derived proinflammatory and cytotoxic factors in MPP^+-treated MES 23.5 cell membranes (Zhang et al., 2011).

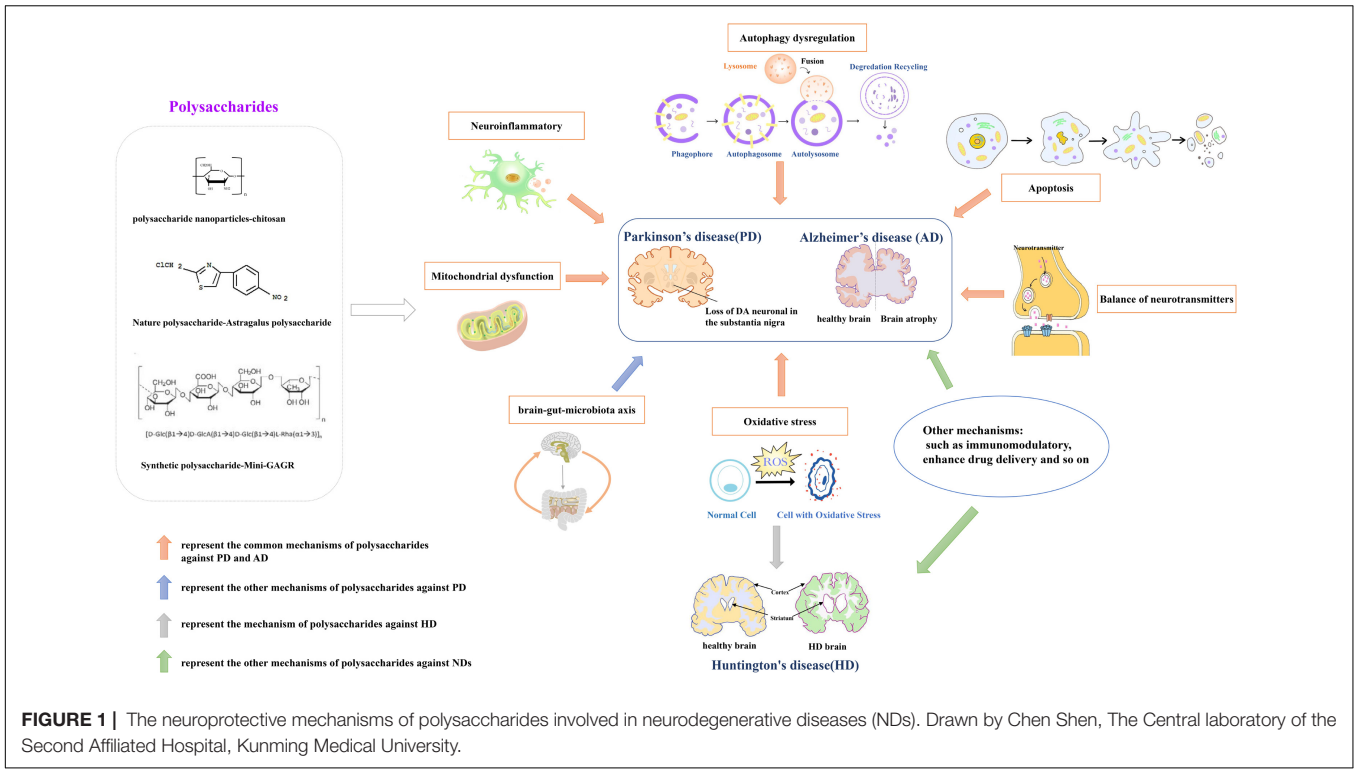

FIGURE 1 | The neuroprotective mechanisms of polysaccharides involved in neurodegenerative diseases (NDs). Drawn by Chen Shen, The Central laboratory of the Second Affiliated Hospital, Kunming Medical University.

Apoptosis occurs normally during development and aging and as a homeostatic mechanism to maintain cell populations, including normal cell turnover, proper development and functioning of the immune system, hormone-dependent atrophy, embryonic development and chemical-induced cell death (Elmore, 2007), and apoptosis and caspase-mediated cell death are important mediators of neuronal death in NDs. Traditional herbal medicine has been used for centuries in China to treat PD and remains in use, suggesting that medicinal herbs may be a good source of drug candidates for the treatment of PD (Chen et al., 2007). *Gynostemma pentaphyllum* Makino is a well-known edible and medicinal plant in Asia (Su et al., 2021), its extract polysaccharides decreased Bax/Bcl2 ratio, attenuated the activation of caspase-3/9, and improved PC12 cell viability of MPP^+ – induced PD cell model (Deng and Yang, 2014). *Lycium barbarum* polysaccharides reduced apoptosis to reverse the decreased viability of PC12 cells in a vitro PD model (Gao et al., 2014).

Autophagy is a cellular basic metabolic process that degrades the aggregated or misfolded proteins and abnormal organelles in cells. The abnormal regulation of neuronal autophagy is accompanied by the accumulation and deposition of irregular proteins, leading to changes in neuron homeostasis and neurodegeneration. Autophagy is a unique mechanism for cells to protect themselves. When autophagy is weakened, abnormal protein aggregation will accelerate the onset of PD; and when autophagy is too strong, it will lead to the autophagy death of nerve cells. Studies show that PTEN-induced putative kinase 1 (PINK1) and E3 ubiquitin protein ligase (Parkin) participate in mitochondrial autophagy, mutations in PINK1 and Parkin genes result in defective mitochondria and trigger early onset PD (Meka et al., 2015). Ren et al. has reported that *G. lucidum* extract attenuated autophagy, and declined in the expression of PINK1 and Parkin, improved behavioral performance in PD model (Ren et al., 2019).

Polymannuronic acid (PM) is a water-soluble homopolysaccharide and can be easily separated *via* pH fractionation from alginate hydrolyzate (Li et al., 2013), it increased gut microbial diversity and fecal SCFAs production, improved the integrity of the intestinal barrier and BBB, prevented DA neuronal loss and improved motor functions in MPTP-induced PD mice (Dong et al., 2020).

To date, a number of literatures have been reported for the possible mechanism of traditional Chinese medicine in treating PD (Rai et al., 2021). As shown in **Table 2**, current research in PD show that polysaccharides play neuroprotective roles *via* inhibiting cell apoptosis, neuroinflammatory responses and oxidative stress, reversing mitochondrial dysfunction, regulating microbiome and its metabolic product, improving autophagy and other mechanisms.

The Role of Polysaccharides in Alzheimer's Disease

Alzheimer's disease is a common degenerative disease of the nervous system with insidious onset and progressive development worldwide. The AD progression develops from initial short-term memory loss to behavioral problems, gradual loss of physical function, and finally death (Tarawneh and Holtzman, 2012). It is believed that the pathogenesis of AD includes the excessive aggregation of Aβ and neurofibrillary tangles formed by hyperphosphorylation of Tau protein

TABLE 2 | Polysaccharides and their effects on PD.

Experimental models	Source of polysaccharides	Effects	References
MPTP-induced mouse	*Momordica charantia*	Inhibit oxidative stress and increase DA levels	Guo et al., 2021
MPTP-induced mouse	*spirulina platensis*	Inhibit oxidative stress	Zhang et al., 2015
6-OHDA-induced mouse	*Antrodia camphorata*	Inhibit oxidative stress	Han et al., 2020
H_2O_2-induced PC12 cells	*Cynomorium songaricum*	Reduce oxidative stress	Wang F. et al., 2016
H_2O_2-induced PC12 cells	*Platycodon grandiflorum*	Attenuate intracellular ROS formation	Sheng et al., 2017
MPP^+ -induced PC-12 cells	Radix Ophiopogonis	Reverse oxidative stress and ER stress rise	Liu and Li, 2018
Rotenone-induced SH-SY5Ycells	Low molecular weight Sulfated chitosan	Suppress mitochondrial dysfunction	Manigandan et al., 2019
Rotenone-induced Sprague-Dawley Rat	Focoidan	Enhance mitochondrial respiratory function	Zhang L. et al., 2018
6-OHDA-induced mice	*Schisandra chinensis*	Suppress neuroinflammation	Yan et al., 2021
MPP^+-treated MES 23.5 cell membranes	*Ganoderma lucidum*	prevent the production of microglia-derived proinflammatory	Zhang et al., 2011
MPP^+-inducedPC12 cells	*Gynostemma pentaphyllum*	Inhibit apoptosis	Deng and Yang, 2014
6-OHDA-induced PC12 cells	*Lycium barbarum*	Decrease apoptosis	Gao et al., 2014
MPTP-induced mouse;MPP^+-inducedneuro-2a.	*Ganoderma lucidum*	Attenuate autophagy	Ren et al., 2019
6-OHDA-induced PC12 cells	*Astragalus*	Increase autophagy	Tan et al., 2020
MPTP-induced mouse	Polymannuronic acide	Modulate brain-gut-microbiota axis, increase gut microbial diversity and increase fecal SCFAs production.	Dong et al., 2020

(Zhang et al., 2021), release of pro-inflammatory cytokines (Bellucci et al., 2004), mitochondrial dysfunction (Kukreja et al., 2014), oxidative stress (Guix et al., 2012; Wahlster et al., 2013), apoptosis (Zhu et al., 2006), autophagy (Plaza-Zabala et al., 2017), and so on.

The cause of AD remains unclear, and all current medications only relieve the symptoms or delay its development. Aβ is produced and released from the axon terminals of neurons already afflicted with tau pathology (Braak and Del Tredici, 2013). FDA approved AD drugs such as acetylcholinesterase (AChE) inhibitors and *N*-methyl-D-aspartate receptor antagonists only alleviate symptoms in about half of the patients for approximately 6–12 months (Winslow et al., 2011).

In amyloid precursor protein/presenin 1 (APP/PS1), a double transgenic mouse model of AD, *Codonopsis pilosula* polysaccharide decreased the expression of Aβ42 and Aβ40 in the hippocampus and alleviated cognitive impairment through the restoration of synaptic plasticity (Wan et al., 2020). *Maitake* polysaccharide, an edible/medicinal mushroom, activated microglia and astrocytes, promoted the recruitment of microglia to Aβ plaques, enhanced Aβ phagocytosis to reduce Aβ load, increased the number of surviving neurons and maintained the histomorphology of the hippocampus, finally improved learning and memory impairment in APP/PS1 mice (Bai et al., 2019). Furthermore, polysaccharides also have been found to have the same effect in cellular models. *Lycium barbarum* polysaccharide reduced the expression of Aβ42/Aβ40 against β-amyloid peptide neurotoxicity in N2a/APP695 cells (mouse neuroblastoma N2a cells stably expressing human APP695; Wu et al., 2021a). A novel pectin polysaccharide from *Polygala tenuifolia* enhanced the expression of insulin-degradation enzyme and Neprilysin (NEP) to attenuate Aβ42 production and inhibit Aβ42 aggregation (Zeng et al., 2020). Moreover, polysaccharide obtained from *Coptis chinensis* Franch could inhibit the deposition of Aβ *via* the reduction of Aβ-induced toxicity and delaying of the aging in a transgenic *Caenorhabditis elegans* (*C. elegans*) model of AD (Li Y. et al., 2018).

The presence of tau pathology and its correlation with cognitive deficits encouraged the statement of the "tau hypothesis" of AD (Kametani and Hasegawa, 2018). Tau is a microtubule-related protein that aggregates tubulin into microtubules, maintains complex neuronal cell microstructure promoting neuron maturation and regulating synaptic function (Dawson et al., 2001; Castellani and Perry, 2019), changes in synaptic distribution and interruption of interaction with synaptic proteins, damage neuron function and even lead to AD. Previous studies showed that polysaccharides from various plants alleviate cognitive impairment and pathological alterations in AD animal models (Ho et al., 2010; Zhang J. et al., 2016). In an adeno-associated virus serotype 2 (AAV2)-induced expression of human full-length Tau (hTau) in C57/BL6 mice to mimic AD tau pathology, *C. pilosula* polysaccharide significantly increased protein phosphatase-2A (PP2A) activity to attenuate tau phosphorylation in the hippocampus of mice (Zhang Q. et al., 2018). Polysaccharides, extracted from an edible fungus *Pleurotus ostreatus*, decreased Aβ accumulation and tau phosphorylation by increasing the expression of PP2A and glycogen synthase kinase 3beta (GSK3), alleviated cognitive impairment in AD rats (Zhang Y. et al., 2016). An intranasally applied polysaccharide Mini-GAGR can cross BBB to increase

antioxidant enzymes in the hippocampus and cortex, decrease phosphorylated-tau (p-tau) and improve memory in AD mice (Murphy et al., 2018). Similarly, another 4.7 KD polysaccharide Midi-GAGR also penetrated the BBB to reduce free reactive radicals and microglia cells, increased neurite outgrowth and phosphorylated cAMP responsive element binding protein, decreased hyperphosphorylated tau for neuroprotection in the transgenic AD mouse model (Makani et al., 2016).

Acetylcholine (Ach) is a signal transmitter of cholinergic neurons, its metabolic processes influence learning and memory in AD brain (Ferreira-Vieira et al., 2016). A commonly used traditional Chinese herb *Angelica sinensis* is widely used for nourishing the blood. *Angelica* polysaccharide regulated the balance of neurotransmitters by decreasing AChE level and increasing Ach and acetyltransferase (ChAT), eventually meliorated spatial learning and memory deficiency in AD rats (Du et al., 2020). Porphyran, from red algae *Pyropia haitanensis*, increased ChAT activity and decreased AChE activity in the cortical and hippocampal, significantly ameliorated the learning and memory impairment induced by Aβ1-40 of AD mice (Zhang et al., 2020c). The changes of chAT and AchE activity are considered to be important indicators to indirectly reflect the cholinergic biochemical changes in AD (Mantzavinos and Alexiou, 2017).

In Aβ-induced AD rats, marine brown seaweed fucoidan, a complex sulfated polysaccharide, increased of Bcl2/Bax ratio and decreased of caspase-3, inhibited cell apoptosis followed by improving the learning and memory abilities (Gao et al., 2012). Non-saponin fraction with rich polysaccharides from ginseng ameliorated mitochondrial deficit in Aβ-treated HT22 cells and enhanced and restored the cognitive function of healthy and AD mice (Shin et al., 2021). Furthermore, study has shown that many natural polysaccharides are also called immune polysaccharides due to their immunological activity. Polysaccharides from *Schisandra Chinensis Fructus* significantly reduced the deposition of Aβ, improved the cognition and histopathological changes *via* downregulating the expression of pro-inflammatory cytokines such as IL-1β, IL-6, and TNF-α, and the activation of glial cells in the hippocampus of AD mice (Xu et al., 2019). Moreover, *G. lucidum* polysaccharides *via* oral administration promoted neural progenitor cell proliferation to enhance neurogenesis and alleviated cognitive deficits in transgenic AD mice, and also improved locomotor functions and prolonged the life span of *Drosophila* Aβ42-AD model (Huang et al., 2017).

As reported, the promotion of autophagy initiation and autolysosome formation can reduce the aggregate-prone proteins aggregation and its neurotoxicity in AD model (Nixon, 2013). Two trehalose analogs including lactulose and melibiose increase autophagy by upregulating the LC3II/LC3I and downregulating the p62, decrease neuroinflammation, eventually attenuated the short-term memory and the learning retrieval in AD mice (Lee et al., 2021). Moreover, In AD-like symptom C57BL/6J mice, polysaccharides from *Taxus chinensis* var. *mairei* Cheng et L.K.Fu (Taxaceae) inhibited oxidative stress, restored the impaired learning and cognitive function *via* regulating the expression of NF-E2-related factor 2 (Nrf2) which plays an important role in cell defense against oxidative stress in CNS (Zhang et al., 2020a). A fungal species *Inonotus obliquus* polysaccharide also decreased oxidative stress *via* Nrf2 signaling, improved the pathological behaviors related memory, and cognition in APP/PS1 mice (Han et al., 2019).

In conclusion, AD seriously threatens aged people's health. As shown in **Table 3**, we speculate that polysaccharides can reduce oxidative stress, apoptosis and neuroinflammation, regulate the balance of neurotransmitters, increase autophagy, ultimately decrease Aβ peptide formation and tau phosphorylation, alleviate cognitive impairment in AD models. Consequently, it is plausible to recommend polysaccharide as one of the promising tools in the development of drug therapy for AD.

Huntington's Disease

Huntington's disease is a single-gene autosomal dominant neurodegenerative disorder with the disease-causing gene IT-15 (the *HTT* gene). The HD gene has been mapped in 4p16.3, which is abnormally amplified in CAG trinucleotide repeats in HD. When the number of CAG copies is abnormally increased due to gene mutation, the polyglutamine (polyQ) chain at the amino-terminal of the mutant Htt (mHtt) protein is prolonged and abnormally folded. The β lamellae structure is formed to cause the loss of normal function and toxic effect of mHtt protein (Southwell and Patterson, 2011). HD usually presents in midlife with chorea, dementia, and weight loss, with death typically occurring 15–20 years after symptom onset (Walker, 2007), the dance-like movements that are a primary clinical symptom of HD. Nonetheless, the therapies currently available to HD patients only moderate symptom relief and do not affect disease progression.

A prominent pathological feature of HD is the accumulation of mHtt in neurons, and mHtt plays a cytotoxic role by affecting transcription, mitochondrial function, synaptic transmission, and axon transport (Ramakrishnan and Gupta, 2021). Compared with ordinary Htt, mHtt has a longer polyQ (>36) extension at the N-terminal (Ross, 2002). mHtt undergoes proteolysis, misfolding, accumulation, self-aggregation, and eventually forms inclusion bodies (Cortes and La Spada, 2014). mHtt engages in various aberrant interactions that lead to the pathological gain of toxic functions and loss of normal functions. The study found that reduced AKT phosphorylation and inhibited AKT activity are involved in mHtt-induced cell death. *Lycium barbarum* polysaccharide alleviated the cytotoxicity of mHtt by activating AKT and reduceing mHtt levels in HD-transgenic mice (Fang et al., 2016). *Astragalus membranaceus* polysaccharide reduced polyQ aggregation and alleviated the associated neurotoxicity in *C. elegans* (Zhang et al., 2012). *Peganum harmala* L. polysaccharide inhibited polyQ aggregation through proteasome-mediated protein degradation, alleviated the neurotoxicity of *C. elegans* (Guo et al., 2020).

Soluble and aggregative mHtt has cytotoxicity, manifests primarily as excessive intracellular oxidative stress response leading to cell apoptosis in the mitochondrial pathway (Reijonen et al., 2008; Ayala-Peña, 2013), increases expression of apoptosis-related genes (Bae et al., 2005), and continuous degeneration of neurons caused by cell cycle re-entry (Pelegrí et al.,

TABLE 3 | Polysaccharides and their effects on AD.

Experimental models	Source of polysaccharides	Mechanism	References
APP/PSI transgenic mice	*Codonopsis pilosula*	Restore synaptic plasticity	Wan et al., 2020
APP/PSI transgenic mice	*Maitake*	Promote the recruitment of microglia to Aβ plaques	Bai et al., 2019
N2a/APP695 cells	*Lycium barbarum*	Reduce Aβ peptide neurotoxicity	Wu et al., 2021a
CHO/APPBACE1 and HEK293-APPsw cells	*Polygala tenuifolia*	Enhance main enzymes (IDE and NEP) involved in Aβ degradation expression	Zeng et al., 2020
transgenic *C. elegans*	*Coptis chinensis*	Reduce Aβ-induced toxicity	Li Y. et al., 2018
AAV2-hTau-infected C57/BL6 mice	Codonopsis pilosula	Attenuate Tau phosphorylation by increasing PP2A activity	Zhang Q. et al., 2018
Male Wistar rats	*Pleurotus ostreatus*	Decrease Tau phosphorylation by elevating PP2A and reducing APP, BACE1, GSK3 expression	Zhang Y. et al., 2016
3xTg-AD mice	Mini-GAGR	Increase antioxidant enzymes decrease and p-Tau	Murphy et al., 2018
3xTg-AD mice	Midi-GAGR	Penetrate the BBB to reduce free reactive radicals and microglia cells	Makani et al., 2016
Male Sprague-Dawley rats	*Angelica sinensis*	Regulate the balance of neurotransmitters	Du et al., 2020
Aβ1-40 of AD mice	Porphyran	Increase ChAT activity and decreases AChE activity	Zhang et al., 2020c
Sprague-Dawley rats	Fucoidan	Inhibit cell apoptosis	Gao et al., 2012
Male KM mice	*Schisandra Chinensis Fructus*	Decrease neuroinflammation	Xu et al., 2019
transgenic AD mice;transgenic Drosophila	*Ganoderma lucidum*	Enhance neurogenesis	Huang et al., 2017
C57BL/6J mice	lactulose and melibiose	Attenuate autophagy	Lee et al., 2021
C57BL/6J mice	Taxus chinensis var. mairei Cheng et L.K.Fu	Decrease oxidative stress	Zhang et al., 2020a
APP/PSI transgenic mice	*Inonotus obliquus*	Inhibit oxidative stress	Han et al., 2019

2008). Polysaccharide is capable of inhibiting behavioral dysfunction mediated by reducing polyQ aggregation. The study found that a kind of traditional Chinese medicine – epimedium is a genus of plants in the family *Berberidaceae*, and its polysaccharide enhanced antioxidant enzyme activities, decreased lipid peroxidation product and oxidative stress, increased the survival rates, attenuated behavioral dysfunction in polyQ transgenic *C. elegans* HD models (Xiang et al., 2017). In the similar HD models, the polysaccharide from a medicinal mushroom *Dictyophora indusiata* was capable of reducing ROS levels and alleviating chemosensory behavior deficits (Zhang J. et al., 2016). 3-nitropropionic acid (3-NP) induces a selective striatal pathology in HD, and has been widely used as an animal model of HD. Ginseng saponins decreased intracellular Ca^{2+} and cytotoxicity of striatal neurons, significantly improved behavioral impairment, and extended the survival of 3-NP-induced HD rats (Kim et al., 2005). Furthermore, polysaccharides and their effects on HD are shown in **Table 4**.

DISCUSSION

Previous studies suggest that polysaccharides are employed to protect against NDs. Herein, this review presents multiform polysaccharides protect against NDs *via* mediating various mechanisms. Despite many signaling pathways involved in, the common mechanisms of polysaccharides mainly include neuroinflammation, oxidative stress, autophagy, apoptosis and mitochondrial dysfunction in PD and AD for neuroprotective effects. And, HD related studies are still rare. In the above literatures, a majority of polysaccharide in NDs have been studied *in vitro*. Most polysaccharides have a poor BBB permeability besides chitosan nanoparticles and LPS. Therefore, it is rarely reported that the polysaccharides directly activate polysaccharides receptors in the CNS of NDs. How do the polysaccharides work in the CNS? Up to now, only polysaccharide receptor TLR-4 has been reported to be bind with LPS to increase accumulation of Aβ in AD. Based on above studies and the metabolism of polysaccharides, the polysaccharides may directly penetrate BBB to act on the polysaccharide receptors or mediate intestinal microorganism and metabolites to activate downstream signaling for neuroprotective effect in NDs. Whereas, the related studies are still limited.

Most NDs patients develop gastrointestinal motility abnormalities and constipation, hence intestinal flora might be closely related to the development of NDs. The imbalance also affects the intestinal mucosal barrier, triggers intestinal and peripheral neuroinflammatory responses. These phenomena may lead to neuroinflammation or neurodegeneration in CNS (Pellegrini et al., 2018). Polysaccharide molecules are closely related to the regulation of intestinal flora, the role of the microbiota provides new therapeutic targets for NDs (Sun et al., 2020). Nerves, immunity, and the endocrine system could alter the microbiota-gut-brain axis. The intestine, the brain and immune system dysfunctions promotes the development and progression of NDs. The intestinal microbiota and its primary metabolites SCFAs affect brain activity and behavior *via* endocrine, vagus nerve, immune pathways and other humoral pathways (Shaik et al., 2020). SCFAs promote the development and growth of brain microglia, play a central role in brain development and the maintenance of CNS homeostasis (Erny et al., 2015). Natural polysaccharides have received increasing attention and have become popular dietary

TABLE 4 | Polysaccharides and their effects on HD.

Experimental models	Source of polysaccharides	Effects	References
HD-transgenic mice	*Lycium barbarum*	Alleviate the cytotoxicity of mHtt	Fang et al., 2016
C. elegans	*Astragalus membranaceus*	Reduce polyQ aggregation and alleviate neurotoxicity	Zhang et al., 2012
C. elegans	*Peganum harmala*	Inhibit polyQ aggregation and alleviate the neurotoxicity	Guo et al., 2020
C. elegans	*epimedium*	Reduce oxidative stress	Xiang et al., 2017
transgenic *C. elegans*	*Dictyophora indusiata*	Reduce oxidative stress	Zhang J. et al., 2016
3-NP-induced SD rats	Ginseng saponins	Alleviate cytotoxicity of striatal neurons	Kim et al., 2005

nutrients because of their various biological functions. Some natural polysaccharides are favorable for the proliferation of SCFA-producing bacteria, the presence of which improves the intestinal microenvironment. Moreover, natural polysaccharides also suppress excessive inflammatory responses by improving the intestinal microbiota composition, promoting SCFAs production, strengthening intestinal barrier function and reducing pro-inflammatory mediators (Tang et al., 2019). A plant polysaccharide from *Cistanche deserticola* improves cognitive function in mice in a D-galactose induced aging model by restoring homeostasis of the gut-microbiota-brain axis (Gao et al., 2021). Therefore, polysaccharides may mediate intestinal flora and related metabolites against NDs.

The natural polysaccharides contain polysaccharides and their derivatives (such as nanoparticles). Using polysaccharides nanoparticles for drug delivery can enhance the aqueous solubility of the drug (Kang et al., 2015). Additionally, specific polysaccharides can provide targeting mechanisms due to receptor recognition and binding (Yadav et al., 2008), mucosal adhesion and transport (Feng et al., 2015), site specific enzymatic degradation (Castelli et al., 2008). Polysaccharide-based drug delivery, specially, polysaccharide nanoparticle has been improved the uptake and specificity of drugs and the bioavailability of poorly soluble drugs. Such as, polysaccharide chitosan as the only essentially natural cationic polysaccharide is useful for chemical modification and electrostatic interactions in drug delivery systems in NDs (Sarvaiya and Agrawal, 2015; Liu et al., 2017; Raj et al., 2018). Starch is a glucose-based polysaccharide produced by many green plants to store energy, often as an excipient in pharmaceutical products, have been used to modify the properties of drug delivery systems to improve sustained release and directly to enhance drug delivery in PD (Odeniyi et al., 2018; Becker et al., 2021). An energy storage polysaccharide Inulin is found in plants of the *Compositae* family, and also indigestible to humans and digested by the enzymes of bacteria in the gut, allowing to be exploited for colon targeted delivery (Castelli et al., 2008). Polysaccharides represent a platform for therapeutic delivery applications, and these multiple functions are likely to be increasingly applied in the future.

There are growing evidences on the fact that distinct immune responses, involving the adaptive as well as the innate immune system, are crucially implicated in NDs (Chitnis and Weiner, 2017), and immunotherapy is one of the most studied therapeutic strategies in NDs (Ciccocioppo et al., 2020). Moreover, microglia and astrocytes protect the brain from infectious agents, while their prolonged activation causes neuroinflammation that promote neurodegeneration (Barbalace et al., 2019). Neuroinflammation significantly initiates and enhances neurodegenerative pathological change, natural anti-inflammatory compounds may be good candidates for the development of successful therapeutic strategies. Polysaccharides have significant pharmaceutical importance due to their strong anti-inflammatory and immunomodulatory properties (Hou C. et al., 2020). The polysaccharides in AD, PD, and HD share a common mechanism – oxidative stress. Growing reports have demonstrated that oxidative stress is implicated in the development and progression of many chronic diseases, and oxidative stress is a condition of imbalance between ROS formation and cellular antioxidant capacity due to enhance ROS generation or dysfunction of the antioxidant system. Many polysaccharides are reported to have potent reducing power and free radical scavenging ability *in vitro*, and reduce the levels of ROS and associated peroxidation products in cellular and animal models under oxidative stress. Furthermore, oxidative stress can interact with many other stresses to induce neurodegeneration, so antioxidant polysaccharides play significant role as a pharmacological potential in treatment NDs.

In addition, the polysaccharides also develop for clinical applications. Acemannan, the main bioactive polysaccharide of *Aloe vera*, is a neuroprotective immunomodulator and antioxidant, and improved the cognitive performances of middle-aged patients suffering from mental fatigue (Liu et al., 2019). Furthermore, chitosan as a biomaterial for the development of a flexible, thin film, laser-activated surgical adhesive termed surgical adhesive, are FDA approved and successfully used in a variety of biomedical applications and products. Therefore, chitosan is an alternative to microsurgery for peripheral nerve reconstruction (Foster and Karsten, 2012). Chitosan nerve tube can improve peripheral sensory nerve regeneration of the patients in traumatic sensory nerve lesions of the hand (Neubrech et al., 2018). So polysaccharides and their mechanisms deserve further study as potential candidates for preventing and treating NDs.

AUTHOR CONTRIBUTIONS

YW wrote the manuscript. NZ and JY contributed to writing and review by the manuscript. RC, QW, and XC were implied in collecting and sorting literatures and references. ZY wrote a small part and offered some ideas for the first manuscript, and

improved language, revised, refined the manuscript in the process of revision. All authors read and approved the final manuscript.

FUNDING

This work is supported by the National Natural Science Foundation Program of China (grant no. 31860274), Department of Science and Technology of Yunnan Province (grant nos. 202101AT070251, 202201AS070084, 202005AC160058, and 2019FI016).

ACKNOWLEDGMENTS

We sincerely thank Chen Shen (The Central laboratory of the Second Affiliated Hospital, Kunming Medical University) for drawing the graphical summary.

REFERENCES

Ahmadi, S., Mainali, R., Nagpal, R., Sheikh-Zeinoddin, M., Soleimanian-Zad, S., Wang, S., et al. (2017). Dietary polysaccharides in the amelioration of gut microbiome dysbiosis and metabolic diseases. *Obes. Control Ther.* 4:10.15226/2374-8354/4/2/00140. doi: 10.15226/2374-8354/4/2/00140

Ayala-Peña, S. (2013). Role of oxidative DNA damage in mitochondrial dysfunction and Huntington's disease pathogenesis. *Free Radic. Biol. Med.* 62, 102–110. doi: 10.1016/j.freeradbiomed.2013.04.017

Bae, B. I., Xu, H., Igarashi, S., Fujimuro, M., Agrawal, N., Taya, Y., et al. (2005). p53 mediates cellular dysfunction and behavioral abnormalities in Huntington's disease. *Neuron* 47, 29–41. doi: 10.1016/j.neuron.2005.06.005

Bai, Y., Chen, L., Chen, Y., Chen, X., Dong, Y., Zheng, S., et al. (2019). A Maitake (Grifola frondosa) polysaccharide ameliorates Alzheimer's disease-like pathology and cognitive impairments by enhancing microglial amyloid-β clearance. *RSC Adv.* 9, 37127–37135. doi: 10.1039/c9ra08245j

Balestrino, R., and Schapira, A. (2020). Parkinson disease. *Eur. J. Neurol.* 27, 27–42. doi: 10.1111/ene.14108

Bandopadhyay, R., Mishra, N., Rana, R., Kaur, G., Ghoneim, M. M., Alshehri, S., et al. (2022). Molecular mechanisms and therapeutic strategies for levodopa-induced dyskinesia in Parkinson's disease: a perspective through preclinical and clinical evidence. *Front. Pharmacol.* 13:805388. doi: 10.3389/fphar.2022.805388

Barbalace, M. C., Malaguti, M., Giusti, L., Lucacchini, A., Hrelia, S., and Angeloni, C. (2019). Anti-Inflammatory activities of marine algae in neurodegenerative diseases. *Int. J. Mol. Sci.* 20:3061. doi: 10.3390/ijms20123061

Becker, A., Pierre Schmartz, G., Groger, L., Grammes, N., Galata, V., Philippeit, H., et al. (2021). Effects of resistant starch on symptoms, fecal markers and gut microbiota in Parkinson's disease - the RESISTA-PD trial. *Genomics Proteomics Bioinform.* S1672-0229(21)00245-X. [Online ahead of print], doi: 10.1016/j.gpb.2021.08.009

Bellucci, A., Westwood, A. J., Ingram, E., Casamenti, F., Goedert, M., and Spillantini, M. G. (2004). Induction of inflammatory mediators and microglial activation in mice transgenic for mutant human P301S tau protein. *Am. J. Pathol.* 165, 1643–1652. doi: 10.1016/S0002-9440(10)63421-9

Bird, T. D. (2018). *Alzheimer Disease Overview. GeneReviews®[Internet]*. Seattle, DC: University of Washington.

Blume, T., Filser, S., Jaworska, A., Blain, J.-F., Koenig, G., Moschke, K., et al. (2018). BACE1 inhibitor MK-8931 alters formation but not stability of dendritic spines. *Front. Aging Neurosci.* 10:229. doi: 10.3389/fnagi.2018.00229

Braak, H., and Del Tredici, K. (2013). Amyloid-β may be released from non-junctional varicosities of axons generated from abnormal tau-containing brainstem nuclei in sporadic Alzheimer's disease: a hypothesis. *Acta Neuropathol.* 126, 303–306. doi: 10.1007/s00401-013-1153-2

Burudi, E. M., and Régnier-Vigouroux, A. (2001). Regional and cellular expression of the mannose receptor in the post-natal developing mouse brain. *Cell Tissue Res.* 303, 307–317. doi: 10.1007/s004410000311

Cai, G., Wusiman, A., Gu, P., Mao, N., Xu, S., Zhu, T., et al. (2021). Supplementation of Alhagi honey polysaccharides contributes to the improvement of the intestinal immunity regulating the structure of intestinal flora in mice. *Food Funct.* 12, 9693–9707. doi: 10.1039/d1fo01860d

Cardinali, D. P., Vigo, D. E., Olivar, N., Vidal, M. F., and Brusco, L. I. (2014). Melatonin therapy in patients with Alzheimer's disease. *Antioxidants (Basel, Switzerland)* 3, 245–277. doi: 10.3390/antiox3020245

Cash, J. L., White, G. E., and Greaves, D. R. (2009). Chapter 17. Zymosan-induced peritonitis as a simple experimental system for the study of inflammation. *Methods Enzymol.* 461, 379–396. doi: 10.1016/S0076-6879(09)05417-2

Cass, S. P. (2017). Alzheimer's disease and exercise: a literature review. *Curr. Sports Med. Rep.* 16, 19–22.

Castellani, R. J., and Perry, G. (2019). Tau biology, tauopathy, traumatic brain injury, and diagnostic challenges. *J. Alzheimers Dis.* 67, 447–467. doi: 10.3233/JAD-180721

Castelli, F., Sarpietro, M. G., Micieli, D., Ottimo, S., Pitarresi, G., Tripodo, G., et al. (2008). Differential scanning calorimetry study on drug release from an inulin-based hydrogel and its interaction with a biomembrane model: pH and loading effect. *Eur. J. Pharm. Sci.* 35, 76–85. doi: 10.1016/j.ejps.2008.06.005

Chen, L. W., Wang, Y. Q., Wei, L. C., Shi, M., and Chan, Y. S. (2007). Chinese herbs and herbal extracts for neuroprotection of dopaminergic neurons and potential therapeutic treatment of Parkinson's disease. *CNS Neurol. Disord. Drug Targets* 6, 273–281. doi: 10.2174/187152707781387288

Chen-Plotkin, A. S. (2014). Unbiased approaches to biomarker discovery in neurodegenerative diseases. *Neuron* 84, 594–607. doi: 10.1016/j.neuron.2014.10.031

Chitnis, T., and Weiner, H. L. (2017). CNS inflammation and neurodegeneration. *J. Clin. Invest.* 127, 3577–3587. doi: 10.1172/JCI90609

Ciccocioppo, F., Bologna, G., Ercolino, E., Pierdomenico, L., Simeone, P., Lanuti, P., et al. (2020). Neurodegenerative diseases as proteinopathies-driven immune disorders. *Neural Regen. Res.* 15, 850–856. doi: 10.4103/1673-5374.268971

Cortes, C. J., and La Spada, A. R. (2014). The many faces of autophagy dysfunction in Huntington's disease: from mechanism to therapy. *Drug Discov. Today* 19, 963–971. doi: 10.1016/j.drudis.2014.02.014

Dawson, H. N., Ferreira, A., Eyster, M. V., Ghoshal, N., Binder, L. I., and Vitek, M. P. (2001). Inhibition of neuronal maturation in primary hippocampal neurons from tau deficient mice. *J. Cell Sci.* 114(Pt 6), 1179–1187. doi: 10.1242/jcs.114.6.1179

De La Torre, J. C. (2010). The vascular hypothesis of Alzheimer's disease: bench to bedside and beyond. *Neurodegener. Dis.* 7, 116–121. doi: 10.1159/000285520

Dean, M., and Sung, V. W. (2018). Review of deutetrabenazine: a novel treatment for chorea associated with Huntington's disease. *Drug Des. Devel. Ther.* 12, 313–319. doi: 10.2147/DDDT.S138828

Deng, Q., and Yang, X. (2014). Protective effects of *Gynostemma pentaphyllum* polysaccharides on PC12 cells impaired by MPP(+). *Int. J. Biol. Macromol.* 69, 171–175. doi: 10.1016/j.ijbiomac.2014.05.049

Dhahri, M., Alghrably, M., Mohammed, H. A., Badshah, S. L., Noreen, N., Mouffouk, F., et al. (2022). Natural polysaccharides as preventive and therapeutic horizon for neurodegenerative diseases. *Pharmaceutics* 14:1. doi: 10.3390/pharmaceutics14010001

Dickson, D. W. (2018). Neuropathology of Parkinson disease. *Parkinsonism Relat. Disord.* 46(Suppl. 1), S30–S33. doi: 10.1016/j.parkreldis.2017.07.033

Donaldson, G. P., Ladinsky, M. S., Yu, K. B., Sanders, J. G., Yoo, B. B., Chou, W. C., et al. (2018). Gut microbiota utilize immunoglobulin A for mucosal colonization. *Science* 360, 795–800. doi: 10.1126/science.aaq0926

Dong, X. L., Wang, X., Liu, F., Liu, X., Du, Z. R., Li, R. W., et al. (2020). Polymannuronic acid prevents dopaminergic neuronal loss via brain-gut-microbiota axis in Parkinson's disease model. *Int. J. Biol. Macromol.* 164, 994–1005. doi: 10.1016/j.ijbiomac.2020.07.180

Dröge, W. (2002). Free radicals in the physiological control of cell function. *Physiol. Rev.* 82, 47–95. doi: 10.1152/physrev.00018.2001

Du, Q., Zhu, X., and Si, J. (2020). Angelica polysaccharide ameliorates memory impairment in Alzheimer's disease rat through activating BDNF/TrkB/CREB pathway. *Exp. Biol. Med. (Maywood)* 245, 1–10. doi: 10.1177/1535370219894558

Dutta, G., Zhang, P., and Liu, B. (2008). The lipopolysaccharide Parkinson's disease animal model: mechanistic studies and drug discovery. *Fundamental Clin. Pharmacol.* 22, 453–464. doi: 10.1111/j.1472-8206.2008.00616.x

Elmore, S. (2007). Apoptosis: a review of programmed cell death. *Toxicol. Pathol.* 35, 495–516. doi: 10.1080/01926230701320337

Emamzadeh, F. N. (2016). Alpha-synuclein structure, functions, and interactions. *J. Res. Med. Sci. Off. J. Isfahan Univ. Med. Sci.* 21, 29–29. doi: 10.4103/1735-1995.181989

Erny, D., Hrabě De Angelis, A. L., Jaitin, D., Wieghofer, P., Staszewski, O., David, E., et al. (2015). Host microbiota constantly control maturation and function of microglia in the CNS. *Nat. Neurosci.* 18, 965–977. doi: 10.1038/nn.4030

Fang, F., Peng, T., Yang, S., Wang, W., Zhang, Y., and Li, H. (2016). Lycium barbarum polysaccharide attenuates the cytotoxicity of mutant huntingtin and increases the activity of AKT. *Int. J. Dev. Neurosci.* 52, 66–74. doi: 10.1016/j.ijdevneu.2016.05.004

Feng, C., Li, J., Kong, M., Liu, Y., Cheng, X. J., Li, Y., et al. (2015). Surface charge effect on mucoadhesion of chitosan based nanogels for local anti-colorectal cancer drug delivery. *Colloids Surf. B Biointerfaces* 128, 439–447. doi: 10.1016/j.colsurfb.2015.02.042

Ferreira-Vieira, T. H., Guimaraes, I. M., Silva, F. R., and Ribeiro, F. M. (2016). Alzheimer's disease: targeting the cholinergic system. *Curr. Neuropharmacol.* 14, 101–115. doi: 10.2174/1570159x13666150716165726

Filatova, E. V., Alieva, A., Shadrina, M. I., Shulskaya, M. V., Fedotova, E. Y., Illarioshkin, S. N., et al. (2014). [Analysis of mutations in patients with suspected autosomal dominant form of the Parkinson disease]. *Mol. Gen. Mikrobiol. Virusol.* 29, 1–3.

Foster, L. J., and Karsten, E. (2012). A chitosan based, laser activated thin film surgical adhesive, 'SurgiLux': preparation and demonstration. *J. Vis. Exp.* 3527. doi: 10.3791/3527

Gao, K., Liu, M., Cao, J., Yao, M., Lu, Y., Li, J., et al. (2014). Protective effects of Lycium barbarum polysaccharide on 6-OHDA-induced apoptosis in PC12 cells through the ROS-NO pathway. *Molecules* 20, 293–308. doi: 10.3390/molecules20010293

Gao, Y., Li, B., Liu, H., Tian, Y., Gu, C., Du, X., et al. (2021). Cistanche deserticola polysaccharides alleviate cognitive decline in aging model mice by restoring the gut microbiota-brain axis. *Aging (Albany NY)* 13, 15320–15335. doi: 10.18632/aging.203090

Gao, Y., Li, C., Yin, J., Shen, J., Wang, H., Wu, Y., et al. (2012). Fucoidan, a sulfated polysaccharide from brown algae, improves cognitive impairment induced by infusion of Aβ peptide in rats. *Environ. Toxicol. Pharmacol.* 33, 304–311. doi: 10.1016/j.etap.2011.12.022

Guix, F. X., Wahle, T., Vennekens, K., Snellinx, A., Chávez-Gutiérrez, L., Ill-Raga, G., et al. (2012). Modification of γ-secretase by nitrosative stress links neuronal ageing to sporadic Alzheimer's disease. *EMBO Mol. Med.* 4, 660–673. doi: 10.1002/emmm.201200243

Guo, D., Zhou, J., Zhang, M., Taximaimaiti, R., Wang, X., and Wang, H. (2021). *Momordica Charantia* polysaccharides attenuates MPP+-Induced injury in Parkinson's disease mice and cell models by regulating TLR4/MyD88/NF-κB pathway. *Int. J. Polym. Sci.* 2021:5575636.

Guo, S. S., Cui, X. L., and Rausch, W. D. (2016). *Ganoderma* Lucidum polysaccharides protect against MPP(+) and rotenone-induced apoptosis in primary dopaminergic cell cultures through inhibiting oxidative stress. *Am. J. Neurodegener. Dis.* 5, 131–144.

Guo, X., Yuan, J., Song, X., Wang, X., Sun, Q., Tian, J., et al. (2020). Bacteria metabolites from Peganum harmala L. polysaccharides inhibits polyQ aggregation through proteasome-mediated protein degradation in C. elegans. *Int. J. Biol. Macromol.* 161, 681–691. doi: 10.1016/j.ijbiomac.2020.06.091

Han, C., Shen, H., Yang, Y., Sheng, Y., Wang, J., Li, W., et al. (2020). Antrodia camphorata polysaccharide resists 6-OHDA-induced dopaminergic neuronal damage by inhibiting ROS-NLRP3 activation. *Brain Behav.* 10:e01824. doi: 10.1002/brb3.1824

Han, Y., Nan, S., Fan, J., Chen, Q., and Zhang, Y. (2019). Inonotus obliquus polysaccharides protect against Alzheimer's disease by regulating Nrf2 signaling and exerting antioxidative and antiapoptotic effects. *Int. J. Biol. Macromol.* 131, 769–778. doi: 10.1016/j.ijbiomac.2019.03.033

Ho, Y. S., Yu, M. S., Yang, X. F., So, K. F., Yuen, W. H., and Chang, R. C. (2010). Neuroprotective effects of polysaccharides from wolfberry, the fruits of Lycium barbarum, against homocysteine-induced toxicity in rat cortical neurons. *J. Alzheimers Dis.* 19, 813–827. doi: 10.3233/JAD-2010-1280

Hou, C., Chen, L., Yang, L., and Ji, X. (2020). An insight into anti-inflammatory effects of natural polysaccharides. *Int. J. Biol. Macromol.* 153, 248–255. doi: 10.1016/j.ijbiomac.2020.02.315

Hou, X., Watzlawik, J. O., Fiesel, F. C., and Springer, W. (2020). Autophagy in Parkinson's disease. *J. Mol. Biol.* 432, 2651–2672. doi: 10.1016/j.jmb.2020.01.037

Huang, S., Mao, J., Ding, K., Zhou, Y., Zeng, X., Yang, W., et al. (2017). Polysaccharides from ganoderma lucidum promote cognitive function and neural progenitor proliferation in mouse model of Alzheimer's disease. *Stem Cell Rep.* 8, 84–94. doi: 10.1016/j.stemcr.2016.12.007

Huang, S., Yuan, H., Li, W., Liu, X., Zhang, X., Xiang, D., et al. (2021). *Polygonatum sibiricum* polysaccharides protect against MPP-Induced neurotoxicity via the Akt/mTOR and Nrf2 pathways. *Oxid. Med. Cell Longev.* 2021:8843899. doi: 10.1155/2021/8843899

Huang, W. J., Chen, W. W., and Zhang, X. (2016). Huntington's disease: molecular basis of pathology and status of current therapeutic approaches. *Exp. Ther. Med.* 12, 1951–1956. doi: 10.3892/etm.2016.3566

Husemann, J., and Silverstein, S. C. (2001). Expression of scavenger receptor class B, type I, by astrocytes and vascular smooth muscle cells in normal adult mouse and human brain and in Alzheimer's disease brain. *Am. J. Pathol.* 158, 825–832. doi: 10.1016/S0002-9440(10)64030-8

Hwang, Y. H., Jang, S. A., Lee, A., Cho, C. W., Song, Y. R., Hong, H. D., et al. (2020). Polysaccharides isolated from lotus leaves (LLEP) exert anti-osteoporotic effects by inhibiting osteoclastogenesis. *Int. J. Biol. Macromol.* 161, 449–456. doi: 10.1016/j.ijbiomac.2020.06.059

Jenner, P. (2002). Pharmacology of dopamine agonists in the treatment of Parkinson's disease. *Neurology* 58(Suppl. 1), S1–S8. doi: 10.1212/wnl.58.suppl_1.s1

Jiang, M. H., Zhu, L., and Jiang, J. G. (2010). Immunoregulatory actions of polysaccharides from Chinese herbal medicine. *Expert Opin. Ther. Targets* 14, 1367–1402. doi: 10.1517/14728222.2010.531010

Jimenez-Sanchez, M., Licitra, F., Underwood, B. R., and Rubinsztein, D. C. (2017). Huntington's disease: mechanisms of pathogenesis and therapeutic strategies. *Cold Spring Harb. Perspect. Med.* 7:a024240. doi: 10.1101/cshperspect.a024240

Kametani, F., and Hasegawa, M. (2018). Reconsideration of amyloid hypothesis and tau hypothesis in Alzheimer's disease. *Front. Neurosci.* 12:25. doi: 10.3389/fnins.2018.00025

Kang, B., Opatz, T., Landfester, K., and Wurm, F. R. (2015). Carbohydrate nanocarriers in biomedical applications: functionalization and construction. *Chem. Soc. Rev.* 44, 8301–8325. doi: 10.1039/c5cs00092k

Kim, J., Karthivashan, G., Kweon, M. H., Kim, D. H., and Choi, D. K. (2019). The ameliorative effects of the Ethyl acetate extract of Salicornia europaea L. and its bioactive candidate, Irilin B, on LPS-induced microglial inflammation and MPTP-intoxicated PD-like mouse model. *Oxid. Med. Cell Longev.* 2019:6764756. doi: 10.1155/2019/6764756

Kim, J. H., Kim, S., Yoon, I. S., Lee, J. H., Jang, B. J., Jeong, S. M., et al. (2005). Protective effects of ginseng saponins on 3-nitropropionic acid-induced striatal degeneration in rats. *Neuropharmacology* 48, 743–756. doi: 10.1016/j.neuropharm.2004.12.013

Kukreja, L., Kujoth, G. C., Prolla, T. A., Van Leuven, F., and Vassar, R. (2014). Increased mtDNA mutations with aging promotes amyloid accumulation and brain atrophy in the APP/Ld transgenic mouse model of Alzheimer's disease. *Mol. Neurodegener.* 9:16. doi: 10.1186/1750-1326-9-16

Kumar, A., Kumar, V., Singh, K., Kumar, S., Kim, Y. S., Lee, Y. M., et al. (2020). Therapeutic advances for Huntington's disease. *Brain Sci.* 10:43. doi: 10.3390/brainsci10010043

Kwon, M. J., Kim, S., Han, M. H., and Lee, S. B. (2016). Epigenetic changes in neurodegenerative diseases. *Mol. Cells* 39, 783–789. doi: 10.14348/molcells.2016.0233

Lee, S. W., Park, H. J., Im, W., Kim, M., and Hong, S. (2018). Repeated immune activation with low-dose lipopolysaccharide attenuates the severity of Huntington's disease in R6/2 transgenic mice. *Anim. Cells Syst.* 22, 219–226. doi: 10.1080/19768354.2018.1473291

Lee, Y. S., Lai, D. M., Huang, H. J., Lee-Chen, G. J., Chang, C. H., Hsieh-Li, H. M., et al. (2021). Prebiotic lactulose ameliorates the cognitive deficit in Alzheimer's disease mouse model through macroautophagy and chaperone-mediated autophagy pathways. *J. Agric. Food Chem.* 69, 2422–2437. doi: 10.1021/acs.jafc.0c07327

Lesage, S., and Brice, A. (2009). Parkinson's disease: from monogenic forms to genetic susceptibility factors. *Hum. Mol. Genet.* 18, R48–R59. doi: 10.1093/hmg/ddp012

Li, G., Zhou, Y., Yang, W. Y., Zhang, C., Hong, L., and Jia, L. (2021). Inhibitory effects of sulfated polysaccharides from the sea cucumber cucumaria frondosa against Aβ40 aggregation and cytotoxicity. *ACS Chem. Neurosci.* 12, 1854–1859. doi: 10.1021/acschemneuro.1c00223

Li, Q., Li, C., Yang, C., Liu, C., Yu, G., and Guan, H. (2013). Preparation, characterization and antioxidant activities of polymannuronic acid phosphate, H-phosphonate and sulfate. *Int. J. Biol. Macromol.* 62, 281–286. doi: 10.1016/j.ijbiomac.2013.09.012

Li, R., Yin, F., Guo, Y., Ruan, Q., and Zhu, Q. (2018). Angelica polysaccharide protects PC-12 cells from lipopolysaccharide-induced injury via down-regulating microRNA-223. *Biomed. Pharmacother.* 108, 1320–1327. doi: 10.1016/j.biopha.2018.09.147

Li, X., Chen, C., Leng, A., and Qu, J. (2021). Advances in the extraction, purification, structural characteristics and biological activities of Eleutherococcus senticosus polysaccharides: a promising medicinal and edible resource with development value. *Front. Pharmacol.* 12:753007.

Li, Y., Guan, S., Liu, C., Chen, X., Zhu, Y., Xie, Y., et al. (2018). Neuroprotective effects of *Coptis chinensis* Franch polysaccharide on amyloid-beta (Aβ)-induced toxicity in a transgenic *Caenorhabditis* elegans model of Alzheimer's disease (AD). *Int. J. Biol. Macromol.* 113, 991–995. doi: 10.1016/j.ijbiomac.2018.03.035

Lin, Y. R., Guan, Q. Y., Li, L. Y., Tang, Z. M., Zhang, Q., and Zhao, X. H. (2021). In vitro immuno-modulatory potentials of purslane (*Portulaca oleracea* L.) polysaccharides with a chemical selenylation. *Foods* 11:14. doi: 10.3390/foods11010014

Liu, C., Cui, Y., Pi, F., Cheng, Y., Guo, Y., and Qian, H. (2019). Extraction, purification, structural characteristics, biological activities and pharmacological applications of acemannan, a polysaccharide from Aloe vera: a review. *Molecules* 24:1554. doi: 10.3390/molecules24081554

Liu, H., Chen, S., Guo, C., Tang, W., Liu, W., and Liu, Y. (2018). Astragalus polysaccharide protects neurons and stabilizes mitochondrial in a mouse model of Parkinson disease. *Med. Sci. Monit.* 24, 5192–5199. doi: 10.12659/MSM.908021

Liu, J., Liu, W., Lu, Y., Tian, H., Duan, C., Lu, L., et al. (2018). Piperlongumine restores the balance of autophagy and apoptosis by increasing BCL2 phosphorylation in rotenone-induced Parkinson disease models. *Autophagy* 14, 845–861. doi: 10.1080/15548627.2017.1390636

Liu, J., Pu, H., Liu, S., Kan, J., and Jin, C. (2017). Synthesis, characterization, bioactivity and potential application of phenolic acid grafted chitosan: a review. *Carbohydr. Polym.* 174, 999–1017. doi: 10.1016/j.carbpol.2017.07.014

Liu, L., Sha, X. Y., Wu, Y. N., Chen, M. T., and Zhong, J. X. (2020). Lycium barbarum polysaccharides protects retinal ganglion cells against oxidative stress injury. *Neural Regen. Res.* 15, 1526–1531. doi: 10.4103/1673-5374.274349

Liu, R., and Li, X. (2018). Radix Ophiopogonis polysaccharide extracts alleviate MPP(+)-induced PC-12 cell injury through inhibition of Notch signaling pathway. *Int. J. Clin. Exp. Pathol.* 11, 99–109.

Luk, K. C., Kehm, V., Carroll, J., Zhang, B., O'brien, P., Trojanowski, J. Q., et al. (2012). Pathological α-synuclein transmission initiates Parkinson-like neurodegeneration in nontransgenic mice. *Science* 338, 949–953. doi: 10.1126/science.1227157

Luo, T., Wu, J., Kabadi, S. V., Sabirzhanov, B., Guanciale, K., Hanscom, M., et al. (2013). Propofol limits microglial activation after experimental brain trauma through inhibition of nicotinamide adenine dinucleotide phosphate oxidase. *Anesthesiology* 119, 1370–1388. doi: 10.1097/ALN.0000000000000020

Makani, V., Jang, Y. G., Christopher, K., Judy, W., Eckstein, J., Hensley, K., et al. (2016). BBB-permeable, neuroprotective, and neurotrophic polysaccharide, Midi-GAGR. *PLoS One* 11:e0149715. doi: 10.1371/journal.pone.0149715

Mandemakers, W., Morais, V. A., and De Strooper, B. (2007). A cell biological perspective on mitochondrial dysfunction in Parkinson disease and other neurodegenerative diseases. *J. Cell. Sci.* 120(Pt 10), 1707–1716. doi: 10.1242/jcs.03443

Manigandan, V., Nataraj, J., Karthik, R., Manivasagam, T., Saravanan, R., Thenmozhi, A. J., et al. (2019). Low molecular weight sulfated chitosan: neuroprotective effect on rotenone-induced in vitro Parkinson's disease. *Neurotox Res.* 35, 505–515. doi: 10.1007/s12640-018-9978-z

Mantzavinos, V., and Alexiou, A. (2017). Biomarkers for Alzheimer's disease diagnosis. *Curr. Alzheimer Res.* 14, 1149–1154.

Margolis, R. L., and Ross, C. A. (2003). Diagnosis of Huntington disease. *Clin. Chem.* 49, 1726–1732. doi: 10.1373/49.10.1726

Marsh, A. P. (2019). Molecular mechanisms of proteinopathies across neurodegenerative disease: a review. *Neurol. Res. Pract.* 1:35.

Marsh, B. J., and Stenzel-Poore, M. P. (2008). Toll-like receptors: novel pharmacological targets for the treatment of neurological diseases. *Curr. Opin. Pharmacol.* 8, 8–13. doi: 10.1016/j.coph.2007.09.009

Meka, D. P., Müller-Rischart, A. K., Nidadavolu, P., Mohammadi, B., Motori, E., Ponna, S. K., et al. (2015). Parkin cooperates with GDNF/RET signaling to prevent dopaminergic neuron degeneration. *J. Clin. Invest.* 125, 1873–1885. doi: 10.1172/JCI79300

Menozzi, E., Macnaughtan, J., and Schapira, A. H. V. (2021). The gut-brain axis and Parkinson disease: clinical and pathogenetic relevance. *Ann. Med.* 53, 611–625. doi: 10.1080/07853890.2021.1890330

Morris, G. P., Clark, I. A., and Vissel, B. (2014). Inconsistencies and controversies surrounding the amyloid hypothesis of Alzheimer's disease. *Acta Neuropathol. Commun.* 2:135. doi: 10.1186/s40478-014-0135-5

Mozammil Hasnain, S. M., Hasnain, M. S., and Nayak, A. K. (2019). "Chapter 1 - Natural polysaccharides: sources and extraction methodologies," in *Natural Polysaccharides in Drug Delivery and Biomedical Applications*, eds M. S. Hasnain and A. K. Nayak (Cambridge, MA: Academic Press), 1–14. doi: 10.1007/978-1-0716-1398-6_16

Muddapu, V. R., Dharshini, S. A. P., Chakravarthy, V. S., and Gromiha, M. M. (2020). Neurodegenerative diseases – is metabolic deficiency the root cause? *Front. Neurosci.* 14:213. doi: 10.3389/fnins.2020.00213

Murphy, K., Llewellyn, K., Wakser, S., Pontasch, J., Samanich, N., Flemer, M., et al. (2018). Mini-GAGR, an intranasally applied polysaccharide, activates the neuronal Nrf2-mediated antioxidant defense system. *J. Biol. Chem.* 293, 18242–18269. doi: 10.1074/jbc.RA117.001245

Nagatsu, T., and Sawada, M. (2006). Molecular mechanism of the relation of monoamine oxidase B and its inhibitors to Parkinson's disease: possible implications of glial cells. *J. Neural Transm. Suppl.* 71, 53–65. doi: 10.1007/978-3-211-33328-0_7

Neubrech, F., Sauerbier, M., Moll, W., Seegmüller, J., Heider, S., Harhaus, L., et al. (2018). Enhancing the outcome of traumatic sensory nerve lesions of the hand by additional use of a chitosan nerve tube in primary nerve repair: a randomized controlled bicentric trial. *Plastic Reconstruct. Surg.* 142, 415–424. doi: 10.1097/PRS.0000000000004574

Ngwuluka, N., Pillay, V., Du Toit, L. C., Ndesendo, V., Choonara, Y., Modi, G., et al. (2010). Levodopa delivery systems: advancements in delivery of the gold standard. *Expert Opin. Drug Deliv.* 7, 203–224. doi: 10.1517/17425240903483166

Nimmrich, V., and Eckert, A. (2013). Calcium channel blockers and dementia. *Br. J. Pharmacol.* 169, 1203–1210. doi: 10.1111/bph.12240

Nixon, R. A. (2013). The role of autophagy in neurodegenerative disease. *Nat. Med.* 19, 983–997. doi: 10.1038/nm.3232

Odeniyi, M. A., Omoteso, O. A., Adepoju, A. O., and Jaiyeoba, K. T. (2018). Starch nanoparticles in drug delivery: a review. *Polim. Med.* 48, 41–45. doi: 10.17219/pim/99993

Ostadkarampour, M., and Putnins, E. E. (2021). Monoamine oxidase inhibitors: a review of their anti-inflammatory therapeutic potential and mechanisms of action. *Front. Pharmacol.* 12:676239. doi: 10.3389/fphar.2021.676239

Page, M. J., Kell, D. B., and Pretorius, E. (2022). The role of lipopolysaccharide-induced cell signalling in chronic inflammation. *Chronic Stress (Thousand Oaks, Calif.)* 6:24705470221076390. doi: 10.1177/24705470221076390

Pelegrí, C., Duran-Vilaregut, J., Del Valle, J., Crespo-Biel, N., Ferrer, I., Pallàs, M., et al. (2008). Cell cycle activation in striatal neurons from Huntington's disease patients and rats treated with 3-nitropropionic acid. *Int. J. Dev. Neurosci.* 26, 665–671. doi: 10.1016/j.ijdevneu.2008.07.016

Pellegrini, C., Antonioli, L., Colucci, R., Blandizzi, C., and Fornai, M. (2018). Interplay among gut microbiota, intestinal mucosal barrier and enteric

neuro-immune system: a common path to neurodegenerative diseases? *Acta Neuropathol.* 136, 345–361. doi: 10.1007/s00401-018-1856-5

Perez-Pardo, P., Dodiya, H. B., Engen, P. A., Forsyth, C. B., Huschens, A. M., Shaikh, M., et al. (2019). Role of TLR4 in the gut-brain axis in Parkinson's disease: a translational study from men to mice. *Gut* 68, 829–843. doi: 10.1136/gutjnl-2018-316844

Plaza-Zabala, A., Sierra-Torre, V., and Sierra, A. (2017). Autophagy and microglia: novel partners in neurodegeneration and aging. *Int. J. Mol. Sci.* 18:598. doi: 10.3390/ijms18030598

Poewe, W., Seppi, K., Tanner, C. M., Halliday, G. M., Brundin, P., Volkmann, J., et al. (2017). Parkinson disease. *Nat. Rev. Dis. Primers* 3:17013. doi: 10.1038/nrdp.2017.13

Potkin, K. T., and Potkin, S. G. (2018). New directions in therapeutics for Huntington disease. *Future Neurol.* 13, 101–121. doi: 10.2217/fnl-2017-0035

Qin, Y., Xiong, L., Li, M., Liu, J., Wu, H., Qiu, H., et al. (2018). Preparation of bioactive polysaccharide nanoparticles with enhanced radical scavenging activity and antimicrobial activity. *J. Agric. Food Chem.* 66, 4373–4383. doi: 10.1021/acs.jafc.8b00388

Rai, S. N., Singh, P., Varshney, R., Chaturvedi, V. K., Vamanu, E., Singh, M. P., et al. (2021). Promising drug targets and associated therapeutic interventions in Parkinson's disease. *Neural Regen. Res.* 16, 1730–1739. doi: 10.4103/1673-5374.306066

Raj, R., Wairkar, S., Sridhar, V., and Gaud, R. (2018). Pramipexole dihydrochloride loaded chitosan nanoparticles for nose to brain delivery: development, characterization and in vivo anti-Parkinson activity. *Int. J. Biol. Macromol.* 109, 27–35. doi: 10.1016/j.ijbiomac.2017.12.056

Ramakrishnan, S., and Gupta, V. (2021). Trinucleotide repeat disorders. *StatPearls.* Trinucleotide repeat disorders. *Annu. Rev. Neurosci.* 30, 575–621.

Reijonen, S., Putkonen, N., Nørremølle, A., Lindholm, D., and Korhonen, L. (2008). Inhibition of endoplasmic reticulum stress counteracts neuronal cell death and protein aggregation caused by N-terminal mutant huntingtin proteins. *Exp. Cell. Res.* 314, 950–960. doi: 10.1016/j.yexcr.2007.12.025

Reith, W. (2018). [Neurodegenerative diseases]. *Radiologe* 58, 241–258. doi: 10.1007/s00117-018-0363-y

Ren, F., Yang, Y., Wu, K., Zhao, T., Shi, Y., Song, M., et al. (2021). The effects of dandelion polysaccharides on iron metabolism by regulating hepcidin via JAK/STAT signaling pathway. *Oxid. Med. Cell. Longev.* 2021:7184760. doi: 10.1155/2021/7184760

Ren, X., and Butterfield, D. A. (2021). Fidelity of the PINK1 knockout rat to oxidative stress and other characteristics of Parkinson disease. *Free Radic. Biol. Med.* 163, 88–101. doi: 10.1016/j.freeradbiomed.2020.12.004

Ren, Z. L., Wang, C. D., Wang, T., Ding, H., Zhou, M., Yang, N., et al. (2019). Ganoderma lucidum extract ameliorates MPTP-induced parkinsonism and protects dopaminergic neurons from oxidative stress via regulating mitochondrial function, autophagy, and apoptosis. *Acta Pharmacol. Sin.* 40, 441–450. doi: 10.1038/s41401-018-0077-8

Roberts, J. S., Patterson, A. K., and Uhlmann, W. R. (2020). Genetic testing for neurodegenerative diseases: ethical and health communication challenges. *Neurobiol. Dis.* 141:104871. doi: 10.1016/j.nbd.2020.104871

Ross, C. A. (2002). Polyglutamine pathogenesis: emergence of unifying mechanisms for Huntington's disease and related disorders. *Neuron* 35, 819–822. doi: 10.1016/s0896-6273(02)00872-3

Salamon, A., Zádori, D., Szpisjak, L., Klivényi, P., and Vécsei, L. (2022). What is the impact of catechol-O-methyltransferase (COMT) on Parkinson's disease treatment? *Expert Opin. Pharmacother.* 1–6. [Online ahead of print], doi: 10.1080/14656566.2022.2060738

Sarvaiya, J., and Agrawal, Y. K. (2015). Chitosan as a suitable nanocarrier material for anti-Alzheimer drug delivery. *Int. J. Biol. Macromol.* 72, 454–465. doi: 10.1016/j.ijbiomac.2014.08.052

Sha, X., Xu, X., Liao, S., Chen, H., and Rui, W. (2022). Evidence of immunogenic cancer cell death induced by honey-processed Astragalus polysaccharides in vitro and in vivo. *Exp. Cell Res.* 410:112948. doi: 10.1016/j.yexcr.2021.112948

Shaik, L., Kashyap, R., Thotamgari, S. R., Singh, R., and Khanna, S. (2020). Gut-Brain axis and its neuro-psychiatric effects: a narrative review. *Cureus* 12:e11131. doi: 10.7759/cureus.11131

Sharma, K. (2019). Cholinesterase inhibitors as Alzheimer's therapeutics (Review). *Mol. Med. Rep.* 20, 1479–1487. doi: 10.3892/mmr.2019.10374

Shen, W. D., Li, X. Y., Deng, Y. Y., Zha, X. Q., Pan, L. H., Li, Q. M., et al. (2021). Polygonatum cyrtonema Hua polysaccharide exhibits anti-fatigue activity via regulating osteocalcin signaling. *Int. J. Biol. Macromol.* 175, 235–241. doi: 10.1016/j.ijbiomac.2021.01.200

Sheng, Y., Liu, G., Wang, M., Lv, Z., and Du, P. (2017). A selenium polysaccharide from Platycodon grandiflorum rescues PC12 cell death caused by H(2)O(2) via inhibiting oxidative stress. *Int. J. Biol. Macromol.* 104(Pt A), 393–399. doi: 10.1016/j.ijbiomac.2017.06.052

Sheng, Z. H. (2017). The interplay of axonal energy homeostasis and mitochondrial trafficking and anchoring. *Trends Cell Biol.* 27, 403–416. doi: 10.1016/j.tcb.2017.01.005

Shin, S. J., Nam, Y., Park, Y. H., Kim, M. J., Lee, E., Jeon, S. G., et al. (2021). Therapeutic effects of non-saponin fraction with rich polysaccharide from Korean red ginseng on aging and Alzheimer's disease. *Free Radic. Biol. Med.* 164, 233–248. doi: 10.1016/j.freeradbiomed.2020.12.454

Southwell, A. L., and Patterson, P. H. (2011). Gene therapy in mouse models of huntington disease. *Neuroscientist* 17, 153–162. doi: 10.1177/1073858410386236

Spires-Jones, T. L., and Hyman, B. T. (2014). The intersection of amyloid beta and tau at synapses in Alzheimer's disease. *Neuron* 82, 756–771. doi: 10.1016/j.neuron.2014.05.004

Su, C., Li, N., Ren, R., Wang, Y., Su, X., Lu, F., et al. (2021). Progress in the medicinal value, bioactive compounds, and pharmacological activities of *Gynostemma pentaphyllum*. *Molecules* 26:6249. doi: 10.3390/molecules26206249

Sun, Q., Cheng, L., Zeng, X., Zhang, X., Wu, Z., and Weng, P. (2020). The modulatory effect of plant polysaccharides on gut flora and the implication for neurodegenerative diseases from the perspective of the microbiota-gut-brain axis. *Int. J. Biol. Macromol.* 164, 1484–1492. doi: 10.1016/j.ijbiomac.2020.07.208

Sun, X. Z., Liao, Y., Li, W., and Guo, L. M. (2017). Neuroprotective effects of ganoderma lucidum polysaccharides against oxidative stress-induced neuronal apoptosis. *Neural Regen. Res.* 12, 953–958. doi: 10.4103/1673-5374.208590

Tan, Y., Yin, L., Sun, Z., Shao, S., Chen, W., Man, X., et al. (2020). Astragalus polysaccharide exerts anti-Parkinson via activating the PI3K/AKT/mTOR pathway to increase cellular autophagy level in vitro. *Int. J. Biol. Macromol.* 153, 349–356. doi: 10.1016/j.ijbiomac.2020.02.282

Tang, C., Ding, R., Sun, J., Liu, J., Kan, J., and Jin, C. (2019). The impacts of natural polysaccharides on intestinal microbiota and immune responses - a review. *Food Funct.* 10, 2290–2312. doi: 10.1039/c8fo01946k

Tarawneh, R., and Holtzman, D. M. (2012). The clinical problem of symptomatic Alzheimer disease and mild cognitive impairment. *Cold Spring Harb. Perspect. Med.* 2:a006148. doi: 10.1101/cshperspect.a006148

Theocharopoulou, G. (2020). The ubiquitous role of mitochondria in Parkinson and other neurodegenerative diseases. *AIMS Neurosci.* 7, 43–65. doi: 10.3934/Neuroscience.2020004

Tiwari, P. C., and Pal, R. (2017). The potential role of neuroinflammation and transcription factors in Parkinson disease. *Dialogues Clin. Neurosci.* 19, 71–80. doi: 10.31887/DCNS.2017.19.1/rpal

Wahlster, L., Arimon, M., Nasser-Ghodsi, N., Post, K. L., Serrano-Pozo, A., Uemura, K., et al. (2013). Presenilin-1 adopts pathogenic conformation in normal aging and in sporadic Alzheimer's disease. *Acta Neuropathol.* 125, 187–199. doi: 10.1007/s00401-012-1065-6

Walker, F. O. (2007). Huntington's disease. *Lancet* 369, 218–228. doi: 10.1016/S0140-6736(07)60111-1

Wan, L., Zhang, Q., Luo, H., Xu, Z., Huang, S., Yang, F., et al. (2020). Codonopsis pilosula polysaccharide attenuates Aβ toxicity and cognitive defects in APP/PS1 mice. *Aging (Albany NY)* 12, 13422–13436. doi: 10.18632/aging.103445

Wang, F., Liu, Q., Wang, W., Li, X., and Zhang, J. (2016). A polysaccharide isolated from Cynomorium songaricum Rupr. protects PC12 cells against H2O2-induced injury. *Int. J. Biol. Macromol.* 87, 222–228. doi: 10.1016/j.ijbiomac.2016.02.011

Wang, J., Liu, H., Zhang, X., Li, X., Geng, L., Zhang, H., et al. (2017). Sulfated hetero-polysaccharides protect SH-SY5Y cells from H_2O_2-Induced apoptosis by affecting the PI3K/Akt signaling pathway. *Mar. Drugs* 15:110. doi: 10.3390/md15040110

Wang, L., Yao, C., Wu, F., Lin, X., Shen, L., and Feng, Y. (2015). Targeting delivery of Radix Ophiopogonis polysaccharide to ischemic/reperfused rat myocardium

by long-circulating macromolecular and liposomal carriers. *Int. J. Nanomed.* 10, 5729–5737. doi: 10.2147/IJN.S89445

Wang, P.-C., Zhao, S., Yang, B.-Y., Wang, Q.-H., and Kuang, H.-X. (2016). Anti-diabetic polysaccharides from natural sources: a review. *Carbohydrate Polym.* 148, 86–97. doi: 10.1016/j.carbpol.2016.02.060

Wang, Z., Sun, Q., Zhang, H., Wang, J., Fu, Q., Qiao, H., et al. (2021). Insight into antibacterial mechanism of polysaccharides: a review. *LWT* 150:111929.

Wen, L., Sheng, Z., Wang, J., Jiang, Y., and Yang, B. (2022). Structure of water-soluble polysaccharides in spore of Ganoderma lucidum and their anti-inflammatory activity. *Food Chem.* 373(Pt A):131374. doi: 10.1016/j.foodchem.2021.131374

Winslow, B. T., Onysko, M. K., Stob, C. M., and Hazlewood, K. A. (2011). Treatment of Alzheimer disease. *Am. Fam. Physician* 83, 1403–1412.

Wu, J., Lin, C., Chen, X., Pan, N., and Liu, Z. (2021b). Polysaccharides isolated from Bangia fuscopurpurea induce apoptosis and autophagy in human ovarian cancer A2780 cells. *Food Sci. Nutr.* 9, 6707–6719. doi: 10.1002/fsn3.2621

Wu, J., Chen, T., Wan, F., Wang, J., Li, X., Li, W., et al. (2021a). Structural characterization of a polysaccharide from Lycium barbarum and its neuroprotective effect against β-amyloid peptide neurotoxicity. *Int. J. Biol. Macromol.* 176, 352–363. doi: 10.1016/j.ijbiomac.2021.02.016

Wu, J. H., Xu, C., Shan, C. Y., and Tan, R. X. (2006). Antioxidant properties and PC12 cell protective effects of APS-1, a polysaccharide from Aloe vera var. chinensis. *Life Sci.* 78, 622–630. doi: 10.1016/j.lfs.2005.05.097

Xiang, Y., Zhang, J., Li, H., Wang, Q., Xiao, L., Weng, H., et al. (2017). Epimedium polysaccharide alleviates polyglutamine-induced neurotoxicity in *Caenorhabditis* elegans by reducing oxidative stress. *Rejuvenation Res.* 20, 32–41. doi: 10.1089/rej.2016.1830

Xu, M., Yan, T., Fan, K., Wang, M., Qi, Y., Xiao, F., et al. (2019). Polysaccharide of Schisandra Chinensis Fructus ameliorates cognitive decline in a mouse model of Alzheimer's disease. *J. Ethnopharmacol.* 237, 354–365. doi: 10.1016/j.jep.2019.02.046

Xue, Y., Wang, N., Zeng, Z., Huang, J., Xiang, Z., and Guan, Y.-Q. (2020). Neuroprotective effect of chitosan nanoparticle gene delivery system grafted with acteoside (ACT) in Parkinson's disease models. *J. Mater. Sci. Technol.* 43, 197–207.

Yadav, A. K., Mishra, P., and Agrawal, G. P. (2008). An insight on hyaluronic acid in drug targeting and drug delivery. *J. Drug Target* 16, 91–107. doi: 10.1080/10611860802095494

Yan, H., Ma, X., Mi, Z., He, Z., and Rong, P. (2022). Extracellular polysaccharide from *Rhizopus* nigricans inhibits hepatocellular carcinoma via miR-494-3p/TRIM36 axis and cyclin E ubiquitination. *J. Clin. Transl. Hepatol.*

Yan, T., Mao, Q., Zhang, X., Wu, B., Bi, K., He, B., et al. (2021). Schisandra chinensis protects against dopaminergic neuronal oxidative stress, neuroinflammation and apoptosis via the BDNF/Nrf2/NF-κB pathway in 6-OHDA-induced Parkinson's disease mice. *Food Funct.* 12, 4079–4091. doi: 10.1039/d0fo02836c

Zeng, H., Li, P., Zhou, L., and Ding, K. (2020). A novel pectin from Polygala tenuifolia blocks Aβ(42) aggregation and production by enhancing insulin-degradation enzyme and neprilysin. *Int. J. Biol. Macromol.* 161, 35–43. doi: 10.1016/j.ijbiomac.2020.05.212

Zhang, F., Lu, J., Zhang, J.-G., and Xie, J.-X. (2015). Protective effects of a polysaccharide from Spirulina platensis on dopaminergic neurons in an MPTP-induced Parkinson's disease model in C57BL/6J mice. *Neural Regener. Res.* 10, 308–313. doi: 10.4103/1673-5374.152387

Zhang, H., Pan, N., Xiong, S., Zou, S., Li, H., Xiao, L., et al. (2012). Inhibition of polyglutamine-mediated proteotoxicity by Astragalus membranaceus polysaccharide through the DAF-16/FOXO transcription factor in Caenorhabditis elegans. *Biochem. J.* 441, 417–424. doi: 10.1042/BJ20110621

Zhang, H., Wei, W., Zhao, M., Ma, L., Jiang, X., Pei, H., et al. (2021). Interaction between Aβ and Tau in the pathogenesis of Alzheimer's disease. *Int. J. Biol. Sci.* 17, 2181–2192. doi: 10.7150/ijbs.57078

Zhang, J., Shi, R., Li, H., Xiang, Y., Xiao, L., Hu, M., et al. (2016). Antioxidant and neuroprotective effects of Dictyophora indusiata polysaccharide in Caenorhabditis elegans. *J. Ethnopharmacol.* 192, 413–422. doi: 10.1016/j.jep.2016.09.031

Zhang, L., Hao, J., Zheng, Y., Su, R., Liao, Y., Gong, X., et al. (2018). Fucoidan protects dopaminergic neurons by enhancing the mitochondrial function in a rotenone-induced rat model of Parkinson's disease. *Aging Dis.* 9, 590–604. doi: 10.14336/AD.2017.0831

Zhang, Q., Xia, Y., Luo, H., Huang, S., Wang, Y., Shentu, Y., et al. (2018). *Codonopsis pilosula* polysaccharide attenuates tau hyperphosphorylation and cognitive impairments in hTau infected mice. *Front. Mol. Neurosci.* 11:437. doi: 10.3389/fnmol.2018.00437

Zhang, R., Xu, S., Cai, Y., Zhou, M., Zuo, X., and Chan, P. (2011). Ganoderma lucidum protects dopaminergic neuron degeneration through inhibition of microglial activation. *Evid. Based Complement. Alternat. Med.* 2011:156810. doi: 10.1093/ecam/nep075

Zhang, S., Pei, R., Li, M., Su, H., Sun, H., Ding, Y., et al. (2022). Cocktail polysaccharides isolated from *Ecklonia kurome* against the SARS-CoV-2 infection. *Carbohydr. Polym.* 275:118779. doi: 10.1016/j.carbpol.2021.118779

Zhang, Y., Yang, X., Jin, G., Yang, X., and Zhang, Y. (2016). Polysaccharides from Pleurotus ostreatus alleviate cognitive impairment in a rat model of Alzheimer's disease. *Int. J. Biol. Macromol.* 92, 935–941. doi: 10.1016/j.ijbiomac.2016.08.008

Zhang, Z., Liu, H., Yu, B., Tao, H., Li, J., Wu, Z., et al. (2020b). Lycium barbarum polysaccharide attenuates myocardial injury in high-fat diet-fed mice through manipulating the gut microbiome and fecal metabolome. *Food Res. Int.* 138(Pt B):109778. doi: 10.1016/j.foodres.2020.109778

Zhang, Z., Wang, X., Pan, Y., Wang, G., and Mao, G. (2020c). The degraded polysaccharide from Pyropia haitanensis represses amyloid beta peptide-induced neurotoxicity and memory in vivo. *Int. J. Biol. Macromol.* 146, 725–729. doi: 10.1016/j.ijbiomac.2019.09.243

Zhang, S., Li, L., Hu, J., Ma, P., and Zhu, H. (2020a). Polysaccharide of *Taxus chinensis* var. mairei Cheng et L.K.Fu attenuates neurotoxicity and cognitive dysfunction in mice with Alzheimer's disease. *Pharm. Biol.* 58, 959–968. doi: 10.1080/13880209.2020.1817102

Zhao, Y., Yan, B., Wang, Z., Li, M., and Zhao, W. (2020). Natural polysaccharides with immunomodulatory activities. *Mini Rev. Med. Chem.* 20, 96–106. doi: 10.2174/1389557519666190913151632

Zhou, C., Sun, X., Hu, Y., Song, J., Dong, S., Kong, D., et al. (2019). Genomic deletion of TLR2 induces aggravated white matter damage and deteriorated neurobehavioral functions in mouse models of Alzheimer's disease. *Aging (Albany NY)* 11, 7257–7273. doi: 10.18632/aging.102260

Zhu, X., Raina, A. K., Perry, G., and Smith, M. A. (2006). Apoptosis in Alzheimer disease: a mathematical improbability. *Curr. Alzheimer Res.* 3, 393–396. doi: 10.2174/156720506778249470

Zhu, Y., Yu, X., Ge, Q., Li, J., Wang, D., Wei, Y., et al. (2020). Antioxidant and anti-aging activities of polysaccharides from *Cordyceps* cicadae. *Int. J. Biol. Macromol.* 157, 394–400. doi: 10.1016/j.ijbiomac.2020.04.163

Zou, Q., Zhang, X., Liu, X., Li, Y., Tan, Q., Dan, Q., et al. (2020). Ficus carica polysaccharide attenuates DSS-induced ulcerative colitis in C57BL/6 mice. *Food Funct.* 11, 6666–6679. doi: 10.1039/d0fo01162b

Conflict of Interest: The authors declare that the research was conducted in the absence of any commercial or financial relationships that could be construed as a potential conflict of interest.

Publisher's Note: All claims expressed in this article are solely those of the authors and do not necessarily represent those of their affiliated organizations, or those of the publisher, the editors and the reviewers. Any product that may be evaluated in this article, or claim that may be made by its manufacturer, is not guaranteed or endorsed by the publisher.

frontiers | Frontiers in Aging Neuroscience

ORIGINAL RESEARCH
published: 04 July 2022
doi: 10.3389/fnagi.2022.905115

Growth Differentiation Factor 15 Regulates Oxidative Stress-Dependent Ferroptosis Post Spinal Cord Injury by Stabilizing the p62-Keap1-Nrf2 Signaling Pathway

Mingjie Xia[1†], Qinyang Zhang[2,3†], Yanan Zhang[2,3†], Rulin Li[2,3], Tianyu Zhao[2,3], Lingxia Chen[4], Qiangxian Liu[1], Shengnai Zheng[1], Haijun Li[3,5], Zhanyang Qian[6,7*] and Lei Yang[3,5,8*]*

[1] Department of Orthopedics, Nanjing First Hospital, Nanjing Medical University, Nanjing, China, [2] Postgraduate School, Dalian Medical University, Dalian, China, [3] Department of Orthopedics, Taizhou People's Hospital, Nanjing Medical University, Taizhou, China, [4] Department of Cardiology, Nanjing University of Chinese Medicine, Nanjing, China, [5] Taizhou Clinical Medical School of Nanjing Medical University, Taizhou, China, [6] Department of Orthopedics, Zhongda Hospital of Southeast University, Nanjing, China, [7] School of Medicine, Southeast University, Nanjing, China, [8] School of Biomedical Engineering and Informatics, Nanjing Medical University, Nanjing, China

Background: Spinal cord injury (SCI) is a severe traumatic disorder of the central nervous system (CNS) that causes irreversible damage to the nervous tissue. The consequent hemorrhage contributed by trauma induces neuronal ferroptosis post SCI, which is an important death mode to mediate neuronal loss. Growth differentiation factor 15 (GDF15) is a cytokine that regulates cell proliferation, differentiation, and death. However, the specific role of GDF15 in neuronal ferroptosis post SCI remains unknown.

Materials and Methods: Neuronal ferroptosis *in vitro* was measured by detection of lipid peroxidation, glutathione, iron content, and reactive oxidative stress. *In vivo*, western blotting and immunofluorescence (IF) staining was utilized to measure ferroptosis post SCI. IF staining, TUNEL staining, hematoxylin-eosin staining, and Nissl staining were used to measure neurological damage. Finally, locomotor function recovery was analyzed using the Basso Mouse Scale and Louisville Swim Scale.

Results: GDF15 was significantly increased in neuronal ferroptosis and silencing GDF15 aggravated ferroptosis both *in vitro* and *in vivo*. Besides, GDF15-mediated inhibition of neuronal ferroptosis is through p62-dependent Keap1-Nrf2 pathway. In SCI mice, knockdown of GDF15 significantly exacerbated neuronal death, interfered with axon regeneration and remyelination, aggravated ferroptosis-mediated neuroinflammation, and restrained locomotor recovery.

Conclusion: GDF15 effectively alleviated neuronal ferroptosis post SCI *via* the p62-Keap1-Nrf2 signaling pathway and promoted locomotor recovery of SCI mice, which is suggested as a potential target on SCI pathogenesis and treatment.

Keywords: spinal cord injury, GDF15, oxidative stress, ferroptosis, p62-Keap1-Nrf2 pathway

OPEN ACCESS

Edited by:
Min Tang,
Jiangsu University, China

Reviewed by:
Alamgeer,
University of the Punjab, Pakistan
Francesco Paolo Busardò,
Marche Polytechnic University, Italy
Weinan Zhou,
University of Illinois at Urbana-Champaign, United States

***Correspondence:**
Haijun Li
13901436563@139.com
Zhanyang Qian
spineqzy@126.com
Lei Yang
leiyang@njmu.edu.cn

† These authors have contributed equally to this work

Specialty section:
This article was submitted to Neurocognitive Aging and Behavior, a section of the journal Frontiers in Aging Neuroscience

Received: *26 March 2022*
Accepted: *31 May 2022*
Published: *04 July 2022*

Citation:
Xia M, Zhang Q, Zhang Y, Li R, Zhao T, Chen L, Liu Q, Zheng S, Li H, Qian Z and Yang L (2022) Growth Differentiation Factor 15 Regulates Oxidative Stress-Dependent Ferroptosis Post Spinal Cord Injury by Stabilizing the p62-Keap1-Nrf2 Signaling Pathway. Front. Aging Neurosci. 14:905115. doi: 10.3389/fnagi.2022.905115

INTRODUCTION

Spinal cord injury (SCI) is an extremely serious traumatic disease leading to high rates of mortality and disability (Ahuja et al., 2017; Rong et al., 2021b). Following trauma, the disruption of microvessels causes erythrocyte leakage, which produces excess iron (Silva et al., 2014; Yu et al., 2022). The latter insults neurons, contributing to the intracellular iron metabolism disorder and the generation of reactive oxygen species (ROS), which destroy cellular functions and lead to ferroptosis (Zhang et al., 2022). Consequently, a large amount of neuronal loss caused by ferroptosis affects motor and sensory function post SCI (Huang et al., 2020; Feng et al., 2021). However, the intact mechanism of neuronal ferroptosis after SCI remains elusive.

Ferroptosis is an iron-dependent type of programmed cell death that was put forward by Dixon in 2012 (Dixon et al., 2012; Yang and Stockwell, 2016), of which the nature is oxidative damage, accumulation of iron-stimulated ROS, and lipid peroxidation (Mou et al., 2019). Ferroptosis is involved in the pathogenesis of multiple central nervous system (CNS) diseases like Alzheimer's disease and subarachnoid hemorrhage (Lane et al., 2021; Qu et al., 2021). Interestingly, ferroptosis also plays an important role in mouse models of SCI, and inhibition of ferroptosis attenuates damage to nervous tissue and promotes neuronal functional recovery (Li et al., 2017; Zille et al., 2017; Chen et al., 2020).

Growth and differentiation factor 15 (GDF15), a cytokine of the transforming growth factor-β (TGF-β) superfamily, is associated with various pathophysiological processes (Emmerson et al., 2018; Wang et al., 2021). GDF15 plays a multifunctional role in proliferation, apoptosis, aging, inflammatory response, and malignancy (Luan et al., 2019; Tarfiei et al., 2019; Borner et al., 2020). In addition, evidence demonstrated that GDF15 was related to the level of hepcidin, which could degrade iron transporter ferroportin (Jiang et al., 2014). Although GDF15 has been investigated in various diseases, whether it has an impact on regulating the pathological process of oxidative stress-dependent neuronal ferroptosis after SCI remains elusive.

In this study, we found that GDF15 was significantly increased in neuronal ferroptosis both *in vitro* and *in vivo* and that silencing GDF15 aggravated neuronal ferroptosis. Furthermore, we first demonstrated that GDF15 inhibits oxidative stress-dependent ferroptosis in neurons post SCI through the p62-Keap1-Nrf2 signaling pathway and alleviates neurological damage, which consequently promotes locomotor function recovery in SCI mice. Therefore, GDF15 is suggested as a potential target on regulating neuronal ferroptosis, and our findings may provide a new insight into SCI pathogenesis and treatment.

MATERIALS AND METHODS

Extraction and Culture of Primary Neurons

The primary neurons were extracted from the cerebral cortex of fetal mice according to a previous study (Pu et al., 2020). Briefly, an 18-day pregnant mouse was anesthetized and a cesarean was performed, then its fetal mice were sacrificed in 75% ethanol. The cerebral cortex was removed from the fetal mice, digested with 2 mg/ml papainase (Sigma-Aldrich, St. Louis, MO, United States) dissolved in Dulbecco's modified Eagle medium (DMEM; KeyGEN, Nanjing, China) for 30 min, then the mixed cell group suspended in DMEM supplemented 10% fetal bovine serum (FBS; Gibco, Grand Island, NY, United States) were seeded in 6-well plates (Corning, NY, United States). After 4 h culture, the neurons were cultured with the neurobasal medium (Gibco) supplemented 1% glutamine and B27 (Gibco). Then the primary neurons were treated with Hemin (100 μM, MedChemExpresss, Weehawken, NJ, United States) for 24 h.

Spinal Cord Injury Model

Total of 50 C57BL/6J adult mice (males, average weight of 20 g, 8 weeks of age) were acquired from Charles River (Beijing, China). All mice were given free food and water and housed at 50% humidity as well as 22°C ± 1°C temperature with a 12 h/12 h light-dark cycle. The operation of SCI was the same as our previous study (Jiang et al., 2021). Our animal protocol was approved by the Institutional Animal Care and Use Committee of Southeast University (Approval No.: 20210302042). In brief, ketamine (80 mg/kg) was utilized to anesthetize mice before the skin was prepared for disinfection, and then the back skin was incised to expose the lamina at T10. Finally, a moderate contusion (5 g × 5 cm) was created by an impactor (RWD, Shenzhen, China). Spinal cord hemorrhage, hindlimb extension, and delayed paralysis suggest successful modeling. Only laminectomy was performed in the Sham group.

Analysis of Cell Viability

Cell viability was assessed by Cell Counting Kit-8 (CCK-8) assay (Biosharp, Hefei, China). Primary neurons were treated with different concentrations of Hemin for 24 h and CCK-8 (10 μl) was added in neurons for a 1 h incubation at 37°C. The absorbance was detected by a microplate reader (BioTek Instruments, Inc., Winooski, VT, United States) at 450 nm.

Regulation of Growth Differentiation Factor 15 and p62 Expression

The short hairpin (sh) RNAs targeting GDF15 and p62 (BIOG, Changzhou, China) for knockdown were loaded in plasmids, respectively, and transfected into primary neurons by RFect Plasmid Transfection Reagent (BIOG) for 24 h. Recombinant GDF15 (rGDF5; ab202199, Abcam, Cambridge, MA, United States) was used to provide exogenetic expression of GDF15 *in vitro* (Li H. et al., 2021). The shRNA-GDF15 loaded in adeno-associated virus (AAV) vectors was obtained from Genechem CO., LTD (Shanghai, China). The AAV containing shRNA-GDF15 were delivered into mice at 1 week before SCI modeling *via* the intracortical injections (Lewandowski and Steward, 2014). Briefly, the scalp was clipped and a small piece of skull was removed after anesthesia. Then, 1 μl of AAVshRNA-GDF15 (10^8 genome copies/ml) was injected 0.8 mm underneath the brain surface at 1 mm anterior to bregma and 2 mm lateral to the midline.

Real-Time Quantitative Reverse-Transcription PCR

A TRIzol reagent (YiFeiXue Biotechnology, Nanjing, China) was employed to extract RNA of spinal cords according to the manufacturer's guidance. After the RNA concentration was measured, a reverse transcription kit and a qPCR Kit (YiFeiXue Biotechnology) were utilized to carry out qRT-PCR in the Roche LightCycler 480 (Roche, Basel, Switzerland). The primer sequences of GDF15, p62, and GAPDH were as follows: GDF15: forward: CTGGCAATGCCTGAACAACG; reverse: GGTCGGGACTTGGTTCTGAG; p62: forward: GAGGCAC CCCGAAACATGG; reverse: ACTTATAGCGAGTTCCCACCA; GAPDH: forward: TGACCTCAACTACATGGTCTACA; reverse: CTTCCCATTCTCGGCCTTG.

Western Blotting

Total protein from the primary neurons and the spinal cords was extracted using a Total Protein Extraction Kit (Keygen). The concentrations of proteins were determined by Enhanced BCA Protein Assay Kit (Beyotime, Shanghai, China). Total of 60 μg proteins in each group were used for WB analysis. The main primary and secondary antibodies used in WB are as follows: anti-GDF15 (1:1,000, 32005, Singalway Antibody, CollegePark, MD, United States), anti-ACSL4 (1:1,000, ab155282, Abcam), anti-FTH-1 (1:1,000, 32180, Singalway Antibody), anti-GPX4 (1:1,000, ab125066, Abcam), anti-p62 (1:10,000, ab109012, Abcam), anti-Keap1 (1:1,000, 41626, Singalway Antibody), anti-Nrf2 (1:1,000, 66504, Proteintech, Rosemount, IL, United States), anti-HO-1 (1:1,000, 86806, Cell Signaling Technology, Boston, MA, United States), anti-GAPDH (1:10,000, HRP-60004, Proteintech), anti-β-Tubulin (1:10,000, HRP-66240, Proteintech), and HRP Goat-anti-Rabbit secondary antibody (1:10,000, YFSA02, YiFeiXue Biotechnology). The bands were captured using a Gel Document System (SYNGENE, Cambridge, United Kingdom), and the protein density was then analyzed using the ImageJ software (National Institutes of Health, Bethesda, MD, United States).

Lipid Peroxidation, Glutathione, and Iron Content Detection

MDA and 4-HNE, the main products of lipid peroxidation, were measured by their detection kits (S0131M, Beyotime, and ab238538, Abcam) (Rong et al., 2021a). Briefly, for MDA detection, the samples were mixed with the working solution pre-prepared, then heated at 100°C for 15 min and cooled to room temperature. The absorbance at 532 nm was measured under a microplate reader (BioTek). For 4-HNE detection, after adding 50 μl of the diluted anti-4-HNE antibody and 100 μl diluted secondary antibody to samples, respectively, and incubating for 1 h, we washed the mixture and stopped the reaction. The absorbance at 450 nm was detected on a microplate reader (BioTek). The relative GSH level was tested by the GSH assay kit (S0053, Beyotime). Analogously, the sample was mixed with the GSH working solution, and the absorbance at 405 nm was measured on a microplate reader (BioTek). The relative Fe^{2+} concentration was detected by an iron assay kit (ab83366, Abcam). For iron detection, 5 μl of assay buffer was added to each sample and then incubated at 37°C for 30 min, followed by adding 100 μl iron probe to the mixture and incubated at 37°C for 60 min in the dark. Finally, the absorbance at 593 nm was measured on a microplate reader (BioTek).

Detection of Reactive Oxygen Species

DCFH-DA (YFX0707, YiFeiXue Biotechnology) was diluted with serum-free medium to reach the final concentration of 10 μmol/L. The cell culture medium was replaced by the DCFH-DA solution, followed by a 20 min incubation at 37°C. Washed three times by serum-free medium, the neurons were collected and resuspended by PBS for flow cytometry (FACSVerse 8, BD).

Immunofluorescence Staining

Neurons and paraffin sections of cords were incubated with primary antibodies overnight at 4°C after blocking with immunol staining blocking buffer (Beyotime) for 1 h, followed by incubation with fluorescent secondary antibodies in the dark for 1 h. The antibodies used were as follows: anti-GDF15 (1:100, 32005, Singalway Antibody), anti-ACSL4 (1:100, ab155282, Abcam), anti-p62 (1:1,000, ab109012, Abcam), anti-Nrf2 (1:100, 66504, Proteintech), anti-GPX4 (1:100, ab125066, Abcam), anti-NeuN (1:100, ab177487; Abcam), anti-IBA-1 (1:500, ab178847; Abcam), anti-GFAP (1:600, 3670; Cell Signaling Technology), anti-NF200 (1:200, ab82259; Abcam), anti-MBP (1:600, ab7349; Abcam), 488 AffiniPure Fab Fragment Goat-anti-Rabbit secondary antibody (1:500, 111-547-003, Jackson ImmunoResearch, PA, United States), and 594 AffiniPure Fab Fragment Goat Anti-Rabbit secondary antibody (1:500, 111-587-003, Jackson ImmunoResearch). After counterstaining with diaminobenzidine (DAPI), the samples were observed under a fluorescent microscope (Leica, Oskar, Germany).

TUNEL Staining

The death of neurons in injured spinal cords was detected by a TUNEL Staining Kit (Servicebio, Wuhan, China). Briefly, after treating with 0.1% TritonX-100 (Biosharp) for 20 min, the paraffin slices of spinal cords were incubated with the mixture including terminal deoxynucleotidyl transferase (TDT, Servicebio) enzyme, deoxyuridine triphosphates (dUTP, Servicebio), and buffer at a ratio of 1:5:50 at 37°C for 2 h. The sections were counterstained with DAPI and observed under a fluorescence microscope (Leica).

Hematoxylin-Eosin Staining

The integrity of nervous tissue was assessed with an H&E Staining Kit (Servicebio). Briefly, after paraffin sections were dewaxed, H&E was used to stain nuclei and cytoplasm.

Nissl Staining

A Nissl Staining Reagent (Servicebio) was utilized to measure the number of neurons in spinal cords at 7 or 28 days post injury (dpi). Briefly, Toluidine Blue was used to stain the sections for 2–5 min, and 1% glacial acetic acid was added. Then, the sections were washed, mounted with neutral balm, and observed under a microscope (Leica).

Behavioral Assessment

The Basso Mouse Scale (BMS) and Louisville Swim Scale (LSS) were used to assess the locomotor function of mice hindlimbs post SCI (Basso et al., 2006; Smith et al., 2006). BMS scores ranged from 0 (no ankle movement) to 9 (normal movement). LSS had 15 gradings to assess forelimb dependency and hindlimb function (Kong et al., 2020). All the mice in the study were assessed in an open field or a water tank at 1, 3, 7, 14, 21, and 28 dpi.

Statistical Analysis

The experimental data were exhibited as the mean ± standard deviation (SD) values and analyzed using the Prism software, version 8.3 (GraphPad, San Diego, CA, United States). Comparisons between two groups were analyzed by unpaired *t*-tests, and among more than two groups using one-way or two-way ANOVAs followed by Tukey's *post hoc* test. P-value < 0.05 were regarded as significance.

RESULTS

Growth Differentiation Factor 15 Was Increased in Spinal Cord Injury and Neuronal Ferroptosis

Ferroptosis inducer Hemin was used to treat with primary neurons for 24 h. The result showed that Hemin obviously decreased the cell viability (**Figure 1A**). Besides, qRT-PCR and WB analysis revealed that both the mRNA and protein expressions of GDF15 were increasing within a week post SCI and peaked at 7 dpi (**Figures 1B–D**). To further determine the expression of GDF15 in neuronal ferroptosis, we treated the neurons with Hemin within 24 h *in vitro*, finding that GDF15 significantly upgraded after Hemin treatment (**Figures 1E,F**). In addition, the ferroptosis-related protein ACSL4 was increased but the other two markers FTH1 and GPX4 decreased after Hemin treatment (**Figures 1G–I**). Then, we measured the lipid peroxidation, GSH, and iron content in Hemin-treated neurons medium. The results exhibited that the expression of GSH markedly reduced, which linked to the obviously increased Fe^{2+} content as well as the lipid peroxidation products MDA and 4-HNE after Hemin treatment, indicating that neuronal ferroptosis was effectively stimulated (**Figures 1J–M**).

Growth Differentiation Factor 15 Effectively Alleviated Oxidative Stress-Dependent Neuronal Ferroptosis *in vitro*

To research the function of GDF15 in oxidative stress-induced neuronal ferroptosis, we transfected neurons with plasmids loaded with sh-GDF15 to knock down GDF15 expression (KD-GDF15). The mRNA and protein levels of GDF15 were significantly decreased after knockdown compared to control group (**Figures 2A–C**). WB results revealed that the expression of ACSL4 increased more, but FTH1 and GPX4 decreased more in KD-GDF15 neurons compared to the untreated neurons after Hemin insult. However, the above results were relieved by rGDF15 supplement (**Figures 2D–F**). IF staining also showed that rGDF15 increased the expression of ACSL4 inhibited by KD-GDF15 (**Figure 2G**). Additionally, GSH level was significantly reduced, but the expression of MDA, 4-HNE, and Fe^{2+} were increased markedly after KD-GDF15 treatment compared with Hemin group, whereas the results were reversed by rGDF15 (**Figures 2H–K**). The detection of ROS also confirmed the above results (**Figures 2L,M**).

Growth Differentiation Factor 15 Mitigates Hemin-Induced Reactive Oxygen Species Production and Ferroptosis in Neurons Through the p62-Keap1-Nrf2 Signaling Pathway

The P62-Keap1-Nrf2 signaling axis has been reported to be associated with ferroptosis (Ren et al., 2021). We next investigated whether GDF15 inhibited ferroptosis by regulating the p62-Keap1-Nrf2 signaling pathway. We transfected sh-p62 to hemin-treated neurons to silence p62 expression, and both the mRNA and protein levels of p62 were markedly decreased compared with control group (**Figures 3A,B**). In agreement with previous studies, our results showed that the p62-Keap1-Nrf2 signaling axis was activated with ferroptosis occurring after Hemin treatment. In addition, rGDF15 further increased the expression of p62, followed by the decrease of Keap1 and increase of Nrf2 and HO-1, which indicated that GDF15 promoted the activation of the p62-Keap1-Nrf2 signaling pathway and alleviated oxidative stress in neuronal ferroptosis (**Figures 3C–F**). Besides, in consistent with previous findings, rGDF15 reduced the level of ferroptosis; however, ferroptosis level was increased again when p62 was knocked down, which showed that GDF15-mediated inhibition of ferroptosis was p62-dependent (**Figures 3G–I**). We next used IF to detect the expression of p62 and Nrf2 in neuronal ferroptosis. The results displayed that rGDF15 increased the protein level of p62 and Nrf2 compared to Hemin-treated group, which was in accordance with WB results (**Figure 3J**). In addition, the ROS level was prominently decreased by treatment with rGDF15, whereas that reversely increased after the knockdown of p62 (**Figures 3K,L**).

Silencing Growth Differentiation Factor 15 Aggravated Ferroptosis After Spinal Cord Injury *via* Destabilizing p62 and Nrf2 Level

We next researched the role of GDF15 in SCI mice. The AAV containing shRNA-GDF15 was injected to mice, and the mRNA expression of GDF15 was significantly decreased compared to Sham group (**Figure 4A**). At 1 dpi, WB revealed that SCI obviously increased the protein expression of ACSL4 and decreased the protein expression of GPX4 and FTH1 when compared with the Sham group. Notably, KD-GDF15 further deteriorated ferroptosis (**Figures 4B–E**). Furthermore, the p62-Keap1-Nrf2 signaling pathway was activated after SCI. However, KD-GDF15 significantly

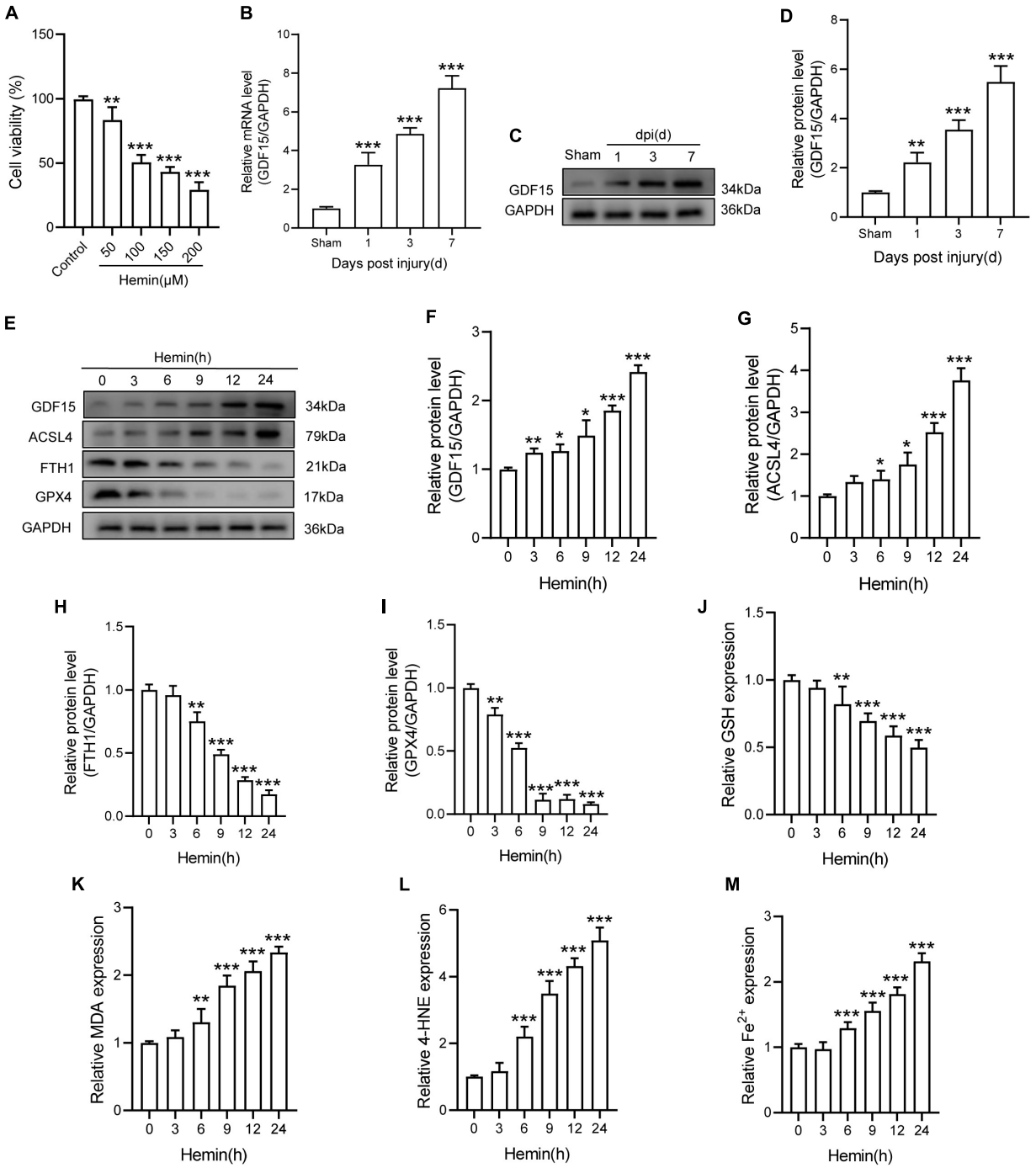

FIGURE 1 | GDF15 was increased in SCI and neuronal ferroptosis. **(A)** Cell viability was detected by CCK-8 ($n = 6$). **(B)** Relative mRNA level of GDF15 in the spinal cord within a week post-injury ($n = 6$). **(C)** Western blotting of GDF15 protein levels in the spinal cord within a week post-injury ($n = 6$). **(D)** Bar graph showing a quantitative analysis of GDF15 expression ($n = 6$). **(E)** Western blotting of GDF15 and ferroptosis-associated proteins including ACSL4, FTH1, and GPX4 in Hemin-stimulated primary neurons within 24 h ($n = 3$). GAPDH was used as the control. **(F–I)** Bar graph showing quantitative analysis of GDF15, ACSL4, FTH1, and GPX4 ($n = 3$). **(J–M)** The values of GSH, MDA, 4-HNE, and Fe^{2+} concentrations were determined; $n = 6$. The error bars represent the SD. $^{*}p < 0.05$ vs. control group by one-way ANOVA followed by Tukey's *post hoc* analysis ($^{*}p < 0.05$, $^{**}p < 0.01$, and $^{***}p < 0.001$). Sham: Only laminectomy was performed.

decreased the protein level of p62, Nrf2, and HO-1 but increased the protein level of Keap1, which indicated that SCI-induced ferroptosis was deteriorative (**Figures 4F–K**). We next used IF staining of GPX4 and NeuN to detect neuronal ferroptosis after SCI. The results displayed that the expression of GPX4 in neurons was reduced after SCI, and silencing

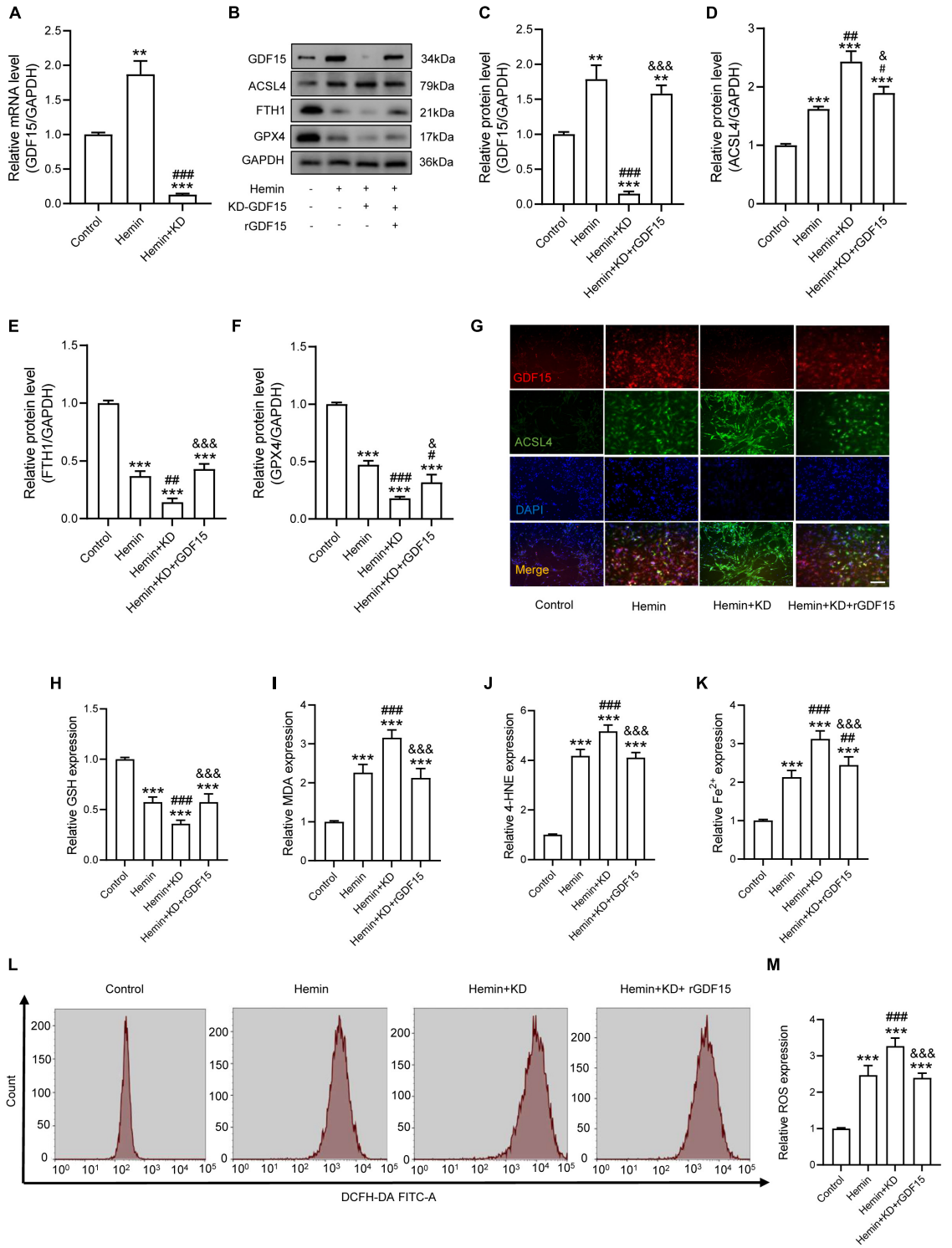

FIGURE 2 | GDF15 effectively alleviated oxidative stress-dependent neuronal ferroptosis *in vitro*. **(A)** Relative mRNA level of GDF15 after knockdown ($n = 6$). **(B)** Western blotting performed for GDF15 and ferroptosis-associated proteins including ACSL4, FTH1, and GPX4 in Hemin-activated primary neurons after transfection of KD-GDF15 or adding rGDF15 ($n = 3$). GAPDH was used as the control. **(C–F)** Bar graph showing quantitative analysis of GDF15, ACSL4, FTH1, and GPX4 ($n = 3$). **(G)** Representative immunofluorescence labeling images for GDF15 (red) and ACSL4 (green) in Hemin-activated primary neurons after transfection of KD-GDF15 or adding rGDF15 (Scale bar = 50 μm). **(H–K)** The values of GSH, MDA, 4-HNE, and Fe^{2+} concentrations were determined ($n = 6$). **(L)** The value of ROS was determined ($n = 6$). **(M)** Bar graph showing quantitative analysis of ROS expression ($n = 6$). The error bars represent the SD. $^{**}p < 0.01$, $^{***}p < 0.001$, vs. control group; $^{\#}p < 0.05$, $^{\#\#}p < 0.01$, $^{\#\#\#}p < 0.001$, vs. Hemin group; $^{\&}p < 0.05$, $^{\&\&\&}p < 0.001$, vs. Hemin + KD group by one-way ANOVA followed by Tukey's *post hoc* analysis.

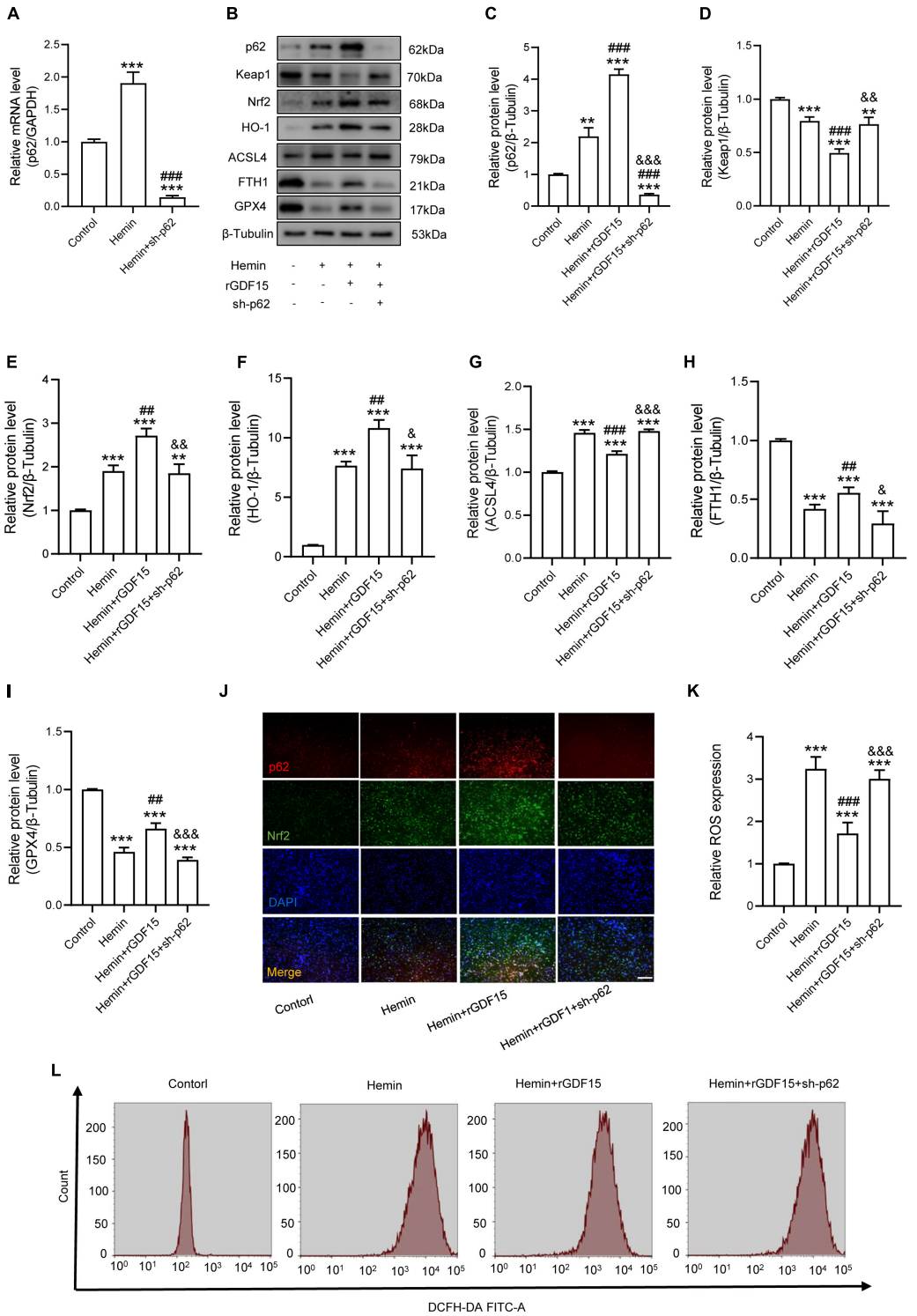

FIGURE 3 | GDF15 mitigates Hemin-induced ROS production and ferroptosis in neurons through the p62-Keap1-Nrf2 signaling pathway. **(A)** Relative mRNA level of p62 after knockdown (n = 6). **(B)** Western blotting performed for p62, Keap1, Nrf2, HO-1, ACSL4, FTH1, and GPX4 in Hemin-activated primary neurons after adding rGDF15 or transfection of sh-p62 (n = 3). β-Tubulin was used as the control. **(C–I)** Bar graph showing quantitative analysis of p62, Keap1, Nrf2, HO-1, ACSL4, FTH1, and GPX4 (n = 3). **(J)** Representative immunofluorescence labeling images for p62 (red) and Nrf2 (green) in Hemin-activated primary neurons after adding rGDF15 or transfection of sh-p62 (Scale bar = 200 μm). **(K)** Bar graph showing quantitative analysis of ROS expression (n = 6). **(L)** The value of ROS was determined (n = 6). The error bars represent the SD. $^{**}p < 0.01$, $^{***}p < 0.001$, vs. control group; $^{\#\#}p < 0.01$, $^{\#\#\#}p < 0.001$, vs. Hemin group; $^{\&}p < 0.05$, $^{\&\&}p < 0.01$, $^{\&\&\&}p < 0.001$, vs. Hemin + rGDF15 group by one-way ANOVA followed by Tukey's *post hoc* analysis.

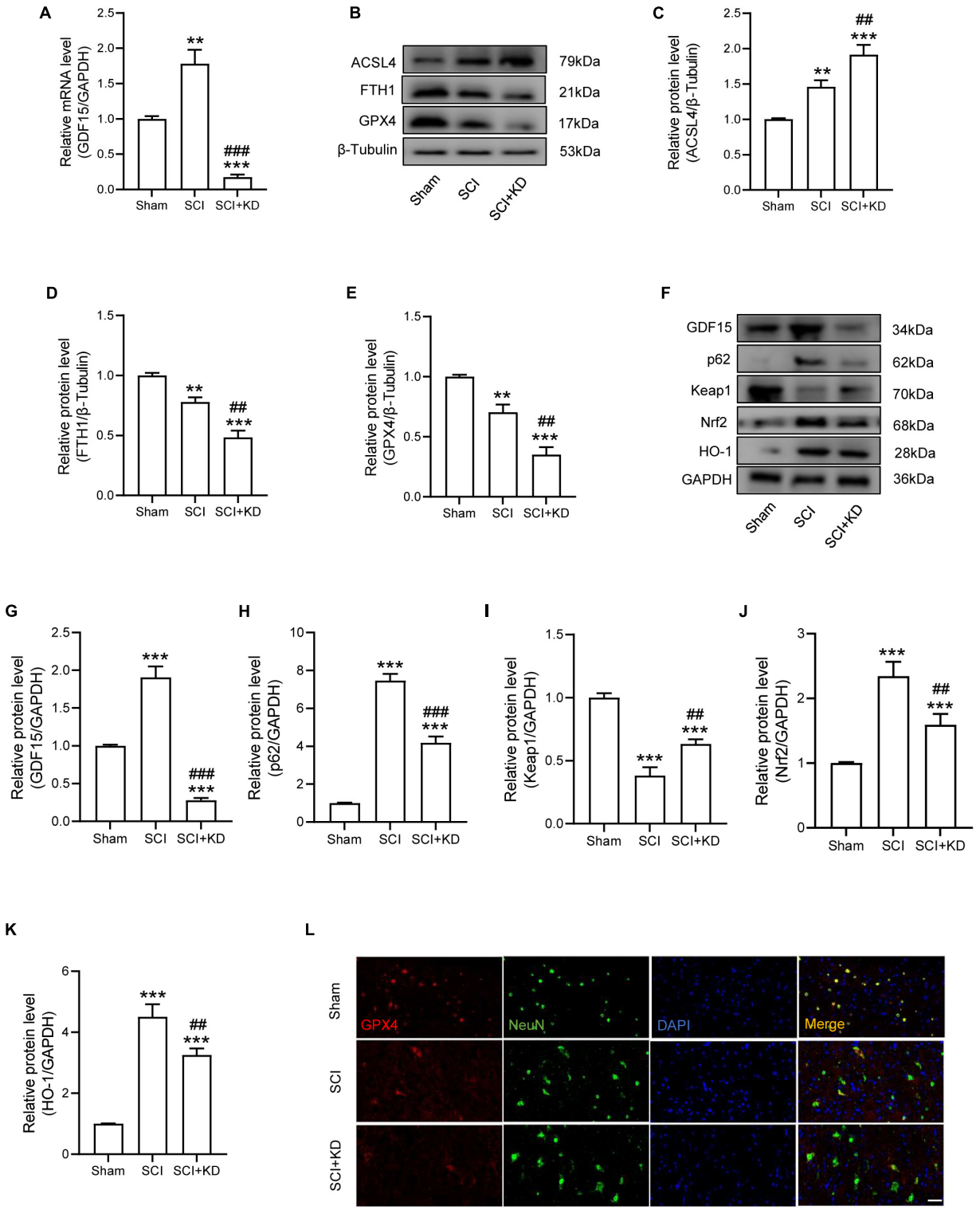

FIGURE 4 | Silencing GDF15 aggravated ferroptosis after SCI *via* destabilizing p62 and Nrf2 level. **(A)** Relative mRNA level of GDF15 in SCI mice after knockdown ($n = 6$). **(B)** Western blotting of ACSL4, FTH1, and GPX4 protein levels at 1 dpi in Sham, SCI, and SCI + KD mice ($n = 3$). **(C–E)** Bar graph showing a quantitative analysis of ACSL4, FTH1, and GPX4 ($n = 3$). **(F)** Western blotting performed for GDF15, p62, Keap1, Nrf2, and HO-1 at 1 dpi in Sham, SCI, and SCI + KD mice ($n = 3$). **(G–K)** Bar graph showing a quantitative analysis of GDF15, p62, Keap1, Nrf2, and HO-1 ($n = 3$). **(L)** Double IF of GPX4-1 (red) and NeuN (green), obtained from longitudinal sections centered around central canal at 1 dpi in Sham, SCI, and SCI + KD mice (Scale bar = 40 μm). The error bars represent the SD. $^{**}p < 0.01$, $^{***}p < 0.001$, vs. Sham group; $^{\#\#}p < 0.01$, $^{\#\#\#}p < 0.001$, vs. SCI group by one-way ANOVA followed by Tukey's *post hoc* analysis.

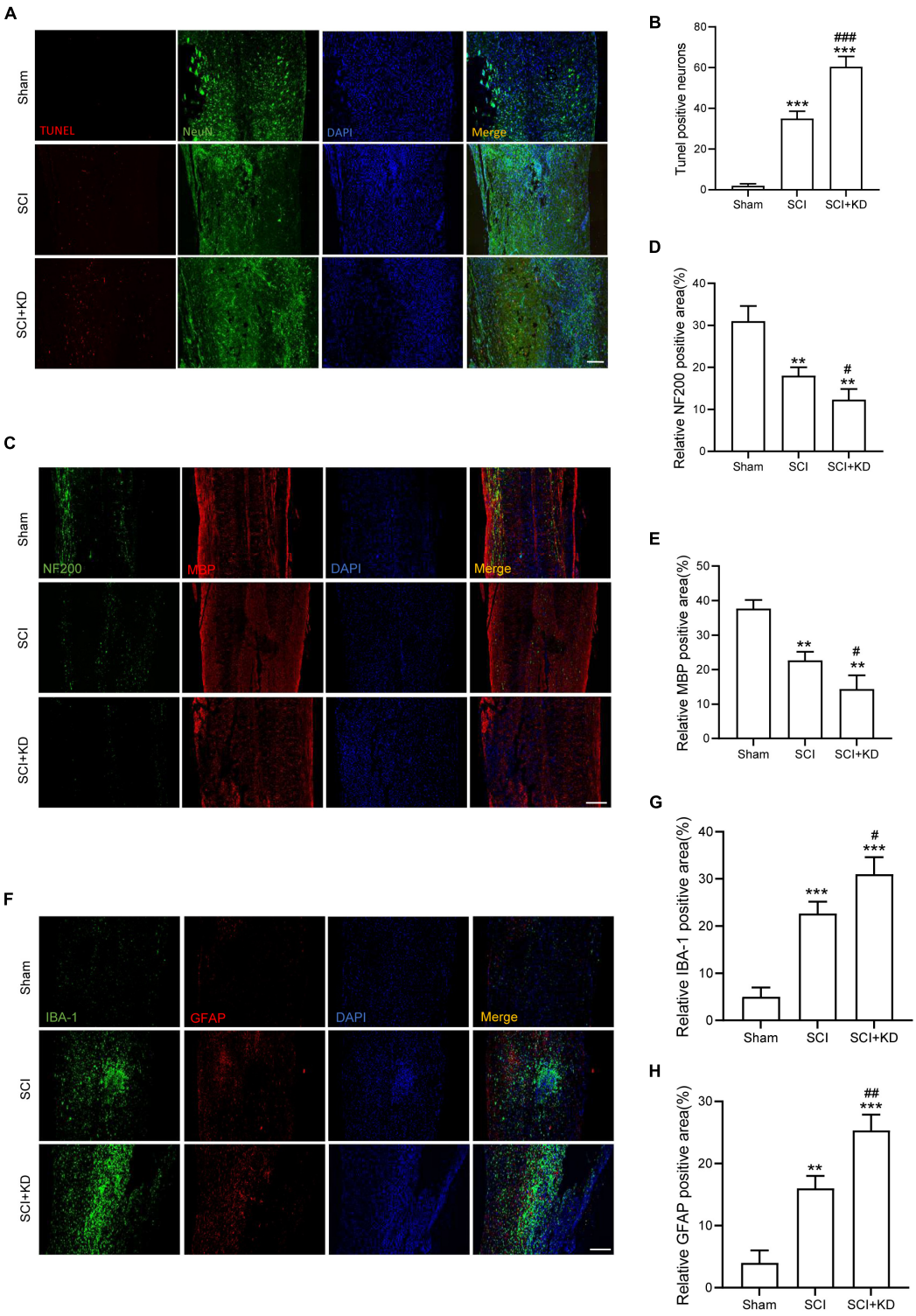

FIGURE 5 | Inhibition of GDF15 aggravated neurological damage and neuroinflammation. **(A)** Neuronal death determined by TUNEL assay at 7 dpi in Sham, SCI, and SCI + KD mice (Scale bar = 200 μm). **(B)** Quantitative analysis of TUNEL-positive neurons. **(C)** Representative immunofluorescence labeling of neurofilaments for NF200 (green) and myelin sheath for MBP (red) and obtained from longitudinal sections centered around the injured core 1.5 mm at 28 dpi (Scale bar = 300 μm). **(D)** Quantitative analysis of NF200 positive area at 28 dpi ($n = 6$). **(E)** Quantitative analysis of MBP positive area at 28 dpi ($n = 6$). **(F)** Double immunofluorescence labeling of microglia for IBA-1 (green) and astrocytes for GFAP (red) obtained from longitudinal sections centered around the injured core 3 mm at 7 dpi (Scale bar = 300 μm). **(G)** Quantitative analysis of IBA-1 positive area at 7 dpi. **(H)** Quantitative analysis of GFAP positive area at 7 dpi. The error bars represent the SD. $^{**}p < 0.01$, $^{***}p < 0.001$, vs. Sham group; $^{\#}p < 0.05$, $^{\#\#}p < 0.01$, $^{\#\#\#}p < 0.001$, vs. SCI group by t-test, one-way ANOVA followed by Tukey's *post hoc* analysis.

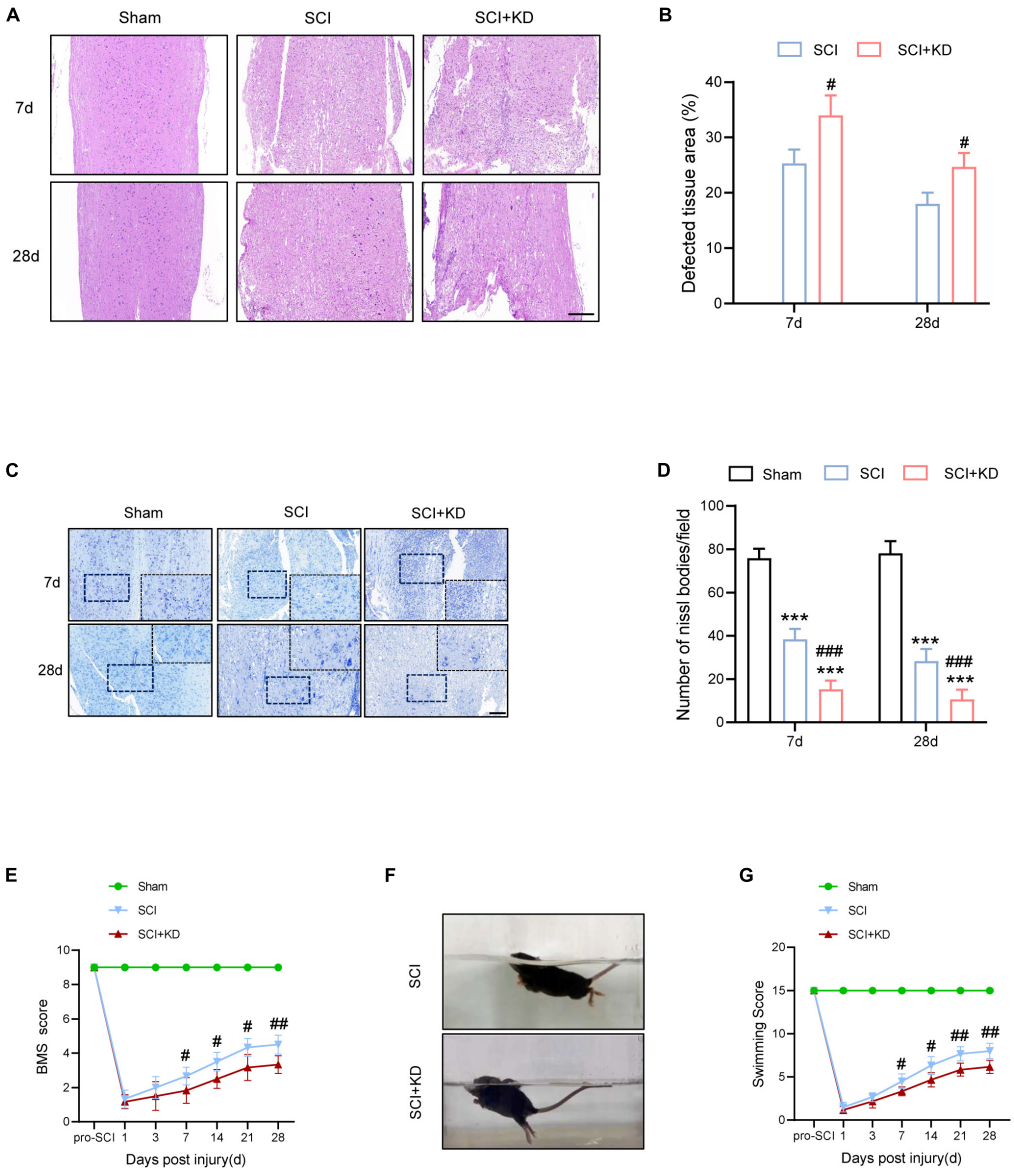

FIGURE 6 | Knockdown of GDF15 interferes locomotor recovery by aggravated neuronal loss in SCI mice. **(A)** H&E staining images of cords centered around the injured core 3 mm obtained at 7 and 28 dpi (Scale bar = 300 μm). **(B)** Quantitative analysis of the defected area at 7 and 28 dpi (n = 6). **(C)** Representative images for Nissl staining obtained from longitudinal sections centered around the injured core 1.5 mm at 7 and 28 dpi in Sham, SCI, and SCI + KD mice (Scale bar = 200 μm). **(D)** Quantitative analysis of the amounts of survived neurons at 7 and 28 dpi (n = 6). **(E)** The BMS score post SCI in Sham, SCI, and SCI + KD mice. **(F,G)** Photographs of Swimming at 28 dpi, showing the worse trunk instability and uncoordinated action in SCI mice, and statistical analysis of the Louisville Swim Scale over a period of 28 days (n = 6). $^{***}p < 0.001$, vs. Sham group; $^{\#}p < 0.05$, $^{\#\#}p < 0.01$, $^{\#\#\#}p < 0.001$, vs. SCI group by two-way ANOVA followed by Tukey's *post hoc* analysis.

GDF15 caused the further reduction of GPX4 expression in neurons (**Figure 4L**).

Inhibition of Growth Differentiation Factor 15 Aggravated Neurological Damage and Neuroinflammation

At 7 dpi, TUNEL staining results showed that Tunel-positive neurons was significantly increased after SCI and KD-GDF15 further aggravated neuronal death (**Figures 5A,B**). Additionally, KD-GDF15 caused lower levels of axon numbers and myelin sheath numbers labeled by NF-200 and MBP, respectively, when compared with SCI group, which indicated axon regeneration and remyelination, were significantly inhibited (**Figures 5C–E**). Previous studies have reported that excessive accumulation of iron promoted the activation of microglia and thus exacerbated neuroinflammation (Wang et al., 2022). We have verified silencing GDF15 aggravated ferroptosis after SCI,

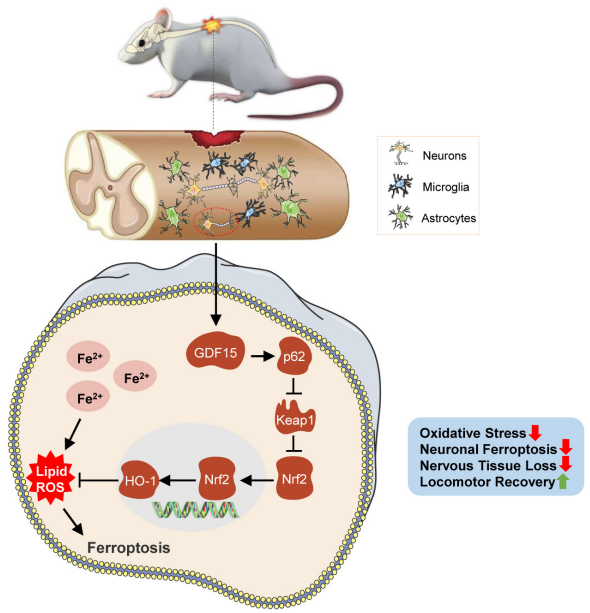

FIGURE 7 | GDF15 alleviates SCI-induced neuronal ferroptosis by regulating the p62-Keap1-Nrf2 signaling pathway. After SCI, cracked blood vessels at the injured cords result in the lysis and destruction of erythrocytes, which release a large amount of iron. Excessive iron accumulated in neurons produces superfluous ROS and causes neuronal ferroptosis, which promotes the activation of the p62-Keap1-Nrf2 signaling pathway. Besides, GDF15 in neurons further facilitates the activation of the p62-Keap1-Nrf2 pathway by stabilizing p62 and increased Nrf2 and HO-1 inhibit the accumulation of ROS and thus alleviate neuronal ferroptosis. GDF15 is suggested as a potential target on mitigating nervous tissue loss and promoting locomotor recovery post SCI.

and we next analyzed whether GDF15 affected ferroptosis-mediated neuroinflammation. Neuroinflammation after SCI is characterized by high expression of activated microglia and astrocytes (Qian et al., 2022); our results showed that both the expressions of IBA-1, a biological marker of microglia, glial fibrillary acidic protein (GFAP), and a characteristic marker of astrocytes were significantly increased when inhibition of GDF15 compared with SCI only, which suggested that silencing GDF15 further aggravated the ferroptosis-mediated neuroinflammation (**Figures 5F–H**).

Knockdown of Growth Differentiation Factor 15 Interferes Locomotor Recovery by Aggravated Neuronal Loss in Spinal Cord Injury Mice

At 7 and 28 dpi, H&E staining showed more defective tissue area in KD-GDF15 mice compared to SCI alone, indicating that knockdown of GDF15 aggravated nervous tissue loss post SCI (**Figures 6A,B**). Additionally, Nissl staining also demonstrated that SCI caused neuronal loss compared with the Sham group, which was further deteriorated by KD-GDF15 (**Figures 6C,D**). The BMS and LSS were employed to evaluate the locomotor recovery of SCI mice. The results showed low scores within 3 days post SCI. Interestingly, the scores of KD-GDF15 mice were significantly less than the SCI mice starting on 7 dpi and lasting until 28 dpi (**Figure 6E**). The LSS also displayed that the KD-GDF15 SCI mice exhibited worse body balance, weaker hindlimb alternation, and larger body-surface angle starting at 7 dpi. Briefly, silencing of GDF15 led to more neuronal loss and consequently affected locomotor recovery post SCI (**Figures 6F,G**).

DISCUSSION

In this study, we first reported the functional role of GDF15 in inhibiting oxidative stress-dependent neuronal ferroptosis post SCI by regulating ferroptosis levels through targeting the p62-Keap1-Nrf2 signaling pathway. Neuronal death and the damage of nervous tissue have always been the severe pathologic process of SCI that significantly impairs motor and sensory function of patients and causes high mortality and bring great burden to the patients and their families (Li C. et al., 2021; Haque et al., 2022; Valeri et al., 2022). Ferroptosis has been previously reported a form of neuronal death in SCI. The pathogenesis of cell rupture, hemorrhaging, hemolysis, and supernumerary iron post SCI caused excess ROS accumulation, which results in ferroptosis occurrence (Hu et al., 2021; Ge et al., 2022). Our results showed that ferroptosis-related protein GPX4, primarily expressed in neurons, significantly decreased while ACSL4 increased both *in vitro* and *in vivo*. Hence, inhibiting ferroptosis is a central link to alleviate neuronal death after SCI.

Previous studies have reported that GDF15, a cytokine associated with cell growth and differentiation, might effectively predicated the prognosis of colorectal cancer patients as a ferroptosis-related gene (Shao et al., 2021). Besides, GDF15 plays a vital role in metabolic disorders (Chow et al., 2022), inflammatory process (Sanchez-Infantes et al., 2021), tumor progression (Jin et al., 2021), and interestingly, neurodegenerative diseases (Rochette et al., 2020). Therefore, GDF15 may mediate the processes of iron metabolism and thus affect the occurrence and development of ferroptosis in CNS disorders. However, the mechanism of GDF15 in neuronal ferroptosis after SCI remains unknown. To examine the effect of GDF15 in SCI, we detected the level of GDF15 in injured spinal cords and the results displayed that both mRNA and protein levels of GDF15 were significantly elevated post SCI. Interestingly, we found that GDF15 protein levels were also significantly increased in neuronal ferroptosis *in vitro*. We then showed that knockdown of GDF15 significantly aggravated ferroptosis, which was rescued by rGDF15. This also identified that GDF15 is closely linked to ferroptosis. We demonstrated that GDF15 alleviates neuronal ferroptosis after SCI, but its specific regulatory mechanism needs to be further studied.

As what mentioned before, SCI is a complex pathologic process involving neuronal ferroptosis with iron-induced lipid peroxidation and production of large amounts of ROS (Ebrahimi et al., 2022; Liao et al., 2022). Exploration of potential intervention targets to ferroptosis is promising for the treatment

of many clinical diseases. The p62-Keap1-Nrf2 signaling axis was reported to effectively inhibit ROS accumulation and oxidative stress thus alleviating ferroptosis (Hou et al., 2021; Zhao et al., 2021; Yuan et al., 2022). Sun et al. (2016) have reported that activating the p62-Keap1-Nrf2 axis can effectively inhibit ferroptosis in liver cancer. Mechanically, Keap1 inhibits Nrf2 expression through ubiquitination under normal conditions. When ferroptosis occurs, increasing p62 promotes the autophagy degradation of Keap1, which facilitates Nrf2 to be released into the nucleus. Nrf2 activates downstream transcription factors such as HO-1, which further restrains the production of ROS, thus inhibiting ferroptosis (Sun et al., 2020; Zhang et al., 2021). In agreement with previous studies, we found that the p62-Keap1-Nrf2 signaling axis was stimulated in neuronal ferroptosis both *in vitro* and *in vivo*. Markedly, rGDF15 treatment further promotes the expression of p62, followed by the increased protein levels of Nrf2 and HO-1 *in vitro*. Oppositely, knockdown of GDF15 in SCI mice significantly inhibited the p62-Keap1-Nrf2 signaling pathway and consequently aggravated ferroptosis. To examine the regulatory mechanism between GDF15 and p62, we silenced p62 on the basis of rGDF15 and found that not only the activation of the pathway was inhibited, but also the level of ferroptosis was conversely increased. These results also suggested that GDF15 reduced ferroptosis by regulating the expression of p62.

In this study, neuronal ferroptosis was observed after SCI. We sought to investigate the neuroprotective role of GDF15 post SCI and found that the death of neurons was more severe after knockdown of GDF15 at both 7 and 28 dpi. Deteriorative loss of neurons can lead to inevitable damage to nervous tissue followed by demyelination and motor system disorders (Feng et al., 2021; Rong et al., 2021a). We found that silencing GDF15 impeded axonal regeneration and remyelination and aggravated nervous tissue loss post SCI. Previous studies have shown that overloaded iron-induced ferroptosis promoted the activation of microglia by a ROS-independent mechanism and the latter caused the secretion of pro-inflammatory cytokines such as tumor necrosis factor-α (TNF-α) and interleukin-1β (IL-1β), which triggered neuroinflammation (Ko et al., 2021). In our study, we observed that after deteriorative ferroptosis caused by the knockdown of GDF15, neuroinflammation post SCI was also more severe, which suggested that GDF15 was associated with ferroptosis-mediated neuroinflammation. However, the specific role of GDF15 in neuroinflammation post SCI needs to be further researched. Finally, both BMS and LSS showed delayed locomotor recovery in KD-GDF15 mice, which demonstrated that KD-GDF15 further inhibited the recovery of motor function in SCI mice by aggravating neuronal ferroptosis (**Figure 7**).

CONCLUSION

Growth differentiation factor 15 is a neuroprotective factor that regulates oxidative stress-dependent ferroptosis post SCI by stabilizing the p62-Keap1-Nrf2 signaling pathway. Silencing GDF15 aggravates neuronal ferroptosis, increases nervous tissue damage, and interferes with locomotor recovery in SCI mice. Our results revealed the specific role of GDF15 in neuronal ferroptosis, which may be a promising treatment target for SCI. However, other regulatory effects of GDF15 involved in neuronal ferroptosis and neuroinflammation after SCI remain uncertain. Thus, further studies of GDF15 in SCI need to be implemented in the future.

DATA AVAILABILITY STATEMENT

The original contributions presented in this study are included in the article/supplementary material, further inquiries can be directed to the corresponding authors.

ETHICS STATEMENT

The animal study was reviewed and approved by the Institutional Animal Care and Use Committee of Southeast University (Approval No. 20210302042).

AUTHOR CONTRIBUTIONS

LY, ZQ, and MX conceived and designed the experiments. MX, QZ, YZ, RL, and TZ performed the experiments. SZ analyzed the data. MX wrote the manuscript. QL and LC maintained the mice colonies. HL and LY funded and supervised the study. All authors read and approved the final manuscript for publication.

FUNDING

This study was supported by Scientific Research Project of Health Commission of Jiangsu Province of China (No. LGY2020068) and the Natural Science Foundation of Jiangsu Province (No. SBK2022022488 to HL).

ACKNOWLEDGMENTS

We thank for the technology support from the Central Lab of Taizhou People's Hospital, China.

REFERENCES

Ahuja, C. S., Wilson, J. R., Nori, S., Kotter, M., Druschel, C., Curt, A., et al. (2017). Traumatic spinal cord injury. *Nat. Rev. Dis. Primers* 3:17018. doi: 10.1038/nrdp.2017.18

Basso, D. M., Fisher, L. C., Anderson, A. J., Jakeman, L. B., McTigue, D. M., and Popovich, P. G. (2006). Basso Mouse Scale for locomotion detects differences in recovery after spinal cord injury in five common mouse strains. *J. Neurotrauma.* 23, 635–659. doi: 10.1089/neu.2006.23.635

Borner, T., Shaulson, E. D., Ghidewon, M. Y., Barnett, A. B., Horn, C. C., Doyle, R. P., et al. (2020). GDF15 induces anorexia through nausea and emesis. *Cell Metab.* 31, 351–362. doi: 10.1016/j.cmet.2019.12.004

Chen, Y., Liu, S., Li, J., Li, Z., Quan, J., Liu, X., et al. (2020). The latest view on the mechanism of ferroptosis and its research progress in spinal

cord injury. *Oxid. Med. Cell. Longev.* 2020:6375938. doi: 10.1155/2020/6375938

Chow, C., Guo, X., Asthana, P., Zhang, S., Wong, S., Fallah, S., et al. (2022). Body weight regulation via MT1-MMP-mediated cleavage of GFRAL. *Nat. Metab.* 4, 203–212. doi: 10.1038/s42255-022-00529-5

Dixon, S. J., Lemberg, K. M., Lamprecht, M. R., Skouta, R., Zaitsev, E. M., Gleason, C. E., et al. (2012). Ferroptosis: an iron-dependent form of nonapoptotic cell death. *Cell* 149, 1060–1072. doi: 10.1016/j.cell.2012.03.042

Ebrahimi, N., Adelian, S., Shakerian, S., Afshinpour, M., Chaleshtori, S. R., Rostami, N., et al. (2022). Crosstalk between ferroptosis and the epithelial-mesenchymal transition: implications for inflammation and cancer therapy. *Cytokine Growth Factor Rev.* 64:33–45. doi: 10.1016/j.cytogfr.2022.01.006

Emmerson, P. J., Duffin, K. L., Chintharlapalli, S., and Wu, X. (2018). GDF15 and growth control. *Front. Physiol.* 9:1712. doi: 10.3389/fphys.2018.01712

Feng, Z., Min, L., Chen, H., Deng, W., Tan, M., Liu, H., et al. (2021). Iron overload in the motor cortex induces neuronal ferroptosis following spinal cord injury. *Redox Biol.* 43:101984. doi: 10.1016/j.redox.2021.101984

Ge, H., Xue, X., Xian, J., Yuan, L., Wang, L., Zou, Y., et al. (2022). Ferrostatin-1 alleviates white matter injury via decreasing ferroptosis following spinal cord injury. *Mol. Neurobiol.* 59, 161–176. doi: 10.1007/s12035-021-02571-y

Haque, A., Das, A., Samantaray, S., Matzelle, D., Capone, M., Wallace, G., et al. (2022). Premarin reduces neurodegeneration and promotes improvement of function in an animal model of spinal cord injury. *Int. J. Mol. Sci.* 23:2384. doi: 10.3390/ijms23042384

Hou, K., Shen, J., Yan, J., Zhai, C., Zhang, J., Pan, J. A., et al. (2021). Loss of TRIM21 alleviates cardiotoxicity by suppressing ferroptosis induced by the chemotherapeutic agent doxorubicin. *EBioMedicine* 69:103456. doi: 10.1016/j.ebiom.2021.103456

Hu, X., Xu, Y., Xu, H., Jin, C., Zhang, H., Su, H., et al. (2021). Progress in understanding ferroptosis and its targeting for therapeutic benefits in traumatic brain and spinal cord injuries. *Front. Cell Dev. Biol.* 9:705786. doi: 10.3389/fcell.2021.705786

Huang, H., Young, W., Skaper, S., Chen, L., Moviglia, G., Saberi, H., et al. (2020). Clinical neurorestorative therapeutic guidelines for spinal cord injury (IANR/CANR version 2019). *J. Orthop. Translat.* 20, 14–24. doi: 10.1016/j.jot.2019.10.006

Jiang, F., Yu, W. J., Wang, X. H., Tang, Y. T., Guo, L., and Jiao, X. Y. (2014). Regulation of hepcidin through GDF-15 in cancer-related anemia. *Clin. Chim. Acta* 428, 14–19. doi: 10.1016/j.cca.2013.10.015

Jiang, S., Wu, Y., Wu, S., Ye, S., Kong, R., Chang, J., et al. (2021). Silencing TAK1 reduces MAPKs-MMP2/9 expression to reduce inflammation-driven neurohistological disruption post spinal cord injury. *Cell Death Discov.* 7:96. doi: 10.1038/s41420-021-00481-5

Jin, Y., Jung, S. N., Lim, M. A., Oh, C., Piao, Y., Kim, H. J., et al. (2021). Transcriptional regulation of GDF15 by EGR1 promotes head and neck cancer progression through a positive feedback loop. *Int. J. Mol. Sci.* 22:11151. doi: 10.3390/ijms222011151

Ko, C. J., Gao, S. L., Lin, T. K., Chu, P. Y., and Lin, H. Y. (2021). Ferroptosis as a major factor and therapeutic target for neuroinflammation in parkinson's disease. *Biomedicines* 9:1679. doi: 10.3390/biomedicines9111679

Kong, F. Q., Zhao, S. J., Sun, P., Liu, H., Jie, J., Xu, T., et al. (2020). Macrophage MSR1 promotes the formation of foamy macrophage and neuronal apoptosis after spinal cord injury. *J. Neuroinflamm.* 17:62. doi: 10.1186/s12974-020-01735-2

Lane, D., Metselaar, B., Greenough, M., Bush, A. I., and Ayton, S. J. (2021). Ferroptosis and NRF2: an emerging battlefield in the neurodegeneration of Alzheimer's disease. *Essays Biochem.* 65, 925–940. doi: 10.1042/EBC20210017

Lewandowski, G., and Steward, O. (2014). AAVshRNA-mediated suppression of PTEN in adult rats in combination with salmon fibrin administration enables regenerative growth of corticospinal axons and enhances recovery of voluntary motor function after cervical spinal cord injury. *J. Neurosci.* 34, 9951–9962. doi: 10.1523/JNEUROSCI.1996-14.2014

Li, C., Qin, T., Liu, Y., Wen, H., Zhao, J., Luo, Z., et al. (2021). Microglia-Derived exosomal microRNA-151-3p enhances functional healing after spinal cord injury by attenuating neuronal apoptosis via regulating the p53/p21/CDK1 signaling pathway. *Front. Cell Dev. Biol.* 9:783017. doi: 10.3389/fcell.2021.783017

Li, H., Tang, D., Chen, J., Hu, Y., Cai, X., and Zhang, P. (2021). The clinical value of GDF15 and its prospective mechanism in sepsis. *Front. Immunol.* 12:710977. doi: 10.3389/fimmu.2021.710977

Li, Q., Han, X., Lan, X., Gao, Y., Wan, J., Durham, F., et al. (2017). Inhibition of neuronal ferroptosis protects hemorrhagic brain. *JCI Insight* 2:e90777. doi: 10.1172/jci.insight.90777

Liao, P., Wang, W., Wang, W., Kryczek, I., Li, X., Bian, Y., et al. (2022). CD8(+) T cells and fatty acids orchestrate tumor ferroptosis and immunity via ACSL4. *Cancer Cell* 40, 365–378.e6. doi: 10.1016/j.ccell.2022.02.003

Luan, H. H., Wang, A., Hilliard, B. K., Carvalho, F., Rosen, C. E., Ahasic, A. M., et al. (2019). GDF15 is an Inflammation-Induced central mediator of tissue tolerance. *Cell* 178, 1231–1244. doi: 10.1016/j.cell.2019.07.033

Mou, Y., Wang, J., Wu, J., He, D., Zhang, C., Duan, C., et al. (2019). Ferroptosis, a new form of cell death: opportunities and challenges in cancer. *J. Hematol. Oncol.* 12:34. doi: 10.1186/s13045-019-0720-y

Pu, A., Mishra, M. K., Dong, Y., Ghorbanigazar, S., Stephenson, E. L., Rawji, K. S., et al. (2020). The glycosyltransferase EXTL2 promotes proteoglycan deposition and injurious neuroinflammation following demyelination. *J. Neuroinflamm.* 17:220. doi: 10.1186/s12974-020-01895-1

Qian, Z., Chen, H., Xia, M., Chang, J., Li, X., Ye, S., et al. (2022). Activation of glucagon-like peptide-1 receptor in microglia attenuates neuroinflammation-induced glial scarring via rescuing Arf and Rho GAP adapter protein 3 expressions after nerve injury. *Int. J. Biol. Sci.* 18, 1328–1346. doi: 10.7150/ijbs.68974

Qu, X. F., Liang, T. Y., Wu, D. G., Lai, N. S., Deng, R. M., Ma, C., et al. (2021). Acyl-CoA synthetase long chain family member 4 plays detrimental role in early brain injury after subarachnoid hemorrhage in rats by inducing ferroptosis. *CNS Neurosci. Ther.* 27, 449–463. doi: 10.1111/cns.13548

Ren, X., Li, Y., Zhou, Y., Hu, W., Yang, C., Jing, Q., et al. (2021). Overcoming the compensatory elevation of NRF2 renders hepatocellular carcinoma cells more vulnerable to disulfiram/copper-induced ferroptosis. *Redox Biol.* 46:102122. doi: 10.1016/j.redox.2021.102122

Rochette, L., Zeller, M., Cottin, Y., and Vergely, C. (2020). Insights into mechanisms of GDF15 and receptor GFRAL: therapeutic targets. *Trends Endocrinol Metab.* 31, 939–951. doi: 10.1016/j.tem.2020.10.004

Rong, Y., Fan, J., Ji, C., Wang, Z., Ge, X., Wang, J., et al. (2021a). USP11 regulates autophagy-dependent ferroptosis after spinal cord ischemia-reperfusion injury by deubiquitinating Beclin 1. *Cell Death Differ.* [Online ahead of print]. doi: 10.1038/s41418-021-00907-8

Rong, Y., Ji, C., Wang, Z., Ge, X., Wang, J., Ye, W., et al. (2021b). Small extracellular vesicles encapsulating CCL2 from activated astrocytes induce microglial activation and neuronal apoptosis after traumatic spinal cord injury. *J. Neuroinflamm.* 18:196. doi: 10.1186/s12974-021-02268-y

Sanchez-Infantes, D., Nus, M., Navas-Madronal, M., Fite, J., Perez, B., Barros-Membrilla, A. J., et al. (2021). Oxidative stress and inflammatory markers in abdominal aortic aneurysm. *Antioxidants* 10:602. doi: 10.3390/antiox10040602

Shao, Y., Jia, H., Huang, L., Li, S., Wang, C., Aikemu, B., et al. (2021). An original Ferroptosis-Related gene signature effectively predicts the prognosis and clinical status for colorectal cancer patients. *Front. Oncol.* 11:711776. doi: 10.3389/fonc.2021.711776

Silva, N. A., Sousa, N., Reis, R. L., and Salgado, A. J. (2014). From basics to clinical: a comprehensive review on spinal cord injury. *Prog. Neurobiol.* 114, 25–57. doi: 10.1016/j.pneurobio.2013.11.002

Smith, R. R., Burke, D. A., Baldini, A. D., Shum-Siu, A., Baltzley, R., Bunger, M., et al. (2006). The Louisville Swim Scale: a novel assessment of hindlimb function following spinal cord injury in adult rats. *J. Neurotrauma.* 23, 1654–1670. doi: 10.1089/neu.2006.23.1654

Sun, X., Ou, Z., Chen, R., Niu, X., Chen, D., Kang, R., et al. (2016). Activation of the p62-Keap1-NRF2 pathway protects against ferroptosis in hepatocellular carcinoma cells. *Hepatology* 63, 173–184. doi: 10.1002/hep.28251

Sun, Y., He, L., Wang, T., Hua, W., Qin, H., Wang, J., et al. (2020). Activation of p62-Keap1-Nrf2 pathway protects 6-Hydroxydopamine-Induced ferroptosis in dopaminergic cells. *Mol. Neurobiol.* 57, 4628–4641. doi: 10.1007/s12035-020-02049-3

Tarfiei, G. A., Shadboorestan, A., Montazeri, H., Rahmanian, N., Tavosi, G., and Ghahremani, M. H. (2019). GDF15 induced apoptosis and cytotoxicity in A549

cells depends on TGFBR2 expression. *Cell Biochem. Funct.* 37, 320–330. doi: 10.1002/cbf.3391

Valeri, A., Chiricosta, L., Gugliandolo, A., Pollastro, F., and Mazzon, E. (2022). Will cannabigerol trigger neuroregeneration after a spinal cord injury? An in vitro answer from NSC-34 scratch-injured cells transcriptome. *Pharmaceuticals* 15:117. doi: 10.3390/ph15020117

Wang, C., Chen, S., Guo, H., Jiang, H., Liu, H., Fu, H., et al. (2022). Forsythoside a mitigates alzheimer's-like pathology by inhibiting ferroptosis-mediated neuroinflammation via Nrf2/GPX4 axis activation. *Int. J. Biol. Sci.* 18, 2075–2090. doi: 10.7150/ijbs.69714

Wang, D., Day, E. A., Townsend, L. K., Djordjevic, D., Jorgensen, S. B., and Steinberg, G. R. (2021). GDF15: emerging biology and therapeutic applications for obesity and cardiometabolic disease. *Nat. Rev. Endocrinol.* 17, 592–607. doi: 10.1038/s41574-021-00529-7

Yang, W. S., and Stockwell, B. R. (2016). Ferroptosis: death by lipid peroxidation. *Trends Cell Biol.* 26, 165–176. doi: 10.1016/j.tcb.2015.10.014

Yu, Q., Jiang, X., Liu, X., Shen, W., Mei, X., Tian, H., et al. (2022). Glutathione-modified macrophage-derived cell membranes encapsulated metformin nanogels for the treatment of spinal cord injury. *Mater. Sci. Eng. C.* 18:112668. doi: 10.1016/j.msec.2022.112668

Yuan, L., Li, S., Chen, Q., Xia, T., Luo, D., Li, L., et al. (2022). EBV infection-induced GPX4 promotes chemoresistance and tumor progression in nasopharyngeal carcinoma. *Cell Death Differ.* [Online ahead of print]. doi: 10.1038/s41418-022-00939-8

Zhang, M., Zhang, T., Song, C., Qu, J., Gu, Y., Liu, S., et al. (2021). Guizhi Fuling Capsule ameliorates endometrial hyperplasia through promoting p62-Keap1-NRF2-mediated ferroptosis. *J. Ethnopharmacol.* 274:114064. doi: 10.1016/j.jep.2021.114064

Zhang, Y., Khan, S., Liu, Y., Zhang, R., Li, H., Wu, G., et al. (2022). Modes of brain cell death following intracerebral hemorrhage. *Front. Cell. Neurosci.* 16:799753. doi: 10.3389/fncel.2022.799753

Zhao, Y., Lu, J., Mao, A., Zhang, R., and Guan, S. (2021). Autophagy inhibition plays a protective role in ferroptosis induced by alcohol via the p62-Keap1-Nrf2 pathway. *J. Agric. Food Chem.* 69, 9671–9683. doi: 10.1021/acs.jafc.1c03751

Zille, M., Karuppagounder, S. S., Chen, Y., Gough, P. J., Bertin, J., Finger, J., et al. (2017). Neuronal death after hemorrhagic stroke in vitro and in vivo shares features of ferroptosis and necroptosis. *Stroke* 48, 1033–1043. doi: 10.1161/STROKEAHA.116.015609

Conflict of Interest: The authors declare that the research was conducted in the absence of any commercial or financial relationships that could be construed as a potential conflict of interest.

Publisher's Note: All claims expressed in this article are solely those of the authors and do not necessarily represent those of their affiliated organizations, or those of the publisher, the editors and the reviewers. Any product that may be evaluated in this article, or claim that may be made by its manufacturer, is not guaranteed or endorsed by the publisher.

frontiers | Frontiers in Aging Neuroscience

ORIGINAL RESEARCH
published: 07 July 2022
doi: 10.3389/fnagi.2022.949083

Hub Genes, Diagnostic Model, and Predicted Drugs Related to Iron Metabolism in Alzheimer's Disease

Xuefeng Gu[1,2,3*†], *Donglin Lai*[1,2,3†], *Shuang Liu*[1,2,3], *Kaijie Chen*[1,2,3], *Peng Zhang*[1,4], *Bing Chen*[5], *Gang Huang*[1*], *Xiaoqin Cheng*[6*] and *Changlian Lu*[1,2*]

[1] Shanghai Key Laboratory of Molecular Imaging, Zhoupu Hospital, Shanghai University of Medicine and Health Sciences, Shanghai, China, [2] School of Pharmacy, Shanghai University of Medicine and Health Sciences, Shanghai, China, [3] School of Health Science and Engineering, University of Shanghai for Science and Technology, Shanghai, China, [4] School of Clinical Medicine, Shanghai University of Medicine and Health Sciences, Shanghai, China, [5] Department of Neurosurgery, Affiliated Hospital of Guangdong Medical University, Zhanjiang, China, [6] Department of Neurology, Zhongshan Hospital, Fudan University, Shanghai, China

Alzheimer's disease (AD), the most common neurodegenerative disease, remains unclear in terms of its underlying causative genes and effective therapeutic approaches. Meanwhile, abnormalities in iron metabolism have been demonstrated in patients and mouse models with AD. Therefore, this study sought to find hub genes based on iron metabolism that can influence the diagnosis and treatment of AD. First, gene expression profiles were downloaded from the GEO database, including non-demented (ND) controls and AD samples. Fourteen iron metabolism-related gene sets were downloaded from the MSigDB database, yielding 520 iron metabolism-related genes. The final nine hub genes associated with iron metabolism and AD were obtained by differential analysis and WGCNA in brain tissue samples from GSE132903. GO analysis revealed that these genes were mainly involved in two major biological processes, autophagy and iron metabolism. Through stepwise regression and logistic regression analyses, we selected four of these genes to construct a diagnostic model of AD. The model was validated in blood samples from GSE63061 and GSE85426, and the AUC values showed that the model had a relatively good diagnostic performance. In addition, the immune cell infiltration of the samples and the correlation of different immune factors with these hub genes were further explored. The results suggested that these genes may also play an important role in immunity to AD. Finally, eight drugs targeting these nine hub genes were retrieved from the DrugBank database, some of which were shown to be useful for the treatment of AD or other concomitant conditions, such as insomnia and agitation. In conclusion, this model is expected to guide the diagnosis of patients with AD by detecting the expression of several genes in the blood. These hub genes may also assist in understanding the development and drug treatment of AD.

Keywords: Alzheimer's disease, iron metabolism, hub gene, diagnostic, drug, immune

OPEN ACCESS

Edited by:
Tao Huang,
Shanghai Institute of Nutrition and Health (CAS), China

Reviewed by:
Meijing Li,
Shanghai Maritime University, China
Huiqian Huang,
Zhejiang University, China

***Correspondence:**
Changlian Lu
lvcl@sumhs.edu.cn
Xiaoqin Cheng
cxq19850429@aliyun.com
Gang Huang
huangg@sumhs.edu.cn
Xuefeng Gu
guxf@sumhs.edu.cn

[†] These authors have contributed equally to this work

Specialty section:
This article was submitted to Alzheimer's Disease and Related Dementias, a section of the journal Frontiers in Aging Neuroscience

Received: *23 May 2022*
Accepted: *14 June 2022*
Published: *07 July 2022*

Citation:
Gu X, Lai D, Liu S, Chen K, Zhang P, Chen B, Huang G, Cheng X and Lu C (2022) Hub Genes, Diagnostic Model, and Predicted Drugs Related to Iron Metabolism in Alzheimer's Disease. Front. Aging Neurosci. 14:949083. doi: 10.3389/fnagi.2022.949083

INTRODUCTION

Alzheimer's disease (AD), the most common form of dementia, is a neurodegenerative disease associated with aging. According to a report in 2020, there are an estimated 5.8 million people aged 65 and older with AD in the United States, and this number could increase to 13.8 million by the middle of this century (Zhang T. et al., 2021). Typical AD occurs after the age of 65 years, and <5% of AD cases occur earlier in life, among which 1–2% occur in familial clusters (Long and Holtzman, 2019). The pathology of this disease is characterized by amyloid plaques comprised of amyloid-β (Aβ) peptides and neurofibrillary tangles (NFTs) containing hyperphosphorylated tau proteins (DeTure and Dickson, 2019). Various drugs available to treat AD, such as donepezil, galantamine, memantine, rivastigmine, and aducanumab (also known as Aduhelm), are not very effective (Barthold et al., 2020; Mullard, 2021). Therefore, finding new effective molecules to improve the diagnosis and treatment of AD is urgent.

As the second most abundant metal on the Earth's crust after aluminum, iron is one of the trace metals essential for human beings. Iron is an important component of hemoglobin, which is involved in oxygen transport. Iron is also involved in the metabolism of catecholamine neurotransmitters and the formation of myelin sheaths in the nervous system (Thirupathi and Chang, 2019; Peng et al., 2021). Iron homeostasis is maintained by a variety of complex mechanisms, such as iron regulatory proteins and hepcidin (Pantopoulos et al., 2012). Disruption of this homeostasis leads to excessive accumulation of intracellular iron, which can damage DNA, proteins, and lipids through the production of oxidative stress and free radicals (Ward et al., 2014). Abnormal iron accumulation has been observed in different brain regions of patients with AD (Mills et al., 2010; Apostolakis and Kypraiou, 2017; Lee and Lee, 2019). In AD, excessive accumulation of iron in the brain aggravates amyloid protein deposition and tau protein hyperphosphorylation, which leads to neuronal damage and cognitive impairment (Gong et al., 2019; Yan and Zhang, 2019; Choi et al., 2021; Peng et al., 2021). Iron can also directly induce oxidative damage to neurons (Thirupathi and Chang, 2019). In conclusion, there is a non-negligible relationship between iron metabolism and AD.

Based on abundant public resources and bioinformatics methods, this study identified nine hub genes associated with iron metabolism and AD by differential analysis and WGCNA of GSE132903. GO and GSEA analyses were applied to further investigate the biological processes and pathways. Stepwise regression and logistic regression analyses were performed to screen four of them and construct a diagnostic model for AD, which was validated in two other blood sample datasets, GSE63061 and GSE85426. The AUC values indicated that this model has relatively good diagnostic performance and thus had a potential application in the clinical diagnosis of AD. Neuroinflammation, an important pathological feature of AD, is closely related to immunity. Therefore, we further explored the immune infiltration of these samples and the correlation of different immune factors with these hub genes. In addition, eight drugs targeting these hub genes were retrieved from the DrugBank database, which has implications for the pharmacological treatment of AD. The workflow of this study is shown in **Figure 1**.

MATERIALS AND METHODS

Data Acquisition

Gene expression data were obtained from the NCBI Gene Expression Omnibus public database (GEO). GSE132903 contained RNA expression data annotated by GPL10558 in the middle temporal gyrus, which included 97 AD samples and 98 ND controls. Samples from two datasets GSE63061 and GSE85426 were extracted from peripheral blood. GSE63061 annotated by GPL10558 included 139 AD samples and 134 ND samples, and GSE85426 annotated by GPL14550 included 90 AD samples and 90 ND samples.

Differential Expression Analysis

Differential expression analysis of AD and ND samples was performed using the "limma" package in R software. Genes with $p\_adj < 0.01$ and $abs(logFC) > 0.585$ were considered as DEGs. Heat maps and volcano plots of DEGs were created using the "pheatmap" and "ggplot2" packages.

Iron Metabolism-Related Genes

Fourteen iron metabolism-related gene sets were extracted from the Molecular Signatures Database v7.5.1 (MSigDB; Liberzon et al., 2015), including GOBP_CELLULAR_IRON_ION_HOMEOSTASIS, GOBP_HEME_METABOLIC_PROCESS, GOBP_IRON_COORDINATION_ENTITY_TRANSPORT, GOBP_IRON_ION_HOMEOSTASIS, GOBP_IRON_ION_IMPORT_ACROSS_PLASMA_MEMBRANE, GOBP_IRON_ION_TRANSPORT, GOBP_RESPONSE_TO_IRON_ION, GOMF_2_IRON_2_SULFUR_CLUSTER_BINDING, GOMF_4_IRON_4_SULFUR_CLUSTER_BINDING, GOMF_IRON_ION_BINDING, HALLMARK_HEME_METABOLISM, HEME_BIOSYNTHETIC_PROCESS, MODULE_540, and REACTOME_IRON_UPTAKE_AND_TRANSPORT (Mou et al., 2020). After removing the overlapping genes, the gene sets associated with iron metabolism contained 520 genes (**Supplementary Table 1**).

Weighted Correlation Network Analysis (WGCNA)

To explore the co-expression relationships among the genes and the relationship between the genes and the phenotypes, a gene co-expression network was constructed using the "WGCNA" package in R software (Langfelder and Horvath, 2008). Based on the cluster trees, abnormal samples were removed. The top 5,000 genes with a median absolute deviation (MAD) > 1 were retained. The correlation coefficient between each gene pair was calculated to construct a similarity matrix. To ensure the construction of a scale-free network, a suitable soft threshold

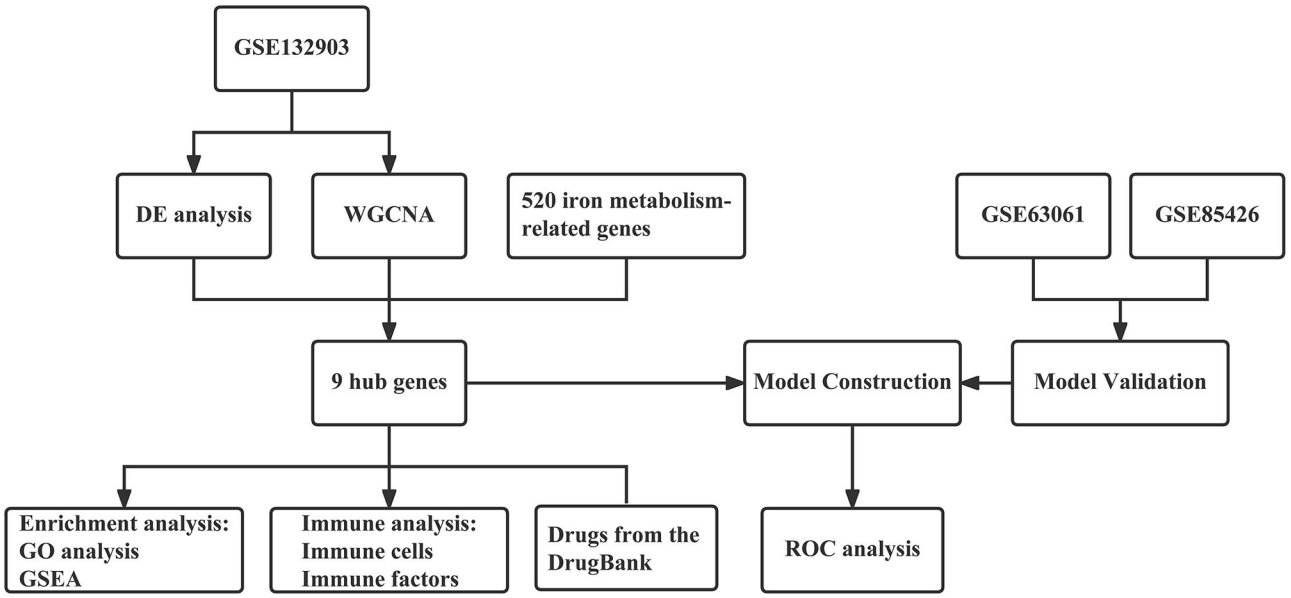

FIGURE 1 | The workflow of the analyses.

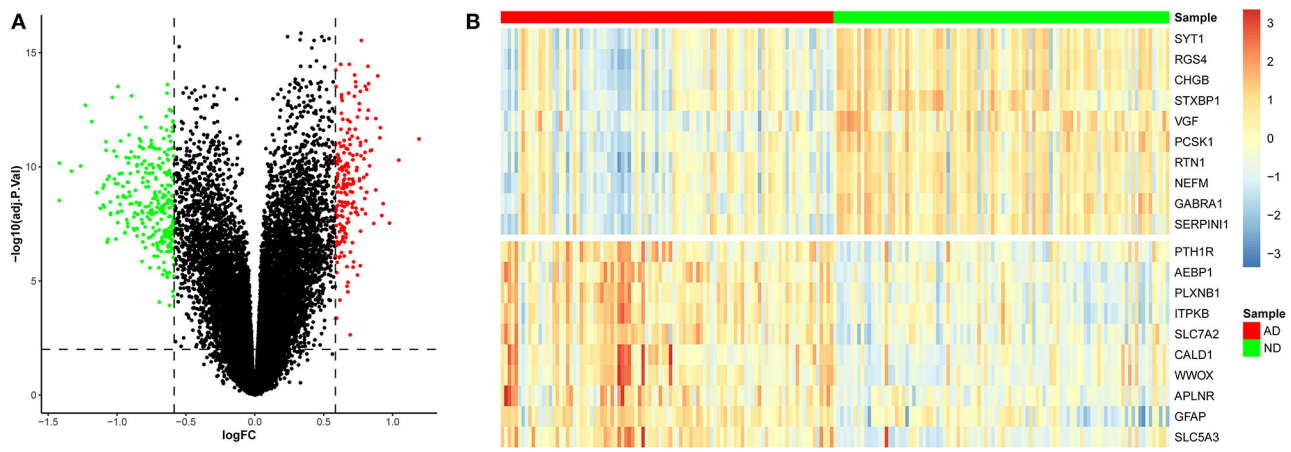

FIGURE 2 | Differentially expressed genes between AD and ND samples. **(A)** Red genes represent significantly high expression in AD, green genes represent significantly high expression in ND, and gray genes indicate insignificant changes. **(B)** The heatmap shows the top 20 genes significantly highly expressed in AD or ND samples.

was chosen to transform the similarity matrix into an adjacency matrix. Subsequently, a topological overlap matrix (TOM) was created to measure the mean network connectivity of each gene. Based on the relevant parameters of the blockwiseModules function, such as minModuleSize and mergeCutHeight, genes with similar expression profiles were grouped into different modules using the dynamic tree cutting method. Each module was depicted in a different color, where the genes in gray modules represented genes that cannot be assigned to any module. The gene expression profile of each module was represented by the first principal component called the module eigengene (ME). MEs were used to assess the association between the modules and phenotypes. The module with the highest absolute value of the correlation coefficient was identified as the key module for further analysis. Module membership (MM) is the correlation coefficient between the expression value of a gene and the ME of a module, representing the correlation between this gene and this module. Gene significance (GS) was the correlation coefficient between the expression value of a gene and a phenotype, representing the association between genes and phenotypes.

Identification of Hub Genes

To obtain hub genes associated with both iron metabolism and AD, the intersection of DEGs, genes obtained by WGCNA, and genes in the iron metabolism gene sets were taken using the "VennDiagram" package in R software. Differences in the

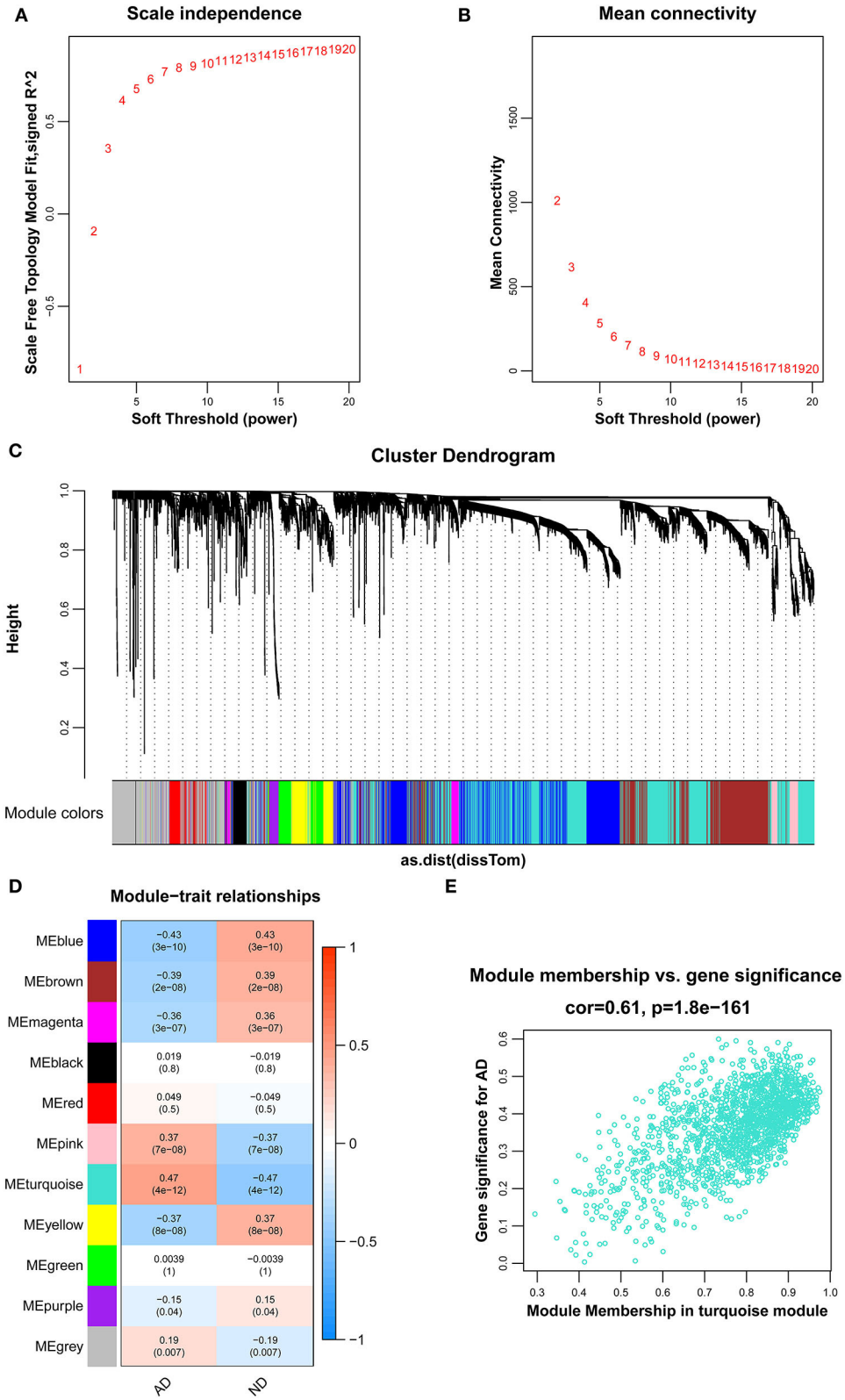

FIGURE 3 | Results of the WGCNA. **(A)** The corresponding scale-free topological model fit indices at different soft threshold powers. **(B)** The corresponding mean connectivity values at different soft threshold powers. **(C)** Cluster dendrogram of genes. **(D)** Correlations between different modules and clinical traits. Red represents a positive correlation, and blue represents a negative correlation. **(E)** Correlation of module membership and gene significance in the turquoise module.

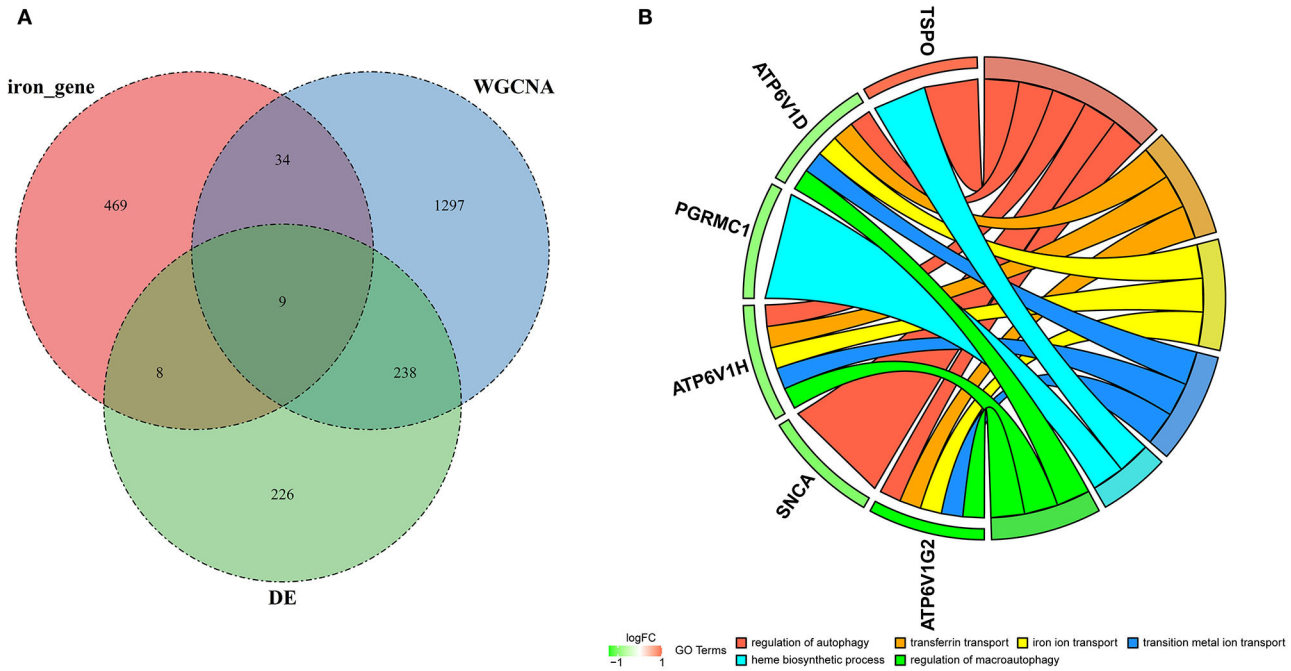

FIGURE 4 | Hub genes and GO analysis. **(A)** Nine hub genes were obtained by taking the intersections of the DEGs, MEturquoise module genes of the WGCNA, and iron metabolism-related genes. **(B)** Biological processes in which the hub genes were involved.

expressions of hub genes between the AD and ND samples were represented by violin plots. The hypothesis tests used were the *t*-test and the Mann-Whitney *U*-test. The former was used if the data conformed to a normal distribution, and the latter if not. Significance was defined as $p < 0.05$.

Enrichment Analysis

To investigate the biological mechanisms of the hub genes affecting AD, functional enrichment analyses were conducted. We first analyzed the biological processes (BP) of Gene Ontology (GO) in which these genes are involved, and the final results were presented in a chord diagram using the "GOplot" package in R software. Next, the respective functions of each gene were revealed by Gene Set Enrichment Analysis (GSEA). Samples were distinguished into two groups based on median values of hub gene expression levels, including the low expression group and the high expression group. Genes were sorted by logFC from the highest to the lowest, and the background gene sets were downloaded from MSigDB (Liberzon et al., 2015). The final results were presented using the "enrichplot" package in R software. All these analyses were conducted using the "clusterProfiler" package in R software, and the screening condition was $p\_adj < 0.05$.

Logistic Regression Model

Logistic regression is a generalized linear regression analysis model that can be used for the automatic diagnosis of diseases. In this study, logistic regression with two response variables was used, representing the AD sample when the response variable was 1 and the ND sample when it was 0. Stepwise regression analysis was first used to eliminate factors that were not significant for the response variable, and only those that were significant were retained to simplify the model. The stepwise regression iteratively added or removed variables from the model until the statistical value of Akaike information criterion (AIC) was minimized. Afterward, logistic regression was used to fit the relationship between these significant factors and the response variable. Finally, the diagnostic efficacy of the model was evaluated using receiver operating characteristic curves (ROCs) and the area under the ROC curve (Coat et al., 2015; Lai et al., 2021). These analyses were performed with the "stats" and "pROC" packages in R software.

Immune Infiltration and Immune-Related Factors

Immune cell infiltration in the microenvironment was assessed using CIBERSORT, which contains 547 biomarkers and 22 human immune cells, including plasma, B cell, T cell, and myeloid cell subpopulations. The tool is based on the linear support vector regression principle for deconvolution analysis of the expression matrix of immune cells. This study used expression data from GSE132903 and quantified the relative proportions of the 22 immune cells in each sample. In addition, Spearman correlation analysis was performed between hub genes and immune infiltration, and immune factors. This analysis was performed using the "psych" package in R software, and the results were displayed as heatmaps. Different immune factors were downloaded from the TISIDB database (Ru et al., 2019), including 24 immunoinhibitors, 45 immunostimulators, and 41 chemokines (**Supplementary Table 2**).

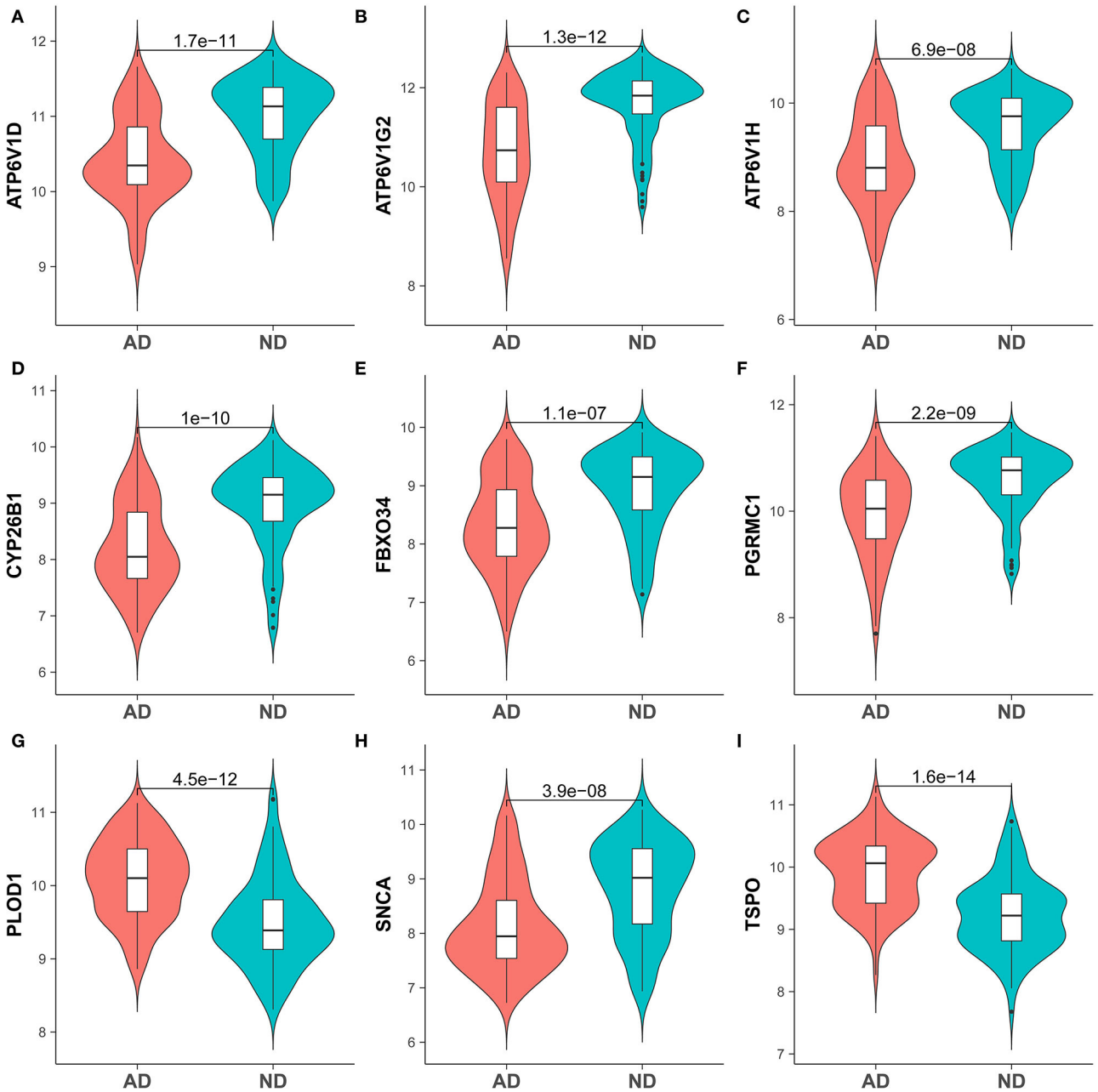

FIGURE 5 | Expression of hub genes in the AD and ND groups of brain tissue samples GSE132903. **(A)** ATP6V1D, **(B)** ATP6V1G2, **(C)** ATP6V1H, **(D)** CYP26B1, **(E)** FBXO34, **(F)** PGRMC1, **(G)** PLOD1, **(H)** SNCA, and **(I)** TSPO.

Drugs From the DrugBank

Drugs targeting hub genes were retrieved from the DrugBank database. The DrugBank database is a cheminformatics and bioinformatics repository containing detailed information on drugs and their targets. The database collects more than 7,800 drugs, including nutraceuticals, experimental drugs, FDA-approved small-molecule drugs, and FDA-approved biotech drugs (Wishart et al., 2018). The DrugBank also has a large collection of SNP drugs useful for pharmacogenomic studies.

Statistical Analysis

All analyses were performed in R software. The *t*-test and Mann–Whitney *U*-test were selected according to whether the data conformed to a normal distribution. Significance was usually defined as $p < 0.05$.

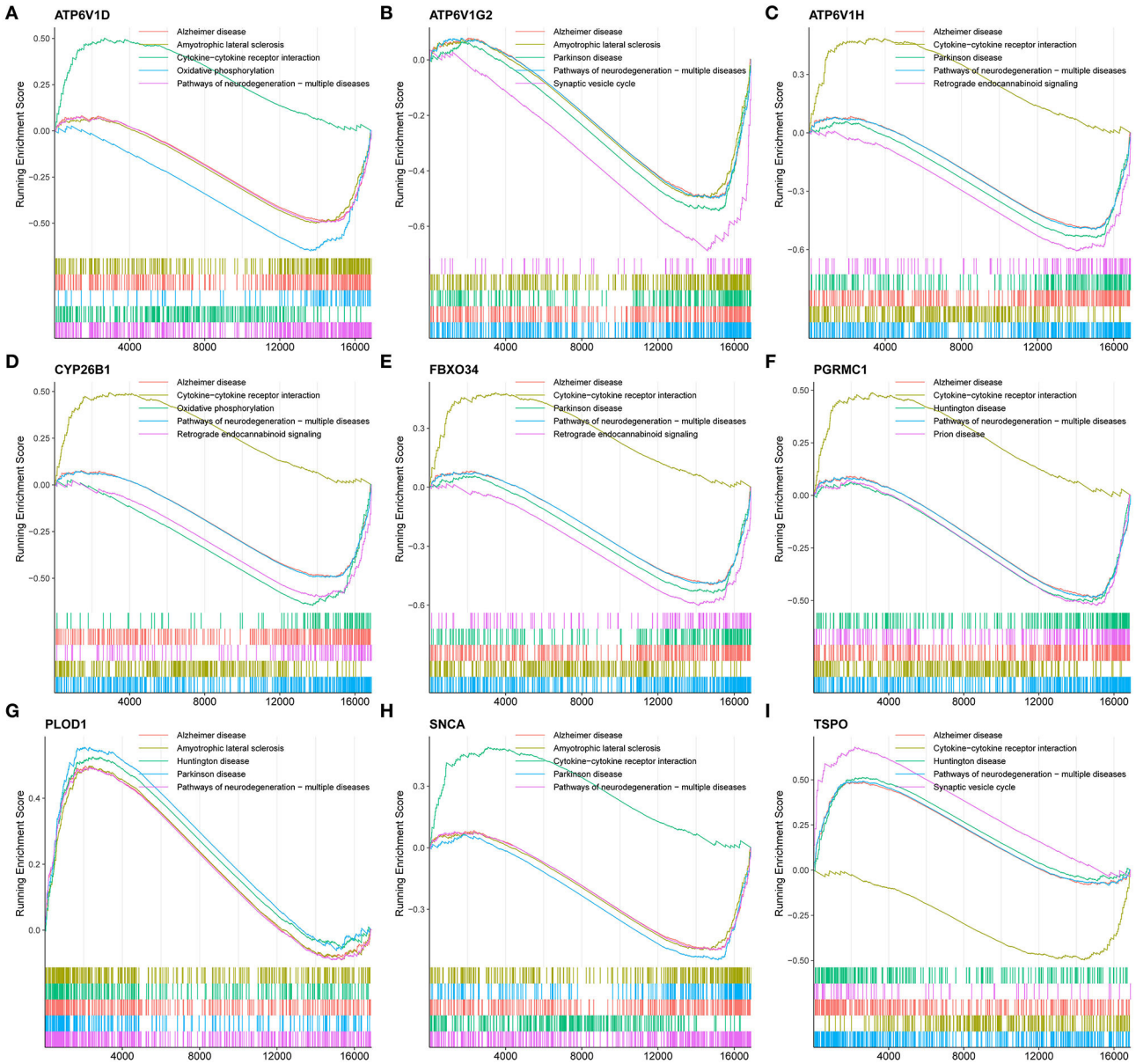

FIGURE 6 | GSEA revealed the enriched pathways of the hub genes. **(A)** ATP6V1D, **(B)** ATP6V1G2, **(C)** ATP6V1H, **(D)** CYP26B1, **(E)** FBXO34, **(F)** PGRMC1, **(G)** PLOD1, **(H)** SNCA, and **(I)** TSPO.

RESULTS

Identification of Hub Genes Associated With AD and Iron Metabolism

To identify genes related to AD, we first obtained 481 differentially expressed genes from GSE132903 with the screening conditions "p_adj $<$ 0.01 and abs(logFC) $>$ 0.585" (**Supplementary Table 3**). These DEGs were presented in a volcano plot (**Figure 2A**). A heatmap of the top 20 differentially expressed genes was plotted (**Figure 2B**). After removing abnormal samples and filtering the genes, the expression profiles of 5,000 genes and 195 samples were extracted from GSE132903 and used for the construction of a weighted gene co-expression network. When the soft threshold power was set to 14, the scale independence reached 0.858 and the average connection value was 30.124 (**Figures 3A,B**). When the cut height was set to 0.25 and the minimum module size was set to 50, 11 different co-expression modules were obtained by dynamic tree cutting (**Figure 3C**). Then, correlation analyses of each module with clinical traits were performed. The MEturquoise module had the highest positive correlation with AD ($r = 0.47$, $p = 4e{-}12$), while the MEblue module had the highest negative correlation with AD ($r = -0.43$, $p = 3e{-}10$; **Figure 3D**). Here, the MEturquoise module, containing 1,578 genes with the largest absolute value

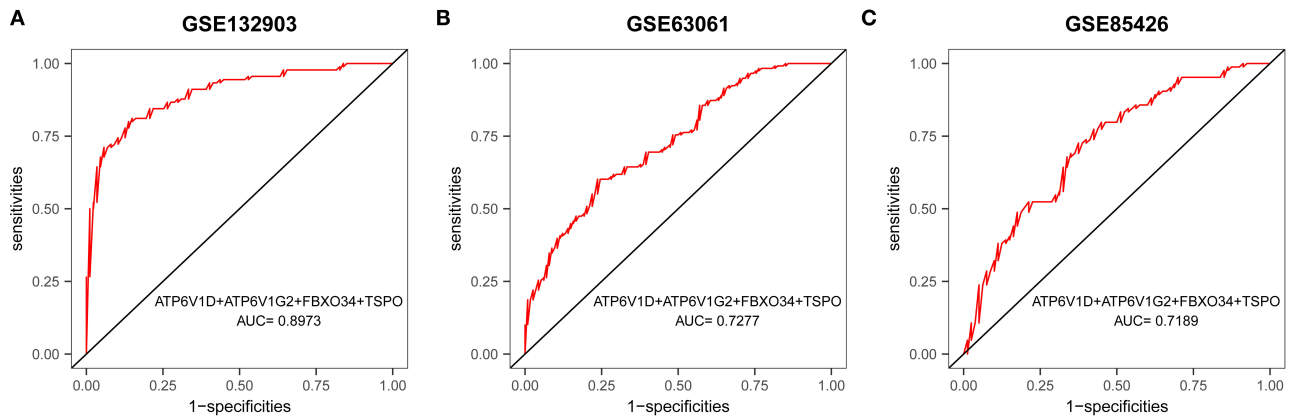

FIGURE 7 | ROC curves and corresponding AUC values for the three expression cohorts. **(A)** Brain tissue samples from GSE132903. **(B)** Blood samples from GSE63061. **(C)** Blood samples from GSE85426.

of correlation coefficient, was selected for further analysis. Additionally, correlation analysis between MM and GS showed that these genes were highly correlated with both module and phenotype (cor = 0.61, p = 1.8e−161; **Figure 3E**). Nine hub genes associated with iron metabolism and AD were obtained by taking the intersections of 481 DEs, 1,578 MEturquoise module genes, and 520 iron metabolism-related genes from 14 iron metabolism-related gene sets (**Figure 4A**). Violin plots showed that *TSPO* and *PLOD1* were highly expressed in AD, and the other seven genes were expressed at lower levels than in the ND group in GSE132903 (**Figure 5**). In addition, the expression of these genes in blood samples from GSE63061 and GSE85426 is shown in **Supplementary Figures 1**, **2**.

Biological Processes and Pathways Enriched for the Hub Genes

To understand the potential biological roles of these genes, enrichment analyses were performed. GO analysis revealed that six of the nine genes were involved in autophagy-related biological processes, including regulation of autophagy and macroautophagy, and iron metabolism-related biological processes, including transferrin transport, iron ion transport, transition metal ion transport, and heme biosynthetic process (**Figure 4B**). GSEA of these genes has shown that they are associated with several neurodegenerative diseases (AD, amyotrophic lateral sclerosis, Parkinson's disease, Prion disease, and Huntington's disease), neurological related pathways (the synaptic vesicle cycle, retrograde endocannabinoid signaling, retrograde endocannabinoid signaling, and pathway of neurodegeneration), and other pathways (cytokine–cytokine receptor interaction and oxidative phosphorylation; **Figure 6**).

Construction and Blood Validation of a Diagnostic Model

A multigene prediction model was constructed by a logistic regression algorithm based on GSE132903. Using stepwise regression analysis, four of these nine genes, including *ATP6V1D*, *ATP6V1G2*, *FBXO34*, and *TSPO*, were selected to obtain the best model. The results showed that the predictive model constructed from these four genes had good diagnostic performance, with an AUC of 0.8973 (**Figure 7A**). The model was then further validated in blood samples. The AUCs of the models in GSE63061 and GSE85426 were relatively high, 0.7277 and 0.7189, respectively (**Figures 7B,C**). Brain tissue samples tended to be more representative of AD pathology than blood samples, which may explain the better diagnostic performance of the former. However, it was difficult to obtain brain tissue *in vivo*. The good results in blood samples suggested that this model has a certain guiding significance for the diagnosis of patients with AD in clinical applications.

Immune Infiltration and Immune-Related Factors

The microenvironment consists of immune cells, extracellular matrix, inflammatory factors, and various growth factors that have an important impact on the clinical therapeutic sensitivity and disease diagnosis. In this study, the proportion of 22 immune cells in 97 AD samples and 98 ND samples was estimated by the CIBERSORT algorithm, which can be seen in the histogram (**Figure 8A**). The immune cell infiltration of AD and ND samples was compared in a boxplot (**Figure 8B**). The results showed that the AD group had significantly higher proportions of naive B cells (p = 0.0210), M1 macrophages (p = 0.0090), neutrophils (p = 0.0497), CD4 naive T cells (p = 0.0101), and gamma delta T cells (p = 0.0070), and lower proportions of plasma cells (p = 0.0056) and follicular helper T cells (p = 0.0314) than the ND group. Next, the relationship between the hub genes and immune infiltration, and immune factors was analyzed. *PLOD1* and *TSPO* were significantly negatively associated with follicular helper T cells, CD8 T cells, and activated dendritic cells, and positively associated with resting NK cells, M1 macrophages, M0 macrophages, and naive B cells, while the opposite was true for the other downregulated genes (**Figure 9A**). The correlation heatmaps showed a significant correlation between the hub

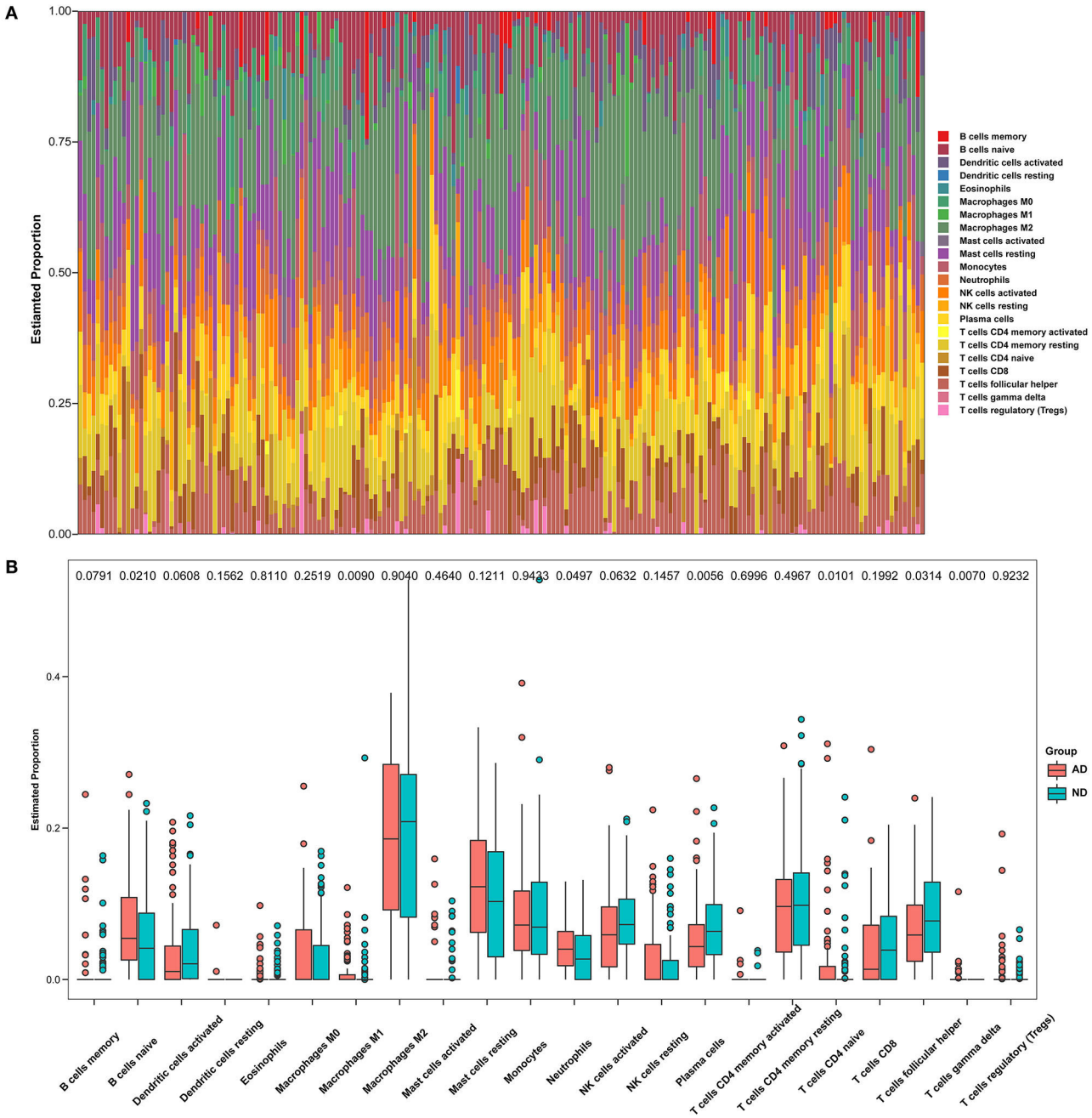

FIGURE 8 | Immune infiltration between AD and ND samples. **(A)** The relative percentage of 22 immune cells in each sample. **(B)** Differences in immune infiltration between AD and ND samples.

genes and most immune factors, including immunoinhibitors, immunostimulators, and chemokines (**Figures 9B–D**). These results suggested that the hub genes may play an important role in the immune microenvironment.

Drugs From the DrugBank

Based on drug and target information from the DrugBank database, eight drugs targeting these nine hub genes were identified (**Figure 10**). Among these drugs, six drugs were approved, one was an investigational drug, and one was withdrawn. Tiludronic acid (DB01133), an inhibitor of *ATP6V1D*, *ATP6V1G2*, and *ATP6V1H*, is used for the treatment of Paget's disease of the bone. Tretinoin (DB00755) targeting *CYP26B1* is used to treat fine wrinkles, acne vulgaris, and certain types of promyelocytic leukemia. Dextromethorphan (DB00514) is a binder of *PGRMC1* used to treat cases of dry cough. Ascorbic acid (DB00126) is a

FIGURE 9 | Correlation of hub genes with immune cells and different immune factors. **(A)** Immune cells, **(B)** immunoinhibitors, **(C)** immunostimulators, and **(D)** chemokines.

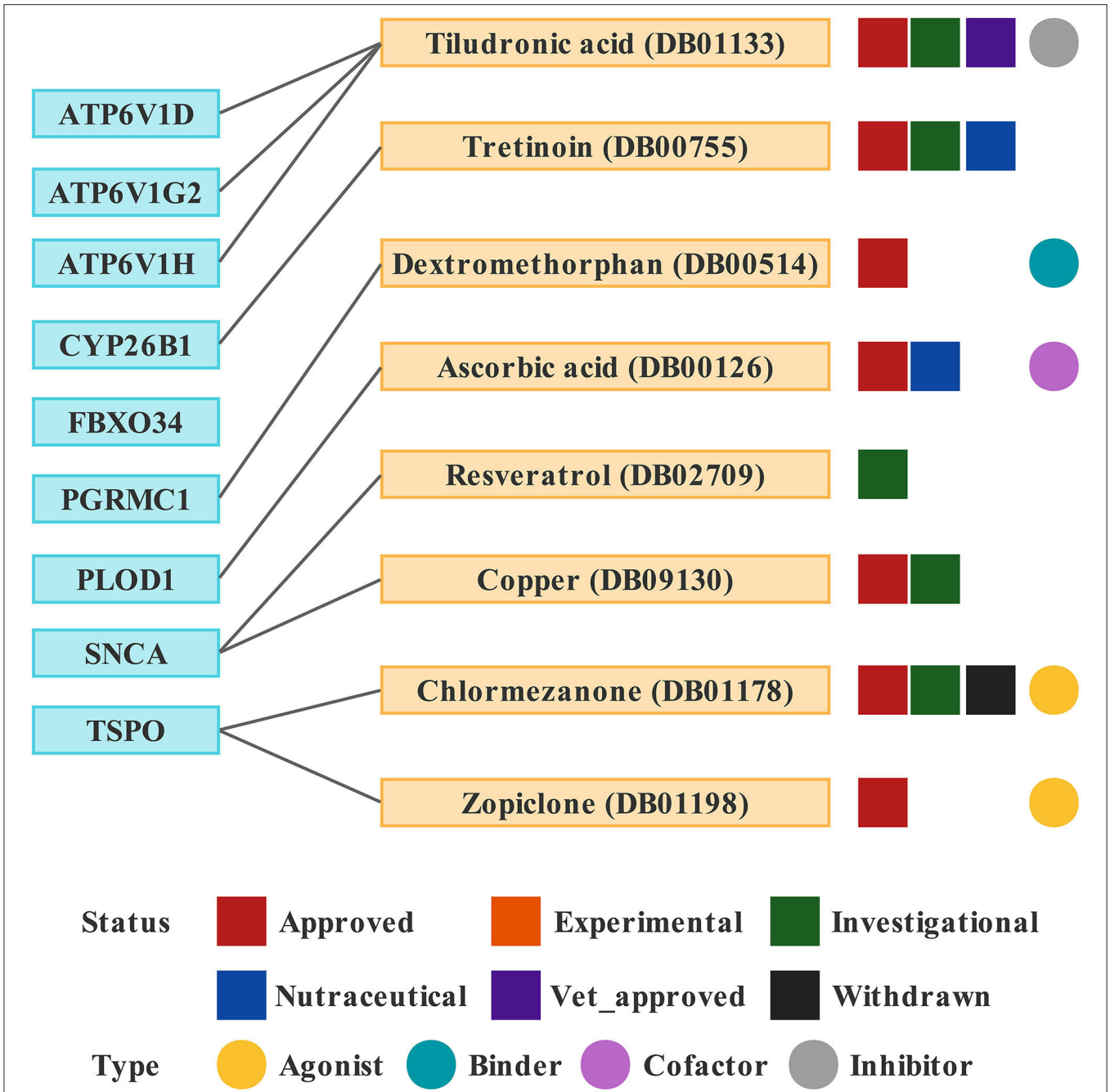

FIGURE 10 | Drugs targeting these nine hub genes obtained from the DrugBank database. Drug statuses, including approved, experimental, investigational, nutraceutical, vet_approved and withdrawn, are indicated by colored squares. Drug types, including agonist, binder, cofactor, and inhibitor, are indicated by colored circles.

cofactor of *PLOD1* used to correct vitamin C deficiency and increase intestinal absorption of iron. Resveratrol (DB02709) targeting *SNCA* was investigated for the treatment of herpes labialis infections (cold sores). Both chlormezanone (DB01178) and zopiclone (DB01198) are agonists of *TSPO*. Chlormezanone is used to manage anxiety and treat muscle spasms, while zopiclone is used to treat insomnia (**Supplementary Table 4**).

DISCUSSION

Iron is involved in myelination, neurotransmitter synthesis, and mitochondrial respiration in the nervous system and could contribute to oxidative stress. Both iron overload and iron deficiency have adverse effects and may lead to neurological disorders. Relevant studies have found that increases in ferritin and iron, most likely ferritin-bound iron, are present in several

brain regions involved in AD (Quintana and Gutiérrez, 2010; Galazka-Friedman et al., 2012; Raven et al., 2013).

In this study, nine genes linking AD and iron metabolism were screened. GO analysis showed that they were involved in autophagy-related and iron metabolism-related biological processes. A decrease in neuronal autophagy leads to an inability to clear pathological proteins, such as beta-amyloid (Aβ) and tau proteins (Feng et al., 2015). Several key proteins involved in the regulation of autophagy are closely associated with the development of AD (Majumder et al., 2011; Lucin et al., 2013; Heras-Sandoval et al., 2014; Sepe et al., 2014). Restoration of parkin-mediated mitophagy prevents cognitive decline (Goudarzi et al., 2021). Some neuroprotective drugs exert their effects by modulating mitophagy (Wang et al., 2018; Hirano et al., 2019; Han et al., 2020; Sun C. et al., 2020). When intracellular iron levels fall, ferritin is degraded to release free iron, a process called ferritinophagy. Biasiotto et al. proposed that abnormal ferritinophagy may be a link between impaired autophagy and dysfunctional iron homeostasis in several neurodegenerative diseases (Biasiotto et al., 2016). In addition, the GSEA showed that these hub genes were all associated with neurodegenerative diseases, especially AD, which validates the accuracy of the selection of these genes to some extent (**Figure 6**).

Four of the nine genes, including *ATP6V1D*, *ATP6V1G2, FBXO34,* and *TSPO*, were screened to construct a diagnostic model, which may be useful to guide the diagnosis of AD in clinical applications. Both *ATP6V1G2* and *ATP6V1D* encode a component of vacuolar ATPase (V-ATPase). In addition to acting as an H+ pump, V-ATPase is also involved in enzyme activity, the coupled transport of substrates across membranes, and the dissociation of ligands from receptors (Huynh and Grinstein, 2007; Vahlensieck et al., 2021). A deficiency of V-ATPase can lead to central nervous system disorders such as AD and PD (Lee et al., 2010; Williamson and Hiesinger, 2010). *ATP6V1G2* is downregulated in AD as a key metabolic gene and is involved in lysosomal transport, transporting protons from the cytoplasm to the lysosome, and maintaining lysosomal acidification (Li et al., 2020). *ATP6V1D* is associated with mitochondrial function and impaired bioenergetic metabolism (Alves et al., 2015). *FBXO34* belongs to the F-box protein family, and F-box proteins are junction proteins for Skp1-Cul1-FBP (SCF)-type E3 ubiquitin ligases, directing the ubiquitination of numerous proteins (Randle and Laman, 2016). Ubiquitinated proteins are found in neurofibrillary tangles and oligomeric Aβ plaques, and a mutation of the ubiquitin-B+1 gene leads to neuronal degeneration, which is associated with spatial reference memory impairment (van Tijn et al., 2011) and AD (Tan et al., 2007). The ubiquitin–proteasome system is also related to several neuronal signaling pathways (Zhao et al., 2003; Patrick, 2006). The ubiquitin–proteasome system and tau phosphorylation in AD are closely related (Ciechanover and Kwon, 2015; Kumar P. et al., 2015). Gong et al. found that FBXO2 ubiquitinates β-secretase, which leads to protein degradation and reduced Aβ production (Gong et al., 2016). *TSPO* is mainly found in the outer mitochondrial membrane. In response to inflammatory stimulation, *TSPO* expression is highly upregulated in various inflammatory diseases, including AD (Rupprecht et al., 2010; Selvaraj and Stocco, 2015). *TSPO* is shown to be increased in postmortem brain samples from patients with AD (Venneti et al., 2009; Gui et al., 2020), which is consistent with our study. *TSPO* deficiency does not affect Aβ production, but it does accelerate Aβ deposition, leading to more senile plaques (Zhang H. et al., 2021). Studies have shown the presence of the rs6971 single nucleotide polymorphism (SNP) in *TSPO*, which produces different radioligand binding affinities (Owen et al., 2011; Tournier et al., 2020). Currently, *TSPO* is the primary target for PET and SPECT *in vivo* neuroinflammatory imaging to monitor the inflammatory state in the brain (Tournier et al., 2020; López-Picón et al., 2022). According to one of the hypotheses of AD pathogenesis, mitochondrial dysfunction occurs in the early stages, and thus, maintaining mitochondrial function may be a therapeutic strategy for AD (Readnower et al., 2011; Eckert et al., 2012; Kumar A. et al., 2015). Kim et al. identified novel *TSPO* ligands that can restore Aβ-induced mitochondrial dysfunction and improve cognitive impairment in mouse models with AD (Kim et al., 2021).

Intrinsic immune cells such as microglia and astrocytes, as well as peripheral immune cells, are involved in the neuroinflammation associated with AD (Calsolaro and Edison, 2016; Dionisio-Santos et al., 2019; Wyatt-Johnson and Brutkiewicz, 2020; Leng and Edison, 2021). Here, immune cell infiltration and immune factors were further explored. Box plots showed significant differences in multiple immune cells between the AD and the ND groups. M1 macrophages were found to be elevated in AD, which is consistent with a previous study (Liu et al., 2022). When stimulated by pro-inflammatory factors, macrophages are converted to the M1 phenotype. Upon recognition by specific receptors, it in turn secretes other pro-inflammatory mediators that further promote the conversion of unpolarized macrophages to M1, thus forming a positive pro-inflammatory feedback loop (Gate et al., 2010; Weisser et al., 2013; Sanz et al., 2020). In addition, neutrophils and gamma delta T cells were also upregulated in AD. Increased neutrophil accumulation was found in AD brains and AD model mice, and neutrophil hyperactivity is thought to be a feature of AD (Katayama, 2020; Kong et al., 2020). Katayama found that neutrophils appear to be drivers of AD and they secrete large amounts of reactive oxygen species (Katayama, 2020). Interleukin-17 (IL-17)-producing cells, mainly γδ T cells, accumulate in the brain and meninges of women with AD, accompanied by a cognitive decline (Brigas et al., 2021). IL-17-producing cells have been identified as key players in disease progression, as they promote a local immune amplification loop in the meninges and cause disruption of the blood–brain barrier (Shichita et al., 2009; Sutton et al., 2009; Gelderblom et al., 2012; Benakis et al., 2016). Heatmaps showed a strong correlation between these hub genes and different immune factors. IL-10 single nucleotide polymorphisms were found to affect the susceptibility to AD pathology (Babić Leko et al., 2020; Yang et al., 2021). When stimulated by anti-inflammatory cytokines, macrophages are converted to the M2 phenotype. Upon recognition by specific receptors, it in turn secretes other anti-inflammatory factors that promote the conversion

of unpolarized macrophages to M2, thus forming a positive feedback mechanism for the anti-inflammatory response (Gordon and Martinez, 2010; Mulder et al., 2014; Murray et al., 2014). In addition, a promising lead compound promoting IL-10 activity was provided, confirming that promoting IL-10 expression may be useful to treat AD and stroke (Sun P. et al., 2020). The interaction between astrocytic CXCL1 and neuronal CXCR2 receptors exacerbates the synaptotoxic effects of Aβ and is expected to serve as a novel target for the treatment of AD (Perez-Nievas et al., 2021). CX3CL1 was found to be decreased in the cerebrospinal fluid of patients with AD (Perea et al., 2018), which is consistent with our findings. CX3CL1 has been shown to be a strong activator of adult neurogenesis, reducing neuronal loss and improving the cognitive function of patients with AD (Fan et al., 2020). In addition, the critical roles of CX3CL1/CX3CR1 and ATP/$P2X_7R$ in regulating microglial activation in AD have been reviewed (Suresh et al., 2021).

Finally, eight drugs targeting the above genes were retrieved from the DrugBank database. Zopiclone (DB01198) is a non-benzodiazepine hypnotic used for the short-term treatment of insomnia. Several studies have found zopiclone to be helpful for insomnia in patients with AD, thereby improving their quality of life (Katsunuma et al., 1998; Richardson et al., 2021; Louzada et al., 2022). Tiludronic acid (DB01133), a bisphosphonate, was first described for the treatment of Paget's disease of the bone (Reginster et al., 1988). A study found that tiludronic acid and olsalazine may be potential drugs for the treatment of AD through *in silico* predictions, but further experimental validation is needed (G et al., 2020). Ascorbic acid (DB00126) is highly concentrated in the brain as a neuroprotective compound and may combat neurotoxic and neurodegenerative diseases, including AD (Moretti and Rodrigues, 2021). Jang *et al.* found that a mixture of Schisandra Chinensis extract and ascorbic acid improves mitochondrial function and memory and can also be used to alleviate AD and aging-related memory decline (Jang et al., 2020). Dextromethorphan (DB00514) is an NMDA receptor antagonist. Deuterated dextromethorphan/quinidine (AVP-786) is a promising and well-tolerated treatment option for agitation in AD, having completed two phase III trials (Garay and Grossberg, 2017; Khoury et al., 2021; Khoury, 2022). Resveratrol (DB02709), a polyphenolic phytoalexin, has been reported to affect several AD-related- and neuroprotective genes (Dennison et al., 2022). Resveratrol can improve AD-associated pathologies and produce therapeutic effects (Gomes et al., 2018; Rahman et al., 2020; Yan et al., 2020; Fang et al., 2021; Gu et al., 2021; Jang et al., 2021; Abozaid et al., 2022). Copper (DB09130) is a transition metal and a trace element in the body. Copper imbalance is associated with the pathogenesis of AD, which is an avenue for new therapeutic strategies (Ejaz et al., 2020; Zhu et al., 2020; Zubčić et al., 2020; Lei et al., 2021; Pal et al., 2021).

CONCLUSION

Through bioinformatics approaches, we obtained nine hub genes linking iron metabolism and AD. The biological processes and pathways in which they are involved were explored, which will help in understanding the development of AD. However, further experimental validation is required to verify these functions. Based on the logistic regression analysis, we constructed a diagnostic model that can diagnose patients with AD by detecting the expression of several genes in the blood. In addition, these hub genes have been found to be associated with different immune factors, suggesting that they may also have an important role in the immune microenvironment. However, further studies are needed to explore their specific roles. Currently, only a few drugs targeting these hub genes are predicted to alleviate AD, suggesting that additional drugs need to be developed.

DATA AVAILABILITY STATEMENT

The original contributions presented in the study are included in the article/**Supplementary Material**, further inquiries can be directed to the corresponding authors.

AUTHOR CONTRIBUTIONS

XG, XC, and CL conceived and designed the study. DL, KC, and SL were responsible for the collection and assembly of data, data analysis, and interpretation. DL and XG were involved in the writing of the manuscript. BC, PZ, and GH provided help in revising the manuscript. All authors read and approved the final manuscript.

FUNDING

This work was supported by the National Natural Science Foundation of China (81772829 and 81830052), the Special Program for Collaborative Innovation, the Construction Project of Shanghai Key Laboratory of Molecular Imaging (18DZ2260400), the Top-100 Talent Cultivation Plan of Shanghai University of Medicine and Health Sciences, Funding Scheme for Training Young Teachers in Shanghai Colleges, and Innovative Team of Intelligent Inspection and Active Health (ITIH).

SUPPLEMENTARY MATERIAL

The Supplementary Material for this article can be found online at: https://www.frontiersin.org/articles/10.3389/fnagi.2022.949083/full#supplementary-material

Supplementary Figure 1 | Expression of hub genes in the AD and ND groups of blood samples from GSE63061. **(A)** ATP6V1D. **(B)** ATP6V1G2. **(C)** ATP6V1H. **(D)** CYP26B1. **(E)** FBXO34. **(F)** PGRMC1. **(G)** PLOD1. **(H)** SNCA. **(I)** TSPO.

Supplementary Figure 2 | Expression of hub genes in the AD and ND groups of blood samples GSE85426. **(A)** ATP6V1D. **(B)** ATP6V1G2. **(C)** FBXO34. **(D)** PGRMC1. **(E)** PLOD1. **(F)** SNCA. **(G)** TSPO.

Supplementary Table 1 | Five hundred twenty genes obtained from 14 iron metabolism-related gene sets.

Supplementary Table 2 | Different immune factors were downloaded from the TISIDB database.

Supplementary Table 3 | Differentially expressed genes between AD and ND samples in GSE132903.

Supplementary Table 4 | Information on drugs targeting these nine hub genes.

REFERENCES

Abozaid, O. A. R., Sallam, M. W., El-Sonbaty, S., Aziza, S., Emad, B., and Ahmed, E. S. A. (2022). Resveratrol-selenium nanoparticles alleviate neuroinflammation and neurotoxicity in a rat model of Alzheimer's disease by regulating Sirt1/miRNA-134/GSK3β expression. *Biol. Trace Element Res.* 21:7. doi: 10.1007/s12011-021-03073-7

Alves, C. J., Dariolli, R., Jorge, F. M., Monteiro, M. R., Maximino, J. R., Martins, R. S., et al. (2015). Gene expression profiling for human iPS-derived motor neurons from sporadic ALS patients reveals a strong association between mitochondrial functions and neurodegeneration. *Front. Cell. Neurosci.* 9:289. doi: 10.3389/fncel.2015.00289

Apostolakis, S., and Kypraiou, A. M. (2017). Iron in neurodegenerative disorders: being in the wrong place at the wrong time? *Rev. Neurosci.* 28, 893–911. doi: 10.1515/revneuro-2017-0020

Babić Leko, M., Nikolac Perković, M., Klepac, N., Štrac, D., Borovečki, F., Pivac, N., et al. (2020). IL-1β, IL-6, IL-10, and TNFα single nucleotide polymorphisms in human influence the susceptibility to Alzheimer's disease pathology. *J. Alzheimer's Dis.* 75, 1029–1047. doi: 10.3233/JAD-200056

Barthold, D., Joyce, G., Ferido, P., Drabo, E. F., Marcum, Z. A., Gray, S. L., et al. (2020). Pharmaceutical treatment for Alzheimer's disease and related dementias: utilization and disparities. *J. Alzheimer's Dis.* 76, 579–589. doi: 10.3233/JAD-200133

Benakis, C., Brea, D., Caballero, S., Faraco, G., Moore, J., Murphy, M., et al. (2016). Commensal microbiota affects ischemic stroke outcome by regulating intestinal γδ T cells. *Nat. Med.* 22, 516–523. doi: 10.1038/nm.4068

Biasiotto, G., Di Lorenzo, D., Archetti, S., and Zanella, I. (2016). Iron and neurodegeneration: is ferritinophagy the link? *Mol. Neurobiol.* 53, 5542–5574. doi: 10.1007/s12035-015-9473-y

Brigas, H. C., Ribeiro, M., Coelho, J. E., Gomes, R., Gomez-Murcia, V., Carvalho, K., et al. (2021). IL-17 triggers the onset of cognitive and synaptic deficits in early stages of Alzheimer's disease. *Cell Rep.* 36:109574. doi: 10.1016/j.celrep.2021.109574

Calsolaro, V., and Edison, P. (2016). Neuroinflammation in Alzheimer's disease: current evidence and future directions. *Alzheimer's Dement.* 12, 719–732. doi: 10.1016/j.jalz.2016.02.010

Choi, D. H., Kwon, K. C., Hwang, D. J., Koo, J. H., Um, H. S., Song, H. S., et al. (2021). Treadmill exercise alleviates brain iron dyshomeostasis accelerating neuronal amyloid-β production, neuronal cell death, and cognitive impairment in transgenic mice model of Alzheimer's disease. *Mol. Neurobiol.* 58, 3208–3223. doi: 10.1007/s12035-021-02335-8

Ciechanover, A., and Kwon, Y. T. (2015). Degradation of misfolded proteins in neurodegenerative diseases: therapeutic targets and strategies. *Exp. Mol. Med.* 47:e147. doi: 10.1038/emm.2014.117

Coat, J., Demoersman, J., Beuzit, S., Cornec, D., Devauchelle-Pensec, V., Saraux, A., et al. (2015). Anti-B lymphocyte immunotherapy is associated with improvement of periodontal status in subjects with rheumatoid arthritis. *J. Clin. Periodontol.* 42, 817–823. doi: 10.1111/jcpe.12433

Dennison, J. L., Volmar, C. H., Ke, D., Wang, J., Gravel, E., Hammond-Vignini, S., et al. (2022). JOTROL, a novel formulation of resveratrol, shows beneficial effects in the 3xTg-AD mouse model. *J. Alzheimer's Dis.* 86, 173–190. doi: 10.3233/JAD-215370

DeTure, M. A., and Dickson, D. W. (2019). The neuropathological diagnosis of Alzheimer's disease. *Mol. Neurodegener.* 14:32. doi: 10.1186/s13024-019-0333-5

Dionisio-Santos, D. A., Olschowka, J. A., and O'Banion, M. K. (2019). Exploiting microglial and peripheral immune cell crosstalk to treat Alzheimer's disease. *J. Neuroinflam.* 16:74. doi: 10.1186/s12974-019-1453-0

Eckert, G. P., Renner, K., Eckert, S. H., Eckmann, J., Hagl, S., Abdel-Kader, R. M., et al. (2012). Mitochondrial dysfunction–a pharmacological target in Alzheimer's disease. *Mol. Neurobiol.* 46, 136–150. doi: 10.1007/s12035-012-8271-z

Ejaz, H. W., Wang, W., and Lang, M. (2020). Copper toxicity links to pathogenesis of Alzheimer's disease and therapeutics approaches. *Int. J. Mol. Sci.* 21:20766. doi: 10.3390/ijms21207660

Fan, Q., He, W., Gayen, M., Benoit, M. R., Luo, X., Hu, X., et al. (2020). Activated CX3CL1/Smad2 signals prevent neuronal loss and Alzheimer's tau pathology-mediated cognitive dysfunction. *J. Neurosci.* 40, 1133–1144. doi: 10.1523/JNEUROSCI.1333-19.2019

Fang, Y., Su, Z., Si, W., Liu, Y., Li, J., and Zeng, P. (2021). Network pharmacology-based study of the therapeutic mechanism of resveratrol for Alzheimer's disease. *Nan fang yi ke da xue xue bao* 41, 10–19. doi: 10.12122/j.issn.1673-4254.2021.01.02

Feng, L., Zhang, J., Ding, Q., Zhu, N., Wang, P., and Shen, Y. (2015). Autophagy involved in overexpressed tau and okadaic acid-induced hyperphosphorylated tau degradation. *Chin Pharm Bull.* 31, 356–362. doi: 10.3969/j.issn.1001-1978.2015.03.013

G, N. S. H., Ganesan Rajalekshmi, S., Murahari, M., and Burri, R. R. (2020). Reappraisal of FDA approved drugs against Alzheimer's disease based on differential gene expression and protein interaction network analysis: an *in silico* approach. *J. Biomol. Struct. Dyn.* 38, 3972–3989. doi: 10.1080/07391102.2019.1671231

Galazka-Friedman, J., Bauminger, E. R., Szlachta, K., and Friedman, A. (2012). The role of iron in neurodegeneration–Mössbauer spectroscopy, electron microscopy, enzyme-linked immunosorbent assay and neuroimaging studies. *J. Phys.* 24:244106. doi: 10.1088/0953-8984/24/24/244106

Garay, R. P., and Grossberg, G. T. (2017). AVP-786 for the treatment of agitation in dementia of the Alzheimer's type. *Expert Opin. Investig. Drugs* 26, 121–132. doi: 10.1080/13543784.2017.1267726

Gate, D., Rezai-Zadeh, K., Jodry, D., Rentsendorj, A., and Town, T. (2010). Macrophages in Alzheimer's disease: the blood-borne identity. *J. Neural Transmission* 117, 961–970. doi: 10.1007/s00702-010-0422-7

Gelderblom, M., Weymar, A., Bernreuther, C., Velden, J., Arunachalam, P., Steinbach, K., et al. (2012). Neutralization of the IL-17 axis diminishes neutrophil invasion and protects from ischemic stroke. *Blood* 120, 3793–3802. doi: 10.1182/blood-2012-02-412726

Gomes, B. A. Q., Silva, J. P. B., Romeiro, C. F. R., Dos Santos, S. M., Rodrigues, C. A., Gonçalves, P. R., et al. (2018). Neuroprotective mechanisms of resveratrol in Alzheimer's disease: role of SIRT1. *Oxid. Med. Cell. Longevity* 2018:8152373. doi: 10.1155/2018/8152373

Gong, B., Radulovic, M., Figueiredo-Pereira, M. E., and Cardozo, C. (2016). The ubiquitin-proteasome system: potential therapeutic targets for Alzheimer's disease and spinal cord injury. *Front. Mol. Neurosci.* 9:4. doi: 10.3389/fnmol.2016.00004

Gong, N. J., Dibb, R., Bulk, M., van der Weerd, L., and Liu, C. (2019). Imaging beta amyloid aggregation and iron accumulation in Alzheimer's disease using quantitative susceptibility mapping MRI. *NeuroImage* 191, 176–185. doi: 10.1016/j.neuroimage.2019.02.019

Gordon, S., and Martinez, F. O. (2010). Alternative activation of macrophages: mechanism and functions. *Immunity* 32, 593–604. doi: 10.1016/j.immuni.2010.05.007

Goudarzi, S., Hosseini, A., Abdollahi, M., and Haghi-Aminjan, H. (2021). Insights into parkin-mediated mitophagy in Alzheimer's disease: a systematic review. *Front. Aging Neurosci.* 13:674071. doi: 10.3389/fnagi.2021.674071

Gu, J., Li, Z., Chen, H., Xu, X., Li, Y., and Gui, Y. (2021). Neuroprotective effect of trans-resveratrol in mild to moderate Alzheimer disease: a randomized, double-blind trial. *Neurol. Therapy* 10, 905–917. doi: 10.1007/s40120-021-00271-2

Gui, Y., Marks, J. D., Das, S., Hyman, B. T., and Serrano-Pozo, A. (2020). Characterization of the 18 kDa translocator protein (TSPO) expression in post-mortem normal and Alzheimer's disease brains. *Brain Pathol.* 30, 151–164. doi: 10.1111/bpa.12763

Han, Y., Wang, N., Kang, J., and Fang, Y. (2020). β-Asarone improves learning and memory in Aβ(1-42)-induced Alzheimer's disease rats by regulating PINK1-Parkin-mediated mitophagy. *Metabol. Brain Dis.* 35, 1109–1117. doi: 10.1007/s11011-020-00587-2

Heras-Sandoval, D., Pérez-Rojas, J. M., Hernández-Damián, J., and Pedraza-Chaverri, J. (2014). The role of PI3K/AKT/mTOR pathway in the modulation of autophagy and the clearance of protein aggregates in neurodegeneration. *Cell. Signal.* 26, 2694–2701. doi: 10.1016/j.cellsig.2014.08.019

Hirano, K., Fujimaki, M., Sasazawa, Y., Yamaguchi, A., Ishikawa, K. I., Miyamoto, K., et al. (2019). Neuroprotective effects of memantine *via* enhancement of autophagy. *Biochem. Biophys. Res. Commun.* 518, 161–170. doi: 10.1016/j.bbrc.2019.08.025

Huynh, K. K., and Grinstein, S. (2007). Regulation of vacuolar pH and its modulation by some microbial species. *Microbiol. Mol. Biol. Rev.* 71, 452–462. doi: 10.1128/MMBR.00003-07

Jang, B. G., Lee, J., Choi, B., Koh, Y. H., and Kim, M. J. (2021). Unexpected beta-amyloid production by middle doses of resveratrol through stabilization of APP protein and AMPK-mediated inhibition of trypsin-like proteasome activity in a cell model of Alzheimer's disease. *Food Chem. Toxicol.* 152:112185. doi: 10.1016/j.fct.2021.112185

Jang, Y., Lee, J. H., Lee, M. J., Kim, S. J., Ju, X., Cui, J., et al. (2020). Schisandra extract and ascorbic acid synergistically enhance cognition in mice through modulation of mitochondrial respiration. *Nutrients* 12:40897. doi: 10.3390/nu12040897

Katayama, H. (2020). Anti-interleukin-17A and anti-interleukin-23 antibodies may be effective against Alzheimer's disease: role of neutrophils in the pathogenesis. *Brain Behav.* 10:e01504. doi: 10.1002/brb3.1504

Katsunuma, H., Shimizu, T., Ogawa, K., Kubo, H., Ishida, H., and Yoshihama, A. (1998). Treatment of insomnia by concomitant therapy with Zopiclone and Aniracetam in patients with cerebral infarction, cerebroatrophy, Alzheimer's disease and Parkinson's disease. *Psychiatr. Clin. Neurosci.* 52, 198–200. doi: 10.1111/j.1440-1819.1998.tb01028.x

Khoury, R. (2022). Deuterated dextromethorphan/quinidine for agitation in Alzheimer's disease. *Neural Regener. Res.* 17, 1013–1014. doi: 10.4103/1673-5374.324842

Khoury, R., Marx, C., Mirgati, S., Velury, D., Chakkamparambil, B., and Grossberg, G. T. (2021). AVP-786 as a promising treatment option for Alzheimer's Disease including agitation. *Expert Opin. Pharmacother.* 22, 783–795. doi: 10.1080/14656566.2021.1882995

Kim, T., Morshed, M. N., Londhe, A. M., Lim, J. W., Lee, H. E., Cho, S., et al. (2021). The translocator protein ligands as mitochondrial functional modulators for the potential anti-Alzheimer agents. *J. Enzyme Inhibit. Med. Chem.* 36, 831–846. doi: 10.1080/14756366.2021.1900158

Kong, Y., Liu, K., Hua, T., Zhang, C., Sun, B., and Guan, Y. (2020). PET imaging of neutrophils infiltration in Alzheimer's disease transgenic mice. *Front. Neurol.* 11:523798. doi: 10.3389/fneur.2020.523798

Kumar, A., Singh, A., and Ekavali, A. (2015). A review on Alzheimer's disease pathophysiology and its management: an update. *Pharmacol. Rep.* 67, 195–203. doi: 10.1016/j.pharep.2014.09.004

Kumar, P., Jha, N. K., Jha, S. K., Ramani, K., and Ambasta, R. K. (2015). Tau phosphorylation, molecular chaperones, and ubiquitin E3 ligase: clinical relevance in Alzheimer's disease. *J. Alzheimer's Dis.* 43, 341–361. doi: 10.3233/JAD-140933

Lai, D., Tan, L., Zuo, X., Liu, D., Jiao, D., Wan, G., et al. (2021). Prognostic ferroptosis-related lncRNA signatures associated with immunotherapy and chemotherapy responses in patients with stomach cancer. *Front. Genet.* 12:798612. doi: 10.3389/fgene.2021.798612

Langfelder, P., and Horvath, S. (2008). WGCNA: an R package for weighted correlation network analysis. *BMC Bioinformat.* 9:559. doi: 10.1186/1471-2105-9-559

Lee, J. H., and Lee, M. S. (2019). Brain iron accumulation in atypical Parkinsonian syndromes: *in vivo* MRI evidences for distinctive patterns. *Front. Neurol.* 10:74. doi: 10.3389/fneur.2019.00074

Lee, J. H., Yu, W. H., Kumar, A., Lee, S., Mohan, P. S., Peterhoff, C. M., et al. (2010). Lysosomal proteolysis and autophagy require presenilin 1 and are disrupted by Alzheimer-related PS1 mutations. *Cell* 141, 1146–1158. doi: 10.1016/j.cell.2010.05.008

Lei, P., Ayton, S., and Bush, A. I. (2021). The essential elements of Alzheimer's disease. *J. Biol. Chem.* 296:100105. doi: 10.1074/jbc.REV120.008207

Leng, F., and Edison, P. (2021). Neuroinflammation and microglial activation in Alzheimer disease: where do we go from here? *Nat. Rev. Neurol.* 17, 157–172. doi: 10.1038/s41582-020-00435-y

Li, W. X., Li, G. H., Tong, X., Yang, P. P., Huang, J. F., Xu, L., et al. (2020). Systematic metabolic analysis of potential target, therapeutic drug, diagnostic method and animal model applicability in three neurodegenerative diseases. *Aging* 12, 9882–9914. doi: 10.18632/aging.103253

Liberzon, A., Birger, C., Thorvaldsdóttir, H., Ghandi, M., Mesirov, J. P., and Tamayo, P. (2015). The molecular signatures database (MSigDB) hallmark gene set collection. *Cell Syst.* 1, 417–425. doi: 10.1016/j.cels.2015.12.004

Liu, C., Zhang, X., Chai, H., Xu, S., Liu, Q., Luo, Y., et al. (2022). Identification of immune cells and key genes associated with Alzheimer's disease. *Int. J. Medical Sci.* 19, 112–125. doi: 10.7150/ijms.66422

Long, J. M., and Holtzman, D. M. (2019). Alzheimer disease: an update on pathobiology and treatment strategies. *Cell* 179, 312–339. doi: 10.1016/j.cell.2019.09.001

López-Picón, F. R., Keller, T., Bocancea, D., Helin, J. S., Krzyczmonik, A., Helin, S., et al. (2022). Direct comparison of [(18)F]F-DPA with [(18)F]DPA-714 and [(11)C]PBR28 for neuroinflammation imaging in the same Alzheimer's disease model mice and healthy controls. *Mol. Imaging Biol.* 24, 157–166. doi: 10.1007/s11307-021-01646-5

Louzada, L. L., Machado, F. V., Quintas, J. L., Ribeiro, G. A., Silva, M. V., Mendonça-Silva, D. L., et al. (2022). The efficacy and safety of zolpidem and zopiclone to treat insomnia in Alzheimer's disease: a randomized, triple-blind, placebo-controlled trial. *Neuropsychopharmacology* 47, 570–579. doi: 10.1038/s41386-021-01191-3

Lucin, K. M., O'Brien, C. E., Bieri, G., Czirr, E., Mosher, K. I., Abbey, R. J., et al. (2013). Microglial beclin 1 regulates retromer trafficking and phagocytosis and is impaired in Alzheimer's disease. *Neuron* 79, 873–886. doi: 10.1016/j.neuron.2013.06.046

Majumder, S., Richardson, A., Strong, R., and Oddo, S. (2011). Inducing autophagy by rapamycin before, but not after, the formation of plaques and tangles ameliorates cognitive deficits. *PLoS ONE* 6:e25416. doi: 10.1371/journal.pone.0025416

Mills, E., Dong, X.-P., Wang, F., and Xu, H. (2010). Mechanisms of brain iron transport: insight into neurodegeneration and CNS disorders. *Future Med Chem.* 2, 51–64. doi: 10.4155/fmc.09.140

Moretti, M., and Rodrigues, A. L. S. (2021). Functional role of ascorbic acid in the central nervous system: a focus on neurogenic and synaptogenic processes. *Nutr. Neurosci.* 2021, 1–11. doi: 10.1080/1028415X.2021.1956848

Mou, Y., Zhang, Y., Wu, J., Hu, B., Zhang, C., Duan, C., et al. (2020). The landscape of iron metabolism-related and methylated genes in the prognosis prediction of clear cell renal cell carcinoma. *Front. Oncol.* 10:788. doi: 10.3389/fonc.2020.00788

Mulder, R., Banete, A., and Basta, S. (2014). Spleen-derived macrophages are readily polarized into classically activated (M1) or alternatively activated (M2) states. *Immunobiology* 219, 737–745. doi: 10.1016/j.imbio.2014.05.005

Mullard, A. (2021). Landmark Alzheimer's drug approval confounds research community. *Nature* 594, 309–310. doi: 10.1038/d41586-021-01546-2

Murray, P. J., Allen, J. E., Biswas, S. K., Fisher, E. A., Gilroy, D. W., Goerdt, S., et al. (2014). Macrophage activation and polarization: nomenclature and experimental guidelines. *Immunity* 41, 14–20. doi: 10.1016/j.immuni.2014.06.008

Owen, D. R., Gunn, R. N., Rabiner, E. A., Bennacef, I., Fujita, M., Kreisl, W. C., et al. (2011). Mixed-affinity binding in humans with 18-kDa translocator protein ligands. *J. Nucl. Med.* 52, 24–32. doi: 10.2967/jnumed.110.079459

Pal, A., Rani, I., Pawar, A., Picozza, M., Rongioletti, M., and Squitti, R. (2021). Microglia and astrocytes in Alzheimer's disease in the context of the aberrant copper homeostasis hypothesis. *Biomolecules* 11:111598. doi: 10.3390/biom11111598

Pantopoulos, K., Porwal, S. K., Tartakoff, A., and Devireddy, L. (2012). Mechanisms of mammalian iron homeostasis. *Biochemistry* 51, 5705–5724. doi: 10.1021/bi300752r

Patrick, G. N. (2006). Synapse formation and plasticity: recent insights from the perspective of the ubiquitin proteasome system. *Curr. Opin. Neurobiol.* 16, 90–94. doi: 10.1016/j.conb.2006.01.007

Peng, Y., Chang, X., and Lang, M. (2021). Iron homeostasis disorder and Alzheimer's disease. *Int. J. Mol. Sci.* 22:12442. doi: 10.3390/ijms222212442

Perea, J. R., Lleó, A., Alcolea, D., Fortea, J., Ávila, J., and Bolós, M. (2018). Decreased CX3CL1 levels in the cerebrospinal fluid of patients with Alzheimer's disease. *Front. Neurosci.* 12:609. doi: 10.3389/fnins.2018.00609

Perez-Nievas, B. G., Johnson, L., Beltran-Lobo, P., Hughes, M. M., Gammallieri, L., Tarsitano, F., et al. (2021). Astrocytic C-X-C motif chemokine ligand-1 mediates β-amyloid-induced synaptotoxicity. *J. Neuroinflam.* 18:306. doi: 10.1186/s12974-021-02371-0

Quintana, C., and Gutiérrez, L. (2010). Could a dysfunction of ferritin be a determinant factor in the aetiology of some neurodegenerative diseases? *Biochim. Biophys. Acta* 1800, 770–782. doi: 10.1016/j.bbagen.2010.04.012

Rahman, M. H., Akter, R., Bhattacharya, T., Abdel-Daim, M. M., Alkahtani, S., Arafah, M. W., et al. (2020). Resveratrol and neuroprotection: impact and its therapeutic potential in Alzheimer's disease. *Front. Pharmacol.* 11:619024. doi: 10.3389/fphar.2020.619024

Randle, S. J., and Laman, H. (2016). F-box protein interactions with the hallmark pathways in cancer. *Semin. Cancer Biol.* 36, 3–17. doi: 10.1016/j.semcancer.2015.09.013

Raven, E. P., Lu, P. H., Tishler, T. A., Heydari, P., and Bartzokis, G. (2013). Increased iron levels and decreased tissue integrity in hippocampus of Alzheimer's disease detected *in vivo* with magnetic resonance imaging. *J. Alzheimer's Dis.* 37, 127–136. doi: 10.3233/JAD-130209

Readnower, R. D., Sauerbeck, A. D., and Sullivan, P. G. (2011). Mitochondria, amyloid β, and Alzheimer's disease. *Int. J. Alzheimer's Dis.* 2011:104545. doi: 10.4061/2011/104545

Reginster, J. Y., Jeugmans-Huynen, A. M., Albert, A., Denis, D., Deroisy, R., Lecart, M. P., et al. (1988). Biological and clinical assessment of a new bisphosphonate, (chloro-4 phenyl) thiomethylene bisphosphonate, in the treatment of Paget's disease of bone. *Bone* 9, 349–354. doi: 10.1016/8756-3282(88)90115-9

Richardson, K., Savva, G. M., Boyd, P. J., Aldus, C., Maidment, I., Pakpahan, E., et al. (2021). Non-benzodiazepine hypnotic use for sleep disturbance in people aged over 55 years living with dementia: a series of cohort studies. *Health Technol. Assess.* 25, 1–202. doi: 10.3310/hta25010

Ru, B., Wong, C. N., Tong, Y., Zhong, J. Y., Zhong, S. S. W., Wu, W. C., et al. (2019). TISIDB: an integrated repository portal for tumor-immune system interactions. *Bioinformatics* 35, 4200–4202. doi: 10.1093/bioinformatics/btz210

Rupprecht, R., Papadopoulos, V., Rammes, G., Baghai, T. C., Fan, J., Akula, N., et al. (2010). Translocator protein (18 kDa) (TSPO) as a therapeutic target for neurological and psychiatric disorders. *Nat. Rev. Drug Discov.* 9, 971–988. doi: 10.1038/nrd3295

Sanz, M., Marco Del Castillo, A., Jepsen, S., Gonzalez-Juanatey, J. R., D'Aiuto, F., Bouchard, P., et al. (2020). Periodontitis and cardiovascular diseases: consensus report. *J. Clin. Periodontol.* 47, 268–288. doi: 10.1111/jcpe.13189

Selvaraj, V., and Stocco, D. M. (2015). The changing landscape in translocator protein (TSPO) function. *Trends Endocrinol. Metabol.* 26, 341–348. doi: 10.1016/j.tem.2015.02.007

Sepe, S., Nardacci, R., Fanelli, F., Rosso, P., Bernardi, C., Cecconi, F., et al. (2014). Expression of Ambra1 in mouse brain during physiological and Alzheimer type aging. *Neurobiol. Aging* 35, 96–108. doi: 10.1016/j.neurobiolaging.2013.07.001

Shichita, T., Sugiyama, Y., Ooboshi, H., Sugimori, H., Nakagawa, R., Takada, I., et al. (2009). Pivotal role of cerebral interleukin-17-producing gammadeltaT cells in the delayed phase of ischemic brain injury. *Nat. Med.* 15, 946–950. doi: 10.1038/nm.1999

Sun, C., Qiu, X., Wang, Y., Liu, J., Li, Q., Jiang, H., et al. (2020). Long-term oral melatonin alleviates memory deficits, reduces amyloid-β deposition associated with downregulation of BACE1 and mitophagy in APP/PS1 transgenic mice. *Neurosci. Lett.* 735:135192. doi: 10.1016/j.neulet.2020.135192

Sun, P., Zhou, W., Yue, H., Zhang, C., Ou, Y., Yang, Z., et al. (2020). Compound AD110 acts as therapeutic management for Alzheimer's disease and stroke in mouse and rat models. *ACS Chem. Neurosci.* 11, 929–938. doi: 10.1021/acschemneuro.9b00651

Suresh, P., Phasuk, S., and Liu, I. Y. (2021). Modulation of microglia activation and Alzheimer's disease: CX3 chemokine ligand 1/CX3CR and P2X(7)R signaling. *Tzu chi Med. J.* 33, 1–6. doi: 10.4103/tcmj.tcmj_144_20

Sutton, C. E., Lalor, S. J., Sweeney, C. M., Brereton, C. F., Lavelle, E. C., and Mills, K. H. (2009). Interleukin-1 and IL-23 induce innate IL-17 production from gammadelta T cells, amplifying Th17 responses and autoimmunity. *Immunity* 31, 331–341. doi: 10.1016/j.immuni.2009.08.001

Tan, Z., Sun, X., Hou, F. S., Oh, H. W., Hilgenberg, L. G., Hol, E. M., et al. (2007). Mutant ubiquitin found in Alzheimer's disease causes neuritic beading of mitochondria in association with neuronal degeneration. *Cell Death Different.* 14, 1721–1732. doi: 10.1038/sj.cdd.4402180

Thirupathi, A., and Chang, Y. Z. (2019). Brain iron metabolism and CNS diseases. *Adv. Exp. Med. Biol.* 1173, 1–19. doi: 10.1007/978-981-13-9589-5_1

Tournier, B. B., Tsartsalis, S., Ceyzériat, K., Garibotto, V., and Millet, P. (2020). *In vivo* TSPO signal and neuroinflammation in Alzheimer's disease. *Cells* 9:1941. doi: 10.3390/cells9091941

Vahlensieck, C., Thiel, C. S., Adelmann, J., Lauber, B. A., Polzer, J., and Ullrich, O. (2021). Rapid transient transcriptional adaptation to hypergravity in jurkat T cells revealed by comparative analysis of microarray and RNA-seq data. *Int. J. Mol. Sci.* 22:168451. doi: 10.3390/ijms22168451

van Tijn, P., Hobo, B., Verhage, M. C., Oitzl, M. S., van Leeuwen, F. W., and Fischer, D. F. (2011). Alzheimer-associated mutant ubiquitin impairs spatial reference memory. *Physiol. Behav.* 102, 193–200. doi: 10.1016/j.physbeh.2010.11.001

Venneti, S., Wiley, C. A., and Kofler, J. (2009). Imaging microglial activation during neuroinflammation and Alzheimer's disease. *J. Neuroimmune Pharmacol.* 4, 227–243. doi: 10.1007/s11481-008-9142-2

Wang, H., Jiang, T., Li, W., Gao, N., and Zhang, T. (2018). Resveratrol attenuates oxidative damage through activating mitophagy in an *in vitro* model of Alzheimer's disease. *Toxicol. Lett.* 282, 100–108. doi: 10.1016/j.toxlet.2017.10.021

Ward, R. J., Zucca, F. A., Duyn, J. H., Crichton, R. R., and Zecca, L. (2014). The role of iron in brain ageing and neurodegenerative disorders. *Lancet Neurol.* 13, 1045–1060. doi: 10.1016/S1474-4422(14)70117-6

Weisser, S. B., McLarren, K. W., Kuroda, E., and Sly, L. M. (2013). Generation and characterization of murine alternatively activated macrophages. *Methods Mol. Biol.* 946, 225–239. doi: 10.1007/978-1-62703-128-8_14

Williamson, W. R., and Hiesinger, P. R. (2010). On the role of v-ATPase V0a1-dependent degradation in Alzheimer disease. *Commun. Integr. Biol.* 3, 604–607. doi: 10.4161/cib.3.6.13364

Wishart, D. S., Feunang, Y. D., Guo, A. C., Lo, E. J., Marcu, A., Grant, J. R., et al. (2018). DrugBank 5.0: a major update to the DrugBank database for 2018. *Nucl. Acids Res.* 46, D1074–d1082. doi: 10.1093/nar/gkx1037

Wyatt-Johnson, S. K., and Brutkiewicz, R. R. (2020). The complexity of microglial interactions with innate and adaptive immune cells in Alzheimer's disease. *Front. Aging Neurosci.* 12:592359. doi: 10.3389/fnagi.2020.592359

Yan, N., and Zhang, J. (2019). Iron metabolism, ferroptosis, and the links with Alzheimer's disease. *Front. Neurosci.* 13:1443. doi: 10.3389/fnins.2019.01443

Yan, Y., Yang, H., Xie, Y., Ding, Y., Kong, D., and Yu, H. (2020). Research progress on Alzheimer's disease and resveratrol. *Neurochem. Res.* 45, 989–1006. doi: 10.1007/s11064-020-03007-0

Yang, R., Duan, J., Luo, F., Tao, P., and Hu, C. (2021). IL-6, IL-8 and IL-10 polymorphisms may impact predisposition of Alzheimer's disease: a meta-analysis. *Acta Neurol. Belgica* 121, 1505–1512. doi: 10.1007/s13760-020-01369-4

Zhang, H., Wang, H., Gao, F., Yang, J., Xu, Y., Fu, Y., et al. (2021). TSPO deficiency accelerates amyloid pathology and neuroinflammation by impairing microglial phagocytosis. *Neurobiol. Aging* 106, 292–303. doi: 10.1016/j.neurobiolaging.2021.06.020

Zhang, T., Liu, N., Wei, W., Zhang, Z., and Li, H. (2021). Integrated analysis of weighted gene co-expression network analysis identifying six genes as novel biomarkers for Alzheimer's disease. *Oxid. Med. Cell. Longevity* 2021:9918498. doi: 10.1155/2021/9918498

Zhao, Y., Hegde, A. N., and Martin, K. C. (2003). The ubiquitin proteasome system functions as an inhibitory constraint on synaptic strengthening. *Current biology : CB.* 13, 887–898. doi: 10.1016/S0960-9822(03)00332-4

Zhu, X., Victor, T. W., Ambi, A., Sullivan, J. K., Hatfield, J., Xu, F., et al. (2020). Copper accumulation and the effect of chelation treatment on cerebral amyloid angiopathy compared to parenchymal amyloid plaques. *Metallomics : integrated biometal science.* 12, 539–546. doi: 10.1039/c9mt00306a

Zubčić, K., Hof, P. R., Šimić, G., and Jazvinšćak Jembrek, M. (2020). The Role of Copper in Tau-Related Pathology in Alzheimer's Disease. *Frontiers in molecular neuroscience.* 13: 572308. doi: 10.3389/fnmol.2020.572308

Conflict of Interest: The authors declare that the research was conducted in the absence of any commercial or financial relationships that could be construed as a potential conflict of interest.

Publisher's Note: All claims expressed in this article are solely those of the authors and do not necessarily represent those of their affiliated organizations, or those of the publisher, the editors and the reviewers. Any product that may be evaluated in this article, or claim that may be made by its manufacturer, is not guaranteed or endorsed by the publisher.

frontiers | Frontiers in Aging Neuroscience

ORIGINAL RESEARCH
published: 07 July 2022
doi: 10.3389/fnagi.2022.934283

Development and Validation of a Website to Guide Decision-Making for Disorders of Consciousness

*Junwei Kang†, Yuan Zhong†, Gengfa Chen†, Lianghua Huang, Yunliang Tang, Wen Ye and Zhen Feng**

Department of Rehabilitation Medicine, First Affiliated Hospital of Nanchang University, Nanchang, China

Background: This study aimed to develop and validate a nomogram and present it on a website to be used to predict the overall survival at 16, 32, and 48 months in patients with prolonged disorder of consciousness (pDOC).

Methods: We retrospectively analyzed the data of 381 patients with pDOC at two centers. The data were randomly divided into training and validation sets using a ratio of 6:4. On the training set, Cox proportional hazard analyses were used to identify the predictive variables. In the training set, two models were screened by COX regression analysis, and based on clinical evidence, model 2 was eventually selected in the nomogram after comparing the receiver operating characteristic (ROC) of the two models. In the training and validation sets, ROC curves, calibration curves, and decision curve analysis (DCA) curves were utilized to measure discrimination, calibration, and clinical efficacy, respectively.

Results: The final model included age, Glasgow coma scale (GCS) score, serum albumin level, and computed tomography (CT) midline shift, all of which had a significant effect on survival after DOCs. For the 16-, 32-, and 48-month survival on the training set, the model had good discriminative power, with areas under the curve (AUCs) of 0.791, 0.760, and 0.886, respectively. For the validation set, the AUCs for the 16-, 32-, and 48-month survival predictions were 0.806, 0.789, and 0.867, respectively. Model performance was good for both the training and validation sets according to calibration plots and DCA.

Conclusion: We developed an accurate, efficient nomogram, and a corresponding website based on four correlated factors to help clinicians improve their assessment of patient outcomes and help personalize the treatment process and clinical decisions.

Keywords: clinical prediction, nomogram, Glasgow coma scale score, disorders of consciousness (DOC), website

OPEN ACCESS

Edited by:
Tao Huang,
Shanghai Institute of Nutrition and Health (CAS), China

Reviewed by:
Jinhua Cai,
Children's Hospital of Chongqing Medical University, China
Hao Zhang,
The Second Affiliated Hospital of Harbin Medical University, China

***Correspondence:**
Zhen Feng
fengzhen@email.ncu.edu.cn

†These authors have contributed equally to this work

Specialty section:
This article was submitted to Neurocognitive Aging and Behavior, a section of the journal Frontiers in Aging Neuroscience

Received: *02 May 2022*
Accepted: *30 May 2022*
Published: *07 July 2022*

Citation:
Kang J, Zhong Y, Chen G, Huang L, Tang Y, Ye W and Feng Z (2022) Development and Validation of a Website to Guide Decision-Making for Disorders of Consciousness. Front. Aging Neurosci. 14:934283. doi: 10.3389/fnagi.2022.934283

INTRODUCTION

The treatment of disorders of consciousness (DOCs) is a global challenge. Prolonged DOC (pDOC) refers to the loss of consciousness for more than 28 days, which usually occurs after traumatic brain injury, especially when severe (Kondziella et al., 2020). There is currently no effective treatment for DOCs, and most patients are bedridden and require long-term and arduous care. The cost of treatment and care from injury to death may be as high as US$1 million (Ragnarsson, 2002).

Globally, the number of patients with pDOC is staggering. Reportedly, there are ∼100,000–300,000 patients with pDOC in the United States (Giacino et al., 2018), whereas in Europe, the proportion is about 0.2–6.1 cases for every 100,000 people (Erp et al., 2015). No accurate reports exist on the matter in China, but it is commonly thought that the incidence and prevalence of pDOC are increasing. This poses a challenge for clinical medicine and places a large burden on the local economy. The prognosis of DOC is directly related to the decisions made by the patients' family members and clinicians, which form the basis for further neurological rehabilitation. Therefore, objective and sound prognostication is important and urgently needed. However, accurately predicting the outcomes of patients with DOCs remains a challenge.

At present, evaluation of the clinical prognosis of patients with DOC mainly relies on scales and clinical manifestations, but this has disadvantages, such as high subjectivity and poor accuracy. Song et al. (2018) studied the relationship between resting-state cerebral functional MRI (fMRI) and the 1-year outcome of patients with pDOC. Certain patterns found in the sleep electroencephalogram (EEG) can be used to predict the short-term outcome of pDOC patients (Yang et al., 2020). Anderson et al. (2020) found that three biomarkers (GFAP, UCH-L1, and MAP-2) were related to the recovery of patients with pDOC within 6 months. Unfortunately, today no universally applicable scoring system for predicting mortality in patients with DOCs is available. Therefore, the goal of our study was to develop and validate a system for scoring the risk of death in patients with pDOC. Such a system can help to identify patients at high risk of death, which, in turn, will contribute to their clinical management.

The characteristic of a nomogram is that it contains many variables and can predict the probability of an event in a single patient (Kattan, 2002). In this study, we developed a website to predict the survival rate of patients with pDOC based on a nomogram. In addition, two data sets were used to evaluate the performance, discrimination, and calibration of the model. The model is simple and practical, and can be used as an early warning and prediction system for patients with DOC.

METHODS

Study Participants

This study involved participants from two research centers, the First Affiliated Hospital of Nanchang University and Shangrao Hospital of Traditional Chinese Medicine. The keywords, "coma" and "disorder of consciousness," were entered into the medical record information system, and all the patients admitted from January 1, 2016, to January 1, 2021, who met these conditions were considered. Patients with pDOC caused by anoxic, traumatic, or vascular events, and with a course of at least 28 days (Giacino et al., 2018), were included in this study.

Patients with a history of craniocerebral injury or DOC not caused by craniocerebral injury, as well as those without follow-up data, information on cause of death, and incomplete medical records were excluded from this study. A total of 381 patients

TABLE 1 | Comparison of baseline data between the training set and validation set.

Features	Training set (n = 229)	Validation set (n = 152)	P-value
Age (years)	52.14 ± 14.75	53.52 ± 15.04	0.374
Sex			0.629
Male	162 (70.7%)	104 (68.4%)	
Female	67 (29.3%)	48 (31.6%)	
Level of consciousness			0.492
VS	152 (66.4%)	106 (69.6%)	
MCS	77 (33.6%)	46 (30.4%)	
Etiology			0.743
Trauma	115 (50.2%)	72 (47.4%)	
Stroke	92 (40.2%)	67 (44.1%)	
Anoxia	22 (9.6%)	13 (8.5%)	
GCS total score	9.00 (6.00, 9.00)	8.00 (6.00, 9.00)	0.618
CRS-R total score	5.00 (3.00, 8.00)	5.00 (4.00, 8.00)	0.754
Serum albumin			0.326
≥35 g/L	147 (64.2%)	90 (59.2%)	
<35 g/L	82 (35.8%)	62 (40.8%)	
Epilepsy			0.685
Presence	24 (10.5%)	14 (9.2%)	
Absence	205 (89.5%)	138 (90.8%)	
Hydrocephalus			0.077
Presence	33 (14.4%)	12 (7.9%)	
Absence	196 (85.6%)	140 (92.1%)	
Multiple injuries			0.398
Presence	88 (38.4%)	65 (42.8%)	
Absence	141 (61.6%)	87 (57.2%)	
Midline shift			0.275
Presence	52 (22.7%)	42 (27.6%)	
Absence	177 (77.3%)	110 (72.4%)	
Hypertension			0.752
Presence	85 (37.1%)	54 (35.5%)	
Absence	144 (62.9%)	98 (64.5%)	
Diabetes			0.404
Presence	63	36	
Absence	166	116	
Smoking history			0.119
Presence	33 (%)	13 (%)	
Absence	196 (%)	139 (%)	
Subarachnoid hemorrhage			0.471
Presence	85	62	
Absence	144	90	
Craniotomy			0.739
Presence	106	73	
Absence	123	79	
Pupillary light reflex			0.507
One or both absent	56	30	
Presence	173	122	
State			0.332
Death	61	33	
Survival	168	119	

TABLE 2 | Cox regression analyses of prognostic factors in patients with prolonged disorders of consciousness in the training set.

Variable	Univariate		Multivariate	
	HR (95%CI)	*P*-value	HR (95%CI)	*P*-value
Age (years)	1.041 (1.022–1.061)	0.000	1.022 (1.002–1.044)	0.0305
Sex				
Female	Ref			
Male	0.787 (0.439–1.410)	0.421		
Level of consciousness				
VS	Ref		Ref	
MCS	0.386 (0.196–0.762)	0.006	0.525 (0.222–1.243)	0.143
Etiology				
Trauma	Ref			
Stroke	1.123 (0.657–1.918)	0.671		
Anoxia	1.509 (0.661–3.447)	0.328		
GCS total score	0.798 (0.717–0.889)	0.000	0.874 (0.783–0.976)	0.0162
CRS-R total score	0.819 (0.449–1.494)	0.514		
Serum albumin(g/L)				
<35	Ref		Ref	
≥35	0.434 (0.262–0.717)	0.001	0.580 (0.342–0.984)	0.0433
Epilepsy				
Presence	Ref			
Absence	1.363 (0.546–3.403)	0.507		
Hydrocephalus				
Presence	Ref			
Absence	0.554 (0.304–1.007)	0.053		
Multiple injuries				
Presence	Ref			
Absence	1.698 (0.970–2.974)	0.064		
Midline shift				
Presence	Ref		Ref	
Absence	0.417 (0.248–0.700)	0.001	0.557 (0.319–0.971)	0.039
Hypertension				
Presence	Ref			
Absence	0.622 (0.376–1.029)	0.065		
Diabetes				
Presence	Ref		Ref	
Absence	0.485 (0.290–0.813)	0.006	0.618 (0.366–1.045)	0.073
Smoking history				
Presence	Ref			
Absence	0.643 (0.342–1.209)	0.170		
Pupillary light reflex				
One or both absent	Ref			
Presence	0.644 (0.373–1.111)	0.114		
Subarachnoid hemorrhage				
Presence	Ref			
Absence	1.045 (0.619–1.763)	0.869		
Craniotomy				
Presence	Ref			
Absence	0.990 (0.599–1.637)	0.969		

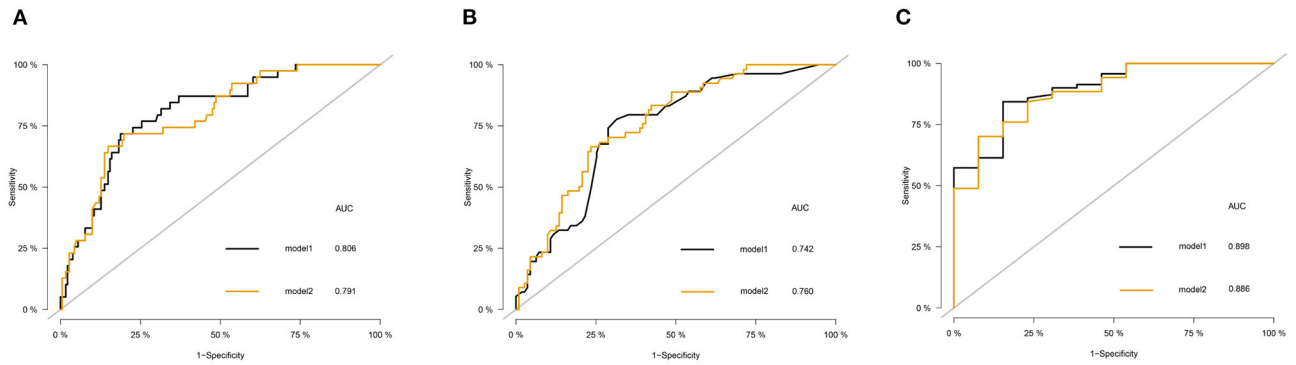

FIGURE 1 | The receiver operating characteristic (ROC) curve of the model 1 and model 2 in the training set. **(A)** Comparison of ROC curves of model 1 and model 2 for predicting the survival of patients with disorder of consciousness (DOC) at 16 months. **(B)** Comparison of ROC curves of model 1 and model 2 for predicting the survival of patients with DOC at 32 months. **(C)** Comparison of ROC curves of model 1 and model 2 for predicting the survival of patients with DOC at 48 months.

were finally included and randomized into training (60%) and validation (40%) cohorts.

Data Collection

Seventeen potential predictors were collected in detail from the electronic medical records of the selected patients, including baseline demographic data (age, sex, and etiology such as trauma, stroke, or hypoxia), patient status at admission [state of consciousness such as vegetative state (VS) or minimally concious state (MCS), Glasgow coma scale (GCS) and Coma Recovery Scale-Revised (CRS-R) scores, and pupillary light reflex], laboratory test results (albumin and lateral shift of cerebral midline structures), complications (epilepsy, hydrocephalus, cobwebs, and submembranous hemorrhage), and medical history (hypertension, diabetes, smoking history, multiple trauma, and history of craniotomy). The duration of survival and survival status of each patient were also extracted. To reduce sampling bias, data were obtained with consultation, involving effective communication and cross-checking, of the medical staff.

Statistical Analysis

In order to improve the accuracy of our statistical analysis, and to reduce the bias caused by missing data, this paper made multiple data imputations (Sterne et al., 2009). Patients were randomly divided into training and validation cohorts using a ratio of 6:4. The comparability of the two groups was assessed (**Table 1**). Continuous data conforming to the normal distribution were presented as mean ± standard deviation (m ± s), and independent samples *t*-tests were used to infer differences between the training and validation sets. For those with skewed distribution, the median (1st quartile, 3rd quartile) was used to describe them, and the Mann-Whitney U test was used to compare the two groups. Categorical variables were expressed as frequencies (proportions), and the chi-squared test or Fisher's exact test was used for their comparison.

To screen predictors, we performed Cox proportional hazards analyses in the training set. Variables with a *p*-value of <0.05 in the multivariate Cox regression were used as independent predictors (Abougergi et al., 2018). However, it is important to consider both clinical and statistical significance when selecting covariates for inclusion. Therefore, we used the state of consciousness with a *p*-value of >0.05 in the Cox regression analysis in our model, based on sufficient clinical evidence (Giacino et al., 2018). We combined variables with significant differences in the Cox regression and variables based on clinical evidence to develop two predictive models. In order to select the optimal model, Delong's test was used to compare the area under the receiver operating characteristic (ROC) curve of model 1 and model 2, and finally incorporate the optimal model into the nomogram. For both the training and validation groups, the performance of the nomogram was evaluated with calibration plots and decision curve analysis (DCA). All analyses were performed using R software (version 3.6.3).

Based on the scores for each factor in the nomogram, an overall risk score was calculated for each patient in the entire cohort. Patients were divided into two groups according to their risk: low and high risks (a restricted cubic spline was used to model the non-linear relationship between the overall risk score and the survival of patients with DOC). The Kaplan-Meier and log-rank methods were used to compare the survival of the two groups.

RESULTS

Baseline Patient Characteristics

A total of 381 patients from the two centers were included. The general data of the training and validation cohorts are shown in **Table 1**. During the follow-up period, 61 deaths were recorded for the training cohort, representing a mortality rate of 26.6%. For the validation cohort, 33 deaths were recorded, representing a mortality rate of 21.7%.

Development of Nomogram for DOC

Univariate analysis showed that age, GCS score, state of consciousness, diabetes, albumin, and computed tomography (CT) midline shift were associated with the risk of death from

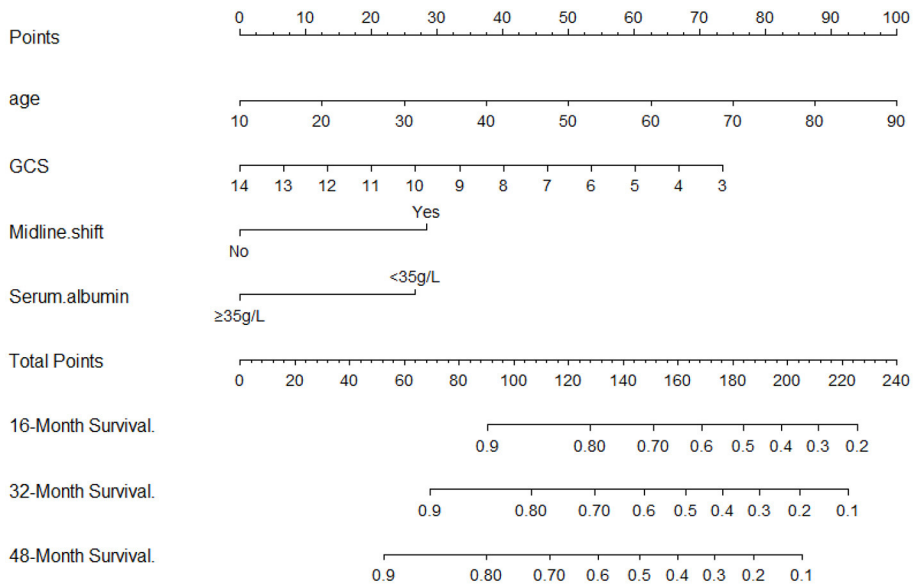

FIGURE 2 | A clinical feature model was used to develop a nomogram.

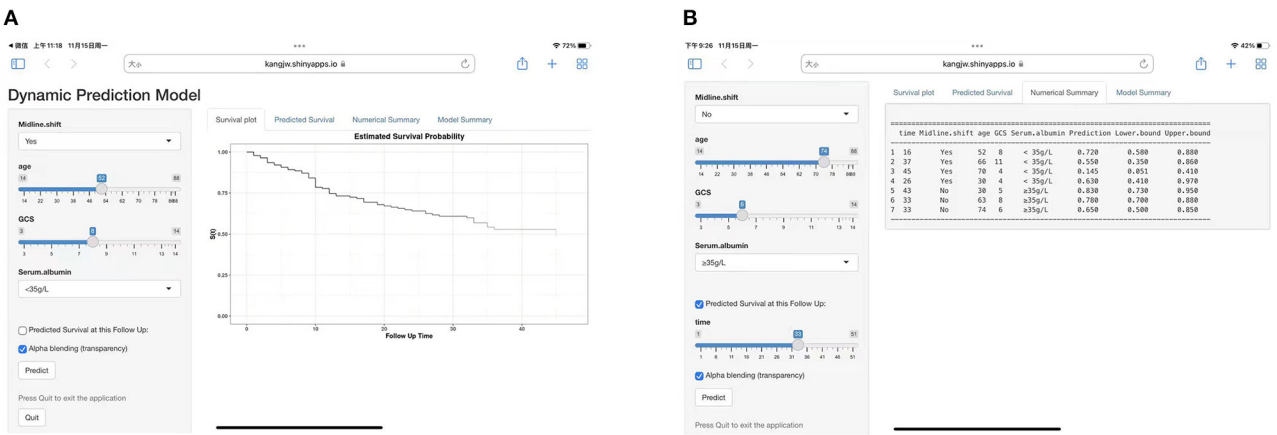

FIGURE 3 | Construction of a web-based calculator for predicting DOC's disease survival based on the model (https://kangjw.shinyapps.io/P-Doc/). **(A)** Web survival rate calculator. **(B)** 95% confidence interval (CI) of the web survival rate calculator.

a DOC. Multivariate Cox regression analysis revealed that four of these variables (age, GCS score, CT midline shift, and albumin) were independent risk factors for DOC death (**Table 2**). The state of consciousness did not show a significant difference in the multivariate analysis. However, based on clinical evidence, we combined the variables with significant differences during Cox regression and variables based on clinical evidence to develop two predictive models—model 1: age + CT midline shift + albumin + GCS + state of consciousness; model 2: age + CT Midline shift + albumin + GCS. The individual performance and comprehensive performance of the two models were analyzed using ROC curves to determine which one was optimal. The ROC curves of models 1 and 2 at 16, 32, and 48 months were similar: 80.6 vs. 79.1, $p = 0.075$; 74.2 vs. 76, $p = 0.162$; and 89.8 vs. 88.6, $p = 0.270$, respectively (**Figure 1**). Since the best model should be the simplest and with fewer variables (Van, 2018), we selected the four variables of model 2 and incorporated them into the nomogram (**Figure 2**), which is an intuitive visual model. According to the nomogram, age had the greatest impact on DOC prognosis, followed by the GCS score, midline shift, and albumin. The total score was the sum of the individual scores of these four variables, and the specific probabilities of survival at 16, 32, and 48 months were finally derived based on the score.

Establishment of a Website

To facilitate the use of the nomogram in clinical settings, we built a website (https://kangjw.shinyapps.io/P-Doc/). For example: at 52 years of age, with midline shift, GCS score of 8, and albumin

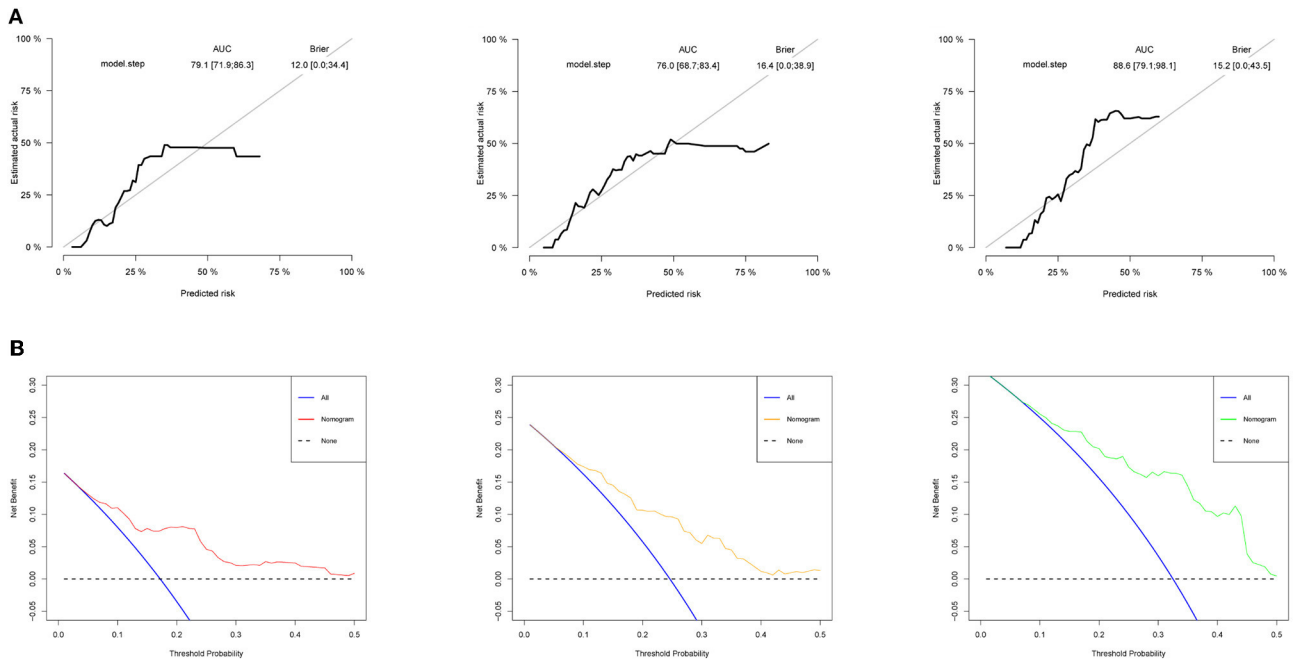

FIGURE 4 | Model performance in the training set. **(A)** Calibration curves of 16-, 32-, and 48-month specific survival. **(B)** Decision curve analyses (DCA) for predicting the survival of patients with DOC at 16, 32, and 48 months by nomogram.

concentration of <35 g/l, the 16-month survival rate was ∼72% [95% confidence interval (CI): 58–88.0%] (**Figure 3**).

Model Performance on the Training Set

The ROC curve was used to evaluate the detection performance of the model in the training set. The area under the curve (AUC) values for predicting the 16-, 32-, and 48-month survival rates were 0.791, 0.760, and 0.886, respectively (**Figure 1**), indicating that the nomogram was effective at predicting prognosis. The calibration curve based on the training set showed that the nomogram had good calibration capabilities (**Figure 4A**). In addition, the DCA curves showed that the nomogram could be used for valuable judgments (**Figure 4B**). The management of patients with DOCs will benefit from this predictive model.

Model Performance on the Validation Set

We used the validation cohort to evaluate the predictive models. The discrimination, calibration, and clinical effectiveness of nomograms were evaluated using the ROC curves, calibration curves, and DCA, respectively. Model 2 showed good discrimination for prognostic prediction, with AUCs of 0.806, 0.789, and 0.867 for the 16-, 32-, and 48-month survival rates, respectively (**Figure 5A**). In addition, we performed a calibration curve analysis, whose results showed that the model had good probabilistic agreement between the predictions and observations on the validation set (**Figure 5B**). The model was better at predicting DOC survival (**Figure 5C**).

Risk Stratification by Nomogram

For the training set, the nomogram was used to calculate the total prognosis score. Classification was performed using a restricted cubic spline assessment (**Figure 6A**), and the total prognostic scores were divided into two risk groups to predict mortality (group A: 0–100 points, group B: >100 points). For both the training and validation sets, the survival analysis of patients with low-risk disease showed significantly better outcomes than those with high-risk disease ($p < 0.0001$ and $p = 0.0011$; **Figures 6B,C**).

DISCUSSION

With the continuous improvement of current diagnosis and treatment systems, the mortality rate of high-risk diseases, such as traumatic brain injury and cerebral apoplexy, has been declining, but the number of patients with DOC tends to increase. Predicting the survival time of patients with DOCs will aid in the development of appropriate healthcare and DOC management guidelines and will be highly beneficial for clinicians in personalizing DOC management and optimizing limited health resources. Through a retrospective study of DOC patients in two centers, we comprehensively evaluated the relationships between routine clinical scores, laboratory tests, and DOC mortality rates. An optimal predictive model for predicting DOC-related mortality with satisfactory consistency and accuracy was successfully developed and carefully evaluated.

Available evidence suggests that the prognosis of patients can be judged simply and intuitively from a nomogram, which makes it convenient for clinical personnel to use and interpret its results (Lei et al., 2016; Chen et al., 2019). To the best of our knowledge,

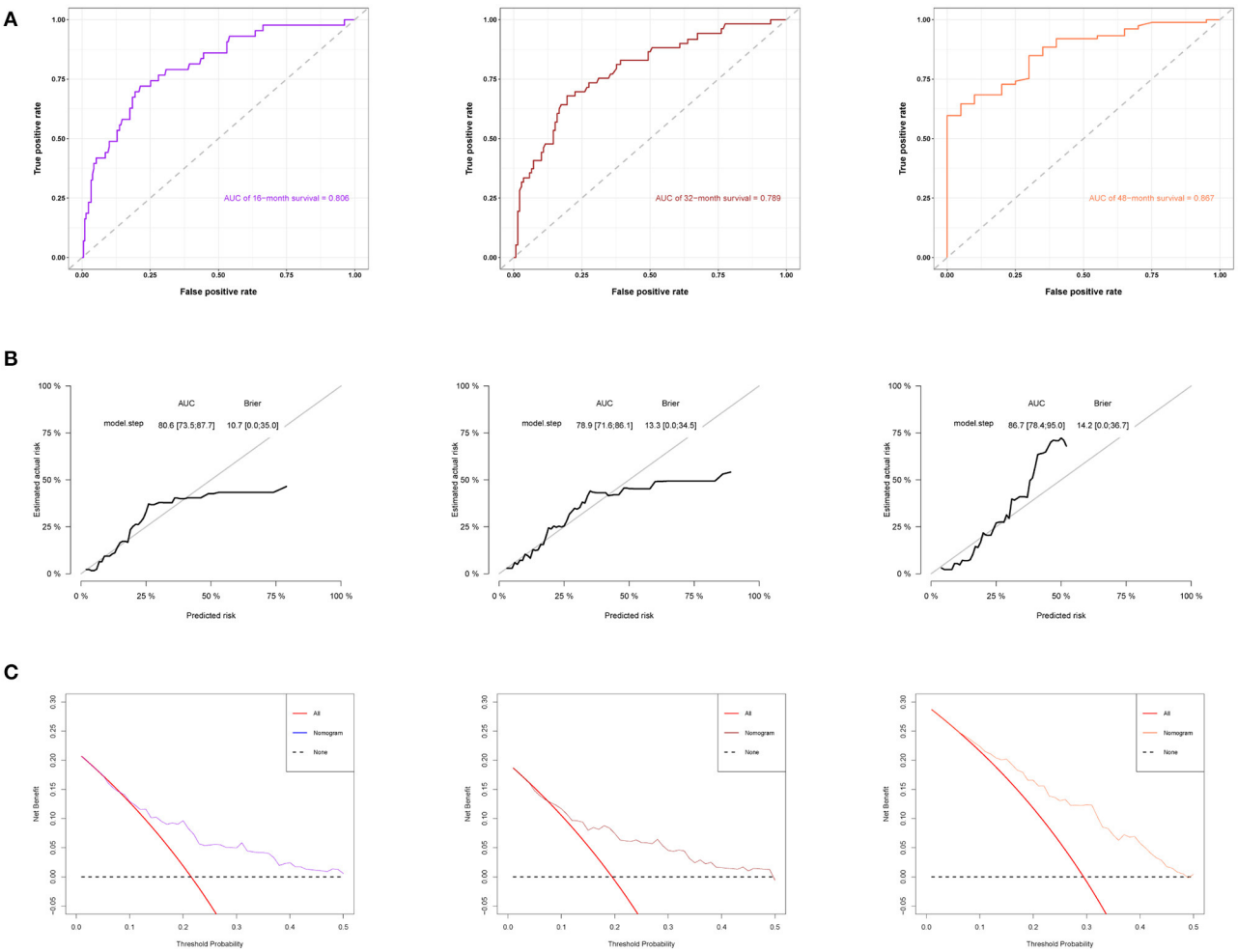

FIGURE 5 | Model discrimination and performance in the validation set. **(A)** ROC curves for nomogram-based prognostic prediction. **(B)** Calibration curve of 16-, 32-, and 48-month specific survival. **(C)** DCA of this nomogram in the validation set.

our current model is the first to be used to develop a nomogram to predict DOC survival probability using simple and readily available metrics. We developed a multivariate Cox proportional hazards regression model (model 2) based on our observation that age, GCS score, midline shift, and low albumin concentration were independently associated with mortality related to DOC. In addition, there was no clear association between consciousness status and death outcome in our multivariate Cox proportional hazards regression model. However, we included them in model 1 based on clinical evidence. By comparing the areas under the ROC curves of models 1 and 2, we finally settled with model 2 as our final model. Model 2 was based on four features (age, GCS, midline shift, and albumin concentration), and it showed good discriminative ability for both the training and validation sets. For the training set, the AUCs for the 16-, 32-, and 48-month survival rates were 0.791, 0.760, and 0.886, respectively. For the validation set, the AUCs for the 16-, 32-, and 48-month survival rates were 0.806, 0.789, and 0.867, respectively. Model performance was also evaluated using calibration curves and DCA for both the datasets. Our results suggest that the model can serve as a cost-effective tool to predict the prognosis of DOC and assist in clinical decision-making.

So far, few studies have been done on the markers of survival outcomes in patients with DOC. Therefore, the variables selected are the most readily available and easy to ascertain for widespread clinical application. For our model, we identified four variables for the survival prediction of DOC. First, age had the largest strongest association. Previous studies have shown that prognosis deteriorates with age in patients with DOC. The possible reason is that meningeal fibrosis is more severe in older patients than in young patients due to the decline in circulatory and metabolic capacity with age. This affects the circulation and absorption of cerebrospinal fluid, in addition to the significantly weaker resistance to disease progression than in younger patients (Hao et al., 2016). Therefore, age is considered the greatest risk factor for DOC mortality.

The second variable is the GCS score, which is one of the most widely used tools for examining a patient's level of consciousness

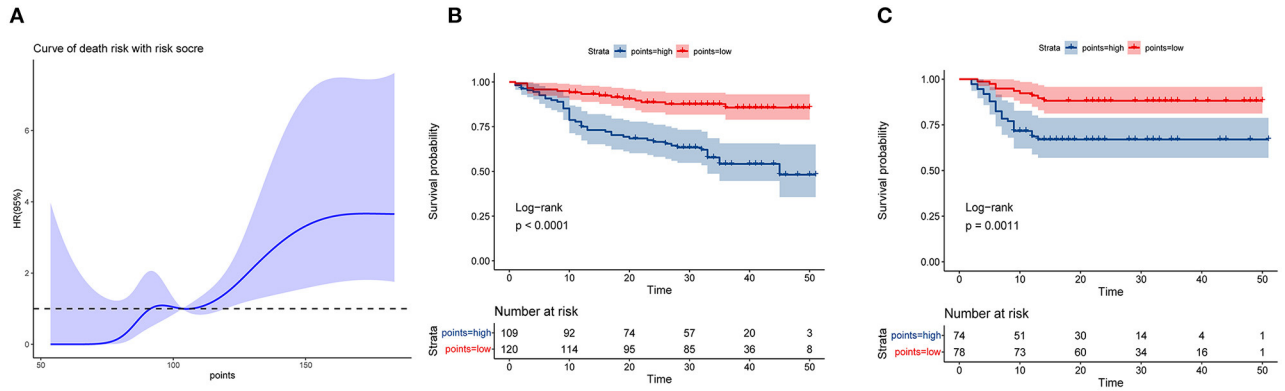

FIGURE 6 | Performance of the nomogram in stratifying the risk of patients. **(A)** Restricted cubic spline analysis of the total risk score in the training set. **(B)** Kaplan–Meier survival analysis between the low- and high-risk groups in the training set. **(C)** Kaplan–Meier survival analysis between the low- and high-risk groups in the validation set.

(Perel et al., 2008; Dijkland et al., 2019). Our study showed a significant correlation between the GCS score and patient survival outcomes, which is consistent with previous reports. Our third variable, brain midline shift, refers to changes in the position of the midline structures of the brain, which are closely related to the hypothalamic-pituitary axis, the efferent and afferent pathways, and the centers that regulate important life activities such as breathing and heart rate. Brain midline shift can lead to abnormalities in the frequency, rhythm, and amplitude of the heartbeat and respiration of patients. In addition, the patient may also experience endocrine dysfunction, which is a serious threat to life and causes a poor prognosis. Therefore, in our study, we found that the survival outcomes of patients with a midline shift were significantly different from those without it. The fourth variable is hypoproteinemia. This is not an independent disease, but a negative nitrogen balance due to various reasons. Albumin accounts for two-thirds of the total plasma protein and plays an important role in the transport and binding of many molecules. Patients with pDOC may have low serum albumin concentrations because of the following causes (Corrigan et al., 2016; Sorby-Adams et al., 2017). First, bleeding: trauma leads to vascular damage, which may involve the blood-brain barrier, which causes loss of albumin and hemoglobin. Second, the strong stress after traumatic brain injury may also lead to the release of inflammatory mediators, thereby enhancing vascular permeability. This may promote the transfer of albumin from the blood vessels to the interstitial space. Hypoalbuminemia can seriously impair the defense and immune function of patients with DOC and cause various complications such as pulmonary infection (Sung et al., 2004), which seriously affects the prognosis of DOC.

Predicting the outcome of patients with DOC is challenging. Joint prediction of multiple variables can reduce errors and improve overall accuracy. At present, in the neuroscience community, the most explored brain monitoring technologies are fMRI, positron emission tomography, and EEG (Stender et al., 2014; Wang et al., 2015; Song et al., 2020). However, these technologies are not only difficult to operate but also expensive, which makes them prohibitive for medical institutions of different levels. Furthermore, there are currently no multivariate models to predict mortality outcomes.

The prediction model established in this study is based on four clinical parameters. Previous studies have shown that the level of consciousness and CRS-R score are correlated with the prognosis of DOC (Giacino et al., 2018). However, in this study, the CRS-R score showed no significant difference in either univariate or multivariate Cox regression, while the consciousness status was only statistically different for univariate Cox analysis, which may be related to its heterogeneity. Our study has several important characteristics. First, the nomogram is a model with the ability to predict prognosis that integrates meaningful variables, provides graphs and visualizations of data, and predicts individual outcomes in a very detailed and intuitive way. We distributed our nomogram via a website, which is convenient for clinical use. Second, previous studies have focused on predicting the probability of improvement in DOC, and this study is the first to develop a model to predict DOC survival outcomes. Our study provides foundational insights for clinical decision-making of patients with DOC. In addition, our model used clinical variables that are easy to obtain. Through verification, we found that this model had good clinical application value.

This study had limitations. First, it was a retrospective cohort study involving a small sample. Therefore, it was subject to information bias and selection bias, which is also the inherent limitation of retrospective research. To validate our model, it is necessary to carry out a prospective study with a larger sample size in multiple centers. Second, GCS and albumin concentration in our model may not have been stable throughout the follow-up period, which may have affected the accuracy of prediction to an extent. Third, the characteristics of patients with impaired consciousness may differ with medical settings and regions. Our study participants were exclusively Chinese and limited to Jiangxi Province, which may limit the generalizability of our findings to a wider population. Therefore, it is still necessary to

select multicenter experiments in different regions to verify the accuracy and effectiveness of the model.

In conclusion, our study identified age, GCS score, CT midline shift, and albumin concentrations as significant predictors of the survival outcomes of DOC. A website based on a nomogram was developed to use this model easily in clinical settings. In addition, as the model can distinguish the patients with DOC who have a high risk of mortality, it is useful for use during the follow-up periods. This model may facilitate decision-making, preventive strategies, and individualized treatment for DOC.

DATA AVAILABILITY STATEMENT

The datasets generated or analyzed during this study are available from the corresponding author on reasonable request.

ETHICS STATEMENT

The studies involving human participants were reviewed and approved by Ethics Committee of the First Affiliated Hospital of Nanchang University. The patients/participants provided their written informed consent to participate in this study.

AUTHOR CONTRIBUTIONS

JK conducted experiments and wrote manuscripts. YZ and GC designed the study and collected the data. LH performed the statistical analysis of the data. YT and WY searched the relevant literature. ZF secured funding for the project. All authors have read and approved the final manuscript.

FUNDING

The study was funded by the Major Research Development Program of Jiangxi Province (Grant No. 20202BBG72002), National Natural Science Foundation of China (Grant No. 82160437), Youth Talent Cultivation Project of First Affiliated Hospital of Nanchang University (Grant No. PRJ-20211017170929794), and Science and Technology Project of Jiangxi Provincial Health Commission (Grant No. 202210362).

REFERENCES

Abougergi, M. S., Peluso, H., and Saltzan, J. R. (2018). Thirty-day readmission among patients with non-variceal upper gastrointestinal hemorrhage and effects on outcomes. *Gastroenterology* 155, 38–46. doi: 10.1053/j.gastro.2018.03.033

Anderson, T. N., Hwang, J., Munar, M., Papa, L., Hinson, H. E., and Vaughan, A., et al. (2020). Blood-based biomarkers for prediction of intracranial hemorrhage and outcome in patients with moderate or severe traumatic brain injury. *J. Trauma Acute Care* 89, 80–86. doi: 10.1097/TA.0000000000002706

Chen, L., Cai, B. B., Zhou, C. J., Hou, X. Q., Hu, S. P., and Fang, G., et al. (2019). A sample model established by S-index predicting overall survival after curative resection of primary hepatocellular carcinoma. *Cancer Manag. Res.* 11, 693–703. doi: 10.2147/CMAR.S193593

Corrigan, F., Mander, K. A., Leonard, A. V., and Vink, R. (2016). Neurogenic inflammation after traumatic brain injury and its potentiation of classical inflammation. *J. Neuroinflamm.* 13, 264. doi: 10.1186/s12974-016-0738-9

Dijkland, S. A., Foks, K. A., Polinder, S., Dippel, D., and Steyerberg, E. W. (2019). Prognosis in moderate and severe traumatic brain injury: a systematic review of contemporary models and validation studies. *J. Neurotraum.* 37, 1–13. doi: 10.1089/neu.2019.6401

Erp, W., Lavrijsen, J., van de Laar, F. A., Vos, P. E., Laureys, S., and Koopmans, R. (2015). The vegetative state/unresponsive wakefulness syndrome: a systematic review of prevalence studies. *Eur. J. Neurol.* 21, 1361–1368. doi: 10.1111/ene.12483

Giacino, J., Katz, D., Schiff, N., Whyte, J., Ashman, E., and Ashwal, S., et al. (2018). Comprehensive systematic review update summary: disorders of consciousness: report of the guideline development, dissemination, and implementation subcommittee of the american academy of neurology; the American congress of rehabilitation medicine; and the national institute on disability, independent living, and rehabilitation research. *Arch. Phys. Med. Rehab.* 99, 1710–1719. doi: 10.1016/j.apmr.2018.07.002

Hao, X., Junwen, W., Jiaqing, L., Ran, L., Zhuo, Z., and Yimin, H., et al. (2016). High fibrosis indices in cerebrospinal fluid of patients with shunt-dependent post-traumatic chronic hydrocephalus. *Transl. Neurosci.* 7, 92–97. doi: 10.1515/tnsci-2016-0015

Kattan, M. W. (2002). Nomograms. Introduction. *Semin. Urol. Oncol.* 20, 79–81.

Kondziella, D., Bender, A., Diserens, K., Erp, W. V., Estraneo, A., and Formisano, R., et al. (2020). European Academy of Neurology guideline on the diagnosis of coma and other disorders of consciousness. *Eur. J. Neurol.* 27, 741–756. doi: 10.1111/ene.14151

Lei, Z., Li, J., Dong, W., Yong, X., Wang, Q., and Si, A., et al. (2016). Nomogram for preoperative estimation of microvascular invasion risk in hepatitis b virus–related hepatocellular carcinoma within the milan criteria. *JAMA Surg.* 151, 356–363. doi: 10.1001/jamasurg.2015.4257

Perel, P., Arango, M., Clayton, T., Edwards, P., and Komolafe, E. (2008). Predicting outcome after traumatic brain injury: Practical prognostic models based on large cohort of international patients. *BMJ* 336, 425–429. doi: 10.1136/bmj.39461.643438.25

Ragnarsson, K. T. (2002). Results of the NIH consensus conference on "Rehabilitation of persons with traumatic brain injury". *Restor. Neurol. Neurosci.* 20, 103–108.

Song, M., Yang, Y., Yang, Z., Cui, Y., Yu, S., and He, J., et al. (2020). Prognostic models for prolonged disorders of consciousness: an integrative review. *Cell. Mol. Life Sci.* 77, 3945–3961. doi: 10.1007/s00018-020-03512-z

Song, M., Yi, Y., He, J., Yang, Z., Shan, Y., and Xie, Q., et al. (2018). Prognostication of chronic disorders of consciousness using brain functional networks and clinical characteristics. *eLife Sci.* 7, e36173. doi: 10.7554/eLife.36173

Sorby-Adams, A. J., Marcoionni, A. M., Dempsey, E. R., Woenig, J. A., and Turner, R. J. (2017). The role of neurogenic inflammation in Blood-Brain barrier disruption and development of cerebral oedema following acute central nervous system (CNS) injury. *Int. J. Mol. Sci.* 18, 1788. doi: 10.3390/ijms18081788

Stender, J., Gosseries, O., Bruno, M., Charland-Verville, V., Vanhaudenhuyse, A., and Demertzi, A., et al. (2014). Diagnostic precision of PET imaging and functional MRI in disorders of consciousness: a clinical validation study. *Lancet* 384, 514–522. doi: 10.1016/S0140-6736(14)60042-8

Sterne, J. A., White, I. R., Carlin, J. B., Spratt, M., Royston, P., and Kenward, M. G., et al. (2009). Multiple imputation for missing data in epidemiological and clinical research: potential and pitfalls. *BMJ* 338, b2393. doi: 10.1136/bmj.b2393

Sung, J., Bochicchio, G. V., Joshi, M., Bochicchio, K., and Scalea, T. M. (2004). Admission serum albumin is predicitve of outcome in critically ill trauma patients. *Am Surg.* 70, 1099–1102.

Van, D. B. H. A. (2018). Occam's razor: from Ockham's via moderna to modern data science. *Sci. Progress* 101, 261–272. doi: 10.3184/003685018X15295002645082

Wang, F., Di, H., Hu, X., Jing, S., Thibaut, A., and Perri, C. D., et al. (2015). Cerebral response to subject's own name showed high prognostic value in traumatic vegetative state. *BMC Med.* 13, 1–13. doi: 10.1186/s12916-015-0330-7

Yang, X. A., Song, C. G., Yuan, F., Zhao, J. J., and Jiang, W. (2020). Prognostic roles of sleep electroencephalography pattern and circadian rhythm biomarkers in the recovery of consciousness in patients with coma: a prospective cohort study. *Sleep Med.* 69, 204–212. doi: 10.1016/j.sleep.2020.01.026

Conflict of Interest: The authors declare that the research was conducted in the absence of any commercial or financial relationships that could be construed as a potential conflict of interest.

frontiers | Frontiers in Aging Neuroscience

ORIGINAL RESEARCH
published: 03 August 2022
doi: 10.3389/fnagi.2022.925072

Molecular Mechanism of *Xingnao Kaiqiao* Pill for Perioperative Neurocognitive Disorder and Its Correlation With Immune and Inflammatory Signaling Pathways Based on Network Pharmacology and Molecular Docking

Weiwei Zhang[1,2†], Gaoxiang Shi[1,2†], Hui Wang[1,2], Miaomiao Feng[1,2], Xiang Gao[1,2], Qipeng Xie[1,2], Ning Zhang[1,2] and Zhigan Lv[1,2]*

[1] Shanxi Bethune Hospital, Tongji Shanxi Hospital, Third Hospital of Shanxi Medical University, Shanxi Academy of Medical Sciences, Taiyuan, China, [2] Tongji Medical College, Tongji Hospital, Huazhong University of Science and Technology, Wuhan, China

To investigate the molecular mechanism of *Xingnao Kaiqiao* Pill in the treatment of perioperative neurocognitive disorder (PND) from the perspective of network pharmacology and molecular docking technology. Active ingredients of *Xingnao Kaiqiao* Pill were screened from the traditional Chinese medicine database and analysis platform, and the putative targets were predicted. The GeneCards database was searched to obtain PND-related targets. The genes corresponding to the targets were searched and annotated on the UniProt database. The VennDiagram package in R was employed to obtain common target genes. The overlap genes were introduced into STRING to obtain a protein-protein interaction (PPI) network; thus, key targets were screened. The target relationship network of "*Xingnao Kaiqiao* Pill–traditional Chinese medicine–compound–common target" was constructed by Cytoscape software. Using R language package Bioconductor, Gene Ontology (GO) and pathway enrichment analysis (Kyoto Encyclopedia of Genes and Genomes Pathway, KEGG Pathway) were performed on the common target genes. A total of 45 active ingredients of *Xingnao Kaiqiao* Pill were screened, with 182 potential targets, and 1,579 PND-related targets were retrieved from the GeneCards databases (Score $\geq$ 1). Using VennDiagram, 132 overlap genes were gotten. *Xingnao Kaiqiao* Pill mainly acted on targets, such as MAPK and JUN. GO enrichment analysis displayed G protein-coupled amine receptor activity, nuclear receptor activity, ligand-activated transcription factor activity, G protein-coupled neurotransmitter receptor activity, steroid hormone receptor activity, and cytokine receptor activity. KEGG enrichment analysis exhibited 157 signaling pathways. The regulation of interleukin 17, tumor necrosis factor, hypoxia-inducible factor-1, and MAPK signaling pathways affected central nervous system (CNS) inflammatory response,

OPEN ACCESS

Edited by:
Min Tang,
Jiangsu University, China

Reviewed by:
Jian Su,
Nanjing University of Information Science and Technology, China
Xinyan Wang,
Xi'an Peihua University, China
Zhixin Zhou,
Hangzhou Dianzi University, China

***Correspondence:**
Zhigan Lv
sxbqeyylzg@gmail.com

† These authors have contributed equally to this work and share first authorship

Specialty section:
This article was submitted to Neuroinflammation and Neuropathy, a section of the journal Frontiers in Aging Neuroscience

Received: *21 April 2022*
Accepted: *22 June 2022*
Published: *03 August 2022*

Citation:
Zhang W, Shi G, Wang H, Feng M, Gao X, Xie Q, Zhang N and Lv Z (2022) Molecular Mechanism of Xingnao Kaiqiao Pill for Perioperative Neurocognitive Disorder and Its Correlation With Immune and Inflammatory Signaling Pathways Based on Network Pharmacology and Molecular Docking. Front. Aging Neurosci. 14:925072. doi: 10.3389/fnagi.2022.925072

cellular immunity, tumor-related signaling pathways, protected neurons, and inhibited PND. The active ingredients of *Xingnao Kaiqiao* Pill adjust interleukin 17, tumor necrosis factor, hypoxia-inducible factor-1, and MAPK signaling pathways by acting on cell targets, such as JUN, MAPK, AKT1, etc., and finally exert a therapeutic effect on PND.

Keywords: network pharmacology, perioperative neurocognitive disorder, drug targets, inflammatory factors, molecular docking

INTRODUCTION

With the increased number of elderly surgical patients, brain dysfunction after general anesthesia has been paid more and more attention in clinical practice. Neurocognitive changes related to surgery and anesthesia are mainly composed of postoperative delirium (POD) and postoperative cognitive dysfunction (POCD) (Kong et al., 2022). Since 2018, perioperative neurocognitive disorder (PND) has been used internationally to describe cognitive function changes during the perioperative period (Evered et al., 2018). PND is mainly manifested as a decline in postoperative cognitive function, which is reflected in impaired memory, attention, comprehension, and reduced ability to process information. The pathophysiological mechanism of PND is still unclear, among which neuroinflammation may be the most important mechanism (Subramaniyan and Terrando, 2019). Cytokines in the central nervous system (CNS), such as IL-6, may contribute to neuroinflammation and PND (Pereira et al., 2022). Nevertheless, there is, currently, a lack of specific therapeutic medicines.

With the clinical development of integrated traditional Chinese and western medicine, traditional Chinese medicine compound preparations have been extensively utilized in the clinical treatment and prevention of PND. For patients with PND, traditional Chinese medicine preparations *Xingnao Kaiqiao* Pill, *Angong Niuhuang* Pill, and *Buyang Huanwu* Decoction are utilized for intervention, and have certain clinical effects (Zhu and Feng, 2018). *Xingnao Kaiqiao* Pill is composed of *Gastrodiaelata Bl., Bovis Calculus, Arum Ternatum Thunb, Acoritataninowii Rhizoma, Caulis Bambusae in Taenia, Arisaematis Rhizoma, Trichosanthes Kirilowii Maxim, Coptidis Rhizoma,* and *Polygalae Radix. Xingnao Kaiqiao* Pill can calm the mind, strengthen the body resistance, eliminate pathogenic factors, suppress the hyperactive liver, relieve endogenous wind, regulate qi, resolve depression, strengthen the brain, and tonify the kidney. Modern pharmacology has found that active ingredients of above-mentioned Chinese medicines can regulate immunity, inhibit inflammation, adjust autophagy/apoptosis, and protect neurons (Hu et al., 2014; Yu et al., 2014).

With the continuous maturity of computer and database technology, the traditional Chinese medicine database and analysis platform (TCMSP) was built based on the big data of traditional Chinese medicines. The molecular network of various complex components constructed by network pharmacology and the protein/gene interactions based on multilevel targets can explain the material basis and functions of traditional Chinese medicine. Network pharmacology analysis is becoming an important method for studying complex diseases caused by multiple genes and multiple factors, such as PND. This study investigated the mechanism of *Xingnao Kaiqiao* Pill in the treatment of PND, explained the scientificity and feasibility of traditional Chinese medicine empirical medication from the perspective of molecular biology, and provided a reference for the development of targeted medicines using the TCMSP and the latest technology of Chinese medicine compound prescriptions.

MATERIALS AND METHODS

Collection and Screening of Active Ingredients of *Xingnao Kaiqiao* Pill

The TCMSP database[1] was employed to search the active ingredients of the *Xingnao Kaiqiao* Pill formula (*Arum Ternatum Thunb, Acoritataninowii Rhizoma, Caulis Bambusae in Taenia, Arisaematis Rhizoma, Trichosanthes Kirilowii Maxim, Coptidis Rhizoma, Bovis Calculus, Gastrodiaelata Bl,* and *Polygalae Radix*) (Ru et al., 2014). Two parameters related to ADME (absorption, distribution, metabolism, and excretion), i.e., oral bioavailability (OB) greater than or equal to 30% and drug-likeness (DL) greater than or equal to 0.18 were set to screen the obtained active ingredients.

Investigation and Prediction of Compound-Related Targets

Chemoinformatics was employed to predict the targets of the Chinese medicine components in *Xingnao Kaiqiao* Pill using the TCMSP platform and the DrugBank database. For compounds whose targets were not found in the TCMSP, the *Pharmacopoeia* was retrieved, and literature search was conducted, and then the Pharm Mapper database was used for target prediction. The sdf format of the active ingredients was uploaded to the Pharm Mapper platform, with the property of "homo sapiens" set, and the putative targets could be obtained.

Screening of Perioperative Neurocognitive Disorder-Related Targets

The full name of PND was entered as a search term, and the disease-related targets could be retrieved on the GeneCards database. The output results of GeneCards used a relevance score greater than 1 as the screening criteria. Considering that PND has used names, such as POD and POCD, in the past, "postoperative delirium" and "postoperative cognitive dysfunction" were also

[1]http://tcmspw.com/tcmsp.php

input as search terms to prevent omission; the search results were summarized, and the targets were merged.

Annotation of Gene Names

The active ingredients of the above-mentioned medicines and the targets corresponding to the diseases were searched on the UniProt database.[2] The UniProt ID and Gene Name were annotated for each target. The Hash function of the Perl script was employed for automatic annotation of the above targets so as to perform further analysis.

Determination of Compound-Disease Overlap Genes

The VennDiagram package in R software was employed to calculate the overlap between the targets of *Xingnao Kaiqiao* Pill and PND, and the intersection genes corresponding to the compound disease were screened out as common target genes to determine the potential targets of *Xingnao Kaiqiao* Pill acting on PND.

Construction of "*Xingnao Kaiqiao* Pill—Traditional Chinese Medicine—Compound—Common Target" Relationship Network

The drug names, active ingredients, and the common target genes between drug and disease were imported into the Cytoscape 3.9.1 software to construct the network diagram of "*Xingnao Kaiqiao* Pill—traditional Chinese medicine—compound—common target" relationship network for visual analysis (Shannon et al., 2003).

Construction and Analysis of Protein-Protein Interaction Network

The above-mentioned common target genes were uploaded to the STRING 11.5 database,[3] with the limitation of "*Homo sapiens*" as the species, and the interaction score greater than 0.9. The protein—protein interaction network was imported to the Cytoscape 3.9.1 software, and the CytoHubba plug-in was used to screen key targets encoded by hub genes. We employed four algorithms, namely, Degree, Betweenness, Closeness, and MCC to rank key targets or hub genes. The Degree value of a node shows the number of connections to that node in the network. The higher the value is, the more likely the target to be the key target.

Gene Ontology and Kyoto Encyclopedia of Genes and Genomes Enrichment Analysis of Common Targets

GO and KEGG enrichment analyses of common target genes were performed using the ClusterProfiler package in the R software to obtain the relevant functions and pathways with false discovery rate (FDR) less than 0.05 (Wu et al., 2021). The GO enrichment categories of common target genes include biological process (BP), cellular component (CC), and molecular function (MF). The barplots, dotplots, and pathway plots were drawn by using the ggplot2 package in R, and the common target genes, namely, drug-disease intersection genes were marked on the pathway plots.

Molecular Docking Simulation

In order to further verify the interaction between the active components of *Xingnao Kaiqiao* Pill and key targets encoded by hub genes, The RCSB PDB database (错误!超链接引用无效。was utilized to query large proteins. The structure of small molecules was obtained from the PubChem database.[4] Potential targets and corresponding components were used to simulate molecular docking. The software programs used were AutoDock-4.2 and AutoDockTools-1.5.7 (Morris et al., 2009).

RESULTS

Collection and Screening of Active Ingredients and Predictive Targets of Chinese Herbal Medicines in *Xingnao Kaiqiao* Pill

TCMSP and literature retrieval were employed to get the basic information of Chinese herbal medicines contained in *Xingnao Kaiqiao* Pill, as is shown in **Table 1**. The same components and targets were analyzed in **Table 2**. After deleting the duplicate values, 45 effective chemical components of all the single medicine in *Xingnao Kaiqiao* Pill and 182 predicted targets were determined.

[2]https://www.uniprot.org/

[3]https://string-db.org/

[4]https://pubchem.ncbi.nlm.nih.gov

TABLE 1 | Information of ingredients in *Xingnao Kaiqiao* Pill and their putative targets.

Chinese name	Latin name	Compound number	Predict target number
Banxia	*Arum Ternatum Thunb*	12	172
Changpu	*Acoritataninowii Rhizoma*	4	103
Danxing	*Arisaematis Rhizoma*	6	81
Gualou	*Trichosanthes Kirilowii Maxim*	10	35
Huanglian	*Coptidis Rhizoma*	11	285
Niuhuang	*Bovis Calculus*	5	18
Yuanzhi	*Polygalae Radix*	1	4

TABLE 2 | Single Chinese medicine with repeated targets.

Mol ID	Single Chinese medicine	Predict target number
MOL000358	*Arum Ternatum Thunb, Arisaematis Rhizoma*	38
MOL000449	*Arum Ternatum Thunb, Arisaematis Rhizoma*	31
MOL000953	*Bovis Calculus, Arisaematis Rhizoma*	4
MOL003578	*Arum Ternatum Thunb, Acoritataninowii Rhizoma*	1

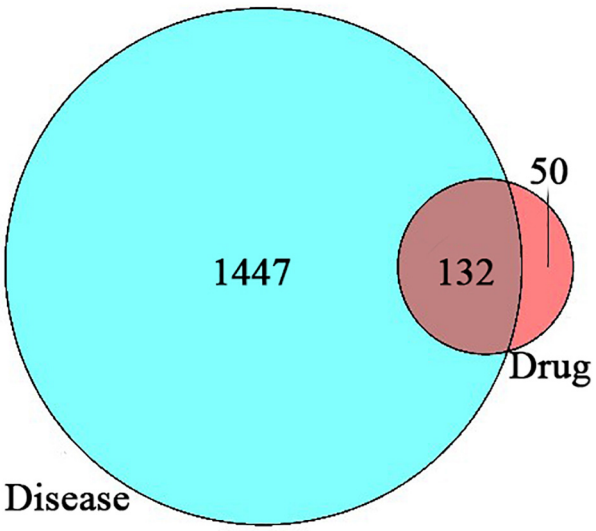

FIGURE 1 | The Venn diagram of intersection targets.

Perioperative Neurocognitive Disorder-Related Targets

The GeneCards database was searched using Relevance scores $\geq$ 1 as the screening criteria. The search term "perioperative neurocognitive disorders" was searched to get 124 targets, and "postoperative delirium" and "postoperative cognitive dysfunction" as the search terms to get 1,572 targets. After the results were combined and the duplicates were deleted, 1,579 PND-related targets were obtained.

Compound-Disease Overlap Genes

Using VennDiagram, 132 overlap genes were obtained, that was, 132 potential targets of *Xingnao Kaiqiao* Pill for PND were determined, as is shown in **Figure 1**.

"Xingnao Kaiqiao Pill—Traditional Chinese Medicine—Compound-Common Target" Relationship Network

There were 234 nodes and 573 edges in the network, as is shown in **Figure 2**. Yellow represented the targets, blue represented the active ingredients, and green represented the medicines. The denser the connections, the more important the node is. According to the results of network analysis, stigmasterol, quercetin, beta-sitosterol, kaempferol, and baicalein determined to be the main active components of *Xingnao Kaiqiao* Pill.

Construction and Analysis of Protein-Protein Interaction Network

To shed light on the potential mechanisms through which *Xingnao Kaiqiao* Pill acts on PND, a PPI network generated from the STRING database was constructed. Cytoscape (version 3.9.1) was used to visualize the network, and the size of the nodes was proportional to the degree centrality obtained from topology analysis. As is shown in **Figure 3A**, the PPI network consisted of 106 non-isolated nodes and 373 edges. The top ten genes derived from the four network analysis algorithms are shown

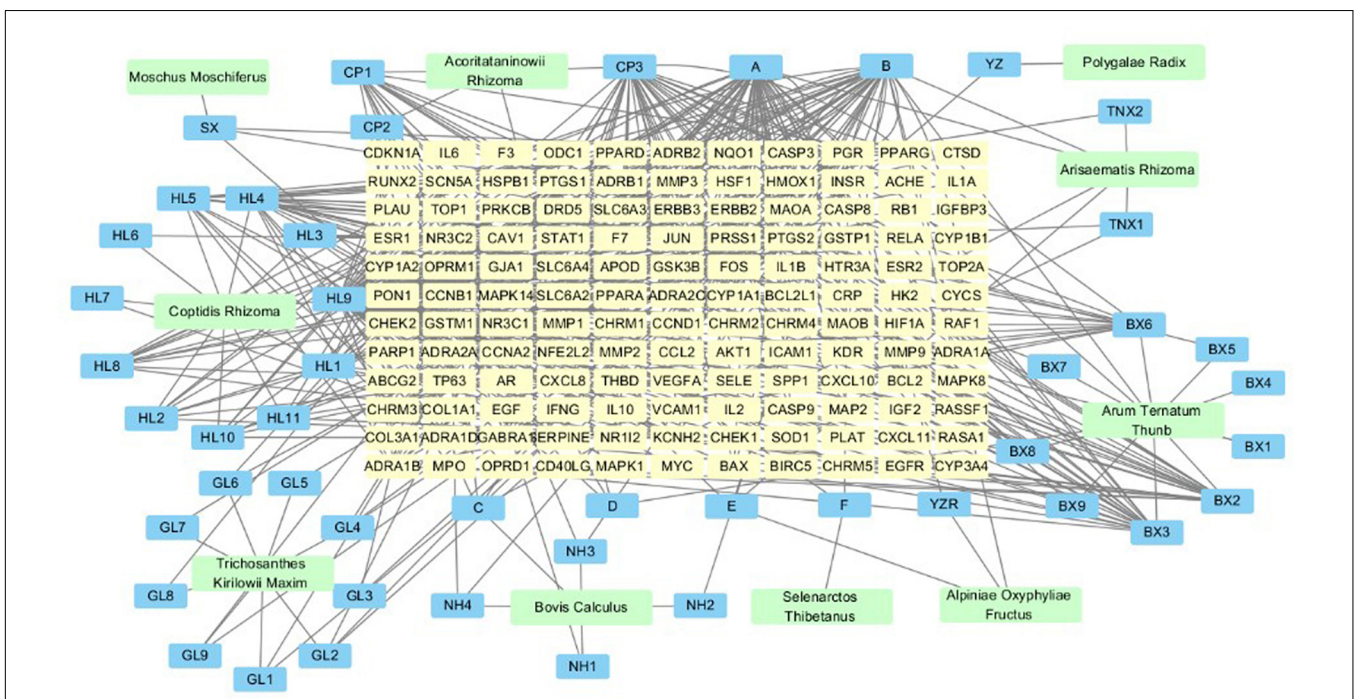

FIGURE 2 | *Xingnao Kaiqiao* Pill- tradition Chinese medicine—compound-common target relationship network.

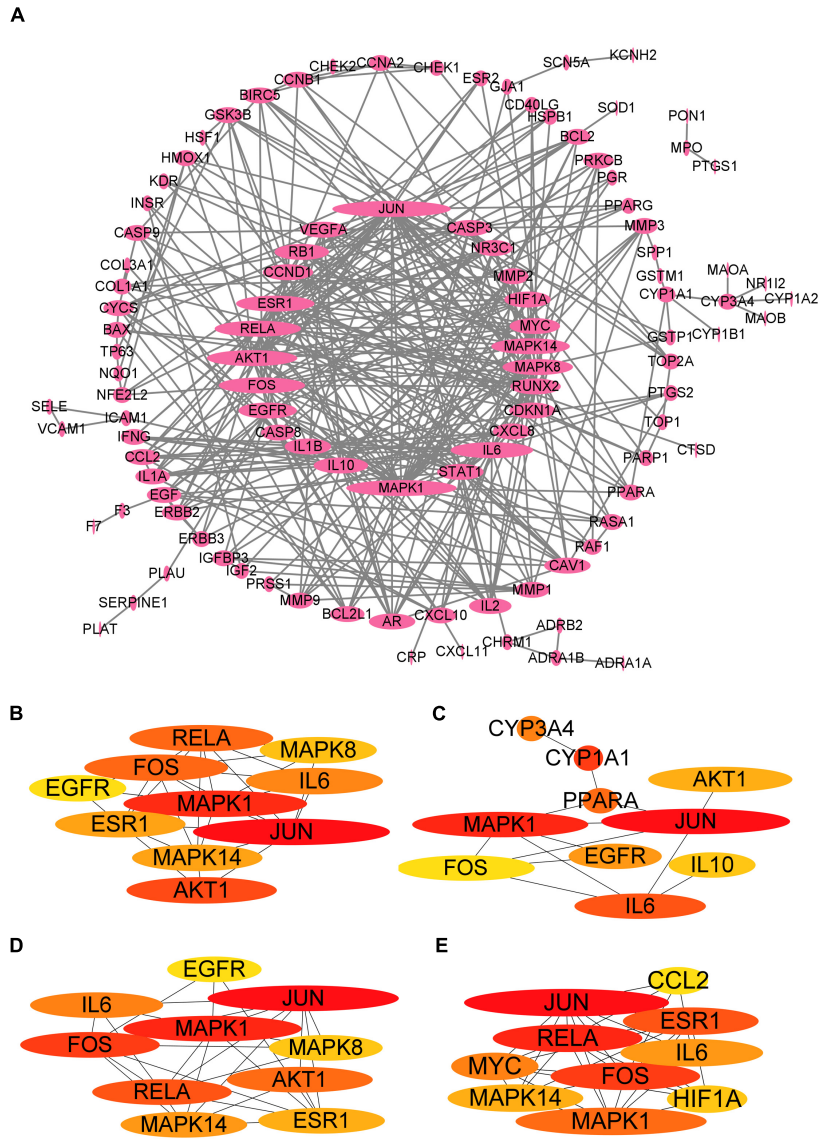

FIGURE 3 | PPI network visualization and analysis. **(A)** PPI network. **(B)** The top 10 genes of Degree algorithm. **(C)** The top 10 genes of Betweeness algorithm. **(D)** The top 10 genes of Closeness algorithm. **(E)** The top 10 genes of MCC algorithm.

in **Figures 3B–E**, and the degree values of the first 10 genes are shown in **Table 3**. Topology analysis indicated that JUN, MAPK1, AKT1, RELA, IL6, FOS, ESR1, MAPK14, MAPK8, and EGFR were the top 10 shared targets from the perspective of degree centrality. We selected the top five targets as molecular docking targets.

Gene Ontology Enrichment Results

GO analysis results demonstrated that 132 targets were enriched in 154 GO items; these targets primarily existed in the membrane raft, the membrane microdomain, the caveola, the plasma membrane raft, the postsynaptic membrane, the organelle outer membrane, the outer membrane, the integral component of the postsynaptic membrane, and other regions of the cells. Secondly, these targets were involved in metabolism, energy pathways, apoptosis, and other biological processes. Moreover, G protein-coupled amine receptor activity, DNA-binding transcription factor binding, nuclear receptor activity, and other functions are the principal molecular functions of *Xingnao Kaiqiao* Pill against PND. The results of the top 10 in the above three aspects are shown in **Figure 4**.

Kyoto Encyclopedia of Genes and Genomes Enrichment Results

The results of KEGG pathway analysis of common target genes exhibited that 125 targets were enriched in 157 signaling pathways or biological processes. According to the count value and *P*-value, the first 20 items were selected, as shown in

TABLE 3 | Analysis of PPI network results.

Symbol	Degree
JUN	30
MAPK1	28
AKT1	23
RELA	22
IL6	22
FOS	21
ESR1	20
MAPK14	20
MAPK8	18
EGFR	15

Figure 5, among which important pathways mainly involve the AGE-RAGE signaling pathway, the tumor signaling pathway, the interleukin 17 (IL-17) signaling pathway, the tumor necrosis factor (TNF) signaling pathway, the hypoxia-inducible factor-1 (HIF-1) signaling pathway, and signal pathways closely related to fluid shear stress and atherosclerosis, endocrine resistance, bladder cancer, prostate cancer, etc., which mainly play an important role in inhibiting inflammatory reaction, hormone, and endocrine regulation. The signaling pathways related to cellular immunity and inflammation consisted of the AGE-RAGE signaling pathway, the IL-17 signaling pathway, and the TNF signaling pathway; there are common targets and synergies between these signaling pathways. In conclusion, the effect of *Xingnao Kaiqiao* Pill on PND seems to have a close association with immune response and metabolism of immune molecules. The details of the above three signaling pathways are displayed from **Figures 6**–**8**, and the compound-disease intersection genes are shown in red.

Molecular Docking Verification

In this study, we used molecular docking stimulation to identify the binding ability between bioactive components of *Xingnao Kaiqiao* Pill and key targets encoded by hub genes. According to **Figure 9** and **Table 4**, all the bioactive components of *Xingnao Kaiqiao* Pill demonstrated good binding with the key targets. Beta-sitosterol had a strong binding ability with two hub genes, i.e., AKT1 and RELA. Stigmasterol showed good binding ability with MAPK1 and IL6. Kaempferol showed good binding ability with JUN.

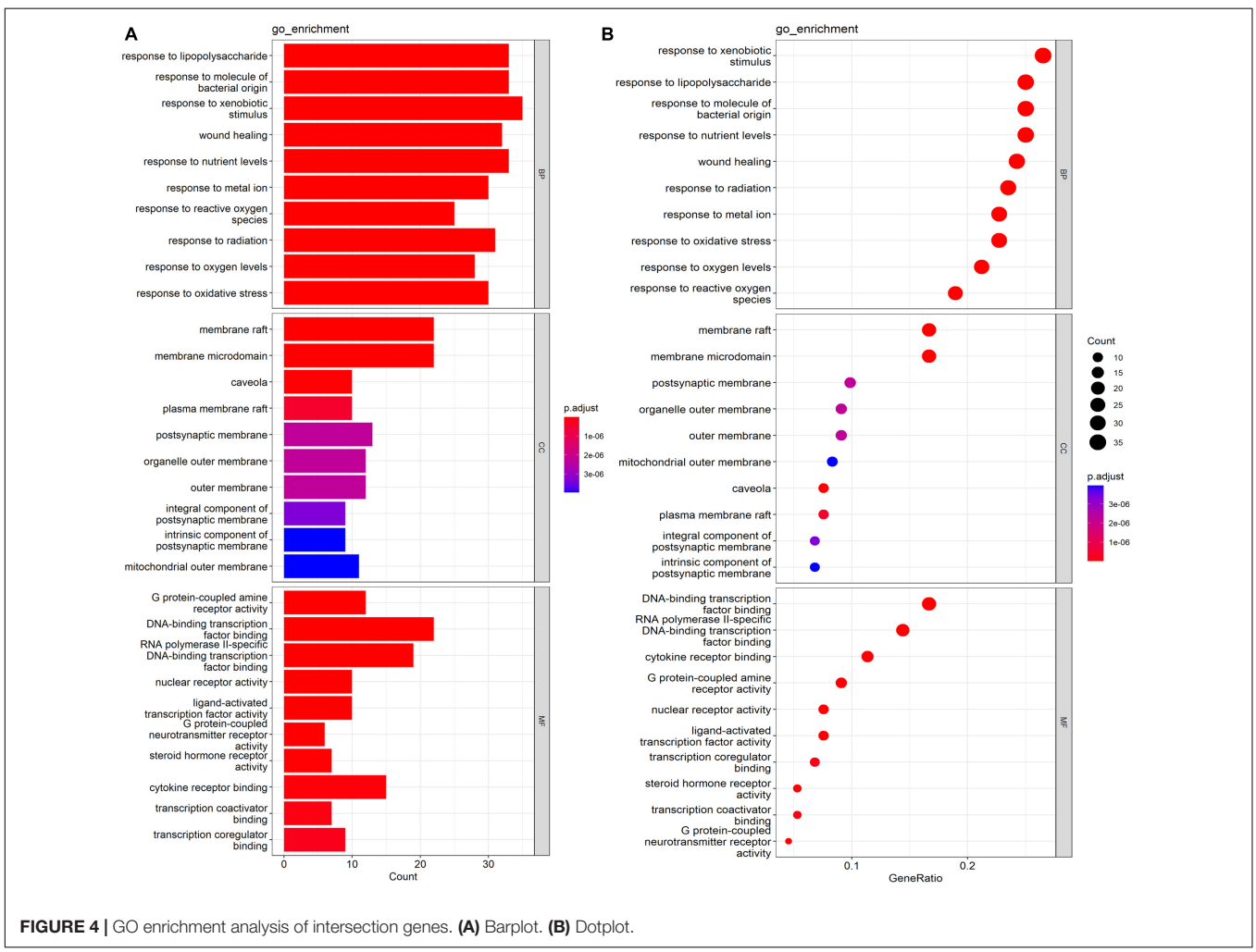

FIGURE 4 | GO enrichment analysis of intersection genes. **(A)** Barplot. **(B)** Dotplot.

FIGURE 5 | KEGG enrichment analysis of intersection genes. **(A)** Barplot. **(B)** Dotplot.

DISCUSSION

PND, a CNS complication, presents many clinical manifestations; the deterioration of cognitive function involves cognitive, memory, motor function, attention, and concentration. According to the universally recognized pathogenesis, PND can be considered as a neuroinflammation disease (Subramaniyan and Terrando, 2019; Li et al., 2022). It has been found that there is a close connection between the nervous system and the immune system, and inhibiting the expression level of inflammatory factors or suppressing the immune response can reduce the symptoms of PND or the occurrence of PND (Mu et al., 2015).

There is no clear record of this disease in Chinese medicine. Some scholars believe that PND should be classified as "dementia," "forgetfulness," and "epilepsy" on the basis of its clinical manifestations (Han et al., 2011), and classified early delirium in PND as the category of "manic-depressive psychosis" in traditional Chinese medicine.

Chinese medicine treatment of PND is generally based on pathophysiological characteristics and clinical manifestations of the elderly after surgery. In a study of PND, Chinese medicine syndrome in elderly patients with bowel cancer, clinical patients were roughly divided into five syndrome types, namely, kidney essence deficiency syndrome, phlegm turbidity blocking orifice syndrome, blood stasis blocking collaterals syndrome, viscera stagnation, and turbid retention syndrome, *qi*, and blood deficiency syndrome. Elderly people frequently experience liver and kidney deficiency, insufficient *qi*, and blood. Furthermore, surgical trauma can break *qi*, consume blood, damage the collaterals, cause deficiency of *qi* and blood circulation, stagnation of blood stasis, and result in cerebral collateral blockage and mental function failure. The treatment should invigorate *qi*, activate blood, dispel blood stasis, and dredge collaterals. If the patient suffers from heart and kidney deficiency, *yin* deficiency, blood insufficiency, and internal disturbance of deficiency and fire, the treatment should nourish

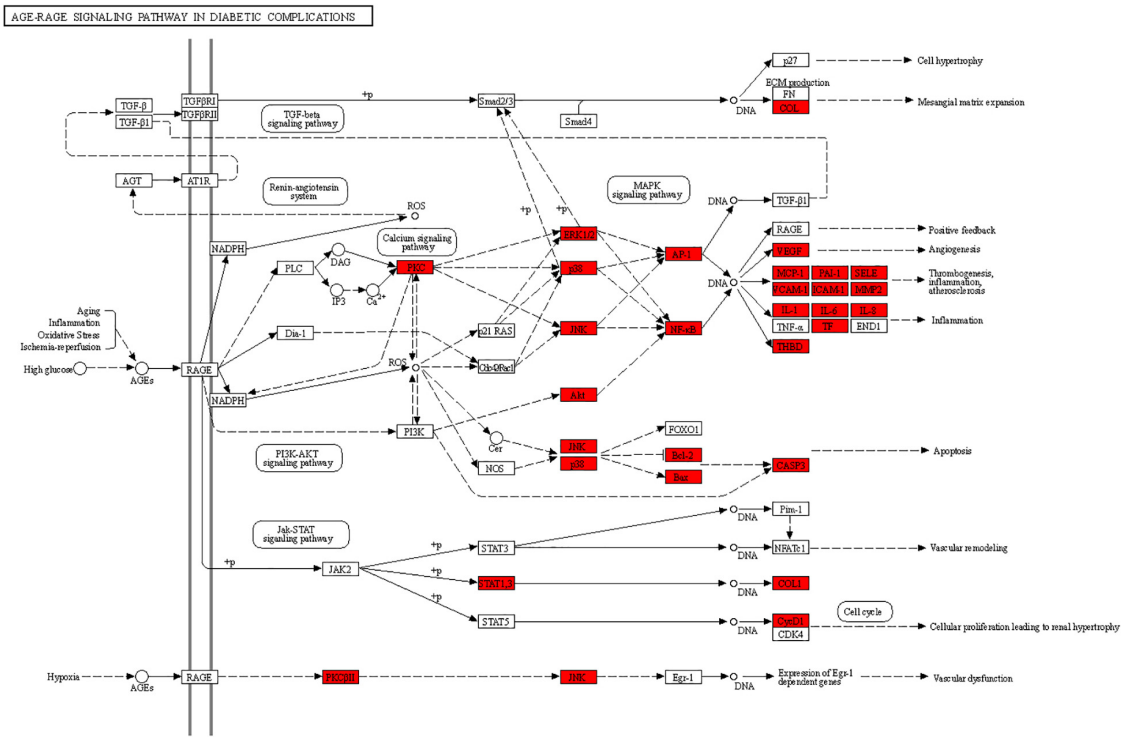

FIGURE 6 | The AGE-RAGE signaling pathway.

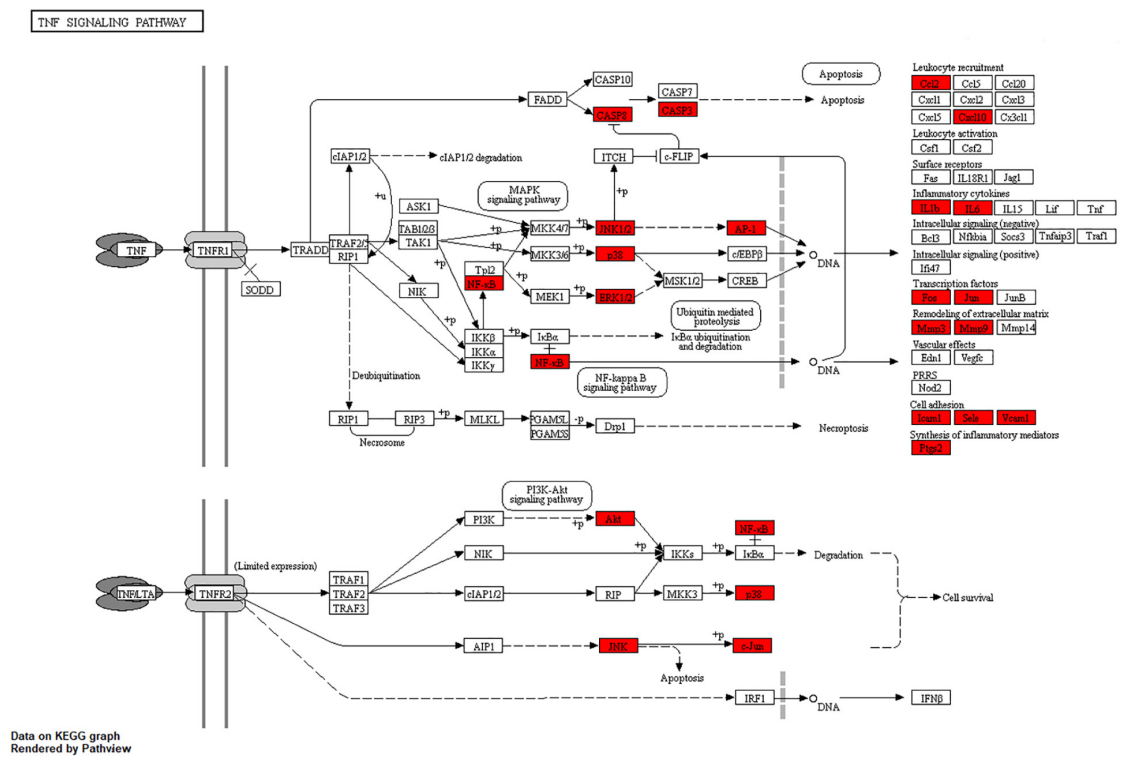

FIGURE 7 | The TNF signaling pathway.

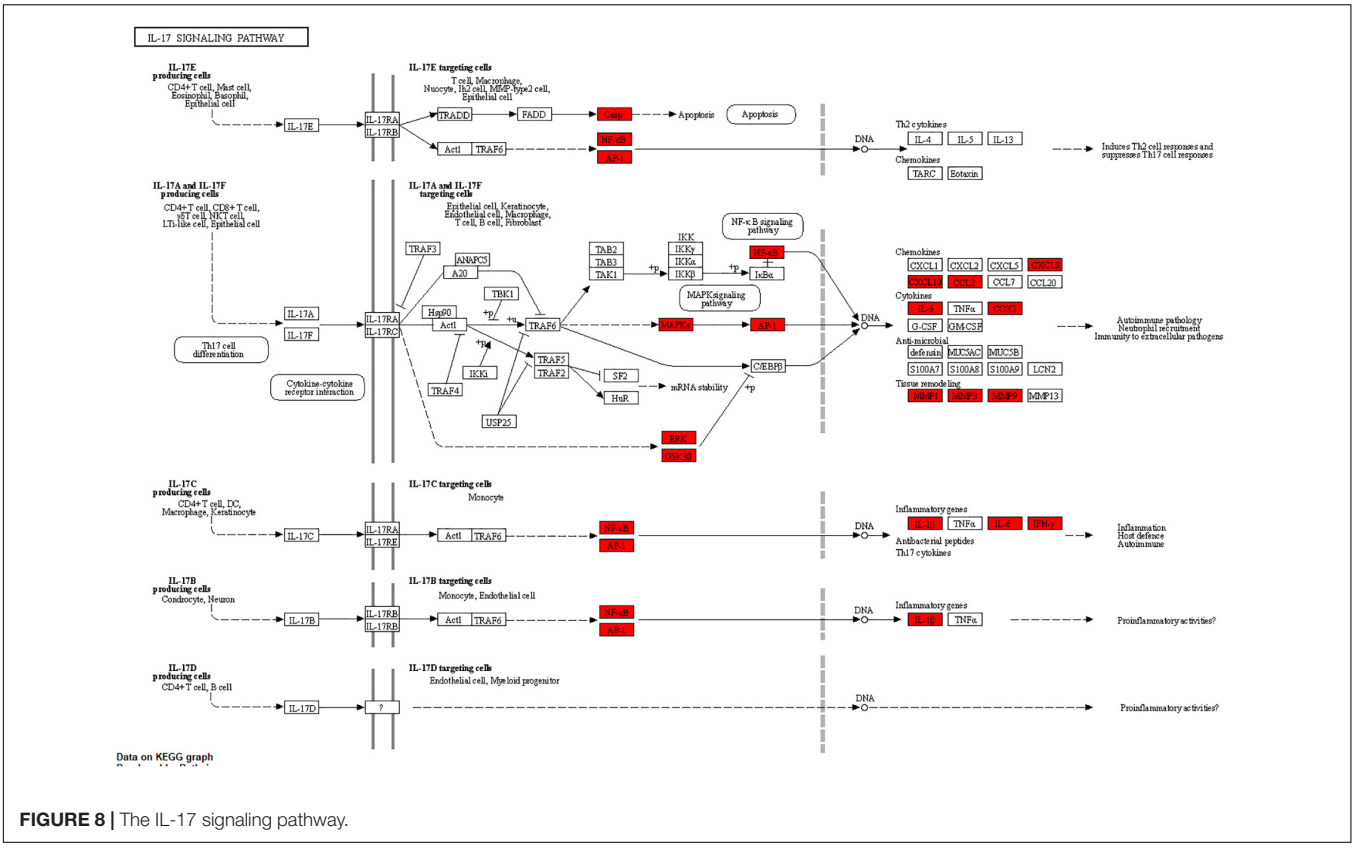

FIGURE 8 | The IL-17 signaling pathway.

yin, blood, the heart, and focus on tranquilization. Chinese medicine compound preparation *Xingnao Kaiqiao* pill can tranquilize the emotional distress, strengthen body resistance, eliminate pathogenic factors, suppress the hyperactive liver for calming endogenous wind, regulate *qi*, dispel stagnation, tonify the kidney, and invigorate the brain. *Xingnao Kaiqiao* pill has the characteristics of overall regulation, multiple targets, multiple pathways, and multiple mechanisms, and has advantages in improving cognition and perioperative quality of life. More than 50 patients with PND, who had been consulted at the Department of Traditional Chinese Medicine in our hospital since 2020, received the treatment with *Xingnao Kaiqiao* pill and achieved good results.

Numerous research results demonstrated that PND may be induced by various factors, and its pathogenesis is not yet fully clear. Animal experiments and clinical trials have shown that PND pathogenesis is associated with increased immune inflammatory response of the CNS, abnormal neurotransmitters or receptors, abnormal cholinergic nerve function, β-amyloid formation, noxious stimulation, and stress response (Uchino et al., 2014). It is currently believed that neuroinflammatory response and excessive activation of microglia are the main factors that trigger PND in elderly patients (Subramaniyan and Terrando, 2019). Microglia are the innate immune cells of the CNS. Their excessive activation induces the release of neurotoxic substances, and then alters the normal transmission of neurotransmitters and synaptic plasticity, and ultimately leads to PND (Niraula et al., 2017). The excessive activation of microglia is strongly associated with the activation of MAPK and other inflammatory signaling pathways caused by the release of inflammatory factors in the CNS (Zhang et al., 2020).

MAPK is a class of intracellular serine/threonine protein kinases, an important signaling system that mediates extracellular signals to intracellular responses, and plays a key role in immunity, inflammation, apoptosis, and angiogenesis. The MAPK signaling pathway plays an important role in the pathophysiological process of cognitive impairment (Xiang et al., 2020). IL-6 is a multipotent cytokine with a wide range of functions; it can regulate the growth and differentiation of many kinds of cells; regulate immune response, acute phase response, and hematopoiesis; and plays an important role in immune response. Following surgery, local cytokine-driven inflammation occurs, as part of the normal healing process. Cytokines in the CNS, such as IL-6 and IL-8, may also be elevated. Perioperative changes in cytokines have a role in the development of PND (Pereira et al., 2022).

The GO analysis results confirmed that intersection genes mainly enriched in the G protein-coupled amine receptor activity, nuclear receptor activity, ligand-activated transcription factor activity, G protein-coupled neurotransmitter receptor activity, steroid hormone receptor activity, and cytokine receptor activity may be associated with abnormal neurotransmitter or receptor and abnormal cholinergic nerve function in the pathogenesis of PND (Uchino et al., 2014).

In the results of KEGG pathway enrichment, PND-related body immunity and inflammation signaling pathways include

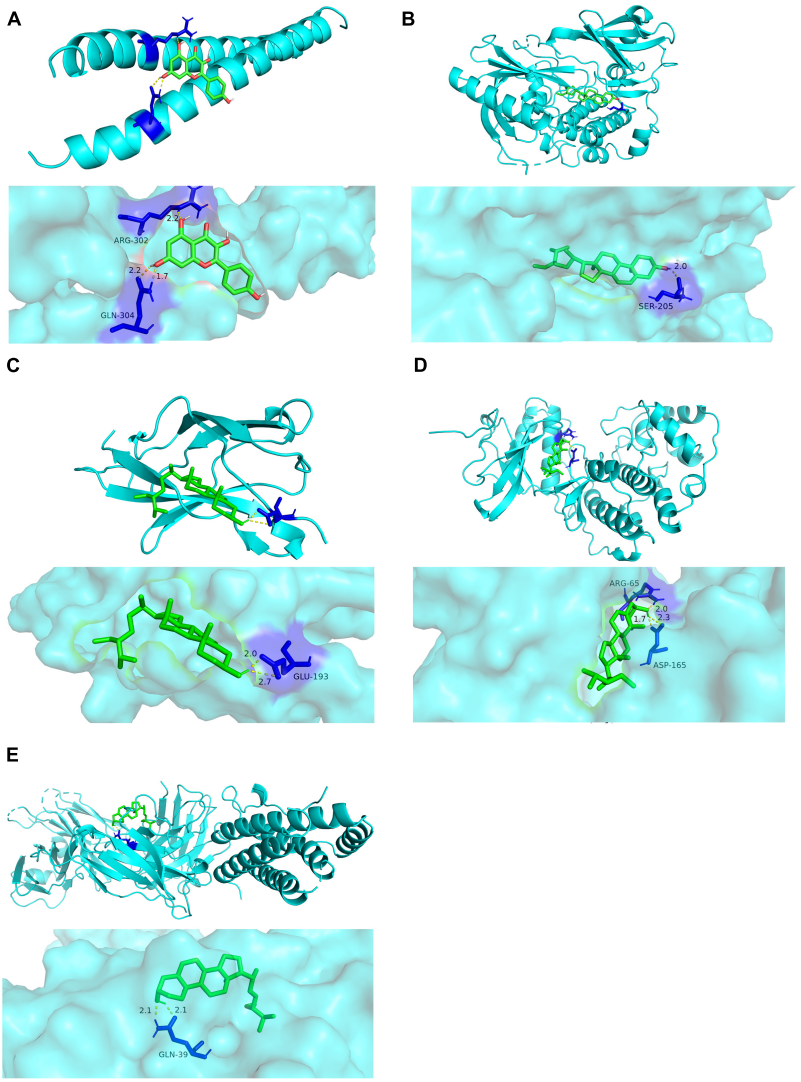

FIGURE 9 | Detailed target-compound interactions with the highest molecular docking affinities. **(A)** The binding pattern between JUN and kaempferol. **(B)** The binding pattern between AKT1 and beta-sitosterol. **(C)** The binding pattern between RELA and beta-sitosterol. **(D)** The binding pattern between MAPK1 and stigmasterol. **(E)** The binding pattern between IL6 and stigmasterol.

TABLE 4 | Docking scores of the active ingredients of *Xingnao Kaiqiao* Pill with their potential targets.

Molecular name	Affinity (kcal/mol)				
	JUN	MAPK1	AKT1	RELA	IL6
Stigmasterol	–4.67*	–8.44	–10.96	–7.11	–9.00
Quercetin	–3.81	–6.58	–7.49	–6.37	–6.96
Beta-sitosterol	–3.32	–7.59	–11.00	–7.18	–8.19
Kaempferol	–4.12	–6.76	–7.71	–6.50	–7.45
Baicalein	–3.16	–6.74	–6.12	–6.54	–6.78

**No hydrogen bonds formed.*

the AGE-RAGE signaling pathway, the TNF signaling pathway, and the IL-17 signaling pathway. Notably, we found the MAPK signaling pathway embedded in these pathways above. The significant indicators indicate a high correlation with the pathophysiological mechanism of PND and the pharmacological effects of *Xingnao Kaiqiao* Pill. These signaling pathways above do not exist in isolation, but have many intersections and protein interactions. The interaction of multiple signaling pathways has a key impact on the activation of downstream signaling pathways, the activation of microglia, the release of neurotoxic substances, and the impairment of cognitive function (Ding et al., 2017; Gong et al., 2020).

IL-17 is an important member of the new inflammatory cytokine family, and a proinflammatory cytokine extensively present in various inflammatory pathways (McGeachy et al., 2019). The IL-17 family is composed of six members of IL-17 (A∼F). The results of the KEGG pathway enrichment in this study exhibited that MAPK, NF-κB, GSK3β, and CASP3 sites in the compound-disease targets were crucial receptors

in IL-17 target cells. Moreover, there are many types of inflammatory mediators, cytokines, and chemokines released by IL-17-mediated target cells. Among them, 10 types, such as IL-1β, IL-6, IFN-γ, etc., are visibly identified as common medicine-disease targets (Gu and Wu, 2013).

Microglia are immune cells in the CNS, and their activation pathways include three states: classic activation, alternative activation, and acquired activation. The classic activation pathway is strongly associated with TNF. The results of the KEGG pathway enrichment in this study displayed that NF-κB, JNK1/2, and Akt sites in the compound-disease target are crucial receptors in TNF target cells. There are many types of inflammatory mediators, cytokines, and chemokines released by TNF-mediated target cells. Among them, 12 types, such as IL-1β, IL-6, Jun, etc., are clearly identified as compound-disease targets.

Cellular hypoxia linked to cognitive impairment. HIF-1 is an important regulator of cells, adapting to hypoxic environment (Eltzschig and Carmeliet, 2011). HIF-1α could resist the toxic effect of Aβ, inhibits tau hyperphosphorylation, and promotes microglial activation (Schubert et al., 2009). However, the current research on the relationship between hypoxia and PND is relatively lacking.

CONCLUSION

In summary, the mechanism of *Xingnao Kaiqiao* Pill in the treatment of PND is mainly associated with the regulation of CNS inflammation, and the involved signaling pathways have many intersections and protein interactions. MAPK1, JUN, AKT1, IL6, and RELA are core targets of active ingredients acting on the main related signaling pathways. Due to the limitations of the database and the algorithm, further experimental investigations are needed to verify the results from this analysis.

DATA AVAILABILITY STATEMENT

The original contributions presented in this study are included in the article/supplementary material, further inquiries can be directed to the corresponding author.

AUTHOR CONTRIBUTIONS

WZ and GS managed the literature searches, designed the study, interpreted the statistical analyses, and wrote the first draft of the manuscript. HW and MF contributed to the data administration. XG edited the language to improve the clarity of the manuscript. ZL instructed in the study approach and supervised the statistical analyses and their interpretation. All authors have contributed to and approved the final manuscript.

FUNDING

This research was supported by the Scientific Research Project of Shanxi Provincial Health Commission (#2022068 to WZ).

REFERENCES

Ding, Y., Shi, C., Chen, L., Ma, P., Li, K., Jin, J., et al. (2017). Effects of andrographolide on postoperative cognitive dysfunction and the association with NF-kappaB/MAPK pathway. *Oncol. Lett.* 14, 7367–7373. doi: 10.3892/ol.2017.7088

Eltzschig, H. K., and Carmeliet, P. (2011). Hypoxia and inflammation. *N. Engl. J. Med.* 364, 656–665.

Evered, L., Silbert, B., Knopman, D. S., Scott, D. A., DeKosky, S. T., and Rasmussen, L. S. (2018). Recommendations for the Nomenclature of Cognitive Change Associated with Anaesthesia and Surgery-2018. *Anesthesiology* 129, 872–879.

Gong, M., Wang, G., Li, G., Liu, J., Sun, P., Xu, L., et al. (2020). Dysfunction of inflammation-resolving pathways is associated with postoperative cognitive decline in elderly mice. *Behav. Brain Res.* 386:112538. doi: 10.1016/j.bbr.2020.112538

Gu, C., and Wu, L. (2013). IL-17 family: cytokines, receptors and signaling. *Cytokine* 64, 477–485.

Han, S. H., Li, H., and Liu, L. T. (2011). [Therapeutic efficacy assessment of Chinese medicine on mild cognitive impairment]. *Zhongguo Zhong Xi Yi Jie He Za Zhi* 31, 608–617.

Hu, Y., Li, C., and Shen, W. (2014). Gastrodin alleviates memory deficits and reduces neuropathology in a mouse model of Alzheimer's disease. *Neuropathology* 34, 370–377. doi: 10.1111/neup.12115

Kong, H., Xu., L. M., and Wang, D.-X. (2022). Perioperative neurocognitive disorders: A narrative review focusing on diagnosis, prevention, and treatment. *CNS Neurosci. Ther.* [Epub ahead of print]. doi: 10.1111/cns.13873

Li, Z., Zhu, Y., Kang, Y., Qin, S., Chai, J., et al. (2022). Neuroinflammation as the Underlying Mechanism of Postoperative Cognitive Dysfunction and Therapeutic Strategies. *Front. Cell Neurosci.* 16:843069. doi: 10.3389/fncel.2022.843069

Morris, G. M., Huey, R., Lindstrom, W., Sanner, M. F., Belew, R. K., Goodsell, D. S., et al. (2009). AutoDock4 and AutoDockTools4: Automated docking with selective receptor flexibility. *J. Comput. Chem.* 30, 2785–2791. doi: 10.1002/jcc.21256

McGeachy, M. J., Cua, D. J., and Gaffen, S. L. (2019). The IL-17 Family of Cytokines in Health and Disease. *Immunity* 50, 892–906.

Mu, J. L., Lee, A., and Joynt, G. M. (2015). Pharmacologic agents for the prevention and treatment of delirium in patients undergoing cardiac surgery: systematic review and metaanalysis. *Crit. Care Med.* 43, 194–204.

Niraula, A., Sheridan, J. F., and Godbout, J. P. (2017). Microglia Priming with Aging and Stress. *Neuropsychopharmacology* 42, 318–333.

Pereira, C., Dani, M., Taylor-Robinson, S. D., and Fertleman, M. (2022). Putative Involvement of Cytokine Modulation in the Development of Perioperative Neurocognitive Disorders. *Int. J. Gen. Med.* 15, 5349–5360. doi: 10.2147/IJGM.S364954

Ru, J., Li, P., Wang, J., Zhou, W., Li, B., Huang, C., et al. (2014). TCMSP: a database of systems pharmacology for drug discovery from herbal medicines. *J. Cheminform* 6:13.

Schubert, D., Soucek, T., and Blouw, B. (2009). The induction of HIF-1 reduces astrocyte activation by amyloid beta peptide. *Eur. J. Neurosci.* 29, 1323–1334.

Shannon, P., Markiel, A., Ozier, O., Baliga, N. S., Wang, J. T., and Ramage, D. (2003). Cytoscape: a software environment for integrated models of biomolecular interaction networks. *Genom. Res.* 13, 2498–2504. doi: 10.1101/gr.1239303

Subramaniyan, S., and Terrando, N. (2019). Neuroinflammation and Perioperative Neurocognitive Disorders. *Anesth. Analg.* 128, 781–788.

Uchino, H., Nagashima, F., Nishiyama, R., Ishida, Y., Saiki, I., Yara, M., et al. (2014). [Pathophysiology and mechanisms of postoperative cognitive dysfunction]. *Masui* 63, 1202–1210.

Wu, T., Hu, E., Xu, S., Chen, M., Guo, P., Dai, Z., et al. (2021). clusterProfiler 4.0: A universal enrichment tool for interpreting omics data. *Innovation* 2:100141. doi: 10.1016/j.xinn.2021.100141

Xiang, Y., Dai, L., Yuan, J., Zhu, J., and Deng, C. (2020). Effects of P38/MAPK pathway on cognitive function and inflammation in rats with cerebral small vascular disease. *Panminerva Med.* 62, 273–275. doi: 10.23736/S0031-0808.19.03647-4

Yu, L., Sun, L., and Chen, S. (2014). Protective effect of senegenin on splenectomy-induced postoperative cognitive dysfunction in elderly rats. *Exp. Ther. Med.* 7, 821–826. doi: 10.3892/etm.2014.1501

Zhang, Y., Meng, Q., Yin, J., Zhang, Z., Bao, H., and Wang, X. (2020). Anthocyanins attenuate neuroinflammation through the suppression of MLK3 activation in a mouse model of perioperative neurocognitive disorders. *Brain Res.* 1726:146504. doi: 10.1016/j.brainres.2019.146504

Zhu, X., and Feng, Q. (2018). Research progress of traditional Chinese medicine in the treatment of mild cognitive impairment in recent five years. *Linchuang Yixue Yanjiu Yu Shijian* 3, 153–155.

Conflict of Interest: The authors declare that the research was conducted in the absence of any commercial or financial relationships that could be construed as a potential conflict of interest.

Publisher's Note: All claims expressed in this article are solely those of the authors and do not necessarily represent those of their affiliated organizations, or those of the publisher, the editors and the reviewers. Any product that may be evaluated in this article, or claim that may be made by its manufacturer, is not guaranteed or endorsed by the publisher.

frontiers | Frontiers in Aging Neuroscience

TYPE Original Research
PUBLISHED 18 August 2022
DOI 10.3389/fnagi.2022.971528

OPEN ACCESS

EDITED BY
Min Tang,
Jiangsu University, China

REVIEWED BY
Qianqian Song,
Wake Forest School of Medicine, United States
You Guo,
First Affiliated Hospital of Gannan Medical University, China
Huaidong Cheng,
Second Hospital of Anhui Medical University, China

*CORRESPONDENCE
Wenzhou Zhang
hnzzzwzx@sina.com
Xuan Wu
xuanw91_zzu@126.com

†These authors have contributed equally to this work

SPECIALTY SECTION
This article was submitted to Parkinson's Disease and Aging-related Movement Disorders, a section of the journal Frontiers in Aging Neuroscience

RECEIVED 17 June 2022
ACCEPTED 03 August 2022
PUBLISHED 18 August 2022

CITATION
Li D, Liang J, Guo W, Zhang Y, Wu X and Zhang W (2022) Integrative analysis of DNA methylation and gene expression data for the diagnosis and underlying mechanism of Parkinson's disease. *Front. Aging Neurosci.* 14:971528. doi: 10.3389/fnagi.2022.971528

Integrative analysis of DNA methylation and gene expression data for the diagnosis and underlying mechanism of Parkinson's disease

Ding Li[1,2,3†], Jiaming Liang[4†], Wenbin Guo[5], Yongna Zhang[1,2,3], Xuan Wu[6*] and Wenzhou Zhang[1,2,3*]

[1]Department of Pharmacy, The Affiliated Cancer Hospital of Zhengzhou University, Henan Cancer Hospital, Zhengzhou, China, [2]Henan Engineering Research Center for Tumor Precision Medicine and Comprehensive Evaluation, Henan Cancer Hospital, Zhengzhou, China, [3]Henan Provincial Key Laboratory of Anticancer Drug Research, Henan Cancer Hospital, Zhengzhou, China, [4]Department of Internal Medicine, The Second Affiliated Hospital of Guangzhou Medical University, Guangzhou, China, [5]Department of Pathology, Pingtan Comprehensive Experimental Area Hospital, Fuzhou, China, [6]Academy of Medical Science, Zhengzhou University, Zhengzhou, China

Background: Parkinson's disease (PD) is the second most common progressive neurodegenerative disorder and the leading cause of disability in the daily activities. In the management of PD, accurate and specific biomarkers in blood for the early diagnosis of PD are urgently needed. DNA methylation is one of the main epigenetic mechanisms and associated with the gene expression and disease initiation of PD. We aimed to construct a methylation signature for the diagnosis of PD patients, and explore the potential value of DNA methylation in therapeutic options.

Materials and methods: Whole blood DNA methylation and gene expression data of PD patients as well as healthy controls were extracted from Gene Expression Omnibus database. Next, differentially expressed genes (DEGs) and differentially methylated genes (DMGs) between PD patients and healthy controls were identified. Least absolute shrinkage and selection operator cox regression analysis was carried out to construct a diagnostic signature based on the overlapped genes. And, the receiver operating characteristic (ROC) curves were drawn and the area under the curve (AUC) was used to assess the diagnostic performance of the signature in both the training and testing datasets. Finally, gene ontology and gene set enrichment analysis were subsequently carried out to explore the underlying mechanisms.

Results: We obtained a total of 9,596 DMGs, 1,058 DEGs, and 237 overlapped genes in the whole blood between PD patients and healthy controls. Eight methylation-driven genes (HIST1H4L, CDC42EP3, KIT, GNLY, SLC22A1, GCM1,

INO80B, and ARHGAP26) were identified to construct the gene expression signature. The AUCs in predicting PD patients were 0.84 and 0.76 in training dataset and testing dataset, respectively. Additionally, eight methylation-altered CpGs were also identified to construct the CpGs signature which showed a similarly robust diagnostic capability, with AUCs of 0.8 and 0.73 in training dataset and testing dataset, respectively.

Conclusion: We conducted an integrated analysis of the gene expression and DNA methylation data, and constructed a methylation-driven genes signature and a methylation-altered CpGs signature to distinguish the patients with PD from healthy controls. Both of them had a robust prediction power and provide a new insight into personalized diagnostic and therapeutic strategies for PD.

KEYWORDS

neurodegenerative disease, Parkinson's disease, DNA methylation, methylation-driven gene, diagnostic signature

Introduction

As the second most diagnosed neurodegenerative disease, Parkinson's disease (PD) is characteristic by a complex, age-related disease with more than six million patients worldwide and is the main cause of neurological dysfunction (Bloem et al., 2021). Currently, the diagnosis of PD is mainly based on clinical criteria, which have been updated many times to improve the diagnostic accuracy (Tolosa et al., 2021). The advances of gene microarray technology allow researchers to rapidly measure the expression data of thousands of genes in various diseases, helping to gain a deeper understanding of disease pathogenesis at the genetic level (Behzadi and Ranjbar, 2019). Given that specific and accurate molecular biomarkers could greatly contribute to the early diagnosis and therapy will have a greater chance of success in the early stages of disease. Thus, there is an urgent need to identify potential biomarkers for the diagnosis of PD.

Abbreviations: PD, Parkinson's disease; SNCA, Synuclein Alpha; LRRK2, Leucine Rich Repeat Kinase 2; MAPT, Microtubule Associated Protein Tau; GBA, Glucosylceramidase Beta; NPAS2, Neuronal PAS Domain Protein 2; CYP2E1, Cytochrome P450 Family 2 Subfamily E Member 1; PGC1-α, PPARG Coactivator 1 Alpha; DEGs, differentially expressed genes; DMGs, differentially methylated genes; LASSO, least absolute shrinkage and selection operator; AUC, area under the curve; GO, Gene Ontology; BP, biological process; MF, molecular function; CC, cellular component; GSEA, Gene Set Enrichment Analysis; CpGs, 5′-C-phosphate-G-3′; HIST1H4L, H4 clustered histone 13; CDC42EP3, CDC42 effector protein 3; KIT, receptor tyrosine kinase; GNLY, Granulysin; SLC22A1, solute carrier family 22 member 1; GCM1, glial cells missing transcription factor 1; INO80B, INO80 complex subunit B; ARHGAP26, Rho GTPase activating protein 26; KEGG, Kyoto Encyclopedia of Genes and Genomes.

Genetic variants and epigenetic changes play crucial roles in the initiation and progression of PD by through affecting endosomal, lysosomal, and mitochondrial function in pathophysiology (Dutta et al., 2021). The altered epigenetic modification or abnormal expression of PD-related genes, such as SNCA, LRRK2, MAPT, and GBA, have been reported to be closely related to PD (Bloem et al., 2021). Abnormal deposition of SNCA/α-synuclein is verified to be associated with the pathogenesis of PD (Ho et al., 2020). And all SNCA mutations were associated with the earlier age of onset and faster disease progression (Jowaed et al., 2010). Furthermore, hypomethylation of the SNCA promotor region has been reported in substantia nigra of PD patients (Matsumoto et al., 2010). The mutations in LRRK2 associated with increased kinase activity are the most common cause of autosomal dominant PD (Tolosa et al., 2020). Genome-wide association studies have implicated MAPT is a major susceptibility locus for idiopathic PD (Mata et al., 2014). Furthermore, the hypermethylation of the MAPT is neuroprotective by reducing MAPT expression (Coupland et al., 2014). Variants in GBA, encoding the enzyme glucocerebrosidase, are closely related to Lewy body diseases including PD and Lewy body dementia (Blauwendraat et al., 2020). Epigenomic changes associated with other genes including hypomethylation of NPAS2 and CYP2E1, and hypermethylation of PGC1-α, have also been implicated in PD (Lin et al., 2012).

Epigenetic mechanism, particularly DNA methylation, plays an important role in the molecular etiology of neurodegenerative diseases, including PD. DNA methylation in PD-related genes have been widely studied to explore the

mechanisms in disease progression and identify potential biomarkers for early diagnosis (Kaut et al., 2012). Initial studies have explored the correlations between the regulated genes and DNA methylation in PD brain tissue (Nalls et al., 2014; Young et al., 2019). However, recent studies have described the concordant DNA methylation patterns between brain tissue and blood sample (Masliah et al., 2013; Henderson-Smith et al., 2019). While the blood sample is less invasive and easier to obtain, the blood-based biomarkers confer a number of advantages compared with the tissue-based ones (Chahine et al., 2014). And, the previous researches have revealed that some reliable biomarkers for PD also exist in blood (Su et al., 2015). Here, we conducted an integrative analysis of gene expression data and DNA methylation data based on the 5′-C-phosphate-G-3′ (CpGs) in blood between PD patients and healthy controls to identify the molecules as well as their epigenetic changes underlying PD and constructed two diagnostic signatures to distinguish the patients with PD from healthy controls.

Materials and methods

Data collection and procession

The DNA methylation dataset GSE145361 (1,001 PD patients and 973 health controls), and the gene expression dataset GSE99039 (205 PD patients and 233 normal blood samples) were downloaded from Gene Expression Omnibus (GEO) database[1] on May 10, 2022. In addition, the blood DNA methylation dataset GSE111629 (335 PD patients and 237 normal blood samples), and the blood gene expression dataset of GSE6613 with 50 PD patients and 23 healthy controls were also downloaded from GEO to validate the accuracy and specificity of our signature. All the above data was downloaded using R package "GEOquery" and then preprocessed using the method described in the previous study (Henderson-Smith et al., 2019; Wang et al., 2019).

Differential methylation and expression analysis

The differential methylation and expression analyses were performed using the method previously described (Wang et al., 2019). The gene methylation level in this study was measured according to CpGs. The differentially methylated genes (DMGs) between PD patients and normal controls in the GSE145361 dataset were identified with the thresholds of adjusted p-value <0.001 and fold-change >1 using R package "ChAMP." We identified the differentially expressed genes (DEGs) between PD patients and normal controls in the GSE99039 dataset using R package "limma" with the cutoff value of adjusted $p < 0.05$ and fold-change >1.

Construction of the Parkinson's disease diagnostic signature based on overlapped genes

After the overlapping analysis based on the DMGs and DEGs of the PD patients compared to the normal controls, we constructed the diagnostic signature through applying least absolute shrinkage and selection operator (LASSO) Cox regression analysis and stepwise logistics regression to these overlapped genes of DMGs and DEGs to eliminate the genes highly correlated with each other to avoid overfitting. Finally, the signature was constructed with eight DNA methylation-driven genes and their coefficients.

The receiver operating characteristic (ROC) curves were drawn and area under the curve (AUC) was used to measure the performance of the gene signature in the diagnosis of PD using R package "pROC."

Functional enrichment analysis of differentially expressed DNA methylated genes

In order to explore the potential molecular mechanism of the differentially expressed DNA methylation-driven genes, we performed Gene ontology (GO) analysis under three terms, including biological process (BP), molecular function (MF), and cellular component (CC), using R package "clusterProfiler" (Chen et al., 2017; Wang et al., 2019; Kanehisa et al., 2021). A adjust p value <0.05 was set as the cutoffs of different parameters.

Construction of the Parkinson's disease diagnostic signature based on the DNA methylation sites

The 77 DNA methylation sites of the eight signature genes developed in GSE99039 were used as candidate sites to construct the signature. Then, in the GSE145361 dataset, LASSO analysis was carried out in the candidate sites with the R package 'glmnet'. Finally, the signature was constructed with eight methylation sites and their coefficients. We used the AUCs of ROC curves to measure the quality of the methylation

1 http://www.ncbi.nlm.nih.gov/geo

site signature in the diagnosis of PD based on the R package "pROC."

Validation of the gene expression and methylation site signatures in the testing datasets

To further validate the accuracy and specificity of the gene expression and methylation site signatures, we calculated the risk score of each sample based on the signature and used the AUCs of ROC curves to measure the diagnostic value in the GSE6613 and GSE111629 datasets.

Gene set enrichment analysis

Gene set enrichment analysis (GSEA) was performed to analyze the enrichment of datasets between high- and low-expression groups of hub genes, according to the gene sets files from the KEGG databases. A adjust *P* value <0.05 was set as the cutoffs of different parameters.

Statistical analysis

The R software version 3.6.1 and R Studio software were used to perform the statistical analyses and figures output. The false discovery rate (FDR) was used to adjust the *p*-value obtained by the Mann–Whitney *U* test. Adjusted *p*-value <0.001 were set as cutoff criteria for DMGs, and adjusted *p*-value <0.05 as threshold for DEGs. Adjust *P* value <0.05 was set as a cutoff value to identify significant biological pathways in GO and GESA analysis. Student's *t* tests were used to determine statistical significance among two groups.

Results

Identification of the differentially methylated genes

To identify the DMGs based on the whole blood sample between PD patients and normal controls, GSE145361 dataset with a large sample size (1,001 PD patients and 973 health controls) was downloaded from the GEO database. We obtained a total of 9,596 DMGs, in which 5,164 DMGs are hypo-methylated and 4,432 DMGs are hyper-methylated (**Figure 1A**).

Distribution of hypo- and hyper-methylated sites in genomic regions relative to transcription start sites (TSSs) and CpG islands are shown in **Figures 1B–E**, respectively. The hyper-methylated CpGs notably tended to be located in gene bodies (60.3%) and CpGs open sea (59.5%). While, hypo-methylated CpGs notably tended to be located in the promoters (TSS1500, TSS200, 5UTR, and 1stExon) (59.0%) and CpG islands (37.0%).

Identification of the differentially expressed genes

Next, we carried out a differential expression analysis to identify genes altered in PD patients. A linear model was applied to determine the DEGs based on the whole blood sample of 205 PD patients compared to 233 normal controls from the GSE99039 dataset. We identified 1,058 significant DEGs, including 129 downregulated genes and 929 upregulated genes (**Figure 2A**). Furthermore, we cross-linked DMGs and DEGs to determine 237 differentially methylation-driven genes (**Figure 2B** and **Supplementary Table 1**). To evaluate the correlation between expression levels and methylation levels of the overlapped genes, we assigned these 237 overlapped genes to four groups: hypermethylated and upregulated gene group (n = 140, **Supplementary Table 2**), hypermethylated and downregulated gene group (n = 18, **Supplementary Table 3**), hypomethylated and upregulated gene group (n = 202, **Supplementary Table 4**), and hypomethylated and downregulated gene group (n = 22, **Supplementary Table 5**). As shown in **Figures 2C–F**, the hypo-up genes were notably more than other group genes, which suggested that hypomethylation might be the key epigenetic modification involved in PD.

Functional enrichment analysis of differentially expressed DNA methylation-driven genes

To further explore the underlying mechanism of differentially expressed DNA methylation-driven genes, we performed GO analysis based on these 237 overlapped genes. The GO analysis revealed these overlapped genes were primarily enriched in BP terms, including neutrophil activation involved in immune response, neutrophil activation, positive regulation of cytokine production, neutrophil mediated immunity, antigen processing and presentation of endogenous antigen (**Figure 3A**). CC terms include integral component of lumenal side of endoplasmic reticulum membrane, secretory granule membrane, lumenal side of membrane, MHC protein complex, phagocytic vesicle, and cell leading edge (**Figure 3B**). MF terms include peptide antigen binding, calcium-dependent protein serine/threonine kinase activity, cytokine binding, hydrolase activity, calcium-dependent protein binding, and GTPase regulator activity (**Figure 3C**).

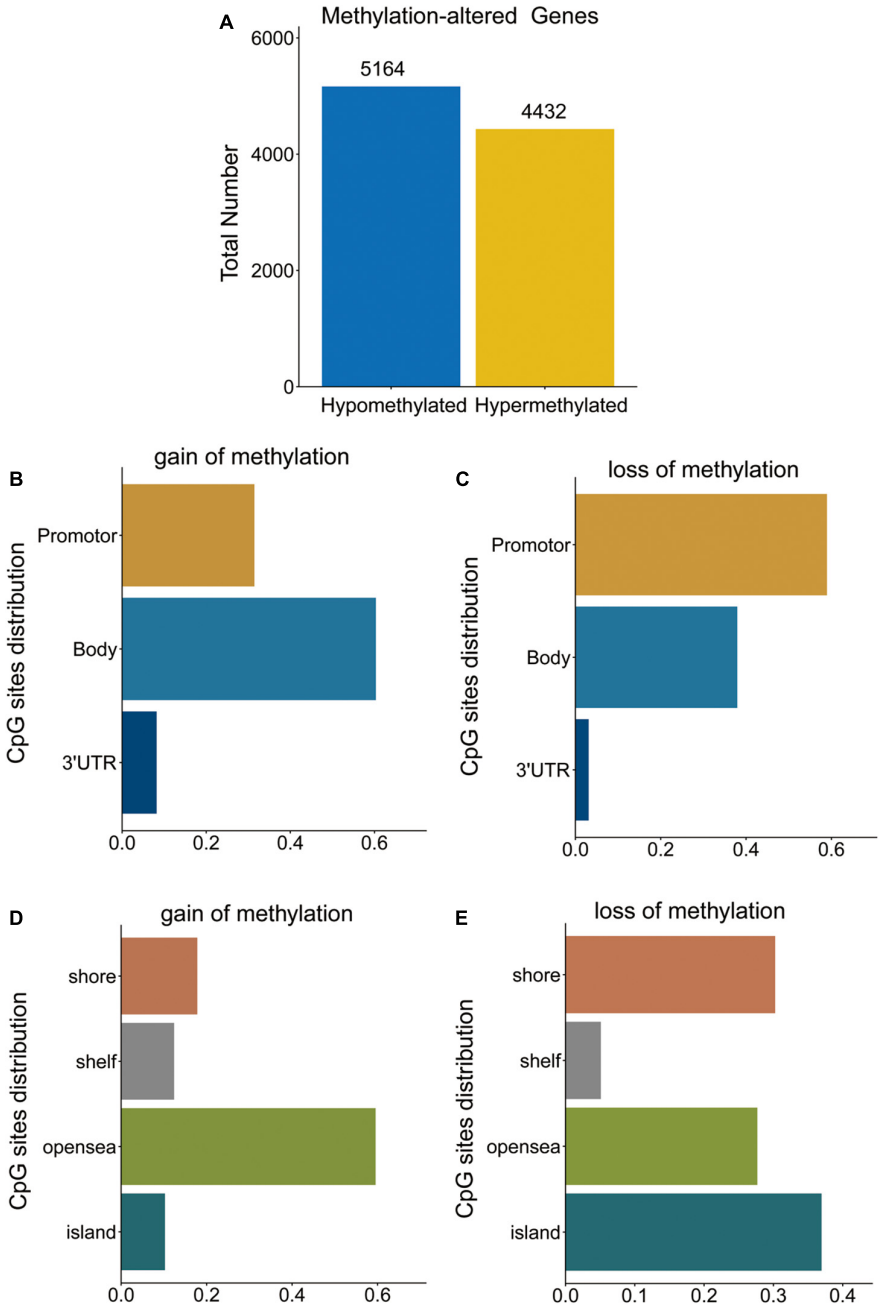

FIGURE 1
DMGs in PD patients. **(A)** Bar plot for DMGs in PD patients and healthy controls. **(B,C)** Distribution of DNA methylation changes in all genomic compartments. **(D,E)** Distribution of DNA methylation changes in varying CpG content and neighborhood context.

Construction and validation of the diagnostic signature based on eight methylation-driven genes

Least absolute shrinkage and selection operator regression and stepwise logistic regression analysis were applied to these 237 overlapped genes model to determine the most accurate predictive methylation-driven genes. Finally, eight methylation-driven genes HIST1H4L (H4 Clustered Histone 13), CDC42EP3 (CDC42 Effector Protein 3), KIT (receptor tyrosine kinase), GNLY (Granulysin), SLC22A1 (Solute Carrier Family 22 Member 1), GCM1 (Glial Cells Missing Transcription Factor 1), INO80B (INO80 Complex Subunit B), and ARHGAP26 (Rho GTPase Activating Protein 26) were identified. Subsequently, the signature was constructed based on the expression level and the relative coefficient of each signature

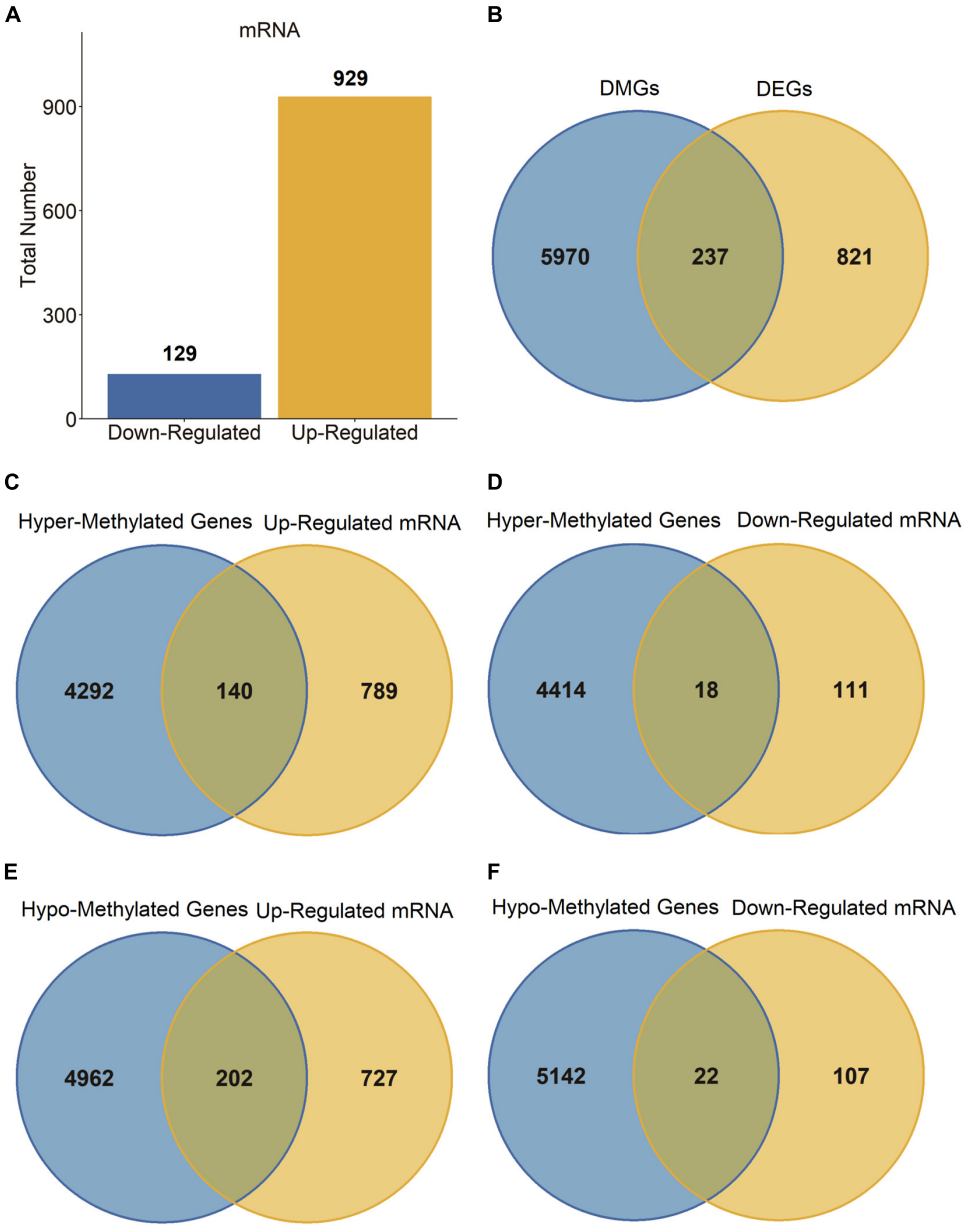

FIGURE 2
DEGs in PD patients. **(A)** Bar plot for DEGs in PD patients and healthy controls. **(B–F)** Venn diagram of DMGs and DEGs.

gene (Figures 4A–E). The risk scoring formula was as following: risk score = (0.796331667 × ARHGAP26) + (0.772781522 × INO80B) + (0.613379779 × GCM1) + (0.608204371 × SLC22A1) + (0.602134411 × GNLY) + (0.524810413 × KIT) + (0.408771389 × CDC42EP3) + (−0.82230679 × HIST1H4L).

To evaluate the performance of the gene expression signature in the diagnosis of PD, the ROC curve was plotted and AUC achieved 0.84 when applied to the training dataset GSE99039 (Figure 4F). The AUC was 0.76 when applied to the other independent PD-associated blood gene expression dataset GSE6613 (Figure 4G), which demonstrated that the signature had accuracy predictive power for PD patients.

Gene set enrichment analysis of the high- and low-risk groups based on the diagnostic signature

To explore the potential biological pathways and processes involved in the molecular heterogeneity, GSEA was carried

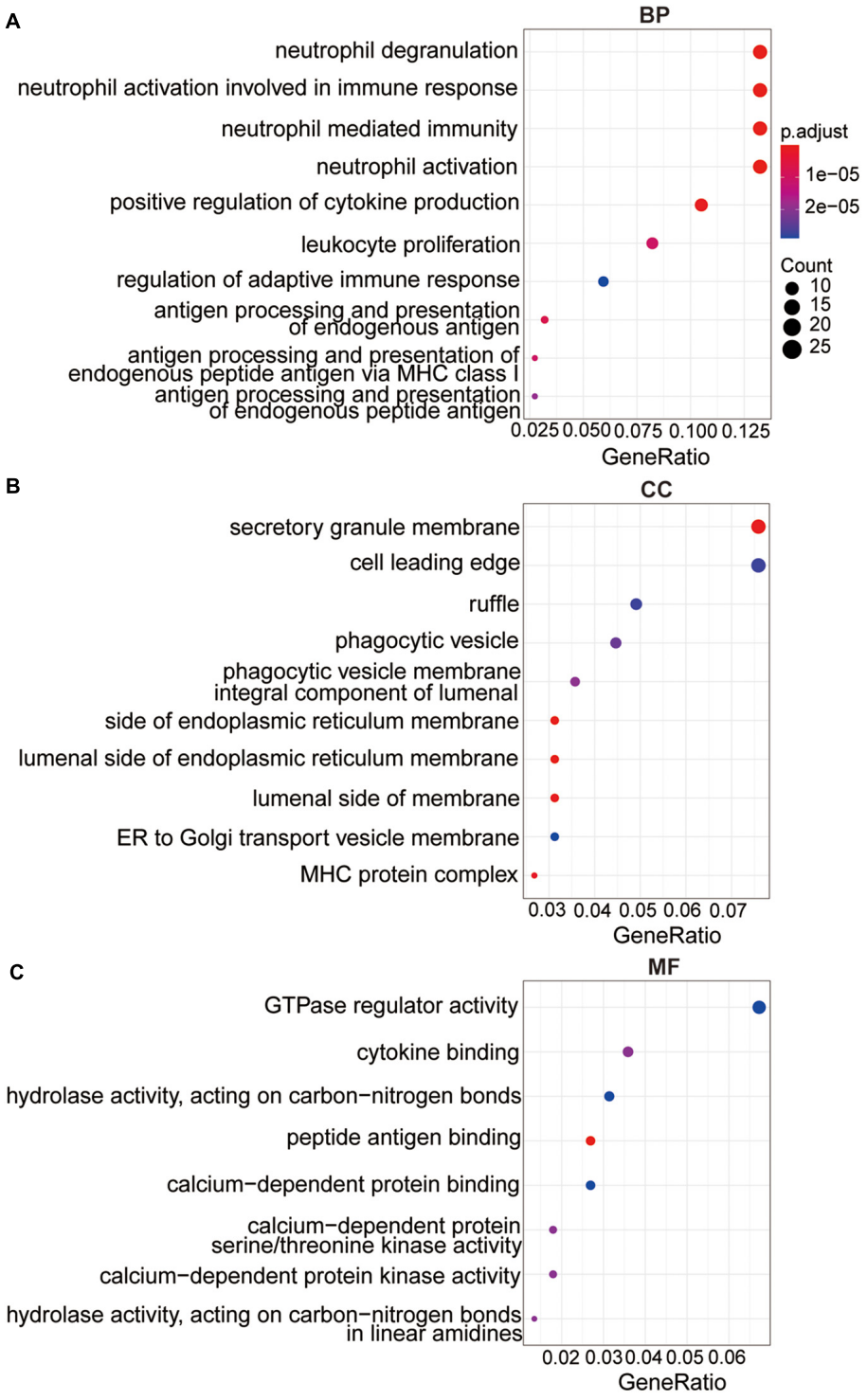

FIGURE 3
The functional analysis of the methylation-driven genes. **(A)** Top 10 of biological process enrichment. **(B)** Top 10 of cellular component enrichment. **(C)** Top 10 of molecular function enrichment.

out between the two risk groups in the training dataset GSE99039. As shown in Figure 5, the top KEGG (Kyoto Encyclopedia of Genes and Genomes) signaling pathways enriched in the high-risk group were associated with PD, neurotrophic signaling pathway, ubiquitin mediated proteolysis, B cell receptor signaling pathway, Toll like receptor signaling

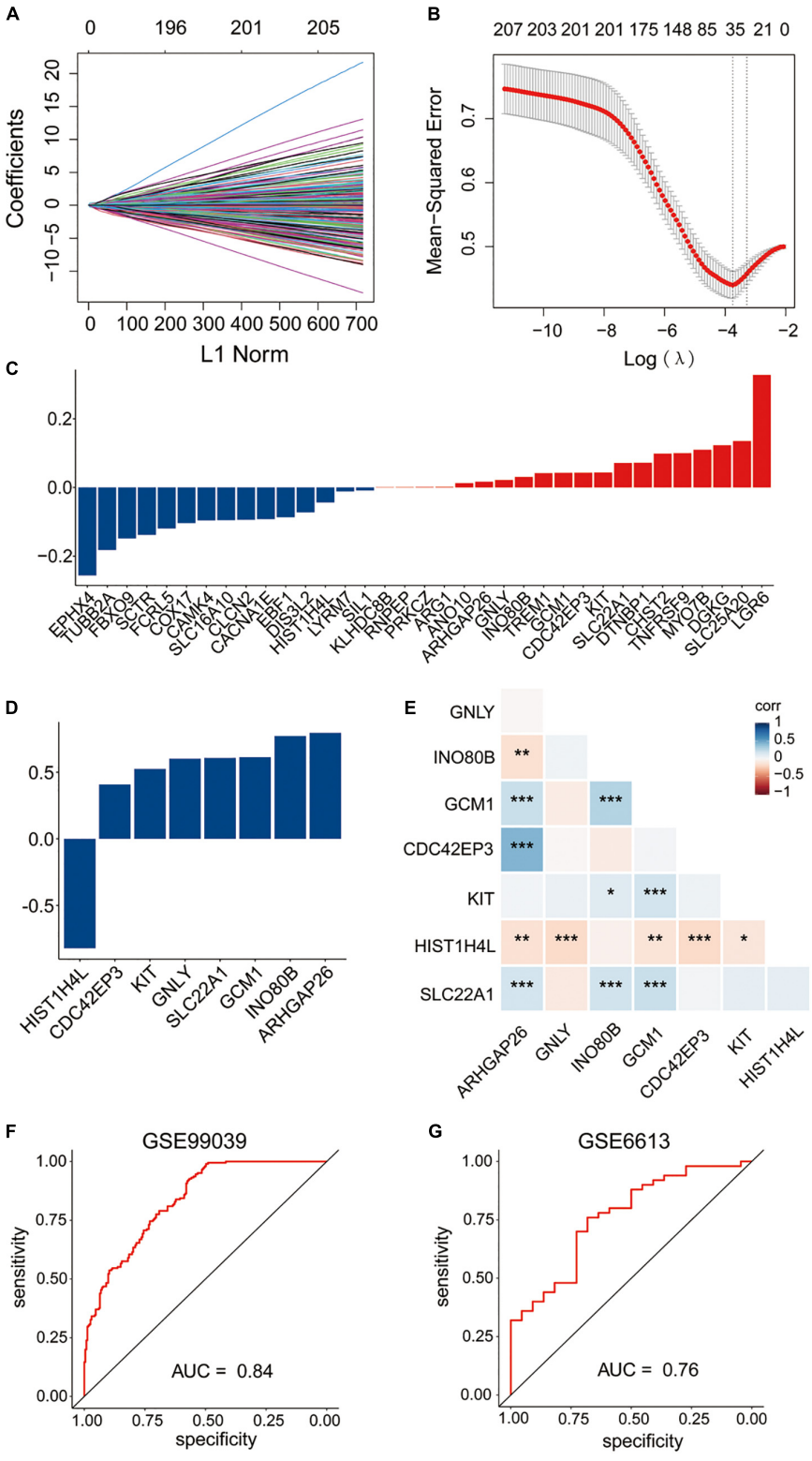

FIGURE 4
Construction of the diagnostic signature based on methylation-driven genes. **(A,B)** LASSO regression was performed to calculate the coefficients **(A)** and minimum criteria **(B)**. **(C)** Coefficients of 35 methylation-driven genes selected by LASSO regression. **(D)** Coefficients of eight methylation-driven genes in the signature selected by the stepwise logistic regression analysis. **(E)** Spearman correlation analysis of the eight genes. **(F)** ROC curve of the signature in the training set GSE99039. **(G)** ROC curve of the signature in the testing set GSE6613.

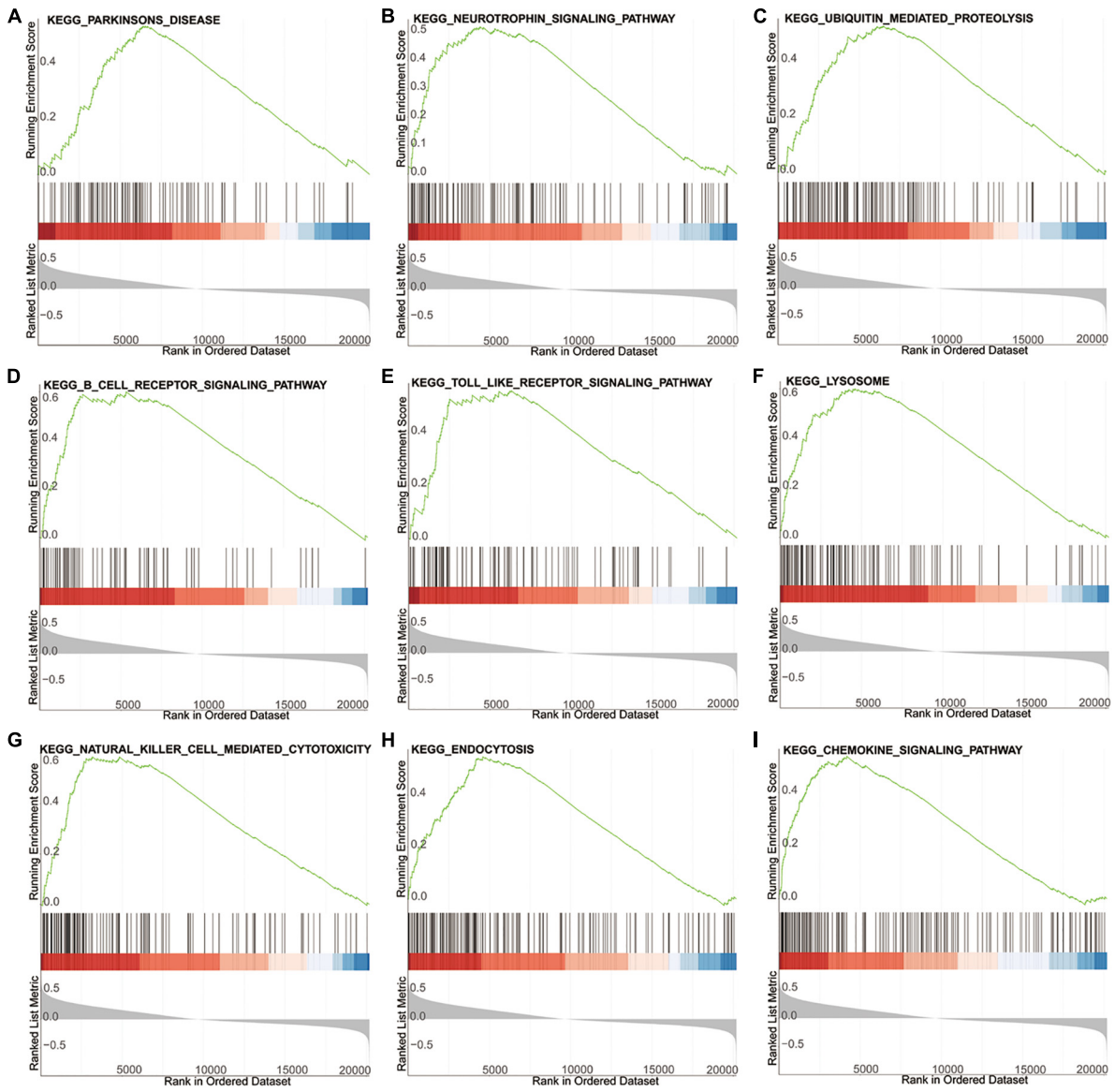

FIGURE 5
GSEA of the high- and low-risk group based on the diagnostic signature. **(A–I)** The top KEGG signaling pathways in high-risk group.

pathway, natural killer cell mediated cytotoxicity, lysosome, endocytosis, chemokine signaling pathway. These results provided new insights into pathogenesis and prevention for PD patients.

Construction and validation of the diagnostic signature based on DNA methylation sites

In the GSE145361 dataset, 77 methylation-altered CpGs associated with the eight methylation-driven genes in the gene expression signature were used in the LASSO regression model. Then, 33 CpGs obtained were further analyzed in the stepwise logistic regression model. Finally, eight CpGs were acquired to construct the signature (Figures 6A–D). The risk scoring formula was as following: risk score = (−32.323837 × cg07023902) + (−5.3875735 × cg05469695) + (4.1370905 × cg12307314) + (3.0167468 × cg13286582) + (2.6430882 × cg01204911) + (2.4635395 × cg27579771) + (2.0870986 × cg10087973) + (1.761926332 × cg04188241).

The AUC of ROC curve to distinguish the PD patients from the health controls achieved 0.8 when applied to the training dataset GSE145361 (Figure 6E). In addition, we also validated the accuracy of the CpGs signature in the other independent PD-associated blood DNA methylation dataset. The AUC of

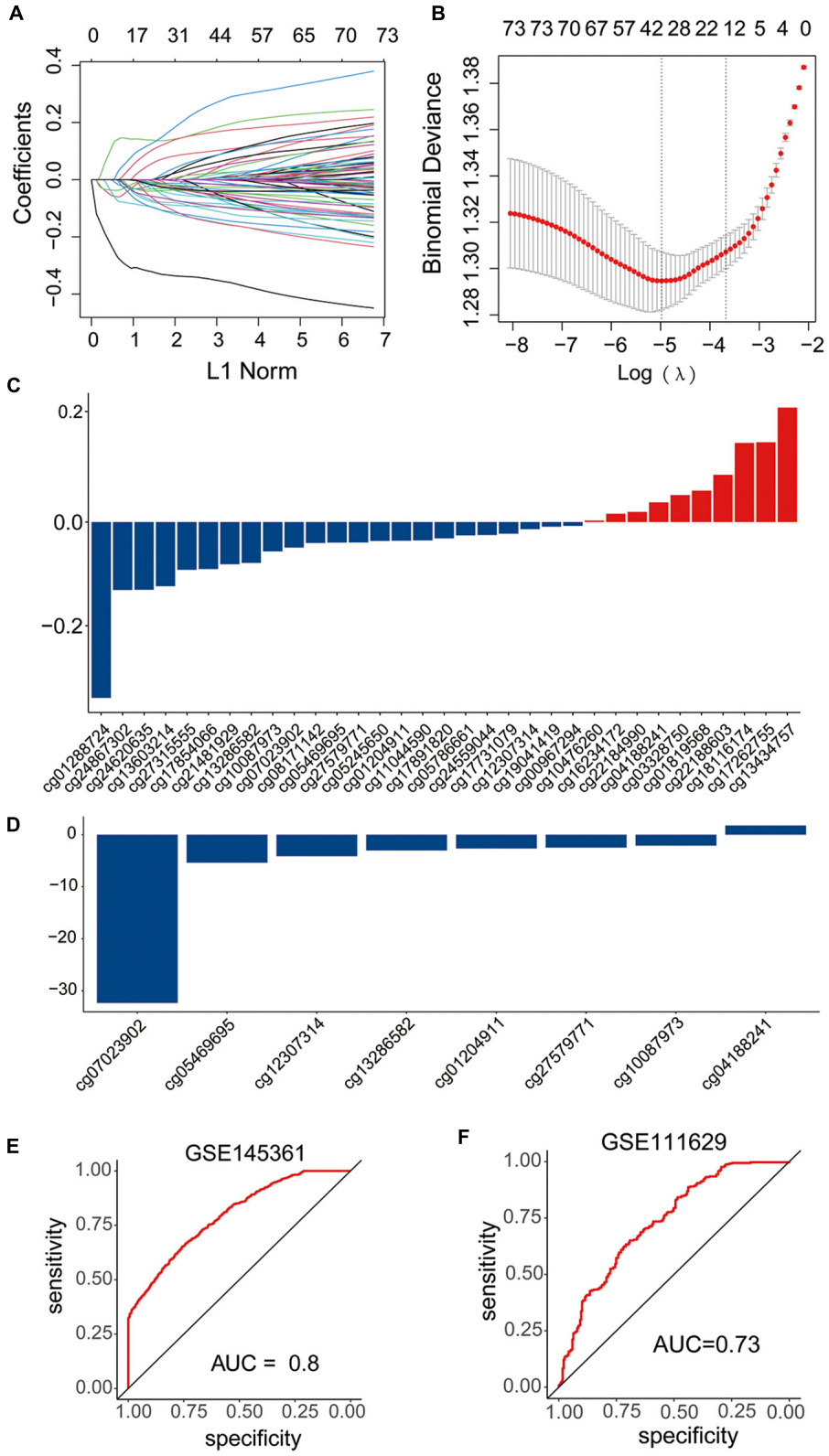

FIGURE 6
Construction and validation of the diagnostic signature based on DNA methylation sites. **(A–C)** LASSO regression was performed to calculate the **(A,B)** minimum criteria and **(C)** coefficients. **(D)** Coefficients of eight DNA methylation sites in the signature selected by the stepwise logistic regression analysis. **(E,F)** ROC curves of the signature in the training set GSE145361 and testing set GSE111629.

ROC curve achieved 0.73 when applied to GSE111629 dataset (**Figure 6F**), which indicated that the CpG signature was also efficient for PD.

Discussion

A growing number of aberrant genome or epigenome mechanisms are associated with carcinogenesis and progression. However, the specific mechanism of methylation in neurodegenerative disease still remains poorly described. The diagnosis of PD patients mainly relies on the clinical symptoms, which hinders detection of the early stages of the disease that often had the greatest therapeutic effect. It is of great value to explore potential methylated blood biomarkers for the diagnosis of PD patients.

Omics approaches play increasingly important roles in the management of disease (Amariuta et al., 2020). Biomarkers commonly used as part of routine clinical practice can complement clinical examination and contribute to the management of various diseases. The advance of the new sequencing approach and access to some huge genetic and epigenetic databases including TCGA and GEO, are providing potential biomarkers options and the focus is shifting to a combination of several or more biomarkers, rather than a single marker that researchers have concentrated on in the past (Conway and Wong, 2020; Vincent et al., 2020; Bian et al., 2022). In this study, we conducted an integrative analysis of gene expression and DNA methylation data, and identified the DMGs and DEGs between PD patients and healthy controls. Furthermore, LASSO regression analysis was carried out to further construct the methylation-driven gene signature. Finally, an eight methylation- driven genes risk signature was developed, and the AUCs in evaluating the predictive accuracy of the signature were high (0.84 in training dataset, 0.76 in testing dataset, respectively).

Among the eight methylation-driven signature genes, ARHGAP26 is a GTPase-activating protein and inhibits the activity of Rho GTPases to affect tumorigenesis and progression of various tumors (Zhang et al., 2022). Recently, it was reported to be significantly associated with neuropsychiatric diseases and neurodegenerative diseases, including PD (Wang et al., 2022). SLC22A1 facilitates the transport, distribution, and elimination of levodopa, which is significantly associated with the occurrence of adverse events of dopaminergic treatment in PD (Redenšek et al., 2019). INO80B regulates trophoblast differentiation and embryonic stem cell self-renewal, implicating in tumorigenesis, pre-eclampsia, and avoidant personality disorder (Wang et al., 2014; Oudejans et al., 2015). GCM1 encodes a DNA-binding protein with a gcm-motif, which is associated with the epigenetic regulation of Hes5 transcription by DNA demethylation. Loss of GCM1 leads to the impaired induction of neural stem cells (Hitoshi et al., 2011). GNLY, an immune-regulator, has a close correlation with methylation and expression change, and has previously been implicated in spontaneous abortions (Novakovic et al., 2011). Oncogene KIT mediates cellular responses, such as cell survival, proliferation, and differentiation (Roskoski, 2018). It was reported that hyper-methylation in the promoter region of c-KIT proto-oncogene would result in the down-regulation of gene expression in most cancer tissues (Huang et al., 2015). CDC42EP3, one of five CDC42 effector proteins, acts as a key regulator of the activities of CDC42 (Farrugia and Calvo, 2017). Previous studies have indicated that the bio functional roles of CDC42EP3 in regulating cell shape change, actomyosin contractility and pathological fibroblast activation (Farrugia and Calvo, 2016). Additionally, CDC42EP3 is also associated with the occurrence and progression of human cancers, such as colorectal cancer (Feng et al., 2021), ovarian cancer (Yan et al., 2021), and glioma (Yang et al., 2022). HIST1H4L, known as H4 Clustered Histone 13 (H4C13), is essential nuclear proteins responsible for the nucleosome structure of the chromosomal fiber in eukaryotes. Dysregulation of HIST1H4L may lead to the alternative histone modifications and aberrant gene expression and has been identified as a senescence-related gene in lung adenocarcinoma (Wang et al., 2021; Lin et al., 2022). Overall, HIST1H4L, CDC42EP3, KIT, GNLY, GCM1, and INO80B have not been previously elucidated to be involved in PD, which provides additional insights in the underlying molecular mechanism of PD.

Despite the data came from distinct samples, and was obtained using different analytical means, some genes were overlapped between DEGs and DMGs. Notably, majority of the overlapped genes were hypomethylated and upregulated, which demonstrated that the hypomethylation was the key epigenetic modification associated with PD and hypomethylation of some PD-related genes result in the upregulation of these genes. Moreover, dominant methylation-altered regions of the genes were remarkably different. In addition, some genes had multiple dominant DNA methylation-altered regions, while others had a single dominant methylation-altered region. Therefore, to further explore the clinical value of CpGs in PD, eight significant dominant methylation-altered CpGs were used to construct a gene methylation signature. The ROC analyses demonstrated that the signature also had a superior prediction power for PD (AUCs of 0.8 in training dataset, and 0.73 in testing dataset, respectively).

To explore the underlying biological functions and signaling pathways involved in the signature, GO and GSEA analyses were performed. The results revealed that the neutrophil function and the relevant signaling pathway were significantly enriched in both GO and GSEA analyses. As the protagonists in chronic inflammation (Soehnlein et al., 2017), neutrophil activation stimulates the local and systemic inflammation, promotes proinflammatory cytokines

induction and causes neuroinflammation (Kanashiro et al., 2020). Neuroinflammation has been shown to contribute to the progression of neurodegeneration in PD (Tansey and Romero-Ramos, 2019; Hirsch and Standaert, 2021). Previous evidences proved that neutrophil activation played an important role in various diseases, including cancer (Rosell et al., 2021), cardiovascular disease (Bonaventura et al., 2019), and Alzheimer's disease (Dong et al., 2019). And many studies demonstrated that, compared with healthy controls, PD patients had a high neutrophil count, which was consistent to the results of our study (Ataç Uçar et al., 2017; Muñoz-Delgado et al., 2021). Our study showed that neutrophil activation could be an indicator of the inflammatory status and peripheral immune dysregulation in PD, but whether it is a cause or a consequence of PD progression remains unclear.

Currently, several biomarkers for PD diagnosis were available. Caldi et al. identified a miRNA signature in PD cerebrospinal fluid (Caldi Gomes et al., 2021). Shao et al. identified a metabolite panel in PD plasma samples (Shao et al., 2021). In comparison, there are also some strengthens in our study. First, we constructed the diagnostic signature based on a dataset with a large sample size. Second, we integrated the gene expression and DNA methylation data, which is more stable than a single data form. Third, the signature was based on the whole blood sample, which could be obtained with a non-invasive, convenient and easy method. Furthermore, the signature has a higher accuracy and specificity, and contains fewer genes, which is more promising for clinical application.

However, there are some limitations should be noticed in our study. First, this study was performed based on the public database and was driven by the analysis of available retrospective data. And, the optimal cutoff value was required to be defined before clinical application. In addition, our study only focused on the methylated genes. However, there are many other epigenetic modifications in disease pathology. It is of great value to integrate more modifications together. In future study, *in vivo* and/or *in vitro* experiments based on the constructed mouse model and a large number of patient blood samples are planned to validate the identified signature and elucidate the underlying mechanisms in PD.

Conclusion

In conclusion, we performed an integrated analysis of the gene expression data and DNA methylation data, constructed a methylation-driven genes signature and a methylation-altered CpGs signature to distinguish PD patients from healthy controls. All of them have a good prediction power for PD and provide a new insight into personalized diagnostic and therapeutic strategies for PD.

Data availability statement

The datasets presented in this study can be found in online repositories. The names of the repository/repositories and accession number(s) can be found in the article/**Supplementary material**.

Author contributions

XW, DL, and WZ designed the research. JL, YZ, and WG analyzed the data. DL and XW wrote the manuscript with contributions from all the authors. All authors have read and approved the manuscript.

Funding

This study was supported by the Henan Provincial Science and Technology Research Project (202102310157).

Acknowledgments

We are grateful to the contributors of the public databases used in the study.

Conflict of interest

The authors declare that the research was conducted in the absence of any commercial or financial relationships that could be construed as a potential conflict of interest.

Publisher's note

Supplementary material

The Supplementary Material for this article can be found online at: https://www.frontiersin.org/articles/10.3389/fnagi.2022.971528/full#supplementary-material

References

Amariuta, T., Luo, Y., Knevel, R., Okada, Y., and Raychaudhuri, S. (2020). Advances in genetics toward identifying pathogenic cell states of rheumatoid arthritis. *Immunol. Rev.* 294, 188–204. doi: 10.1111/imr.12827

Ataç Uçar, C., Gökçe Çokal, B., Ünal Artık, H. A., İnan, L. E., and Yoldaş, T. K. (2017). Comparison of neutrophil-lymphocyte ratio (NLR) in Parkinson's disease subtypes. *Neurol. Sci.* 38, 287–293. doi: 10.1007/s10072-016-2758-8

Behzadi, P., and Ranjbar, R. (2019). DNA microarray technology and bioinformatic web services. *Acta Microbiol. Immunol. Hungarica* 66, 19–30. doi: 10.1556/030.65.2018.028

Bian, S., Ni, W., Zhu, M., Zhang, X., Qiang, Y., Zhang, J., et al. (2022). Flap endonuclease 1 facilitated hepatocellular carcinoma progression by enhancing USP7/MDM2-mediated P53 Inactivation. *Int. J. Biol. Sci.* 18, 1022–1038. doi: 10.7150/ijbs.68179

Blauwendraat, C., Reed, X., Krohn, L., Heilbron, K., Bandres-Ciga, S., Tan, M., et al. (2020). Genetic modifiers of risk and age at onset in GBA associated Parkinson's disease and Lewy body dementia. *Brain* 143, 234–248. doi: 10.1093/brain/awz350

Bloem, B. R., Okun, M. S., and Klein, C. (2021). Parkinson's disease. *Lancet* 397, 2284–2303. doi: 10.1016/S0140-6736(21)00218-X

Bonaventura, A., Montecucco, F., Dallegri, F., Carbone, F., Lüscher, T. F., Camici, G. G., et al. (2019). Novel findings in neutrophil biology and their impact on cardiovascular disease. *Cardiovasc. Res.* 115, 1266–1285. doi: 10.1093/cvr/cvz084

Caldi Gomes, L., Roser, A. E., Jain, G., Pena Centeno, T., Maass, F., Schilde, L., et al. (2021). MicroRNAs from extracellular vesicles as a signature for Parkinson's disease. *Clin. Transl. Med.* 11:e357. doi: 10.1002/ctm2.357

Chahine, L. M., Stern, M. B., and Chen-Plotkin, A. (2014). Blood-based biomarkers for Parkinson's disease. *Parkinson. Relat. Disord.* 20(Suppl. 1), S99–S103. doi: 10.1016/S1353-8020(13)70025-7

Chen, L., Zhang, Y. H., Wang, S., Zhang, Y., Huang, T., and Cai, Y. D. (2017). Prediction and analysis of essential genes using the enrichments of gene ontology and KEGG pathways. *PLoS One* 12:e0184129. doi: 10.1371/journal.pone.0184129

Conway, S. R., and Wong, H. R. (2020). Biomarker panels in critical care. *Crit. Care Clin.* 36, 89–104. doi: 10.1016/j.ccc.2019.08.007

Coupland, K. G., Mellick, G. D., Silburn, P. A., Mather, K., Armstrong, N. J., Sachdev, P. S., et al. (2014). DNA methylation of the MAPT gene in Parkinson's disease cohorts and modulation by vitamin E in vitro. *Mov. Disord.* 29, 1606–1614. doi: 10.1002/mds.25784

Dong, X., Nao, J., Shi, J., and Zheng, D. (2019). Predictive value of routine peripheral blood biomarkers in Alzheimer's disease. *Front. Aging Neurosci.* 11:332. doi: 10.3389/fnagi.2019.00332

Dutta, S., Hornung, S., Kruayatidee, A., Maina, K. N., Del Rosario, I., Paul, K. C., et al. (2021). α-Synuclein in blood exosomes immunoprecipitated using neuronal and oligodendroglial markers distinguishes Parkinson's disease from multiple system atrophy. *Acta Neuropathol.* 142, 495–511. doi: 10.1007/s00401-021-02324-0

Farrugia, A. J., and Calvo, F. (2016). The Borg family of Cdc42 effector proteins Cdc42EP1-5. *Biochem. Soc. Trans.* 44, 1709–1716. doi: 10.1042/BST20160219

Farrugia, A. J., and Calvo, F. (2017). Cdc42 regulates Cdc42EP3 function in cancer-associated fibroblasts. *Small GTPases* 8, 49–57. doi: 10.1080/21541248.2016.1194952

Feng, Q., Xu, D., Zhou, M., Wu, Z., Wu, Z., Wang, Z., et al. (2021). CDC42EP3 promotes colorectal cancer through regulating cell proliferation, cell apoptosis and cell migration. *Cancer Cell Int.* 21:169. doi: 10.1186/s12935-021-01845-8

Henderson-Smith, A., Fisch, K. M., Hua, J., Liu, G., Ricciardelli, E., Jepsen, K., et al. (2019). DNA methylation changes associated with Parkinson's disease progression: outcomes from the first longitudinal genome-wide methylation analysis in blood. *Epigenetics* 14, 365–382. doi: 10.1080/15592294.2019.1588682

Hirsch, E. C., and Standaert, D. G. (2021). Ten unsolved questions about neuroinflammation in Parkinson's disease. *Mov. Disord.* 36, 16–24. doi: 10.1002/mds.28075

Hitoshi, S., Ishino, Y., Kumar, A., Jasmine, S., Tanaka, K. F., Kondo, T., et al. (2011). Mammalian Gcm genes induce Hes5 expression by active DNA demethylation and induce neural stem cells. *Nat. Neurosci.* 14, 957–964. doi: 10.1038/nn.2875

Ho, P. W., Leung, C. T., Liu, H., Pang, S. Y., Lam, C. S., Xian, J., et al. (2020). Age-dependent accumulation of oligomeric SNCA/α-synuclein from impaired degradation in mutant LRRK2 knockin mouse model of Parkinson disease: role for therapeutic activation of chaperone-mediated autophagy (CMA). *Autophagy* 16, 347–370. doi: 10.1080/15548627.2019.1603545

Huang, W. Y., Hsu, S. D., Huang, H. Y., Sun, Y. M., Chou, C. H., Weng, S. L., et al. (2015). MethHC: a database of DNA methylation and gene expression in human cancer. *Nucleic Acids Res.* 43, D856–D861. doi: 10.1093/nar/gku1151

Jowaed, A., Schmitt, I., Kaut, O., and Wüllner, U. (2010). Methylation regulates alpha-synuclein expression and is decreased in Parkinson's disease patients' brains. *J. Neurosci.* 30, 6355–6359. doi: 10.1523/JNEUROSCI.6119-09.2010

Kanashiro, A., Hiroki, C. H., da Fonseca, D. M., Birbrair, A., Ferreira, R. G., Bassi, G. S., et al. (2020). The role of neutrophils in neuro-immune modulation. *Pharmacol. Res.* 151:104580. doi: 10.1016/j.phrs.2019.104580

Kanehisa, M., Furumichi, M., Sato, Y., Ishiguro-Watanabe, M., and Tanabe, M. (2021). KEGG: integrating viruses and cellular organisms. *Nucleic Acids Res.* 49, D545–D551. doi: 10.1093/nar/gkaa970

Kaut, O., Schmitt, I., and Wüllner, U. (2012). Genome-scale methylation analysis of Parkinson's disease patients' brains reveals DNA hypomethylation and increased mRNA expression of cytochrome P450 2E1. *Neurogenetics* 13, 87–91. doi: 10.1007/s10048-011-0308-3

Lin, Q., Ding, H., Zheng, Z., Gu, Z., Ma, J., Chen, L., et al. (2012). Promoter methylation analysis of seven clock genes in Parkinson's disease. *Neurosci. Lett.* 507, 147–150. doi: 10.1016/j.neulet.2011.12.007

Lin, Z., Yu, B., Yuan, L., Tu, J., Shao, C., and Tang, Y. (2022). RAGE is a potential biomarker implicated in immune infiltrates and cellular senescence in lung adenocarcinoma. *J. Clin. Lab. Analysis* 36:e24382. doi: 10.1002/jcla.24382

Masliah, E., Dumaop, W., Galasko, D., and Desplats, P. (2013). Distinctive patterns of DNA methylation associated with Parkinson disease: identification of concordant epigenetic changes in brain and peripheral blood leukocytes. *Epigenetics* 8, 1030–1038. doi: 10.4161/epi.25865

Mata, I. F., Leverenz, J. B., Weintraub, D., Trojanowski, J. Q., Hurtig, H. I., Van Deerlin, V. M., et al. (2014). APOE, MAPT, and SNCA genes and cognitive performance in Parkinson disease. *JAMA Neurol.* 71, 1405–1412. doi: 10.1001/jamaneurol.2014.1455

Matsumoto, L., Takuma, H., Tamaoka, A., Kurisaki, H., Date, H., Tsuji, S., et al. (2010). CpG demethylation enhances alpha-synuclein expression and affects the pathogenesis of Parkinson's disease. *PLoS One* 5:e15522. doi: 10.1371/journal.pone.0015522

Muñoz-Delgado, L., Macías-García, D., Jesús, S., Martín-Rodríguez, J. F., Labrador-Espinosa, M., Jiménez-Jaraba, M. V., et al. (2021). Peripheral immune profile and neutrophil-to-lymphocyte ratio in Parkinson's disease. *Mov. Disord.* 36, 2426–2430. doi: 10.1002/mds.28685

Nalls, M. A., Pankratz, N., Lill, C. M., Do, C. B., Hernandez, D. G., Saad, M., et al. (2014). Large-scale meta-analysis of genome-wide association data identifies six new risk loci for Parkinson's disease. *Nat. Genet.* 46, 989–993. doi: 10.1038/ng.3043

Novakovic, B., Yuen, R. K., Gordon, L., Penaherrera, M. S., Sharkey, A., Moffett, A., et al. (2011). Evidence for widespread changes in promoter methylation profile in human placenta in response to increasing gestational age and environmental/stochastic factors. *BMC Genom.* 12:529. doi: 10.1186/1471-2164-12-529

Oudejans, C. B., Michel, O. J., Janssen, R., Habets, R., Poutsma, A., Sistermans, E. A., et al. (2015). Susceptibility allele-specific loss of miR-1324-mediated silencing of the INO80B chromatin-assembly complex gene in pre-eclampsia. *Hum. Mol. Genet.* 24, 118–127. doi: 10.1093/hmg/ddu423

Redenšek, S., Flisar, D., Kojovič, M., Gregorič Kramberger, M., Georgiev, D., Pirtošek, Z., et al. (2019). Dopaminergic pathway genes influence adverse events related to dopaminergic treatment in Parkinson's disease. *Front. Pharmacol.* 10:8. doi: 10.3389/fphar.2019.00008

Rosell, A., Aguilera, K., Hisada, Y., Schmedes, C., Mackman, N., Wallén, H., et al. (2021). Prognostic value of circulating markers of neutrophil activation, neutrophil extracellular traps, coagulation and fibrinolysis in patients with terminal cancer. *Sci. Rep.* 11:5074. doi: 10.1038/s41598-021-84476-3

Roskoski, R. Jr. (2018). The role of small molecule Kit protein-tyrosine kinase inhibitors in the treatment of neoplastic disorders. *Pharmacol. Res.* 133, 35–52. doi: 10.1016/j.phrs.2018.04.020

Shao, Y., Li, T., Liu, Z., Wang, X., Xu, X., Li, S., et al. (2021). Comprehensive metabolic profiling of Parkinson's disease by liquid chromatography-mass spectrometry. *Mol. Neurodegener.* 16:4. doi: 10.1186/s13024-021-00425-8

Soehnlein, O., Steffens, S., Hidalgo, A., and Weber, C. (2017). Neutrophils as protagonists and targets in chronic inflammation. *Nat. Rev. Immunol.* 17, 248–261. doi: 10.1038/nri.2017.10

Su, X., Chu, Y., Kordower, J. H., Li, B., Cao, H., Huang, L., et al. (2015). PGC-1α promoter methylation in Parkinson's disease. *PLoS One* 10:e0134087. doi: 10.1371/journal.pone.0134087

Tansey, M. G., and Romero-Ramos, M. (2019). Immune system responses in Parkinson's disease: early and dynamic. *Eur. J. Neurosci.* 49, 364–383. doi: 10.1111/ejn.14290

Tolosa, E., Garrido, A., Scholz, S. W., and Poewe, W. (2021). Challenges in the diagnosis of Parkinson's disease. *Lancet Neurol.* 20, 385–397. doi: 10.1016/S1474-4422(21)00030-2

Tolosa, E., Vila, M., Klein, C., and Rascol, O. (2020). LRRK2 in Parkinson disease: challenges of clinical trials. *Nat. Rev. Neurol.* 16, 97–107. doi: 10.1038/s41582-019-0301-2

Vincent, J. L., Bogossian, E., and Menozzi, M. (2020). The future of biomarkers. *Crit. Care Clin.* 36, 177–187. doi: 10.1016/j.ccc.2019.08.014

Wang, C., Chen, L., Yang, Y., Zhang, M., and Wong, G. (2019). Identification of potential blood biomarkers for Parkinson's disease by gene expression and DNA methylation data integration analysis. *Clin. Epigenet.* 11:24. doi: 10.1186/s13148-019-0621-5

Wang, K., Lu, Y., Morrow, D. F., Xiao, D., and Xu, C. (2022). Associations of ARHGAP26 polymorphisms with Alzheimer's disease and cardiovascular disease. *J. Mol. Neurosci.* 72, 1085–1097. doi: 10.1007/s12031-022-01972-5

Wang, L., Du, Y., Ward, J. M., Shimbo, T., Lackford, B., Zheng, X., et al. (2014). INO80 facilitates pluripotency gene activation in embryonic stem cell self-renewal, reprogramming, and blastocyst development. *Cell Stem Cell* 14, 575–591. doi: 10.1016/j.stem.2014.02.013

Wang, Y., Li, Z., Yang, G., Cai, L., Yang, F., Zhang, Y., et al. (2021). The study of alternative splicing events in human induced pluripotent stem cells from a down's syndrome patient. *Front. Cell Dev. Biol.* 9:661381. doi: 10.3389/fcell.2021.661381

Yan, Y., Liang, Q., Xu, Z., and Yi, Q. (2021). Integrative bioinformatics and experimental analysis revealed down-regulated CDC42EP3 as a novel prognostic target for ovarian cancer and its roles in immune infiltration. *PeerJ* 9:e12171. doi: 10.7717/peerj.12171

Yang, Z., Xu, T., Xie, T., Yang, L., Wang, G., Gao, Y., et al. (2022). CDC42EP3 promotes glioma progression via regulation of CCND1. *Cell Death Dis.* 13:290. doi: 10.1038/s41419-022-04733-9

Young, J. I., Sivasankaran, S. K., Wang, L., Ali, A., Mehta, A., Davis, D. A., et al. (2019). Genome-wide brain DNA methylation analysis suggests epigenetic reprogramming in Parkinson disease. *Neurol. Genet.* 5:e342. doi: 10.1212/NXG.0000000000000342

Zhang, L., Zhou, A., Zhu, S., Min, L., Liu, S., Li, P., et al. (2022). The role of GTPase-activating protein ARHGAP26 in human cancers. *Mol. Cell. Biochem.* 477, 319–326. doi: 10.1007/s11010-021-04274-3

frontiers | Frontiers in Aging Neuroscience

TYPE Original Research
PUBLISHED 01 September 2022
DOI 10.3389/fnagi.2022.944195

OPEN ACCESS

EDITED BY
Jialiang Yang,
Geneis (Beijing) Co., Ltd., China

REVIEWED BY
Zhi-xin Wang,
Affiliated Hospital of Qinghai University, China
Jingwei Zhang,
Fengxian District Central Hospital, China
Xu Wang,
Beijing Aiyuhua Maternal and Children Hospital, China

*CORRESPONDENCE
Mingfeng Cao
18653192961@163.com
Yuzhen Xu
tianyayizhe@126.com

†These authors have contributed equally to this work

SPECIALTY SECTION
This article was submitted to Cellular and Molecular Mechanisms of Brain-aging, a section of the journal Frontiers in Aging Neuroscience

RECEIVED 14 May 2022
ACCEPTED 08 August 2022
PUBLISHED 01 September 2022

CITATION
Huang J, Lin W, Sun Y, Wang Q, He S, Han Z, Lu L, Kang X, Chen Y, Guo H, Cui Z, Sun C, Go K, Wu J, Yao M, Cao M and Xu Y (2022) Quercetin targets VCAM1 to prevent diabetic cerebrovascular endothelial cell injury. *Front. Aging Neurosci.* 14:944195. doi: 10.3389/fnagi.2022.944195

Quercetin targets VCAM1 to prevent diabetic cerebrovascular endothelial cell injury

Jiebin Huang[1†], Weiwei Lin[2†], Yuxing Sun[3†], Qian Wang[4†], Shidian He[5†], Zhihua Han[6†], Lixing Lu[7†], Xueran Kang[7†], Yisheng Chen[8], Haoran Guo[9], Zhiyong Cui[10], Chenyu Sun[11], Ken Go[12], Junyi Wu[13], Mengxuan Yao[14], Mingfeng Cao[15]* and Yuzhen Xu[16]*

[1]Ruijin Hospital, Shanghai Jiao Tong University School of Medicine, Shanghai, China, [2]Department of Neurosurgery, Second Affiliated Hospital of Zhejiang University School of Medicine, Zhejiang University, Hangzhou, China, [3]Department of Otorhinolaryngology Head and Neck Surgery, Shanghai Ninth People's Hospital, Shanghai Jiao Tong University School of Medicine, Shanghai, China, [4]Postdoctoral Workstation, Department of Central Laboratory, The Affiliated Tai'an City Central Hospital of Qingdao University, Tai'an, China, [5]College of Bioinformatics Science and Technology, Harbin Medical University, Harbin, China, [6]Department of Orthopedics, Shanghai General Hospital, Shanghai Jiao Tong University School of Medicine, Shanghai Jiao Tong University, Shanghai, China, [7]Department of Otorhinolaryngology Head and Neck Surgery, Shanghai Ninth People's Hospital, Shanghai Jiao Tong University School of Medicine Shanghai, Shanghai, China, [8]Department of Sports Medicine, Huashan Hospital, Fudan University, Shanghai, China, [9]Chinese PLA Medical School, Beijing, China, [10]Shanghai Jiao Tong University, Shanghai, China, [11]AMITA Health Saint Joseph Hospital Chicago, Chicago, IL, United States, [12]St. Marianna Hospital, Tokyo, Japan, [13]Department of General Surgery, Shanghai General Hospital, Shanghai Jiao Tong University School of Medicine, Shanghai, China, [14]Department of Orthopaedic Surgery, The Third Hospital of Hebei Medical University, Shijiazhuang, China, [15]Department of Endocrinology, The Second Affiliated Hospital of Shandong First Medical University Tai'an, Tai'an, China, [16]Department of Rehabilitation, The Second Affiliated Hospital of Shandong First Medical University, Tai'an, China

Introduction: Endothelial cells play important roles in neurodegenerative diseases caused by diabetes, therefore, we aimed at investigating the mechanisms through which endothelial cells are involved in diabetes development.

Methods: Single cell analysis was performed to identify the major endothelial cell subtypes in cardiovascular tissues that are involved in diabetes development. A cell-cell communication approach was then used to identify ligand-receptor interaction pairs between these cell types. Differential expression analysis between the two experimental groups [standard chow diet group and diabetogenic diet with cholesterol (DDC) group] was used to identify diabetes-related differentially expressed genes (DEGs). The upregulated genes were used to identify candidate ligands or receptors, as well as the corresponding cell types. Cell trajectory inference was performed to identify the stage of cell development and changes in expression of candidate ligands or receptors during cell development. Gene set enrichment analysis (GSEA) was conducted to investigate the biological functions of genes of purpose. Finally, molecular dynamics simulations

(MDSs) were used to predict potential drugs with the ability to target the proteins of purpose.

Results: Seven cell types, including five endothelial cell subtypes (EC_1, EC_2, EC_3, EC_4, and EC_EndMT), were identified from endothelial cell-enriched single cell samples from the heart and aorta of mice. Cell-cell communication analysis revealed the potential ligand-receptor interactions between these cell types while five important ligand-receptor-associated genes, including Fn1, Vcam1, Fbn1, Col4a1, and Col4a2, were established by differential expression analysis. Among them, Vcam1 is mainly expressed in EC_EndMT and is involved in interactions between EC_EndMT and other cells. Cell trajectory extrapolation analysis revealed a shift from EC_2/EC_4 to EC_EndMT and a shift from EC_EndMT to EC_3/EC_1 during the progression of diabetes. GSEA analysis revealed that upregulation of VCAM1 may have inhibitory effects on cell growth and energy metabolism.

Conclusion: EC_EndMT subtypes have a complex role in neurodegenerative diseases caused by diabetes. Through mechanisms involved in cell-cell communication, Vcam1 may play an important role in dysregulation of biological functions of EC_ EndMT. Molecular docking results of the quercetin-VCAM1 complex suggest that quercetin may be an effective drug for targeting this protein.

KEYWORDS

diabetes mellitus, endothelial cell, single cell analysis, VCAM1, quercetin, brain aging, neurodegenerative diseases

Introduction

Diabetes is a metabolic disease that is associated with abnormally high blood glucose levels, which can lead to various tissue lesions, including cardiovascular, renal and neurological complications (Huo et al., 2016; Bell and Goncalves, 2020; Chao et al., 2021; Bradley et al., 2022). In recent years, the prevalence of diabetes in China has significantly increased, from 10.9 to 12.4%. When combined with the prevalence of pre-diabetes, the total prevalence can reach 50.5%, with the number of people with the disease increasing from 90 million in 2011 to 140 million in 2021, the total prevalence can reach 56% (Gong et al., 2019; Li et al., 2020; Wang et al., 2021). Among these, cognitive impairment is becoming an important complication of diabetes, what's more, patients with diabetes are more likely to develop neurodegenerative disease as well as brain aging, such as dementia, amyotrophic lateral sclerosis, Alzheimer's disease, and Parkinson's disease (Biessels et al., 2006; Saltiel and Olefsky, 2017; Cheong et al., 2020). Neurodegenerative disease caused by diabetes requires long-term clinical management, therefore, it has become a major public health and social problem.

Through various mechanisms, including endothelial dysfunction, arterial damage and systemic or local inflammatory responses, diabetes has been shown to cause cerebrovascular damage, which causes neurodegenerative diseases. It can also aggravate atherosclerosis, which can in turn exacerbate ischemic diseases of the brain, such as stroke (Bradley et al., 2022; Ferket et al., 2022). Various pathways are involved in these processes, including the production of reactive oxygen species, mitochondrial dysfunction and upregulation of vasoconstrictor endothelin-1 as well as MMP-9 expressions (Bhatti et al., 2017; Hougaard et al., 2020; Urner et al., 2020; D'Onofrio et al., 2021). The current management options for diabetes include appropriate diet, exercise, medication, and insulin therapy, all of which are aimed at controlling blood glucose to achieve suitable therapeutic effects (Ling et al., 2022). Herbal medicines have received increasing attention, however, it has yet to be established whether they can improve diabetic neurodegenerative diseases. It is possible to prevent cognitive impairment and diabetes complications by using herbs (Ling et al., 2022; Tao et al., 2022). Tang G. et al. (2022) showed that naringenin alleviated p2y14 receptor-mediated diabetic cardiac autonomic neuropathy in the superior cervical

Abbreviations: GEO, Gene Expression Omnibus; DEGs, Differentially expressed genes; GSEA, Gene Set Enrichment Analysis; scRNA-seq, Single cell RNA sequencing; EndMT, Endothelial-mesenchymal transition; EC, Endothelial cell.

ganglion to improve diabetic transitions. As an adjunct for Dasatinib, quercetin improves diabetic nephropathy (Hickson et al., 2019). Ginsenosides can reduce diabetic cerebrovascular damage by improving endothelial functions (Yang et al., 2022). Therefore, herbal medicines have positive effects with regards to management of diabetes.

In summary, diabetes can affect neurodegenerative diseases caused by diabetes through endothelial cells, and active molecules of herbs can improve diabetes by improving the function of endothelial cells. Active ingredients of Chinese medicine affect disease progression by activating downstream pathways, mainly through ligand receptor binding, to influence cellular secretory functions (Chen et al., 2022a; Zhang et al., 2022). Therefore, in order to further elaborate the possible mechanisms of the occurrence of neurodegenerative diseases and to illustrate the possible mechanisms of the involvement of Chinese medicine in the prevention of neurodegenerative diseases in diabetes, new theoretical support is provided for the precise treatment of diabetes with Chinese medicine.

Materials and methods

Data acquisition

Datasets were downloaded from the Gene Expression Omnibus (GEO)[1], an international public repository for genomic data (Barrett et al., 2012). In the GEO database, the keyword "diabetes mellitus" was used to retrieve diabetes-related studies and RNA transcriptomic datasets. The data sets for bioinformatics analysis met the following criteria: i. There had a set of normal controls and ii. Their RNA transcript data could be accessed. Bulk RNA-seq data for dermal endothelial cells from four type 2 diabetic patients and six normoglycaemic controls were obtained from the GSE92724 dataset. Transcriptomic data from this dataset were stored in a TPM format and were further log-transformed for subsequent differential gene expression analyses to identify diabetes-associated differentially expressed genes (DEGs). The scRNA-seq data from the GSE169332 dataset was processed *via* the standard 10X Genomics Cell Ranger process. The GSE169332 dataset has single-cell RNA-seq data enriched with endothelial cells from the heart and aorta of Ldlr null ($Ldlr^{-/-}$) mice (Zhao et al., 2021). Mice were assigned into two groups of three each. A group of mice fed on a standard chow (Chow) diet was used as the control group for no diabetic atherosclerosis; another group of mice fed on a diabetogenic diet with cholesterol (DDC) was diagnosed with diabetic atherosclerosis after 12 weeks of feeding, which was characterized by weight gain, impaired glucose tolerance and insulin sensitivity. This single-cell RNA-seq (scRNA-seq) dataset package is composed of transcripts from 1986 cells and was used to explore diabetes-related gene transcriptional differences in endothelial cells at the single-cell level.

Single cell analysis

Cellular integration, dimensionality reduction, clustering, and cellular annotation of scRNA-seq data from this mouse were performed using standard single-cell analysis procedures based on the "Seurat" package as previous researches (Stuart et al., 2019; Chen et al., 2022b). First, quality control of scRNA-seq data was based on cell quality filtering criteria from previous studies. The exclusion criteria were: i. Cells expressing less than 300 genes or more than 4,000 genes; ii. Cells containing more than 10% of unique molecular identifiers (UMIs) derived from the mitochondrial genome; iii. Cells expressing more than 1% of hemoglobin-related genes; and iv. Gene features expressed by no more than 10 cells. A total of 1,670 cells were obtained and 12,494 genetic features were included for further analyses. Then, quality-controlled scRNA-seq data were integrated using the "SCTransform" function. Cell integration was assessed by applying the uniform manifold approximation and projection (UMAP) after running the "RunPCA" and "RunUMAP" functions (Becht et al., 2018). The "FindNeighbors" and "FindClusters" functions were used to cluster the cells and select the appropriate resolution value to establish the number of clusters.

Finally, each cell cluster was annotated using the SingleR (v. 1.4) R package and marker genes of the cell lineage (Aran et al., 2019). The first attempt involved using the SingleR package for cellular annotation of mouse scRNA-seq data based on the ImmGenData and MouseRNAseqData reference datasets, respectively. The final cell annotation was completed using previously reported cell lineage marker genes (Zhao et al., 2021). Among them, marker genes for endothelial cells are Cdh5, Pecam1, Tek, Vwf, Tie1, and Col4a1; marker genes for mesenchymal cells are Fn1, Tgfbr2, and Eln; marker genes for fibroblasts are Dcn and Col1a1 while marker genes for macrophages are Cd68, Adgre1, and Lgals3. After identification of cell types, proportions of each cell type to all cells in both groups were evaluated.

Gene differential expression analysis

Differential expression analysis of bulk RNA-seq data from human dermal vascular endothelial cells was performed using the "limma" R package to identify diabetes-associated DEGs (Zhao et al., 2021). The up- and down-regulated mRNAs at the time of brain hemorrhage were compared to their levels 3 days after brain hemorrhage. Expressions of DEGs were considered to be significant at $p < 0.05$. Fold change (FC) > 1 was used

1 https://www.ncbi.nlm.nih.gov/geo/

to identify up-regulated DEGs. Endothelial cells as well as their subpopulations were extracted from the scRNA-seq data and separately analyzed for differential gene expressions at the single cell level. The "FindMarker" function from the Seurat package was used to calculate DEGs in endothelial cells between DDC and Chow groups. $p < 0.05$ and $|\log FC| > 0.25$ were set as the thresholds for significance.

Cell-cell communication analysis

Cell-cell communication analysis was used to explore context-dependent crosstalk across endothelial cell subtypes and other cell types during diabetes development and to identify genes that alter important physiological processes in endothelial cells (Chen et al., 2022b). CellPhoneDB, a database that can calculate ligand and receptor interactions between cells, was used to perform cell-cell communication analyses (Efremova et al., 2020). Gene expression matrices and cell type text information for each endothelial cell subtype as well as other cell types identified in the dataset were used as input files to predict potential ligand-receptor interactions between these cells. The predicted ligand-receptor interaction pairs were further screened for up-regulated genes in differential analysis of bulk RNA-seq and scRNA-seq. These up-regulated genes were included as significant genes in subsequent analyses.

Cell trajectory inferences

Cell trajectory inference analyses of EC-enriched single-cell RNA-seq data from mouse heart and aortic tissues were performed using monocle3 (v. 1.0) and monocle2 (v. 2.4) (Trapnell et al., 2014; Qiu et al., 2017; Cao et al., 2019; Lin et al., 2021). Trajectory inference (TI), also known as pseudotime analysis, learns cell trajectories by measuring the distance of transcriptional differences between cells and further identifies different cell states. We separately performed cell trajectory inference analysis on all endothelial cells and EC_EndMT, after which we used all DEGs to learn cell trajectories. Based on test grouping and cell subtype distributions, the appropriate root was determined to calculate the pseudotime of all cells, relative to the root. Further identification of pseudotime-related genes was based on ordering of single cell pseudotimes. The DDRTree plot was used for visualization of cell trajectories as well as pseudotimes of cells.

Gene set enrichment analysis

Gene set enrichment analysis (GSEA) is used to explore the biological processes in which important genes of interest are involved (Subramanian et al., 2005). Based on median expression values of genes of interest, samples were divided into two groups. Then, the fold change was calculated for each gene between the groups after which all genes were sorted based on FC value and used as the input file for GSEA. The "c2.cp.v7.2.symbols.gmt [Curated]" gene set in MSigDB Collections was used as the reference gene set for functional pathway annotation.[2]

Protein and small molecule structure preparation and molecular docking

The corresponding structure information of the protein was obtained from Uniport,[3] get the entry of P19320 and download the corresponding Alphafold2 protein structure file as previous studies (Burley et al., 2019; Tunyasuvunakool et al., 2021; Kang et al., 2022; Lu et al., 2022; Tang G.-Y. et al., 2022). Under B3LYP/6-31G* basis set conditions, the quantitative software (Orca) was used for quantum chemical optimization of the small molecule (Quercetin), involving corrections for bond lengths, bond angles, dihedral angles, and calculations of RESP2.0 fixed charges (Neese et al., 2020). The smina software was carried out to achieve small molecule docking selection (Masters et al., 2020). Briefly, the ligand with polar hydrogen addition is docked to the correctly protonated protein with a box center of (17. 31, 91.29, 14.42), an x/y/z size of 126 and an exhaustiveness of 8 after which the lowest energy conformation is chosen as the final conformation to start kinetic simulation.

Molecular dynamics simulation and energy calculation

MD simulations were performed using the Gromacs2019.4 software. Amber14sb was selected as the protein stance while the Gaff2 stance was selected for small molecules. The TIP3P water model was used to create the water box and add the sodium ion equilibrium system into the system of quercetin-VCAM1 (Van Der Spoel et al., 2005). The Coulomb force cut-off distance and van der Waals radius cut-off distance were both 1.4 nm. Finally, the system was equilibrated using a regular system (NVT) and an isothermal isobaric system (NPT), followed by a 100 ns MD simulation at room temperature and pressure. During MD simulations, the involved hydrogen bonds were constrained using the LINCS algorithm with an integration step of 2 fs. Electrostatic interactions were calculated using the Particle-mesh Ewald (PME) method with a cut-off value of 1.2 nm. The non-bond interaction cut-off value was 10 Å. The V-rescale temperature coupling method was used to control the simulated

2 https://www.gsea-msigdb.org/gsea/msigdb/
3 https://www.uniprot.org/uniprot

temperature to 300 K while the Berendsen method was used to control the pressure to 1 bar. Finally, a 100 ns simulation of the finished MD of the protein-ligand complex system was performed. Visualization of simulation results was performed using the Gromacs embedded program and Pymol 2.4. Free binding energy between protein and ligands was calculated using the MM/GBSA method (Valdés-Tresanco et al., 2021). In this study, the 25–30 ns MD trajectory was used in calculation, as follows:

$$\begin{aligned}\Delta G_{\text{bind}} &= \Delta G_{\text{complex}} - (\Delta G_{\text{receptor}} + \Delta G_{\text{ligand}}) \\ &= \Delta E_{\text{internal}} + \Delta E_{\text{VDW}} + \Delta E_{\text{elec}} + \Delta G_{\text{GB}} + \Delta G_{\text{SA}}\end{aligned}$$

Whereby, $\Delta E_{\text{internal}}$ represents internal energy, ΔE_{VDW} represents van der Waals interactions and ΔE_{elec} represents electrostatic interactions. Internal energies include Ebond, Eangle, and Etorsion; ΔG_{GB} and ΔG_{GA} are collectively referred to as free energy of solvation. Among them, G_{GB} is the polar solvation free energy while G_{SA} is the non-polar solvation free energy. For ΔG_{GB}, the GB model developed by Nguyen et al. (2015) was used for calculations (igb = 8). The non-polar solvation free energy (G_{SA}) was calculated as the product of surface tension (γ) and solvent accessible surface area (SA), $G_{\text{SA}} = 0.0072 \times \Delta\text{SASA}$ (Weiser et al., 1999). We ignored entropy variation in this study because of its high consumption of computational resources and low accuracy.

Statistical analysis

All plotting was done using the R software (v. 4.0.2). The "VennDiagram" R package was used for plotting the Venn diagrams. Differences in proportions of cell types between the two groups were evaluated by the chi-square test. $p \leq 0.05$ was the threshold for statistical significance, unless otherwise stated.

Results

The endothelial cell subtypes

The distributions of characteristics in EC-enriched single cells from mouse heart and aorta before and after quality control are shown in **Supplementary Figure 1**. Single cell transcript data integration (**Figure 1A** and **Supplementary Figure 2A**) and cell clustering were performed and 12 cell clusters were identified (**Supplementary Figure 2B**), with 12 clusters in the Chow group and 11 clusters in the DDC group (**Figure 1B**). Automatic annotation of cell clusters using SingleR revealed three main cell types; endothelial cells, fibroblasts, and monocytes/macrophages (**Supplementary Figure 2C**). Then, expressions of marker genes for appeal cell lineages were analyzed in each cell cluster (**Supplementary Figures 2D, 3**). Cluster 4 was identified as fibroblasts, due to its high expressions of fibroblast marker genes (Dcn and Col1a1). Cluster 7 was identified as macrophages, due to its high expression of macrophage marker genes (Cd68, Adgre1, and Lgals3). Apart from cluster 10, the other clusters were identified as endothelial cells due to their high expressions of endothelial cell marker genes (Cdh5, Pecam1, Tek, Vwf, Tie1, and Col4a1). Clusters 8, 9, and 11 were identified as endothelial-mesenchymal transition (EndMT) ECs, based on their expressions of mesenchymal marker genes (Fn1, Tgfbr2, and Eln). Ultimately, 7 cell types, including five EC subtypes (EC_1, EC_2, EC_3, EC_4, and EC_EndMT) were identified from this single cell RNA-seq data (**Figure 1C**). Expressions of selected marker genes for each cell type were consistent between the groups (**Figure 1D**).

Proportions of each endothelial cell subtype differed between the two groups

The proportion of EC_1 was highest in both the Chow (33.89%) and DDC (62.31) groups and was significantly higher in DDC group, relative to Chow group (**Figure 2A**, $p < 0.001$). Moreover, EC_3 levels were markedly high in the DDC group than in the Chow group (15.15% vs. 4.9%, $p < 0.001$). However, EC_2 and EC_4 were essentially only present in the Chow group and, in particular, EC_2 was only present in the Chow group. The abundance of EC_EndMT was significantly higher in the DDC group, relative to the Chow group (10.69% vs. 5.53%, $p < 0.001$). Differences in proportions of fibroblasts between the groups were insignificant ($p = 0.38$). These findings show that the abundance of each endothelial cell subtype differed between the DDC and Chow groups, suggesting altered endothelium functions during diabetes progression.

Ligand-receptor interactions in endothelial cells

Differential analysis of bulk RNA-seq data based on dermal endothelial cells revealed 981 upregulated genes in DM, of which 23 were included in the predicted ligand-receptor pairs from cell-cell communication analysis. Based on differential analysis of endothelial cell scRNA-seq data and cell-cell communication analysis, eight up-regulated genes were included in the predicted ligand-receptor pairs. Intersection analyses of these two sets of genes revealed five endothelium-associated upregulated genes important in DM development (**Figure 2B**). Differential expressions of the five important genes (Fn1, Vcam1, Fbn1, Col4a1, and Col4a2) in dermal endothelial cells bulk RNA-seq and endothelial cell scRNA-seq are presented in volcano and scatter plots, respectively (**Figures 2C,D**). During DM development, these five genes

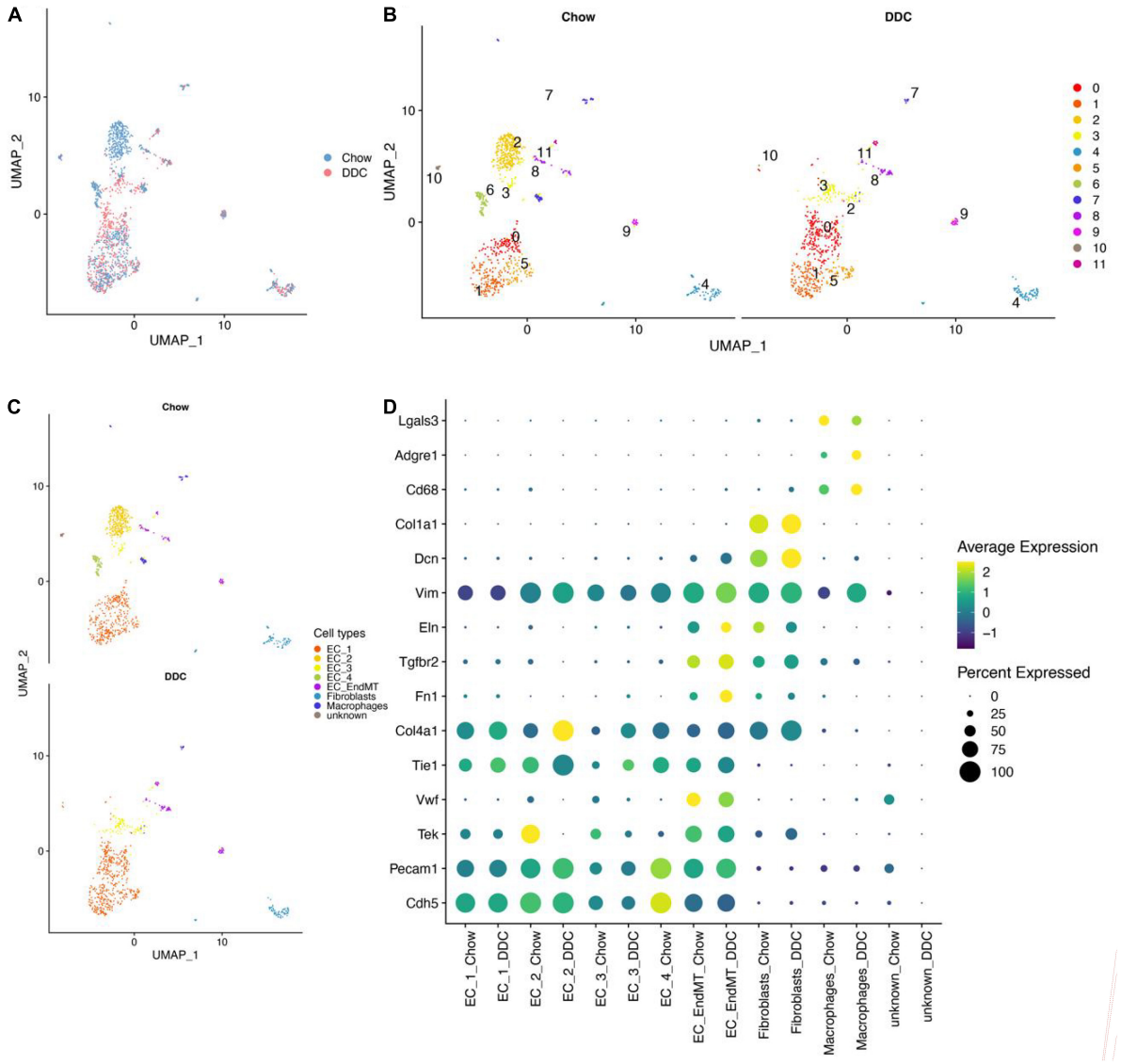

FIGURE 1
EC-enriched single-cell RNA-seq analysis of mouse heart and aorta. **(A)** UMAP plot showed cell aggregation in the Chow group and DDC group. The colors represent different groups. **(B)** UMAP plot showed the clusters of cells from the Chow and DDC groups after cell clustering. Different colors indicated different cell clusters; the Chow group showed 12 clusters of cells, while the DDC group showed 11 clusters. **(C)** UMAP plot showed 7 cell types identified in the Chow and DDC groups, among others, containing 5 endothelial cell subtypes (EC_1, EC_2, EC_3, EC_4, EC_EndMT). **(D)** Dot plots showed the expressions of selected marker genes for each cell type between the groups. Dot sizes indicated the percentage of cells expressing each gene while dot color represented the average expression level in each group. The vertical axis showed the endothelial cell marker genes (Cdh5, Pecam1, Tek, Vwf, Tie1, and Col4a1), mesenchymal marker genes (Fn1, Tgfbr2, and Eln), fibroblast marker genes (Dcn and Col1a1) and macrophage marker genes (Cd68, Adgre1, and Lgals3).

are involved in dysregulation of endothelial cell functions through ligand-receptor interactions. Ligand-receptor pairs in which these five genes are located, and the cell type pairs in which they correspond to, are shown in Figure 2E. Among them, Fbn1 and Vcam1 were enriched in interactions of EC_EndMT and fibroblasts. Vcam1 was highly expressed in EC_EndMT (Figures 2F,G). In summary, the elevated levels and dysregulated functions of EC_EndMT may play important roles in diabetes development, while Vcam1 may be involved in mediating the functions of EC_EndMT through ligand-receptor interactions.

Expressions of the 5 genes in various endothelial cell subtypes

The abundance of EC_1 and EC_3 subtypes were high in the DDC group, relative to the Chow group. Differential

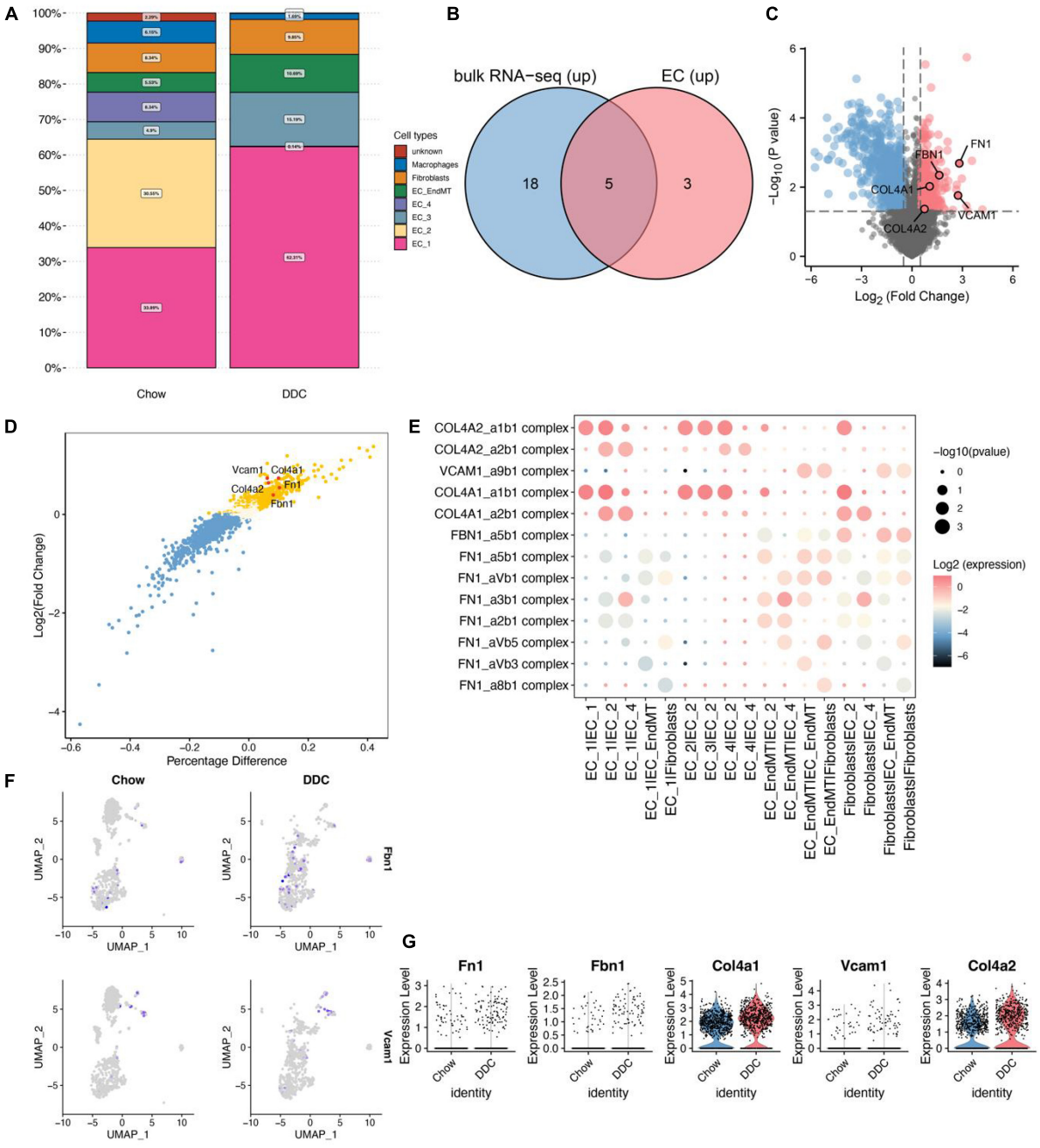

FIGURE 2
Identification of up-regulated genes in the DM group based on cellular communication ligand-receptor analysis. **(A)** Proportions of each cell type in Chow and DDC groups. **(B)** Differential analysis based on bulk RNA-seq data and endothelial cell scRNA-seq data revealed that 23/8 genes from predicted ligand-receptor pairs were upregulated in the DM group. Intersection analysis revealed five up-regulated important genes in the DM group. **(C)** Volcano plot showed the results of differential analysis of the five important genes (*FN1*, *VCAM1*, *FBN1*, *COL4A1*, and *COL4A2*) based on bulk RNA-seq data. **(D)** The results showed differential analysis of the 5 important genes based on scRNA-seq data from endothelial cells. **(E)** Dot plots showed that ligand-receptor pairs contain the five important genes in cell receptor-ligand interaction analysis and corresponding pairs of interacting cell types. **(F)** UMAP plots showed the expressions of Fbn1 and Vcam1 in endothelial cells. **(G)** Violin plots showed the expressions of the 5 important genes between the Chow and DDC groups.

expression analysis revealed that Fbn1, Col4a1 and Col4a2 expressed by EC_1 were upregulated in DDC group, compared to Chow group (Supplementary Figures 4A,B); Expressions of Fn1, Col4a1 and Col4a2 were upregulated in EC_3 (Supplementary Figures 4C,D). The EC_2 and EC_4 isoforms are predominantly present in the DDC group

and are characterized by expressions of Col4a1 and Col4a2 (**Supplementary Figures 4E,F**). Therefore, the EC_2 and EC_4 endothelial cell subtypes may play important roles in maintaining normal endothelial tissue functions while EC_1 and EC_3 may be involved in diabetes progression. In addition, ligand-receptor interaction pairs related to Fbn1 and Fn1 may play a role in conversion of the biological functions of endothelial cells.

Conversion of each endothelial cell subtype between Chow and diabetogenic diet with cholesterol groups

All endothelial trajectories between the groups were inferred (Trajectory inference) based on different transcriptional characteristics of endothelial cells and the group, endothelial cell subtypes and pseudo-temporal characteristics were projected onto the DDRTree plot (**Figures 3A,C**). The UMAP was used for further visualization of the distribution of each endothelial cell subtype (**Supplementary Figure 5A**). The DDRTree plot showed the 3 stages (states) and pseudotimes (**Supplementary Figures 5B–D**) of the endothelium. The cell state in which EC_2 and EC_4 were unique to the Chow group is defined as the root. Thus, it could be postulated that endothelial cells transition from EC_2/EC_4 to EC_EndMT and subsequently to EC_3/EC_1 (**Figure 3B**). The UMAP showed the grouping of endothelial cells (**Figure 3D**) and the transformation trajectory of endothelial cells (**Figure 3E**). The appearance of the EC_EndMT isoform throughout the endothelial cell trajectory could be seen in multiple locations and cellular stages, indicating its complex role in progression of diabetes. Changes in expressions of the top 50 genes that were associated with pseudo-temporal sorting of cells were shown in **Supplementary Figure 5E**. Among them, Vcam1, Fn1, and Fbn1 were found to be upregulated in the pseudo-time-based intermediate segment of the trajectory (**Figures 3F–H**), while Vcam1 was predominantly expressed in the EC_EndMT isoform.

Trajectory inference for the endothelial-mesenchymal transition endothelial cell subtype

Cellular trajectory analysis was performed to investigate the role of the EC_EndMT subtype in diabetes development. First, differential expression analysis showed that Vcam1 and Fn1 expressed by EC_EndMT were upregulated in the DDC group (**Figures 4A,B**). Then, EndMT ECs were subjected to trajectory learning and cell stage identification (**Supplementary Figure 5F**). DDRTree plots showed the distributions of trajectories of EC_EndMT, along with the groups in which they belong to and their pseudotime (**Figures 4C,D**). Vcam1 and Fn1 were highly expressed at intermediate pseudo-time periods (**Figures 4E,F**). Pseudo-time periods corresponded to cellular stages at states 2, 3, and 4 (**Figure 4G**). These findings imply that Vcam1 is involved in dysregulation of biological functions of EC_EndMT through cell-cell communication during diabetes development.

VCAM1 has inhibitory roles on cell growth and energy metabolism

GSEA showed that in samples with upregulated VCAM1, IFNA signaling was upregulated, while retrograde neurotrophin signaling, FGFR1 mutant receptor activation and downstream signaling of activated FGFR4 pathways associated with cell growth were downregulated (**Figure 5A**). In addition, cytoplasmic ribosomal proteins were upregulated, while energy and metabolism-related pathways, such as electron transport chain: OXPHOS system in the mitochondria and dicarboxylate metabolism, and triglyceride biosynthesis were downregulated (**Figure 5B**). These findings imply that elevated VCAM1 inhibits cell growth and energy metabolism, thereby, playing a role in diabetes development.

Analysis of molecular dynamics simulation results

Findings from molecular docking of the quercetin-VCAM1 complex were shown in **Figure 6A**. Molecular dynamics simulation (MDS) is an important method for studying the stability and kinetic characteristics of complexes in aqueous solutions. Atomic root mean square deviation (RMSD) provides a measure of the stability of the system. RMSD values fluctuated at roughly 5, 50, and 82 ns, where they started as a result of transient instability obtained from balanced docking, and then entered a steady state at 20 ns and a final steady state at 80 ns (**Figure 6B**). Root mean square fluctuations (RMSF) allow the system to be observed as local sites change configuration during simulation (**Figure 6C**). With a cut-off value of 0.25 fluctuations, amino acids 26–32, 75–78, 101–107, 142–146, and 176–185 could be seen to be highly volatile. The radius of gyration (Rg) is an important indicator for evaluating the tightness of the structure of the system. Rg analysis of the Quercetin-VCAM1 complex revealed a fluctuation at 5/50 ns each, corresponding to the ripple in RMSD, indicating that the system is undergoing a transition from multiple instabilities to platforms at this moment (**Figure 6D**). A steady decrease in Solvent Accessible Surface on Protein Surface (SASA) was found for proteins from 0 to 100 ns, indicating favorable binding and progressive protein

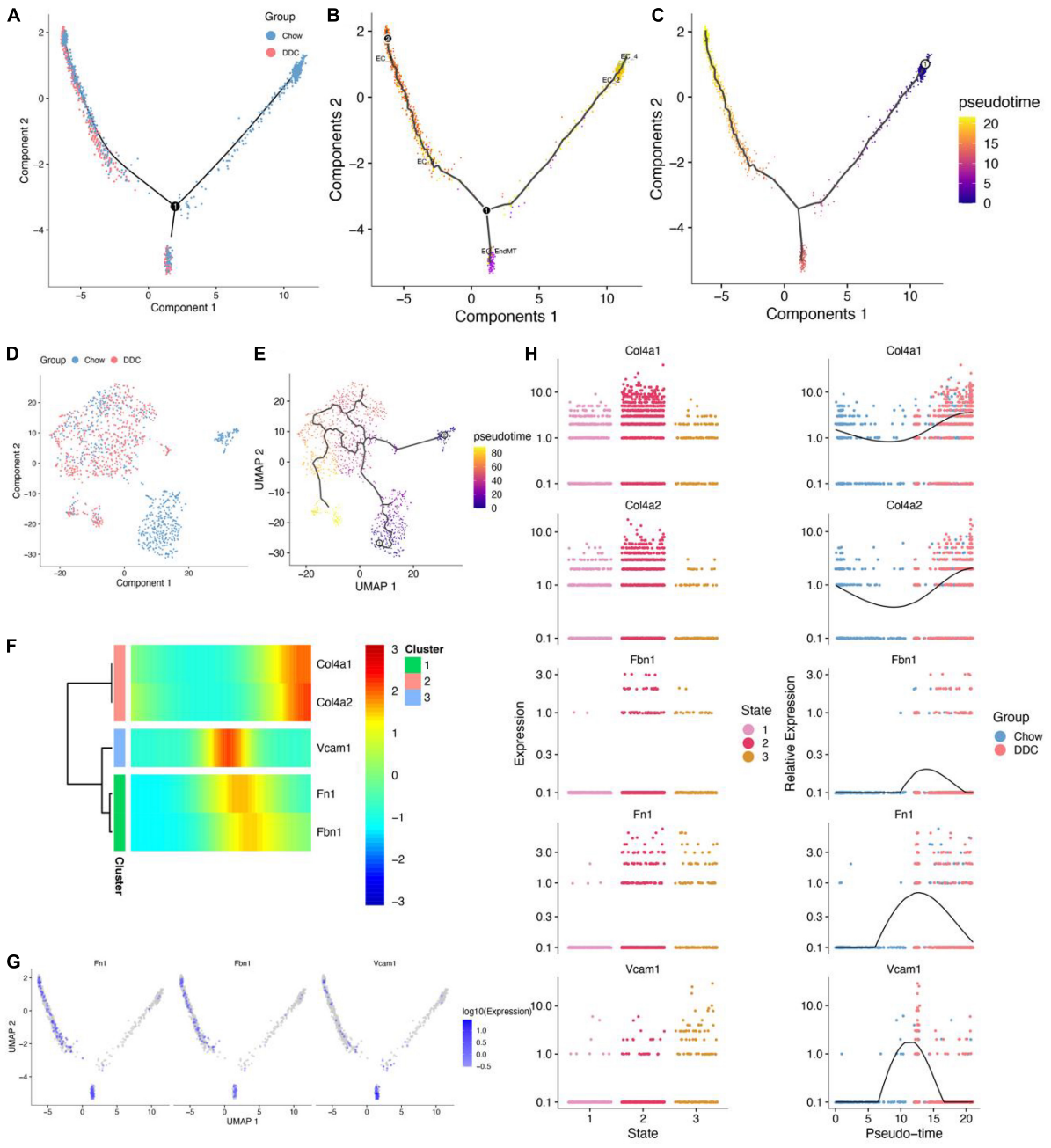

FIGURE 3
Cell trajectory analysis of five endothelial cell subtypes. **(A)** DDRTree plot of endothelial cells between Chow and DDC groups. **(B)** DDRTree plot showed the various cell subtypes of endothelial cells. **(C)** DDRTree plot showed the pseudotime of endothelial cells. **(D)** UMAP plot showed endothelial cells between Chow and DDC groups based on Monocle 2. **(E)** UMAP plot of pseudotime of endothelial cells. **(F)** Five important genes (Col4a1, Col4a2, Vcam1, Fn1, and Fbn1) were associated with pseudotime and cell trajectory differentiation of endothelial cells. **(G)** DDRTree plots of expressions of Fn1, Fbn1, and Vcam1 in endothelial cells. **(H)** Five important genes were differentially expressed between cell states and their expressions were accompanied by pseudotime. Expressions of Fbn1 and Vcam1 were the highest in the middle segment of the cell trajectory based on pseudotime.

tightening (Figure 6E). The hydrogen bonding change curve showed that the quercetin-VCAM1 complex has 2–3 hydrogen bonds in the steady state (Figure 6F). The above analyses imply that the quercetin-VCAM1 complex system becomes more stable after a series of transformations as MDS proceeds. The middle and both ends of the ligand-bound protein have red areas, therefore, this kinetic simulation causes a distal change in protein conformation.

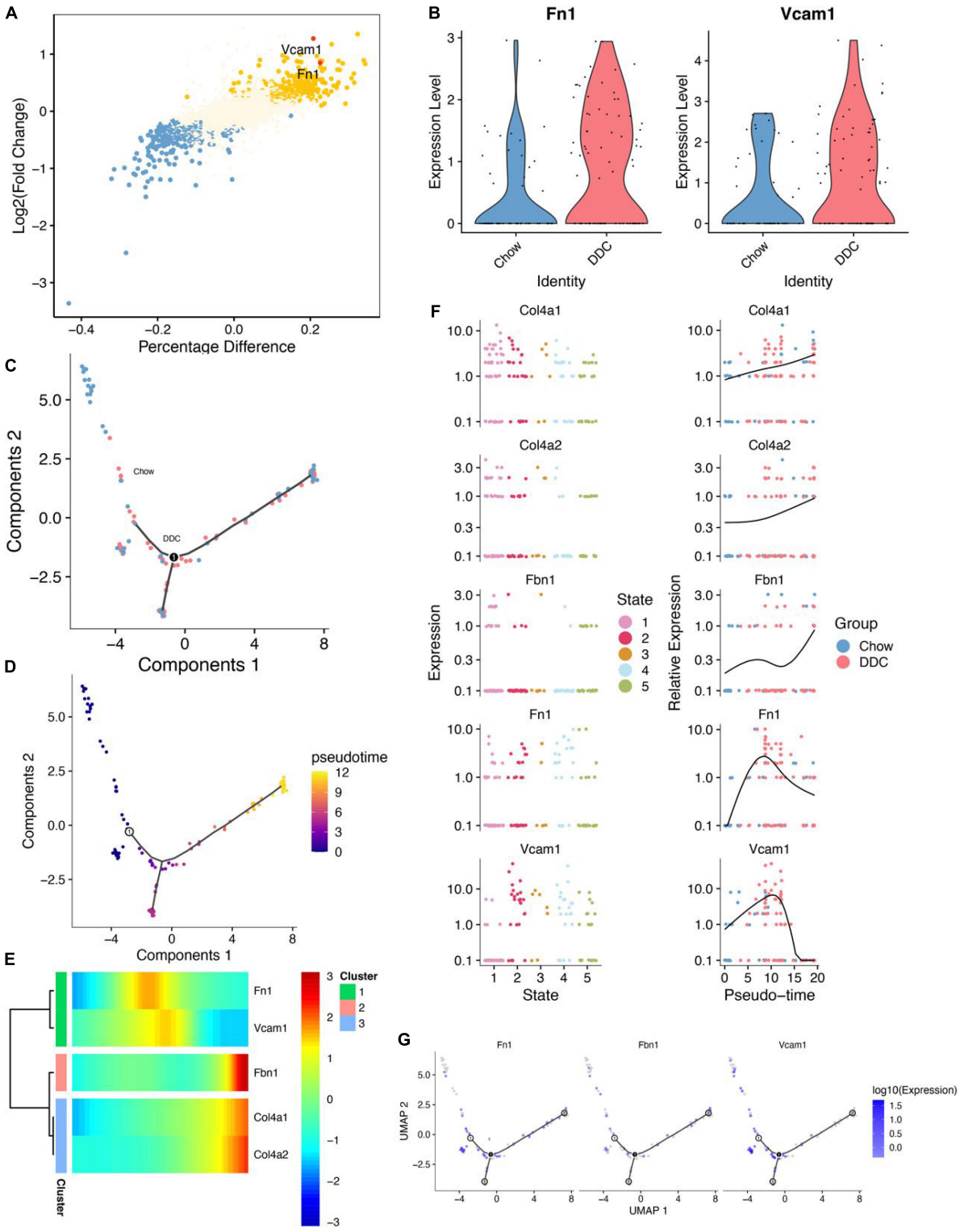

FIGURE 4
Cell trajectory inference analysis of EC_EndMT. **(A)** The results showed differential analysis of Vcam1 and Fn1. **(B)** Vcam1 and Fn1 were upregulated in DDC group compared to Chow group. **(C)** DDRTree plot showed the distributions of EC_EndMT subtypes between Chow and DDC groups. **(D)** DDRTree plot of pseudotime of EC_EndMT subtypes. **(E)** Expressions of 5 important genes in EC_EndMT were accompanied by changes in the sorting of pseudotime. **(F)** Expressions of these five important genes between cell states (left), and their expressions were accompanied by changes in the sorting of pseudotime (right). **(G)** DDRTree plots for Fn1, Fbn1, and Vcam1 expressions in EC_EndMT.

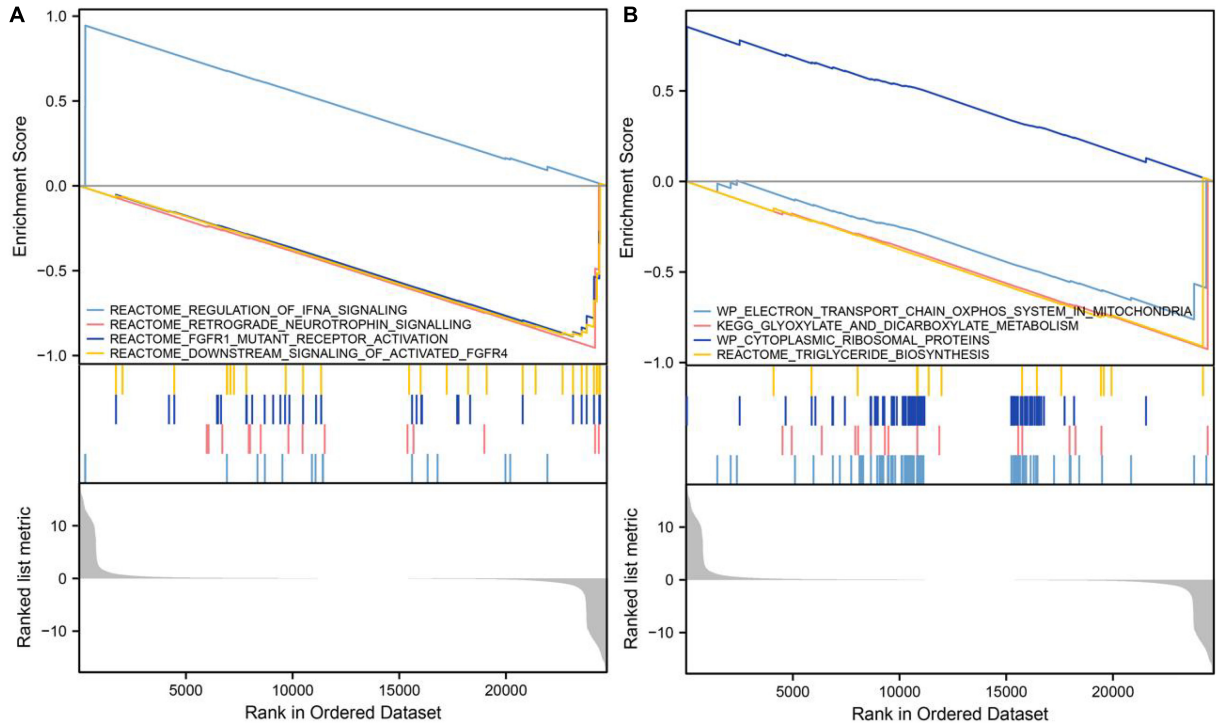

FIGURE 5
Gene set enrichment analysis of VCAM1. **(A)** Upregulation of VCAM1 was accompanied by inhibition of pathways associated with promotion of cell growth. **(B)** Upregulation of VCAM1 was accompanied by inhibition of energy and metabolism-related pathways.

Molecular dynamics simulation of secondary structures and binding free energy analysis

Secondary structure analysis based on MDS revealed that this simulation involves structures such as coil, B-sheet, B-bridge, bend, turn, and 3-helix, where the overall number of structures becomes less as simulation progresses, b-sheet and 3-helix decreases, but the number of coil and bend increases (Figure 7A). After calculating the free energy of binding between protein-ligand complexes, we calculated the differences in free energy of binding between two solvated molecules in the bound and unbound states and compared the free energies of different solvated conformations of the same molecule (Figure 7B). Analysis of the data on variations of binding free energy with MDS revealed that the energies were all negative in TOTAL free energy, suggesting a strong possibility of interactions between the protein and the small molecule. To break down each small item, "GGAS" represents the gas-phase free energy, which is negative, and is calculated by combining VDWAALS ("van der Waals energy") and EEl ("Electrostatic energy"). VDWAALS and Eel are both < 0, indicating that both hydrophobic and electrostatic interactions contribute to binding, while electrostatic interactions inhibit binding. In contrast, GSOLV represents "Total solvation free energy" which is positive, indicating unfavorable binding. GSOLV resulted from interactions of ESURF ("Non-polar solvation energy") and EGB ("Polar solvation energy"), with positive EGB values indicating that polar solvation is not conducive for binding. Breaking down each contact residue, it was shown that ILE-177 acts as a barrier to binding while ARG-10, LEU-12, GLU-87, and ASP-178 promote binding (Figure 7C). The contribution of ASP-178 was significant, thus, further keyframe analysis was performed and 22 ns as well as 73.4 ns were selected as key frames for analysis. At 22 ns, HIS-176, and ASP-122 were linked by hydrogen bonding polarity from the head and tail of the small molecule, respectively. Both are small molecules with H as the hydrogen donor and the protein as the hydrogen acceptor (Figure 7D). At 73.4 ns, after a 50 ns perturbation, the small molecule finally proceeded to the steady state (Figure 7E). At this point, the complex system remained in the previous cavity pocket while the small molecule changes position, with ARG-123 inheriting the previous active role of ASP-122 having hydrogen bonding with the small molecule. The GLU-179 and ASP-178 interacted with the small molecule to jointly stabilize it, where GLU-179 and Arg-123 act as hydrogen co-donors and ASP-178 acts as a hydrogen acceptor.

In summary, VCAM1 plays an important role in diabetic neurovascular complications through the endothelial cell

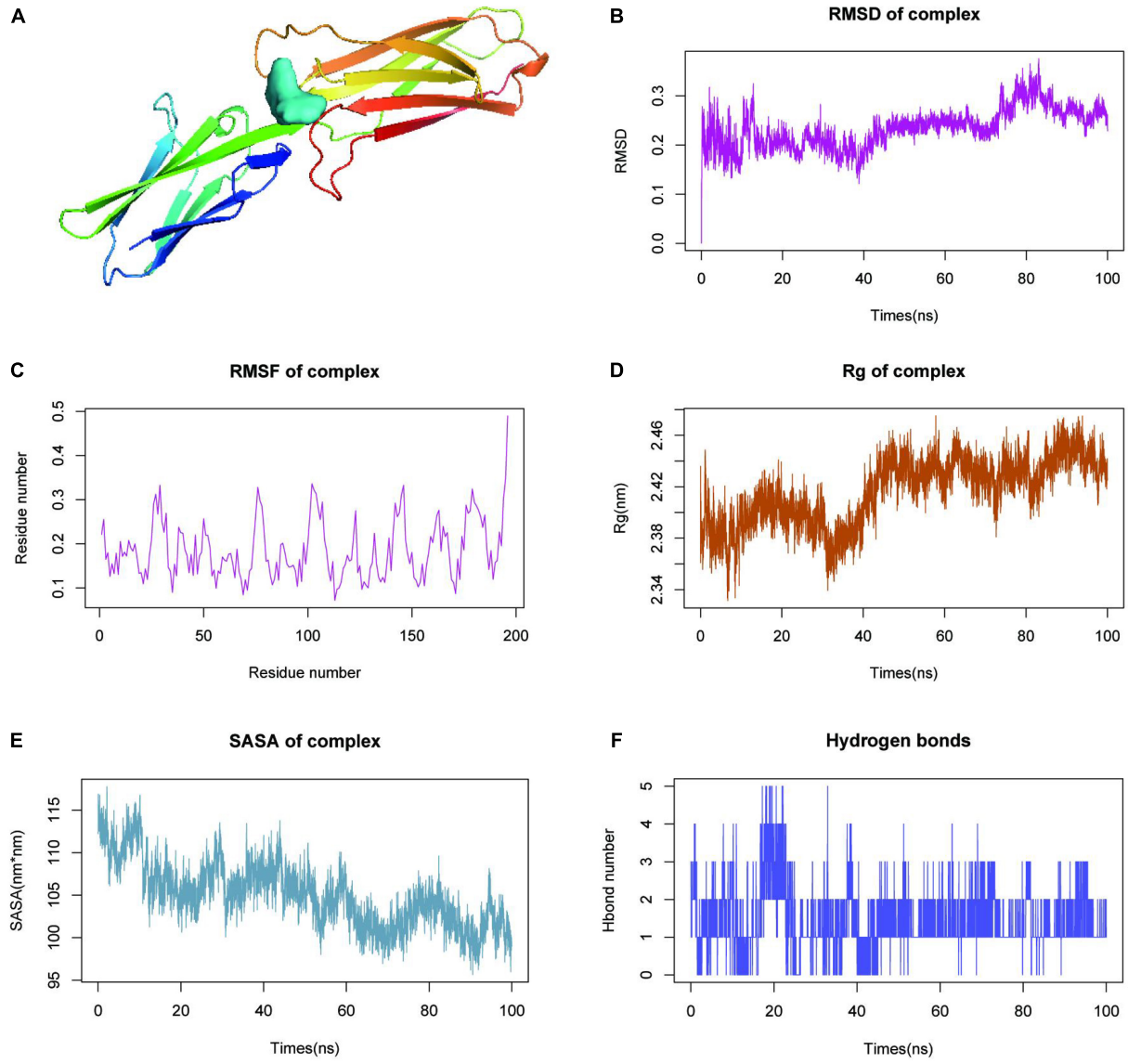

FIGURE 6
Molecular dynamics simulation (MDS) analysis of VCAM1-quercetin. **(A)** Molecular docking results of quercetin-VCAM1 complex. **(B)** Root-mean-square deviation of quercetin-VCAM1 complex MDS. **(C)** Root-mean-square fluctuation plot of quercetin-VCAM1 complex MDS. **(D)** Plot of Rg changes in MDS of quercetin-VCAM1 complex. **(E)** SASA changes of proteins in quercetin-VCAM1 complex MDS 0–100 ns. **(F)** Changes in hydrogen bonding in steady state of quercetin-VCAM1 complex.

subtype EC_EndMT, and quercetin can prevent diabetic neurovascular complications by targeting VCAM1.

Discussion

We identified the endothelial cell types associated with neurodegenerative diseases of diabetes and further identified five important genes, *FN1*, *VCAM1*, *FBN1*, *COL4A1*, and *COL4A2*. The *FN1* gene encodes the fibronectin protein, which is involved in cell adhesion and migration. FN1 is involved in the development and progression of various diseases, including spondyloepiphyseal dysplasia, corner fracture type and glomerulopathy with fibrin deposition (Zollinger and Smith, 2017). Moreover, it plays a roles in progression of diabetic nephropathy, however, the involved mechanisms are unclear (Yang et al., 2021). In addition, FN1 can influence the development of amyotrophic lateral sclerosis, one of the neurodegenerative diseases, by affecting the NF-κB pathway (Lin et al., 2020). *FBN1* encodes fibrillin, which can act as a structural component of calcium-bound microfibrils that provide load-bearing structural support in elastic and

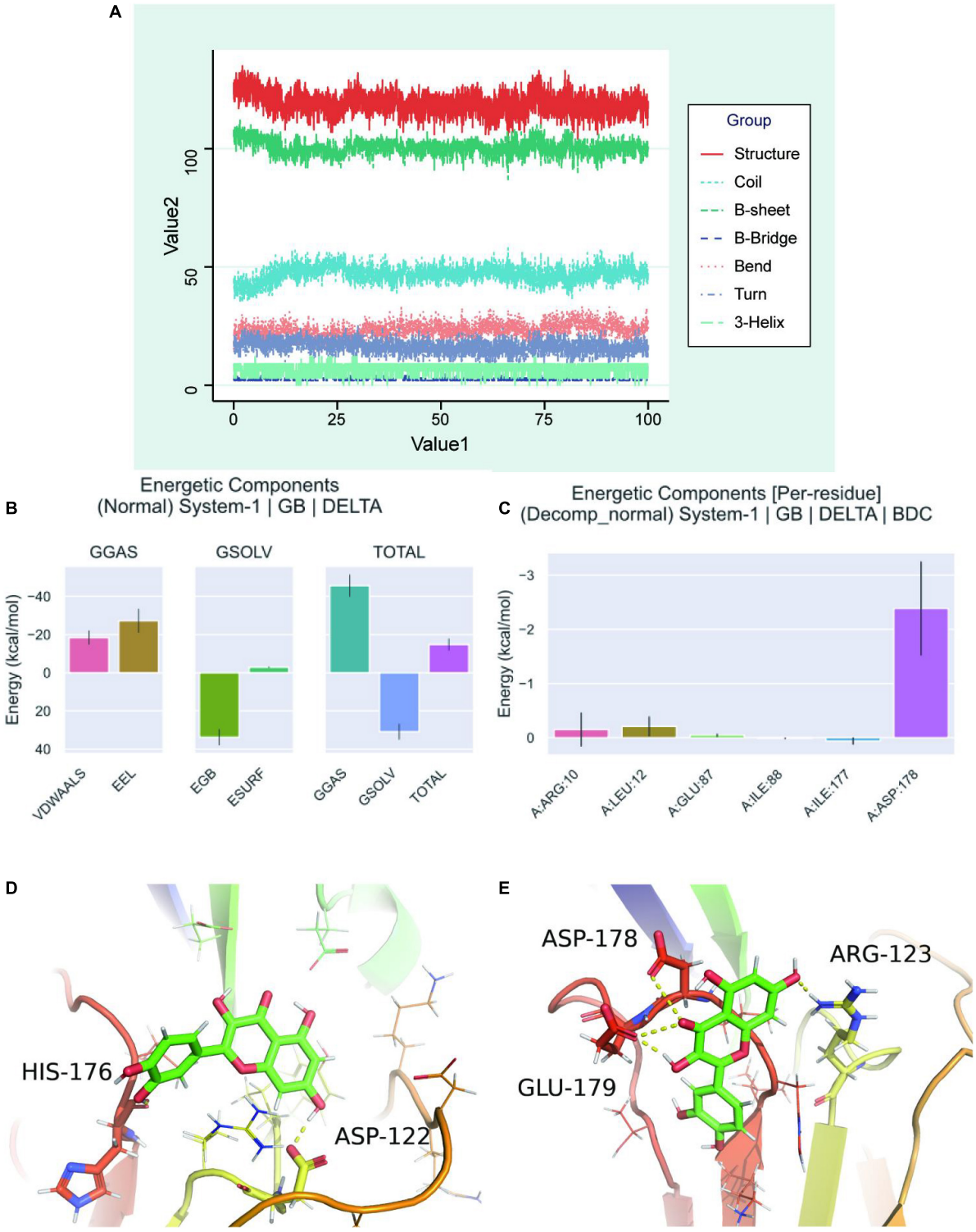

FIGURE 7
Molecular dynamics simulation analysis of secondary structure. **(A)** A graph showed the change of individual secondary structures of proteins over time in MDS system. **(B)** Free energy of binding between protein-ligand complexes. VDWAALS, "van der Waals energy"; Eel, "Electrostatic energy"; EGB, "Polar solvation energy"; ESURF, "Non-polar solvation energy"; GGAS, "Total gas phase free energy"; GSOLV, "Total solvation free energy"; TOTAL, The free energy item: "GSOLV + GGAS." **(C)** Relationship between each contact residue with binding energy. **(D)** Binding of quercetin-VCAM1 complex at critical frame of 22 ns. **(E)** Binding of quercetin-VCAM1 complex at critical frame of 73.4 ns.

inelastic connective tissues. The FBN1-associated diseases include Marfan syndrome and skin stiffness syndrome (Judge and Dietz, 2005; Sakai et al., 2016; Yu et al., 2020). It has been reported that FBN1 can initiate the development of obesity-induced diabetes (Hoffmann et al., 2020). *COL4A1* and *COL4A2* can encode different subunits of type IV collagen, a major structural component of the mucosa, and are associated with various diseases, including retinal artery tortuosity, cerebral small vessel disease with or without ocular abnormalities, cerebral small vessel disease and cerebral hemorrhage, which is closely associated with vascular disease (Volonghi et al., 2010; Kuo et al., 2012; Meuwissen et al., 2015). COL4A1 is involved in diabetic nephropathy while COL4A2 is involved in diabetic cardiovascular disease development (Adams et al., 2014; Rizvi et al., 2014). VCAM1, a member of the Ig superfamily, encodes a cell surface salivary gland glycoprotein expressed by endothelial cells, whose main function is to participate in cell adhesion and signaling, and possibly in neurodegenerative diseases of diabetes (Willeit et al., 2017; Kong et al., 2018; Niedzielski et al., 2020). We found that Fbn1 interact with Vcam1 mainly at EC_EndMT and fibroblasts. Further cell trajectory studies revealed that Vcam1 may play important roles in dysregulation of biological functions of EC_EndMT *via* cell-cell communication. Other studies have suggested that Vcam1 could be a marker for transitional obesity and diabetic nephropathy (Fadel et al., 2021). In the presence of hyperinsulinemia in type 2 diabetes, it activates the MAPK signaling pathway, which in turn activates the expressions VCAM1 and E-selectin and induces the production of ROS, involved in vascular damage in diabetes, including the neurodegenerative diseases (Potenza et al., 2009). We found that VCAM1 can inhibit endothelial cell growth and energy metabolism, suggesting that VCAM1 can promote the development of neurodegenerative diseases of diabetes. Therefore, we used VCAM1 as a site for action and performed MDSs of its potential action as a drug and realized that quercetin has a large binding potential to VCAM1.

Quercetin, a major constituent of many traditional Chinese medicines, has certain anti-tumor and anti-platelet aggregation effects. It is a flavonol compound with multiple biological activities, which can exert antioxidant effects by activating the NrF-2-ARE pathway or by promoting the expressions of antioxidant proteins (CAT and SOD) to improve the symptoms of several diseases, including neurodegenerative diseases, tumors, inflammatory diseases, obesity and diabetes (Wang et al., 2013; Kumar et al., 2016; Mukhopadhyay et al., 2018; Yarahmadi et al., 2018; Ebrahimpour et al., 2020; Abdou et al., 2022). Quercetin suppresses inflammation by reducing the expressions of pro-inflammatory factors, including IL-6 and IL-1β (Cheng et al., 2019). In addition, it can reduce MDA and NO levels, inhibit PI3K/PKB expressions to regulate glucose metabolism and reduce oxidative damage, as well as inhibit the NF-κB signaling pathway to improve islet functions. Above all, quercetin could improve the neurovascular symptoms of diabetes and reduce the incidence of neurodegenerative diseases in diabetic patients. Therefore, quercetin is a potential treatment option for type 2 diabetes and the complications of diabetes (Mukhopadhyay et al., 2018; Pathak et al., 2018). In addition, quercetin suppressed VCAM1 as well as ROS levels and delayed the progression of neurovascular complication of diabetes (Lotito et al., 2011; Wei et al., 2020). These studies suggest that quercetin has some complication-reducing effects in diabetes, and that for neurodegenerative diseases, quercetin can improve diabetic neurovascular damage by targeting VCAM1.

In summary, we identified key cells and factors involved in the progression of diabetes and its complications through single cell sequencing analysis data for the first time, providing a new theoretical basis for the diagnosis and treatment of diabetes. However, this study has some limitations. *In vivo* and *ex vivo* assays should be performed to further investigate the molecular mechanisms of action of quercetin.

Conclusion

We identified a complex role for EC_EndMT subtypes in progression of diabetes. Furthermore, it revealed the potential role in the development of neurodegenerative diseases of diabetes and developed a new Chinese medicine against the target, provided theoretical support for traditional Chinese medicine treatment of neurovascular complications. Through mechanisms involved in single cell analysis and cell-cell communication, VCAM1 may play an important role in neurodegenerative diseases of diabetes, and quercetin may be an effective drug for precise treatment of neurodegenerative diseases.

Data availability statement

The original contributions presented in this study are included in the article/**Supplementary material**, further inquiries can be directed to the corresponding author/s.

Author contributions

JH, WL, YS, QW, SH, ZH, LL, and XK: conceptualization, methodology, software, investigation, formal analysis, and writing—original draft. YC, HG, and ZC: data curation and

writing—original draft. CS, KG, JW, MY, and MC: visualization and investigation. YX: conceptualization, funding acquisition, resources, supervision, and writing—review and editing. All authors contributed to the article and approved the submitted version.

Funding

This work was supported by the Nursery Project of the Affiliated Tai'an City Central Hospital of Qingdao University (2022MPM06), the Shandong Medical and Health Technology Development Fund (202103070325), and the Shandong Province Major Science and Technology Public Relations Program (2015GSF118139).

Conflict of interest

The authors declare that the research was conducted in the absence of any commercial or financial relationships that could be construed as a potential conflict of interest.

Publisher's note

Supplementary material

The Supplementary Material for this article can be found online at: https://www.frontiersin.org/articles/10.3389/fnagi.2022.944195/full#supplementary-material

SUPPLEMENTARY FIGURE 1
Quality control of single-cell RNA-seq data. **(A)** Maps showed the distribution of the main features of cells before quality control. Red dashed line represented the threshold used to perform data filtering. **(B–E)** Data quality assessment after single-cell RNA-seq data filtering.

SUPPLEMENTARY FIGURE 2
Cell clustering and annotation process for single cell analysis. **(A)** UMAP plot showed cell aggregation in Chow and DDC groups. **(B)** UMAP plot showed the number and distribution of cell clusters after cell clustering. **(C)** UMAP plots showed the initial cell annotation of cell clusters by application of SingleR. The left side was based on MouseRNAseqData reference dataset, while the right side was based on ImmGenData reference dataset. **(D)** Violin plots of cell cluster and lineage marker gene.

SUPPLEMENTARY FIGURE 3
Visualization display of expressions of endothelial cell, mesenchymal, fibroblast and macrophage marker genes. Cdh5, Pecam1, Tek, Vwf, Tie1, and Col4a1 were marker genes for endothelial cell; Fn1, Tgfbr2, and Eln were marker genes for mesenchymal: Dcn and Col1a1 were marker genes for fibroblast; Cd68, Adgre1, and Lgals3 were marker genes for macrophage.

SUPPLEMENTARY FIGURE 4
Differential expression analysis of the five important genes in endothelial cell subtypes (EC_1, EC_2, EC_3, and EC_4). **(A,B)** Differential expression analysis of genes in EC_1. **(C,D)** Differential expression analysis of genes in EC_3. **(E)** Expressions of the five genes in EC_2. **(F)** Expressions of the five genes in EC_4 in the Chow group.

SUPPLEMENTARY FIGURE 5
Single-cell trajectories inferential analysis of endothelial cells. **(A)** UMAP plot showed individual cell types in cell clustering based on Monocle 2. **(B)** DDRtree plots showed the 3 cell states in endothelial cells. **(C)** DDRTree plot showed pseudotime values for endothelial cells. **(D)** The cell subtypes of endothelial cells in DDRtree plot. **(E)** Changes in expressions of the top 50 genes that were most associated with sorting of pseudotime. **(F)** DDRtree plot showed 5 cell states in the EC_EndMT.

References

Abdou, H. M., Hamaad, F. A., Ali, E. Y., and Ghoneum, M. H. (2022). Antidiabetic efficacy of Trifolium alexandrinum extracts hesperetin and quercetin in ameliorating carbohydrate metabolism and activating IR and AMPK signaling in the pancreatic tissues of diabetic rats. *Biomed. Pharmacother.* 149:112838. doi: 10.1016/j.biopha.2022.112838

Adams, J. N., Raffield, L. M., Freedman, B. I., Langefeld, C. D., Ng, M. C., Carr, J. J., et al. (2014). Analysis of common and coding variants with cardiovascular disease in the diabetes heart study. *Cardiovasc. Diabetol.* 13:77. doi: 10.1186/1475-2840-13-77

Aran, D., Looney, A. P., Liu, L., Wu, E., Fong, V., Hsu, A., et al. (2019). Reference-based analysis of lung single-cell sequencing reveals a transitional profibrotic macrophage. *Nat. Immunol.* 20, 163–172. doi: 10.1038/s41590-018-0276-y

Barrett, T., Wilhite, S. E., Ledoux, P., Evangelista, C., Kim, I. F., Tomashevsky, M., et al. (2012). NCBI GEO: Archive for functional genomics data sets—update. *Nucleic Acids Res.* 41:D991–D995. doi: 10.1093/nar/gks1193

Becht, E., McInnes, L., Healy, J., Dutertre, C.-A., Kwok, I. W. H., Ng, L. G., et al. (2018). Dimensionality reduction for visualizing single-cell data using UMAP. *Nat. Biotechnol.* 37, 38–44. doi: 10.1038/nbt.4314

Bell, D. S. H., and Goncalves, E. (2020). Stroke in the patient with diabetes (part 1) – Epidemiology, etiology, therapy and prognosis. *Diabetes Res. Clin. Pract.* 164:108193. doi: 10.1016/j.diabres.2020.108193

Bhatti, J. S., Bhatti, G. K., and Reddy, P. H. (2017). Mitochondrial dysfunction and oxidative stress in metabolic disorders — A step towards mitochondria based therapeutic strategies. *Biochim. Biophys. Acta Mol. Basis Dis.* 1863, 1066–1077. doi: 10.1016/j.bbadis.2016.11.010

Biessels, G. J., Staekenborg, S., Brunner, E., Brayne, C., and Scheltens, P. (2006). Risk of dementia in diabetes mellitus: A systematic review. *Lancet Neurol.* 5, 64–74. doi: 10.1016/S1474-4422(05)70284-2

Bradley, S. A., Spring, K. J., Beran, R. G., Chatzis, D., Killingsworth, M. C., and Bhaskar, S. M. M. (2022). Role of diabetes in stroke: Recent advances in pathophysiology and clinical management. *Diabetes Metab. Res. Rev.* 38:e3495. doi: 10.1002/dmrr.3495

Burley, S. K., Berman, H. M., Bhikadiya, C., Bi, C., Chen, L., Di Costanzo, L., et al. (2019). RCSB Protein Data Bank: Biological macromolecular structures enabling research and education in fundamental biology, biomedicine, biotechnology and energy. *Nucleic Acids Res.* 47:D464–D474. doi: 10.1093/nar/gky1004

Cao, J., Spielmann, M., Qiu, X., Huang, X., Ibrahim, D. M., Hill, A. J., et al. (2019). The single-cell transcriptional landscape of mammalian organogenesis. *Nature* 566, 496–502. doi: 10.1038/s41586-019-0969-x

Chao, M.-L., Luo, S., Zhang, C., Zhou, X., Zhou, M., Wang, J., et al. (2021). S-nitrosylation-mediated coupling of G-protein alpha-2 with CXCR5 induces Hippo/YAP-dependent diabetes-accelerated atherosclerosis. *Nat. Commun.* 12:4452. doi: 10.1038/s41467-021-24736-y

Chen, Y., Luo, Z., Lin, J., Qi, B., Sun, Y., Li, F., et al. (2022a). Exploring the Potential Mechanisms of Melilotus officinalis (L.) Pall. in Chronic Muscle Repair Patterns Using Single Cell Receptor-Ligand Marker Analysis and Molecular Dynamics Simulations. *Dis. Markers* 2022:9082576. doi: 10.1155/2022/9082576

Chen, Y., Sun, Y., Luo, Z., Chen, X., Wang, Y., Qi, B., et al. (2022b). Exercise Modifies the Transcriptional Regulatory Features of Monocytes in Alzheimer's Patients: A Multi-Omics Integration Analysis Based on Single Cell Technology. *Front. Aging Neurosci.* 14:881488. doi: 10.3389/fnagi.2022.881488

Cheng, S.-C., Huang, W.-C. S., Pang, J.-H., Wu, Y.-H., and Cheng, C.-Y. (2019). Quercetin Inhibits the Production of IL-1β-Induced Inflammatory Cytokines and Chemokines in ARPE-19 Cells via the MAPK and NF-κB Signaling Pathways. *Int. J. Mol. Sci.* 20:2957. doi: 10.3390/ijms20122957

Cheong, J. L. Y., de Pablo-Fernandez, E., Foltynie, T., and Noyce, A. J. (2020). The Association Between Type 2 Diabetes Mellitus and Parkinson's Disease. *J. Parkinsons Dis.* 10, 775–789. doi: 10.3233/JPD-191900

D'Onofrio, N., Sardu, C., Trotta, M. C., Scisciola, L., Turriziani, F., Ferraraccio, F., et al. (2021). Sodium-glucose co-transporter2 expression and inflammatory activity in diabetic atherosclerotic plaques: Effects of sodium-glucose co-transporter2 inhibitor treatment. *Mol. Metab.* 54:101337. doi: 10.1016/j.molmet.2021.101337

Ebrahimpour, S., Zakeri, M., and Esmaeili, A. (2020). Crosstalk between obesity, diabetes, and alzheimer's disease: Introducing quercetin as an effective triple herbal medicine. *Ageing Res. Rev.* 62:101095. doi: 10.1016/j.arr.2020.101095

Efremova, M., Vento-Tormo, M., Teichmann, S. A., and Vento-Tormo, R. (2020). CellPhoneDB: Inferring cell–cell communication from combined expression of multi-subunit ligand–receptor complexes. *Nat. Protoc.* 15, 1484–1506. doi: 10.1038/s41596-020-0292-x

Fadel, M. M., Abdel Ghaffar, F. R., Zwain, S. K., Ibrahim, H. M., and Badr, E. A. E. (2021). Serum netrin and VCAM-1 as biomarker for Egyptian patients with type II diabetes mellitus. *Biochem. Biophys. Rep.* 27:101045. doi: 10.1016/j.bbrep.2021.101045

Ferket, B. S., Hunink, M. G. M., Masharani, U., Max, W., Yeboah, J., Burke, G. L., et al. (2022). Lifetime Cardiovascular Disease Risk by Coronary Artery Calcium Score in Individuals With and Without Diabetes: An Analysis From the Multi-Ethnic Study of Atherosclerosis. *Diabetes Care* 45, 975–982. doi: 10.2337/dc21-1607

Gong, Q., Zhang, P., Wang, J., Ma, J., An, Y., Chen, Y., et al. (2019). Morbidity and mortality after lifestyle intervention for people with impaired glucose tolerance: 30-year results of the Da Qing Diabetes Prevention Outcome Study. *Lancet Diabetes Endocrinol.* 7, 452–461. doi: 10.1016/S2213-8587(19)30093-2

Hickson, L. J., Langhi Prata, L. G. P., Bobart, S. A., Evans, T. K., Giorgadze, N., Hashmi, S. K., et al. (2019). Senolytics decrease senescent cells in humans: Preliminary report from a clinical trial of Dasatinib plus Quercetin in individuals with diabetic kidney disease. *EBioMedicine* 47, 446–456. doi: 10.1016/j.ebiom.2019.08.069

Hoffmann, J. G., Xie, W., and Chopra, A. R. (2020). Energy Regulation Mechanism and Therapeutic Potential of Asprosin. *Diabetes* 69, 559–566. doi: 10.2337/dbi19-0009

Hougaard, A., Younis, S., Iljazi, A., Haanes, K. A., Lindberg, U., Vestergaard, M. B., et al. (2020). Cerebrovascular effects of endothelin-1 investigated using high-resolution magnetic resonance imaging in healthy volunteers. *J. Cereb. Blood Flow Metab.* 40, 1685–1694. doi: 10.1177/0271678X19874295

Huo, X., Gao, L., Guo, L., Xu, W., Wang, W., Zhi, X., et al. (2016). Risk of non-fatal cardiovascular diseases in early-onset versus late-onset type 2 diabetes in China: A cross-sectional study. *Lancet Diabetes Endocrinol.* 4, 115–124. doi: 10.1016/S2213-8587(15)00508-2

Judge, D. P., and Dietz, H. C. (2005). Marfan's syndrome. *Lancet* 366, 1965–1976. doi: 10.1016/S0140-6736(05)67789-6

Kang, X., Sun, Y., Yi, B., Jiang, C., Yan, X., Chen, B., et al. (2022). Based on Network Pharmacology and Molecular Dynamics Simulations, Baicalein, an Active Ingredient of Yiqi Qingre Ziyin Method, Potentially Protects Patients With Atrophic Rhinitis From Cognitive Impairment. *Front. Aging Neurosci.* 14:880794. doi: 10.3389/fnagi.2022.880794

Kong, D.-H., Kim, Y., Kim, M., Jang, J., and Lee, S. (2018). Emerging Roles of Vascular Cell Adhesion Molecule-1 (VCAM-1) in Immunological Disorders and Cancer. *Int. J. Mol. Sci.* 19:1057. doi: 10.3390/ijms19041057

Kumar, A. D. N., Bevara, G. B., Kaja, L. K., Badana, A. K., and Malla, R. R. (2016). Protective effect of 3-O-methyl quercetin and kaempferol from Semecarpus anacardium against H2O2 induced cytotoxicity in lung and liver cells. *BMC Complement. Altern. Med.* 16:376. doi: 10.1186/s12906-016-1354-z

Kuo, D. S., Labelle-Dumais, C., and Gould, D. B. (2012). COL4A1 and COL4A2 mutations and disease: Insights into pathogenic mechanisms and potential therapeutic targets. *Hum. Mol. Genet.* 21:R97–R110. doi: 10.1093/hmg/dds346

Li, Y., Teng, D., Shi, X., Qin, G., Qin, Y., Quan, H., et al. (2020). Prevalence of diabetes recorded in mainland China using 2018 diagnostic criteria from the American Diabetes Association: National cross sectional study. *BMJ* 369:m997. doi: 10.1136/bmj.m997

Lin, J., Huang, P., Chen, W., Ye, C., Su, H., and Yao, X. (2020). Key Molecules and Pathways Underlying Sporadic Amyotrophic Lateral Sclerosis: Integrated Analysis on Gene Expression Profiles of Motor Neurons. *Front. Genet.* 11:578143. doi: 10.3389/fgene.2020.578143

Lin, W., Wang, Y., Chen, Y., Wang, Q., Gu, Z., and Zhu, Y. (2021). Role of Calcium Signaling Pathway-Related Gene Regulatory Networks in Ischemic Stroke Based on Multiple WGCNA and Single-Cell Analysis. *Oxid. Med. Cell. Longev.* 2021:8060477. doi: 10.1155/2021/8060477

Ling, C., Bacos, K., and Rönn, T. (2022). Epigenetics of type 2 diabetes mellitus and weight change — a tool for precision medicine? *Nat. Rev. Endocrinol.* 18, 433–448. doi: 10.1038/s41574-022-00671-w

Lotito, S. B., Zhang, W.-J., Yang, C. S., Crozier, A., and Frei, B. (2011). Metabolic conversion of dietary flavonoids alters their anti-inflammatory and antioxidant properties. *Free Radic. Biol. Med.* 51, 454–463. doi: 10.1016/j.freeradbiomed.2011.04.032

Lu, L., Kang, X., Yi, B., Jiang, C., Yan, X., Chen, B., et al. (2022). Exploring the Mechanism of Yiqi Qingre Ziyin Method in Regulating Neuropeptide Expression for the Treatment of Atrophic Rhinitis. *Dis. Markers* 2022:4416637. doi: 10.1155/2022/4416637

Masters, L., Eagon, S., and Heying, M. (2020). Evaluation of consensus scoring methods for AutoDock Vina, smina and idock. *J. Mol. Graph. Model.* 96:107532. doi: 10.1016/j.jmgm.2020.107532

Meuwissen, M. E. C., Halley, D. J. J., Smit, L. S., Lequin, M. H., Cobben, J. M., de Coo, R., et al. (2015). The expanding phenotype of COL4A1 and COL4A2 mutations: Clinical data on 13 newly identified families and a review of the literature. *Genet. Med.* 17, 843–853. doi: 10.1038/gim.2014.210

Mukhopadhyay, P., Maity, S., Mandal, S., Chakraborti, A. S., Prajapati, A. K., and Kundu, P. P. (2018). Preparation, characterization and in vivo evaluation of pH sensitive, safe quercetin-succinylated chitosan-alginate core-shell-corona nanoparticle for diabetes treatment. *Carbohydr. Polym.* 182, 42–51. doi: 10.1016/j.carbpol.2017.10.098

Neese, F., Wennmohs, F., Becker, U., and Riplinger, C. (2020). The ORCA quantum chemistry program package. *J. Chem. Phys.* 152:224108. doi: 10.1063/5.0004608

Nguyen, H., Pérez, A., Bermeo, S., and Simmerling, C. (2015). Refinement of generalized born implicit solvation parameters for nucleic acids and their complexes with proteins. *J. Chem. Theory Comput.* 11, 3714–3728. doi: 10.1021/acs.jctc.5b00271

Niedzielski, M., Broncel, M., Gorzelak-Pabiś, P., and Woźniak, E. (2020). New possible pharmacological targets for statins and ezetimibe. *Biomed. Pharmacother.* 129:110388. doi: 10.1016/j.biopha.2020.110388

Pathak, S., Regmi, S., Nguyen, T. T., Gupta, B., Gautam, M., Yong, C. S., et al. (2018). Polymeric microsphere-facilitated site-specific delivery of quercetin prevents senescence of pancreatic islets in vivo and improves transplantation outcomes in mouse model of diabetes. *Acta Biomater.* 75, 287–299. doi: 10.1016/j.actbio.2018.06.006

Potenza, M., Gagliardi, S., Nacci, C., Carratu, M., and Montagnani, M. (2009). Endothelial Dysfunction in Diabetes: From Mechanisms to Therapeutic Targets. *Curr. Med. Chem.* 16, 94–112. doi: 10.2174/092986709787002853

Qiu, X., Hill, A., Packer, J., Lin, D., Ma, Y.-A., and Trapnell, C. (2017). Single-cell mRNA quantification and differential analysis with Census. *Nat. Methods* 14, 309–315. doi: 10.1038/nmeth.4150

Rizvi, S., Raza, S. T., and Mahdi, F. (2014). Association of genetic variants with diabetic nephropathy. *World J. Diabetes* 5:809–816. doi: 10.4239/wjd.v5.i6.809

Sakai, L. Y., Keene, D. R., Renard, M., and De Backer, J. (2016). FBN1: The disease-causing gene for Marfan syndrome and other genetic disorders. *Gene* 591, 279–291. doi: 10.1016/j.gene.2016.07.033

Saltiel, A. R., and Olefsky, J. M. (2017). Inflammatory mechanisms linking obesity and metabolic disease. *J. Clin. Investig.* 127, 1–4. doi: 10.1172/JCI92035

Stuart, T., Butler, A., Hoffman, P., Hafemeister, C., Papalexi, E., Mauck, W. M., et al. (2019). Comprehensive Integration of Single-Cell Data. *Cell* 177, 1888–1902.e21. doi: 10.1016/j.cell.2019.05.031

Subramanian, A., Tamayo, P., Mootha, V. K., Mukherjee, S., Ebert, B. L., Gillette, M. A., et al. (2005). Gene set enrichment analysis: A knowledge-based approach for interpreting genome-wide expression profiles. *Proc. Natl. Acad. Sci. U.S.A.* 102, 15545–15550. doi: 10.1073/pnas.0506580102

Tang, G., Pi, L., Guo, H., Hu, Z., Zhou, C., Hu, Q., et al. (2022). Naringin Relieves Diabetic Cardiac Autonomic Neuropathy Mediated by P2Y14 Receptor in Superior Cervical Ganglion. *Front. Pharmacol.* 13:873090. doi: 10.3389/fphar.2022.873090

Tang, G.-Y., Yu, P., Zhang, C., Deng, H.-Y., Lu, M.-X., and Le, J.-H. (2022). The Neuropeptide-Related HERC5/TAC1 Interactions May Be Associated with the Dysregulation of lncRNA GAS5 Expression in Gestational Diabetes Mellitus Exosomes. *Dis. Markers* 2022:8075285. doi: 10.1155/2022/8075285

Tao, P., Ji, J., Gu, S., Wang, Q., and Xu, Y. (2022). Progress in the Mechanism of Autophagy and Traditional Chinese Medicine Herb Involved in Dementia. *Front. Pharmacol.* 12:825330. doi: 10.3389/fphar.2021.825330

Trapnell, C., Cacchiarelli, D., Grimsby, J., Pokharel, P., Li, S., Morse, M., et al. (2014). The dynamics and regulators of cell fate decisions are revealed by pseudotemporal ordering of single cells. *Nat. Biotechnol.* 32, 381–386. doi: 10.1038/nbt.2859

Tunyasuvunakool, K., Adler, J., Wu, Z., Green, T., Zielinski, M., Žídek, A., et al. (2021). Highly accurate protein structure prediction for the human proteome. *Nature* 596, 590–596. doi: 10.1038/s41586-021-03828-1

Urner, S., Ho, F., Jha, J. C., Ziegler, D., and Jandeleit-Dahm, K. N. A. D. P. H. (2020). Oxidase Inhibition: Preclinical and Clinical Studies in Diabetic Complications. *Antioxid. Redox Signal.* 33, 415–434. doi: 10.1089/ars.2020.8047

Valdés-Tresanco, M. S., Valdés-Tresanco, M. E., Valiente, P. A., and Moreno, E. (2021). gmx MMPBSA: A New Tool to Perform End-State Free Energy Calculations with GROMACS. *J. Chem. Theory Comput.* 17, 6281–6291. doi: 10.1021/acs.jctc.1c00645

Van Der Spoel, D., Lindahl, E., Hess, B., Groenhof, G., Mark, A. E., and Berendsen, H. J. C. (2005). GROMACS: Fast, flexible, and free. *J. Comput. Chem.* 26, 1701–1718. doi: 10.1002/jcc.20291

Volonghi, I., Pezzini, A., Del Zotto, E., Giossi, A., Costa, P., Ferrari, D., et al. (2010). Role of COL4A1 in Basement-Membrane Integrity and Cerebral Small-Vessel Disease. The COL4A1 Stroke Syndrome. *Curr. Med. Chem.* 17, 1317–1324. doi: 10.2174/092986710790936293

Wang, L., Peng, W., Zhao, Z., Zhang, M., Shi, Z., Song, Z., et al. (2021). Prevalence and Treatment of Diabetes in China, 2013-2018. *JAMA* 326, 2498–2506. doi: 10.1001/jama.2021.22208

Wang, W., Wang, C., Ding, X.-Q., Pan, Y., Gu, T.-T., Wang, M.-X., et al. (2013). Quercetin and allopurinol reduce liver thioredoxin-interacting protein to alleviate inflammation and lipid accumulation in diabetic rats: Quercetin and allopurinol inhibit TXNIP. *Br. J. Pharmacol.* 169, 1352–1371. doi: 10.1111/bph.12226

Wei, J., Zhang, Y., Li, D., Xie, T., Li, Y., Li, J., et al. (2020). Integrating Network Pharmacology and Component Analysis Study on Anti-Atherosclerotic Mechanisms of Total Flavonoids of *Engelhardia roxburghiana* Leaves in Mice. *Chem. Biodivers.* 17:e1900629. doi: 10.1002/cbdv.201900629

Weiser, J., Shenkin, P. S., and Still, W. C. (1999). Approximate atomic surfaces from linear combinations of pairwise overlaps (LCPO). *J. Comput. Chem.* 20, 217–230. doi: 10.1002/(SICI)1096-987X(19990130)20:2<217::AID-JCC4<3.0.CO;2-A

Willeit, K., Pechlaner, R., Willeit, P., Skroblin, P., Paulweber, B., Schernthaner, C., et al. (2017). Association Between Vascular Cell Adhesion Molecule 1 and Atrial Fibrillation. *JAMA Cardiol.* 2:516. doi: 10.1001/jamacardio.2017.0064

Yang, C., Chen, X.-C., Li, Z.-H., Wu, H.-L., Jing, K.-P., Huang, X.-R., et al. (2021). SMAD3 promotes autophagy dysregulation by triggering lysosome depletion in tubular epithelial cells in diabetic nephropathy. *Autophagy* 17, 2325–2344. doi: 10.1080/15548627.2020.1824694

Yang, F., Yang, M.-Y., Le, J.-Q., Luo, B.-Y., Yin, M.-D., Chao-Li, et al. (2022). Protective Effects and Therapeutics of Ginsenosides for Improving Endothelial Dysfunction: From Therapeutic Potentials, Pharmaceutical Developments to Clinical Trials. *Am. J. Chin. Med.* 50, 749–772. doi: 10.1142/S0192415X22500318

Yarahmadi, A., Khademi, F., Mostafavi-Pour, Z., and Zal, F. (2018). In-Vitro Analysis of Glucose and Quercetin Effects on m-TOR and Nrf-2 Expression in HepG2 Cell Line (Diabetes and Cancer Connection). *Nutr. Cancer* 70, 770–775. doi: 10.1080/01635581.2018.1470654

Yu, Y., He, J., Hu, L., Jiang, L., Fang, L., Yao, G., et al. (2020). Placensin is a glucogenic hormone secreted by human placenta. *EMBO Rep.* 21:e49530. doi: 10.15252/embr.201949530

Zhang, Q., Yang, J., Yang, C., Yang, X., and Chen, Y. (2022). Eucommia ulmoides Oliver-Tribulus terrestris L. drug pair regulates ferroptosis by mediating the neurovascular-related ligand-receptor interaction pathway- a potential drug pair for treatment hypertension and prevention ischemic stroke. *Front Neurol.* 13:833922. doi: 10.3389/fneur.2022.833922

Zhao, G., Lu, H., Liu, Y., Zhao, Y., Zhu, T., Garcia-Barrio, M. T., et al. (2021). Single-Cell Transcriptomics Reveals Endothelial Plasticity During Diabetic Atherogenesis. *Front. Cell Dev. Biol.* 9:689469. doi: 10.3389/fcell.2021.689469

Zollinger, A. J., and Smith, M. L. (2017). Fibronectin, the extracellular glue. *Matrix Biol.* 6, 27–37. doi: 10.1016/j.matbio.2016.07.011

Advantages of publishing in Frontiers

OPEN ACCESS
Articles are free to read for greatest visibility and readership

FAST PUBLICATION
Around 90 days from submission to decision

HIGH QUALITY PEER-REVIEW
Rigorous, collaborative, and constructive peer-review

TRANSPARENT PEER-REVIEW
Editors and reviewers acknowledged by name on published articles

Frontiers
Avenue du Tribunal-Fédéral 34
1005 Lausanne | Switzerland

Visit us: www.frontiersin.org
Contact us: frontiersin.org/about/contact

REPRODUCIBILITY OF RESEARCH
Support open data and methods to enhance research reproducibility

DIGITAL PUBLISHING
Articles designed for optimal readership across devices

FOLLOW US
@frontiersin

IMPACT METRICS
Advanced article metrics track visibility across digital media

EXTENSIVE PROMOTION
Marketing and promotion of impactful research

LOOP RESEARCH NETWORK
Our network increases your article's readership